Lecture Notes in Physics 880

Allen Hunt
Robert Ewing
Behzad Ghanbarian

Percolation Theory for Flow in Porous Media

Third Edition

With Forewords by John Selker, Robert Horton and Muhammad Sahimi

Springer

Lecture Notes in Physics

Volume 880

For further volumes:
www.springer.com/series/5304

The Lecture Notes in Physics

The series Lecture Notes in Physics (LNP), founded in 1969, reports new developments in physics research and teaching—quickly and informally, but with a high quality and the explicit aim to summarize and communicate current knowledge in an accessible way. Books published in this series are conceived as bridging material between advanced graduate textbooks and the forefront of research and to serve three purposes:

- to be a compact and modern up-to-date source of reference on a well-defined topic
- to serve as an accessible introduction to the field to postgraduate students and nonspecialist researchers from related areas
- to be a source of advanced teaching material for specialized seminars, courses and schools

Both monographs and multi-author volumes will be considered for publication. Edited volumes should, however, consist of a very limited number of contributions only. Proceedings will not be considered for LNP.

Volumes published in LNP are disseminated both in print and in electronic formats, the electronic archive being available at springerlink.com. The series content is indexed, abstracted and referenced by many abstracting and information services, bibliographic networks, subscription agencies, library networks, and consortia.

Proposals should be sent to a member of the Editorial Board, or directly to the managing editor at Springer:

Christian Caron
Springer Heidelberg
Physics Editorial Department I
Tiergartenstrasse 17
69121 Heidelberg/Germany
christian.caron@springer.com

Allen Hunt • Robert Ewing • Behzad Ghanbarian

Percolation Theory for Flow in Porous Media

Third Edition

Springer

Allen Hunt
Department of Earth and Environmental Sciences
Wright State University
Dayton, OH, USA

Behzad Ghanbarian
Department of Earth and Environmental Sciences
Wright State University
Dayton, OH, USA

Robert Ewing
Department of Agronomy
Iowa State University
Ames, IA, USA

ISSN 0075-8450
ISSN 1616-6361 (electronic)
Lecture Notes in Physics
ISBN 978-3-319-03770-7
ISBN 978-3-319-03771-4 (eBook)
DOI 10.1007/978-3-319-03771-4
Springer Cham Heidelberg New York Dordrecht London

Library of Congress Control Number: 2014931418

Printed on acid-free paper

Springer is part of Springer Science+Business Media (www.springer.com)

Foreword to the Third Edition

Flow and transport phenomena in porous media arise in many diverse fields of science. What makes this field so fascinating is the fact that, in order to truly understand any given phenomenon in a porous medium, one must account for the complex pore structure of the medium and its interaction with its fluid content. It is this interaction that controls the distribution, flow, displacement of one or more fluids, or dispersion (mixing) of one fluid in or by another fluid. If the fluid is reactive or, for example, carries ions or particles of various shapes, sizes, and electrical charges, or if it is under a large enough force that may go under deformation, the pore structure of the medium may change due to the reaction of the fluid with the pore surface, or the physicochemical interaction between the particles and the pore surface.

In the early years of studying flow phenomena in porous media, it was almost always invariably assumed that the heterogeneities were randomly distributed, and not correlated with each other. Moreover, it was also routinely assumed that the heterogeneities occur over length scales that are much smaller than the overall linear size of the system, so that one could always write down well-defined averaged equations governing any phenomenon based on the classical equations of hydrodynamics. However, strong evidence, accumulated over decades, suggested that rock and other types of porous media do not conform to such simplistic assumptions. They exhibit correlations in their properties that are often present at all the length scales. The existence of such correlations necessitated the introduction of fractal distributions that have enabled us to understand how the spatial distributions of the various properties depend on the length scale of observations and are correlated with one another.

But, correlations and scale-dependence are only half the story. The other half is the connectivity. In natural, and often many man-made, porous media the pores are connected in a complex fashion. Clearly, if the connected pores cannot provide a sample-spanning path for the fluids to flow, there will be no macroscopic flow. The same thing happens in large-scale porous media, such as those at field scale. In such a porous medium the permeabilities of the various regions often follow a broad distribution. Thus, although parts of the medium may be highly permeable, other segments may be practically impermeable, or allow very little fluid to go through.

This implies that, for large-scale fluid flow and transport take place in such porous media, the permeable regions must be connected. The language and the tools for taking into account the effect of the connectivity are provided by percolation theory.

The book by Hunt, Ewing, and Ghanbarian demonstrates the crucial role that the connectivity and correlations play in fluid flow in porous media, and how percolation theory may be used fruitfully to address many complex phenomena in porous media. They bring out the history of the applications of percolation theory to fluid flow in porous media, a history that is now about 40 years old, and take us through an amazing collection of problems in porous media, ranging from the characterization of their morphology—their pore connectivity, pore geometry, and surface roughness—to various fluid flow and transport phenomena in their pore space. In each case, they discuss very convincingly why correlations and power laws that are characteristics of percolation systems are relevant concepts, and how they are used to address many problems that might have seemed hopelessly complex to solve just three or four decades ago. I have always believed that there is hardly any problem in any disordered porous medium to which percolation theory and the effect of connectivity and correlations are not relevant. The book by Hunt, Ewing, and Ghanbarian amply confirms my belief. Part of the book represents the important contributions that the authors themselves have made to this research areas. Other parts reflect the tremendous progress that has been made over the past few decades.

The field of porous media and in particular the application of percolation theory to their characterization and modeling and fluid flow therein is still highly active and thriving. Thus, this book, now in its third edition and more complete than ever before, is a most welcome addition to this rapidly growing literature, which will be highly useful to both practitioners of the field, as well as those who wish to become familiar with the concepts and ideas of percolation theory, and how they are used to address complex phenomena in porous media.

University of Southern California Muhammad Sahimi
Los Angeles, USA

Foreword to the Second Edition

Scientists specialize. In attempting to isolate and understand individual processes, we risk losing sight of the whole. In essence, most of us study isolated trees rather than considering the whole forest. This specialization is evident in the science of porous media: most studies focus on just one or a few specific media, with only occasional papers addressing a broad class of media. Thus we have specialists in natural media such as soil, fractured rock, and granular materials, while others focus on powders, foodstuffs, paper and textiles, ceramics, building materials, and so on.

Percolation theory has been touted as providing a general framework for describing generalized transport in all types of media. Can this general framework be applied to a specific class of porous media, with at least as much success as the accumulated insights of decades of more conventional approaches? If the answer is yes, then applying percolation theory to transport processes in porous media will yield great scientific progress.

To illustrate this point, I will briefly consider the porous media that I study. Soils are a growth medium for plants, and so they support most terrestrial life. More than six billion people depend on soils for food, for storing and purifying water, for recycling waste, and for holding us up. This vital layer covering the earth's terrestrial surface is fragile. Often less than a meter thick, soils develop slowly but are easily damaged by accelerated erosion, compaction, tillage, and pollution. Thus knowledge of soils and their wise management is crucial for sustaining civilization.

But soils are tremendously complex and variable. To describe a transport process in the soil, one must first define the time scale and the sample size; only then can the relevant scale(s) of climate, geology, landscape position, vegetation, and management be considered. The interface between air and land, between vegetable and mineral, routinely encounters extremes of heat and cold, wet and dry, growth and decay. Transport is irregular and incessant: heat, water, both as liquid and vapor, organic and inorganic carbon are constantly on the move.

Conceptual and mathematical models describing these transport processes have grown increasingly complex. Attempting to describe a greater range of behaviors, soil scientists have incorporated macropores (wormholes, drying cracks), aggregates, clay flocs and tactoids, and mineral-specific surface chemistry into our mod-

els. While our predictions have (on average) improved, the model parameters have become more numerous, more difficult to quantify, and arguably less physically defensible. Continuous, volume-averaged functions gloss over important details: the ubiquitous nonlinear behaviors appear to be driven by discrete events, discrete pore pathways, and discrete "tipping points."

When I first met Robert (Toby) Ewing about 15 years ago, I invited him to present a guest lecture to students in my graduate-level soil physics course, which covers heat transfer, water flow, chemical transport, and coupled processes. Over the ensuing years I invited Toby to expand his role in the course. His contributions grew in quantity and quality, and now we effectively co-teach the course. I focus on continuous mathematical approaches following Fick, Fourier, Buckingham, Taylor, Richards, and others. Toby focuses on discrete mathematical approaches for flow and transport, including network models, percolation theory, and critical path analysis.

Toby sometimes chides me about being stuck on "old" approaches (playfully using words like ancient and Neanderthal). I respond that the so-called "old" ways are tested and trustworthy, while his "new" approaches lack measurement support and substantive application. However, my defense of the 'old' ways has been weakening since Toby met Allen Hunt about eight years ago. Allen has been at the forefront of applying percolation theory to transport in (mainly geological) porous media. Allen and Toby have developed a fruitful collaboration; this book, rich in insights, is one such fruit. They present examples of percolation theory applied to gas transfer, water retention and flow, electrical conductivity, heat transfer, and dispersion. Over time I have come to appreciate the potential power of their work.

From time to time in science some new concept rings a bell, and scientists rush to engage the new concept. I want to help "ring the bell" for this excellent work of Hunt and Ewing. In soil science we have focused on empirical descriptions of flow and transport. Hunt and Ewing offer percolation theory as a foundational description of how to proceed with a unifying approach. Can percolation theory prove to be a unifying theory in porous media? Perhaps. The theory is sound, but applications of the theory to real porous media will require care and wisdom. The theory is unifying, but like all theories it carries restrictions of simplifying assumptions. Questions of when and when not, how and how not to apply the theory are valid and important questions. Hunt and Ewing provide a foundation, and invite others to engage in the iterative process of applying, evaluating, and advancing the theory.

The foundations of percolation theory presented in this book allow for the study of isolated trees, but Hunt and Ewing also connect the trees to the forest. I encourage the broad range of porous media scientists to study this book. I think the book provides new ways to consider the processes occurring in porous media, and it will inspire new thought, analysis, and exploration of flow in porous media.

Curtiss Distinguished Professor of Agriculture
Ames, IA, USA Robert Horton
Eve of Thanksgiving (November) 2008

Foreword to the First Edition

Though a sledge hammer may be wonderful for breaking rock, it is a poor choice for driving a tack into a picture frame. There is a fundamental, though often subtle, connection between a tool and the application. When Newton and Leibniz developed the Calculus they created a tool of unprecedented power. The standard continuum approach has served admirably in the description of fluid behavior in porous media: the conservation of mass and linear response to energy gradients fit conveniently, and are solid foundations upon which to build. But to solve these equations we must characterize the up-scaled behavior of the medium at the continuum level. The nearly universal approach has been to conceive the medium as a bundle of capillary tubes. Some authors made the tubes porous, so they could fill and drain through their walls; others "broke and reconnected" them so each tube had a range of diameters along its length. In the end it must be admitted that the marriage of tool (capillary tube bundles) and task (to derive the constitutive relations for porous media) has not yet proven to be entirely satisfactory. Lacking in these conceptual models is a framework to describe the fluid-connected networks within the medium which evolve as functions of grain size distribution, porosity, saturation, and contact angle. This is fundamentally a geometry problem: how to concisely describe the particular nature of this evolving, sparse, dendritic, space-filling network.

Recognizing this basic problem, the community flocked to the fractal models as they became better understood in the 1990s. But fractals alone were not enough, as the real problem was to understand not the geometry of the medium, but the geometry of the fluids within the medium, and moreover, to correctly identify the geometry of the locations that control the flow.

I met Allen Hunt in the late 1990s, and over coffee he described his ideas about critical path analysis for the development of constitutive relationships for unsaturated conductivity. I was immediately sold: it was transparent that the geometric model (with the equally important framework for mathematical analysis) was ideally suited to the problem at hand. Since resistance to flow is a function of the fourth power of the pore aperture, clearly the key was to systematize the determination of the "weak link" to compute overall resistance to flow. Paths that had breaks were irrelevant; and paths that contained very small pores provided negligible contribu-

tion. The permeability should be proportional to the fourth power of the radius of the smallest pore in the connected path which has the largest small pore. Read that sentence twice: we are looking for the path of least resistance, and that paths resistance will be a function of the smallest pore in that path. Allen had the tool to identify this path as a function of fluid content. A very useful, appropriately sized, hammer had arrived for our nail. Over the following years Allens work showed the power of using the right tool: he could explain the relationship between the geometry of the medium and liquid content versus permeability, residual fluid content, electrical resistance, diffusion of solutes, and even the thorny issues of the scale of a representative elementary unit. Critical path analysis is not a panacea, but due to the focus on the controlling geometric features, it provides a remarkably concise parameterization of fluid–medium relationships based on physically measurable properties that accurately predict many of the basic ensemble properties.

A fundamental problem in having these results be broadly understood and adopted is sociological. Consider how much time we spend learning calculus to solve the occasional differential equation. Critical path analysis requires calculus, but also understanding of the mathematics of fractals, and the geometric strategy of percolation theory. When Allen started his remarkably productive march into flow through porous media he deftly employed these tools that none of our community had mastered. There is a natural inertia to any discipline since re-tooling requires major investments of time. From this perspective I have long encouraged Allen to help the community make use of this essential set of tools by providing a primer on their application to flow though porous media. In this book Allen has once again moved forward strategically, and with great energy. He has provided an accessible tutorial that not only provides the bridge for the hydrologist to these new tools, but also the physicist a window into the specialized considerations of flow through natural porous media.

Learning new mathematical constructs is much like learning a new language. There is a great deal of investment, and the early effort has few rewards. Ultimately, however, without language there is no communication. Without mathematics, there is no quantitative prediction. If understanding the behavior of liquids in porous media is central to your work, I urge you to make the investment in learning this material. By way of this book Allen provides a direct and efficient avenue in this venture. Your investment will be well beyond repaid.

Corvallis, Oregon John Selker
April, 2005

Preface to the Third Edition

The first edition of "Percolation theory for flow in porous media" was short and focused. The point of the book was primarily to introduce readers to a suite of techniques, by which the author believed essentially all problems of flow, conduction, and diffusion in porous media could be solved, although it was also admitted that many problems that were in principle soluble by these techniques, were as yet unsolved. The strategy that was presented integrated critical path analysis with cluster statistics of percolation and scaling relationships. In the second edition we determined that some of the problems that we had left out could also be addressed in the general framework that was put forth, the most notable addition being the dispersion of solutes during advective transport. At the same time it was becoming clear to the authors that there was an entire suite of problems of interest to a number of different research communities that we had not even touched on, even though we had tried to expand the range of problems addressed. In this third edition we continue in the same vein as in the second, namely in a demonstration of the widening range of problems that we have tackled within this framework for solving problems. The principle motivation remains the same, however, to show that this particular combination of techniques from percolation theory can unify solutions of a wide range of problems. Although this preface therefore need not be long, we do wish to point out that we have greatly expanded the portions involving experimental verification of results, especially in the cases of air permeability, hydraulic conductivity, diffusion, and dispersion. And we have shown that our results for the spatio-temporal scaling of solute velocities give excellent predictions of the scaling of surface reaction rates over ten orders of magnitude of time scales. This, frankly unexpected, result means that the theoretical framework for dispersion of *non-reactive solutes* introduced in the previous edition, has relevance far beyond what was originally imagined, since the chemical weathering of silicate minerals in the earth's crust is among the reactions whose scaling behavior is described. And silicate weathering has an important role in many global phenomena, such as soil production and surface denudation rates, but most notably

for the global carbon cycle, with its implications for climate change and extinctions.

October 2013

Allen Hunt
Robert Ewing
Behzad Ghanbarian

Preface to the Second Edition

Why would we wish to start a 2nd edition of "*Percolation Theory for Flow in Porous Media*" only two years after the first one was finished? There are essentially three reasons:

(1) Reviews in the soil physics community have pointed out that the introductory material on percolation theory could have been more accessible. Our additional experience in teaching this material led us to believe that we could improve this aspect of the book. In the context of rewriting the first chapter, however, we also expanded the discussion of Bethe lattices and their relevance for "classical" exponents of percolation theory, thus giving more of a basis for the discussion of the relevance of hyperscaling. This addition, though it will not tend to make the book more accessible to hydrologists, was useful in making it a more complete reference, and these sections have been marked as being possible to omit in a first reading. It also forced a division of the first chapter into two. We hope that physicists without a background in percolation theory will now also find the introductory material somewhat more satisfactory.

(2) We have done considerable further work on problems of electrical conductivity, thermal conductivity, and electromechanical coupling. The electrical conductivity may in more complex media than those addressed in the first edition lead to the relevance of nonuniversal exponents of percolation theory, while the thermal conductivity may be strongly affected by complex structures such as capillary bridges or pendular rings between grains. Neither of these subjects in morphology was discussed in detail in the first edition.

Our additional research into the saturation dependence of the electrical conductivity appeared to confirm the relevance of universal scaling to a much wider range of materials than we knew about at the time of the first edition. However, a related subject long considered important in petroleum engineering is diagenesis, which was handled in some detail in Sahimi's 1993 review. It is possible to make models of rock formation in which the connectivity of the pore space scarcely changes, while the width of the pores diminishes rapidly with diminishing porosity. Such models

allow, at least in principle, the possibility of nonuniversal exponents of percolation theory.

The reason that pendular structures could be relevant, especially to the thermal conductivity of geological porous media, is that the solid fraction generally has a higher thermal conductivity than the fluid phase (e.g., air or water), while the thermal resistance between neighboring grains may be quite high. Thus, small amounts of fluid at these junctions—pendular structures—may produce a rather large increase in the thermal conductivity, and this increase may have nothing to do with percolation theory as such, since the topology of the connected network might not initially change with increasing fluid content, although critical path analysis may still be useful for this problem. The large increase in material covered in the original Chap. 4 also led to its division into the current Chaps. 5 and 6.

(3) We have recently addressed the problem of dispersion in porous media, which brings up the relevance of some additional topological aspects of percolation theory, in particular, the relationship of the tortuosity of the backbone cluster to the distribution of passage times. Because this was not addressed in the first edition, the introductory chapters mentioned the topic only briefly. As a consequence the preface to the first edition is now more dated as dispersion was implied to be a problem that could be omitted. In fact, inclusion of dispersion into the second edition has made a significant advance in the unity of the theoretical approach here.

We also bring in an additional problem (Sect. 11.4) addressing the question of how to generate a realistic prediction in horizontal and vertical K distributions for a topical waste management problem, which uses output parameters from a smallscale upscaling to generate appropriate input parameters in a large-scale upscaling. We hope it is useful to see how difficult practical problems in applying percolation theory at multiple scales might be managed.

In order to give the book a wider relevance, it is useful to embed the discussions of the relevance of universal exponents in a wider context. This is accomplished by looking at a wider range of models of porous media, a wider range of properties, and a wider range of experiments. As a consequence, the introductory review chapters needed to be rewritten in order to accommodate a more widely applicable theory.

Finally, it has been noted that solutions to the problems are not provided. It was our intention, except in the introductory chapters, to suggest mostly problems whose solutions could be published, so these problems have not yet been attempted.

Besides the people acknowledged in the first edition, one of us would like to thank the staff of the library at Wright State University.

Preface to the First Edition

The focus of research in porous media is largely on phenomena. How do you explain fingering? What causes preferential flow? What "causes" the scale effect on the hydraulic conductivity? Why can the incorporation of 5% of hydrophobic particles into soil make the soil water repellent? Where do long tails in dispersion come from? These are merely a few examples of a very long list of questions asked. The approach to "solving" problems is frequently to (1) take standard differential equations such as the advection-diffusion equation for solute transport, or Richards' equation for water transport; (2) substitute results for what are called constitutive relations such as the hydraulic conductivity, K, molecular diffusion constants, or air permeability as functions of saturation, and pressure-saturation curves, including hysteresis, etc.; (3) apply various models for the variability and the spatial correlations of these quantities at some scale; and (4) solve the differential equations numerically according to prescribed initial and/or boundary conditions. In spite of continuing improvement in numerical results, this avenue of research has not led to the hoped-for increase in understanding. In fact there has been considerable speculation regarding the reliability of the fundamental differential equations (with some preferring fractional derivatives in the advection-diffusion equation, and some authors questioning the validity of Richards' equation) while others have doubted whether the hydraulic conductivity can be defined at different scales.

Although other quite different approaches have thus been taken, let us consider these "constitutive" relations. The constitutive relationships used traditionally are often preferred because (1) they generate well-behaved functions and make numerical treatments easier; (2) they are flexible. This kind of rationale for using a particular input to a differential equation is not likely to yield the most informative solution. The most serious problem associated with traditional constitutive relations is that researchers use such concepts as connectivity and tortuosity (defined in percolation theory) as means to adjust theory to experimental results. But the appropriate spatial "averaging" scheme is inextricably connected to the evaluation of connectivity. In fact, when percolation theory is used in the form of critical path analysis, it is not the spatial "average" of flow properties which is relevant, but the most resistive elements on the most conductive paths, i.e. the dominant resistances on the

paths of least resistance. An additional problem is that usual constitutive relations often cover simultaneous moisture regimes in which the represented physics is not equilibrium, and thus time-dependent, as well as those moisture regimes where the dominant physics is equilibrium, so that they must be overprescribed (while still not describing temporal effects). Finally, there has been no progress in making the distributions and spatial correlations of, e.g. K, consistent with its values at the core scale, because there is no systematic treatment of the connectivity of the optimally conducting regions of the system. This book shows a framework that can be used to develop a self-consistent and accurate approach to predict these constitutive relationships, their variability, spatial correlations and size dependences, allowing use of standard differential equations in their continuum framework (and, it is hoped, at all spatial scales).

Although applications of percolation theory have been reviewed in the porous media communities (e.g. Sahimi, 1993; Sahimi and Yortsos, 1990) (in fact, percolation theory was invented for treating flow in porous media, Broadbent and Hammersley, 1957) it tends to be regarded as of limited applicability to real systems. This is partly a result of these summaries themselves, which state for example that "Results from percolation theory are based on systems near the percolation threshold and the proximity of real porous rocks to the threshold and the validity of the critical relationships away from the threshold are matters of question," (Berkowitz and Balberg, 1993). However, it is well-known that percolation theory provides the most accurate theoretical results for conduction also, in strongly disordered systems far above the percolation threshold (using critical path analysis). The novelty in this course is the combined use of both scaling and critical path applications of percolation theory to realistic models of porous media; using this combination it is possible to address porous media under general conditions, whether near the percolation threshold or not.

This book will show how to use percolation theory and critical path analysis to find a consistent and accurate description of the saturation dependence of basic flow properties (hydraulic conductivity, air permeability), the electrical conductivity, solute and gas diffusion, as well as the pressure-saturation relationships, including hysteresis and non-equilibrium effects. Using such constitutive relationships, results of individual experiments can be predicted and more complex phenomena can be understood. Within the framework of the cluster statistics of percolation theory it is shown how to calculate the distributions and correlations of K. Using such techniques it becomes easy to understand some of the phenomena listed above, such as the "scale" effect on K, as well.

This work does not exist in a vacuum. In the 1980s physicists and petroleum engineers addressed basic problems by searching for examples of scaling that could be explained by percolation theory, such as Archie's law (Archie, 1942) for the electrical conductivity, or invasion percolation for wetting front behavior, hysteresis, etc. or by using the new fractal models for porous media. The impetus for further research along these lines has dwindled, however, and even the basic understanding of hysteresis in wetting and drainage developed in the 1980s is lacking today, at least if one inquires into the usual literature. In addition, the summaries of the work

done during that time suggest that the percolation theoretical treatments are not flexible enough for Archie's law (predict universal exponents), or rely on non-universal exponents from continuum percolation theory without a verifiable way to link those exponents with the medium and make specific predictions. An identifiable problem has been the inability of researchers to separate connectivity effects from poresize effects. This limitation is addressed here by applying percolation scaling and critical path analysis simultaneously. While there may have been additional problems in the literature of the 1980s (further discussed here in the Chapter on hysteresis), it is still not clear to me why this (to me fruitful) line of research was largely abandoned in the 1990s. This book represents an attempt to get percolation theory for porous media back "on track."

It is interesting that many topics dealt with as a matter of course by hydrologists, but in a rather inexact manner, are explicitly treated in percolation theory. Some examples are:

1. upscaling the hydraulic conductivity = calculating the conductivity from microscopic variability,
2. air entrapment = lack of percolation of the air phase,
3. residual water, oil residuals = critical moisture content for percolation, sum of cluster numbers,
4. grain supported medium = percolation of the solid phase;
5. Representative Elementary Volume = the cube of the correlation length of percolation theory,
6. tortuosity = tortuosity,
7. flow channeling = critical path.

These concepts and quantities are not, in general, treatable as optimization functions or parameters in percolation theory because their dependences are prescribed. Note that in a rigorous perspective for disordered systems, however, one does not "upscale" K. The difficulty here is already contained within the language; what is important are the optimal conducting paths, not the conductivities of certain regions of space. The conductivity of the system as a whole is written in terms of the rate-limiting conductances on the optimal paths and the frequency of occurrence of such paths. Defining the conductivity of the system as a whole in terms of the conductivities of its components is already a tacit assumption of homogeneous transport. Further, some elementary rigorous results of percolation theory are profoundly relevant to understanding flow in porous media. In two-dimensional systems it is not possible for even two phases to percolate simultaneously (in a grainsupported medium there is no flow or diffusion!), while in three dimensions a number of phases can percolate simultaneously. As percolation thresholds are approached, such physical quantities as the correlation length diverge, and these divergences cause systematic dependences of flow and transport properties on system size that can only be analyzed through finite-size scaling. Thus it seems unlikely that treatments not based on percolation theory can be logically generalized from 2D to 3D.

I should mention that a book with a similar title, "Percolation Models for Transport in Porous Media," by Selyakov and Kadet (1996) also noted that percolation

theory could have relevance further from the percolation threshold, but overlooked the existing literature on critical path analysis, and never mentioned fractal models of the media, thereby missing the importance of continuum percolation as well. As a consequence, these authors did not advance in the same direction as this present course.

The organization of this book is as follows. The purpose of Chap. 1 is to provide the kind of introduction to percolation theory for hydrologists which (1) gives all the necessary basic results to solve the problems presented later; and which (2) with some effort on the part of the reader, can lead to a relatively solid foundation in understanding of the theory. The purpose of Chap. 2 is to give physicists an introduction to the hydrological science literature, terminology, experiments and associated uncertainties, and finally at least a summary of the general understanding of the community. This general understanding should not be neglected as, even in the absence of quantitative theories, some important concepts have been developed and tested. Thus these lecture notes are intended to bridge the gap between practicing hydrologists and applied physicists, as well as demonstrate the possibilities to solve additional problems, using summaries of the background material in the first two chapters. Subsequent chapters give examples of critical path analysis for concrete system models Chap. 3; treat the "constitutive relationships for unsaturated flow," including a derivation of Archie's law Chap. 4; hysteresis, non-equilibrium properties and the critical volume fraction for percolation Chap. 5; applications of dimensional analysis and apparent scale effects on K Chap. 6; spatial correlations and the variability of the hydraulic conductivity Chap. 7; and multiscale heterogeneity Chap. 8.

I wish to thank several people for their help in my education in hydrology and soil physics, in particular: Todd Skaggs, whose simulation results have appeared in previous articles and also in this book; John Selker, who showed me the usefulness of the Rieu and Sposito model for the pore space; Glendon Gee, who helped me understand experimental conditions and obtain data from the Hanford site; Eugene Freeman for providing additional Hanford site data; Bill Herkelrath, again for data; Toby Ewing, whose simulations for diffusion were invaluable; Tim Ellsworth for showing me the relevance of the experiments of Per Moldrup; Per Moldrup for giving me permission to republish his figures; Max Hu for providing me with his diffusion data; and Sally Logsdon for her data on soil structure; Alfred Huebler for giving me a forum among physicists to discuss these ideas. I also thank my wife, Beatrix Karthaus-Hunt, for her support.

Dayton Allen G. Hunt
April, 2005

Contents

1 Percolation Theory: Topology and Structure 1
1.1 What Is Percolation? 1
1.2 Some Examples 2
1.3 Qualitative Descriptions 4
1.4 What Are the Basic Variables? 6
1.5 What Is Scale Invariance and why Is It so Important? 7
1.6 The Correlation Length in One Dimension 9
1.7 The Relationship of Scale Invariance and Renormalization, and the Relationship of the Renormalization Group to Percolation Theory 11
1.8 Cluster Statistics of Percolation Theory 12
1.9 Derivation of One-Dimensional Cluster Statistics and Discussion of Fractal Dimensionality 14
1.10 Argument for Dimensionally-Dependent Scaling Law, Implications for Critical Exponent, τ, and Applications to Critical Exponents 15
1.11 Explicit Calculations of the Second Moment of Cluster Statistics in One Dimension 18
1.12 Calculation of the Correlation Length on a Bethe Lattice 19
1.13 Explicit Calculations of the Second Moment of Cluster Statistics on a Bethe Lattice 22
1.14 Mean-Field Treatment of the Probability of Being Connected to the Infinite Cluster 22
1.15 Cluster Statistics on a Bethe Lattice 23
1.16 Summary of Relationships Between Exponents in One Dimension and in Infinite Dimensions Using Scaling Relationships. Implications for the Validity of Hyperscaling . . . 24
1.17 Calculation of the Critical Site Percolation Probability for the Two-Dimensional Triangular Lattice and of the Critical Exponent for the Correlation Length in Two Dimensions 25

1.18 Value of p_c for Bond Percolation on the Square Lattice 28
1.19 Estimations of p_c for Bond Percolation on the Triangular and Honeycomb Lattices 29
1.20 Summary of Values of p_c 30
1.21 More General Relationships for p_c 31
Problems 32
References 33

2 Properties Relevant for Transport and Transport Applications . . 37
2.1 Exponents Describing Backbone Structure 37
2.2 Exponents for Conduction Properties 39
2.3 Summary of Derived Values of Critical Exponents 43
2.4 Finite-Size Scaling and Fractal Characteristics 44
2.5 Scaling Far from the Threshold 45
2.6 Critical Path Analysis 46
2.6.1 Relation of Critical Path Analysis to Extreme Value Statistics in 1D Systems 47
2.6.2 Critical Path Analysis in 2D 49
2.6.3 Critical Path Analysis in 3D 50
2.6.4 Dimensional Dependence and Similarity to Matheron Conjecture 51
2.6.5 Optimization of the Percolation Network: Contrast Between 2D and 3D 52
2.7 Summary 55
Problems 55
References 56

3 Porous Media Primer for Physicists 59
3.1 How Does Percolation Theory Relate to Porous Media? 59
3.2 Kinds of Porous Media 60
3.3 Properties of Porous Media Independent of Fluid 61
3.3.1 Porosity 62
3.3.2 Bulk & Particle Density, Particle Size Distribution 63
3.3.3 What Is a Pore? 65
3.3.4 Pore Size Distribution 66
3.3.5 Surface Area and Surface Chemistry 68
3.4 Single-Fluid Transport Properties 68
3.4.1 Permeability 72
3.4.2 Dispersion 75
3.4.3 Electrical Conductivity 78
3.5 Multiple-Fluid Properties and the Role of Pore Occupancy 79
3.5.1 Wettability, Pore Size, and Capillarity 79
3.5.2 The Pressure-Saturation or Water Retention Curve (WRC) 82
3.5.3 Obtaining a Pore Size Distribution 84
3.5.4 Widely Used Equations for the Water Retention Curve . . 86
3.5.5 Unsaturated Hydraulic Conductivity, $K(\theta)$ 89

3.6 Conceptual Models of Porous Media . . . 91
3.7 Conclusion . . . 93
Problems . . . 94
References . . . 94

4 Fractal Models of Porous Media . . . 103
4.1 Fractal Approaches to Porous Media Modeling . . . 103
4.2 The Rieu and Sposito (RS) Fractal Model . . . 106
4.3 Water Retention Using the RS Model . . . 111
4.4 Other Fractal Models of the WRC . . . 115
4.4.1 de Gennes [13] . . . 115
4.4.2 Tyler and Wheatcraft [60] . . . 116
4.4.3 Perrier et al. [51] . . . 117
4.4.4 Perfect [46] . . . 117
4.4.5 Bird et al. [5] . . . 118
4.4.6 Millán and González-Posada [38] . . . 120
4.4.7 Cihan et al. [11] . . . 120
4.4.8 Deinert et al. [17] . . . 122
4.5 A General Fractal Model for the Soil Water Retention Curve . . . 122
4.6 Assumptions in WRC Measurement and Modeling . . . 123
4.6.1 Finite-Size Effects at High Saturations . . . 124
4.6.2 Non-equilibrium Condition at the Dry End . . . 124
4.6.3 Contact Angle Assumptions . . . 125
4.6.4 The Power-Law Form of the WRC . . . 126
4.7 Conclusions . . . 126
References . . . 127

5 Specific Examples of Critical Path Analysis . . . 131
5.1 r-Percolation . . . 132
5.2 r–E-Percolation (Variable-Range Hopping) . . . 140
5.3 Saturated Hydraulic Conductivity . . . 143
5.4 Unsaturated Hydraulic Conductivity . . . 147
5.5 Hydraulic Conductivity for Geologic Media: Parallel vs. Series . . . 149
5.6 Summary . . . 152
Problems . . . 153
References . . . 154

6 Hydraulic and Electrical Conductivity: Conductivity Exponents and Critical Path Analysis . . . 157
6.1 Background . . . 157
6.2 Hydraulic and Electrical Conductivities, and Electrokinetic Coupling: Universal and Non-universal Exponents . . . 160
6.2.1 Balberg Non-universality . . . 164
6.2.2 Transition from Critical Path Analysis to Percolation Scaling . . . 166
6.2.3 Comparison with Experiment . . . 167

6.2.4 Cross-over Moisture Content for the Electrical Conductivity . . . 178
6.2.5 Return to Balberg Non-universality . . . 178
6.2.6 Inferences on Porosity Dependences at Full Saturation: Archie's Law . . . 179
6.2.7 Universal Exponents Masquerading as Non-universal . . . 181
6.2.8 Regions of Applicability . . . 184
6.3 Electrical Conductivity as a Function of Saturation: Trends and Potential Complications in Experimental Data . . . 187
6.3.1 Comparison with Experiment . . . 191
6.4 Effects of Arbitrary Pore-Size Distributions . . . 199
6.5 Water Film Issues . . . 202
6.6 Electrical Conductivity for $\theta < \theta_t$ . . . 208
Problems . . . 208
Appendix: Calculation of Water Retention and Unsaturated Hydraulic Conductivity for Pore-Solid Fractal Model with Two Fractal Regimes . . . 209
Water Retention Curve . . . 209
Unsaturated Hydraulic Conductivity . . . 211
References . . . 214

7 Other Transport Properties of Porous Media . . . 219
7.1 Air Permeability . . . 219
7.2 Thermal Conductivity . . . 234
7.2.1 General Comments on the Saturation Dependence of Thermal Conductivity . . . 234
7.3 Solute and Gas Diffusion . . . 242
7.4 Electrical Conductivity of Hydrated Clay Minerals . . . 249
7.4.1 r-Percolation and E-Percolation . . . 252
7.4.2 Percolation Calculation of E_a . . . 255
7.5 Geophysical Applications . . . 262
7.6 Summary . . . 265
References . . . 268

8 Pressure Saturation Curves and the Critical Volume Fraction for Percolation: Accessibility Function of Percolation Theory . . . 273
8.1 Structural Hysteresis . . . 274
8.2 Hydraulic Conductivity-Limited Equilibration, and Dry-End Deviations from Fractal Scaling . . . 278
8.3 Analysis of Water-Retention Curves in Terms of the Critical Moisture Content for Percolation . . . 285
8.4 Wet-End Deviations from Fractal Scaling of Water-Retention Curves, and Discussion of the Critical Volume Fraction for Percolation . . . 288
8.5 General Formulation for Equilibrium and Analogy to Ideal Glass Transition . . . 292

8.6 Oil Residuals . . . 294
Problems . . . 294
References . . . 295

9 Applications of the Correlation Length: Scale Effects on Flow . . . 297
9.1 Representative Elementary Volume (REV) . . . 298
9.2 Isolation of Geologic and Percolation Effects on a Correlation Length . . . 298
9.3 Effects of Dimensional Cross-Overs on Conductivity . . . 299
9.4 Comparison with Field Data . . . 305
9.5 Effects of Hydrophobicity on Water Uptake of Porous Media . . . 308
Problem . . . 309
References . . . 310

10 Applications of the Cluster Statistics . . . 313
10.1 Spatial Statistics and Variability of K from Cluster Statistics of Percolation Theory . . . 313
10.2 Cluster Statistics Treatment of Non-equidimensional Volumes and Anisotropy . . . 320
10.3 Semi-variograms and Cross-Covariance . . . 326
Problems . . . 330
References . . . 330

11 Properties Based on Tortuosity . . . 333
11.1 Tortuosity . . . 334
11.1.1 Tortuosity Theory . . . 335
11.1.2 Comparisons of Calculated Tortuosity with Experiment and with Simulations . . . 338
11.2 Longitudinal Dispersion of Solutes in Porous Media . . . 342
11.2.1 Scope and Definition . . . 342
11.2.2 Background Information . . . 343
11.2.3 Theoretical Descriptions . . . 346
11.2.4 Comparison with Simulations . . . 355
11.2.5 Comparison with Experiments . . . 357
11.3 Spatial Distribution at an Instant in Time and Its Moments . . . 362
11.4 Comparison of Dispersivity Values with Experiments . . . 363
11.5 Typical System Crossing Times and the Scaling of Solute Velocities . . . 369
11.5.1 Comparison with Typical System Crossing Times in Transient Photoconductivity Experiments . . . 369
11.5.2 Comparison with the Scaling of Chemical Reaction Rates 374
11.6 Dispersion Coefficient as a Function of Time . . . 390
11.7 Hydraulic Conductivity . . . 393
11.8 Asymptotic Treatment of Diffusion Effects . . . 394
11.8.1 Theoretical Considerations . . . 394
11.8.2 Results . . . 396
11.9 Discussion . . . 398

Appendix Basic CTRW and Gaussian Results 399
References 400

12 Effects of Multi-scale Heterogeneity 409
12.1 Soil Structure 410
12.2 Variable Moisture Content 415
12.3 A Schematic Hierarchical Problem 418
12.4 A More Realistic Hierarchical Problem 420
Problems 425
References 426

13 Misconceptions 429
13.1 Some Misconceptions at the Pore Scale 430
13.2 Some Misconceptions at the Geological Scale 431
13.3 Summary 432
References 434

Index 435

Chapter 1
Percolation Theory: Topology and Structure

1.1 What Is Percolation?

Percolation theory describes emergent properties related to the connectivity of large numbers of objects. These objects typically have some spatial extent, and their spatial relationships are relevant and statistically prescribed. Percolation theory is thus related to graph (e.g. [12]) and network (e.g. [14]) theories. All of these exist within the intersection of probability theory and topology. For the present purpose, the chief relevance of percolation theory is its ability to deliver global properties from local specifications. Here the global properties sought describe flow, conduction and other transport properties of porous media. The relationships between local and global properties are not trivial: sometimes the global properties relate to universal topological properties, and sometimes to system-dependent properties.

In percolation theory the topology is customarily referenced to some d-dimensional spatial structure with an existence independent of the probabilistic characteristics of the theory. Examples of such structures include regular grids (known in solid state physics as lattices), consisting of nodes (sites) connected by bonds. In porous media the pore space (filled, e.g., with water or air) corresponds to a random lattice, viewed already in the 1950s [17] as a network. The typical twist from percolation theory is to take such a known structure with simple topology, characterized by as few as one or two parameters, and make the presence of, e.g., bonds a probabilistic affair, which generates quite complex topologies.

Percolation theory comes in three basic varieties: bond, site, and continuum, with the first two versions linked by name to the grids mentioned above. We will consider all three varieties. Percolation theory also has some interesting and potentially relevant variants, including bootstrap percolation (an early reference is [9]), gradient percolation [35], and invasion percolation [10, 30, 52]. Bootstrap and gradient percolation are ignored here, while invasion percolation theory is applied in a few places. Invasion percolation was developed in the context of wetting and drying of porous media, in order to describe phenomena related to, e.g., wetting fronts, where the wetting fluid enters the medium from one side. It should become clear that a great deal of unification was already provided by the basic percolation theory as

A. Hunt et al., *Percolation Theory for Flow in Porous Media*,
Lecture Notes in Physics 880, DOI 10.1007/978-3-319-03771-4_1,

formulated by Flory [19] and Broadbent and Hammersley [7]. Nevertheless, this book describes some new combinations of uses of percolation theory. In order to understand these combinations it is important to understand clearly the basic applications of percolation theory, particularly to conduction. These applications have some basis in the topology of the system being examined. Our introduction is made more accessible by considering specific physical examples.

A system is said to be at percolation, or to percolate, when a sufficient fraction of the entities in question (sites, bonds, etc.) is connected locally that a global connection emerges. This global connection is a continuous string of locally connected entities which is unbounded in size except as may result from limitations of a finite-sized system. As is often the case in mathematics, percolation theory has some surprises. Here the simplest result, at least conceptually, is that precisely one global connection develops [2, 22, 24] exactly at a specific fraction, p_c, of local connections known as the critical fraction. Such a simple result is also profound, and decades elapsed before it was proven.

1.2 Some Examples

A simple bond percolation problem can be represented by a window screen which maps out a square grid (lattice). Imagine cutting at random a fraction p of the elements of this grid. At some critical fraction $p \equiv p_c$ (which will turn out to be 0.5), the window screen will lose its connectedness and fall apart. Percolation theory addresses directly the question, "at what fraction of cut bonds does the screen fall apart?" (i.e., what is p_c?), and related questions such as, "what is the largest hole in the screen if the cut fraction p is less than p_c," and "what is the structure of such holes?". Percolation theory also readily provides the electrical conductivity of such an incompletely connected network of (conducting) bonds, or what the diffusion coefficient of a network of the same structure would be if the elements were water-filled tubes rather than wires. Answers to the latter questions are given in terms of p, p_c, and the conductivity or diffusivity of the individual bonds.

A simple site percolation problem can be represented by the random emplacement of equal-sized metallic and plastic spheres in a large container. If two metal spheres touch each other, a current can pass from one to the other. Here the relevant percolation variable is the fraction, p, of spheres that is conducting. If the fraction of metallic spheres exceeds a critical value, a continuous conducting pathway will be formed. The larger the fraction of metallic spheres, the better connected the path will be and the greater the electrical conductivity of the system. Percolation theory generates the electrical conductivity as a function of the fraction of the spheres made of metal. Site and bond percolation problems can be defined on either regular grids, like a square-lattice window screen, or irregular grids like a random sphere pack. They can also be defined on tree structures with constant branching ratios known as Bethe lattices.

A continuum percolation problem receiving attention already in the 1970's is a network of sintered glass and metallic particles. The glass particles may have different sizes and shapes from the metallic particles (which are typically smaller), while the sintering process tends to change the shapes of the particles, producing a net flow of material into the pore space. The irregularity of the particle shapes can thus be contrasted with the regular geometry of the site percolation problem described above. Such networks have relevance in the xerox industry. In the above continuum percolation problem the relevant percolation variable becomes the volume fraction, p, taken up by the metallic particles. If the detailed structure is known, percolation theory can account for some aspects of the electrical conductivity of these systems as well [4, 25, 31]. Other real systems whose electrical properties can be treated in terms of continuum percolation include piezoelectric ceramics [20, 43]. The continuum percolation problem that we will be most interested in here is that of water flowing in variably saturated porous media. Porous media are often far from the percolation threshold whereas piezoelectric ceramics are extremely close to it.

Across these applications of percolation theory, we may see the values of p_c vary widely from system to system. However, the same relationships are still used to determine, e.g., the size of the largest hole in the screen, or the electrical conductivity as a function of $p - p_c$, where p is the fraction of conducting portions, and p_c its critical value for percolation. Relationships that are functions of the difference $p - p_c$ are normally (with isolated exceptions) termed "universal" [45, 47]. Here universal means that the property is independent of the details of the system and depends only on its dimensionality, d. We wish to demonstrate how percolation theory can be used to solve practical problems relating to transport in porous media.

It had earlier been hoped that the universal behavior exhibited by most models near the percolation threshold could be used to guide understanding of real physical systems across the entire range of connectivities (see, for example, [6, 36, 37]). But as has been frequently pointed out, it is not clear how close real systems are to the percolation threshold. Thus it is important to emphasize at the outset that this book will explain the use of percolation theory to calculate transport properties not merely near the percolation transition, but also far from it. Far from the percolation transition it is frequently non-universal aspects of percolation theory, i.e. the value of p_c and the statistical characteristics of the medium, which control transport; near the percolation threshold it is the universal aspects that dominate. This perspective will be seen to be far more useful than a restriction to either case by itself: it allows calculation of all the transport properties of porous media, as well as their variability and the structure of their spatial correlations.

This first chapter is devoted to the development of basic methods and concepts from percolation theory that refer to the structure of topology of percolation. The material here is drawn from many sources, but most importantly from Stauffer [45], Sahimi [36], Stauffer and Aharony [47], and Bunde and Havlin [8]. Some concepts important for the unification of percolation theory will be treated in some depth for the benefit of those readers with a physics background but without detailed experience in percolation theory. These will be pointed out and can be skipped in an initial reading. The second chapter provides an introduction to transport-related aspects of

percolation theory. The third chapter will serve as an introduction to porous media. Subsequent chapters will detail the applications.

1.3 Qualitative Descriptions

Consider a square grid of points, and draw line segments between nearest neighbor points "at random." For very small values of p these segments will only connect pairs of nearest neighbor sites. As p increases more pairs will connect, and gradually clusters of interconnected sites will appear. As p nears p_c many of these clusters will become large, with complex internal structure. What is the occurrence of such clusters as a function of p and their size? We would also like to quantify the structure of the clusters. This structure has been described using various quantities, such as perimeter, density, mass (i.e., number of sites), "chemical path" length, and ramification. The perimeter (the number of sites in the cluster with neighboring sites not in the cluster) has two contributions: one is proportional to the volume [26], while the second, similar to surface area, is proportional to the volume to the $1 - 1/d$ power, where d is the Euclidean dimension [45]. The radius of a large cluster is not given in terms of its volume by the usual relationships valid for Euclidean objects. In fact large clusters at, or near, the percolation threshold are fractal objects, without scale reference except in the small scale limit when the scale of the grid becomes visible.

As p reaches p_c the largest interconnected cluster just reaches infinite size. For p greater than but still close to p_c, most of the sites on the infinite connected cluster are located on what are called "dead ends." Dead ends are connected to the rest of the infinite cluster by only one bond. If current were to flow across the system through the infinite cluster, these dead ends would carry no current. If the dead ends are "pruned" from the cluster, what remains is called the "backbone," the portion of the infinite cluster that carries current. The backbone has a large number of loops, making it a multiply-connected object. The backbone also has "red" bonds, for which no alternate path exists. If a red bond is cut, the current is interrupted. Red bonds are associated with the largest drops in the potential field, which is why they are designated "red" or "hot". If the length scale viewed is not too large, then large finite clusters just below percolation have the same appearance as the infinite cluster just above percolation. Figure 1.1 shows the "infinite" cluster for $p > p_c$ and bond percolation on a square lattice, and Fig. 1.2 shows its backbone.

The backbone cluster itself has been described using the terms "links," "nodes," and "blobs." A pictorial definition of these terms is given in Fig. 1.3. The characteristic separation of nodes, or the length of a link, will be equivalent to the correlation length, defined in Eq. (1.1) below. A heuristic derivation of the exponent for the vanishing of the conductivity [41] is based on the conceptualization of the infinite cluster depicted in Fig. 1.3. Note that considerable work on non-linear effects on the electrical conductivity, as well as the usefulness of effective-medium theoretical descriptions is based on this kind of a pictorial concept. This literature will not be

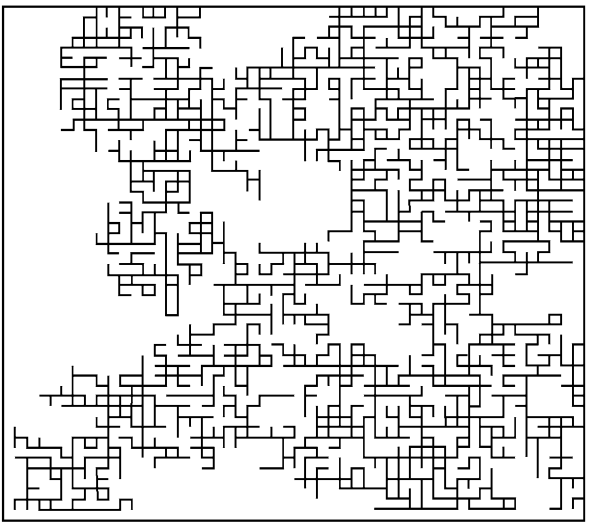

Fig. 1.1 A finite size sample of bond percolation on a square lattice above the percolation threshold

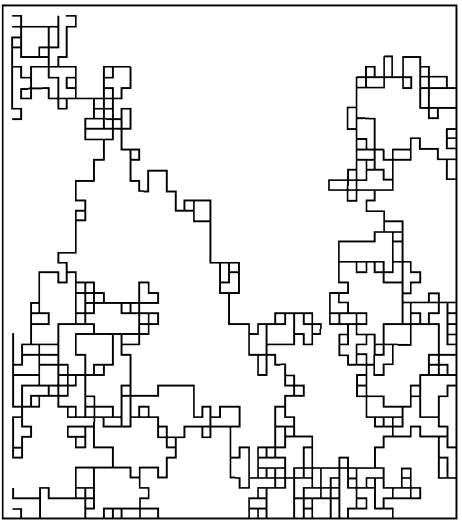

Fig. 1.2 The same system and realization of Fig. 1.1, but for which the dead ends have been removed from the infinite cluster to form the "backbone" cluster. Note the existence of many closed loops (figure from Todd Skaggs, unpublished)

discussed here, and if interested, the reader should consult Shklovskii and Efros [40] or Pollak [33] and the references therein.

The clusters, being fractal objects, have many properties which are best characterized using a fractal dimensionality. While the multiplicity of consequent fractal dimensionalities can be confusing, we will concentrate our attention on three of these: (1) the fractal dimension, d_{f}, associated with the mass distribution of the cluster, (2) the fractal dimension associated with the mass distribution of the backbone, D_{b}, and (3) the fractal dimension associated with the optimal path length along the backbone, D_{min}. The first is relevant to any understanding of the occurrence of

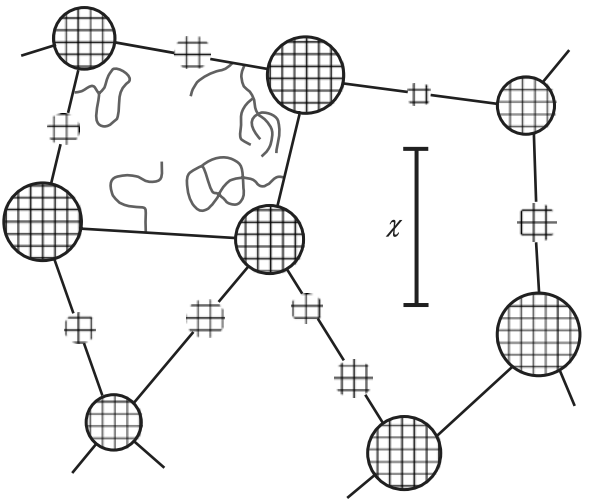

Fig. 1.3 Schematic of a section of the backbone. Links and nodes have conventional meanings from, e.g., Kirchoff's network equations, while blobs are cycles or loops, or collections thereof. Nodes are hatched *circles with borders*. Blobs are hatched *circles without borders*. Links are the *lines* connecting nodes. *Gray lines in the upper left hole* represent dangling ends. The average link length, χ, is also the average hole size

clusters as a function of cluster size, while the second, and perhaps the third, have relevance to calculations of dispersion through descriptions of solute transport along paths of constant flux through porous media.

1.4 What Are the Basic Variables?

The most fundamental variable is p, which for the bond percolation problem is defined to be the fraction of (cut) bonds in the above screen problem, or, equivalently the fraction of bonds emplaced on a background without bonds. In site percolation p normally stands for the fraction of, e.g., the metallic balls mentioned above. It can also stand for the number of lattice (grid) sites marked by some special color, and which "connect" if they happen to be nearest neighbors. (In two dimensions there is little point in distinguishing multiple colors because at most one type of site, bond or continuum can percolate at one time, but in higher dimensions more than one color can percolate simultaneously.) In continuum percolation, p can stand for a fractional volume, for example the water content of a soil. The most important value of p is p_c, the critical value at which percolation occurs. In an infinitely large system, p_c is precisely defined: larger values of p guarantee "percolation," the existence of an infinitely large cluster of interconnected sites (bonds or volume), while smaller values of p guarantee that percolation does not occur. For a given finite sized system this transition may occur at a value of p somewhat greater than or less than p_c. Some authors use this spread in p_c values for finite sized systems as a starting point to discuss finite-size effects on percolation properties; here we use the cluster statistics of percolation as a basis for treating such finite-size effects. Percolation theory has sufficient redundancy to make either approach suitable.

Other basic variables are all functions of the difference $p - p_c$. P_∞ is defined to be the fraction of active bonds (or sites) connected to the infinite cluster (if an

infinite cluster exists, i.e., for $p > p_c$). χ, known as the correlation length, gives the typical linear extent of the largest cluster for $p < p_c$, and the largest hole for $p > p_c$. n_s is defined to be the volume concentration of clusters of sites or bonds with s interconnected elements, and is a function of s and of the difference $p - p_c$. How to obtain such quantities, and how to use them to calculate realistic and often very accurate values of transport coefficients of disordered porous media, is the point of this book.

1.5 What Is Scale Invariance and why Is It so Important?

A core concept of percolation theory, central to much of its theoretical development, is that the correlation length, χ, diverges (goes to infinity) in the limit $p \to p_c$. While, for $p \neq p_c$ χ defines a relevant physical scale, this scale disappears precisely at $p = p_c$. The lack of any length scale, known as scale invariance, also implies the relevance of fractal analysis, or self-similarity. Even for $p \neq p_c$, if a percolation system is viewed at length scales less than χ it appears fractal. Only at length scales greater than χ does the geometry become Euclidean [46]. Another physical meaning of a divergent correlation length is that at $p = p_c$, the largest cluster of interconnected bonds, sites, or volume, just reaches infinite size. Thus it can be said that if one examines the system at length scales smaller than the largest self-similar structure, the medium appears to be self-similar. At the percolation threshold, the largest self-similar structure reaches infinite size, and the self-similar appearance of the medium extends to infinite length scales. Of course no physical medium on the earth can precisely obey such a condition.

Before we define the correlation length, we define first the correlation function $g(r)$ as the mean number of sites at a Euclidean distance r from some arbitrary occupied site, that are also occupied and on the same cluster as that arbitrary site. The sum of $g(r)$ over all values of r will thus yield the total cluster mass. This makes $g(r)$, suitably normalized, a measure of cluster density. Because of the exceedingly complex structure of clusters in higher dimensions, $g(r)$ is cumbersome to construct, except on Bethe lattices and one-dimensional systems.

The correlation length, χ, may be defined as

$$\chi^2 = \frac{\sum_{r=1}^{\infty} r^2 g(r)}{\sum_{r=1}^{\infty} g(r)} \tag{1.1}$$

Thus the correlation length is a root-mean-square (rms) measure of the size of the finite clusters. While Bunde and Havlin [8] take the lower limit of the sum in Eq. (1.1) to be $r = 1$, Stauffer and Aharony [47, Sect. 2.2] use $r = 0$, a distinction which makes no difference in the behavior of any calculated property in the vicinity of the percolation threshold.

Starting from $p > p_c$, the divergence of the correlation length implies that the largest hole in the infinite connected cluster just reaches infinite size and there is

symmetry between $p > p_c$ and $p < p_c$. This symmetry is perfect only in two dimensions, where only one phase, or class, of sites or bonds can percolate simultaneously. The divergence of the correlation length implies that right at percolation there is no finite length scale left in the problem. In reference to the qualitative discussion of Sect. 1.3, this scale invariance shows up also in the shapes and internal structure of the clusters, and is represented through quantities that describe fractal dimensionalities.

What does the lack of a finite length scale at the percolation threshold imply? It requires the use of functions of powers. Powers may appear to have a scale, i.e., under some circumstances the relationship of a conductivity to a length scale, x, can, simply by dimensional analysis, be shown to have a form such as,

$$K = K_0 \left(\frac{x}{x_0} \right)^{-(d-1)} \tag{1.2}$$

where the choice of the power $-(d-1)$ is not intended to be anything beyond illustrative, K is a conductivity, K_0 is a particular value of the conductivity, x is a length, and x_0 is a particular value of x. In contrast to an exponential function, x_0 in this case need not identify a particular "scale," though if used in a judicious fashion it may imply a boundary of the validity of the scale invariance (the existence of a lower limit of the validity of scale-invariance in site and bond percolation problems is clearly required by the finite dimensions of the underlying lattice). On the other hand an exponential function, $K = K_0 \exp(-x/x_0)$, must also have an argument x/x_0. But the particular value of x_0 has completely different consequences in the two equations. For example, as long as x is within a range of lengths for which the power law is valid (Eq. (1.2)), for $d = 3$, doubling the system size will always decrease the conductivity by a factor of four, regardless of the actual values of x_0 or K_0. In the case of the exponential function, the conductivity obtained by doubling the system size will depend on the conductivity of the initial system, and thus on the size ratio of the larger system to x_0; this is in no sense a scale-independent relationship. Notice that in physical systems a power law may have upper *and* lower boundaries. For example, physical objects with fractal characteristics are, strictly speaking, truncated fractals: their fractal nature does not extend to sub-atomic or galactic length scales. We may therefore give their power law description an upper and lower bound, but they are still scale-invariant *within those bounds*. More generally, incorporating a particular scale in a power law equation may provide useful information about one of its bounds without negating its scale invariance within the range under consideration.

The above argument implies that the correlation length must therefore be a power function. The argument of the correlation length is known to be the difference, $p - p_c$, making it simplest to describe the correlation length as in Eq. (1.3),

$$\chi \propto (p - p_c)^{-\nu} \tag{1.3}$$

The negative exponent, $-\nu$, allows χ to diverge at $p = p_c$. The term "universality" can now be understood in a practical way: the form of Eq. (1.3) is the same in all systems and the exponent ν depends only on the dimensionality of the system.

The scale invariance—lack of a length scale—also implies the relevance of fractal analysis, or self-similarity. Self-similarity is especially important because it allows the application of the mathematical techniques of renormalization. Application of renormalization will permit us to estimate some important quantities of percolation theory, and to employ analogies from the existing framework of the theory of critical phenomena. Renormalization and critical phenomena are treated in many books (e.g., [5, 8, 11, 13, 27, 42, 44]). The books by Bunde and Havlin [8] and Sornette [42] address percolation theory, while Sornette [42] specifically links discussion of percolation with critical phenomena, making these references most pertinent here.

In disordered systems that are far above the percolation threshold, it is always possible to define some variable, describing a subset of the system, which is at the percolation threshold. If this variable is defined in such a way as to relate to local transport coefficients, then it will be possible to identify the chief contribution to the transport properties of the medium. Then one has the interesting result that for disordered systems of nearly any structure transport is dominated by connecting paths near the percolation threshold, and the fractal characteristics of percolation can be relevant to transport even in media, which seem to have no resemblance to fractals. The basis for this application, called critical path analysis, is described in the last section of this chapter. Many applications of percolation theory to disordered systems (e.g., [8]) ignore critical path analysis, and so underestimate its value by restricting it to systems near the percolation threshold. The transport property, for which the impact of the fractal structure is greatest is solute dispersion (Chap. 10).

The fact that percolation variables behave as power laws in $p - p_c$, as in Eq. (1.3) means that they must either diverge or vanish at $p - p_c$, depending on whether the exponent is negative or positive. The term singular behavior (in mathematics) or critical behavior (in physics) however, refers to either divergences or zeroes.

It is important to consider some examples of problems that can be solved "exactly," providing a reference point for the more general scaling arguments typically advanced in percolation theory. Most of these exact solutions derive from Essam [15] or Stauffer [46]. We start with one of these, the calculation of the correlation length in 1-dimension.

1.6 The Correlation Length in One Dimension

It is possible to use the definition (Eq. (1.1)) to make a direct calculation of the correlation length in one dimension. That calculation is described nicely in Bunde and Havlin [8]. The calculation was stated explicitly in terms of site percolation, but is essentially the same for bond percolation. Consider a one-dimensional chain, where each site is occupied randomly with probability p. Clusters of length s consist of chains of s consecutive occupied sites. Since any empty site breaks an infinite chain, the percolation probability in one dimension is $p_c = 1$: every single site must be occupied. Recall that the correlation function, $g(r)$, is the mean number of sites on the same cluster at a distance r from an arbitrary occupied site. In order for

another occupied site even to be on the same cluster as the given site, each site in between must be occupied, a situation that occurs with probability p^r in each direction, leading to,

$$g(r) = 2p^r \tag{1.4}$$

Substituting Eq. (1.4) into the definition of the correlation length (Eq. (1.1)) leads to

$$\chi^2 = \frac{\sum_{r=1}^{\infty} r^2 g(r)}{\sum_{r=1}^{\infty} g(r)} = \frac{\sum_{r=1}^{\infty} r^2 p^r}{\sum_{r=1}^{\infty} p^r} \tag{1.5}$$

In this expression the sum of p^r is simply a geometric series that yields the well-known result $1/(1-p)$. The factors r^2 may be verified to be generated from the sum over p^r by the (term by term) operation $p(d/dp)(pd/dp)\sum p^r$, since each derivative generates from p^r a factor r, but steps the power down by 1, requiring each time the compensating operation of subsequent multiplication by the factor p. The second derivative essentially generates $(1-p)^{-3}$ from $(1-p)^{-1}$, while the simple sum generates $(1-p)^{-1}$ in the denominator, and the result for χ^2 is a quotient of the two [8],

$$\chi^2 = \frac{1+p}{(1-p)^2} \quad \text{or} \quad \chi \propto (p_c - p)^{-1} \tag{1.6}$$

The final result ignores the factor of $1+p$ in the numerator for the purpose of finding the critical exponent (the power of $p - p_c$) for the correlation length. Equation (1.6) thus both confirms the proposed functional form of the correlation length as a divergent power of $p - p_c$, and yields the value $\nu = 1$ in one dimension. In the case of power law divergences, the choice of a definition of χ is somewhat arbitrary. See Problem 1.2 for an alternate calculation of χ which leads to the same critical behavior as shown in Eq. (1.6), although the exact result is different. Later we will also find the value of ν by examining the cluster statistics. Percolation allows multiple paths for analysis.

In order to be able to make general application of percolation theory to an arbitrary system of course it is necessary to know the value of such powers under all circumstances. Most of the exponents of percolation theory are the same for all systems in a particular dimension, but differ importantly from dimension to dimension. In other words, for all three dimensional arrangements of bonds and sites, most of the exponents of percolation theory do not vary, but they do vary depending on whether the system sites are arranged in three dimensional space, or on a plane, for example.

Note that the correlation length represents an actual distance as measured in the Euclidean space and is thus a measure of a cluster size. The shortest connecting path that links opposite sides of a cluster has a step-by-step length called the chemical distance, r_l, [3, 28, 32] since this is the actual distance of particle transport.

1.7 The Relationship of Scale Invariance and Renormalization, and the Relationship of the Renormalization Group to Percolation Theory

Renormalization is both a technique and a conceptual foundation for understanding percolation. As a technique it provides many useful results, but its conceptual role is even more important here.

Renormalization as a technique is a rather complex mathematical procedure, corresponding (in real space though not in Fourier space) to a relatively simple physical operation. This operation is a kind of "coarse-graining," caused by the observer drawing back to a greater distance. If the system has true scale-invariance, i.e., is exactly at the percolation threshold, it will be impossible to detect a statistical change in the appearance of the system as the scale of observation is increased. A system with an infinite correlation length looks, in a statistical sense, the same at all finite length scales. But if the system is merely near the percolation threshold, so the correlation length is finite, then drawing back to a greater distance will make the correlation length look smaller. Eventually the observation scale will be greater than the correlation length. This (relative) diminution of the correlation length means that at larger length scales the system must appear as though it were further from the percolation threshold. Thus it must also be possible to redefine p simultaneously to be enough closer to p_c so that the appearance of the system does not change. This concept underlies the assertion that it is possible to define 'scaling' variables.

In the operation of renormalization, systems which are precisely at percolation remain at percolation. However, with increasing length scales, systems not at percolation appear to move away from percolation. Considered in terms of the redefined p as a function of the scale of observation, repeated renormalization leads to completely different trajectories for systems above and below the percolation threshold. The trajectory produced by repeated renormalization of a system at the percolation threshold is a point, since no changes can be observed. But the trajectory produced by such repeated applications of renormalization to a system not at percolation will always be away from the percolation threshold. Specifically, if the starting state has $p > p_c$, the trajectory will always be towards $p = 1$, while if the starting state has $p < p_c$, the trajectory will always be towards $p = 0$. If there is a largest cluster or largest hole size, this cluster (or hole) will look smaller every time the renormalization is applied. If the initial p value is either zero or one, renormalization will not affect p. Thus $p = 0$, $p = p_c$, and $p = 1$ are all "fixed points" of the renormalization procedure (though $p = 0$ and $p = 1$ are "trivial" fixed points, giving no new information). This same behavior is observed at second order phase transitions, for which the correlation length also diverges. While the language and understanding of phase transitions has become more complex since the study of percolation theory commenced, the percolation transition does qualify as a second order phase transition in the traditional definition and the theoretical development for such critical phenomena can be adopted for percolation theory.

1.8 Cluster Statistics of Percolation Theory

Probably the most elegant means to summarize the theory of percolation is to use the scaling theory of percolation clusters [45]. In principle one can formulate most of percolation theory simply in terms of its cluster statistics, and these statistics also allow easy analogies to other phase transitions. The purpose of this section is not to provide a detailed overview; for that the reader is referred to Stauffer's review [45]. What will be discussed here is sufficient to demonstrate the internal consistency of percolation theory, and to provide less experienced readers with multiple avenues for understanding and application.

The cluster statistics of percolation define the concentration n_s of clusters of volume (number of sites) s as a function of p. Consider initially n_s for $p < p_c$, deferring until later in this section the more complicated case including an infinite cluster. The sum $\sum s n_s$ over all cluster sizes must equal p, since it is by definition the total number of occupied sites per unit volume. Clearly as p increases toward p_c the number of large clusters increases. It turns out that precisely at p_c there can be no volume scale, because there is no length scale: n_s must therefore follow a power law in s. So at percolation n_s must obey [18],

$$n_s(p = p_c) \propto s^{-\tau} \tag{1.7}$$

Here τ is an exponent whose value will be discussed later. How does n_s depend on p? For $p \neq p_c$ a length scale exists, and its value is the correlation length χ. Suppose that one increases the observation length scale (reducing χ) and *simultaneously* takes the system closer to p_c (increasing χ); one can recover the original appearance if these operations cancel perfectly. Stauffer [45] states "We assume that the ratio $[\ldots]$ $n_s(p)/n_s(p_c)$ and similar ratios of other cluster properties are a function of the ratio s/s_χ." Here s_χ is a typical cluster volume at p, which, since cluster sizes follow a power law, is proportional to the *limiting* (or largest) cluster volume at p. Since the linear extent of the largest clusters with $s = s_\chi$ is χ, which diverges as $p \to p_c$, the limiting cluster volume must also diverge in the limit $p \to p_c$. The exponent of $(p - p_c)$ which restricts the largest cluster volume is now denoted $-1/\sigma$, allowing the possibility that it is different from $-\nu$. This exponent must also be negative in order that the largest cluster size diverge at $p = p_c$. Thus $(s/s_\chi)^\sigma = s^\sigma (p - p_c) \equiv z$ is the scaling variable that allows the simultaneous effects of a size change and a change in p to cancel precisely. Consequently the ratio of the cluster numbers at p and at p_c can be written

$$\frac{n_s(p)}{n_s(p_c)} = f(z) = f\left[s^\sigma (p - p_c)\right] \tag{1.8}$$

The value of σ is not known a priori. Equation (1.8) may be called semi-empirical in that it was designed to: (1) accommodate results of simulations, which revealed that the cluster numbers n_s decay according to a power law (with exponent τ) precisely at the percolation threshold, and (2) allow simultaneous rescaling of s and p in such a way that the system looks the same, because the product $(p - p_c)s^\sigma$ remains the same. Approximate values of τ and σ can be found from simulations and/or

renormalization procedures. These values will be the same for all systems of a given dimensionality, but have a dependence on spatial dimensionality, d (we will use the notation 1-d, 2-d and 3-d to denote the dimensionality of the Euclidean space, in which the system is embedded).

Substitution of $p = p_c$ in the left hand side of Eq. (1.8) forces $f(0) = 1$. The exact form of the function f was uncertain for a long time, with various approximations proposed. In the Stauffer review it was pointed out that a Gaussian form for f could fit a wide range of data. Thus a useful approximation for $n_s(p)$ is [45]

$$n_s(p) \propto s^{-\tau} \exp\left\{-[z - z_0]^2\right\} \approx s^{-\tau} \exp\left\{-\left[s^{\sigma}(p - p_c)\right]^2\right\} \tag{1.9}$$

The approximation made here, which omits z_0, is motivated by the observation that z_0 must have some dependence on the system investigated and thus cannot be universal Nevertheless the fact that a z_0 exists makes the cluster statistics, in principle, asymmetric about the percolation transition, for which $z = 0$. For bond percolation on a square lattice in two dimensions), however, there is perfect symmetry between connected and unconnected bonds and the existence of a term z_0 would imply that extrema for the clusters of interconnected bonds would occur at different values of p than for clusters of unconnected bonds. However, it must be kept in mind that the neglect of this detail could lead to small discrepancies. The form of Eq. (1.9) makes it apparent that for $p \neq p_c$ the cluster statistics decay as a power law only up to a certain maximum size $s = s_\chi$, which is proportional to $|p - p_c|^{-1/\sigma}$. This provides an explicit context for the scaling arguments above, because clusters of larger volume rapidly become extremely rare when $|s^{\sigma}(p - p_c)| \gg 1$.

One can use Eq. (1.9) in many ways. As a first application let us use Eq. (1.9) to find the fraction of sites connected to the infinite cluster at $p > p_c$. Note that the summation of sn_s from $s = 1$ to infinity is qualitatively different for $p > p_c$ from its form for $p < p_c$. For $p < p_c$, every occupied site (or bond) must be located on some finite cluster, but for $p > p_c$, some fraction P_∞ of occupied sites is found on the infinite cluster, not included in the summation. Thus every site on the lattice is either (1) empty with probability $1 - p$, (2) occupied and on the infinite cluster with probability pP_∞, or (3) occupied but not on the infinite cluster with probability $p(1 - P_\infty) \equiv \sum sn_s$. From these results one finds

$$P_\infty = 1 - \frac{1}{p} \sum_s sn_s \tag{1.10}$$

Stauffer's argument, which has been amply verified, is that it is the "singular" behavior of cluster sums, such as Eq. (1.10), which gives the percolation quantities of interest, such as P_∞, χ, etc. A sum of sn_s with n_s taken from Eq. (1.9) may be approximated by an integral. The functional dependence of such an integral on variables such as $p - p_c$ can be evaluated by transforming the argument of the exponential to dimensionless variables, i.e., z, (no dependence on $p - p_c$). The result then contains one or more terms that are products of a power of $p - p_c$, and a definite integral which integrates to some (unimportant) constant. In such cases, singular behavior refers to the lowest non-analytical power of $p - p_c$. An even easier technique for evaluating the functional dependence of such sums exists, however.

A sum over a power law distribution of s, truncated at a maximum s value, will typically be dominated by the largest s allowed. At large values of its argument, the exponential function is a much more rapidly diminishing function than a power law, but at small values of its argument it is nearly a constant. Thus, the exponential function can be approximated to do nothing except to truncate the sum, or integral, over sn_s at a value of s proportional to $(p - p_c)^{-1/\sigma}$. This argument leads to the following result:

$$\int_1^{(p-p_c)^{\frac{-1}{\sigma}}} s s^{-\tau} ds \propto p\left[1 - (p - p_c)^{\frac{\tau-2}{\sigma}}\right] \tag{1.11}$$

The factor p is included since when $p = p_c$ the integral must yield p. Using Eq. (1.11) in Eq. (1.10) gives,

$$P_\infty = \frac{(p - p_c)^{\frac{\tau-2}{\sigma}}}{p} \propto (p - p_c)^\beta \tag{1.12}$$

The exponent β is customarily used for the critical behavior of P_∞. Equation (1.12) relates β to τ and σ via $\beta = (\tau - 2)/\sigma$. If the cluster statistics of percolation theory are known accurately Eq. (1.12) allows direct calculation of β. Otherwise Eq. (1.12) still gives an important scaling relationship.

Since P_∞ must vanish at $p = p_c$ $\beta \geq 0$. Therefore $\tau \geq 2$. In one dimension, because p_c is exactly 1, there is no regime $p > p_c$, and $\beta = 0$ is allowed, but in all higher dimensions, $\beta > 0$. In systems of practical interest (two and three dimensional systems) $0 < \beta < 1$. However, we will only be able to calculate accurately two values of β, 0 in one dimension and 1 in six dimensions or higher (or on Bethe lattices). Though we only show calculations of selected values of the critical exponents of percolation theory, summaries of values given elsewhere are also provided.

One can, in fact, calculate an entire series of integrals similar to Eq. (1.11). In particular, the kth moment of the cluster distribution is given by,

$$M_k = \int_1^{(p-p_c)^{\frac{-1}{\sigma}}} s^k s^{-\tau} ds \propto |p - p_c|^{\frac{\tau-1-k}{\sigma}} \tag{1.13}$$

Since the lower moments, M_0, M_1, and M_2, all correspond to important physical properties, the values of $(\tau - 1 - k)/\sigma$ for these cases receive special designations. Thus Eq. (1.13) will provide the basis for three scaling relationships that we will use later. The possibility to organize several scaling relationships into a single equation (1.13) makes the cluster statistics formulation of percolation theory so appealing. But further discussion of these scaling relationships is postponed until after we have shown how to calculate n_s in 1-d.

1.9 Derivation of One-Dimensional Cluster Statistics and Discussion of Fractal Dimensionality

In one dimension the critical bond fraction for percolation, $p_c = 1$. This result is necessary because any break in the chain of elements will prevent the formation of

a cluster of infinite size that spreads from negative to positive infinity. A purpose in repeating this fundamental condition is to remind the reader that in 1-d systems expressions containing $1-p$ may be rewritten as $p_c - p$. The next discussion follows Stauffer [45] in its general content. The probability of finding a cluster of s interconnected bonds, all in a row, is

$$n_s = p^s(1-p)^2 \tag{1.14}$$

where the factor $(1-p)^2$ truncates the s-cluster on both ends. In the case that $p_c - p \ll 1$ (p very near p_c), this result can be rewritten to lowest order in $p_c - p$ (noting that $1-p = p_c - p$) as,

$$n_s = s^{-2}\big[1-(p_c-p)\big]^s\big[s^2(p_c-p)^2\big] = s^{-2}\exp\big[-s(p_c-p)\big]\big[s^2(p_c-p)^2\big] \tag{1.15}$$

"Derivation" of Eq. (1.15) from Eq. (1.14) requires also use of the approximation $(1-x)^s = \exp(-sx)$, valid for $x \ll 1$. This approximation is used again when the cluster statistics for a Bethe lattice are derived. The cluster statistics of percolation theory can always be written in the following form,

$$n_s = s^{-\tau} f\big[s^{\sigma}(p-p_c)\big] \tag{1.16}$$

Equation (1.15) and Eq. (1.16) show that for one dimensional systems $\tau = 2$ and $\sigma = 1$. Also, consistent with $\sigma = 1$, one sees that there is a cut-off in the occurrence of clusters for sizes $s > s_{max} \approx 1/(p_c - p)$. In 1-d the length of a cluster of s elements is s (times the fundamental bond length), so that the linear dimension of the largest cluster for $p < p_c$ is also $(p_c - p)^{-1}$. This result then defines the correlation length and yields the value $\nu = 1$ in agreement with Eq. (1.6). Note that the fact that $s_{max} \propto (p_c - p)^{-1/\sigma}$ and that $\chi \propto (p_c - p)^{-\nu}$ implies the result that $s_{max} \propto \chi^{1/\sigma\nu} = \chi^1$ where the equality holds in 1-d. Any time the total "volume" (s) of an object is proportional to its linear dimension (χ) to an exponent, the implication is that the "dimensionality" of the object is that exponent. As a consequence, the combination of exponents, $1/\sigma\nu$ has become known as the fractal dimensionality, d_f, of percolation clusters, i.e., of large clusters near the percolation threshold. This fractal dimensionality has been called a "mass" fractal since it refers to a relationship between volume (proportional to mass) and linear dimension. Since for $d = 1$ $d_f = 1$ as well, in one dimension large clusters near the percolation threshold do not (cannot) have the rough "surface" associated with fractal objects. However, in systems of larger dimensionalities, d_f turns out to be less than d.

1.10 Argument for Dimensionally-Dependent Scaling Law, Implications for Critical Exponent, τ, and Applications to Critical Exponents

The scaling form of Eq. (1.8) for the cluster statistics is independent of the dimensionality of the system. The exponents of percolation theory that appear in Eq. (1.8),

Eq. (1.12) and similar equations below depend only on the dimensionality of the system The scaling laws in Eq. (1.13) do not depend explicitly on the dimensionality allowing, in principle at least, the possibility that the values of the exponents are the same in all dimensions. But there is an important scaling law that does depend on dimensionality. The existence of this scaling law forces a variation of the values of the critical exponents with dimensionality, necessitating the tabulation of values given later in this chapter. Here we derive the dimensionally-dependent scaling law that relates the various critical exponents from percolation theory.

The dimensionally-dependent scaling law relating various critical exponents from percolation theory can be derived starting again from the cluster statistics of percolation, though the cluster statistics are not, by themselves, sufficient for this derivation. We first need to rewrite the cluster statistics of percolation theory in terms of the linear extent of the clusters. A cluster may be defined to have some linear extent N, where N is a number which, when multiplied by a basic length scale (such as a bond length) gives the linear dimension of the cluster. We know that the volume of a cluster of linear extent N is equal to $s = N^{1/\sigma\nu}$, on account of the fractal dimensionality of the clusters. We have derived the form of the cluster statistics in one dimension, and it has been demonstrated that this form is also appropriate in larger dimensions, though with different values of the exponents [45]. Further, the scale-invariance of the system exactly at percolation requires that the cluster statistics follow a power-law decay, so we can write

$$n_s(p = p_c) = s^{-\tau} \tag{1.17}$$

Now use the probabilistic identity,

$$n_s ds = n_N dN \tag{1.18}$$

to obtain,

$$n_N = N^{-\frac{(\tau-1-\sigma\nu)}{\sigma\nu}} \tag{1.19}$$

If one integrates this (unnormalized) probability density function over a range of values from, say, N_0 to $2N_0$, which in a power-law discretization scheme (appropriate for self-similar media) would represent one "size class," one obtains,

$$P(N_0) = N_0^{-\frac{\tau-1}{\sigma\nu}} \tag{1.20}$$

The significance of Eq. (1.20) becomes clear when it is discussed in the context of the self-similarity of the medium at $p = p_c$. At percolation, typically one cluster of linear extent N_0 should be found in a volume N_0^d (for any value of N_0) in order to be (1) consistent with the idea of percolation, i.e., that one can expect percolation to occur in any size system, all the way to infinite size, and (2) consistent with the concepts of self-similarity, i.e., that all such volumes look alike. Thus the concentration of clusters of size N_0 is proportional to N_0^{-d} so that the product of N_0^d and $N_0^{-d} = 1$. The implication is that,

$$\frac{\tau - 1}{\sigma\nu} = d \quad \tau = 1 + \frac{d}{d_f} \tag{1.21}$$

This is the fundamental scaling relationship of percolation theory that cannot be obtained directly from the cluster statistics. It is the only such relationship that involves explicitly the dimensionality of the space, d, in which the percolation problem is embedded. Equation (1.21) relates the fractal dimensionality, $1/\sigma\nu$, to the Euclidean dimensionality, d in terms of how rapidly cluster numbers decay with increasing size.

It is also straightforward to derive the ratio of the number of connected sites of a large cluster to the total number of occupied sites in the volume spanned by that cluster. Such a ratio is proportional to the mass M of the cluster divided by its volume V, and gives thus the cluster's density, ρ (e.g., [36]). In the context of percolation, a "large" cluster has linear extent approximately equal to the correlation length. The result for ρ is

$$\rho = \frac{M}{V} = \frac{\chi^{d_f}}{\chi^d} = \left[(p - p_c)^{-\nu}\right]^{\frac{1}{\sigma\nu}-d} = (p - p_c)^{d\nu-\frac{1}{\sigma}} \equiv (p - p_c)^{\beta} \tag{1.22}$$

Equation (1.22), just above percolation in the limit of a cluster of infinite extent, also gives the fraction of sites, which is connected to the infinite cluster, justifying the final definition in Eq. (1.22). From Eq. (1.22) we can see that

$$\beta = d\nu - \frac{1}{\sigma} \tag{1.23}$$

or

$$d_f = \frac{1}{\sigma\nu} = d - \frac{\beta}{\nu} \tag{1.24}$$

One can combine Eq. (1.21) and Eq. (1.24) to write,

$$\frac{\tau - 2}{\sigma} = \beta \tag{1.25}$$

which is the same result as that derived directly from the cluster statistics. Thus, combining the expression for the density of large clusters with the dimensionally-dependent scaling relationship yields one of the known cluster scaling relationships (from Eq. (1.12)). The implication of this redundancy is that the density of large clusters is dependent on the probability that an arbitrary site is found on the infinite cluster. Therefore the argument leading to Eq. (1.22) only appears to be new.

The conclusion that $\tau > 2$ (after Eq. (1.12) can be drawn simply by examining the definition of n_s. Consider the integral,

$$\int_1^\infty s n_s ds = s^{2-\tau}\Big|_1^\infty \tag{1.26}$$

which represents the total number of connected sites. This integral diverges unless $\tau > 2$. Although in dimensions $d > 1$ this is strictly an inequality, in $d = 1$ the value $\tau = 2$ is allowed. The reason for this is that the percolation probability is identically 1. So there is no regime $p > p_c$ in one dimension. Further, at $p = p_c$ the concentration of clusters of linear size s cannot really follow a power law: all sites are connected, there is only one cluster, and it is infinite in extent. Precisely at p_c in one dimension, then, the infinite cluster must be Euclidean, as implied already from

the equivalence of d and d_f. Equation (1.11), from which the scaling relationship (Eq. (1.12)) for the exponents in n_s was derived, yields in 1-d fundamentally different results in the limit $p \to 1$ and for $p = 1$. In fact, a sudden increase in P_∞ from 0 to 1 over an infinitesimally small increase in p is consistent with a value of $\beta = 0$. Note that $\beta = 0$ is also obtained by application of the scaling equations Eq. (1.23) or Eq. (1.25) consistent with $d = d_f$ or $\tau = 2$. The other immediate implication of the argument from integral 1.26 that $\tau > 2$ is that Eq. (1.21) then requires $d_f < d$.

Finally, the most attractive aspect of the cluster statistics is that it is possible to use the same starting point (Eq. (1.13)) to derive three different scaling relationships. These relationships arise from applying the same techniques to the sums, $\sum s^0 n_s \propto (p - p_c)^{2-\alpha}$, $\sum s^1 n_s \propto (p - p_c)^{\beta}$, $\sum s^2 n_s \propto (p - p_c)^{-\gamma}$. The scaling relationships from the second was already given in Eq. (1.12) (and (1.25)); the first and third can be written in the following forms (see Problems 1.4, 1.5, and 1.9),

$$2 - \alpha = \frac{\tau - 1}{\sigma} = d\nu \tag{1.27}$$

$$\frac{\tau - 3}{\sigma} = -\gamma \tag{1.28}$$

The three sums also have interesting physical significance; for magnetic systems they correspond to the free energy, the magnetization, and the magnetic susceptibility, respectively. In percolation problems, the first is the mean number of clusters, the second yields the fraction of sites on the infinite cluster, while the third yields the mean mass of the clusters. Each then relates an important exponent from experiment to τ and to σ. Using these three scaling relationships (Eq. (1.27), Eq. (1.28), and Eq. (1.12)) and the dimensionally dependent scaling relationship (Eq. (1.21)) it is possible to define all six critical exponents in terms of just two, most simply, for example, τ and σ from the cluster statistics.

1.11 Explicit Calculations of the Second Moment of Cluster Statistics in One Dimension

It will be necessary here to relate the second moment, M_2, of the cluster distribution to a simple sum over $g(r)$. In fact, the sum over $g(r)$ is easy to evaluate; any difficulty comes from the argument of its equivalence to M_2. Together with the results of calculations already shown and the scaling relationships of percolation we will then be able to generate the remaining exponents of percolation theory for the case of one dimensional systems. We will also generate in subsequent sections the exponents of percolation theory for infinite dimensional systems and then use the information generated from the extreme cases to understand the dimensional dependence of the exponent values.

The mean mass of finite clusters is shown in Bunde and Havlin [8] to be proportional to the second moment of the cluster size distribution. How do they show this? They start with the sum $\sum s n_s$ and use the exact expression for n_s in one dimension

to show that this sum over finite cluster sizes (the only clusters that exist in one dimension) is exactly p.

The probability that an arbitrary lattice site belongs to an s-cluster is $sp^s(1-p)^2$. The factor s arises from the possibility that such an arbitrary site can be any of the s sites of the cluster. The authors then construct the corresponding probability per cluster site, which is just $p^s(1-p)^2$. Now construct the sum,

$$w \equiv \sum_{s=1}^{\infty} sn_s = (1-p)^2 \sum_{s=1}^{\infty} sp^s = (1-p)^2 \sum_{s=1}^{\infty} p\frac{d}{dp}p^s = \left(1-p^2\right)p\frac{d}{dp}\sum_{s=1}^{\infty} p^s \tag{1.29}$$

The sum is easily performed with the result

$$w = (1-p)^2 p\frac{d}{dp}\left(\frac{1}{1-p}-1\right) = (1-p)^2 p\left(\frac{1}{1-p}\right)^2 = p \tag{1.30}$$

The mean mass of a cluster can be defined as then

$$S = \sum_{s=1}^{\infty} s\left[\frac{sn_s}{\sum_{s=1}^{\infty} sn_s}\right] \tag{1.31}$$

with the factor in brackets generating the probability of an arbitrary site being found on an s-cluster and the product of this factor with s then giving the expected number of sites on s-clusters. Thus the mean mass is seen to be proportional to the second moment of the cluster distribution (s^2 in the sum).

In one dimension, since $g(r)$ gives the expected number of cluster sites at distance r the mean mass of a cluster is given [8] as follows,

$$S \equiv M_2 = 1 + \sum_{r=1}^{\infty} g(r) = \sum_{r=0}^{\infty} p^r = \frac{1}{1-p} = \frac{1}{p_c - p} \tag{1.32}$$

M_2 is traditionally characterized by the exponent γ, i.e., $S \propto (p_c - p)^{-\gamma}$. Thus $\gamma = 1$. From Eq. (1.28) one has $(\tau - 3)/\sigma = -\gamma$, so this result could be used to infer the value of τ, if one already knew σ (which we found using Eq. (1.15) to be 1). Of course in that derivation we also found τ and ν.

Since we have already shown how to obtain four exponents in one-dimensional systems, we can generate the remaining values. In fact $\alpha = [2 - (\tau - 1)/\sigma] = [2 - (2-1)/1] = 1$, and $\beta = (\tau - 2)/\sigma = (2-2)/1 = 0$. Of course, following Eq. (1.26) we already argued on physical grounds that $\beta = 0$. Thus we have the complete suite of these fundamental exponents for one-dimensional systems.

1.12 Calculation of the Correlation Length on a Bethe Lattice

Sections 1.12 through 1.15 give some exact calculations of exponents of percolation theory for infinite dimensional systems (in particular, Bethe lattices) as well

as a mean-field calculation of the exponent β. This mean-field result for β is independent of dimensionality, d. Using these values together with the scaling relationships (Eqs. (1.25), (1.27) and (1.28)) and one physical argument from Bunde and Havlin [8] allows calculation of all the exponents of percolation theory in infinite dimensional systems. The scaling relationships in Eqs. (1.25), (1.27), and (1.28) are consistent with the values of the exponents for infinite-dimensional systems and the mean-field calculation of β. But these values are consistent with the dimensionally-dependent scaling relationship (Eq. (1.21) only for $d = 6$. This will make it possible (in Sect. 1.16) to define the range of dimensionalities for which the complete set of scaling relationships from percolation theory is accurate. Since this range of dimensionalities turns out to be $1 \leq d \leq 6$, the reader, especially those interested only in application of percolation theory to problems of subsurface flow and transport, may assume that the above framework of scaling relationships is accurate for systems of experimental interest and skip Sects. 1.12 through 1.16 on a first reading. Nevertheless the following material is included here for those readers interested in understanding better the framework of the theoretical results they are encountering. Readers who skip these sections will still encounter five derivations: (1) cluster statistics in one dimension, (2) the correlation length in one dimension, (3) the mean cluster mass in 1-d, (4) the correlation length in two dimensions using renormalization techniques, (5) the relationship between fractal dimensionality and tortuosity. Ability to perform some derivations as well as familiarity with the scaling laws helps cement the understanding of people new to the field of percolation theory.

Percolation problems can be solved rigorously on a Bethe lattice (Cayley tree) as well as in one dimension. In contrast with the one dimensional system, the Bethe lattice has one advantages: $p_c < 1$ (meaning that it is possible to investigate behavior at $p > p_c$ as well as $p < p_c$). In contrast to all other dimensional systems, Bethe lattices have the following advantage: there are no loops in the structure. In addition, the Bethe lattice actually reduces to a one-dimensional system in a particular limit. It is a relatively simple argument to show that the Bethe lattice is otherwise equivalent to an infinite dimensional structure, so that determination of percolation exponents on Bethe lattice in addition to their values in one-dimensional systems gives these exponents in two extreme cases. A Bethe lattice of coordination number Z has a central site from which Z branches of unit length emanate. The end of each branch is another site, which connects through $Z - 1$ branches to new sites. A Bethe lattice with $Z = 3$ is like a family tree: at each generation there are twice as many ancestors as in the previous one, and it radiates out from a single point.

The lack of loops in the system means that two sites can be connected by only one path. One can draw (with some difficulty) a Bethe lattice on a two-dimensional surface, but, as we will see, the Bethe lattice is equivalent in several respects to an infinite dimensional object. Clearly a Bethe lattice is a hierarchical structure, and it is convenient (and consistent with a drawing) to refer to each higher order of the hierarchy as a higher order shell. As Bunde and Havlin [8] point out, the Euclidean distance has no meaning on a Bethe lattice; only the chemical distance, r_l between two sites has any relevance. Thus the correlation length is calculated with respect to a distance measured in shell separations, l. In particular, the chemical distance

between the central site and a site in the lth shell is $r_l = l$. The lth shell of the tree consists of $Z(Z-1)^{l-1}$ sites. For the special case of $Z = 2$ the lth shell thus contains 2 sites, as in a one-dimensional chain, but in all other cases the number of sites increases exponentially since the l dependence shows up *in the exponent*. In a d-dimensional lattice, the number of sites at distance l increases as $l^{\mathrm{d}-1}$ (the surface area of a sphere of radius r being proportional to r^{3-1}, for example). Exponential functions may be expressed in terms of a Taylor series such as $\sum x^{\mathrm{n}}/n!$. As x increases, the power of the dominant term increases as well. As x increases without bound, the dominant term in the series becomes the largest (or infinite) power, meaning that it is consistent to regard a Bethe lattice as an infinite dimensional structure. From the property of universality of the exponents in percolation theory one can thus propose that the exponents derived for the Bethe lattice are the same as for any infinite-dimensional lattice. Moreover, since Toulouse [50] argues that the upper critical dimensionality for percolation is 6 (which we discuss in Sect. 1.16), it can be argued that the results derived for the exponents for the Bethe lattice are relevant to all systems with $d \geq 6$.

Assume that some fraction p of the sites on a Bethe lattice is occupied. The correlation function $g(l)$ is defined to be the mean number of sites on the same cluster at distance l from an arbitrary occupied site. In order for two sites separated by a distance r_l both to belong to the same cluster, each site in between the two sites must be occupied, bringing in a factor p^{l-1}; thus the probability that the second site is occupied and all the intervening sites as well is p^l. The number of sites on the l-th shell is $Z(Z-1)^{l-1}$, making $g(l)$ the product of p^l (the probability that a given site is connected) and $Z(Z-1)^{l-1}$ (the number of possible connected sites). The correlation function, $[p(Z-1)]^l Z/(Z-1)$, being nearly $(p(Z-1))^l$, obviously trends rapidly to zero if the product $p(Z-1) < 1$, while it diverges for $p(Z-1) > 1$. This makes $p_{\mathrm{c}}(Z-1) = 1$ the defining equation for the critical percolation probability, leading to $p_{\mathrm{c}} = 1/(Z-1)$.

Next, the correlation length can be calculated in terms of the variable l as

$$\chi^2 = \frac{\sum_{l=1}^{\infty} l^2 g(l)}{\sum_{l=1}^{\infty} g(l)} \approx \frac{\sum_{l=1}^{\infty} l^2 (Z-1)^l p^l}{\sum_{l=1}^{\infty} (Z-1)^l p^l} \tag{1.33}$$

This sum may be performed by the same techniques as used in the one-dimensional chain, i.e., the geometric sum is now $1/(1-(Z-1)p) = 1/(1-p/p_{\mathrm{c}}) = p_{\mathrm{c}}/(p_{\mathrm{c}}-p)$. The same trick to generate the factor l^2 in one-dimensional lattices works here as well, since differentiation with respect to p leaves the factor $(Z-1)$ alone. Bunde and Havlin [8] then find

$$\chi^2 \propto (p - p_{\mathrm{c}})^{-2} \tag{1.34}$$

and the correlation exponent equals 1 with respect to the chemical distance, l (in l-space). Since the Euclidean dimension has no meaning on the Bethe lattice, there is no purpose to make a direct calculation of the correlation length as an estimate of the Euclidean dimension of the largest cluster for $p < p_{\mathrm{c}}$. But Bunde and Havlin [8] make the argument that on other lattices of high enough dimension (greater than the critical dimension, 6, as it turns out) any path on a cluster behaves like a random

walk (with the number of steps proportional to l), so that $r^2 \propto l$. This argument implies that for $d \geq 6$ (other than Bethe lattices) the correlation length as a function of the Euclidean distance should have exponent $\nu = 1/2$.

1.13 Explicit Calculations of the Second Moment of Cluster Statistics on a Bethe Lattice

The calculation of the mean mass for a Bethe lattice is very similar to its calculation in one-dimensional systems. On a Bethe lattice one has

$$S = 1 + \sum_{l=1}^{\infty} Z(Z-1)^{l-1} p^l = \left(\frac{Z}{Z-1}\right) \sum_{0}^{\infty} \left[p^l (Z-1)^l\right]$$
$$= \left(\frac{p_c}{\frac{p_c}{p_c+1}}\right) \frac{1}{1-(Z-1)p} = \frac{p_c+1}{1-p/p_c} = \frac{p_c(p_c+1)}{p_c - p} \tag{1.35}$$

This result yields once again $\gamma = 1$. On the Bethe lattice this calculation turns out to be quite useful indeed.

The exponent $\beta = 0$ describing the behavior of the infinite cluster in one dimension (and given by the first moment of the cluster statistics) was already inferred in Sect. 1.10. The discussion of the exponent β [8] is slightly more complicated on a Bethe lattice, but the next section gives a derivation valid whenever "mean-field" treatments are appropriate (as it will turn out, for $d \geq 6$, and thus also on the Bethe lattice).

1.14 Mean-Field Treatment of the Probability of Being Connected to the Infinite Cluster

Consider a "mean-field" treatment of the bond percolation problem on a lattice with coordination number (number of nearest neighbors), Z. In mean-field treatments all sites are regarded as equivalent. While all sites were equivalent before the bonds were actually assigned, this equivalence is lost afterwards, and this is a reason why mean-field treatments can fail. Nevertheless, a mean-field treatment does illuminate some important concepts, and we can apply these further.

Assume that an infinite cluster of connected sites exists. Define the probability that some particular site is connected to the infinite cluster as P_∞. Then the probability that it is not connected is $1 - P_\infty$. The probability that the site is connected to one of its nearest neighbors, chosen arbitrarily, is p. According to the mean-field hypothesis, the probability that neighbor site is connected to the infinite cluster is assumed to have the same value P_∞, with the value independent of whether the two sites are actually connected or not. The probability that the given site is connected to the infinite cluster over this particular nearest neighbor is pP_∞, where the product

is used because of the independence of the bond probability and the probability P_∞. The probability that it is not connected to the infinite site over this particular nearest neighbor is $1 - pP_\infty$. The probability that it is not connected to the infinite cluster over any of its nearest neighbors is thus $(1 - pP_\infty)^Z$. Thus we must have,

$$1 - P_\infty = (1 - pP_\infty)^Z \tag{1.36}$$

which states that the probability that a site is not connected to the infinite cluster is equal to the probability that it is not connected over any one of its nearest neighbor sites, and that the probability that each of those neighbor sites is not connected to the infinite cluster is identical. Equation (1.36) can be rewritten as,

$$(1 - P_\infty)^{\frac{1}{Z}} = 1 - pP_\infty \tag{1.37}$$

Note that for $p < 1/Z$, this equation has only one solution, namely, $P_\infty = 0$. If the probability that any arbitrary site is connected to the infinite cluster is 0, there must not be an infinite cluster. If an infinite cluster does not exist, the system must be below the percolation threshold. This indicates that to lowest order $1/Z$ is the percolation threshold. We expand Eq. (1.37) (keeping the first two terms of a Taylor series) in the variable $p - 1/Z = p - p_c$ and assume that $P_\infty \ll 1$.

$$1 + \frac{1}{Z}(-P_\infty) + \frac{1}{2}(-P_\infty)^2\left(\frac{1}{Z}\right)\left(\frac{1}{Z} - 1\right) = 1 - \left(\frac{1}{Z} + p - \frac{1}{Z}\right)P_\infty \tag{1.38}$$

Note that the first two terms on each side of the equation are identical and can be subtracted off. Then we have,

$$P_\infty = \frac{(p - \frac{1}{Z})}{\frac{1}{Z}(1 - \frac{1}{Z})} = \frac{p - p_c}{p_c(1 - p_c)} \tag{1.39}$$

P_∞, like all other percolation quantities, is known to be a power of $p - p_c$. Thus the mean-field treatment directly predicts $p_c = 1/Z$ as can be seen from the numerator. Note the implication that $p_c = 1/Z$ has no dependence on d. This is incorrect. However, we are going to assume that the result that $p_c \propto 1/Z$ is correct and that the proportionality constant may depend on dimensionality. For our purposes this is the most important result of the application of the mean-field treatment to find P_∞ and we will use it later to deduce some further values of p_c.

Comparison of Eq. (1.39) with $P_\infty = (p - p_c)^\beta$ allows the identification $\beta = 1$. $\beta = 1$ is the mean-field result. Like all such "classical" results, it is independent of d. It will be argued to be relevant for systems with $d \geq 6$. $\beta = 1$ can be derived exactly for a Bethe lattice.

1.15 Cluster Statistics on a Bethe Lattice

In a one-dimensional lattice the cluster statistics were easy to develop. They are almost as easy to develop on a Bethe lattice, but one difference is that it is somewhat more difficult to define the perimeter of an s-cluster, i.e., the number of sites

which terminate the cluster. It is, however, relatively easy (for $Z = 3$, at any rate) to convince oneself that a cluster of 1 site has Z empty sites surrounding it, a cluster of 2 sites has $Z + Z - 2$ empty sites surrounding it, and a cluster of s sites has $Z - 2$ more empty sites surrounding it than a cluster of $s - 1$ sites. The number of perimeter (empty, bounding) sites can be called u, and u is thus,

$$u(s) = Z + (s-1)(Z-2) \tag{1.40}$$

Note that $u(s) = Z$ in the case $Z = 2$, for which the Bethe lattice collapses to a 1-d chain. Since an s-cluster again can connect only clusters on shells separated by $l = s$, all sites in between must also be occupied, and

$$n_s = g_x p^s (1-p)^{u(s)} = g_x p^s (1-p)^{Z+(s-1)(Z-2)} \tag{1.41}$$

where g_s is just the number of configurations for an s-site cluster. If $p(1-p)^{Z-2}$ is expanded in a Taylor series around $p_c = 1/(Z-1)$ it is possible to show that [8]

$$n_s \approx n_s(p) f(p) \tag{1.42}$$

where $f(p) = (1 - [(p - p_c)^2/2p_c(1-p_c)])^s$. This expression can be rewritten as $\exp(-s[(p-p_c)^2/2p_c(1-p_c)])$ for p nearly p_c. In order to write this function as a function of the scaling variable $z = (p - p_c)s^\sigma$, one must choose $\sigma = 1/2$ so that the product of the factors $(p - p_c)s^\sigma$ is then squared. Note that the form of the cluster statistics (a Gaussian in $p - p_c$) is the same as the approximate result, Eq. (1.9), from Sect. 1.8.

We now have made calculations of the two exponents γ and σ for the Bethe lattice. We can use one of the scaling relationships to infer the value of τ.

$$\tau = 3 + \sigma\gamma = 3 - 1/2 = 5/2 \tag{1.43}$$

Similarly we can find

$$\alpha = 2 - \left(\frac{\tau - 1}{\sigma}\right) = 2 - \frac{3/2}{1/2} = -1 \tag{1.44}$$

We can thus now find most of the exponents of percolation theory in infinite dimensional systems. The one exponent we do not really know at this point is ν for the correlation length. The dimensionally-dependent scaling relationship cannot give it to us. So, practically speaking, we must rely on the argument cited by Bunde and Havlin [8] to find ν.

1.16 Summary of Relationships Between Exponents in One Dimension and in Infinite Dimensions Using Scaling Relationships. Implications for the Validity of Hyperscaling

The term hyperscaling was invented to describe scaling relationships that explicitly involve the dimension, d. The entire compendium of scaling relationships developed in Sects. 1.8 and 1.10 describe exponents with a dimensional dependence

provided the dimensionally-dependent scaling relationship holds. These scaling relations have been shown to be exact in one and two dimensions and are expected to hold for systems of relatively low dimensionality. The set of exponents derived for Bethe lattices on the other hand, except for $\nu(l)$, has been suggested to be valid for all infinite dimensional systems. Mean-field theories are believed to describe the behavior of the ("classical") exponents of percolation theory in high enough dimensions. If the same set of exponents is used independent of dimensionality for any range of values of d, the dimensionally-dependent scaling relationship, Eq. (1.21), cannot generally be true for that set of exponents. However, that set of exponents might be consistent with Eq. (1.21) for one value of d. Thus the set of exponents derived for Bethe lattices may be assumed to be correct in all dimensionalities greater than some maximum (or critical) $d = d_c$, if it is possible to find a $d = d_c$ for which Eq. (1.21) holds for the classical exponents. Without a value of ν, however, this hypothesis cannot be applied. If the suggestion described by Bunde and Havlin [8] regarding the value of $\nu = 1/2$ for infinite lattices is correct (which it is), then we can check to see for which dimension $(\tau - 1)/\sigma\nu = d$ holds. Using these results one finds that $(\tau - 1)/\sigma\nu = 6 \equiv d_c$ meaning that the hyperscaling exponents must be the same as the classical exponents for $d = 6$. This argument was first given by Toulouse [50], and the additional inference is that for systems of dimensionality 6 or greater, the values for percolation exponents found for Bethe lattices are valid. Note that $d_f = 1/\sigma\nu = 4$ holds independently of d for $d \geq d_c$. Thus, even in an infinite dimensional system, the percolation cluster can be embedded in a 4-dimensional space. This result helps to explain why any path on a cluster behaves like a random walk for $d \geq 6$.

For $d < 6$, where hyperscaling is valid, other means for finding the exponents are required. One of the most productive such means is to apply renormalization group calculations using the so-called epsilon expansion with $\varepsilon = 6 - d$ as an expansion parameter, since the values of the exponents are known in six dimensions when $\varepsilon = 6 - 6 = 0$. $d_c = 6$ then becomes the upper limit of validity of hyperscaling.

1.17 Calculation of the Critical Site Percolation Probability for the Two-Dimensional Triangular Lattice and of the Critical Exponent for the Correlation Length in Two Dimensions

The following discussion is an exercise in the power, but also imprecision, of spatial renormalization techniques. It requires some subsequent discussion. Although the actual results are not quite right, they appear to be reasonable, are very nearly accurate, and help illustrate an earlier state of thinking.

While the following development is expanded from Stauffer [45], his source was Reynolds et al. [34]. Consider the image of the triangular lattice in Fig. 1.4. The circles represent sites. Each site can potentially be connected to six nearest neighbors. Imagine coloring in a fraction p of the sites. Whenever two colored sites are

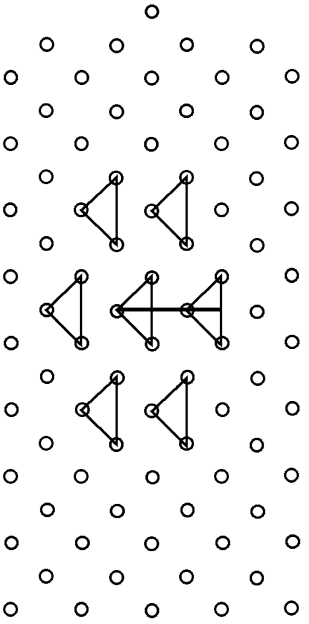

Fig. 1.4 A small portion of a site percolation problem on a triangular lattice. The *circles* are sites. Supersites of a real-space renormalization are located at the centers of the *triangles* shown. The *line* drawn in is an aid to measuring distances using 30-60-90 right *triangles*

nearest neighbors they can be considered to connect (as in the case of metallic balls, which could conduct electricity between them if they were in contact). If a colored site is neighbor to an uncolored site, or two uncolored sites are neighbors, then no connection is made. A renormalization process can be developed, which constructs a new lattice out of "supersites," which replace groupings of three sites as shown. A replacement of three sites by a single site must involve a rescaling of the length, or distance between sites, by the factor $3^{1/2}$. That result can be checked directly in Fig. 1.4 by examining the geometry of the system; the line separating the new sites forms the bisector of the vertex of the triangles, as shown, thus developing 30-60-90 triangles. The sides of these triangles are in the ratios 1, $3^{1/2}$, 2. The ratio of the separation of supersites to that of the simple sites in the original lattice is $2 \times 3^{1/2}/2$. If one moves just far enough away from the lattice that the new "supersites" are exactly as far away from each other as the old simple sites, then the length scale associated with the separation of sites has been reduced by $1/3^{1/2}$.

Now consider how p changes with such a rescaling of the lattice. The approximation that is used here has been called "majority rule." If either two or three sites on the original lattice are colored in, the new site is colored in. Clearly, if all three sites of the original lattice were colored in, a connection could be made across the triangle in any direction, while if two sites are colored in, often a connection across the triangle can still be made, though not in an arbitrary direction. If one or zero sites are colored in on the original lattice, the new site is not colored in, because no connection across the triangle can be made, and in most cases such a triangle will interrupt the continuity of paths constructed across other nearby triangles. The new probability, p', of coloring in a site is thus constructed from the old probability, p.

The above conceptualization is a very reasonable assumption, and nearly precise. It basically means that if you can get across a given "supersite" from one side to the other, presenting potential connections to new sites on both sides, it should be colored in. Otherwise, it should not be. Mathematically this can be represented as,

$$p' = p^3 + 3p^2(1-p) \tag{1.45}$$

The justification for this result is that the probability that all three sites are colored in independently, each with probability p, is p^3. The probability that two particular sites are colored in and the third is not is $p^2(1-p)$. There are three possible locations for the site, which is not colored in, justifying the factor 3. In the case that $p' = p$, the new lattice has precisely the same appearance and statistics as the old, and $p' = p \equiv p_c$. If the substitution $p' = p$ is made in the above equation, it is possible to rewrite the equation as,

$$-2p^3 + 3p^2 - p = 0 \tag{1.46}$$

which can be factored as,

$$-p(2p-1)(p-1) = 0 \tag{1.47}$$

The three roots of this equation are $p = 0$, $p = 1/2$, and $p = 1$. The existence of the "trivial" roots $p = 0$ and $p = 1$ was predicted in Sect. 1.7 (obviously if all sites or no sites are initially colored in, this condition will persist). The root $p = 1/2$ represents p_c.

The divergence of the correlation length must be according to a power law as discussed. The only reasonable form for this relationship is,

$$\chi = \chi_0 |p - p_c|^{-\nu} \tag{1.48}$$

where χ_0 is a scale factor (obviously proportional to the original spacing of the circles marking the fundamental lattice points), which need not concern us here and $\nu > 0$. The value of the critical exponent, ν, can be found through the above renormalization by noting that $-\nu$ is the slope of a graph of the logarithm of χ vs. the logarithm of $p - p_c$. Thus, also for the above change of scale, take p slightly different, e.g., larger than p_c, $p - p_c = \delta$, where $\delta \ll 1$, and find the behavior of $p' - p_c$ as a function of δ. This kind of procedure is known as "linearization," because it will define only the lowest order variability in p'. Using Eq. (1.45) without equating p and p' (because if $p > p_c$, then $p' > p$) write p' as,

$$p' - p_c = (p_c + \delta)^3 + 3(p_c + \delta)^2(1 - p_c - \delta) - p_c \tag{1.49}$$

and expand the result (again in a Taylor series) to first order in δ. The result (the reader should verify this) is that $p' - p_c = (3/2)\delta$. But since $p - p_c = \delta$ by definition, one finds that,

$$\nu = -\frac{\log(\frac{1}{3^{1/2}})}{\log(\frac{3\delta}{2}) - \log(\delta)} = \frac{\log(3^{1/2})}{\log(\frac{3}{2})} = 1.355 \tag{1.50}$$

Note that the value of p_c for the site percolation problem on the triangular lattice is precisely $1/2$, while the value of ν is $4/3 = 1.333$ and the estimate of Eq. (1.50) is only wrong by 2 %.

Consider now also the number of sites on a cluster of linear dimension given by the correlation length. In the renormalization procedure the number of sites on an arbitrary cluster is reduced by the following ratio,

$$\frac{s(p')}{s(p)} = \frac{p'^3 + 3p'^2(1-p')}{3p^3 + 2(3)p^2(1-p) + 3p(1-p^2)} = \frac{1}{3} \tag{1.51}$$

if evaluated right at p_c, i.e. $p = p' = 1/2$. In Eq. (1.51) a standard result for the average number of sites colored in on a given triangle is used, a sum over the product of the probability of occupation and the number of occupied sites. However, if Eq. (1.51) is evaluated at $p = p_c + \delta$, where $\delta \ll 1$, one finds a ratio of $(1/3)(1 + (5/2)\delta)$, which is slightly larger than $1/3$. Equation (1.51) gives a first estimate of the power σ in the cluster statistics, $s_{max} \propto (p - p_c)^{-1/\sigma}$,

$$\frac{1}{\sigma} = -\frac{\log(\frac{1}{3})}{\log(\frac{3\delta}{2}) - \log(\delta)} = 2\nu = 2.711 \tag{1.52}$$

Equation (1.52) for σ cannot be quite right. Consider now these rough results in two dimensions, namely $\nu = 1.355$ and $\sigma = 1/2\nu = 1/2.711$ in the context of the scaling relationships. Use $d_f = 1/\sigma\nu$ to find $d_f = d = 2$! If the fractal dimensionality is the same as the Euclidean dimensionality, then, by Eq. (1.24) just as in one dimension, $\beta = 0$. Then Eq. (1.21) gives $\tau = 2$ as well. In fact, however, $\sigma > 1/2\nu$ (and it turns out that $\beta = 0.14$, not 0). While this difference is not great, and $d_f = 1.9$ for $d = 2$ (only slightly smaller than 2), the difference is obviously very important. So, while the approximate renormalization procedure to find ν appeared at least in 1979 to generate some hope that the value was accurate, in fact the result for the exponent σ is sufficient to show that Eq. (1.50) is merely an approximation.

The statement above Eq. (1.52) that σ is slightly larger than $1/2\nu$, while correct, cannot rigorously be based on the argument provided, since that argument does not produce a consistent power, independent of the value of p. It will turn out that the correct value of $1/\sigma$ is $91/36 = 2.53$, or about 7 % different from the estimate. While this difference is not large, it is critical.

1.18 Value of p_c for Bond Percolation on the Square Lattice

Consider Fig. 1.5. The solid squares form a square lattice. Imagine that a fraction p of the bonds (light lines) have been filled in at random as shown. Next construct the square lattice denoted by the open squares, which are placed at the centers of the individual squares formed by four neighboring solid squares. Imagine that a total of q of the potential bonds on this lattice are connected (heavy lines). Each of these square lattices has the same coordination number, $Z = 4$. Further, every potential bond on each lattice intersects (blocks) exactly one bond on the other lattice, which we can call a dual lattice. Thus p for the first lattice is precisely $1 - q$ for the other lattice and $p + q = 1$. Given the two-dimensional nature of the lattices, however, it is not possible that both can "percolate" simultaneously. Either one lattice percolates

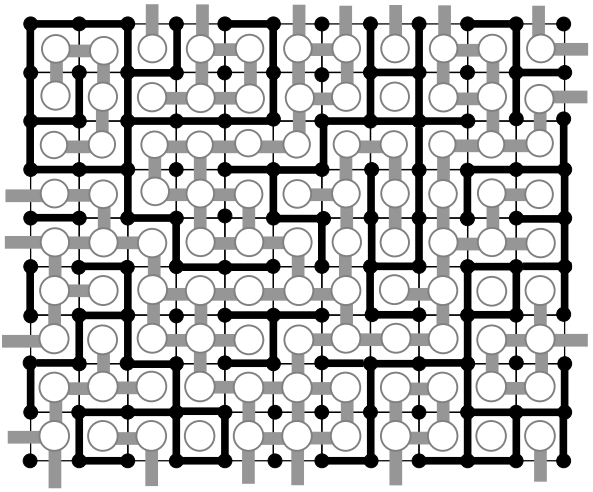

Fig. 1.5 A square lattice (*dark nodes and bonds*) and its dual (*light nodes and bonds*), which is also a square lattice. Note that the bonds of the dual lattice percolate

or the other does. Given the identical natures of the two lattices, however, it does not make sense for $p_c > q_c$, or for $p_c < q_c$. The only alternative is to choose $p_c = q_c = 1/2$. The fact that the square lattice is its own dual lattice means that its percolation probability must be $1/2$. The product of Zp_c for this lattice is 2. Miyazima [29] has constructed an analogous argument to find $p_c = 1/2$ for bond percolation on a four dimensional hypercube (and extended the derivation to $2n$ dimensions).

1.19 Estimations of p_c for Bond Percolation on the Triangular and Honeycomb Lattices

Consider Fig. 1.6. It includes a honeycomb lattice of solid squares ($Z = 3$) and a triangular lattice of open squares ($Z = 6$), which are fully complementary (or each other's duals), as were the two square lattices above. Thus every bond that is connected on the triangular lattice would "break" a bond on the honeycomb lattice and vice-versa. This means that if no bonds from one lattice are allowed to cross bonds from the other one, the bond probability p on the triangular lattice is $1 - q$, with q the bond probability on the honeycomb lattice and $p = 1 - q$. The light lines represent bonds on the triangular lattice, while the heavy lines represent bonds on the honeycomb lattice. As is generally true in two dimensions, either the triangular lattice percolates, or the honeycomb lattice percolates, but not both simultaneously. In the figure the triangular lattice percolates. The result $p + q = 1$ together with the exclusionary result on the two percolation probabilities implies that $p_c + q_c = 1$. But the result from Sect. 1.13 that $p_c \propto 1/Z$ implies that $q_c = 2p_c$. ($p_c \propto 1/Z$ implies that the quantity Zp_c is a constant, which turns out to be a good approximation). Simultaneous solution of these two equations yields $p_c = 1/3$, $q_c = 2/3$. Note that these estimates for p_c are both consistent with the relationship $Zp_c = 2$, but the

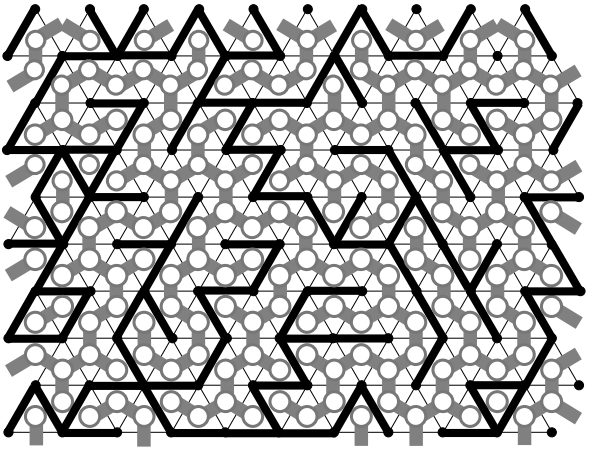

Fig. 1.6 A triangular lattice (*dark nodes and bonds*) and its dual (*gray nodes and bonds*). The dual, a honeycomb lattice, percolates

exact results are $p_c = 0.3473$, $q_c = 0.6527$, for which values $zp_c = 2.08$ and 1.96, making this product only an approximate invariant. Vyssotsky et al. [51] suggested that the product Zp_c should take on the values $d/(d-1)$, for $d \geq 2$, and such an approximate invariant as this can be quite useful if a system, for which p_c is not known and cannot be readily calculated, is encountered.

1.20 Summary of Values of p_c

In general, in a given lattice, a bond has more nearest neighbors than a site. In the square lattice one bond is connected to six nearest neighbor bonds, while a site has only four nearest neighbor sites. Thus large clusters of bonds can be formed more effectively and a lower concentration of bonds is needed to form a spanning cluster, i.e., p_c for bonds is lower than for sites. For the smallest system possible, four squares, the critical percolation probability is 3/4 for site, but 1/2 for bond percolation. Here, the ratio of p_c bond to p_c site is exactly $2/3 = Z_{site}/Z_{bond}$. For infinite sized systems the ratio of critical percolation probabilities is not so simply related to the coordination numbers.

The known results for p_c are summarized in Table 1.1. The four cases, for which simple approximations are known and repeated above are noted. These four cases correspond also to the only exact values of p_c known.

All the *estimated* bond p_c values given are exactly consistent with the Vyssotsky et al. [51] relationship above, though, when compared with the most accurate determinations of p_c that relationship gives values that are accurate only to within about 4 %.

Some of the references for the above values include: Kesten [24] and Essam et al. [16] (triangular bond, honeycomb and triangular site, square bond), Sykes and Wilkinson [49], Adler et al. [1] (bcc bond, simple cubic bond), Ziff and Sapoval [53] (square site), Stauffer [46] (bcc site, fcc site, fcc bond, honeycomb site), Strenski et al. [48] (simple cubic site).

Table 1.1 Tabulated values of p_c

Lattice type	z	p_c bond	Estimated p_c	Zp_c	p_c site (est.)
Honeycomb	3	$1-2\sin(\pi/18)$	2/3	1.96	0.6962
Square	4	1/2	1/2	2	0.5927
Triangular	6	$2\sin(\pi/18)$	1/3	2.08	1/2 (1/2)
Diamond	4	0.3886		1.55	0.4299
Simple Cubic	6	0.2488		1.49	0.3116
BCC	8	0.1795		1.44	0.2464
FCC	12	0.119		1.43	0.199

1.21 More General Relationships for p_c

Some relationships for p_c are mentioned, which may help guide estimations in more complex, but more realistic models.

The lattice structures mentioned so far by no means exhaust the types investigated, and the Vyssotsky relationship is useful only for bond percolation. Galam and Mauger [21] have developed a more general relationship for p_c of the following form, $p_c = p_0[(d-1)(q-1)^{-a}d^b]$. For regular lattices, $q = Z$, the coordination number. For non-periodic tilings, q is an effective value of Z. The relationship is considered to be valid for anisotropic lattices with non-equivalent nearest neighbors, non-Bravais lattices with two atom unit cells and quasi-crystals. The biggest strength of the relationship, however, may be that it can be applied to both site and bond percolation problems. In the former case, $b = 0$, while in the latter $b = a$. The biggest weakness is probably that the known systems fall into two classes, each with different values of p_0 and a. The first class includes 2-d triangle, square and honeycomb lattices with $a = 0.3601$ and $p_0 = 0.8889$ for site percolation and $a = 0.6897$ and $p_0 = 0.6558$ for bond percolation. Two dimensional Kagome and all (hyper)-cubic lattices in $3 \le d \le 6$ constitute the second class with $a = 0.6160$ and $p_0 = 1.2868$ for site and $a = 0.9346$ and $p_0 = 0.7541$ for bond percolation, respectively. But in order to use these results to predict p_c, one must know to which class of lattice a particular system belongs. Nevertheless it is important here to provide guidance for prediction of p_c in new system geometries.

Finally we come to the result of Scher and Zallen [38] for the critical volume fraction for continuum percolation. Such results have the potential to be of great use in percolation problems in porous media. Scher and Zallen [38] found that for regular lattices the critical occupied volume fraction,

$$V_c = p_c f \tag{1.53}$$

where p_c is the critical bond fraction, and f is the filling factor (the fractional volume covered) of a lattice when each site of the lattice is occupied by a sphere in such a way that two nearest neighbor impenetrable spheres touch one another at one point. For a simple cubic lattice the value of this product is 0.163, and in fact the value of this product for all the lattices considered scarcely differed from 0.17. Note

that an analogous model (with different shaped objects) could have direct relevance to porous media with f replaced by the porosity, and there is indeed evidence for the applicability of Eq. (1.53) in this context.

Shante and Kirkpatrick [39] generalized this idea to overlapping spheres, and showed that the average number, B_c, of bonds per site at p_c (equal to the product of Zp_c) is related to the corresponding critical volume fraction by,

$$V_c = 1 - \exp\left[\frac{-B_c}{8}\right] \tag{1.54}$$

Note that the choice of $B_c = 1.5$ for three dimensions yields $V_c = 0.17$. This result is generalized to an arbitrary continuum of spheres by choosing B_c to be the limiting value of $p_c Z$ in the limit $Z \to \infty$. Values of V_c on the order of 0.17 have often been suggested to be relevant to real media. Balberg [4] has developed these ideas further, finding,

$$V_c = 1 - \exp\left[\frac{-B_c V}{V_e}\right] \tag{1.55}$$

where V is the volume of the object and V_e is the excluded volume, i.e., the total volume in which the center of a neighboring volume of the same shape cannot be located without overlapping. For spheres this ratio is $(4/3)\pi r^3/(4/3)\pi(2r)^3 = 1/8$, in agreement with the result of Shante and Kirkpatrick [39].

For results for the critical volume fractions for percolation for a number of anisotropic shapes one can also consult the following web page http://ciks.cbt.nist.gov/~garbocz/paper59/node12.html#SECTION00050000000000000000 (geometrical percolation threshold of overlapping ellipsoids, [23]). These values may be of considerable use in geologic applications, at least to guide conceptualization. In particular, the critical volume fraction for percolation has a strong tendency to diminish for increasing shape anisotropy.

Problems

1.1 Show that at arbitrary p the largest clusters have cluster radius $r_s = s^{\sigma\nu}$, and argue then that for arbitrary p and arbitrary s, $r_s = s^{\sigma\nu} g[s^{\sigma}(p - p_c)]$, where g is an unknown function. Does your result for r_s imply an effective dimension of the clusters?

1.2 Derive Eq. (1.50) from Eq. (1.49).

1.3 Derive Eq. (1.42) from Eq. (1.41).

1.4 The critical exponent α is defined through the singular contribution to $\sum s^0 n_s \propto (p - p_c)^{2-\alpha}$. Find α in terms of known exponents using the results of development of (1.14) and an analogy to Eq. (1.16).

1.5 The critical exponent γ is defined through the singular contribution $\sum s^2 n_s \propto (p - p_c)^{-\gamma}$. Find γ in terms of known exponents.

1.6 Show explicitly that Eq. (1.30) results from Eq. (1.29).

1.7 Verify the scaling relationships for the critical exponents in 1-d, 2-d, and 6-d. Do you expect them to be precisely satisfied in 3-d (where the exponents may not ever be represented in terms of rational fractions)?

1.8 Show that, for one-dimensional systems, definition of χ as

$$\chi = \frac{\sum_{r=1}^{\infty} r p^r}{\sum_{r=1}^{\infty} p^r}$$

leads to $\chi = p/(1-p)$ instead of $\chi = (p+1)/(1-p)$ as obtained from Eq. (1.5). How would you characterize the sensitivity of the scaling behavior of the correlation length relative to the details of its definition?

1.9 The sum in Problem 1.4 has been argued to describe, for a magnetic system, the free energy, while P (the first moment) corresponds to the magnetization, and the sum in Problem 1.5 (the second moment) to the susceptibility. Find an argument for why an increase in the moment of the cluster distribution by one corresponds to a derivative with respect to the applied field.

References

1. Adler, J., Meir, Y., Harris, A.B., Aharony, A.: Bull. Isr. Phys. Soc. **35**, 102 (1989)
2. Aizenman, M., Kesten, H., Newman, C.M.: Uniqueness of the infinite cluster and continuity of connectivity functions for short and long-range percolation. Commun. Math. Phys. **111**(4), 505–531 (1987)
3. Alexandrowizc, Z.: Critically branched chains and percolation clusters. Phys. Lett. A **80**, 284–286 (1980)
4. Balberg, I.: Recent developments in continuum percolation. Philos. Mag. B **30**, 991–1003 (1987)
5. Benfatto, G., Gallavotti, G.: Renormalization Group. Princeton University Press, Princeton (1995)
6. Berkowitz, B., Balberg, I.: Percolation theory and its application to groundwater hydrology. Water Resour. Res. **29**, 775–794 (1993)
7. Broadbent, S.R., Hammersley, J.M.: Percolation processes, 1. Crystals and mazes. Proc. Camb. Philos. Soc. **53**, 629–641 (1957)
8. Bunde, A., Havlin, S.: Percolation I. In: Bunde, A., Havlin, S. (eds.) Fractals and Disordered Systems, Springer, Berlin (1996), 408 pp.
9. Chalupa, J., Leath, P.L., Reich, G.R.: Bootstrap percolation on a Bethe lattice. J. Phys. C, Solid State Phys. **12**, L31–L35 (1979)
10. Chandler, R., Koplik, J., Lerman, K., Willemsen, J.F.: Capillary displacement and percolation in porous media. J. Fluid Mech. **119**, 249–267 (1982)
11. De 'Bell, K., Essam, J.W., Guttman, A.J.: On two dimensional directed percolation. University of Melbourne, Dept. of Mathematics (1988)
12. Diestel, R.: Graph Theory, 3rd edn. Graduate Texts in Mathematics, vol. 173. Springer, Heidelberg (2000)
13. Domb, C., Lebowitz, J.L.: In: Phase Transitions and Critical Phenomena, Academic, London (1988)
14. Du, D.-Z., Hsu, F.: Combinatorial Network Theory. Springer, Berlin (1995)
15. Essam, J.: Rep. Prog. Phys. **43**, 843 (1980)
16. Essam, J.W., Gaunt, D.S., Guttmann, A.J.: Percolation theory at critical dimension. J. Phys. A **11**, 1983–1990 (1978)

17. Fatt, I.: The network model of porous media. Trans. Am. Inst. Min. Metall. Pet. Eng. Inc. **207**, 144–177 (1956)
18. Fisher, M.E.: Physics **3**, 255 (1967)
19. Flory, P.J.: J. Am. Chem. Soc. **63**, 3083 (1941)
20. Gaillard-Groleas, G., Lagier, M., Sornette, D.: Critical behaviour in piezoelectric ceramics. Phys. Rev. Lett. **64**, 1577 (1990)
21. Galam, S., Mauger, A.: A universal formula for percolation thresholds II. Extension to anisotropic and aperiodic lattices. Phys. Rev. E **56**, 322 (1997)
22. Gandolfi, A., Grimmett, G., Russo, L.: On the uniqueness of the infinite cluster in the percolation model. Commun. Math. Phys. **114**, 549–552 (1988)
23. Garboczi, E.J., Snyder, K.A., Douglas, J.F., Thorpe, M.F.: Phys. Rev. E **52**, 819–828 (1995)
24. Kesten, H.: Percolation Theory for Mathematicians. Progress in Probability and Statistics, vol. 2. Birkhauser, Boston (1982), 423 pp. ISBN 3-7643-3107-0
25. Kogut, P.M., Straley, J.: Distribution-induced non-universality of the percolation conductivity exponents. J. Phys. C, Solid State Phys. **12**, 2151–2159 (1979)
26. Kunz, H., Souillard, B.: Phys. Rev. Lett. **40**, 133 (1978)
27. Lesne, A.: Renormalization Methods. Wiley, New York (1998)
28. Middlemiss, K.M., Whittington, S.G., Gaunt, D.C.: Monte-Carlo study of the percolation cluster for the square lattice problem. J. Phys. A **13**, 1835–1840 (1980)
29. Miyazima, S.: An exact percolation point for surface filing in a four-dimensional hyper-cubic lattice. Prog. Theor. Phys. **113**, 1159–1163 (2005)
30. Nickel, B., Wilkinson, D.: Invasion percolation on the Cayley tree—exact solution of a modified percolation model. Phys. Rev. Lett. **51**(2), 71–74 (1983)
31. Pike, G.E.: Conductivity of thick film (cermet) resistors as a function of metallic particle volume fraction. In: Garland, J.C., Tanner, D.B. (eds.) Electrical Transport and Optical Properties of Inhomogeneous Materials, vol. 40, AIP, New York, pp. 366–371 (1978)
32. Pike, R., Stanley, H.E.: Order propagation near the percolation threshold. J. Phys. A **14**, L169–177 (1981)
33. Pollak, M.: Non-crystalline Semiconductors. CRC Press, Boca Raton (1987). Chap. 5ab
34. Reynolds, P.J., Klein, W., Stanley, H.E.: J. Phys. C **10**, L167 (1977)
35. Rosso, M., Gouyet, J.F., Sapoval, B.: Gradient percolation in 3 dimensions and relation to diffusion fronts. Phys. Rev. Lett. **57**, 3195–3198 (1986)
36. Sahimi, M.: Flow phenomena in rocks—from continuum models to fractals, percolation, cellular automata, and simulated annealing. Rev. Mod. Phys. **65**(4), 1393–1534 (1993)
37. Sahimi, M., Yortsos, Y.C.: Applications of fractal geometry to porous media: a review. Paper presented at the 1990 Annual Fall Meeting of the Society of Petroleum Engineers, New Orleans, LA (1990)
38. Scher, H., Zallen, R.: Critical density in percolation processes. J. Chem. Phys. **53**, 3759 (1970)
39. Shante, V.K.S., Kirkpatrick, S.: Adv. Phys. **20**, 325 (1971)
40. Shklovskii, B.I., Efros, A.L.: Electronic Properties of Doped Semiconductors. Springer, Heidelberg (1984)
41. Skal, A.S., Shklovskii, B.I.: Topology of an infinite cluster in the theory of percolation and its relationship to the theory of hopping conduction. Sov. Phys. Semicond. **8**, 1029–1032 (1975)
42. Sornette, D.: Critical Phenomena in Natural Sciences: Chaos, Fractals, Selforganization and Disorder: Concepts and Tools. Springer, Heidelberg (2004)
43. Sornette, D., Lagier, M., Roux, S., Hansen, A.: Critical piezoelectricity in percolation. J. Phys. France **50**, 2201–2216 (1989)
44. Stanley, H.E.: Introduction to Phase Transitions and Critical Phenomena. Oxford University Press, New York (1971)
45. Stauffer, D.: Scaling theory of percolation clusters. Phys. Rep. **54**, 1–74 (1979)
46. Stauffer, D.: Introduction to Percolation Theory. Taylor and Francis, London (1985)
47. Stauffer, D., Aharony, A.: Introduction to Percolation Theory, 2nd edn. Taylor and Francis, London (1994)

48. Strenski, P.N., Bradley, R.M., Debierre, J.M.: Scaling behavior of percolation surfaces in three dimensions. Phys. Rev. Lett. **66**, 1330–1333 (1991)
49. Sykes, M.F., Wilkinson, M.K.: Derivation of series expansions for a study of percolation processes. J. Phys. A **19**, 3415–3424 (1986)
50. Toulouse, G.: Nuovo Cimento B **23**, 234 (1974)
51. Vyssotsky, V.A., Gordon, S.B., Frisch, H.L., Hammersley, J.M.: Critical percolation probabilities (bond problem). Phys. Rev. **123**, 1566–1567 (1961)
52. Wilkinson, D., Willemsen, J.: Invasion percolation: a new form of percolation theory. J. Phys. A, Math. Gen. **16**, 3365–3376 (1983)
53. Ziff, R.M., Sapoval, B.: The efficient determination of the percolation threshold by a frontier-generating walk in a gradient. J. Phys. A **19**, L1169–L1172 (1987)

Chapter 2
Properties Relevant for Transport and Transport Applications

This chapter describes aspects of percolation theory that can be used to predict transport properties of disordered systems. Topics are selected to provide a basis for understanding subsequent applications to porous media, and are thus not meant to be exhaustive. Still, there will at times be hints to subjects that may have relevance to problems not yet considered within the present framework.

2.1 Exponents Describing Backbone Structure

The structure of the backbone is important to such issues as distributions of arrival times of passive solutes (simply carried along by fluid flow). The resulting dispersion is an inevitable aspect of transport, and is frequently of great practical interest. In the soil physics and hydrology literature it is customary to distinguish between "transport" properties (including conduction) and flow properties. In the physics literature all these properties fall under the category of transport.

A number of related properties of the infinite cluster have been investigated in the context of solute dispersion. The mass fractal dimensionality of the backbone cluster is denoted by D_b. This fractal dimensionality has the same fundamental definition as that of percolation clusters generally, but its value lacks the universality of the percolation cluster. In other words the backbone cluster topology can differ significantly depending on whether the percolation model is invasion or random, site or bond and whether the local site or bond probabilities are correlated with each other. The chemical path [30] is the shortest path length between two sites on a large cluster near percolation. Defining travel lengths and times that incorporate measures of the tortuosity of the backbone cluster makes sense in the context of solute transport through porous media, when such solutes are carried passively through percolation structures. The tortuosity of the backbone cluster has been studied since the 1970s. Although later works showed the need to generate greater breadth of classification, the initial way to characterize this tortuosity was to give the length of the shortest

A. Hunt et al., *Percolation Theory for Flow in Porous Media*,
Lecture Notes in Physics 880, DOI 10.1007/978-3-319-03771-4_2,

path, Λ, along the backbone cluster as a function of p and p_c. Stauffer [39] gives this length as follows,

$$\Lambda \propto |p - p_c|^{-\eta} \tag{2.1}$$

with $\eta = 1$ the value of the associated critical exponent (in three dimensions). In fact, the "value" of this exponent has been growing over the last 30 years [15, 36], but any value greater than 0.88 implies that the ratio of the (tortuous) path length to the size of the largest cluster is divergent at $p = p_c$, meaning that the path becomes infinitely tortuous at the percolation threshold. Thus the tortuosity, T, may be defined as the ratio Λ/χ, or,

$$T = \left(\frac{\Lambda}{\chi}\right) = |p - p_c|^{\nu-\eta} \tag{2.2}$$

The value of this exponent can be related to the fractal dimensionality, $D_{\min}$, of an optimal chemical path along the backbone by using the defining equation of fractal dimensionality from Mandelbrot [25]. For a path constructed of steps of length ε, the dimensionality is fractal (and larger than 1) if the total length of the path, L, diverges in the limit that ε approaches zero. In particular, $D_{\min}$ is given by

$$L(\varepsilon) = \varepsilon^{1-D_{\min}} \tag{2.3}$$

We can use this expression to relate $D_{\min}$ to η. As the percolation threshold is approached the correlation length, χ, diverges, whereas the individual step lengths (bond dimensions) are constant. But we can simply rescale the picture by reducing the lengths of the individual steps inversely proportionally to the correlation length. This process maintains the physical size of the cluster but increases the detail at which the cluster is drawn, corresponding to Mandelbrot's definition. Thus $\varepsilon \propto \chi^{-1}$, and

$$T \propto \left(|p - p_c|^{\nu}\right)^{1-D_{\min}} = |p - p_c|^{\nu-\nu D_{\min}} \tag{2.4}$$

which yields $\eta = \nu D_{\min}$.

The mass fractal dimensionality of the backbone cluster, D_b [24], appears to be more appropriate in relating the *time of travel* along such a backbone to the linear extent of the cluster. Thus the time of travel is not simply proportional to the length; it turns out to be even longer than what would be simply predicted by making it proportional to the tortuous length. Further, this time can depend strongly on the type of percolation problem considered.

The argument of Lee et al. [24] is as follows. For particles entering a backbone cluster at one side of a system, the typical velocity v at distance x will scale as $1/n$, where n is the number of bonds at distance x. The number of bonds at distance x is proportional to x^{-1+D_b}. Thus the typical travel time t is

$$t \propto \int \frac{dx}{v} \propto \int dx x^{-1+D_b} = x^{D_b} \tag{2.5}$$

Lee et al. [24] do in fact find from simulations in two dimensions that the typical time, t, that a particle takes in traversing a Euclidean distance x scales as the 1.62

Table 2.1 Fractal dimensionalities associated with chemical path lengths and the backbone percolation cluster in three dimensions (from [36])

Model	$D_{\min}$	D_{b}
Site NTIP	1.37	1.87
Site TIP	1.37	1.86
Bond TIP	1.46	1.46
RP	1.37	1.87
Optimal path	1.43	1.42

Table 2.2 Fractal dimensionalities associated with chemical path lengths and the backbone percolation cluster in two dimensions (from [36])

Model	$D_{\min}$	D_{b}
NTIP	1.1293	1.6422
Site TIP	1.214	1.217
Bond TIP	1.217	1.217
RP	1.1307	1.6432
Optimal paths	1.21	1.21

power of x, very close to the value of $D_{\mathrm{b}} = 1.6432$ found by Grassberger [14] for the backbone cluster in two dimensions, but nowhere near the value, 1.217, for optimal paths (see Table 2.2). Thus a kind of temporal tortuosity factor is given in the same form as Eq. (2.4) but with D_{b} substituted for $D_{\min}$. Such a result will have considerable importance for the discussion in Chap. 11.

Sheppard et al. [36] give values for the mass fractal dimensionality of the sample-spanning cluster and the backbone, D_{b}, as well as the fractal dimensionality of the optimal path, $D_{\min}$, in various percolation models. Presenting the basic information from their summary (Tables 2.1 and 2.2) requires defining their acronyms: IP = invasion percolation, TIP = trapping invasion percolation, NTIP = non-trapping invasion percolation, and RP = random percolation (the focus here). The difference between trapping invasion percolation and non-trapping invasion percolation is that in the former case the "defending" fluid (defending against the "invading" fluid) is incompressible, meaning that it can be trapped (in finite clusters). In the latter case, the defending fluid can always escape, even if it does not percolate, since it can be compressed to zero volume.

In the present case for our dispersion calculations (Chap. 11) we have used several values of the exponent D_{b}. These values for the fractal dimensionality each lead to distinct values for the exponent η.

2.2 Exponents for Conduction Properties

Consider the site percolation problem introduced in Sect. 1.2, and stipulate for simplicity that all the metallic balls are of the same size and composition. Allow them to be placed on a simple cubic lattice. We have not calculated p_{c} for this lattice,

but numerical simulations give the result $p_c = 0.3116$. Thus, in an infinite lattice, if fewer than 31.16 % of the balls emplaced are conducting and the remainder are insulators, the system will not conduct at all. If $p > p_c$, the system will conduct. Clearly the conductivity of the system must follow a functional form, which vanishes (rather than diverges) at $p = p_c = 0.3116$. The result of percolation theory is that the functional form must be a power law (and the arguments given here justify that); what we need to do is predict the exponent.

The most important aspects of this problem treated by percolation theory are probably the connectivity and the tortuosity of the conducting paths, concepts which have been independently (but inconsistently) developed in the porous media communities. Discussions of this topic have occupied a great deal of literature but, as will be seen, the original discussion of Skal and Shklovskii [38] is the simplest introduction, although it does not lead to the most widely accepted result. The following is consistent with the general results of that work.

The electrical conductivity of a system is defined as the ratio of the current per unit area and the applied electrical field. If this ratio is independent of the field (as is normally the case at small field strengths), the system obeys Ohm's law. The current per unit area in the present case involves both the current per path, and the number of connected paths per unit area. The simplest assumption is that the current for each connected path is identical. Then the number of connected paths per unit cross-sectional area (in three-dimensions) is proportional to

$$\chi^{-2} \propto (p - p_c)^{2\nu} \tag{2.6}$$

Since in three dimensions, $\nu = 0.88$, the lowest order estimate of the conductivity is that it should vanish as the $2\nu = 1.76$ power of $p - p_c$. This suggestion is actually fairly close to observation. But the structure of large clusters near the percolation threshold, and by extension the infinite cluster just above the percolation threshold, is fractal for distances below the correlation length (which of course diverges at percolation). This fractality produces a tortuosity in the current-carrying path as well. The distance along a connected path, Λ, over a separation equal to the correlation length is actually longer than the correlation length. Specifically, Λ diverges at the percolation threshold according to [39]

$$\Lambda \propto (p - p_c)^{-\nu D_{\min}} \tag{2.7}$$

Thus, assuming that the resistance of the current-carrying path is just the sum of the resistances of all the metal balls encountered, this resistance per unit system length must actually increase as the percolation threshold is approached, with the increase given by the ratio Λ/χ. This ratio is proportional to $(p - p_c)^{\nu - \nu D_{\min}} = (p - p_c)^{-0.33}$ (using the value for $D_{\min}$ for random percolation, Table 2.1). Such an increase in resistance alters the conductivity to

$$\sigma \propto (p - p_c)^{2\nu + (D_{\min}\nu - \nu)} = (p - p_c)^{2.09} \equiv (p - p_c)^{\mu} \tag{2.8}$$

Here the first contribution to the exponent is essentially a result of the connectivity, or separation of the paths along which current can flow, while the second contribution is due to the tortuosity of these paths. The combined exponent is thus the sum

of two contributions, $1.76 + 0.33 = 2.09 = \mu$. At the time of the original estimate by Skal and Shklovskii [38], it was thought that $\eta = 1$, which leads to $\mu = 1.88$. Nowadays, μ is known at least as accurately as are the constituents that distinguish μ from 2ν, and more modern publications [7, 13] give $\mu = 2$. As pointed out by Berkowitz and Balberg [5], the explanation for the discrepancy $\mu = 2$ instead of $\mu = 2.09$ is quite simple. The discussion up until now has omitted the effects on μ of the "blobs," or finite length parallel paths. But the fact that such blobs become increasingly complex and numerous in the limit of $p \to p_c$ leads to a reduction in the resistance of the backbone cluster, meaning that μ is reduced from 2.09. The presentation of this argument is meant more to provide extra qualitative understanding than to imply a quantitative inference on the effects of these "blobs" on conductivity.

In two dimensions the Skal and Shklovskii [38] argument would start with $\mu \approx \nu$ rather than 2ν, because the relevant current density is defined relative to a perpendicular length (χ) rather than a cross-sectional area (χ^2). Then complications due to a tortuosity would be added. But the exponent μ appears to be smaller in magnitude than ν, making the argument of Skal and Shklovskii [38] more difficult to apply. As Berkowitz and Balberg [5] explain, the structure of the backbone cluster in 2D is different enough to make blobs a more important modification to μ than the tortuosity. As a first approximation to μ one can simply use the exponent for the correlation length, $\nu = 1.33$. Derrida and Vannimenus [8] find that the value of μ in two dimensions is 1.28, while Jerauld et al. [19] find $\mu = 1.27$, and Normand and Herrmann [29] find $\mu = 1.30$. But none of these values for μ in two dimensions differs much from the two-dimensional value for ν. Establishing values for μ will have relevance to (for example) discussions of Archie's law for the electrical conductivity of porous media. This is why it is important to find the best values for these exponents, as well as to determine the conditions under which one expects to observe them. The value for μ in two dimensions (three dimensions) will be assumed here to be 1.3 (2.0).

In one dimension, the conductivity is either zero (if there are any non-conducting elements at all), or a finite value, implying $\mu = 0$. But generally μ is non-universal for one-dimensional systems, meaning that in principle any value of μ can be generated. If there is a variation in the conduction properties of the individual elements (not all resistance values identical), the result $p_c = 1$ implies that the total resistance may be dominated by the resistance of the most resistive element in one dimensional systems. In that case the conductivity is calculated using extreme value statistics. The choice of the extreme value statistic is determined by the statistics of the individual resistances, making one-dimensional systems highly non-universal.

Although the concept of conductivity and the discussion of the value of μ were introduced in the context of electrical conduction, the arguments are perfectly general, and the results could instead be applied to, e.g., the hydraulic conductivity or to air flow. What will turn out to differ among these properties is the conditions under which arguments to invoke Eq. (2.8) actually apply.

Berkowitz and Balberg [4] explicitly demonstrated that models of hydraulic conduction yield Eq. (2.8) for the hydraulic conductivity near the percolation threshold, and found values of the exponents compatible with $\mu = 2$ in 3d and $\mu = 1.3$ in 2D. However, they also found results compatible with non-universal exponents [10, 35] in certain 3d systems.

The Einstein relationship [32] relates diffusion, D, and conductivity, σ, via the number of charge carriers n:

$$\sigma = nD \tag{2.9}$$

where we assume that n is given by the fraction of sites connected to the infinite cluster. From this relationship we find

$$D \propto (p - p_c)^{\mu-\beta} \tag{2.10}$$

The following summary is from ben-Avraham and Havlin [2], and will be important when we address diffusion in Chap. 7. The average diffusion constant near and above the percolation threshold and at very long times, for which the root mean square excursion $R = [\langle R^2(t)\rangle]^{0.5}$ of the walks not restricted to the incipient infinite cluster is much larger than the percolation correlation length, is

$$D(t \to \infty, p) \sim (p - p_c)^{\mu} \tag{2.11}$$

Equation (2.11) includes diffusion in all clusters of the system unrestrictedly. We will show that experimental results conform to Eq. (2.11).

Meanwhile, at the percolation threshold the average diffusion constant follows

$$D(t, p_c) \sim t^{(2-d_w)/d_w} \tag{2.12}$$

where d_w is the random walk fractal dimension. And finally, below the threshold we find

$$D(t \to \infty, p) \sim t^{-1}(p_c - p)^{-2v+\beta} \tag{2.13}$$

For the restricted ensemble, consisting of only the incipient infinite cluster, Eqs. (2.11) and (2.13) change to

$$D(t \to \infty, p) \sim (p - p_c)^{\mu-\beta}, \quad p > p_c \tag{2.14}$$

and

$$D(t \to \infty, p) \sim t^{-1}(p_c - p)^{-2v}, \quad p < p_c \tag{2.15}$$

but Eq. (2.12) remains the same. Curiously, a simple effective-medium theoretical result [20] yields $D \propto (p - p_c)^1$, which has been alleged (as $p(p - p_c)$) to occur in soils [27]. However, typical conditions in porous media make it very difficult to distinguish the Moldrup et al. [27] result from universal scaling predictions, and we argue (Chap. 7) that overall the relevance of universal scaling is best supported. Nevertheless, both on account of this coincidence, and because in fact the effective-medium relationship does hold for $p - p_c > 0.8$, the essence of the Keffer et al. [20] derivation is repeated here.

The lowest order effective medium approximation for the mean diffusivity, D_m, can be obtained via physical arguments [21, 22] or via lattice Green functions [33] as [20]

$$\int_0^\infty \frac{D_m - D}{(\frac{Z}{2} - 1)D_m + D} f(D)dD = 0 \tag{2.16}$$

for mean coordination Z. Keffer et al. [20] use as a distribution of diffusivities (to describe ultimately the diffusion in zeolites),

$$f(D) = p\delta(D - D_b) + (1 - p)\delta(D - D_0) \tag{2.17}$$

where D_b is a very small value and D_0 is relatively large, and for which these authors define $f \equiv D_b/D_0$. We caution that these authors made the unusual (and confusing) choice to use the symbol p for the low diffusion elements! The solution of Eq. (2.16) using Eq. (2.17) for $f(D)$ is,

$$\frac{D_m}{D_0} = \frac{1}{2}\left\{A + \left[A^2 + \frac{4f}{\frac{Z}{2} - 1}\right]^{\frac{1}{2}}\right\} \tag{2.18}$$

where

$$A = 1 - p + fp - \frac{f + p - fp}{\frac{Z}{2} - 1} \tag{2.19}$$

For the case $f = 0$, Eq. (2.19) yields

$$\frac{D_m}{D_0} = \frac{(\frac{Z}{2} - 1) - (\frac{Z}{2})p}{(\frac{Z}{2} - 1)} = \frac{(1 - p) - \frac{2}{Z}}{1 - \frac{2}{Z}} \tag{2.20}$$

which would seem to yield $p_c = 1 - 2/Z$ and a critical exponent of 1. But in another confusing choice these authors exchanged the roles of p and $1 - p$, so the actual result obtained for p_c is $Zp_c = 2$. This would be in agreement with the results of percolation theory except that the constant, 2, is more appropriate for two-dimensions, rather than for the three-dimensional configurations considered. With the transposition noted, Eq. (2.20) becomes $D_m/D_0 = (p - p_c)/(1 - p_c)$! Note also that the conclusion that the critical exponent is 1 is unaffected by the transposition of p and $1 - p$.

In this third edition we will show that nearly all diffusion results in porous media actually conform to Eq. (2.11), eliminating a significant uncertainty in earlier editions.

2.3 Summary of Derived Values of Critical Exponents

While most of the entries in Table 2.3 refer to quantities discussed in Chap. 1, it is not presented there because of its inclusion of the conductivity exponent, μ.

Table 2.3 was constructed synthesizing the tabulated values for these exponents from Sahimi [32] and Stauffer [39], but using $\mu = 2.0$ in three dimensions [7, 13] and $\mu = 1.3$ in two dimensions [29]. Known values, for which the derivations were described here, are underlined and in bold; if the values obtained here are different from the known values, they are given in parentheses.

Table 2.3 Values of critical exponents

Exponent	$d=1$	$d=2$	$d=3$	$d\geq 6$
α	**1**	$-2/3$	-0.62	**−1**
β	**0**	5/36	0.41	**1**
γ	**1**	43/18	1.82	**1**
σ	**1**	$36/91=0.396$ **(0.369)**	0.45	**1/2**
τ	**2**	187/91	2.18	**5/2**
ν	**1**	4/3 **(1.355)**	0.88	1/2
μ	Not universal	1.3 **(1.355)**	2.0 **(1.88)**	3

2.4 Finite-Size Scaling and Fractal Characteristics

Numerical simulations are a common means to generate values of both p_c and of critical exponents in percolation theory. But simulations can be performed only for finite-sized systems. While it is possible to try to extract limiting behavior in the infinite system limit as a means to generate such quantities, a better approach is to generate dependences of, e.g., the conductivity on the system size, then use a known transformation to yield the associated dependences on percolation variables. This technique is often used for treating transport problems. For example, quantities like the conductivity, which vanishes at the percolation threshold, will diminish with increasing system size until the linear dimension of the system exceeds the correlation length. At larger length scales the system is known to be Euclidean, meaning that the property in question becomes independent of system size. The exception of course is right at the percolation threshold, for which the correlation length is infinite and the scale dependence continues to infinite system size.

Originally it was Fisher [11] who showed how to relate percolation quantities for finite sized systems to their behavior as a function of $p-p_c$ in the limit of infinite sized systems. In particular, for a system of finite size L, a percolation quantity ψ, which obeys an arbitrary power law $(p-p_c)^{q_0}$, will behave as

$$\psi \propto L^{-\frac{q_0}{\nu}} h\left[\left(\frac{L}{\chi}\right)^{\frac{1}{\nu}}\right] = L^{-\frac{q_0}{\nu}} h\left(L^{\frac{1}{\nu}}(p-p_c)\right) \tag{2.21}$$

with h an unknown non-singular function. Substitute $L=\chi$ into Eq. (2.21) to obtain,

$$\psi \propto (p-p_c)^{-\nu\frac{-q_0}{\nu}} h[1] = (p-p_c)^{q_0} \tag{2.22}$$

Note that Eq. (2.21) is similar to Eq. (1.8) for the cluster statistics. In particular, the ratio of L to the correlation length enters here, because systems near the percolation threshold obey fractal geometry (with e.g., fractal cluster dimensions) only for length scales smaller than the correlation length. For length scales larger than χ the system follows Euclidean geometry. For example, if a system with $p>p_c$ is smaller than the correlation length, the above finite-size scaling results hold, and transport

quantities (e.g., diffusion constant or conductivity) will trend to zero with increasing system size up to a length scale equal to the correlation length. But at larger system sizes, the transport coefficient will remain constant with any further increase in system size. Only precisely at p_c will the behavior of the transport coefficient continue to diminish indefinitely with increasing system size. But on the way to $p = p_c$, the transport coefficient has taken on values at each size, which were equal to the transport coefficient at that value of the correlation length. Therefore the first factor in Eq. (2.21) gives the behavior of the variable ψ for the condition $L = \chi$, since the second factor does not change with L where L is constrained to equal χ. Thus any such exponent obtained from finite-size simulations (and presented as a function of system size, L) must be multiplied by $-\nu$ to find the value predicted by percolation theory. The similarity of Eq. (2.21) to Eq. (1.8) is a consequence of the relevance to percolation scaling of homogeneous functions, a topic not considered here but treated in the standard references mentioned earlier in this chapter.

2.5 Scaling Far from the Threshold

In most applications in this book we can restrict our attention either to critical path analysis (Sect. 2.6) or the asymptotic results from percolation theory above. But we will see that in the case of the thermal conductivity, measurements are taken so far from the percolation threshold that the asymptotic results no longer apply. In addition, we will find that for the gas diffusion, the normalization factor used in the reporting of the data is determined at porosity 1, also so far from the threshold that a roughly 30 % inconsistency in a purely numerical factor is introduced. Both of these difficulties are removed if we refer back to Kirkpatrick [22]. There it was determined that the percolation scaling of $(p - p_c)$ was most accurate to about $p = 0.8 \equiv \varepsilon_x$. Above this value of p, he showed that a linear dependence in $p - p_c$ was superior, a result that derived from effective medium theories and given in Eq. (2.25). We show what form of the conductivity results in Fig. 2.1. Note that for electrical conductivity, solute and gas diffusion, and air permeability, the largest value of p ever investigated is equal to the porosity, which is typically no greater than 0.6, meaning that the complication is never observed directly. However, in the case of the thermal conductivity, where the solid portion of the medium is at least as conducting as the water, the typical case of $\varphi = 0.4$ means that the observed moisture dependence investigates values of p between 0.6 and 1. This means that the cross-over from the quadratic to the linear dependence will show up in the middle of the range of investigated values. Note that the prefactor, $(1 - \varepsilon_t)(\varepsilon_x - \varepsilon_t)$, in the percolation scaling term is about 1.28 for the typical value of $\varepsilon_t = 0.1\varphi$. At the time of Kirkpatrick's analysis, the scaling exponent μ appeared to take on the value of 1.6. It is now known to be 2. This change in exponent value would force the cross-over to take place at a somewhat lower value of ε, requiring a numerical constant somewhat larger than 1.28. Since these changes would be relatively small, however, we have deferred any investigation to a later time.

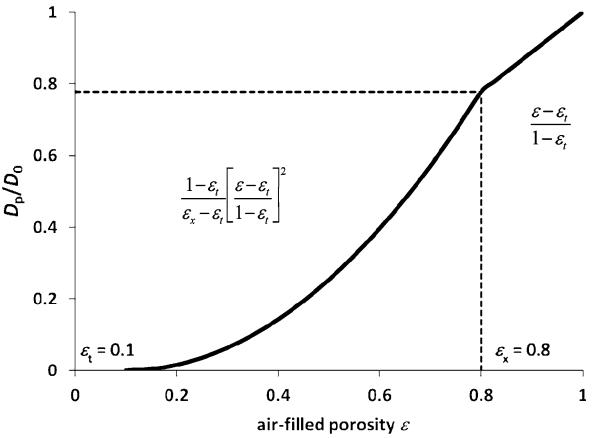

Fig. 2.1 Actual conductivity in three dimensions as a function of p, as compared with the assumption of the validity of percolation scaling. The sharp cross-over at $p = 0.8$ is an artifact of the need to choose the effective-medium result (Eq. (2.20)) for $p > 0.8$ and percolation scaling (Eq. (2.11)) for $p < 0.8$. In actuality we expect a smoother cross-over

2.6 Critical Path Analysis

Although an entire chapter is devoted to Critical Path Analysis (CPA), its introduction here serves to familiarize the reader with its basic concepts. This introduction addresses more general issues, such as effects of the dimensionality of the system, the connectivity of the medium, and the width of a distribution of local conductances, while Chap. 5 treats detailed applications of CPA to systems of experimental relevance.

CPA uses percolation theory to calculate effective conduction properties of a disordered medium. CPA was developed [1, 12, 31] to find the limiting resistance value in a random medium with a wide range of local resistances. The initial work was meant to address the electrical conduction problems of impurity conduction systems in crystalline semiconductors as well as amorphous semiconductors, and so topological disorder was included. The present introduction, however, concentrates on lattice models. Because the connectivity of the more highly conductive regions is a critical input into the calculation of effective properties, the fundamental theory of connectivity is an obvious tool to be employed for such a calculation. Then it is not necessary to add connectivity as an afterthought, or to develop alternative methods to quantify connectivity, such as the Euler number [28]. While the latter has an advantage in that it can be used to identify a percolation transition [28], i.e., when the Euler number changes sign the system crosses p_c, its disadvantage is that there is no known relationship between the Euler number and p. Thus there is no way to express $(p - p_c)$ in terms of Euler numbers, making it impossible to use the Euler number to predict any properties given in percolation theory. Two additional advantages of critical path analysis are that it can be applied to any conductance (or conductivity) distribution, and that it yields results which are most accurate (exact) in the limit of large disorder rather than in the limit of a homogeneous system (although in many cases critical path analysis can be formulated to be exact in both limits).

The gist of critical path analysis is that it defines that interconnected network of conductances which has the largest possible value of the smallest, or bottleneck,

conductance. This value, called the critical conductance, is found by setting an integral over the conductance distribution equal to the critical percolation probability, p_c. The lower limit of this integral is the critical conductance, and the upper limit is the largest conductance. The analysis can be formulated equivalently in terms of a resistance distribution, for which p_c fixes the upper limit of integration while the lower limit is the smallest resistance in the distribution. In critical path analysis p_c is thus the most important parameter, rather than the critical exponents. The critical percolation probability can vary significantly from system to system. Thus there might be important differences in applying critical path analysis in different systems. Important differences do exist in applying critical path analysis in different dimensions.

2.6.1 Relation of Critical Path Analysis to Extreme Value Statistics in 1D Systems

Consider first the case of one-dimensional systems. In infinite one-dimensional systems the conductivity can always be calculated exactly using what is often called the harmonic mean value of the conductance distribution. This value is related to the inverse of the sum of the resistance values, since the effective resistance of resistances in series is their sum. For uniform size characteristics (all bonds the same length, for example) the resistance distribution is a perfect proxy for the resistivity distribution, because the resistance of any bond is some constant times its resistivity. For a wide distribution of resistance values, the harmonic mean is dominated by the largest resistance in the system. For a truncated power-law distribution of resistances, $W(R)$, the harmonic mean conductivity is in fact proportional to the largest resistance value, at least as long as $RW(R)$ is a power of R that is greater than -1. This is simply a property of power-law distributions, and may easily be verified by integration (Problem 2.4). Since $p_c = 1$ in one dimension, critical path analysis requires that the lower limit of integration on the conductance distribution be the smallest conductance in the system (or the largest resistance). In other words it is not possible to connect an infinite path which avoids even the smallest conductance. A single missing element will break the path. Thus critical path analysis quickly reaffirms the relevance of the largest resistance to the system conductivity. For a power-law resistance distribution that extends to infinite resistance the conductivity is zero. In general the conductivity in 1D is given by $\sigma = l/R$, with l the system length and R its total resistance.

In finite-length one-dimensional systems, the problem is more interesting. Again, since in 1D we have $p_c = 1$, the critical conductance g_c is now the smallest actual conductance in the system, rather than the smallest allowed by the distribution. Since it is impossible to avoid even the largest resistance on the path, but this largest resistance can vary from realization to realization, extreme value statistics are implicated in the procedure to find both an ensemble mean conductivity of the system, and a distribution of conductivity values, as a function of the system length. To find an

ensemble mean conductivity it is necessary first to find the dependence on x of the largest expected resistance value, $R_{\max}(x)$ in a system of length x. If $R_{\max}(x)$ is a power of x, then evaluation of the limit of $x/R_{\max}(x)$ for x approaching infinity gives the scaling of the conductivity as a function of length, x. In such cases, the limiting value of $x/R_{\max}(x)$ as x approaches infinity will typically be zero, so that an infinite system does not conduct at all. This is the case in the spatially random hopping conduction system considered below. Whenever the system has a non-zero minimum conductance value, however, the typical resistance of a system of length x is proportional to x, and the system conductivity is non-zero and well-defined.

The following specific system, r-percolation, is discussed in considerably more detail in Sect. 4.1. Here we only give the briefest summary sufficient to actually perform the calculations. Consider a one-dimensional system with resistances connecting every pair of sites, i and $i+1$, where i denotes the position of a site on a linear chain. Let the separation of the sites $r_{i,i+1}$ be a random variable with uniform probability density, $1/b$, where b is the typical separation of sites. Let the resistance $R_{i,i+1} = R_0 \exp[2r_{i,i+1}/a]$, where $a \ll b$ and R_0 are constants with units length and resistance, respectively. While the probability of finding an arbitrary site a distance r (within dr) from site i is dr/b, the probability that site is the nearest neighbor is $(dr/b)\exp(-r/b)$. This probability is normalized over the interval $[0, \infty]$; the nearest neighbor must be somewhere. Now what is the largest likely value of the nearest neighbor distance in a chain of length x? First, the expected number of sites on such a chain is x/b. Thus the number of possible realizations of the nearest neighbor distance is proportional to x/b. This means that the total area under the curve $\exp(-r/b)/b$ would typically be divided into x/b roughly equal areas, meaning that the largest expected resistance value, $R_{\max} = R_0 \exp[2r_{\max}/a]$, would be found by setting the area under the extreme value distribution between $r_{\max}$ and infinity proportional to b/x:

$$\frac{b}{x} \propto \int_{r_{\max}}^{\infty} \frac{dr}{b} \exp\left[\frac{-r}{b}\right] \tag{2.23}$$

Solution of this integration for $r_{\max}$ in terms of x gives

$$r_{\max} \propto b \ln\left(\frac{x}{b}\right) \tag{2.24}$$

Substitution into $R_{\max} = R_0 \exp[2r_{\max}/a]$ leads to

$$R_{\max} \propto R_0 \left[\frac{x}{b}\right]^{\frac{2b}{a}} \tag{2.25}$$

with the result that

$$\sigma(x) \propto x^{1-2b/a} \tag{2.26}$$

Because $b \gg a$, Eq. (2.26) leads to a conductivity which is a negative power of the system length and which vanishes in the limit of an infinite chain [6, 16, 17]. In condensed matter applications, where individual resistance values are typically exponential functions of random variables, the only easy way to generate a power-law

behavior of the conductivity with system size is to invoke extreme value statistics. The only systems in which mean-value statistics appear to be relevant, are one-dimensional systems, because of the fact that $p_c = 1$. Thus one-dimensional systems make a very poor starting point for understanding percolation behavior generally. In the next chapter we will also see (for different reasons) that two-dimensional systems make very poor models of 3d porous media.

2.6.2 Critical Path Analysis in 2D

Now we apply critical path analysis to an idealized conductance distribution on a two-dimensional lattice. An attractive aspect of 2D systems is the direct relationship there between critical conductance and system conductivity. Consider the elementary relationship between the resistance R and the resistivity ρ, for a homogeneous system of length l and cross-sectional area A : $R = \rho l/A$. In two dimensions the analogous relationship is $R = \rho l/z$, where z is the system dimension perpendicular to flow. The particular case of two dimensions, where the sample-dependent property R is equal to the ratio of two lengths times the material property, ρ, is interpreted [40] for the case of disordered systems to imply the equivalence of ρ and R, and thus between the conductance, g, and the conductivity, σ, as well. This makes the system conductivity equal to the critical conductance.

For the bond percolation problem we need the probability density function (pdf), denoted $W(g)$, for finding a conductance between two arbitrary nearest neighbor sites with value between g and $g + dg$. Normalization of this pdf requires,

$$\int_0^\infty W(g)dg = 1 \tag{2.27}$$

Consider the case that $W(g)$ is a log uniform distribution of (electrical or hydraulic) resistance values with width 10 orders of magnitude, e.g., from 10^0 to 10^{10} in arbitrary units. Place each conductance at random between two arbitrary nearest neighbor sites on a square lattice. Each site has four nearest neighbors, $z = 4$, and for the square lattice we know that $p_c = 0.5$. The conductivity of this arrangement is the median conductance value, $g = 10^5$ because it is known that emplacement of a fraction 0.5 of the bonds of this lattice guarantees that the system is at the percolation threshold. The median conductance on this lattice is then the smallest conductance value that cannot be avoided by the current, a value which is more generally known as the critical conductance, g_c. That is, the value of g_c is found from

$$\int_{g_c}^\infty W(g)dg = p_c = 0.5 \tag{2.28}$$

For an infinite square lattice, placement of $1/2$ the conductances into lattice positions at random guarantees existence of a cluster of interconnected conductances which just reaches infinite size; choosing that half of the conductance distribution with the largest conductances yields the path of least resistance. If, in a corresponding physical system all bonds have not only the same length, but also the same cross-sectional area, the median conductance value would correspond rigorously to

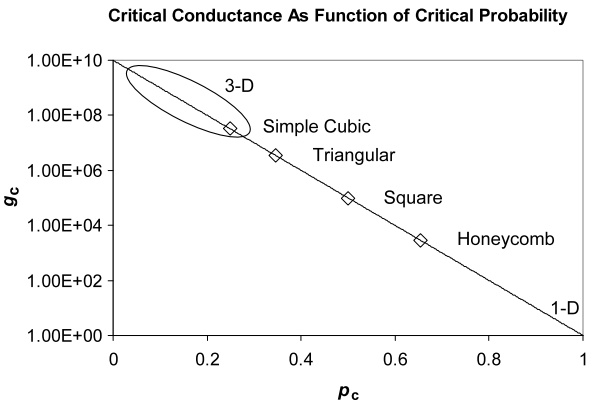

Fig. 2.2 For a log-uniform distribution of conductances the critical (percolating) rate-limiting conductance, g_c, as a function of the critical percolation probability, p_c. Note the rapid diminution of p_c and increase of g_c with increasing dimensionality. Further, if the geometric mean of the distribution is held constant, but the width is increased, all systems to the left of the square lattice will have an increase in K, while all those to the right will experience a decrease

the median conductivity in a distribution of conductivities. Such a picture applies also to media in which the currents are represented numerically in terms of finite difference equations, as long as the medium is divided up into sub-regions of identical squares. Since the effective conductivity of the medium is known in porous media communities as the upscaled conductivity, then under fairly common conditions we can identify the median of a conductivity distribution with the upscaled conductivity in two-dimensions. If the logarithm of K is symmetrically distributed, then the median of the conductivity is also the geometric mean.

These results do not apply for all two-dimensional systems. If the same conductances are placed on a triangular lattice, where each point has six nearest neighbors ($Z = 6$), the dominant conductance value from the distribution is $10^{6.55}$, because p_c is 0.345 and the current avoids the slowest 2/3 of the connections. If the same conductances are placed on a honeycomb lattice, with $Z = 3$, the dominant conductance is $g_c = 10^{3.45}$, because $p_c = 0.655$ and the current avoids only the slowest 1/3 of the connections. Thus in our example, the values of the rate limiting conductances and associated conductivities extend over more than three orders of magnitude in the simplest two dimensional lattices (2D)! In Fig. 2.2 we represent these results pictorially, indicating also the range of likely values for g_c in 3d lattices ($p_c \leq 0.2488$) as well as on a 1D chain (where $p_c = 1$). In 3d the relationship between g_c and system conductivity is more complex, and only in 2D systems can g_c in Fig. 2.2 also be interpreted as the conductivity.

2.6.3 Critical Path Analysis in 3D

In three dimensions we need to be able to write expressions for the conductivity as well. If only enough resistors are placed on the lattice to guarantee the exis-

tence of an infinite cluster ($p = p_c$), then there will be only a single connected path in, say, the x direction over a distance χ in both the y and z directions. But χ diverges right at the percolation threshold. While this path has the largest rate-limiting conductance value possible for a given network topology and conductance distribution, construction of such a critical path does not optimize the conductivity since the conductivity due to a single conducting path in an infinite cross-sectional area (or perpendicular distance in two dimensions) is zero. However, emplacement of a few smaller conductances into their positions in the network reduces χ rapidly while scarcely diminishing the rate-limiting conductance, allowing the possibility of a general optimization procedure. Such an optimization procedure for a three-dimensional lattice is given below. The optimization procedure results in the determination of an optimal value of the conductance, g_{opt}, which is useful as long as g_{opt} is close enough to g_c so that the topology of the conducting paths is described by percolation theory. Nevertheless, the tendency for p_c to be much smaller in 3d than in 2D tends to make the conductivity of 3d systems much higher than in 2D, and we discuss first general tendencies for the conductivity in terms of the dimension of the medium.

2.6.4 *Dimensional Dependence and Similarity to Matheron Conjecture*

In Fig. 2.2 the dimensional dependence of g_c for the proposed log-uniform distribution of conductance values is clear and strong. In two-dimensional square lattices the critical conductance, 10^5, yields the conductivity and is the geometric mean of the distribution $[(10^0)(10^{10})]^{1/2}$. For one dimensional systems g_c is the smallest g in the system, while in 3d systems, it is near the large end of the distribution. This dimensional dependence is reminiscent of that in a classical conjecture of Matheron [26]. The relevance of the geometric mean of a conductivity distribution to the 2D upscaled conductivity is not restricted to a log-uniform distribution, but is repeated for log-normal distributions and power law distributions as well, making it possible to compare the result from critical path analysis to a completely different formulation for upscaling K in heterogeneous media. Assume that the logarithm of the hydraulic conductivity is normally distributed,

$$W(K) \propto \exp\left\{-\left[\frac{(\log(K) - \log(K_0))^2}{2\,\mathrm{Var}(\log(K))}\right]\right\} \tag{2.29}$$

where $\mathrm{Var}[\log(K)]$ is the variance of the distribution of $\log[K]$. Then the lowest order approximation to the hydraulic (or electrical) conductivity is [9]

$$K = K_{gm} \exp\left[\left(\frac{1}{2} - \frac{1}{d}\right)\mathrm{Var}\big(\log(K)\big)\right] = K_0 \exp\left[\left(\frac{1}{2} - \frac{1}{d}\right)\mathrm{Var}\big(\log(K)\big)\right] \tag{2.30}$$

where K_{gm}, the geometric mean of K, is here equal to K_0, the most likely value of K. In fact, De Wit [9] explains that Eq. (2.30) is essentially a perturbation expansion in the (small parameter) $\mathrm{Var}(\log(K))$. Equation (2.30) also implies that the upscaled conductivity in 2D is equal to the geometric mean or to the median value. Further, the hydraulic conductivity increases with increasing variance in 3d and diminishes with increasing variance in 1D, just as in Fig. 2.2. Since all methods generate the hydraulic conductivity in 1-dimensional systems using the inverse of the sum of the resistance values, the two results coincide in 1D as well as in 2D, at least under some circumstances. But in 3d there are some fundamental differences.

In 3d, Eq. (2.30) suggests that the conductivity is independent of the properties of the connectivity of the medium as long as $\log(K)$ is a normally distributed random field. It is known, however, that the connectivity of such fields plays an important role in the upscaling [3, 23, 34, 41]. As can be seen from critical path analysis, the tendency for K to increase with diminishing p_c is not restricted to the effects of increasing dimensionality, but includes effects of larger coordination number as well. Thus increasing the local connectivity reduces p_c and increases K. Further, Eq. (2.30) implies that the conductivity can be represented in terms of the mean value and some parameter describing the variation about the mean. However, it should be apparent from critical path arguments that the important conductance may be far in the tail of the distribution. As mentioned, Eq. (2.30) is not complete: it is believed that Eq. (2.30) represents only the first term in a series [9] of terms proportional to powers of the variance of $\log(K)$. Thus the validity of Eq. (2.30) is subject to an important condition on the magnitude of $\mathrm{Var}(\log(K))$, which must be small. Similarly, even using all the terms in the series is insufficient if the series does not converge, which will be the case for large $\mathrm{Var}(\log(K))$.

2.6.5 *Optimization of the Percolation Network: Contrast Between 2D and 3D*

The idea of critical path analysis is actually not best expressed as an upscaling of the conductivity. In particular, in critical path analysis, one seeks an optimization of an expression for the conductivity, which is based on selection of paths with very small values of the maximum resistance and the separation of those paths. Thus we find the dominant conducting paths, the current (or flow) on those paths, and how many such paths per unit area intersect a plane perpendicular to the flow. We cannot restrict our attention precisely to the paths with the smallest possible values of the maximum resistance, since these paths would be precisely at the percolation threshold and then have infinite separation (leading to a zero conductivity). Incorporating some larger resistances reduces the conductances of these paths, but increases their areal density rapidly from zero. The typical separation of these paths is given in terms of the correlation length, χ. The areal density of the relevant paths is thus χ^{-2}. We will then invert an elementary relationship for the resistance of a homogeneous wire $R = \rho l/A$, with $\rho \equiv \sigma^{-1}$ the resistivity, l the length and A the cross-sectional area,

to obtain the conductivity from R, l and A, i.e., $\sigma = l/RA$. A will thus be the square of the correlation length, and l will be the typical separation of maximal resistances on the path. In that expression for the conductivity, however, all the functions must be written in terms of the maximally valued resistance (or minimum conductance) in order to perform an optimization.

The correlation length is defined in terms of $(p - p_c)$; thus we must have a general expression for $(p - p_c)$, which is written in terms of the resistance distribution itself, in order to apply the optimization procedure.

Define,

$$F(R) \equiv \int_0^R W(R')dR' = p \tag{2.31}$$

Then,

$$F(R_c) = \int_0^{R_c} W(R')dR' = p_c \tag{2.32}$$

Equations (2.31) and (2.32) can be solved in parallel for $p - p_c$. Define a conductance $g \equiv R^{-1}$ and l to be the typical separation of the rate limiting resistances, R. It is then possible to write a relatively simple expression for the conductivity of a three dimensional network, on which a fraction, p, of bonds with the smallest R values possible, is placed at random,

$$\sigma = \frac{l[F(g^{-1}) - F(g_c^{-1})]^{2\nu}}{\chi_0^2} g \tag{2.33}$$

In Eq. (2.33) the factor $[F(g^{-1}) - F(g_c^{-1})]^{2\nu}$ arises from the square of the correlation length in the denominator. Equation (2.33) is, for heterogeneous systems, again equivalent to the result in elementary physics texts for the resistance of a homogeneous wire $R = \rho l/A$, with $\rho \equiv \sigma^{-1}$ the resistivity, l the length and A the cross-sectional area. In Eq. (2.33) $\chi_0^2[F(g^{-1}) - F(g_c^{-1})]^{-2\nu}$ is the square of the correlation length as a function of the smallest conductance included, g. l is actually the separation of rate-limiting resistances on the dominant, current-carrying path and, as such, would seem to involve only the statistics of the resistance values. If the resistance distribution is discretized in steps of the fundamental constant $e = 2.718$, then one could write for l,

$$l \approx \chi_0 \left\{ \frac{\int_0^R W(R)dR}{\int_{-R/e^{1/2}}^{e^{1/2}R} W(R)dR} \right\}^{-\frac{1}{3}} \tag{2.34}$$

in three dimensions. Equation (2.34) actually has a very simple basis. Note that the ratio on the right-hand side is just the inverse of the fraction, f, of emplaced resistances which is in the largest discretization class, so that $l^3 f \approx 1$. In this formulation, the distribution of resistances on the percolating cluster is the same as in the medium generally, so that the volume concentration of the largest resistances is easy to obtain from the appropriate bulk distribution, $W(R)$. Note that l in Eq. (2.33) is thus only a very slowly varying function of p, and not a function of $p - p_c$ at all. For

this reason optimization of Eq. (2.33) is not complicated by consideration of l. Result Eq. (2.33), however, is not generally agreed on. Several authors identify l with the correlation length $\chi = \chi_0[F(g^{-1}) - F(g_c^{-1})]^{-\nu}$, by arguing that the separation of rate-limiting resistances is topologically constrained, rather than a function of the frequency of occurrence of such resistances. The physical basis for this argument is that, in the vicinity of p_c at least, most of the largest resistances are shorted by alternate paths with smaller dominant resistance values, but that, for self-consistency l cannot be larger than χ, otherwise the value of p would have to be changed. This important problem is still not completely settled, with several different perspectives taken in the literature, including an important contribution from a soil physicist [37].

If in Eqs. (2.31) and (2.32) R is an exponential function of a random variable, such as a site separation ($R \propto \exp(2r/a)$ with a a constant length), then $F(R) - F(R_c) \propto \ln(R/R_c) = \ln(g_c/g)$, but if R is a power of, e.g., a tube radius (for hydraulic conduction), then $F(R) - F(R_c) \propto (R - R_c)$ or $g - g_c$ (see the assigned problems). Using Eq. (2.34) for l and optimizing Eq. (2.33) leads, in the first case, to [12]

$$\frac{d\sigma}{dg} = \frac{d}{dg}\left[\frac{l[F(g^{-1}) - F(g_c^{-1})]^{2\nu}}{\chi_0^2} g\right] = \left[\ln\left(\frac{g_c}{g}\right)\right]^{2\nu} - 2\nu\left[\ln\left(\frac{g_c}{g}\right)\right]^{2\nu-1} = 0 \tag{2.35}$$

Solution of Eq. (2.35) yields $\ln(g_c/g) = 2\nu$, or $g = g_c \exp(-2\nu)$. Thus the controlling conductance, g, is closely related to the critical value, g_c, and this value of g can also be substituted into $\chi = \chi_0[F(g^{-1}) - F(g_c^{-1})]^{-\nu}$), to generate an expression for σ in Eq. (2.33). Note that choice above of $l \propto \chi$ would yield $g = g_c \exp(-\nu)$, because the exponent 2ν would be replaced by ν. In two dimensions, the factor χ^2 in the denominator is replaced by χ. If l is taken to be proportional to χ, the two-dimensional case becomes special because l/χ has no dependence on the percolation variables, with the conductivity a universal numerical factor (of order unity) times the critical value of the conductance, g_c. This result does appear to be verified [40], and our own simulations agree [18]. Specific results from critical path analysis will be discussed in Chap. 5 and elsewhere.

Note, however, that in many cases it may be possible to apply critical path analysis without using the above optimization if it is desired only to find the ratio of the critical resistance value at two different values of a changing external parameter such as the moisture content, and under the assumption that far from the percolation threshold the topological aspects affecting the optimization will change only slowly with such external parameters. Predominantly such cases will also be considered in the chapters on applications.

In hydrogeology one of the most important problems is to be able to predict the effective (hydraulic) conductivity, K_{eff}, of a medium from information regarding the variability of K within the medium. This problem is known as "upscaling the hydraulic conductivity." It is often stated that K_{eff} is bounded by its harmonic and arithmetic mean values. The harmonic mean of a collection of resistance values is the value obtained by configuring them all in series. The arithmetic mean of a collection of resistors is the equivalent resistance value when they are all configured in parallel. Geologists often assert that physicists do not comprehend the complexity

of geologic material (which is true), but such an upscaling scheme was obviously developed from the geologic perspective of a subsurface stratified in horizontal geologic units, where horizontal conduction is governed by the arithmetic mean and vertical conduction by the harmonic mean.

Upscaling K in three dimensions as though all resistances were configured in parallel (series) is consistent with assuming that $p_c = 0$ ($p_c = 1$). The latter is valid for one-dimensional systems. Thus regarding the bounds of K as being its harmonic and its arithmetic means corresponds to assuming that the critical bond (or volume) fraction for percolation is between 1 and 0, valid for one and infinite dimensional systems, respectively. This means that typical guidelines for upscaling state only that the critical percolation probability is a probability, or that conduction takes place in a dimension between one and infinity. In this context we can see what potential improvement in theory exists when a perspective based on percolation theory is adopted. The value of p_c for a given system defines what fraction of the (smallest) individual resistances, which must be considered as connected in series, with the remaining $1 - p_c$ fraction of larger resistances connected in parallel. Any information on connectivity should help to estimate the appropriate value of p_c for a system, guiding the upscaling.

2.7 Summary

In predicting transport properties of porous media it is necessary to be able to distinguish the roles of the medium and the fluids within the medium. Likewise, it is essential to be able to calculate inputs from both geometry (e.g., pore size distributions) and topology (specifically fluid connectivity within the pore space). In the framework of this book we can make the following generalizations:

(1) Values of the effective hydraulic conductivity K are strongly affected by the local resistance distribution (obtained at the pore-scale from the pore-size distribution), both at complete saturation, and as a function of saturation.
(2) All other conduction parameters are dominated by fluid connectivity issues, leading to the relevance of universal scaling of percolation for saturation dependences.
(3) When conductance distributions are important, i.e., for K, its effective value is best calculated in critical path analysis. Beyond its aesthetic appeal and greater accuracy of prediction, critical path analysis has the additional advantage of providing a physical interpretation for the "irreducible" moisture content, being mathematically consistent with scaling approaches, and thus allowing parameters to have consistent values across different properties, whether pore-size dominated, or fluid-connectivity dominated.

Problems

2.1 Provide the details of the derivation of Eq. (2.18) and Eq. (2.20) for solute diffusion.

2.2 Verify that $p - p_c \propto \ln(g_c/g)$ if $R \propto \exp(2r/a)$, whereas $p - p_c \propto (g - g_c)$ if $R \propto r^{-4}$. Are there any conditions or restrictions on $W(R)$ for the validity of this derivation? Can you name any systems for which these resistance values are appropriate?

2.3 Repeat the optimization procedure for the conductivity if $R \propto r^4$ and $p - p_c \propto g_c - g$. Note that the optimization procedure described in the text (for the exponential case) is unchanged if the conductivity is represented in terms of R rather than in terms of g. However, the optimization procedure in terms of R fails for the case of the power-law dependence of R. Show this explicitly. What does this failure imply?

2.4 Verify that if $W(R) \propto R^{-\alpha}$ between $R_{\min}$ and $R_{\max}$, such that $-2 < \alpha < -1$, the effective resistance of a 1D chain for this choice of $W(R)$ is proportional to $R_{\max}$.

References

1. Ambegaokar, V.N., Halperin, B.I., Langer, J.S.: Hopping conductivity in disordered systems. Phys. Rev. B **4**, 2612–2621 (1971)
2. ben-Avraham, D., Havlin, S.: Diffusion and Reactions in Fractals and Disordered Systems. Cambridge University Press, New York (2000)
3. Batchelor, G.K.: Transport properties of two-phase materials with stochastic structure. Annu. Rev. Fluid Mech. **6**, 227–255 (1974). doi:10.1146/annurev.fl.06.010174.001303
4. Berkowitz, B., Balberg, I.: Percolation approach to the problem of hydraulic conductivity in porous media. Transp. Porous Media **9**, 275–286 (1992)
5. Berkowitz, B., Balberg, I.: Percolation theory and its application to groundwater hydrology. Water Resour. Res. **29**, 775–794 (1993)
6. Bernasconi, J., Schneider, W.R.: Classical hopping conduction in random one-dimensional systems—non-universal limit-theorems and quasi-localization effects. Phys. Rev. Lett. **47**, 1643–1647 (1981)
7. Clerc, J.P., Podolskiy, V.A., Sarychev, A.K.: Precise determination of the conductivity exponent of 3D percolation using exact numerical renormalization. Eur. Phys. J. B **15**, 507–516 (2000)
8. Derrida, B., Vannimenus, J.: A transfer matrix approach to random resistor networks. J. Phys. A, Math. Gen. **13**, L557–L564 (1982)
9. De Wit, A.: Correlation structure dependence of the effective permeability of heterogeneous porous media. Phys. Fluids **7**(11), 2553–2662 (1995)
10. Feng, S., Halperin, B.I., Sen, P.N.: Transport properties of continuum systems near the percolation threshold. Phys. Rev. B **35**, 197 (1987)
11. Fisher, M.E.: The theory of critical point singularities. In: Green, M.S. (ed.) Critical Phenomena, Proc. 1970 Enrico Fermi Internat. Sch. Phys., Course No. 51, Varenna, Italy, pp. 1–99. Academic Press, New York (1971)
12. Friedman, L., Pollak, M.: The Hall effect in the variable-range hopping system. Philos. Mag. B **44**, 487–507 (1981)
13. Gingold, D.B., Lobb, C.J.: Percolative conduction in three dimensions. Phys. Rev. B **42**(13), 8220–8224 (1990)
14. Grassberger, P.: Conductivity exponent and backbone dimension in 2-d percolation. Physica A **262**, 251–263 (1999)
15. Herrmann, H.J., Stanley, H.E.: The fractal dimension of the minimum path in two-dimensional and three-dimensional percolation. J. Phys. A **21**, L829–L833 (1988)

16. Hunt, A.: One-dimensional hopping conductivity calculations. Philos. Mag. B **64**, 327–334 (1991)
17. Hunt, A.: A general treatment of 1-dimensional hopping conduction. Solid State Commun. **86**, 765–768 (1993)
18. Hunt, A.G.: Applications of percolation theory to porous media with distributed local conductances. Adv. Water Resour. **24**(3,4), 279–307 (2001)
19. Jerauld, G.R., Hatfield, J.C., Scriven, L.E., Davis, H.T.: Percolation and conduction on Voronoi and triangular networks: a case study in topological disorder. J. Phys. C **17**, 1519–1529 (1984)
20. Keffer, D., McCormick, A.V., Davis, H.T.: Diffusion and percolation on zeolite sorption lattices. J. Phys. Chem. US **100**, 967–973 (1996)
21. Kirkpatrick, S.: Phys. Rev. Lett. **27**, 1722 (1971)
22. Kirkpatrick, S.: Percolation and conduction. Rev. Mod. Phys. **45**, 574–588 (1973)
23. Knudby, C., Carrera, J., Bumgardner, J.D., Fogg, G.E.: Binary upscaling—the role of connectivity and a new formula. Adv. Water Resour. **29**, 590–604 (2006)
24. Lee, Y., Andrade, J.S., Buldyrev, S.V., Dokholoyan, N.V., Havlin, S., King, P.R., Paul, G., Stanley, H.E.: Traveling time and traveling length in critical percolation clusters. Phys. Rev. E **60**(3), 3425–3428 (1999)
25. Mandelbrot, B.B.: The Fractal Geometry of Nature. Freeman, San Francisco (1983), 468 pp.
26. Matheron, G.: Éléments Pour Une Théorie des Milieux Poreux. Masson et Cie, Paris (1967)
27. Moldrup, P., Oleson, T., Komatsu, T., Schjoning, P., Rolston, D.E.: Tortuosity, diffusivity, and permeability in the soil liquid and gaseous phases. Soil Sci. Soc. Am. J. **65**, 613–623 (2001)
28. Neuweiler, I., Vogel, H.-J.: Upscaling for unsaturated flow for non-Gaussian heterogeneous porous media. Water Resour. Res. **43**, W03443 (2007)
29. Normand, J.-M., Herrmann, H.J.: Precise numerical determination of the superconducting exponent of percolation in three dimensions. Int. J. Mod. Phys. C **1**, 207–214 (1990)
30. Pike, R., Stanley, H.E.: Order propagation near the percolation threshold. J. Phys. A **14**, L169–L177 (1981)
31. Pollak, M.: A percolation treatment of dc hopping conduction. J. Non-Cryst. Solids **11**, 1–24 (1972). doi:10.1016/0022-3093(72)90304-3
32. Sahimi, M.: Flow phenomena in rocks—from continuum models to fractals, percolation, cellular automata, and simulated annealing. Rev. Mod. Phys. **65**(4), 1393–1534 (1993)
33. Sahimi, M., Hughes, B.D., Scriven, L.E., Davis, H.T.: Real-space renormalization and effective-medium approximation to the percolation conduction problem. Phys. Rev. B **28**, 307–311 (1983)
34. Sanchez-Villa, X., Carrera, J., Girardi, J.P.: Scale effects in transmissivity. J. Hydrol. **183**, 1–22 (1996)
35. Sen, P.N., Roberts, J.N., Halperin, B.I.: Non-universal critical exponents for transport in percolating systems with a distribution of bond strengths. Phys. Rev. B **32**, 3306–3308 (1985)
36. Sheppard, A.P., Knackstedt, M.A., Pinczewski, W.V., Sahimi, M.: Invasion percolation: new algorithms and universality classes. J. Phys. A, Math. Gen. **32**, L521–L529 (1999)
37. Skaggs, T.H.: Effects of finite system size and finite heterogeneity on the conductivity of broadly distributed resistor networks. Physica B **338**, 266–269 (2003)
38. Skal, A.S., Shklovskii, B.I.: Topology of an infinite cluster in the theory of percolation and its relationship to the theory of hopping conduction. Sov. Phys. Semicond. **8**, 1029–1032 (1975)
39. Stauffer, D.: Scaling theory of percolation clusters. Phys. Rep. **54**, 1–74 (1979)
40. Stauffer, D., Aharony, A.: Introduction to Percolation Theory, 2nd edn. Taylor and Francis, London (1994)
41. Torquato, S.: Random Heterogeneous Materials. Springer, Berlin (2002)

Chapter 3
Porous Media Primer for Physicists

3.1 How Does Percolation Theory Relate to Porous Media?

The two disciplines which this book combines—percolation theory and porous media—developed independently, and have only slowly (and seemingly reluctantly) become aware of each other. This despite Broadbent and Hammersley's [14] term "percolation", chosen to evoke the image of water flowing through coffee grounds in a coffee percolator, and their use of porous media as an example application! The previous chapters presented some fundamentals of percolation theory, but did not explicitly relate the theory to porous media. This chapter presents some fundamentals of porous media, without providing the detailed connections with percolation that appear later in this book. The fundamentals have been largely developed in the context of studying pore-scale processes, while extensions to sample scales were typically pursued without applying concepts of percolation theory. To help bridge this apparent disconnect, we start with some conceptual and historical context. It will be seen that the logic of the present development has occasionally been anticipated.

Percolation theory and the study of porous media share two core concepts: networks (what mathematicians call graphs) and emergence. The pores in natural porous materials form a network, and the macro-scale properties of the medium result (emerge) from the local properties and interactions of the component pores. Irwin Fatt [42–44] developed the first network model of porous media, and explicitly calculated how a medium's macroscopic properties emerge from the network of individual pores, although "emergence" was not then an accepted term in the quantitative sciences [30]. Fatt showed how individual events within the pore network combine to produce hysteresis, non-linear relationships between pressure and saturation, and other aspects of porous materials previously found confusing or intractable. Thus the geometrical and topological characteristics of the network itself are relevant to measured properties. Parameters describing pore sizes and pore-connectivity show up most straightforwardly in phenomenologies for the water retention characteristics, which derive from the apportionment of fluids within the medium. This

A. Hunt et al., *Percolation Theory for Flow in Porous Media*,
Lecture Notes in Physics 880, DOI 10.1007/978-3-319-03771-4_3,

subject, including a wide range of influences that confound interpretation is treated in Sect. 3.5.

Direct connections between percolation theory and porous media were not made until 1977, when two groups made the link independently. Larson, Scriven and Davis [86] noted that the size distribution of residual oil blobs in reservoir rock was predicted by percolation theory, and the topology of porous media might be as important as the geometry. Chatzis and Dullien [21] pointed out that the sites and bonds in percolation theory resembled pore bodies and pore throats (see Sect. 3.3) in porous media. Mohanty et al. [100] later formalized this resemblance, showing how in principle one could map a porous medium onto a network. Wilkinson and Willemsen [146] soon developed invasion percolation, a new form of percolation explicitly based on immiscible displacement of fluids in a porous medium, and the two disciplines have drawn inspiration from each other since then, although the connection has never been mainstream in either.

Of the many forms of percolation introduced in Chaps. 1 and 2, which applies to porous media? Of the various techniques for predicting transport properties, which will bear fruit? The answers to the first question will be clearer after we have explored some basic concepts of porous media, both fundamental properties and some processes occurring in them. The answer to the second question is based on analysis of each individual property investigated and is explored in the subsequent chapters.

3.2 Kinds of Porous Media

A porous medium is a composite of solid and void, with the void typically being occupied by one or more fluids. “Most materials are to some extent porous: indeed, it is quite difficult to find or prepare a truly non-porous solid” [114]. Suspensions and slurries are also composites containing solid and fluid, but they differ from porous media in that their solid component is discontinuous, unable to transmit stress. Many materials are useful precisely because they are porous: soil absorbs and stores water, cloth allows air and water vapor to pass through it, and leavened bread sops up gravy. Our focus in this book is on natural granular porous media such as gravel, sand, and soil. Other familiar granular materials include bulk grains like rice and corn, and powders such as flour and baking powder.

Many familiar porous media are not granular, but many concepts examined in this book apply to them as well. Examples include biological tissue (lungs, wood, potatoes), solidified foams (pumice, bread, foam insulation), fibrous media (clothing, paper, fiberglass insulation), crystalline media (granite, some kinds of metal) in which the porosity is mainly at grain boundaries, fractured media (again granite, but focusing on fractures much larger than the individual mineral grains), and sintered materials (ceramics, fritted glass or metal filters). As these examples suggest, porous materials span a wide range of porosity, and they may be isotropic or anisotropic, amorphous or structured, have more than one characteristic length scale, and mediate multiple interesting and interacting processes.

Given the striking complexity and variability of natural porous media, these notes will be limited to soils and rocks, the porous media most familiar to the authors. Soil is so common that people often forget its complexity: it includes both mineral and organic materials, often includes both solids and pores spanning more than four orders of magnitude in length, routinely shifts between water-saturated and air-dry, and has a large and variable surface area that mediates many physical, chemical, and biological reactions. Most processes that occur in some arbitrary porous material also occur naturally in soils, so our use of soils as a common example is not restrictive.

The study of porous materials is the province of many different disciplines. These disciplines, and especially the applied earth sciences (soil science, hydrology, civil and petroleum engineering) have historically focused on applications rather than understanding, and this pragmatic approach has led to some cutting of corners. Furthermore, the different disciplines have different goals, so they have developed their own peculiar vocabulary, insights, and biases. For example, petroleum engineers generally work with consolidated rock, so the concept of a particle size distribution is not as central to their thinking as it is to a soil scientist. Meanwhile, soil scientists working with just two fluids—air and water—often assume that they can get away with assuming that air is infinitely compressible (and has density and viscosity of zero), while petroleum engineers working with multiple flowing gases and liquids must consider all fluid phases in concert. Similarly, engineers may treat geological porous media as disordered systems, while soil scientists focus on soil structure at various scales and object to soil being called disordered. From the perspective of physics, soils are complicated, disordered, composite media.

The purpose of this chapter is to introduce physicists to basic concepts of porous media, especially those found in the applied earth sciences. As such it will show both the successes and the internal inconsistencies of this community. The applied earth science community has come to value flexible formulations of flow and transport above predictive ones: somewhere a combination of parameters must exist that makes "correct" predictions. And in fact, with flexible formulations there may be a large number of such combinations, so a common concern of the community regards the "uniqueness" of parameter determinations. Another advantage of flexible formulations is that experimental error, which is often appreciable, can be readily accommodated. Usually the resulting relationships are recognized in the soil science and hydrology community as being phenomenological only. But the point of a physics-based treatment must be to derive relationships that are both predictive and physically sound, even in the face of complexity.

3.3 Properties of Porous Media Independent of Fluid

We first consider those properties of a porous medium that do not involve any fluid. Historically most properties have been considered to be geometrical: sizes, volumes, surfaces, and so on. But many important properties have a topological aspect as well, and we mention these as appropriate.

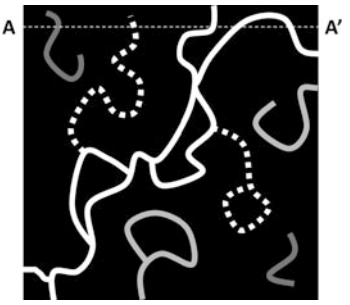

Fig. 3.1 Porosity classified by topology. *White*: infinite cluster, with the backbone *solid* and the dangling ends *dotted*. *Light grey*: edge-connected; *dark grey*: isolated

We caution in passing that even geological porous materials can be dynamic and fragile. For example, soils compress under heavy loads, and clayey soils may swell with increasing moisture content, and shrink upon drying. Ephemeral biological activity can create large macropores that locally dominate the permeability. Collecting and transporting a sample disturbs it, and disturbed samples differ from the *in situ* material (explaining the community's preference for repeated *in situ* measurements, even when the actual techniques are less precise). While of great practical importance, the changeability of these materials is not fundamental to the present discussion, and accounting for it would force the development of more complicated, non-linear techniques. Our implication that these are rigid materials with fixed properties does not make them so.

3.3.1 Porosity

The most fundamental geometrical property of a porous medium is the porosity, the volume fraction that is void rather than solid. Generally denoted ϕ, it is a unitless fraction less than 1. Porosity must describe a finite volume, because a dimensionless point is either completely solid or void. Rock porosity values range from less than a percent in many crystalline rocks such as granite, through 5–15 % in sandstones, to well over 60 % in pumice. Because soils are particulate rather than rigid, the requirement of mechanical stability restricts soil porosity values to a smaller range. Most mineral soils (as opposed to, e.g., peat) have porosities between about 30 % and 60 %, with 40 % to 50 % being a common value near the ground surface.

Porosity is sometimes sub-classified by its size (macropores, mesopores, micropores), its genesis (primary and secondary porosity) or its function (effective porosity, closed porosity). While these have their uses, a more fundamental classification is topological (Fig. 3.1). Pores on the infinite cluster may be on the backbone (fluid would flow through them) or be dangling ends, only singly connected to the infinite cluster. Pores that are not on the infinite cluster may be connected to the "outside" (because porous media, being real rather than mathematical objects, are not infinite), or on finite clusters that connect neither to the outside nor to the infinite cluster. This classification connects explicitly with percolation theory. But note that the topological classification of a given pore can depend on the specific boundaries of the

system: if the medium in Fig. 3.1 were cut at A–A′, one isolated pore would be "promoted" to edge-connected, one dangling end would be promoted to the backbone, and one portion of the backbone would be demoted to edge-connected. These concepts are crucial to studies of, e.g., diffusion into poorly connected media [40, 41], such as the pore space in crystalline rocks.

Porosity can be surprisingly difficult to measure accurately. If the pore space is well connected, then porosity may be measured by measuring the mass of a sample completely occupied in turn by two fluids of known but different densities. For example, the sample may be water-saturated and weighed, then oven-dried and weighed, with the pore volume given by the change in mass times the density difference. But this requires that all pores be completely filled by each fluid in turn, and in fact it takes good experimental technique to guarantee water contents greater than about 0.9ϕ. For example, estimates of saturated moisture contents taken on the same soils by different Department of Energy labs vary by as much as 20 %. Faced with such issues, a physicist must evaluate whether his/her notions of experimental tolerance are realistic.

An alternative method, less susceptible to errors due to wettability and fluid entrapment, is to use gas pycnometry (e.g., [128]): seal the sample into a chamber of known volume, pressurize gas in a different chamber of known volume, measure the gas pressures, then connect the chambers and measure the resulting pressure. From the gas pressures, and the volumes of the chambers, the volume of the solid may be calculated by Boyle's law; if the bulk volume of the sample is also known, one obtains the porosity. This requires that the porespace be connected, which is predominantly the case in soil though less likely in some rocks, e.g. shale. When isolated pores form a non-negligible fraction of the porosity, accurate measurement requires other methods. For example, one may measure the two-dimensional void fraction of a polished section cut through the medium, and equate the result with the three-dimensional porosity via Delesse's theorem [34], although for fractal media (at least), systematic errors result if 2D images are used to estimate the porosity. Alternatively, one may use gamma-ray attenuation [6], or a three-dimensional imaging method such as X-ray CT [91].

3.3.2 Bulk & Particle Density, Particle Size Distribution

The density of the solid phase is denoted ρ_p ($\mathrm{M\,L^{-3}}$, the subscript p means particle, revealing the notation's roots in granular media). The solid phase of a porous medium is often considered constant with respect to material composition, chemistry, and therefore particle density. In contrast, the solid as an ensemble—the bulk material—may be compressible, such that the porosity changes. Changes in porosity must thereby change the bulk density (mass of solids divided by volume of solid plus void), denoted ρ_b:

$$\rho_\mathrm{b} = \rho_\mathrm{p}(1 - \phi) \tag{3.1}$$

In practice porosity is often calculated from this relationship: the bulk density and particle density are relatively easy to measure, and in some materials (for example, soils) the mean particle density is known *a priori* to be within a few percent of the density of quartz, 2.65 $\mathrm{Mg\,m^{-3}}$. The bulk density may be obtained from e.g. the mass of a core of known dimensions, and the particle density can be measured by pulverizing a subsample of that core and using water or gas pycnometry. Pulverizing the sample prior to measuring particle density may connect previously isolated pores above the scale of pulverization.

When the material is granular, it can be useful to know the size distribution of the grains. Because the solid and void form dual networks, knowing the grain size distribution (which is easier to measure) also allows estimation of the pore size distribution. But natural materials have irregular shapes, so the "size" measured is the radius or diameter of an equivalent sphere, with inevitable biases specific to the method used. Particles in the size range 0.05–5.0 mm are usually separated by being passed through a stack of successively finer sieves, but needle-like particles will pass a given sieve only if oriented by sufficiently vigorous shaking; the mode and duration of the shaking therefore affects how different shapes are sieved. Sieving is not practical for particles smaller than about 0.05 mm.

For particles smaller than about 50 μm, surface chemistry and intermolecular forces are relatively strong. These particles may clump together or onto the surface of larger particles, such that they present as larger than they really are. This clumping confounds the main methods used to measure small particles, Stokes settling [48] and laser diffractometry [93], unless particles are first dispersed. The degree of dispersion desired depends on the intended use of the data: for some purposes, the aggregated particle size may be more relevant than the dispersed particle size. A further complication is that particle density and shape may vary systematically with size, because particles classified as clay (<2 μm diameter) are often clay minerals (confusingly, the word "clay" denotes both a size and a mineralogy!), having a sheet-like shape and a lower density than is typical for larger size particles. Again, this systematic change in shape and density requires corrections, which may or may not actually be performed in practice. Finally, use of different methods for different size ranges introduces a new problem: data obtained by two different methods are no longer constrained. Frequently the total weight fraction does not equal 1, so that the cumulative size distribution graph may not accumulate to 1; alternatively there may be regions with apparent negative slope. Since both of these results are unphysical, a protocol must be developed for accepting or rejecting data, or making consistent adjustments to provide a reasonable synthesis.

Some media are composed of a narrow range of particles. For example, loess soils are composed of wind-borne particles that were transported long distances, resulting in soils dominated by a single characteristic particle size. Likewise, industrial processes often produce powders of high uniformity. But where the width of the distribution is as important as the characteristic size (however defined), it is useful to present both aspects of the distribution. In soil science, the particle size is often presented in the form of a "texture class", defined by a region in the "texture triangle". This triangle is defined by breaking the total size range (from 2 μm

to 2 mm) near the geometric mean, which defines 4 bins: <2 μm (clay), 2–50 μm (silt), 50–2000 μm (sand), and >2 mm. (Gravel and coarser material in the >2 mm bin are not defined as part of the soil, because moist soil is considered to be cohesive and cohesive forces between such large particles are negligible. Therefore, only the 3 finer bins are used to construct the ternary diagram.) Plotting a specific soil's bin mass fractions into the ternary diagram places it into one of 12 predefined regions ("textures"). Significant information is clearly lost in this process, but the 12 soil textures have distinct and useful connotations for practitioners. This classification scheme was developed primarily for its relevance to agricultural soils, which need to simultaneously optimize water retention (small pore sizes) and flow (large pore sizes). It has long been recognized that soils with a wide range of particle sizes, incorporating sands, silts and clays, are ideally suited to agriculture.

3.3.3 What Is a Pore?

The emphasis in porous media on the spaces between the particles is complementary to the usual emphasis in e.g., condensed matter physics. The preceding sections mention pores, and the term "porous medium" implies the presence of pores, but we have not defined a pore. It is easy to distinguish between solid and void, so the entire void portion of a given porous medium, its porespace, is defined by difference from the solid. But determining where one pore ends and another begins is somewhat arbitrary. The porespace is continuous, and subdividing it into discrete parts requires arbitrary decisions, like classifying colors or weather. So while we often find it useful to speak of individual pores, those pores might not be uniquely and unambiguously defined.

One might think that in a granular medium (at least) it would be straightforward to define individual pores. The individual grains are roughly convex, so the pores forming the dual network are concave; individual pores may be distinguished by the presence of a minimum between them. In Fig. 3.2a a pore network is shown as Voronoi polygons, defined by the perpendicular bisector of the line connecting the centers of neighboring solid circles. But a pore defined by more than 3 circles (or by more than 4 spheres in the 3 dimensional case) might instead be interpreted as two or more pores, depending on the defining criteria; this is one of the arbitrary choices identified by Mohanty [99]. The issue becomes more complex in 3 dimensions, or when the solids are irregularly shaped.

Often, connections between pores (however defined) are seen to have a converging-diverging geometry. In these cases the large central part is called the pore body, and the narrow connection is called the pore throat (or pore neck). We might (for example) consider that fluid is stored in the pore body, while resistance to flow is given by the pore throat. As Chatzis and Dullien [21] noted, the pore bodies are like the sites of percolation theory, while the pore throats are like the bonds. Building on this analogy, specific pore-scale events or processes are seen to correspond to specific kinds of percolation.

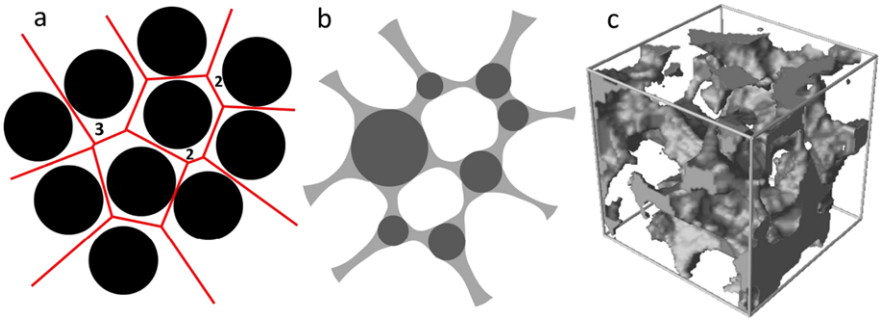

Fig. 3.2 Pores in a granular medium. **a**: An idealized 2D medium with solids shown in *black*, and the void space divided into a pore network (after [100]); **b**: one possible pore network equivalent of **a** with dark pore bodies and lighter pore throats, showing the converging-diverging pore geometry; and **c**: a section of Fontainebleau sandstone with 22 % porosity with solids made transparent, showing only the porespace (from [95]). In **a**, pores marked with a *number* may be interpreted either as that number of distinct pores, or as a single pore, depending on the choice of rules

3.3.4 Pore Size Distribution

The concept of a pore size distribution features prominently throughout this book. Here we briefly consider what it is; in Sect. 3.5.3 we consider various methods for measuring it.

The basic concept seems easy: a pore-size distribution is a cumulative relationship between fractional pore volume and finite ranges of pore size. The difficulty lies in defining precisely what is a "pore size", and precisely what pore volume is associated with that size. Given the difficult issues of assigning a single size to an irregularly-shaped particle (Sect. 3.3.2), and defining a single pore (Sect. 3.3.3), one might anticipate (correctly!) that the pore size distribution is similarly fraught. For example, is the relevant size of a pore the radius of the pore body, or the radius of the pore throat? If the pore body, is the relevant size (for example) the radius of a sphere having the same volume, or perhaps the maximum radius of curvature of a meniscus moving across the pore (but from which pore throat to which other throat, and with what contact angle)? Or, if it's the pore throat, which of the several throats connecting to a pore body (Figs. 3.2b and 3.3) is assigned the volume of the pore? If the chosen throat has an irregular cross-section (as it inevitably will), is its "size" the minimum size reached by a meniscus passing through the throat (and with what contact angle), the square root of the cross-sectional area, or some other value? Often the analysis tacitly assumes that the pore throat is circular, slit-like, or having some other regular geometry; other times the intent is nonetheless to reduce it to some equivalent size of cylinder, slit, or sphere, although most natural media have more than a single type of pore present [9].

We raise these questions to show that the concept of a pore size, a single length used to characterize an irregular (and poorly defined) pore whose identity is questionable, is essentially a necessary fiction. If the pore size is obtained by analysis of 3D data (for example, tomographic information being analyzed by 3DMA

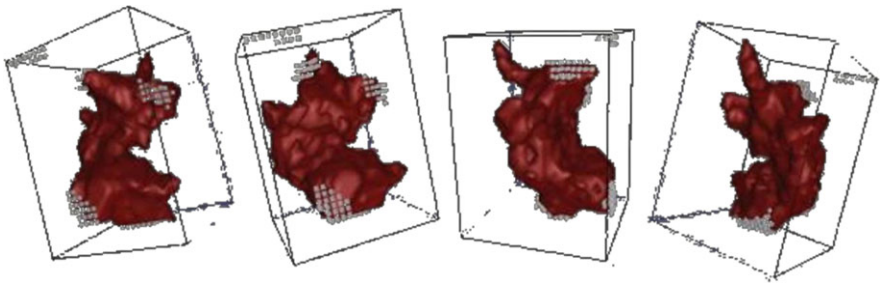

Fig. 3.3 Four views of one individual pore in Fontainebleau sandstone identified by the program 3DMA [88]. The patches of *grey squares* indicate connections to neighboring pores. What single length characterizes this pore?

(Fig. 3.3); [88]), then these questions must be answered unambiguously, but the decisions supporting the answer are still necessarily somewhat arbitrary. Imaging methods [75, 91, 125, 141] involve thresholding or segmenting (e.g., [67]), skeletonizing via medial axis transformation or deformation retract, and using various algorithms to identify and classify pore space components, with each step introducing some ambiguity. A key consideration being the relative scales of the voxels, and the characteristic grains or pores: even at the 5 μm resolution available with synchrotron X-ray imaging [105], pore connections below the image resolution will be missed.

A non-imaging method, small angle neutron scattering (SANS; e.g., [96, 109]), involves different but analogous assumptions in analysis. NMR can be used to track diffusion, and thereby to infer the pore-size distribution [124], but complex and broad distributions are not well handled. Other more common pore-size measurement methods (Sect. 3.5.3), being process-based, assign a pore size to some fraction of the total pore volume based on a combination of measurement protocols and independent assumptions: that is, they define the pore size distribution procedurally rather than rigorously.

While much effort is focused on the pore size distribution, porosity and the pore size distribution are clearly insufficient for characterizing a porous medium. Size distribution is a geometric measure, lacking topological information. Topological input may take the form of a mean coordination number: random packing of uniform spheres produces pores with average coordination in the range 4.7–5.5 [1], depending on how dense the packing is and on precisely how a pore is defined, while lower-porosity sandstones tend to have lower pore coordination [91]. Natural porous media tend to have adjacent pores correlated in size [80], and larger pores tend to have higher coordination [91]; both of these tendencies affect their fluid-holding and transport properties. At a larger scale, soils tend to be "structured," by which is meant two things: first, some pores are larger than the largest grains, and second, a network of large pores may percolate even though they constitute only a small fraction of the total porosity, typically less than the critical fraction for percolation for the smaller "non-structural" pores. The effects of soil structure on hydraulic properties in biologically active soils are considered in Chap. 12. In the

case of swelling clays, these larger "pores" are drying cracks, and such media are not further considered here.

Because it is much easier to measure particles than pores, the pore size distribution is often estimated from the particle size distribution. The simplest approach is to assume a one-to-one correspondence between particles and pores: for every particle with (effective) radius r, there is a corresponding pore with (body or throat) radius ar, for some $a < 1$ [3, 56, 135]. Typical estimates of the numerical value of a run about 0.3, though this value is notoriously variable in terms of the typical particle size; finer soils tend to have a larger proportionality constant than coarser ones due to having relatively greater cohesion. Obviously compaction of a given soil, resulting in a smaller porosity, would reduce a. Further, the proportionality between particle and pore sizes may hold over only part of the range of particle sizes measured, especially if the larger pores are "structural" in nature.

3.3.5 Surface Area and Surface Chemistry

Another basic property is the specific surface area, the surface area per unit mass or volume. This may be of interest because the solid surface catalyzes or otherwise mediates chemical reactions, or because a liquid sorbs to the surface, modifying its properties. For example, in soil the solid surface is often covered by a thin film of water, the thickness of which varies according to the water's energy state. Surface area measurements generally involve monomolecular layer sorption [79], which only measures the connected pores. But in any but the simplest materials, the calculated surface area is also a function of the size of the interrogating molecule [79]. Pore accessibility can also be a function of size—larger molecules being excluded from smaller pores—so multiple measurements of specific surface area using molecules of various sizes will not necessarily give the correct surface fractal dimension.

Many porous media of interest are occupied by more than one fluid. Which fluid occupies which pore varies with (among other things) chemical interactions between the pore surface and the fluid. For example, if the surface chemistry is polar, then occupancy by polar liquids will be favored, and the material would be called "water-wetting". If the surface chemistry is non-polar, the medium may be oil-wetting, and mixed-wet media (in which the solid surface is water-wetting in some places, and oil-wetting in others) are also common. As the terminology implies, this is of particular interest in the petroleum industry, where it is found that oil can be readily pushed out of water-wetting rock by injecting water, but injecting water into oil-wetting rock takes more work and produces little oil.

3.4 Single-Fluid Transport Properties

In this section we consider permeability, dispersion, and electrical conductivity in a medium saturated with a single fluid. The subsequent Sect. 3.5 examines the more

complex case of a medium simultaneously occupied by two immiscible fluids, and restricts discussion to permeability. In both sections the presentation focuses on soil and rock, drawing on classical texts in the field (e.g., [7, 29, 36, 46, 60]) as well as the extensive literature of soil science, hydrology, and petroleum engineering.

The fundamental physics of flow in porous media is classical Newtonian mechanics, even though many natural porous media are not strictly Euclidean. The physics of porous media does not use concepts that are foreign to physicists, although discussions may seem opaque to physicists. The soil science community generally distinguishes between soil *physical* properties (comprehensive descriptions of the pore and particle space as well as mechanical properties), soil *hydraulic* properties (describing the flow of fluids through the medium), and soil *transport* properties (diffusion, electrical conductivity, dispersion, and advection of both sorbing and non-sorbing solutes). Such distinction between flow and transport masks the fact that all conductivities, whether thermal, electrical, or hydraulic, are proportionality coefficients in the same equation in which a flux, J, is proportional to the negative of a potential gradient, $-\nabla\Psi$. While the general problem of flow in porous media is described by the Navier-Stokes equations, at the low Reynolds number flows usually encountered in geological porous media this equation reduces to $J \propto -\nabla\Psi$, with the hydraulic conductivity as the proportionality constant. A major goal of soil science has been to predict hydraulic properties from physical properties, then to predict transport properties from the physical and hydraulic properties. Most treatments ("pedo-transfer functions") have been based either primarily on empiricism or on numerical simulations. This book shows an alternative path to making predictions of flow and transport properties.

It is surprisingly difficult to predict a porous medium's transport properties, as attested by the long history of attempts. For example, consider fluid flowing through a volume of sand, and suppose that the individual pores are short cylindrical tubes that connect at pore bodies. Flow through any individual tube is given by Poiseuille's law,

$$Q = -\frac{\pi r^4}{8\eta}\frac{\Delta P}{L}, \tag{3.2}$$

where Q is the flux (volume of fluid crossing a plane normal to the tube's axis in unit time, having units $\mathrm{L}^3\,\mathrm{T}^{-1}$), r is the tube's radius (L), η is the fluid's dynamic viscosity ($\mathrm{M\,L}^{-1}\,\mathrm{T}^{-1}$), and ΔP is the pressure drop in the fluid over a distance L. In this formulation, pressure is given as energy per unit volume, with units $\mathrm{L\,M}^{-1}\,\mathrm{T}^{-2}$.

If we know the porosity of the sand, and the distribution of r within it, can we predict an effective conductivity for the whole medium? The widely-used Kozeny-Carman equation [19, 82] uses the mean radius of the solid particles, r_s, to give

$$q \equiv \frac{Q}{A} = -\frac{\Phi^2}{45\eta} r_s^2 \phi^3 \frac{\Delta P}{L}, \tag{3.3}$$

where the flux density q has units of velocity, A (L^2) is the cross-sectional area through which flow occurs, and the sphericity Φ of the particles corrects for non-spherical shapes. This relationship works fairly well for laminar flow through a bed

Table 3.1 The three Pythagorean means, and what they imply when applied to a general conductivity g. The weights, given here as volume fractions f_i, are assumed to sum to 1

Mean	Equation	Hölder exponent	Implied topology of a resistor network
Arithmetic	$\langle g_a \rangle = \sum_{i=1}^{N} f_i g_i$	1	Resistors in parallel
Geometric	$\langle g_g \rangle = \prod_{i=1}^{N} g_i^{f_i}$	0	Resistors in a random 2D lattice
Harmonic	$\langle g_h \rangle = 1/\sum_{i=1}^{N} \frac{f_i}{g_i}$	-1	Resistors in series

of randomly packed round particles with a narrow particle size distribution, but as these many qualifiers indicate, this is far from a general relationship. The equation was derived by assuming that the particles form equivalent tubes extending the entire length of the medium, such that flow in each tube is parallel to flow in all other tubes [7]. Semi-empirical corrections then adjust for the tortuosity of the flow (the deviation from straight-line travel along each individual flowpath), the converging-diverging nature of the porespace, and the non-circular cross-sections of the pore throats. If a wide pore size distribution is used, the permeability predictions differ widely from measured values [10].

The Kozeny-Carman equation (Eq. (3.3)) serves to illustrate several points that apply broadly to studies of transport in porous media. First, the field of porous media has a long history of empirical relationships, many of which still form the basis of engineering practice and give reasonable values within their established range of variables. Second, many of these empiricisms predict a property using measurements that are not closely related to the property of interest, but which happen to be available: for example, it is relatively easy to measure porosity and particle size. Third, many semi-empirical methods use good physics reasoning in calculating the behavior of a single pore: for example, in a single-phase flow calculation it makes sense to abstract the porespace as being composed of cylindrical pores, or slit pores if those are more appropriate. Fourth, empirical corrections such as tortuosity often take on a life of their own, although there is little agreement as to what they actually mean or how to assign values to them. And finally, historically the greatest conceptual difficulty has involved the issue of upscaling from a single pore to the whole porous medium.

Upscaling from pore to medium is central to what percolation theory contributes to the field of porous media. However, upscaling is conventionally performed through the use of a mean. The three best-known means, dating back to Pythagoras, are the arithmetic mean, the geometric mean, and the harmonic mean (Table 3.1). When these means are applied to conductivity, each implies a specific topology or connectivity. Clearly the effective conductivity cannot exceed the arithmetic mean, because the pores cannot be more parallel than parallel; neither can the effective conductivity be less than the harmonic mean, because pores cannot be more serial than serial. But these bounding cases represent special topologies that don't represent most natural materials: most porous materials are disordered, intermediate to these two bounding cases. In fact, there is little consensus in the

porous media community regarding which mean (if any) applies to a given physical situation. For example, "The effective conductivity is found to be the harmonic mean for one-dimensional flow, the geometric mean for two-dimensional flow, and [7/6 times the log variance, times] the geometric mean for three-dimensional flow" [55]. This fundamental confusion underlies most of the mistaken efforts in "upscaling."

Scheibe and Yabusaki [121] argued that the upscaled hydraulic conductivity must lie somewhere between the harmonic and the arithmetic mean, and that the appropriate upscaling condition had to be consistent with

$$\langle g \rangle = \left[\sum (g_i)^{-z} \right]^{-z} \tag{3.4}$$

choosing some exponent z in $-1 < z < 1$. They then used extensive modeling to try to identify trends of the exponent z. It is true that for any specific case, some value of z in Eq. (3.4) must yield the correct value of $\langle g \rangle$. However, their conclusion does not follow, as variations in the required value of z do not track observable variables logically or predictably.

Efforts to predict a porous medium's transport properties have often focused on the fact that the actual fluid pathways through the material are typically longer than the straight-line distance. The ratio of these two distances, called the tortuosity and denoted τ (with $\tau \geq 1$), is frequently invoked in derivations, but in practice is often used as a fitting parameter [27], often with physically nonsensical values. Tortuosity and connectivity are considered as separate and independent of the averaging, such that they are then "added in" later, usually in an empirical manner to bring the predictions closer to measurement. Tortuosity and its applications will be discussed more in Chap. 11; for now we simply remark that the concept is widespread but inconsistently used.

The problem of assigning an effective property to an inhomogeneous material is variously called homogenization, effective medium theory, or theory of composites. This area of physics remains largely unknown to most soil scientists and hydrologists, so various empirical approaches have come into practice. These tend to be specific to the problem at hand, developed without explicitly recognizing that homogenization is being performed. Apparently unrelated disciplines may use similar empiricisms, and yet one discipline may use multiple empiricisms for different manifestations of the same underlying physical process. For example, in soil physics, description of three related processes—solute (liquid-phase) diffusion, gas-phase diffusion, and electrical conductivity—use different, unrelated empirical constitutive relationships for their saturation dependence, yet we show here that they all follow the identical relationship, Eq. (2.8) or equivalently, Eq. (2.11).

All measurements take place at some scale, but the soil science and hydrology communities have a mixed record of recognizing this. Geological porous media are quite variable, but traditionally variability has been "handled" by assuming that above some scale, the "representative elementary volume" or REV, the properties become constant and invariant with position. For example, measuring porosity of a sand dune (mean diameter 1 mm) at the μm^3 scale will return values from 0 to 1. At the mm^3 scale, individual measurements will still vary significantly, and not until the

measurement scale is around a cm^3 will individual measurements be close to each other. The REV for a given property is the scale at which repeated measurements return similar results [7]. Similar thinking is found in the field of geostatistics [70], which describes how variability between samples taken from nearby locations is a function of the distance between them. Most geostatistical models assume that beyond some separation distance the samples are independent of each other, so at large distances the sample-to-sample variability reflects a system-scale variance. That is, both the REV and geostatistics reinforce the assumption that variability has an upper scale, above which properties may be averaged. This assumption is both unnecessary, and frequently misleading. What percolation theory has to say about the REV is treated in Chap. 9.

The derivation of an expression for an effective hydraulic or electrical conductivity at a larger scale, in terms of the variability it exhibits at smaller (e.g., pore) scales, is termed "upscaling" in the porous media community. However, we make no distinction between upscaling at the pore scale and upscaling at larger scales, such as field scales in soils or formation scales in rocks. The particular strategy may change with scale, but percolation theory must in principle be relevant at all scales. Interestingly, the porous media community views these two cases quite differently.

3.4.1 Permeability

The permeability of a porous medium is its capacity to transmit a flowing fluid. A medium's permeability is a property of great practical value: for example, it should be low for a dam, but high for a catalytic converter. The science of fluid flow in porous media is based on the Navier-Stokes equations, although the treatment might be more accurate if interactions between the water and the particles were included. For our purposes it is not necessary to consider the full Navier-Stokes equations, because when velocity advection is not important (low Reynolds numbers, laminar flow) the Navier-Stokes equations reduce to linear response, analogous to Fourier's law for heat conduction, Ohm's law for electrical conduction, and Fick's law for diffusion. Considering typical pore radii in the micron to millimeter range, and typical flow velocities less than 10^{-3} cm/s, one finds Reynolds numbers as low as 10^{-5}, and the linear approximation is seldom in jeopardy [7].

In the porous media community, this linear response—the flow is proportional to the pressure gradient—is known as Darcy's law, which in 1D macroscopic form can be written

$$q = -\frac{k}{\eta}\frac{\Delta P}{L}, \tag{3.5}$$

where the coefficient of permeability k (L^2), usually just called the permeability, is considered an intrinsic property of the medium. If pressure is expressed in terms of the height of the water column required to produce it, $h \equiv P/\rho g$, then the pressure gradient is unitless. Conveniently, gravity-driven flow in a column of arbitrary

height, with no water ponded on the surface, produces what is called a unit gradient, i.e., a pressure gradient $\Delta P/L = h/h = 1$. Meanwhile, multiplying k by $\rho g/\eta$ gives the "hydraulic conductivity" K, a proportionality coefficient with units of length per time. Expressing K as a velocity gives a measure of how fast water with a given depth can "infiltrate" into the soil, and also gives an estimate of the pore-scale water velocity.

Because Eq. (3.5) separates the medium's property of permeability from the fluid's property of viscosity, we can in theory measure permeability of a medium using one fluid, and apply that result to a different fluid. But in practice this may not work, because fluids vary in their interaction with the medium. For example, measuring permeability of a clay soil to both air and water will give a higher value for air, because water is much denser than air and wets the clay surfaces whereas air does not; more fluid interaction with the medium results in greater resistance adjacent to the solid surface. This issue can be important, for example in porous media with high specific surface areas when we compare strongly wetting and strongly non-wetting fluids, but we ignore it in this book. We also do not devote much space to the issue of anisotropy, even though it is common in geological materials.

As implied by the units of permeability (L^2), permeability scales with the square of the pore size; the Kozeny-Carman equation's (Eq. (3.3)) squaring the characteristic length makes physical sense. (The fourth power in the Poiseuille equation, Eq. (3.2), is decreased by the square of the radius when we assume that the medium has a constant volume.) More broadly, soil scientists recognize so-called Miller-similarity [97], in which properties of soils that differ only in their characteristic length scale (e.g., mean pore size) can be scaled through simple dimensional analysis.

The experiment which resulted in Darcy's [33] law involved measuring both the flux of water through a vertical column filled with uniform sand, and the pressure drop across the length of the column. The basic procedure has not changed much [110], although nowadays one typically uses samples that are 5–10 cm tall in contrast to Darcy's 3.5 m column. The procedure is subject to several confounding influences that can be difficult to control:

- If the sample is not completely saturated with the test fluid, then the measured permeability will be less than it would be at complete saturation; this is especially true if a wetting liquid is used (because the non-wetting liquid will preferentially partition into larger pores which contribute more to flow; see the next section).
- The porespace must not change over the course of the measurement, as for example by microbial growth clogging the pores, particles being entrained and moved by the flowing fluid, or gas exsolving from the flowing liquid.
- Fluid flow must be slow enough to avoid turbulence, but if it is too slow, especially with flow of a wetting liquid through a high surface area medium, some non-Newtonian artifacts may appear [127].
- When working with a loose material such as sand, packing the column to the correct density is no guarantee that the properties of the native material are reproduced, because both intact and disturbed materials are likely to have some internal stratification which can affect the end result. Additionally, coarse round

particles in a column yield a locally high porosity around the perimeter, and the "wall flow" through this region can significantly increase the flux.

- Loose materials must be held against falling out of the column, and the end cap used for this purpose contributes hydraulic resistance which should be accounted for, but which rarely is in practice. Interestingly, Darcy's [33] experimental setup (his Plate 24, Fig. 3) shows this exact error: he did not separate the pressure drop across the end material from that in the sand, and this same error is still common (e.g., [76]).
- Consolidated materials present their own challenges. For example, if a soil is sampled dry and then wetted, it may expand; if it is sampled moist and then dried for measuring permeability with a gas, it may shrink, creating wall flow artifacts much greater than those seen in a column of loose sand or gravel. So-called shrink-swell soils therefore present additional measurement issues.

Permeability can also be estimated from ancillary data, and such estimates constitute a significant thread in current soil and hydrologic research. The problem is complex because it is not only the texture (particle size distribution) and porosity that determine permeability, but also the degree of randomness of the porespace, which is difficult to quantify and is dynamic in some materials (e.g., soils). The current state of the art uses artificial neural networks, illustrating both the recognition of complexity, and an implicit concession that a sound physically-based method may not be found.

Given the current understanding of the permeability (or hydraulic conductivity) of porous media, there are no exact results for media with an arbitrary microstructure. As a consequence there has been some interest in developing upper and lower bounds of the hydraulic conductivity and exact solutions of simplified problems. A summary of such results is given by Sahimi [115, 116]. These results include slow fluid flow through a dilute cubic array of non-permeable spheres by the Stokes equation [59]; an extension of this result to all three types of cubic lattices [119]; the same problem using a transformation to a set of Fredholm's integral equations of the first kind [150]; harmonic expansions in spherical coordinates for cubic packings [85]; and treatments of Childress [24], Howells [63], and Hinch [62]. Other results are for mixtures in which both components are permeable, including solutions for upper and lower bounds of the hydraulic conductivity [12, 108, 144, 145]. Sahimi comments, "in all cases that have been discussed so far [several more than those mentioned here], the Kozeny-Carman empirical formula falls within 15 % of the results for at least one of the three types of periodic packings if [the porosity is less than half]" [115]. On the other hand, in disordered media the Kozeny-Carman prediction of K came in dead last when compared with treatments by Katz and Thompson [73], Johnson and Schwartz [69], and Bernabé and Revil [11], missing the numerically verified result by orders of magnitude [10].

We mention here the upper bound, k_0, on the permeability of a collection of solid spheres [132], given as

$$k_0 = \frac{2}{9}\frac{\langle r^3\rangle^2}{(1-\phi)\langle r\rangle^2} \approx \frac{2}{9}\left(\frac{5-D_s}{6-D_s}\right)^2\left[1+2\left(\frac{r_0}{r_m}\right)^{5-D} - 2\left(\frac{r_0}{r_m}\right)^{6-D}\right]\frac{r_m^2}{1-\phi} \tag{3.6}$$

Here r refers to the particles, i.e., the solid space. The expression is written explicitly for the Rieu and Sposito model (Chap. 4), and the result for k_0 is, asymptotically in the "polydisperse limit" (large range of sizes), a constant factor times the square of the largest particle size, r_{m}. r_{m} will typically be proportional to the maximum pore radius, with the proportionality constant a diminishing function of the porosity; however, neither ϕ nor $(1-\phi)$ to a negative power is such a function. Clearly Eq. (3.6) is larger than Kozeny-Carman treatments (Eq. (3.3)), consistent with its being an upper bound. The Stokes dilute-limit permeability follows the same general form [132], with slightly different second and third terms in the square brackets. These dilute-limit results do not apply in the limit of small porosity, where the permeability must vanish. But k_0, as in the various theoretical approaches summarized in Bernabé and Bruderer [10], is proportional to the square of a maximum radius. This kind of result is generated by critical path analyses as well [65, 73]. It is interesting that Eq. (3.6), like Eq. (3.3), produces a factor of $1-\phi$ in the denominator, but unlike Eq. (3.3), Eq. (3.6) does not produce a proportionality to ϕ in the numerator.

In strongly disordered media, the weighting function that is applied to local conductivities to generate the system conductivity is not monotonic in the conductivity. The weighting function thus cannot be consistent with a power-law averaging. This has been verified both in solid state applications (see [94, 106]) and for fluid flow in porous media [10]. This non-monotonicity occurs because the quasi-one-dimensional paths, along which the optimal conduction occurs, are dominated by the largest resistances on these paths. Smaller resistances in series are so much smaller that they do not contribute substantially to the total resistance; larger resistances in parallel are never encountered. As stated by Bernabé and Bruderer [10], the pressure field for strongly disordered media is controlled by a few large potential drops due to the critical elements (bottlenecks), making stochastic (small-disorder = homogeneous in the mean) treatments unappealing. Only approaches that are based in percolation theory are consistent with this observation.

3.4.2 Dispersion

Dispersion involves the displacement of one fluid by second with which the first is infinitely miscible. For example, when water with a dissolved contaminant flows into a previously uncontaminated aquifer, the contaminated water disperses into the uncontaminated water. The contaminated water does not propagate as a stable front moving at the mean velocity of the incoming water (what is called "piston flow"); rather, it disperses due to multiple factors. Of these we identify three: the different

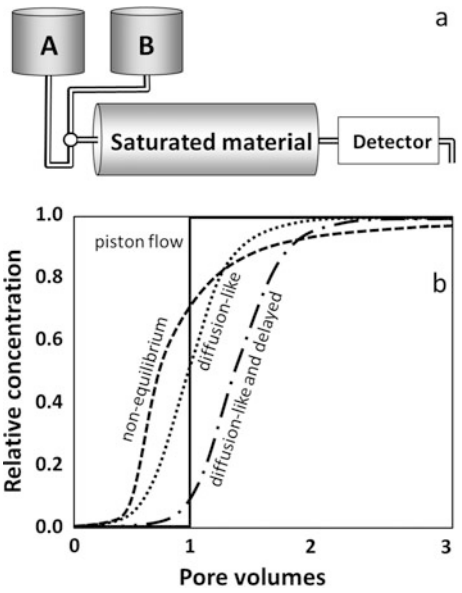

Fig. 3.4 **a**: Simple apparatus for measuring dispersion in saturated flow. **b**: 4 example breakthrough curves

flow velocities operating at multiple scales due to different pore sizes and pore structures, diffusion across what may be a fairly steep concentration gradient, and chemical interactions that may either retard (e.g., sorption) or accelerate (e.g., attaching to a mobile colloid that is excluded from small pores) an individual molecule's movement. In experiments, chemical interactions can be largely eliminated through the use of non-reacting tracers. The relative roles of flow heterogeneity and diffusion depend on the heterogeneity of the porous medium, and the relative rates of advection and diffusion. The observed dispersion—the extent of spreading of the front—varies with time, distance, and flow rate, in addition to various properties of the fluid and the porous medium.

The experimental apparatus needed to measure dispersion is quite simple (Fig. 3.4a). For a simple experiment, the flow rate should remain constant, and there should be minimal mixing of solutions A and B outside the soil column, e.g. in the tubing and end caps of the column. Typically the medium is saturated with solution A, steady-state flow is established with solution A, then the valve changes the input fluid from A to B. The data are generally presented as a "breakthrough curve" (Fig. 3.4b), with the x-axis being the volume of fluid normalized by the pore volume of the sample, and the y-axis being the relative concentration of solution B.

As Danckwerts pointed out, the breakthrough curves typically observed lie between the extremes of piston flow and complete mixing (not shown in Fig. 3.4). Certainly in some specific cases (e.g., a single tube, [129]) the dispersion can be treated as a diffusion analog in a physically consistent manner, so diffusion was an analogy worth examining. But the CDE's failure to capture either the behavior (shape of the curve) or the physics (scaling with time, distance, and velocity) indicates that it is an incorrect phenomenology, and several decades of poor predictions

indicate the need for an improved conceptual model. From this perspective, the CDE is yet another failed attempt to upscale directly from one tube to many tubes to a whole porous medium.

The most common mathematical model used to characterize breakthrough curves is the convection-dispersion equation (CDE; also called the advection-dispersion equation or ADE), typically given in 1-dimensional form as

$$R\frac{\partial C}{\partial t} = D\frac{\partial^2 C}{\partial x^2} - v\frac{\partial C}{\partial x} \tag{3.7}$$

for solute concentration C ($\mathrm{M\,L^{-3}}$), retardation R (unitless), dispersion coefficient D ($\mathrm{L^2\,T^{-1}}$), and constant velocity v ($\mathrm{L\,T^{-1}}$). The CDE is based on the assumption that dispersion in a porous medium is diffusion-like, an analogy that goes back at least to Danckverts [32]. The equation can be readily modified to account for sources and sinks, sorption/desorption and other reactions, and degradation, and analytical solutions have been derived for a variety of initial and boundary conditions (e.g., [149]). The CDE is widely used to predict e.g. dispersion of pollutants in aquifers, but it suffers from many inconsistencies and errors that mainly emerge when comparing across scales. Most notably (1) it is widely observed (e.g., [49, 77, 138]) that the dispersion coefficient increases linearly with velocity, although the equation itself does not show that it should; because of this observation, the propensity of a medium to disperse a solute is often given as the dispersivity α (where $\alpha = D/v$). (2) The spreading (variance) of the solute is ordinarily observed [123] to scale with distance with an exponent 2 rather than the linear dependence predicted by the CDE. And (3) the shape of the breakthrough curve frequently [47] differs from what a diffusion-like process would produce.

Because the CDE often gives poor fits and predictions, alternative models have been developed. The mobile-immobile model (MIM) posits that flow occurs in two separate domains, one dominated by advective flow and the other by diffusion. Flow in the advective domain is governed by the CDE, in tandem with diffusive (or first-order) exchange between the two domains. The MIM produces curves like the "non-equilibrium" curve in Fig. 3.4. This fit some datasets better than the CDE, but at the cost of two additional parameters (the fraction of the porosity that is "mobile", and the mass exchange coefficient). Scaling of the variance with time and/or distance is still linear. Another alternative, the transfer function model (and especially the popular convective lognormal transfer function, CLT; [139]) proposes that flow moves through parallel "streamtubes" that differ in velocity, but with no dispersion within or between streamtubes. The resulting breakthrough curve has a variance that scales with time or distance squared (as is often observed), but because it assumes a specific distribution of velocities it does not always give good fits. Like the other models, it does not explain why dispersion should scale with velocity.

The continuous time random walk (CTRW; [8, 78, 122, 123]) model, developed in the context of hopping transport in semiconductors ([122], for example), provides an alternative to the previous models. The CTRW is a very general transport model that does not make explicit reference to (for example) pores, viscosity, or diffusion. The CTRW can cover a range of scaling behaviors with respect to time or distance,

and a single parameter controls both the shape of the breakthrough curve, and the scaling exponent. This parameter is empirical (fitted) rather than being derived from more fundamental properties of the medium, but aside from this one shortcoming the CTRW is the best solute dispersion model in common use at this time.

As pointed out already 25 years ago [117], percolation scaling, justified by the relevance of critical path analysis, offers a reasonable explanation for the scaling properties of the dispersion. What we will show is that a full percolation treatment, consistent with scaling concepts and critical path analysis, makes a much wider range of verifiable predictions. Although we have not found a simple correspondence between this percolation treatment and CTRW, that correspondence may yet be found.

3.4.3 Electrical Conductivity

To a first approximation, electrons flowing through saturated soil or rock travel through the liquid, rather than through the solids or along the liquid/solid interface. For flow through a tube, electrical conductivity scales with the cross-sectional area available to the current. In the case of a saturated isotropic medium, the cross-sectional area is equal to the porosity, so we might expect that saturated electrical conductivity would scale with the porosity. What is observed, however, is not a linear relationship in ϕ. This is partly because in some media, non-negligible current flows along the interface (e.g., [22, 111]); the other cause is that flowpaths become sparser and more tortuous as porosity decreases, phenomena well described by percolation theory.

In geophysics and petroleum engineering, rock is often characterized by its formation factor F, given as

$$F \equiv \frac{R_0}{R_w} \tag{3.8}$$

where R is electrical resistivity, and the subscripts 0 and w respectively denote the saturated medium and the saturating fluid [29]. In the case of a saturated rock, Archie [2] observed that

$$F = a\phi^{-m} \tag{3.9}$$

where the prefactor a is ascribed to tortuosity, and the exponent m (usually in the range 1.5–2.0) is attributed to the degree of cementation of the rock. This empirical relationship has been accorded the status of a law ("Archie's law") in the geophysics literature, although it lacks a theoretical basis [74]. Archie's law will be further addressed in Chap. 6, where we show the connection with universal scaling of conduction.

In addition to porosity and tortuosity, one may also find discussion of constrictivity [136], the ratio between the radius of a pore body and a pore throat. This is another example of focusing on detailed properties of individual pores, while ignoring the more significant issues involved in upscaling from pore to porous medium.

3.5 Multiple-Fluid Properties and the Role of Pore Occupancy

When a porous medium is occupied by two immiscible fluids, how the fluids are distributed within the pores varies according to specific properties of the solid (pore size distribution, pore connectivity, and surface chemistry), the liquids (especially how polar they are, and their interfacial energy), and the history by which they came to be there. In this section we discuss pore occupancy and its consequences, as it is central to understanding transport in unsaturated media.

Historically, hydrologists and civil engineers have focused mainly on saturated media, where the process of interest is flow. In contrast, soil scientists and petroleum engineers have concentrated on unsaturated media, where retention or storage is equally important and two-phase systems are the norm. The physics of soil is in many ways similar to the physics of petroleum reservoirs, and of aquifers contaminated with a non-polar pollutant: in each case, two different fluids compete to occupy the pores, and the several similar processes lend themselves to similar analyses.

Under most conditions, a geological porous medium's pore space is completely occupied by air and/or water. The volume fraction of the water is usually denoted θ, and the air-filled porosity ε. Assuming a constant volume, $\phi = \theta + \varepsilon$. Again, under most conditions in geological porous media, water is the wetting fluid and air the non-wetting. For simplicity the following is largely presented in terms of air and water, but is not limited to them.

3.5.1 Wettability, Pore Size, and Capillarity

When water and air touch each other and a flat solid surface (Fig. 3.5a) in a static configuration, forces must balance at the contact point as given in Young's equation:

$$\gamma_{sa} = \gamma_{sw} + \gamma_{wa} \cos \alpha, \tag{3.10}$$

where γ is interfacial energy ($\mathrm{M\,T^{-2}}$), α is the contact angle, and the subscripts s, w, and a respectively denote solid, water, and air. Generally one fluid wets (has contact angle $<90°$) the solid, in which case we refer to it as the wetting fluid and the other as the non-wetting fluid. Note that a given fluid may be either wetting or non-wetting, depending on what the other fluid is: oil wets mineral surfaces when competing with air, but not when competing with water. Unless otherwise specified, "saturated" implies saturation with the wetting fluid.

A curved interface between two immiscible fluids indicates a pressure difference. For example, in Fig. 3.5a, the water is at a slightly higher pressure than the air. The pressure difference, called the capillary pressure p_{cap}, is related to the meniscus curvature by the Young-Laplace equation:

$$p_{cap} = p_w - p_a = \gamma_{wa}\left(\frac{1}{r_1} + \frac{1}{r_2}\right), \tag{3.11}$$

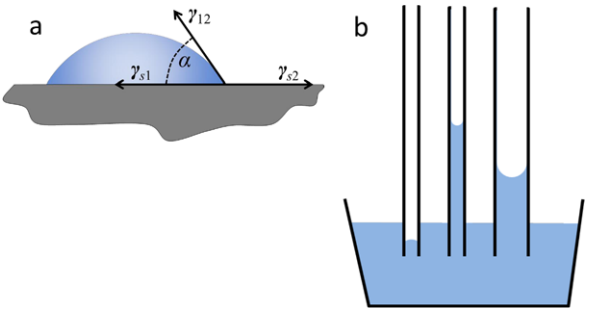

Fig. 3.5 **a**: Forces acting at the contact point of a solid and two fluids. **b**: Capillary rise in three tubes with different radii and contact angles. The *left tube* is hydrophobic, while the *center* and *right tubes* are hydrophilic

where the relevant interfacial energy γ is that between the two fluids, and r denotes the radius of meniscus curvature, with subscripts 1 and 2 denoting (any) two orthogonal directions. For the case of capillary rise, with liquid at equilibrium in a vertical tube with circular cross-section (Fig. 3.5b), the downward force is $\pi r^2 h(\rho_w - \rho_a)g$, balanced by the upward capillary force $2\pi r\gamma \cos(\alpha)$. Rearranging gives the capillary equation

$$h = \frac{2\gamma \cos\alpha}{(\rho_w - \rho_a)gr} \tag{3.12}$$

for height of rise h, gravitational acceleration g, tube radius r, and fluid densities ρ_w and ρ_a. Notice that all water in the tube that is above the free water surface is at a negative pressure. Because pressure is exerted by a standing column of water, earth scientists often express pressure in terms of the height of the water column required to produce it. For a given solid (constant contact angle) and pair of fluids (constant surface energy and density difference), the capillary equation reduces to $h = A/r$. Interpreting h as a capillary pressure, the practical import is that the capillary pressure required to push a non-wetting fluid into a pore, or to pull a wetting fluid out of a pore, is inversely proportional to the pore's (effective) radius.

The physics concept of capillary rise in a tube is related to the concept of water potential in the soil, a unifying concept that goes back to Buckingham [16]. Suppose that a tube (manometer) is connected through a porous cup to a porous medium at a position above the free water surface or water table, as in Fig. 3.6. The height of water in the manometer, $-h$, is negative relative to the height of the porous ceramic cap in the soil, and the water pressure in the soil is less than the atmospheric pressure P_a at the air/water interface by $P = -(\rho_w - \rho_a)gh$. Likewise, the positive height in the manometer having its porous cap below the water table indicates a positive pressure at that location. h is thus energy per unit weight (in a given volume), called pressure head when positive, matric head when negative, or often just head. If instead we used energy per unit volume, we would have a pressure ($\mathrm{M\,L^{-1}\,T^{-2}}$); if we used energy per unit mass, e.g. $\mathrm{J\,kg^{-1}}$, we would have units $\mathrm{L^2\,T^{-2}}$. Because the main components of potential (and the main drivers of flow) in geological porous media are pressure and elevation, it is convenient to express the potential in equivalent heights.

The energy state (potential) of the water in soil is defined with respect to pure water at a reference elevation, and at standard (or some other reference) temperature

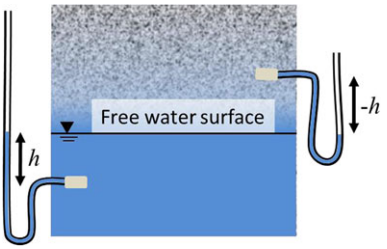

Fig. 3.6 A soil profile, with water at equilibrium with the water table. Water in the manometers connects to the soil water through a porous ceramic cap. Water in the soil above the water table is at a negative pressure given by its height above the water table; water below the water table is at a positive pressure

and pressure. Specifically, the water's potential is the work per unit weight that must be done on an infinitesimally small amount of pure water to bring it into the soil from the reference pressure and elevation. (The stipulation "small amount" is a necessary condition so as to prevent the change in water content from changing the condition of the soil. A similar stipulation applies in electrodynamics, where a field is to be detected with an arbitrarily small test charge.) As this statement implies, the energy state of water is affected by elevation, pressure (positive or negative), the presence of solutes, and temperature. The potential's several components are additive, thus the total potential Ψ is the sum of the elevation potential z, the osmotic potential P, the pressure potential h, and so on.

The presence of solutes in liquid water lowers the partial pressure of water vapor across a flat interface, an effect similar to that of a curved interface as expressed by the Kelvin equation. Note that dissolved salts will change the surface energy and viscosity of the water in addition to decreasing its osmotic potential. The complex effect of temperature, while occasionally acknowledged, is largely ignored in the earth science literature, as is the complex coupling of heat and water movement. Likewise, in this monograph we will largely ignore thermal and osmotic contributions to water potential, focusing on pressure.

Given the questionable assumptions involved in applying the capillary equation to soil and rock, it is remarkable that it has proven so useful. The assumption of a smooth surface is clearly incorrect for most natural materials. The effect of the contact angle is modified by the surface roughness, as manifest in such phenomena as super-hydrophobicity [83]. Calculating capillary rise is more complex even for something as simple as a sinusoidally varying smooth-walled tube [31], so faced with rough surfaces and multiple orientations, one generally makes the very practical assumption that pores are straight and smooth-walled. Likewise, one could assume that pores have non-circular cross-sections (e.g., [133]), but in practice circular cross-sections are almost always assumed. Finally, the assumption of a constant wetting angle is also incorrect for many natural materials. Soils are generally hydrophilic (water-wetting), but organic matter in the soil may be hydrophobic, and the organic matter content in soil changes with depth and position. Similarly, the mineral surfaces in oil reservoirs may change over geological time from hydrophilic to

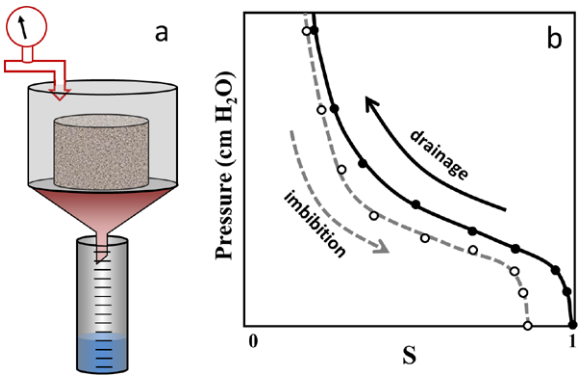

Fig. 3.7 **a**: Sketch of the apparatus for measuring the drainage limb of the pressure-saturation relationship. The porous plate at the bottom of the pressure chamber passes water (wetting fluid) but not air. **b**: An example pressure-saturation relationship, showing both drainage (drying) and imbibition (wetting). The x-axis gives relative saturation, abbreviated S $(= \theta/\phi)$

hydrophobic, for example by tarry substances precipitating into patches on the rock. This gives rise to the so-called "mixed-wet" condition, in which both hydrophobic and hydrophilic patches are found throughout the solid surface [126].

It is convenient to assume that at any given time, a pore is completely occupied by either the wetting or the non-wetting fluid. This useful concept, called the *strong wetting assumption*, is correct mainly at the extremes, when the medium is occupied only by a single fluid. In intermediate cases, a pore that is largely occupied by non-wetting fluid may still have wetting fluid covering the surfaces. For a smooth solid surface this occurs only if the contact angle is zero, but the pits and cracks on rough surfaces may hold non-negligible quantities of water [130]. Water is also held in the form of pendular structures (capillary bridges) around the point of contact of two solid grains [103, 112, 134]. Estimates of the fraction of water in these locales vary, but more important than the quantity is that this non-pore-filling fluid can maintain continuity of a strongly wetting fluid.

3.5.2 The Pressure-Saturation or Water Retention Curve (WRC)

The relationships between capillary rise, pore sizes, and pressure difference across the air/water interface make possible a procedure for measuring the pore size distribution. We start with the observation that, for an imposed pressure difference P between air and water, we can calculate the equivalent head: $P/\rho g = h$. At equilibrium, only those pores with radius $r < A/h$ will contain water.

Removing water from an initially saturated medium requires work, which in a laboratory setting is usually applied in the form of an imposed air pressure. The saturated sample is subjected to sequentially increased air pressures, and the expelled water is measured at each step (Fig. 3.7). The chamber holding the sample must

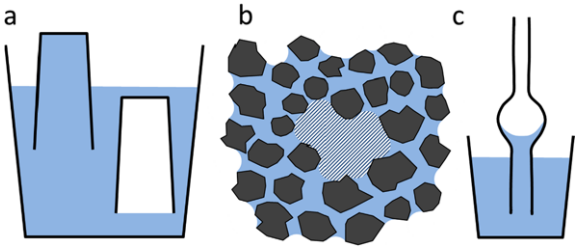

Fig. 3.8 **a**: The drinking cups are prevented from draining or filling solely by accessibility. **b**: A large pore (striped) prevented from draining by water-filled smaller pores surrounding it. **c**: An "inkbottle" pore, a minor contributor to hysteresis in the pressure-saturation curves. Adapted from [66]

withstand the pressure without leaking, as even a small air leak sustained over many days may artifactually dry the sample. A key component is the material on which the sample rests: it must be permeable to water, but not to air, at the pressures applied. In typical laboratory settings this is a sintered glass or ceramic. Sufficient time must be allowed for each step, so the water will drain to equilibrium with the imposed air pressure. For typical soil samples (5–10 cm high), the approach to equilibration at low pressure may take a day, but time to equilibrium increases rapidly as the sample desaturates; this issue is discussed more in Chap. 8.

The relationship shown in Fig. 3.7b, and especially just the drainage curve, is variously called a pressure-saturation curve, a water retention or water release curve (WRC), and a soil water characteristic curve. The saturation may be given as volume fraction of water θ, or as relative saturation $S = \theta/\phi$. The drainage (or drying) curve is faster to measure than the imbibition (or wetting) curve, so often only it is actually measured, and the imbibition curve (if needed) is estimated. When drying starts from saturation a primary drying curve is produced; if instead drying started from the wet end of a wetting curve, a secondary drying curve (not shown) is produced. The relationship is hysteretic, for reasons discussed below.

We note in passing that the WRC shown in Fig. 3.7b violates the usual convention of showing the independent variable (pressure) on the x-axis. The reason is that, displayed this way, the drying curve shows the vertical saturation profile of the medium after it has drained to equilibrium, with the water table at the bottom (zero height = zero pressure).

The drainage process is essentially bond invasion percolation, and a percolation perspective informs our presentation. Draining a water-filled pore requires that three conditions be met (Fig. 3.8): the air pressure must be such that the pore will drain according to the capillary equation, air must be able to enter the pore (the pore must be on the air infinite cluster), and water must be able to leave the pore (the pore must be on the water infinite cluster). This third condition is guaranteed if we consider water flow through films covering the solid surface. The first condition makes the pore "allowable", while the second and third make it "accessible". This perspective is largely lacking in the earth sciences, where only allowability is considered.

Accessibility of a given pore requires it to be on the air/water interface. When a medium is close to saturation (very little air has penetrated into the pores), a large pore may be allowable without being accessible, and consequently will not drain (Fig. 3.8b). When the pore becomes accessible at a higher pressure, the volume of water that drains will be attributed to that higher pressure, resulting in under-estimation of large pores and over-estimation of smaller pores.

Two asymmetries distinguish wetting from drying and contribute to hysteresis. First, draining from an initially saturated state involves just one phase transitions: when air (non-wetting phase) first percolates. As the wetting phase, water is always continuous. But wetting from an initially dry condition involves two phase transitions: one when water first percolates, and one when air no longer percolates. The second asymmetry is that drainage is controlled by the pore necks, while imbibition is controlled by the pore bodies. Specifically, for a pore to be allowed to drain, the meniscus' radius of curvature must be less than the pore throat's radius, while for a pore to be allowed to imbibe, the meniscus radius must be greater than the pore body's radius. Consequently, the water content for a given tension (meniscus curvature) is always higher during drainage than during imbibition. This effect, which is not eliminated by film flow, is called the ink-bottle effect (Fig. 3.8c).

In the soil physics and hydrology literature, hysteresis between the drying and wetting curves is largely attributed to the ink-bottle effect. But the ink-bottle effect can contribute only a scalar shift to the curve [38]. Most hysteresis is caused by the distinction between allowability and accessibility: during imbibition, a small pore surrounded by large pores may not have access to water until the large pores have filled, delaying its filling. Meanwhile, a large pore surrounded by smaller pores (Fig. 3.8b) may not water-fill at all, because air in it is trapped, being unable to leave through the smaller pores. Trapping prevents the wetting curve from attaining full saturation (Fig. 3.7b) [38], a phenomenon which the inkbottle pore concept cannot explain. Both hysteresis and trapping are reduced by higher pore coordination, and by an increase in pore structure (preferential connection of larger pores) [39].

3.5.3 Obtaining a Pore Size Distribution

In principle, and if accessibility constraints are ignored, then analysis of $d\theta/dh$ from a WRC over the full range of h yields the pdf for the pore-size distribution. In the earth sciences it is widely assumed that the pore size distribution can be produced by translating the heights in the pressure-saturation curve into equivalent pore radii via the capillary equation (3.12). This appealing assumption forms the basis of the unsaturated hydraulic conductivity models (e.g. [17, 25, 98, 101]) used in soil, hydrologic, and climate models. But it is based on several questionable assumptions which are rarely acknowledged:

- The pore radius that controls drainage is the same pore radius that controls flow (but recall that each pore may have several throats, while drainage is triggered when the air-water interface passes through just one of them).

- The volume of water drained through a particular pore flows entirely within a pore of that radius (but recall that pores tend to have a converging/diverging geometry).
- The pores are effectively circular in cross-section and smooth-walled, enabling use of the same radius in both Poiseuille's law (3.2) and the capillary equation (3.12).
- The pores have a constant contact angle $\alpha = 0$ throughout the medium, although a different (but still constant) contact angle can be substituted if known.
- All water is pore-filling water (the strong wetting assumption): no water is held in films, surface pits and cracks, capillary bridges, etc.
- During measurement, the sample has time to drain to equilibrium (but equilibrium is reached asymptotically, so this is at best approximately correct).
- During measurement, all water in the sample is at the same matric potential (but this cannot be true, because the sample has non-zero height).
- During measurement, all pores that are allowable are also accessible (but this can be true only for a few special cases, e.g. all pores extend the entire length of the sample. Recall that drainage is an invasion percolation process).
- The sample is representative (which is difficult to assure, given the variability of geological materials).
- There is no effect of sample size on the results obtained (but note the contradiction between needing a large sample to be representative, and a small sample to avoid a height effect).

To echo an earlier comment, given the many questionable assumptions at play, it is remarkable how well predictions often work. Nonetheless, one cannot help but wonder how much better they would be if the physics were more comprehensive and defensible.

There are other methods available for obtaining a pore size distribution. A saturated salt solution can dramatically decrease the partial pressure of water, producing the equivalent of extremely low capillary pressures, such that the dry end of the pressure-saturation curve is sometimes produced by water vapor equilibration over saturated salt solutions (e.g., [72]). After water retention, the most common method used in the earth sciences is mercury intrusion [50, 142], which is analogous to the WRC: mercury (non-wetting) is injected at controlled pressure steps into a dry sample under vacuum (or, more strictly, saturated with mercury vapor). Mercury intrusion is not appropriate for samples that are deformable, as the pressures applied may be quite high. Other methods that are somewhat similar to water retention and mercury intrusion include the vapor equilibration over saturated salt solutions [72] and N_2 isotherms [5], both of which are appropriate for pores in the range (roughly) 0.5 nm to 0.5 μm. All of these methods show some degree of hysteresis and trapping, due to following an invasion percolation-like process. NMR-cryoporometry [143], which incrementally freezes water in the pores and uses NMR to detect the frozen volume, shows hysteresis suggesting an invasion-like pattern, and interpretation of the data is somewhat ambiguous.

Imaging methods such as serial sectioning with reconstruction [148] and X-ray microtomography [91] do not involve an invasion percolation-like process. They can give the entire pore network, from which the pore size distribution can be extracted.

Unfortunately, such methods are expensive, non-trivial to implement and limited by the trade-off between sample size and voxel size to a few orders of magnitude of pore sizes.

There are unfortunately few studies comparing pore size distributions obtained using different methods (e.g., [26]). To our knowledge, Dullien [35, 37] was the first to point out the discrepancy between soil water retention curves measured with different methods, e.g., mercury intrusion porosimetry and photomicrography. He noted that the mercury intrusion method gives the entry pore-size distribution, while the photomicrography technique provides the distribution of pore volume by all pore sizes. Pore-size distribution determined by photomicrography is closer to reality than the entry pore size given by mercury intrusion porosimetry [35]. In a related study, Hall et al. [57] measured the pore-size distribution of shaly rocks with several methods: small-angle neutron and X-ray scattering (SANS and SAXS), nitrogen adsorption, nitrogen desorption, and mercury intrusion porosimetry. They found that pore-size distributions measured by SANS and SAXS techniques were in reasonable agreement with those from the nitrogen adsorption isotherm, but often in disagreement with distributions derived from the nitrogen desorption isotherm and mercury porosimetry. The question "Which method of pore-size distribution measurement should be applied?" thus remains unanswered.

Sahimi [116] concluded that each measurement method has its own strong and weak points. For example, the success of mercury intrusion porosimetry and sorption isotherm methods requires prior knowledge of the pore space connectivity and pore shapes [116]. Pore shape also affects the pore-size distribution derived from scattering methods, and even if the shape is known, the calculated distribution may still be sensitive to the shape [116].

3.5.4 Widely Used Equations for the Water Retention Curve

Because the translation from water retention curve (WRC) to pore size distribution via the capillary equation (Eq. (3.12)) is so widely accepted, to a fair extent WRC models are considered to simultaneously be models of the pore size distribution. Nonetheless, there is an important difference between the two, centered on the concept of residual or irreducible water.

As a medium dries, the fraction of wetting fluid that is actually pore-filling decreases: an increasing fraction of the wetting fluid occurs as films, capillary bridges, and the like. Because film flow is quite slow compared with pore flow (Chap. 6), for practical reasons the dry end of the curve is not measured as frequently. Also recall that the WRC was developed in the context of agricultural soils, and many plants wilt if deprived of water at a pressure less than -1.5 MPa (15 bars, the tension created by a hanging water column some 153 m long), the so-called permanent wilting point. From an agricultural perspective, then, water held more tightly than -1.5 MPa is not worth considering, and soil water retention curves are generally measured only to that tension. In such cases the residual water, denoted θ_r, is specifically identified with the pressure -1.5 MPa. So where the petroleum engineers

speak of relative saturation, $S = \theta/\phi$, the soil scientists more often work with effective saturation, $S_e = (\theta - \theta_r)/(\phi - \theta_r)$.

One of the earliest, and still most widely used, equations for the pore size distribution is that developed by Brooks and Corey [15] (henceforth BC):

$$S_e = \left(\frac{h_A}{h}\right)^{\lambda} \tag{3.13}$$

where h_A is the air entry (also called bubbling) pressure, the smallest air pressure needed to drive air upward through the previously saturated sample, and the exponent λ reflects the width of the pore size distribution. BC explicitly measured h_A with air flowing upward to reduce the effect of the sample's height, considering it to be a physically meaningful parameter. Pressures h and h_A are always positive (like the air pressure in Fig. 3.7). As Brooks and Corey observe, this equation was "discovered by plotting log S_e as a function of log $h\gamma$ "—that is, the equation is empirical. Note that for $h < h_A$, we assume $S_e = 1$: no drainage occurs until the air entry pressure is attained, so the curve has a singularity. While the Brooks and Corey phenomenology was developed pragmatically, its power-law form lends itself easily to interpretations derived from fractal models of the medium, a chief topic of Chap. 4.

Motivated by the need for expressions that were both continuous (for numerical stability) and closed-form (for computational speed), van Genuchten (1980) proposed an empirical function chosen because it is flexible and gives the desired S-shaped curve. The now widely-used expression for the water retention curve (henceforth vG) is

$$S_e = \left[1 + \left(\frac{h}{h_i}\right)^{n}\right]^{-m} \tag{3.14}$$

where the exponent n characterizes the width of the pore size distribution, and m is usually constrained to take the value $m = 1 - 1/n$. The reference pressure h_i is at the curve's inflection point, an important conceptual difference between the BC and vG equations. In practice, vG is fit to data collected using an apparatus like that illustrated in Fig. 3.7a, in which water volume is averaged over the height of the sample. The vG parameters are fitted simultaneously, with θ_r and sometimes even ϕ considered fitted parameters. These changes effectively deprive vG's h_i of much of its physical meaning.

The wet end of the pressure-saturation curve is where h_A is measured; it is also the portion of the curve at which the hydraulic conductivity is greatest, so it bears careful measurement. But it is precisely at the wet end that height averaging is most pronounced. Even if the "real" curve has a BC-like singularity, averaging over progressively taller samples will produce increasingly smoother curves (Fig. 3.9). In a sense, then, the smooth vG is the result of interpreting and restricting data to the scale of measurement [23, 66, 92]. High-resolution pressure-saturation measurements (e.g., [71, 118]) imply that at least for some media, the "real" curve does indeed have a BC-like singularity. Jalbert and Dane [68] developed software for inferring the underlying BC from vG curves, and Cheng and Perfect [23] developed

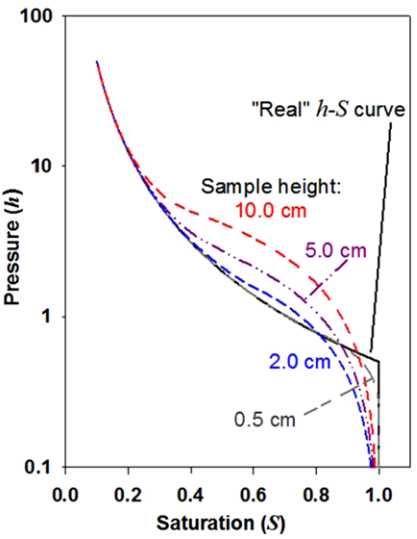

Fig. 3.9 Calculated effect of sample height on a measured pressure-saturation curve

a program for examining height effects on measured pressure-saturation curves of BC soils.

We mention three additional water retention curve models, to show both the range and diverse reasoning behind them. Clapp and Hornberger [25] proposed an expression similar to BC, but with a parabolic section at the wet end to remove the singularity. While their model is little used in soil physics, it is widely implemented in climate models (e.g., [102]). Kosugi [81] proposed that the pore size density distribution had a lognormal shape. His proposed model also attempts to address the difference between BC's h_A and vG's h_i by including both, resulting in a three-parameter model. Grant et al. [53] developed an equation designed to produce an incomplete gamma function when integrated in an unsaturated hydraulic conductivity model: the final function form was more important than dictates of the physical basis.

Because it is easier to measure the particle size distribution than the pore size distribution, there is long history of attempts to predict the pore size distribution (or the water retention curve) from the particle size distribution. Such predictive tools, called pedotransfer functions, are ubiquitous in soil, hydrologic, and climate models. Early point-wise statistical methods used regression models [54] to independently estimate individual points on the water retention curve. Other regression models [20, 25] predict the actual parameters of a water retention model. More recent statistical methods use neural networks [104, 120, 140]. Another class of models, so-called physico-empirical models [3, 45], attempts to construct the water retention curve through a weighted sum of the conjectured water retention curves of component particle-size classes.

3.5.5 Unsaturated Hydraulic Conductivity, $K(\theta)$

Transport through a medium occupied by two immiscible fluids is much more complex than the single-fluid case. Most obviously, the pressure difference that drives fluid flow also drives changes in pore occupancy, such that saturation may vary dynamically along the flowpath, with consequent changes in conductivity. But changes in saturation require fluid continuity: what happens when one fluid is trapped? More broadly, when can one of the two fluids be ignored?

In the simplest analysis, the fluid that is not of interest is assumed to be inert, as if it were part of the solid phase. This effectively changes the porosity and pore size distribution, recasting the problem as a saturated conductivity problem in a different medium. Most methods (our included) implicitly take this approach, although it ignores frictional differences between fluid-fluid and fluid-solid interfaces, including the reciprocal effects of friction due to simultaneous flow of two fluids [113]. However, making this assumption in deriving a $K(\theta)$ relationship does not then require ignoring the second fluid in a two-phase flow simulation!

The unsaturated conductivity is often given relative to the saturated conductivity, as reflected in the petroleum engineer's preferred term, relative permeability. Here we give a brief description of how one popular $K(\theta)$ model, that of Mualem [101], is derived.

Mualem [101] started by assuming that the pore size distribution $W(r)$ was known, from the smallest pore r_0 to the largest r_m, such that

$$\int_{r_0}^{r_\mathrm{m}} W(r)dr = \phi \tag{3.15}$$

He then assumed that at saturation, hydraulic conductivity cannot be given by a simple integration over all pore sizes, because large pores are not continuous across the sample. Instead, he supposed that conductivity was given by a joint probability distribution of $W(r)$ with itself, thereby allowing for random reconnection. At saturation, then, he expected saturated hydraulic conductivity, K_S, to be proportional to

$$K_\mathrm{S} \propto \left[\int_{r_0}^{r_\mathrm{m}} r\,W(r)dr\right]^2 \tag{3.16}$$

Because integration is an arithmetic mean, this implies that all pores are conducting in parallel (Table 3.1). Such an assumption is equivalent to a physical medium consisting of a bundle of (capillary) tubes. We have recently shown [66] what difficulties arise from using such models as a basis for upscaling any pore-scale process to medium scale measurements. This topic is considered in detail in Sect. 3.6.

Mualem then assumed that tortuosity and connectivity together have a multiplicative effect, and that their correction has the functional form $\tau \propto S_\mathrm{e}^l$ for some exponent l. Various values have been given for l; Mualem's choice of 0.5 was largely empirical.

Finally, Mualem assumed that the hydraulic conductivity at any arbitrary degree of saturation is given by changing the integration limits of Eq. (3.16), and adjusting

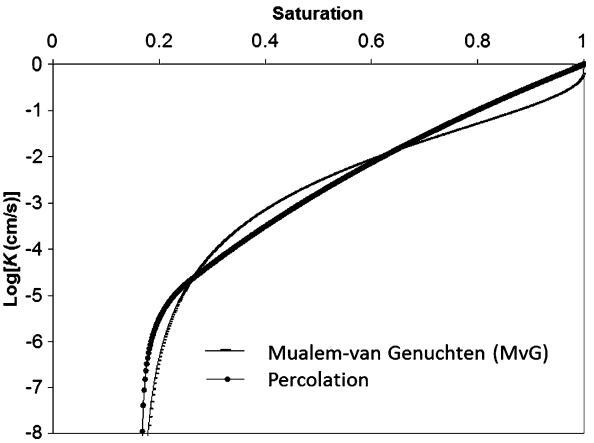

Fig. 3.10 Unsaturated hydraulic conductivity (K) curves predicted by Mualem and van Genuchten (MvG), and by percolation theory combined with critical path analysis. Note that MvG tends to infinite slope at full saturation, in contrast to the percolation-based prediction. The high slope near saturation accommodates the tendency for soil structure (e.g., cracks and wormholes) to strongly enhance K right near saturation

the value of S_e used for the tortuosity correction. Translating through the capillary equation, Mualem's equation for relative permeability is

$$\frac{K(\theta)}{K_S} = S_e^{0.5}\left[\frac{\int_0^\theta \frac{d\theta}{h}}{\int_0^\phi \frac{d\theta}{h}}\right]^2 \tag{3.17}$$

Note that integration from zero implies that pores that are water-filled at θ_r are contributing to flow, even though their "residual" status implies that they cannot drain.

Van Genuchten's [137] WRC equation, Eq. (3.14), allows integration, so using it to replace the integrals in Eq. (3.17) gives (henceforth MvG)

$$\frac{K(\theta)}{K_S} = S_e^{0.5}\left[1-\left(1-S_e^{1/m}\right)^m\right]^2 \tag{3.18}$$

A graphical comparison of Eq. (3.18) with the results for K from critical path analysis (Chap. 5) is given in Fig. 3.10. MvG produces a sigmoidal curve, as is typically observed for the (logarithm of the) hydraulic conductivity as a function of saturation. The parameters n and m $(= 1 - 1/n)$ are known to have some undefined relationship with the pore size distribution. The relationship between m and n relates the curvatures at large and small saturations. We show later that these curvatures must be related, because percolation constraints on the air (water) phase must affect the limits at large (small) saturations. The air and water critical volume fractions appear to be equal for coarse soils, but not for soils with high clay content.

A number of problems exist with the Mualem-van Genuchten relationship (Eq. (3.18)). The argument of the tortuosity/connectivity factor has a dependence on the moisture content consistent with percolation theory, but the power of $1/2$ is far from the appropriate value of 2 [28, 51]. Meanwhile, the second factor is obtained through a simple arithmetic averaging procedure, which as noted is only appropriate with perfect connectivity. Perfect connectivity requires a critical volume fraction of zero, which (a) should then be reflected in the first (connectivity) factor, and (b) is inconsistent with an adjustable residual moisture content [64]. These inconsisten-

cies make the phenomenology capable of matching almost any experimental result, but at the cost of predictive science.

3.6 Conceptual Models of Porous Media

Porous media have been modeled many different ways: as random or regular sphere packs, as bundles of parallel capillary tubes, as pore networks, and with fractal concepts. Experiments are conducted not only on natural materials *in situ* and in the laboratory, but also on artificial porous media such as glass bead packs and etched 2D micromodels.

The capillary tube bundle model deserves special mention. In its simplest form, this model represents the medium as a collection of right circular cylinders, all of the same length, and occurring with a frequency that gives the same volume pdf as the medium. Pressure-saturation relationships are derived by assuming that all tubes with radius $r < A/h$ are filled with water (regardless of height!), while larger tubes are empty: allowability is considered but accessibility is not. The hydraulic conductivity is then calculated as the arithmetic mean conductivity of the water-filled tubes. Additional "physics" may be added in the form of misalignment of tubes to create tortuosity, variable tube radii to generate the inkbottle effect, etc. Despite its obvious shortcomings this model refuses to die: a recent publication [58] endorsed by the National Research Council of Canada recommended abandoning models that are over 100 years old, turning instead to models based on the bundle of capillary tubes! Because each tube spans the entire medium, the "pores" have infinite coordination and zero percolation threshold. It therefore serves as a limiting case of perfect connectivity between pores of any given size, but zero connectivity between pores of different sizes. But as anything other than a teaching tool and a limiting case, the capillary bundle is misleading and physically incorrect. Because this book is a study of how connectivity affects flow and transport in natural media, we will not further examine these models.

Network models of porous media began with Fatt [42–44], as a reaction against unrealistic capillary bundles and mathematically impractical sphere packs. Where Fatt's networks were tubes meeting at a dimensionless point, a "ball-and-tube" configuration soon became common, reflecting the distinction made earlier between storage in pore bodies, and flow through pore throats. More recent pore throat models have a polygonal rather than a circular cross-section section [18, 84, 90], and/or a converging/diverging geometry (e.g., bi-conically shaped throats; [61, 131] rather than a constant cross-section. Early networks were almost all 2D, while modern networks are almost all 3D. This is a critical distinction: in a two-dimensional medium, percolation of only one phase is possible. Thus not only is simultaneous flow of air and water impossible, but if all the grains were in contact with each other (necessary for mechanical stability) no flow at all would be possible! Early networks used regular lattices, with pore radii assigned at random to the bodies and throats, and individual throats pruned (eliminated) at random to yield the desired mean coordination. In contrast, modern treatments often use irregular networks [4], with pore

radii spatially correlated [80] and pore coordination positively correlated with pore size [89]. Network models were used as conceptual tools in petroleum engineering for two decades before their relationship to percolation processes was recognized [21, 87].

The increasing capability of computers, combined with the increasing sophistication of network models, has made it possible to perform numerical flow simulations of rather realistic media, if on a small scale. However, our goal is an analytical framework for prediction, rather than a strictly numerical understanding. Fractal models can represent complex natural media with a paucity of relevant parameters, which is a strong factor in their favor. In fact, fractal models introduced since around 1990 have had some success in modeling both predictions for porosity and the water retention curve, though their relevance for flow properties has not so easily been established. In any case, the basis of the Brooks and Corey (BC) WRC could be shown to lie in the relevance of a power-law pore-size distribution, consistent with the assumptions of certain fractal models. Thus we choose to apply fractal models (Chap. 4) when possible or appropriate.

Suppose we want to model a natural fractal porous medium. Even if the range of fractal properties is restricted to one order of magnitude, the medium cannot be mapped to a regular network because the network has a fundamental scale and associated regularity. The question is, how are natural porous media best modeled? Does the distinction between pore body and pore throat still hold in real media, even if they are fractal? A natural porous medium has a random arrangement of unequal sized and shaped particles, complicating the precise identification of pore bodies and throats. For some real media it has been suggested that a topological definition using, e.g., dual graph theory [52] will yield a consistent distinction. The application of dual graph theory is related to the construction in condensed matter theory for finding the dual of a lattice, in this case for a random medium. Does the distinction hold for fractal media? We assumed implicitly that it does, but what inaccuracies may result from not having a rigorous classification for such a fractal model?

Other practical questions arise. If one uses fractal models to interpret real media, is there a tendency for the fractal dimensionalities to cluster around a single value [147]? Should one use different fractal characteristics in the different ranges of pore sizes corresponding to sand, silt, and clay particles [13], or even a multi-fractal analysis [107]? Many early network models of porous media used log-normal pore size distributions instead of power-law distributions. Which distribution is more common in nature, and does the existence of a power-law pore-size distribution really imply the relevance of a fractal model? Does it make sense to use a power-law pore-radius distribution on a regular grid?

Of course these practical details beg the question: How should one formulate flow and transport theories in such problems? If one starts with a percolation theoretical basis, which form of percolation theory should one choose? Since treatment of fractal media using regular network models would be ill-advised, we chose continuum over site or bond percolation theory, a choice with significant consequences.

As regards the question of whether to use fractal models or more complicated treatments, we have consistently followed an approach of allowing the available data to guide us.

3.7 Conclusion

A person first encountering porous media may be quickly overwhelmed by the variety of materials, the disparate disciplines interested in these materials (and their disparate terminology and assumptions), and the range of porosities, pore sizes, and pore structures. We attempted to avoid this pitfall by restricting ourselves to soil and rocks, while yet examining properties common to all porous media.

We highlight here some recurring themes of this primer, which will recur in later chapters:

- Porous media are largely studied for specific practical reasons, and even now the literature is largely fragmented, empirical, and applied.
- The range of sizes encountered in a given porous material may span several orders of magnitude, such that there is no apparent characteristic length scale.
- We can't define pores unambiguously, and yet we can measure them in the aggregate well enough to make predictions that work, at least sometimes.
- Geometrical properties have been emphasized almost to the exclusion of topological properties.
- Topological disorder of the fluids in the porespace is at the root of many problems in upscaling from the pore scale to the macroscale.
- Fluid flow is a strong function of fluid occupancy.
- There are important asymmetries between the wetting and non-wetting fluids.

More importantly, however, one might ask how the confusion regarding the constitution of porous media and how water is apportioned within them could have contributed to the almost universal failure to recognize the exceptional utility of $\sigma \approx (p - p_c)^2$ in predicting transport properties, as will be seen in Chaps. 6 and 7. We think that this failure has several bases:

(1) Recognition of the overwhelming complexity of porous media together with advances in imaging and numerical modeling have prompted people to follow their natural impulse to classify and define media, and then proceed to developing algorithmic, piecemeal solutions,
(2) Seizing on the relatively simple example of the Brooks-Corey power-law WRC, people have tended to attribute too much importance to the flexibility of fractal models and too little to the topological connections of the fluids within real media. An emphasis on power-law formulations based on medium morphology has been the result,
(3) The failure to recognize that the conditions for the applicability of non-universal power-laws from continuum percolation are quite restrictive, allowing the impression to develop that there is, somewhere, a theoretical basis for choosing an arbitrary power-law phenomenology for an arbitrary property,

(4) A general lack of familiarity with percolation concepts and a commensurate reliance on models and techniques that do not address connectivity,
(5) An almost total ignorance of the reasoning behind critical path analysis,
(6) A hesitation to address the theoretical and practical difficulties inherent in the determination of the critical volume fraction for percolation.

We think that the successes of Chaps. 5–13 should help people overcome various barriers to embracing percolation methodology. It is interesting that the community has recognized the common occurrence of power-law behavior while attributing its cause to fractal morphology. In fact, we show by overwhelming evidence that the ubiquity of power laws is not an evidence for a specific model of a medium, but an expression of the underlying influence of percolation processes. Nevertheless, we agree that fractal medium models can describe a wide range of medium characteristics, distilling a great deal of complexity into a few parameters. Thus we will apply percolation concepts to fractal models, which we discuss in detail in the next chapter. The analyses we develop subsequently are often adequate to distinguish the relative importance of medium and fluid characteristics.

Problems

3.1 Remember that pumice (specific gravity of the solid portion typically ca. 2.65) may float on water. Does this mean that the holes in pumice cannot be connected? Use the Scher and Zallen results (Chap. 1) to set an upper limit on the porosity of a regular pumice, for which all the "holes" are the same size. Assume that the holes are spherical. What lattice would you choose for this calculation?
3.2 Assuming a solid material density of 2.65, calculate the minimum porosity required for the condition that pumice float. Is the Scher and Zallen result useful as a predictor? In a fractal model the porosity of a medium may approach 1. Do you expect that the holes in pumice (due to gas bubbles) are of uniform size, or highly variable?
3.3 If the holes in pumice are due to gas bubbles, did the gas escape? How? Can the relevant porosities for these questions be the porosity not accessible to an infinite cluster instead of the bulk porosity?
3.4 Suppose that the pumice was formed in a violent explosion that resulted when the gas bubbles "percolated." What sort of size distribution of pieces of pumice would you expect to find?

References

1. Al-Raoush, R., Thompson, K., Willson, C.S.: Comparison of network generation techniques for unconsolidated porous media. Soil Sci. Soc. Am. J. **67**, 1687–1700 (2003)

2. Archie, G.E.: The electrical resistivity log as an aid in determining some reservoir characteristics. Trans. Metall. Soc. AIME **146**, 54–61 (1942)
3. Arya, L.M., Paris, J.F.: A physico-empirical model to predict the soil moisture characteristic from particle-size distribution and bulk density data. Soil Sci. Soc. Am. J. **45**, 1023–1030 (1981)
4. Bakke, S., Øren, P.-E.: 3-D pore-scale modelling of sandstones and flow simulations in the pore networks. SPE J. **2**, 136–149 (1997)
5. Barrett, E.P., Joyner, L.G., Halenda, P.P.: The determination of pore volume and area distributions in porous substances. I. Computations from nitrogen isotherms. J. Am. Chem. Soc. **73**(1), 373–380 (1951)
6. Baytaş, A.F., Akbal, S.: Determination of soil parameters by gamma-ray transmission. Radiat. Meas. **35**, 17–21 (2002)
7. Bear, J.: Dynamics of Fluids in Porous Media. Elsevier, New York (1972)
8. Berkowitz, B., Scher, H.: On characterization of anomalous dispersion in porous and fractured media. Water Resour. Res. **31**, 1461–1466 (1995)
9. Bernabé, Y.: The transport properties of networks of cracks and pores. J. Geophys. Res. **100**(B3), 4231–4241 (1995)
10. Bernabé, Y., Bruderer, C.: Effect of the variance of pore size distribution on the transport properties of heterogeneous networks. J. Geophys. Res., Solid Earth **103**(B1), 513–525 (1998)
11. Bernabé, Y., Revil, A.: Pore-scale heterogeneity, energy dissipation and the transport properties of rocks. Geophys. Res. Lett. **22**, 1529–1532 (1995)
12. Berryman, J.G., Milton, G.W.: Normalization constraint for variational bounds on fluid permeability. J. Chem. Phys. **83**, 754–760 (1985)
13. Bittelli, M., Campbell, G.S., Flury, M.: Characterization of particle-size distribution in soils with a fragmentation model. Soil Sci. Soc. Am. J. **63**, 782–788 (1999)
14. Broadbent, S.R., Hammersley, J.M.: Percolation processes, 1. Crystals and mazes. Proc. Camb. Philos. Soc. **53**, 629–641 (1957)
15. Brooks, R.H., Corey, A.T.: Hydraulic properties of porous media. Hydrology Paper 3, Colorado State Univ (1964)
16. Buckingham, E.: Studies on the movement of soil moisture. Bull. No. 38, Bureau of Soils, USDA, Washington, DC (1907)
17. Burdine, N.T.: Relative permeability calculations from pore size distribution data. Petr. Trans. AIME **198**, 71–77 (1953)
18. Camassel, B., Sghaier, N., Prat, M., Ben-Nasrallah, S.: Evaporation in a capillary tube of square cross-section: application to ion transport. Chem. Eng. Sci. **60**, 815–826 (2005)
19. Carman, P.C.: Fluid flow through granular beds. Trans. Inst. Chem. Eng. London **15**, 150–166 (1937)
20. Carsel, R.F., Parrish, R.S.: Developing joint probability distributions of soil water retention characteristics. Water Resour. Res. **24**(5), 755–769 (1988)
21. Chatzis, I., Dullien, F.A.L.: Modelling pore structures by 2-D and 3-D networks with application to sandstones. J. Can. Pet. Technol. **Jan.-Mar.**, 97–108 (1977)
22. Chelidze, T.L., Gueguen, Y., Ruffet, C.: Electrical spectroscopy of porous rocks: a review—II. Experimental results and interpretation. Geophys. J. Int. **137**, 16–34 (1999)
23. Cheng, C.-L., Perfect, E.: Forward prediction of height-averaged capillary pressure-saturation parameters using the BC-vG upscaler. Vadose Zone J. (2013). doi:10.2136/vzj2012.0174
24. Childress, S.: Viscous flow past a random array of spheres. J. Chem. Phys. **56**, 2527 (1972)
25. Clapp, R.B., Hornberger, G.M.: Empirical equations for some soil hydraulic properties. Water Resour. Res. **14**, 601–604 (1978)
26. Clarkson, C.R., Solano, N., Bustin, R.M., Bustin, A.M.M., Chalmers, G.R.L., He, L., Melnichenko, Y.B., Radlinski, A.P., Blach, T.P.: Pore structure characterization of North American shale gas reservoirs using USANS/SANS, gas adsorption, and mercury intrusion. Fuel **103**, 606–616 (2012)

27. Clennell, M.B.: Tortuosity: a guide through the maze. In: Lovell, M.A., Harvey, P.K. (eds.) Developments in Petrophysics, vol. 122, pp. 299–344. Geological Society, London (1997)
28. Clerc, J.P., Podolskiy, V.A., Sarychev, A.K.: Precise determination of the conductivity exponent of 3D percolation using exact numerical renormalization. Eur. Phys. J. B **15**, 507–516 (2000)
29. Collins, R.E.: Flow of Fluids Through Porous Materials. PennWell, Tulsa (1961)
30. Corning, P.A.: The re-emergence of "emergence": a venerable concept in search of a theory. Complexity **7**(6), 18–30 (2002)
31. Czachor, H., Doerr, S.H., Lichner, L.: Water retention of repellent and subcritical repellent soils: new insights from model and experimental investigations. J. Hydrol. **380**(1–2), 104–111 (2010)
32. Danckwerts, P.: Continuous flow systems: distribution of residence times. Chem. Eng. Sci. **2**(1), 1–13 (1953)
33. Darcy, H.: Les Fontaines Publiques de la Ville de Dijon. Dalmont, Paris (1856)
34. Delesse, M.A.: Pour déterminer la composition des roches. Ann. Mines **13**(4), 379–388 (1848)
35. Dullien, F.A.L.: New network permeability model of porous media. AIChE J. **21**, 299–307 (1975)
36. Dullien, F.A.L.: Porous Media: Fluid Transport and Pore Structure, 2nd edn. Academic Press, San Diego (1992)
37. Dullien, F.A.L., Dhawan, G.K.: Characterization of pore structure by a combination of quantitative photomicrography and mercury porosimetry. J. Colloid Interface Sci. **47**(2), 337–349 (1974)
38. Ewing, R.P., Gupta, S.C.: Modeling percolation properties of random media using a domain network. Water Resour. Res. **29**, 3169–3178 (1993)
39. Ewing, R.P., Gupta, S.C.: Percolation and permeability in partially structured networks. Water Resour. Res. **29**, 3179–3188 (1993)
40. Ewing, R.P., Hu, Q., Liu, C.: Scale dependence of intragranular porosity, tortuosity, and diffusivity. Water Resour. Res. **46**, W06513 (2010). doi:10.1029/2009WR008183
41. Ewing, R.P., Liu, C., Hu, Q.: Modeling intragranular diffusion in low-connectivity granular media. Water Resour. Res. **48**, W03518 (2012). doi:10.1029/2011WR011407
42. Fatt, I.: The network model of porous media. I. Capillary pressure characteristics. Trans. Metall. Soc. AIME **207**, 144–159 (1956)
43. Fatt, I.: The network model of porous media. II. Dynamic properties of a single size tube network. Trans. Metall. Soc. AIME **207**, 160–163 (1956)
44. Fatt, I.: The network model of porous media. III. Dynamic properties of networks with tube radius distribution. Trans. Metall. Soc. AIME **207**, 164–177 (1956)
45. Fredlund, M.D., Wilson, G.W., Fredlund, D.G.: Use of the grain-size distribution for estimation of the soil-water characteristic curve. Can. Geotech. J. **39**(5), 1103–1117 (2002)
46. Freeze, R.A., Cherry, J.A.: Groundwater. Prentice-Hall, Englewood Cliffs (1979)
47. Gao, G., Zhan, H., Feng, S., Huang, G., Mao, X.: Comparison of alternative models for simulating anomalous solute transport in a large heterogeneous soil column. J. Hydrol. **377**, 391–404 (2009)
48. Gee, G.W., Or, D.: Particle-size analysis. In: Dane, J.H., Topp, G.C. (eds.) Methods of Soil Analysis, Part 4, Physical Methods, pp. 255–293. Soil Sci. Soc. Am, Madison (2002)
49. Gelhar, L.W., Welty, C., Rehfeldt, K.R.: A critical review of data on field-scale dispersion in aquifers. Water Resour. Res. **28**(7), 1955–1974 (1992)
50. Giesche, H.: Mercury porosimetry: a general (practical) overview. Part. Part. Syst. Charact. **23**, 9–19 (2006)
51. Gingold, D.B., Lobb, C.J.: Percolative conduction in three dimensions. Phys. Rev. B **42**(13), 8220–8224 (1990)
52. Glantz, R., Hilpert, M.: Dual models of pore spaces. Adv. Water Resour. **30**(2), 227–248 (2007)

53. Grant, C.D., Groenevelt, P.H., Robinson, N.I.: Application of the Groenevelt-Grant soil water retention model to predict the hydraulic conductivity. Aust. J. Soil Res. **48**, 447–458 (2010)
54. Gupta, S.C., Larson, W.E.: Estimating soil water retention characteristics from particle size distribution, organic matter percent, and bulk density. Water Resour. Res. **15**, 1633–1635 (1979)
55. Gutjahr, A.L., Gelhar, L.W., Bakr, A.A., MacMillan, J.R.: Stochastic analysis of spatial variability in subsurface flows. 2. Evalution and application. Water Resour. Res. **14**(5), 953–959 (1978)
56. Gvirtzman, H., Roberts, P.V.: Pore scale spatial analysis of two immiscible fluids in porous media. Water Resour. Res. **27**, 1167 (1991)
57. Hall, P.L., Mildner, D.F.R., Borst, R.L.: Small-angle scattering studies of the pore spaces of shaly rocks. J. Geophys. Res. **91**, 2183–2192 (1986)
58. Hansen, D.: Discussion of "On the use of the Kozeny-Carman equation to predict the hydraulic conductivity of soils". Can. Geotech. J. **40**, 616–628 (2004)
59. Hasimoto, H.: On the periodic fundamental solutions of the Stokes equations and their application to viscous flow past a cubic array of spheres. J. Fluid Mech. **5**, 317–328 (1959)
60. Hillel, D.: Fundamentals of Soil Physics. Academic Press, New York (1980)
61. Hilpert, M., Miller, C.T., Gray, W.G.: Stability of a fluid-fluid interface in a biconical pore segment. J. Colloid Interface Sci. **267**, 397–407 (2003)
62. Hinch, E.J.: An averaged-equation approach to particle interactions in a fluid suspension. J. Fluid Mech. **83**, 695–720 (1977)
63. Howells, I.D.: Drag due to the motion of a Newtonian fluid through a sparse random array of small fixed rigid objects. J. Fluid Mech. **64**, 449–475 (1974)
64. Hunt, A.G.: A note comparing van Genuchten and percolation theoretical formulations of the hydraulic properties of unsaturated media. Vadose Zone J. **3**, 1483–1488 (2004)
65. Hunt, A.G., Gee, G.W.: Application of critical path analysis to fractal porous media: comparison with examples from the Hanford site. Adv. Water Resour. **25**, 129–146 (2002)
66. Hunt, A.G., Ewing, R.P., Horton, R.: What's wrong with soil physics? Soil Sci. Soc. Am. J. **77**, 1877–1887 (2013)
67. Iassonov, P., Gebrenegus, T., Tuller, M.: Segmentation of X-ray computed tomography images of porous materials: a crucial step for characterization and quantitative analysis of pore structures. Water Resour. Res. **45**, W09415 (2009). doi:10.1029/2009WR008087
68. Jalbert, M., Dane, J.H.: Correcting laboratory retention curves for hydrostatic fluid distributions. Soil Sci. Soc. Am. J. **65**, 648–654 (2001)
69. Johnson, D.L., Schwartz, L.M.: Unified theory of geometric effects in transport properties of porous media. Paper presented at SPWLA, 30th Annual Logging Symposium, Soc. of Prof. Well Log. Anal, Houston, TX (1989)
70. Journel, A.G., Huijbregts, Ch.J.: Mining Geostatistics. Blackwell, Caldwell (2003)
71. Kang, M., Perfect, E., Cheng, C.-L., Bilheux, H.Z., Lee, J., Horita, J., Warren, J.M.: Multiple pixel-scale soil water retention curves quantified by neutron radiography. Adv. Water Resour. (2014, in press)
72. Kate, J.M., Gokhale, C.S.: A simple method to estimate complete pore size distribution of rocks. Eng. Geol. **84**(1–2), 48–69 (2006)
73. Katz, A.J., Thompson, A.H.: Quantitative prediction of permeability in porous rock. Phys. Rev. B **34**, 8179–8181 (1986)
74. Kennedy, W.D., Herrick, D.C.: Conductivity models for Archie rocks. Geophysics **77**(3), WA109–WA128 (2012)
75. Ketcham, R.A., Carlson, W.D.: Acquisition, optimization and interpretation of X-ray computed tomographic imagery: applications to the geosciences. Comput. Geosci. **27**, 381–400 (2001)
76. Khaleel, R., Relyea, J.F.: Variability of Gardner's alpha for coarse-textured sediments. Water Resour. Res. **37**, 1567–1575 (2001)
77. Khan, A.U.H., Jury, W.A.: A laboratory study of the dispersion scale effect in column outflow experiments. J. Contam. Hydrol. **5**, 119–131 (1990)

78. Kläfter, J., Silbey, R.: Derivation of the continuous-time random walk equation. Phys. Rev. Lett. **44**, 55–58 (1980)
79. Klobes, P., Meyer, K., Munro, R.G.: Porosity and specific surface area measurements for solid materials. US Department of Commerce, Technology Administration, National Institute of Standards and Technology (2006)
80. Knackstedt, M.A., Sheppard, A.P., Sahimi, M.: Pore network modelling of two-phase flow in porous rock: the effect of correlated heterogeneity. Adv. Water Resour. **24**, 257–277 (2001)
81. Kosugi, K.: Three-parameter lognormal distribution model for soil water retention. Water Resour. Res. **30**(4), 891–901 (1994)
82. Kozeny, J.: Über kapillare Leitung des Wassers im Boden. Sitzungsber. Akad. Wiss. Wien **136**(2a), 271–306 (1927)
83. Lafuma, A., Quéré, D.: Superhydrophobic states. Nat. Mater. **2**, 457–460 (2003)
84. Lago, M., Araujo, M.: Threshold pressure in capillaries with polygonal cross-section. J. Colloid Interface Sci. **243**, 219–226 (2001)
85. Larson, R.E., Higdon, J.J.L.: A periodic grain consolidation model of porous media. Phys. Fluids A **1**, 38–47 (1989)
86. Larson, R.G., Scriven, L.E., Davis, H.T.: Percolation theory of residual phases in porous media. Nature **268**, 409–413 (1977)
87. Levine, S., Reed, P., Shutts, G., Neale, G.: Some aspects of wetting/dewetting of a porous medium. Powder Technol. **17**, 163–181 (1977)
88. Lindquist, W.B.: 3DMA General Users Manual. Report No. Report No. SUSB-AMS-99-20, Dept. Applied Math. & Stat., SUNY—Stony Brook (1999)
89. Lindquist, W.B.: Network flow model studies and 3D pore structure. Contemp. Math. **295**, 355–366 (2002)
90. Lindquist, W.B.: The geometry of primary drainage. J. Colloid Interface Sci. **296**, 655–668 (2006)
91. Lindquist, W.B., Venkatarangan, A., Dunsmuir, J., Wong, T.: Pore and throat size distributions measured from synchrotron X-ray tomographic images of Fontainebleau sandstones. J. Geophys. Res. **105**(B9), 21509–21521 (2000)
92. Liu, H.H., Dane, J.H.: Improved computational procedure for retention relations of immiscible fluids using pressure cells. Soil Sci. Soc. Am. J. **59**, 1520–1524 (1995)
93. Ma, Z., Merkus, H.G., de Smet, J.G.A.E., Heffels, C., Scarlett, B.B.: New developments in particle characterization by laser diffraction: size and shape. Powder Technol. **111**, 66–78 (2000)
94. Mallory, K.: Active subclusters in percolative hopping transport. Phys. Rev. B **47**, 7819–7826 (1993)
95. Martys, N.S., Hagedorn, J.G., Goujon, D., Devaney, J.E.: Large-scale simulations of single- and multicomponent flow in porous media. Proc. SPIE 3772, Developments in X-Ray Tomography II, 205 (September 22, 1999) (1999); doi:10.1117/12.363723
96. Melnichenko, Y.B., Wignall, G.D.: Small-angle neutron scattering in materials science: recent practical applications. J. Appl. Phys. **102**(2), 021101 (2007)
97. Miller, E.E., Miller, R.D.: Physical theory for capillary flow phenomena. J. Appl. Phys. **27**, 324–332 (1956)
98. Millington, R.J., Quirk, J.P.: Permeability of porous solids. Trans. Faraday Soc. **57**, 1200–1206 (1961)
99. Mohanty, K.K.: Fluids in porous media: Two-phase distribution and flow. Ph.D. thesis, University of Minnesota (1980)
100. Mohanty, K.K., Davis, H.T., Scriven, L.E.: Physics of oil entrapment in water-wet rock. SPE Reserv. Eng. **2**(1), 113–128 (1987)
101. Mualem, Y.: A new model for predicting the hydraulic conductivity of unsaturated porous media. Water Resour. Res. **12**(3), 513–522 (1976). doi:10.1029/WR012i003p00513
102. Oleson, K.W., Lawrence, D.M., Bonan, G.B., Flanner, M.G., Kluzek, E., Lawrence, P.J., Levis, S., Swenson, S.C., Thornton, P.E., et al.: Technical description of version 4.0 of

the Community Land Model (CLM). NCAR Technical Note NCAR/TN-478+STR, NCAR, Boulder, Colorado (2010)
103. Orr, F.M., Scriven, L.E., Rivas, A.P.: Pendular rings between solids: meniscus properties and capillary force. J. Fluid Mech. **67**(4), 723–742 (1975)
104. Pachepsky, Y.A., Timlin, D., Várallyay, G.: Artificial neural networks to estimate soil water retention from easily measurable data. Soil Sci. Soc. Am. J. **60**, 727–733 (1996)
105. Peth, S., Horn, R., Beckman, F., Donath, T., Fischer, J., Smucker, A.J.M.: Three-dimensional quantification of intra-aggregate pore-space features using synchrotron radiation-based microtomography. Soil Sci. Soc. Am. J. **72**, 897–907 (2008)
106. Pollak, M.: Non-crystalline Semiconductors. CRC Press, Boca Raton (1987). Chap. 5a
107. Posadas, A.N.D., Gimenez, D., Bittelli, M., Vaz, C.M.P., Flury, M.: Multifractal characterization of soil particle-size distributions. Soil Sci. Soc. Am. J. **65**, 1361–1367 (2001)
108. Prager, S.: Viscous flow through porous media. Phys. Fluids **4**, 1477–1482 (1961)
109. Radlinski, A.P., Mastalerz, M., Hinde, A.L., Hainbuchner, M., Rauch, H., Baron, M., Lin, J.S., Fan, L., Thiyagarajan, P.: Application of SAXS and SANS in evaluation of porosity, pore size distribution and surface area of coal. Int. J. Coal Geol. **59**, 245–271 (2004)
110. Reynolds, W.D., Elrick, D.E., Young, E.G., Booltink, H.W.G., Bouma, J.: Saturated and field-saturated water flow parameters. In: Dane, J.H., Topp, G.C. (eds.) Methods of soil analysis, Part 4, Physical methods, pp. 797–878. Soil Sci. Soc. Am., Madison
111. Roberts, J.J., Lin, W.: Electrical properties of partially saturated Topopah Spring tuff: water distribution as a function of saturation. Water Resour. Res. **33**(4), 577–587 (1997)
112. Rose, W.: Volumes and surface areas of pendular rings. J. Appl. Phys. **29**(4), 687–691 (1958)
113. Rose, W.: Myths about later-day extensions of Darcy's law. J. Pet. Sci. Eng. **26**, 187–198 (2000)
114. Rouquerol, J., Avnir, D., Fairbridge, C.W., Everett, D.H., Haynes, J.M., Pernicone, N., Ramsay, J.D.F., Sing, K.S.W., Unger, K.K.: Recommendations for the characterization of porous solids (Technical report). Pure Appl. Chem. **66**(8), 1739–1758 (1994)
115. Sahimi, M.: Flow phenomena in rocks—from continuum models to fractals, percolation, cellular automata, and simulated annealing. Rev. Mod. Phys. **65**(4), 1393–1534 (1993)
116. Sahimi, M.: Flow and Transport in Porous Media and Fractured Rock: From Classical Methods to Modern Approaches. Wiley-VCH, New York (2011), 709 pp.
117. Sahimi, M., Imdakm, A.O.: The effect of morphological disorder on hydrodynamic dispersion in flow through porous media. J. Phys. A, Math. Gen. **21**, 3833–3870 (1988)
118. Sakaki, T., Illangasekare, T.H.: Comparison of height-averaged and point-measured capillary pressure-saturation relations for sands using a modified Tempe cell. Water Resour. Res. **43**, W12502 (2007). doi:10.1029/2006WR005814
119. Sangani, A.S., Acrivos, A.: Slow flow through a periodic array of spheres. Int. J. Multiph. Flow **8**, 343–360 (1982)
120. Schaap, M.G., Leij, F.J., van Genuchten, M.T.: Rosetta: a computer program for estimating soil hydraulic parameters with hierarchical pedotransfer functions. J. Hydrol. **251**, 163–176 (2001)
121. Scheibe, T., Yabusaki, S.: Scaling of flow and transport behavior in heterogeneous groundwater systems. Adv. Water Resour. **22**, 223–238 (1998)
122. Scher, H., Montroll, E.W.: Anomalous transit-time dispersion in amorphous solids. Phys. Rev. B **12**(6), 2455–2477 (1975)
123. Scher, H., Shlesinger, M., Bendler, J.: Time-scale invariance in transport and relaxation. Phys. Today **44**(1), 26–34 (1991). doi:10.1063/1.881289
124. Sen, P.N.: Time-dependent diffusion coefficient as a probe of geometry. Concepts Magn. Reson. A **23A**(1), 1–21 (2004)
125. Silin, D., Patzek, T.: Pore space morphology analysis using maximal inscribed spheres. Physica A **371**, 336–360 (2006)

126. Sutanto, E., Davis, H.T., Scriven, L.E.: Liquid distributions in porous rocks examined by cryo-scanning electron microscopy. Paper 20518-MS, SPE Ann. Tech. Conf. Exhib. New Orleans, LA (1990)
127. Swartzendruber, D.: Non-Darcy behavior in liquid-saturated porous media. J. Geophys. Res. **67**(13), 5205–5213 (1962)
128. Tamari, S.: Optimum design of the constant-volume gas pycnometer for determining the volume of solid particles. Meas. Sci. Technol. **15**, 549–558 (2004)
129. Taylor, G.: Dispersion of soluble matter in solvent flowing slowly through a tube. Proc. R. Soc. Lond. Ser. A, Math. Phys. Sci. **219**(1137), 186–203 (1953)
130. Toledo, P.G., Novy, R.A., Davis, H.T., Scriven, L.E.: Hydraulic conductivity of porous media at low water content. Soil Sci. Soc. Am. J. **54**, 673–679 (1990)
131. Toledo, P.G., Scriven, L.E., Davis, H.T.: Pore space statistics and capillary pressure curves from volume controlled porosimetry. In: Paper SPE 19618, 64th Ann. Tech. Conf. and Exhib. of the SPE, San Antonio, Texas, Oct 8–11 (1989)
132. Torquato, S., Lu, B.: Rigorous bounds on the fluid permeability: effect of polydispersivity in grain size. Phys. Fluids A **2**, 487–490 (1990)
133. Tuller, M., Or, D.: Hydraulic conductivity of variably saturated porous media—laminar film and corner flow in angular pore space. Water Resour. Res. **37**(5), 1257–1276 (2001)
134. Tuller, M., Or, D., Dudley, L.M.: Adsorption and capillary condensation in porous media: liquid retention and interfacial configurations in angular pores. Water Resour. Res. **35**(7), 1949–1964 (1999)
135. Tyler, S.W., Wheatcraft, S.W.: Fractal scaling of soil particle-size distributions—analysis and limitations. Soil Sci. Soc. Am. J. **56**, 362–369 (1992)
136. van Brakel, J., Heertjes, P.M.: Analysis of diffusion in macroporous media in terms of a porosity, a tortuosity and a constrictivity factor. Int. J. Heat Mass Transf. **17**, 1093–1103 (1974)
137. van Genuchten, M.T.: A closed-form equation for predicting the hydraulic conductivity of unsaturated soils. Soil Sci. Soc. Am. J. **44**, 892–898 (1980)
138. Vanderborght, J., Gonzales, C., Vanclooster, M., Mallants, D., Feyen, J.: Effects of soil type and water flux on solute transport. Soil Sci. Soc. Am. J. **61**, 372–389 (1997)
139. Vanderborght, J., Vereecken, H.: Review of dispersivities for transport modeling in soils. Vadose Zone J. **6**, 29–52 (2007). doi:10.2136/vzj2006.0096
140. Vereecken, H., Weynants, M., Javaux, M., Pachepsky, Y., Schaap, M.G., van Genuchten, M.T.: Using pedotransfer functions to estimate the van Genuchten-Mualem soil hydraulic properties: a review. Vadose Zone J. **9**, 795–820 (2010)
141. Vogel, H.-J.: Topological characterization of porous media. In: Morphology of Condensed Matter. Lecture Notes in Physics, vol. 600, pp. 75–92. Springer, Berlin (2002)
142. Washburn, E.W.: Note on a method of determining the distribution of pore sizes in a porous material. Proc. Natl. Acad. Sci. USA **7**(4), 115–116 (1921)
143. Webber, B., Corbettc, P., Sempled, K.T., Ogbonnayad, U., Teele, W.S., Masiellof, C.A., Fisherg, Q.J., Valenza, J.J. II, Song, Y.-Q., Hu, Q.H.: An NMR study of porous rock and biochar containing organic material. Microporous Mesoporous Mater. **178**, 94–98 (2013)
144. Weissberg, H.L., Prager, S.: Viscous flow through porous media. II. Approximate three-point correlation function. Phys. Fluids **5**, 1390–1392 (1962)
145. Weissberg, H.L., Prager, S.: Viscous flow through porous media. III. Upper bounds on the permeability for a simple random geometry. Phys. Fluids **13**, 2958–2965 (1970)
146. Wilkinson, D., Willemsen, J.F.: Invasion percolation: a new form of percolation theory. J. Phys. A, Math. Gen. **16**, 3365–3376 (1983)
147. Wu, Q., Borkovec, M., Sticher, H.: On particle-size distributions in soils. Soil Sci. Soc. Am. J. **57**, 883–890 (1993)

148. Yanuka, M., Dullien, F.A.L., Elrick, D.E.: Serial sectioning and digitization of porous media for two- and three-dimensional analysis and reconstruction. J. Microsc. **135**(2), 159–168 (1984)
149. Yates, S.R.: An analytical solution for one-dimensional transport in heterogeneous porous media. Water Resour. Res. **26**(10), 2331–2338 (1990)
150. Zick, A.A., Homsy, G.M.: Stokes flow through periodic arrays of spheres. J. Fluid Mech. **115**, 13–26 (1982)

Chapter 4
Fractal Models of Porous Media

In the previous chapter we introduced some basic concepts of porous media, and raised the question of how best to model fluid movement in a porous medium. We suggested that fractal concepts might be well suited to such modeling, because of their simple descriptions of highly ramified spaces. In this chapter we examine some fractal models of porous media. After introducing some fractal concepts, we derive one specific random fractal model of the pore size distribution (that of Rieu and Sposito [53]), and show its application to the water retention curve (WRC). We then survey several published fractal WRC models, and develop a general form that includes some existing models as special cases. Finally, we reiterate that there is no simple mapping possible between any measure of the pore space and the soil WRC.

4.1 Fractal Approaches to Porous Media Modeling

Fractal theory provides a promising framework for addressing the complexity of disordered, heterogeneous, hierarchical porous media, such as soils and fracture networks. But natural physical objects can at best only be *approximated* by fractal models, which span an infinite size range and are (often) strictly deterministic. Turcotte [58] elucidated a mechanism by which scale-independent fragmentation processes could form a fractal distribution of particles, giving theoretical legitimacy to the study of fractal models of porous media.

A fractal object is characterized by having a (typically non-integer) dimension less than the Euclidean dimension it is embedded in. It also has the property of self-similarity or self-affinity. If a synthetic fractal object is rescaled in all directions with the same scaling factor, an exactly similar object is reproduced (Fig. 4.1). Self-affinity means that a fractal object has different scaling factors in different directions [55]. Of course, most natural objects that are self-similar or self-affine have that property only in a statistical sense. The concepts of self-similarity and self-affinity have widely been used to model physical and geometrical properties of soils and fracture networks [9, 28, 40, 41, 45, 53, 58]. It has been shown that fracture

A. Hunt et al., *Percolation Theory for Flow in Porous Media*,
Lecture Notes in Physics 880, DOI 10.1007/978-3-319-03771-4_4,

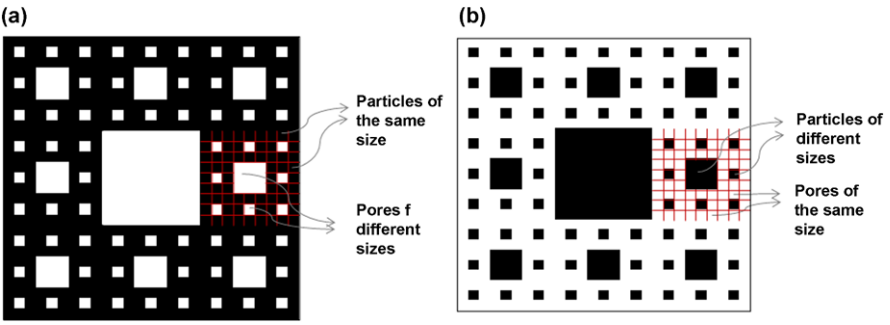

Fig. 4.1 Exactly self-similar Sierpinski carpets after two iterations with fractal dimension $D = 1.893$ and $b = 3$: (**a**) a solid fractal model constructed of particles of the same size but pores of different sizes, (**b**) a pore fractal model built up of particles of different sizes but pores of the same size (after Ghanbarian et al. [21]). The solid matrix is shown in *black*, while pores are *white*

surfaces are statistically self-affine [64]. Poon et al. [52] modeled surface roughness of fractures by means of self-affinity; see Sahimi [55] for a comprehensive review of related work.

A feature of power-law functions that distinguishes them from all other functions is that they are linear when plotted on a log-log scale. The power-law function for describing a fractal number-size distribution is [37]

$$N(\geq l) = kl^{-D}, \quad l_{\min} < l < l_{\max} \tag{4.1}$$

where $N\ (\geq l)$ is the number of fractal objects whose size is equal or greater than l, k is a constant coefficient, and the fractal dimension D typically ranges between 0 and 3 in natural porous materials. Note that Eq. (4.1) is a truncated power-law function: it only applies within the specified range, $l_{\min}$ to $l_{\max}$.

Tyler and Wheatcraft [59] used Eq. (4.1) to estimate the fractal dimensionality of particle-size distributions. To be consistent with Arya and Paris [2], they applied the arithmetic mean particle radius derived from sieve data. Given that counting all particles between two sieve sizes was impractical if not impossible, Tyler and Wheatcraft [59] inferred the number-size distribution from the mass-size distribution. For this purpose, they divided the mass of particles retained on the lower sieve by the mass of a particle with radius equal to the mean of the two sieve sizes. They found that $D > 3$ for 9 of the 10 experiments they analyzed, a physically dubious result because we expect D (even for a number distribution) to be less than E, the Euclidean dimension in which it is embedded.

The fractal dimension over-estimation by Tyler and Wheatcraft [59] and later researchers is likely due to incorrect assumptions used in deducing number-size distributions from mass-size distributions. The first assumption is that particle density is scale-invariant. This assumption would be especially unrealistic if aggregate number-size distribution were derived from aggregate mass-size data. However, analysis of experimental aggregate data by Perfect et al. [48] showed that the assumptions of scale-invariant density and shape were valid for most samples. A second simplifying assumption is ignoring the shape of the aggregates or particles: for

the sake of simplicity, particles are assumed to be spherical, and aggregates cubic. A third assumption is that there are no artifacts in applying the continuous equation (4.1) to discrete data (aggregate and particle sizes). This may produce errors in determining the fractal dimension, because (for example) the $N\ (\geq l)$ value in Eq. (4.1) depends on the choice of sieve size [1], and the arithmetic mean is not the appropriate mean.

The probability density function of fractals—the number of objects whose size is within the range l to $l + \mathrm{d}l$ ($\mathrm{d}N(\geq l) \propto l^{-1-D}$)—is proportional to the first derivative of Eq. (4.1). Generally one writes

$$f(l) = Cl^{-1-D}, \quad l_{\min} < l < l_{\max} \tag{4.2}$$

where $f(l)$ is the probability density function, and C is a constant coefficient which can be found by taking the integral of Eq. (4.2) from $l_{\min}$ to $l_{\max}$ and setting it equal to 1: $C = D/(l_{\min}^{-D} - l_{\max}^{-D})$ [24]. Where $l_{\min} \ll l_{\max}$, as occurs in many natural porous media, the constant coefficient $C \approx Dl_{\min}^{D}$.

While much experimental evidence indicates that the size distribution of particles, aggregates, and pores follows power-law behavior, sometimes the lognormal distribution is assumed instead (see e.g., [34, 36, 56]):

$$f(l) = \frac{1}{\sqrt{2\pi}\sigma l} \exp\left[-\frac{(\ln(l) - \mu)^2}{2\sigma^2}\right], \quad 0 < l < \infty \tag{4.3}$$

where μ is the mean, σ is the standard deviation, and l is the size of the object e.g., pore, particle, or aggregate. In contrast to the power-law distribution, the lognormal distribution has finite mean and variance. With appropriate parameters, the lognormal distribution is similar in shape to the power-law distribution over much of its range. In particular, where variance of the lognormal distribution is large, its cumulative density function may appear linear on a log-log plot for several orders of magnitude [39].

Among the many synthetic fractal objects, the 2D Sierpinski carpet (Fig. 4.1) and its 3D equivalent, the Menger sponge, have been widely used to model porous materials. The Sierpinski carpet is constructed by starting with a square of size L (the "initiator length"). For the first iteration, the operational length scale l is L/b in which the scaling factor $b = 3$ for the traditional Sierpinski carpet (Fig. 4.1). In the exactly self-similar Sierpinski carpet, the central square of size l is removed, thereby creating a square pore of size l. For the next iteration, l is divided by b, and all intact squares of size bl have their central l-size squares removed [23].

Primary fractal models include just two phases, pore and solid, and may be either solid fractal (Fig. 4.1a) or pore fractal (Fig. 4.1b) models [54]. The main characteristic of a solid fractal model is that, within each iteration of its construction, the model is composed of identical-size particles but pores of different sizes (Fig. 4.1a). In such a model, just the solid matrix is fractal whose number-size distribution (and consequently probability density function) follows a power-law function. Although the pore phase in the solid fractal model (Fig. 4.1a) is not geometrically fractal, its number-size distribution is given by a power-law function (Eq. (4.1)) and it has the

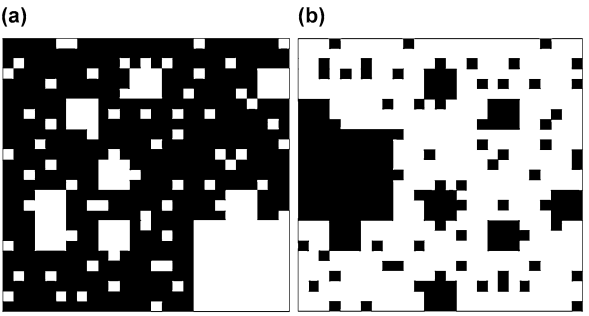

Fig. 4.2 Randomly (statistically) self-similar Sierpinski carpets after two iterations with the same fractal dimension $D = 1.893$ and scale factor $b = 3$ used in Fig. 4.1: (**a**) a solid fractal model, (**b**) a pore fractal model. *Black and white squares* respectively represent solid particles and pores

same fractal dimensionality as the solid phase [54]. So in fact, one fractal dimension scales both solid and pore phases, albeit in different ways. The same argument applies to the pore fractal model (Fig. 4.1b).

The Sierpinski carpets presented in Fig. 4.1 are exactly self-similar. Natural porous media are instead randomly self-similar, but it seems that the same power-law number-size distribution applies. In Fig. 4.2, we show randomly (statistically) self-similar Sierpinski carpets after two iterations for solid (Fig. 4.2a) and pore (Fig. 4.2b) fractal models. Though the fractal dimensionality is identically 1.893 for carpets in both Figs. 4.1 and 4.2, the random carpets shown in Fig. 4.2 are more heterogeneous and complex than the deterministic carpets presented in Fig. 4.1, and appear more similar to real natural porous media.

4.2 The Rieu and Sposito (RS) Fractal Model

Rieu and Sposito [53] (henceforth RS) developed a model of a fractal pore space linked to a fractal particle model. Several studies have subsequently shown that water retention curves (WRCs, also called pressure-saturation curves) can be predicted from particle-size data using the RS model [5, 19, 28]. In the RS notation, d_0 denotes the largest pore size, and d_m the smallest. The reason for this choice is that they use an index i, representing the iteration of the fractal process, which runs from 0 to m. We use their convention for deriving their model, but we use the reverse convention throughout the rest of this book, as it is more intuitive to consider r_0 to be a minimum radius and r_m a maximum.

For simplicity, consider that pores exist only at discretized diameters, d_i. V_i represents the total volume in all pore sizes greater than d_m and less than or equal to d_i. There is a constant ratio N of the number of pores of diameter $d_{i+1} = qd_i$ to the number of pores of diameter d_i. The constant q, the ratio of pore diameters in successive classes, is less than 1. Define the partial volume $P_i \equiv V_i - V_{i+1}$, and denote the total volume as V_0 and the volume of the solid material as V_m. Then one can write

$$V_0 = \sum_{i=0}^{\mathrm{m}} P_i + V_\mathrm{m} \tag{4.4}$$

Self-similarity requires

$$V_i = N V_{i+1} + P_i \tag{4.5}$$

This result allows Eq. (4.4) to be rewritten as

$$V_0 = \sum_{i=0}^{\mathrm{m}-1} N^i P_i + N^{\mathrm{m}} V_{\mathrm{m}} = P_0 \sum_{i=0}^{\mathrm{m}-1} \left(Nq^3\right)^i + \left(Nq^3\right)^{\mathrm{m}} V_0 \tag{4.6}$$

Here, as in the original treatment of Rieu and Sposito, the solid volume is now reinterpreted as $N^{\mathrm{m}} V_{\mathrm{m}}$. One way to think of this is that pores smaller than d_{m} can be ignored; that is, if we could resolve smaller pores, the iteration would proceed further.

The total pore volume, V_{p}, can be written as

$$V_{\mathrm{p}} = P_0\left[1 + Nq^3 + \left(Nq^3\right)^2 + \cdots + \left(Nq^3\right)^{\mathrm{m}-1}\right] = P_0 \frac{1 - (Nq^3)^{\mathrm{m}}}{1 - Nq^3} \tag{4.7}$$

Now we can express the porosity as

$$\phi = \frac{P_0 \frac{1-(Nq^3)^{\mathrm{m}}}{1-Nq^3}}{P_0 \frac{1-(Nq^3)^{\mathrm{m}}}{1-Nq^3} + N^{\mathrm{m}} V_{\mathrm{m}}} \tag{4.8}$$

Solving Eq. (4.6) for P_0 in terms of V_0, we find

$$P_0 = V_0\left(1 - Nq^3\right) \tag{4.9}$$

Using the same substitution in Eq. (4.8) for $N^{\mathrm{m}} V_{\mathrm{m}}$ as in Eq. (4.6), and substituting Eq. (4.9) for P_0, we find

$$\phi = 1 - \left(Nq^3\right)^{\mathrm{m}} \tag{4.10}$$

Now consider the definition of the fractal dimensionality [37, Chap. 13]; [32, Chap. 3]:

$$D = \log(N)/\log(1/q) \tag{4.11}$$

Combine this definition with Eq. (4.10) to obtain

$$D = 3 - \frac{\log(1-\phi)}{\log(q^{\mathrm{m}})} \tag{4.12}$$

The numerical factor q^{m}, however, is nothing more than the ratio of the smallest pore diameter to the largest, d_{m}/d_0, so that

$$D = 3 - \frac{\log(1-\phi)}{\log(\frac{d_{\mathrm{m}}}{d_0})} \tag{4.13}$$

and now Eq. (4.13) may be rewritten as

$$\phi = 1 - \left(\frac{d_{\mathrm{m}}}{d_0}\right)^{3-D} \tag{4.14}$$

Equation (4.14) establishes the RS result for the porosity. This result is very simple, being independent of shape parameters and the choices of N and q. Equation (4.14) can also be used to show that

$$\left(Nq^3\right)^{\mathrm{m}} = \left(q^{\mathrm{m}}\right)^{3-D} \tag{4.15}$$

which simplifies to $N = q^{-D}$. What sort of a distribution of pore sizes does the above analysis lead to? For the partial volume $P(i)$ of pores of size class i, we can write

$$P(i) \propto N^i = q^{-iD} = \left(\frac{d_i}{d_0}\right)^{-D} \tag{4.16}$$

where this last expression uses the relationship between the pore radius r_i and the fractal iteration i: $r_i = q^i r_0$. Equation (4.16) for $P(i)$ could be written as $P(i)\Delta i$ without change, since i is an integral index and $\Delta i = 1$. Then the probability density function $W(d)$ for a pore of diameter d is found by using the transformation $W(i)\mathrm{d}i = W(d)\mathrm{d}d$,

$$W(r) \propto \frac{(\frac{d}{d_0})^{-D}}{d\ln(q)} \propto d^{-D-1} \tag{4.17}$$

We now drop the RS convention, interchanging the meaning of the subscripts 0 and m. We develop a normalized form for a pdf for pore radii, $W(r)$, which generates the same result for the porosity as Eq. (4.14):

$$W(r) = \frac{3-D_{\mathrm{p}}}{r_{\mathrm{m}}^{3-D_{\mathrm{p}}}} r^{-1-D_{\mathrm{p}}} \quad r_0 \le r \le r_{\mathrm{m}} \tag{4.18}$$

Here we have substituted D_{p} for D to specify that the fractal dimensionality concerned applies to the *pore* space. The result for the total porosity derived from Eq. (4.18) is [28]

$$\phi = \frac{3-D_{\mathrm{p}}}{r_{\mathrm{m}}^{3-D_{\mathrm{p}}}} \int_{r_0}^{r_{\mathrm{m}}} r^3 r^{-1-D_{\mathrm{p}}} dr = 1 - \left(\frac{r_0}{r_{\mathrm{m}}}\right)^{3-D_{\mathrm{p}}} \tag{4.19}$$

exactly as in RS. Equation (4.19) is compatible with a volume r^3 for a pore of radius r. That is, if a particular geometry for the pore shape is envisioned, it is possible to change the normalization factor to maintain the result for the porosity, and also maintain the correspondence to RS. This is an important restriction, and is applied because ϕ in the RS treatment is independent of geometry.

Integration of $W(r)r^3$ over the continuous pore size distribution between pr and r, where $p < 1$ is an arbitrary factor, yields the contribution to the porosity from each size class obtained by RS. Integration of $W(r)$ over the same size range yields the probability that an arbitrary pore has a radius of r that is in agreement with the direct calculation of RS. Thus the present model (Eq. (4.19)) is a continuous (and thereby more general) version of the discrete RS model (Eq. (4.14)). The power law distribution of pore sizes is bounded by a maximum radius r_{m}, and a

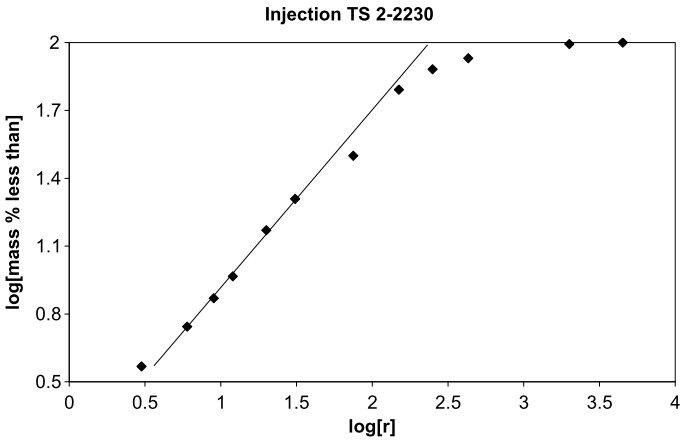

Fig. 4.3 The cumulative particle-size distribution data from the Injection Test Site 2-2230 soil at the US Department of Energy's Hanford Site. Data from Freeman [20]. The *horizontal scale* is in logarithm base 10. The maximum particle radius is very nearly two orders of magnitude larger than the minimum value (Log[2.5] − Log[0.5])

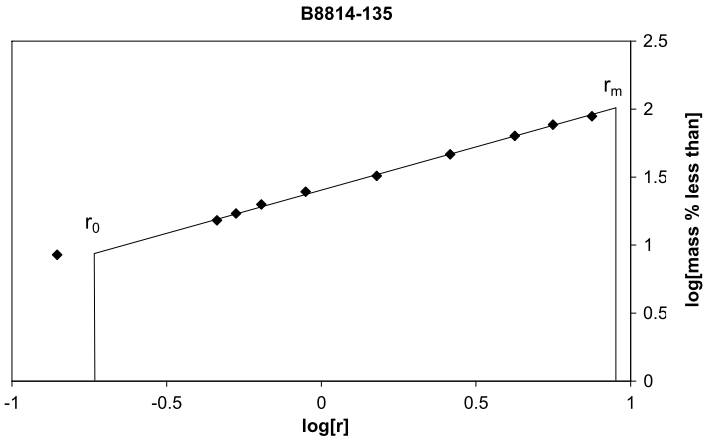

Fig. 4.4 The cumulative particle-size distribution from the B8814-135 soil at the US Department of Energy's Hanford Site

minimum radius r_0. Note that knowledge of ϕ, r_0, and r_m is sufficient to give D explicitly. ϕ is typically obtained through density measurements, and r_0 and r_m are obtained from particle size measurements. Examples of the determination of r_0 and r_m are given in Figs. 4.3, 4.4 and 4.5.

Although the symmetry in shape imposed by the choice of square or cubic volumes for iteration forces equality in the fractal dimensionalities of the pore and solid spaces for idealized fractal models, this equality does not survive the application of a model to a real medium. Using the symmetry in the purely mathematical substitu-

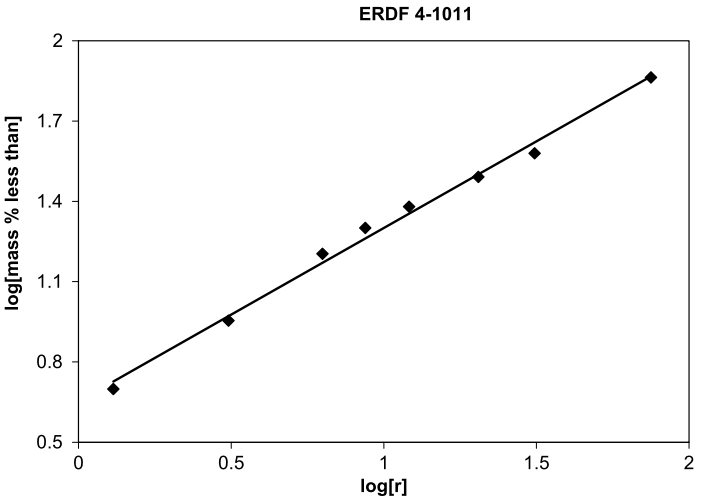

Fig. 4.5 The cumulative particle-size data from the ERDF 4-1011 soil at the US Department of Energy's Hanford Site

tions $\phi \to 1-\phi$ and $D_\mathrm{p} \to D_\mathrm{s}$ (where D_s refers to the fractal dimensionality of the *solid* portion of the medium), we obtain the result [28]

$$\phi = \left(\frac{r_0}{r_\mathrm{m}}\right)^{3-D_\mathrm{s}} \tag{4.20}$$

As a reminder, in Eq. (4.19), r_0 and r_m refer explicitly to the minimum and maximum *pore* sizes, and in Eq. (4.20) to the minimum and maximum *particle* sizes. We have made the common assumption [2, 25, 61] that pore and particle radii are proportional to each other. Under this assumption, the ratio r_0/r_m is the same for both particles and pores, though this assumption is not always justified.

We now have $D_\mathrm{p} = D_\mathrm{s}$ only for the special case that $\phi = 0.5$. For example, Katz and Thompson [33] used optical measurements to detect the range of sizes in the particle space corresponding to the range from r_0 to r_m. They assumed a lower cut-off of $r_0 \approx 2$ nm, and determined values of r_m of up to 100 μm. Then they used Eq. (4.20) (as did Nigmatullin et al. [43]) to relate the porosity, the ratio r_m/r_0, and the fractal dimension, but used the dimensionality of the *pore* volume, D_p, rather than that of the solid volume, D_s, because their model is pore-fractal based (Fig. 4.1b). Their statement, "successful prediction of the porosities from the fractal parameters verifies the assumption that the pore surface and volume are fractals with the same dimension" does not necessarily follow, because Eq. (4.19) and Eq. (4.20) are complementary [27]. Given Eq. (4.19), which relates the fractal dimensionality of the pore space to the porosity, and their assumed values $r_\mathrm{m}/r_0 \approx 10^4$, their fractal dimensionality range from 2.57 to 2.87 would imply porosities between 95 % to 73 %, rather than the values between 5 % to 27 % that they calculated and measured. What this means is that the range of pore-particle interface structures that they mea-

sured, including the fixed lower bound, would not correspond to the range of pore sizes in a pressure-saturation curve. This distinction is made clear in the derivation of the RS model, and supported by its predictions. We have provided two derivations of their result for the porosity above. Further, in addition to our tests on ca. 40 Hanford site soils, which demonstrated that the RS model can be used to predict water retention curves (next section), at least one other group of researchers [19] have also demonstrated that the RS model is predictive in this way.

Where does the typical asymmetry between particles and pores come from? A reasonable hypothesis is that it chiefly arises from the tendency for particles to be positively curved and for the pores to be negatively curved (note the exception of solidified foams such as pumice, for which values of ϕ are probably the largest of all geological porous media). Such a contrast in curvature would tend to produce $\phi < 0.5$. According to Eq. (4.19) and Eq. (4.20), $\phi < 0.5$ is consistent with pore space having a greater fractal dimensionality than that of the particles, a tendency noted also by Rieu and Sposito [53]. In soils, mechanical strength tends to limit porosity to less than 0.5, and the mean porosity of rocks is generally less than that of soils. This discussion is not meant to justify a rule, but only to explain a tendency.

4.3 Water Retention Using the RS Model

As discussed in Sect. 3.5, the water retention curve (as it is known in soil physics and hydrology) or pressure-saturation curve (as it is known in petroleum, chemical, and civil engineering) is assumed to represent the pore-size distribution. Typically either water (a strongly wetting liquid with a contact angle near zero) is drained from the medium, or mercury (a non-wetting liquid with a fairly consistent contact angle on mineral surfaces) is injected into the medium, at controlled pressures. The water retention curve (WRC) relates the incremental pressures to fractions of the pore volume. But because of complex phenomena that are not usually considered—accessibility, hysteresis, wettability, and trapping—the pore-size distribution inferred from a capillary pressure curve may deviate significantly from the true pore size distribution. The RS model for the WRC ignores these complications, assuming perfect wetting (contact angle of 0°) and perfect accessibility.

Assume spherical pores, equilibrium conditions, and a pore radius pdf equal to $W(r)$. Then the total water content in the medium may be written

$$\theta = \int_{r_0}^{A/h} W(r)\left(\frac{4}{3}\pi r^3\right)dr \tag{4.21}$$

where the numerical coefficient A is known for e.g. cylindrical pores, but unknown in a natural medium where the wettability and shapes of pores are typically unknown. In media with non-ideal pores, as long as pore lengths and radii are correlated, the factor r^3 in the integrand is still appropriate. One then finds $d\theta/dh \propto W(r)r^3h^{-2} \propto W(h)(dh/dr)h^{-5} \propto W(h)h^{-3}$, so that to find $W(h)$ (within numer-

ical factors), one simply takes the product of h^3 and the derivative of the water content with respect to h at the given h.

$W(h)$ determined in this way typically contains a region at intermediate saturations which is consistent with power-law behavior and fractal models, but it deviates at the wet and dry ends of the moisture spectrum. These deviations give a sigmoid shape to $W(h)$ (and to $W(r)$), with regions of pronounced curvature at both the wet and dry ends. Such deviations from power-law behavior have led some to conclude that (1) the appropriate distribution of pore volumes is not fractal but, e.g., log-normal, and/or (2) water content changes at the wet end result from the wetting or drying of larger "structural" pores, and at the dry end from water held in thin films, capillary bridges, and surface roughness. Of course, some deviation from the predictions of fractal models must occur at each end, because continuity of the constituent phases is interrupted. That is, such discrepancies are not by themselves sufficient to accept or reject a fractal model. Further, to the extent that such deviations arise from fluid properties and percolation, they may be time-dependent (as discussed in Chap. 8). Incorporation of both time-dependent and time-independent phenomena into a single time-independent phenomenology is by definition inconsistent.

For an RS fractal medium in equilibrium, we proceed from Eq. (4.19) to calculate the fractional water volume at arbitrary pressure $h < 0$ simply by changing the limits of integration:

$$\theta(h) = \frac{3-D}{r_{\mathrm{m}}^{3-D}} \int_{r_0}^{A/h} r^{2-D} dr \tag{4.22}$$

where A/h in the range $r_0 \leq A/h \leq r_{\mathrm{m}}$ determines the largest pore that contains water. For values of h outside this range (A/h larger than r_{m} or smaller than r_0), $\theta = \phi$ or $\theta = 0$. At a particular value of h denoted h_{A} (called the air entry pressure; see Sect. 3.5.4), air could just enter the largest pore if that pore were located at the edge of the sample. Thus, $A/h_{\mathrm{A}} = r_{\mathrm{m}}$, so h_{A} can be related to the porosity:

$$\phi = \frac{3-D}{r_{\mathrm{m}}^{3-D}} \int_{r_0}^{A/h_A} r^{2-D} dr \tag{4.23}$$

Note that for any given soil, there must be some maximum pore size. For $h < h_{\mathrm{A}}$ corresponding to that largest pore, the soil is saturated (as we are still ignoring accessibility issues). Note that there is a saturated region *above* the water table (i.e., $h > 0$) known as the capillary fringe; the height of this region approaches zero in the limit that the largest pore size approaches infinity.

Combining Eq. (4.22) and Eq. (4.23) produces the WRC in terms of relative saturation,

$$S \equiv \frac{\theta}{\phi} = 1 - \frac{1}{\phi}\left[1 - \left(\frac{h_A}{h}\right)^{3-D}\right] \tag{4.24}$$

a relationship also obtained by Rieu and Sposito [53] using their discrete version of this model. Equation (4.24) may be (very roughly) approximated as $S =$

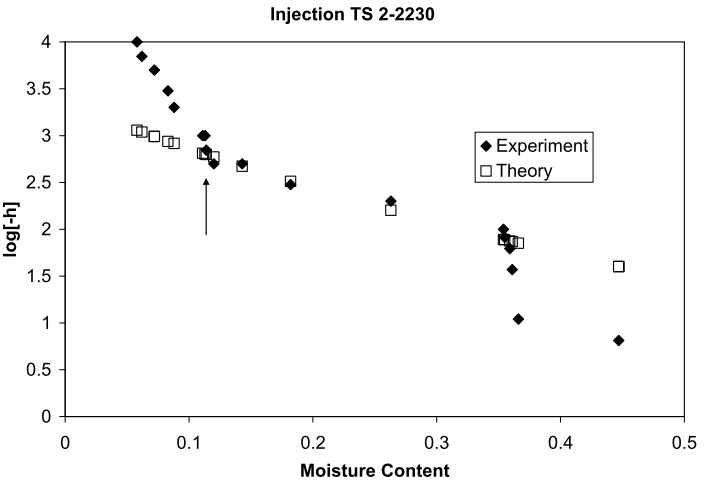

Fig. 4.6 The water retention data for the Injection Test Site 2-2230 soil at the US Department of Energy's Hanford Site. The prediction of the fractal scaling in the *open squares* is taken from the value of D_p determined from the particle-size data in Fig. 4.3; one parameter, h_A, which fixes the vertical scale, was chosen to optimize the fit. The *arrow* denotes the dry-end moisture content at which experiment begins to deviate from the fractal model

$(h_A/h)^{3-D}$, which is precisely the form of the phenomenological relationship proposed by Brooks and Corey [7]. We note in passing that the water content of natural porous media most closely resembles the result of Eq. (4.24) during drainage; the wetting curve has additional complications.

In Figs. 4.6, 4.7 and 4.8 the results of Eq. (4.24) are compared with water retention data from the same media as for Figs. 4.3–4.5. The value of the fractal dimensionality was found from analysis of the particle size data according to Figs. 4.3–4.5, and knowledge of the porosity (Eq. (4.19)). Note that the predicted water retention curve agrees with observation in the middle of the range of saturations, where both the water and the air phase percolate simultaneously, but does not predict the curvature at the wet and dry ends, where complications would be expected due to (among other causes) percolation effects not being included in the RS model. In Chap. 8 we show how, in a large number of tested cases, we can predict the dry end deviations from the RS model using the hydraulic conductivity calculated from the RS model, and the wet end deviations using topological constraints from percolation.

We have found that the RS model is accurate and appropriate for a large number of natural porous media, though certainly we do not assume that it applies to all media. Below we show that for some media, the equilibrium water content predicted by the RS model deviates from experiment at both the wet and dry ends of the spectrum. These observations raise the question: do the observed deviations from prediction stem from defects in the fractal model, or are they due to complications that may be explained by percolation theory? If the latter, the deviations must be recognized as model strengths rather than defects.

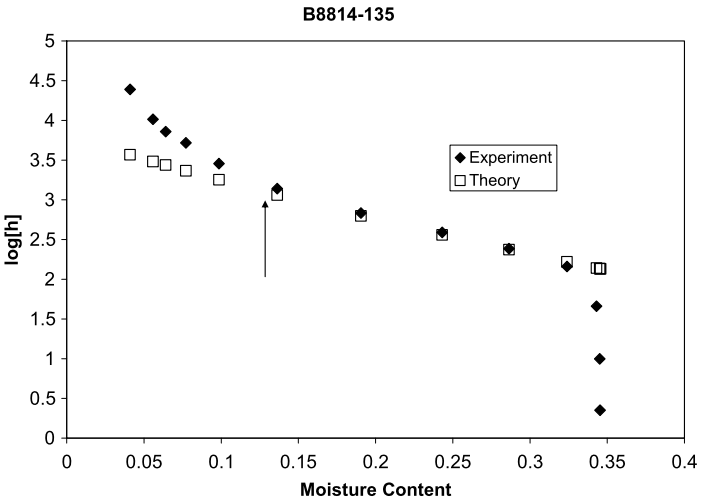

Fig. 4.7 The water retention data for the B8814-135 soil at the US Department of Energy's Hanford Site. The prediction was made analogously to Fig. 4.6

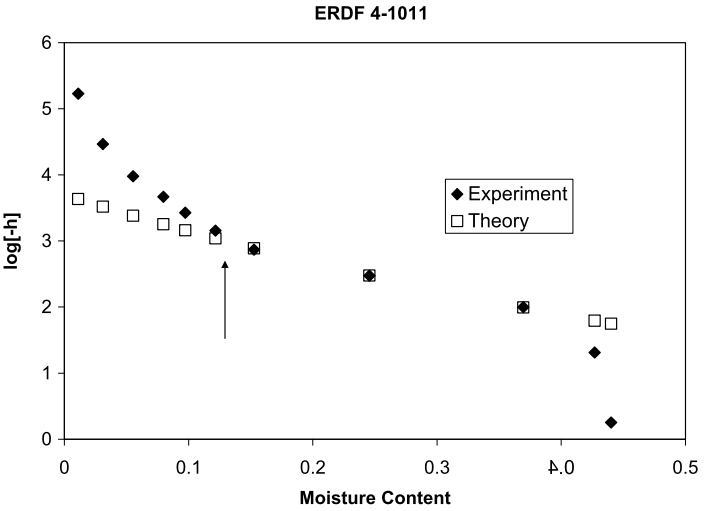

Fig. 4.8 The water retention data for the ERDF 4-1011 soil at the US Department of Energy's Hanford Site. The prediction was again made analogously to Fig. 4.6

We caution that the complicating behavior at the wet and dry ends of the water retention curve need not be due only to percolation behavior. Some pore size distributions may indeed be log-normal. At the wet end, structural pores often *do* complicate the analysis. At the dry end, water present in surface films *may* complicate matters. It is important to keep these uncertainties in mind during analysis, although other than percolation effects, only those effects due to structural pores

will be considered here, and those only in Chap. 12. Before useful conclusions can be drawn from any discrepancies in predictions from the fractal model, however, effects due to percolation must be excluded. Otherwise inferences will be nonsense.

4.4 Other Fractal Models of the WRC

The RS model for the WRC deviates from observations, and it does not describe the whole range of observed water retention curves (WRCs). As we show in Chap. 8, many of the discrepancies are due to issues that are ignored in typical derivations of the WRC, such as finite-size effects and fluid continuity effects at the wet end, and fluid continuity and lack of equilibration at the dry end. But beyond these confounding influences, it is also the case that water can be distributed quite differently at large tension values: appreciable water may reside in capillary bridges, crevices, and surface roughness. Thus the strong wetting assumption (i.e., that all water is pore-filling water) is partially at fault.

Partly in response to the known defects of the strong wetting treatment in the RS model—and without accounting for percolation effects—other WRC models have been developed. At this nascent stage of development and testing of theoretical methods, we have not evaluated under what conditions the deficiencies of the RS model reflect fundamental inadequacies, as opposed to deficiencies due to the strong wetting assumption. Here we consider a wider range of WRC models, hoping to better evaluate where the main limitations of the RS model are found: in its restrictive generating assumptions, in the strong wetting assumption, or perhaps elsewhere.

4.4.1 de Gennes [13]

Pierre-Gilles de Gennes [13], the Nobel Prize winner in physics in 1991, may have been the first to propose a fractal soil water retention model. Using geometrical characteristics of pores for two iterative pits and flocs models, de Gennes [13] indicated that the total volume of pits of size r and less filled with liquid (water) in the iterative pits model is approximately equal to the total volume due to pendular droplets in the iterative flocs model and is

$$V(\leq r) \propto r_{\max}^{D} r^{E-D} \tag{4.25}$$

where D is the surface fractal dimensionality quantifying pore-solid interface roughness (de Gennes [13]), $r_{\max}$ is the largest pore radius in the medium, r is the largest pore radius filled with water, and E is Euclidean dimension equal to 2 and 3 in 2D (e.g., Sierpinski carpet) and 3D (e.g., Menger sponge) systems, respectively.

In the same spirit as Eq. (4.25), the total volume of pores in the medium would be

$$V(\leq r_{\max}) \propto r_{\max}^{E} \tag{4.26}$$

Note that de Gennes [13] ignored any water trapped on the rough surfaces of pores with pore radius larger than r.

Dividing Eq. (4.25) by (4.26) gives

$$\frac{\theta}{\phi} = \left(\frac{r}{r_{\max}}\right)^{E-D} \tag{4.27}$$

Combining Eq. (4.27) with the capillary equation ($h = A/r$, where h is tension head, A is a constant coefficient, and r is the largest pore radius filled with water) and assuming a contact angle of zero yields

$$\frac{\theta}{\phi} = \left(\frac{h}{h_{\min}}\right)^{D-E} \tag{4.28}$$

where $h_{\min}$ can be interpreted as the air entry value. Equation (4.28) is a fractal expression for the water retention curve (also known as capillary pressure curve). Note that Eq. (4.28) has the same form as empirical models proposed by Brooks and Corey [7] (with zero residual water content) and Campbell [8]. However, the exponent $(D - E)$ in Eq. (4.28) has physical meaning.

4.4.2 Tyler and Wheatcraft [60]

Tyler and Wheatcraft [60] proposed a power-law equation having the same form as the de Gennes [13] model (Eq. (4.28)). Despite the formal similarity, the two models have different interpretations. Tyler and Wheatcraft [60] used the solid fractal model and Sierpinski carpet to model hierarchical properties of pore and solid phases. They found porosity at each iteration (ϕ_i) as

$$\phi_i = \frac{n_i}{(b^i)^E} = 1 - \left(b^i\right)^{D-E} \tag{4.29}$$

where n_i is the number of squares (or cubes) which are removed at that iteration step of the Sierpinski carpet (or Menger sponge), i is the number of iterations, and b is the scaling factor ($b = 3$ in the traditional Sierpinski carpet). Tyler and Wheatcraft [60] call D the fractal dimension of the (Sierpinski) carpet.

Tyler and Wheatcraft assumed that the Sierpinski model would be iterated infinite times. This assumption is physically unrealistic for natural porous media, which may be fractal only within a limited range of pore size (e.g., $r_{\min}$ to $r_{\max}$). Infinite iterations cause porosity of the carpet to go to 1 ($\phi = 1$). They then defined water content retained at the ith iteration step (θ_i) of the Sierpinski carpet, and replaced b^i by h_i ($h \propto b^i$) to derive

$$\theta_i = \phi - \phi_i = 1 - \left[1 - \left(b^i\right)^{D-E}\right] \propto h_i^{D-E} \tag{4.30}$$

A special case of Eq. (4.30) is where tension head is equal to the air entry value ($h = h_{\min}$). In such a case the medium is still saturated and $\phi \propto h_{\min}^{D-E}$, which results in the Tyler and Wheatcraft [60] soil water retention model

$$\frac{\theta}{\phi} = \left(\frac{h}{h_{\min}}\right)^{D-E} \tag{4.31}$$

Here we replaced θ_i and h_i by the more general symbols θ and h. The RS model reduces to Eq. (4.31) when $\phi = 1$.

4.4.3 Perrier et al. [51]

Perrier et al. [51] started with the differential pore-size distribution,

$$-\frac{d[V_v > r]}{dr} = K(E - D)r^{E-D-1} \tag{4.32}$$

where $[V_v > r]$ is the volume of pores whose radius is r or greater, K is a positive constant, and D is the pore-solid interface fractal dimension. Integrating Eq. (4.32) and imposing an upper limit value for porosity, Perrier et al. [51] proposed

$$\theta = \phi - \frac{V_{max}}{V_t}\left[1 - \left(\frac{h}{h_{min}}\right)^{D-E}\right] \tag{4.33}$$

in which

$$V_{max} = K r_{max}^{E-D} \tag{4.34}$$

where V_{max} is the upper bound of total pore volume, and V_t is the total volume of a soil sample. As Perrier et al. [51] stated, Eq. (4.33) is a general fractal water retention curve which reduces to the Tyler and Wheatcraft [60] model when V_{max}/V_t is set equal to ϕ, and to the RS model when V_{max}/V_t is set equal to 1.

4.4.4 Perfect [46]

Based on the characteristics of Menger sponge, Perfect [46] defined the water content at the ith step as

$$\theta_i = \left(b^i\right)^{D-3} - \left(b^j\right)^{D-3} \tag{4.35}$$

where b is the scaling factor (for example $b = 3$ in Figs. 4.1 and 4.2), i is the number of iterations, and j is the maximum number of iterations (with $0 \le i \le j$). Perfect [46] called D the mass fractal dimension scaling both pores and solids. The porosity can be defined by setting $i = 0$:

$$\phi = 1 - \left(b^j\right)^{D-3} \tag{4.36}$$

By dividing Eq. (4.35) by Eq. (4.36), Perfect [46] found

$$\frac{\theta_i}{\phi} = \frac{(b^i)^{D-3} - (b^j)^{D-3}}{1 - (b^j)^{D-3}} \tag{4.37}$$

Following Tyler and Wheatcraft [60], one can relate the scaling factor b to minimum and maximum tension heads:

$$\begin{aligned} b^i &= h_i/h_{min} \\ b^j &= h_{max}/h_{min} \end{aligned} \tag{4.38}$$

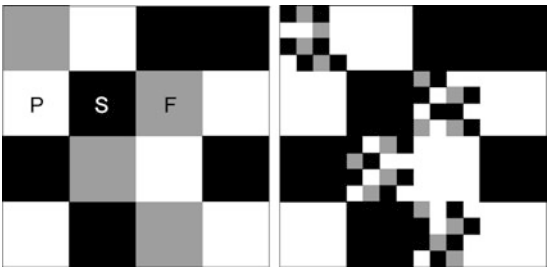

Fig. 4.9 Two-dimensional random pore-solid-fractal (PSF) model (generator on the *left*, and first iteration on the *right*) proposed by Perrier et al. [50]. Here $P = 0.375$ (pore phase portion), $S = 0.375$ (solid phase portion), and $F = 0.25$ (fractal phase portion), and the scaling factor $b = 4$

where $h_{\min}$ and $h_{\max}$ are tensions required to drain the largest and smallest pores, respectively.

Combining Eqs. (4.37) and (4.38) and using more general symbols θ and h result in

$$\frac{\theta}{\phi} = \frac{h^{D-3} - h_{\max}^{D-3}}{h_{\min}^{D-3} - h_{\max}^{D-3}} \tag{4.39}$$

Bird [4] also found Eq. (4.39) using the characteristics of the fragmentation model of Rieu and Sposito [53]. However, in his treatment the residual water content θ_r was included (Eq. (3) in Bird [4]).

As Perfect [46] pointed out, when fitting Eq. (4.39) to water retention data measured from saturation to high tension head (e.g., 3.3×10^5 kPa), in other words the entire accessible range, the fitted fractal dimensions were significantly less than 3. If, on the other hand, Eq. (4.39) was fitted to truncated data (e.g., from saturation to a tension of -1.5 MPa; a more typical measured range of WRC), $D > 3$ was observed. Perfect [46] explained that this systematic error in the fractal dimension estimation might be due to a transition from fractal to nonfractal scaling. In order to estimate the fractal dimension value accurately and reasonably ($D < 3$), Perfect [46] suggested measuring the entire range of water retention curve from saturation to zero water content.

If one subtracts Eq. (4.35) from (4.36) utilizing the results from Eq. (4.38), the RS model equation is obtained. Therefore, the RS and Perfect [46] models are theoretically the same, as also reported by Perfect et al. [49] and Ghanbarian-Alavijeh and Hunt [22].

4.4.5 Bird et al. [5]

All models described so far only include pore and solid phases to model the structure and geometrical properties of porous media. In 1999, Perrier et al. proposed a three-phase model (shown in Fig. 4.9) including pores, solids, and fractals. A remarkable

difference between two-phase (Figs. 4.1 and 4.2) and three-phase PSF (Fig. 4.9) models is that in these so-called pore-solid-fractal (PSF) models, the mass of pore phase and solid phase remains finite even if the model is iterated infinitely many times. Although only the pore-solid interface is geometrically fractal in the PSF approach, the number-size distributions of pore, solid and fractal phases follow the same power-law equation with the same fractal dimensionality.

The porosity of the medium simulated by the PSF model at the ith step would be

$$\phi_i = \frac{P}{P+S}(1-F)^i \tag{4.40}$$

where P $(0 < P < 1)$ and S $(0 < S < 1)$ respectively denote the pore and solid phase portions, and F $(0 < F < 1)$ represents those spatial regions of the generator within which the entire shape is replicated at any given iteration.

For an infinite number of iterations ($i \to \infty$), the porosity reduces to

$$\phi_{i\to\infty} = \frac{P}{P+S} \tag{4.41}$$

In contrast to two-phase fractal models e.g., pore fractal and solid fractal models in which porosity reduces to 0 and 1, respectively, after infinite iteration, the PSF model porosity diminishes to the constant $(P/[P+S])$.

Based on the properties of the PSF approach, Bird et al. [5] presented a new, generalized soil water retention curve which includes the Tyler and Wheatcraft [60] and Rieu and Sposito [53] models as special cases. The Bird et al. [5] model is

$$\theta = \phi - \alpha\left[1 - \left(\frac{h}{h_{\min}}\right)^{D-E}\right] \tag{4.42}$$

where $\alpha = P/[P+S]$, and the pore-solid interface fractal dimension D also scales the pore and solid number-size distributions. The PSF soil water retention curve model (Eq.(4.42)) is similar to the Perrier et al. [51] model, but their physical interpretations are different because Bird et al. [5] is based on a three-phase rather than a two-phase model.

As Bird et al. [5] point out, there are three special cases for Eq. (4.42). First, if $S = 0$, the PSF model reduces to a solid mass fractal model, so the Bird et al. [5] water retention model reduces to the RS model. Second, when $P = 0$, the PSF model would be a pore mass fractal structure where the water retention curve becomes a step function indicating a monosize distribution; all pores are the same size. Third, assume both P and S values are non-zero, and infinite number of iteration. In this case $\alpha = \phi$, and the Bird et al. [5] retention model reduces to the de Gennes [13] and Tyler and Wheatcraft [60] models.

Recently, Hunt et al. [31] extended the PSF approach to model a water retention curve with two fractal regimes (Fig. 4.10). The two-regime PSF model is [31]

$$\theta = \begin{cases} \phi & h < h_{\min} \\ \phi - \alpha_1\left[1 - \left(\frac{h}{h_{\min}}\right)^{D_1-E}\right] & h_{\min} < h < h_{\mathrm{x}} \\ \phi_2 - \alpha_2\left[1 - \left(\frac{h}{h_{\mathrm{x}}}\right)^{D_2-E}\right] & h_{\mathrm{x}} < h < h_{\max} \end{cases} \tag{4.43}$$

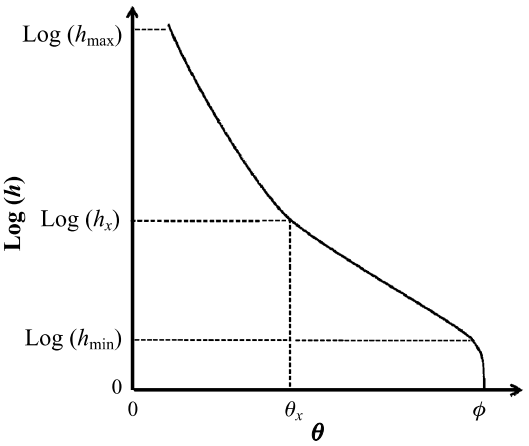

Fig. 4.10 Schematic of a water retention curve with two fractal regimes (after Hunt et al. [31])

where D_1 and D_2 are the pore-solid interface fractal dimension of the first and second regimes, respectively, and ϕ_2 is the porosity of the second regime, equal to the water content at the crossover point whose tension head is h_x.

4.4.6 Millán and González-Posada [38]

Considering that the water retention curve includes both structural and textural pores, and following the power-law model of de Gennes [13], Millán and González-Posada [38] assumed two fractal regimes, and proposed the following piecewise function

$$\theta = \begin{cases} \phi\left(\frac{h}{h_{\min}}\right)^{D_1-E}, & h < h_x \\ \theta_x\left(\frac{h}{h_x}\right)^{D_2-E}, & h > h_x \end{cases} \tag{4.44}$$

where D_1 is the fractal dimensionality of the first regime (which typically captures structural pores), D_2 is the fractal dimensionality of the second regime (textural pores), and θ_x is the water content at the cross-over point (pressure h_x) where scaling behavior changes from structural to textural. Note that h is a tension head (suction or negative pressure) taking a positive value. Equation (4.44) is a special case of Eq. (4.43) where $\alpha_1 = \phi$, and $\alpha_2 = \phi_2 = \theta_2$. Ojeda et al. [44] proposed the same function as Eq. (4.44) for water retention curve model. In general, each regime needs to span at least a couple of orders of magnitude in the independent variable as suggested by Avnir et al. [3].

4.4.7 Cihan et al. [11]

Following Perfect [47] and the fact that in a natural porous medium pores of a given size are not necessarily drained with the same probability of drainage due to bottle-

neck effect or incomplete pore connectivity, Cihan et al. [11] proposed a general scale-variant fractal drainage model, which can be simplified into two scale-variant and scale-invariant models. In their general scale-variant drainage model, the number of pores of a given size l can be expressed as

$$N_p(l) = \left(b^E - b^D\right)\left(b^{i-1}\right)^D \tag{4.45}$$

where D is the mass fractal dimension, b is a scaling factor, and i represents number of iterations.

Considering the probability of drainage (P_d) due to incomplete pore connectivity, Cihan et al. [11] defined the number of drained pores as

$$N_\mathrm{d}(l) = \left(b^E - b^D\right)\left(b^{i-1}\right)^{D_\mathrm{d}} \tag{4.46}$$

where D_d is the fractal dimension for the drained pore space, and P_d is the ratio of the drained pore space to the total pore space ($0 \le P_\mathrm{d} \le 1$).

The cumulative volume of the drained pore would be [11]

$$V_\mathrm{d}(l) = P_\mathrm{d}\left(\frac{b^E - b^D}{b^E - b^{D_\mathrm{d}}}\right)\left(1 - \left(b^i\right)^{D-E}\right) \tag{4.47}$$

Note that they assumed that P_d is constant, which means that the same proportion of pores empties at each iteration.

The volumetric water content at the ith step is determined as

$$\theta_i = \phi - V_\mathrm{d}(l) = \phi - P_\mathrm{d}\left(\frac{b^E - b^D}{b^E - b^{D_\mathrm{d}}}\right)\left(1 - \left(b^i\right)^{D-E}\right) \tag{4.48}$$

Combining Eq. (4.48) with Eq. (4.38), then dividing by total porosity, gives the general scale-variant model of Cihan et al. [11]:

$$\frac{\theta}{\phi} = 1 - \frac{P_\mathrm{d}}{\phi}\left(\frac{b^E - b^D}{b^E - b^{D_\mathrm{d}}}\right)\left(1 - \left(\frac{h}{h_\mathrm{min}}\right)^{D-E}\right) \tag{4.49}$$

Given that porosity is typically known (whether measured or calculated from bulk density and particle density data), Eq. (4.49) includes 5 unknown parameters (i.e., P_d, D, D_d, h_min, and b) whose values cannot be simultaneously determined by direct fitting to measured soil water retention curve.

There are two special cases for Eq. (4.49). First, if one sets $P_\mathrm{d} = 1$ such that all the largest pores drain completely, Eq. (4.49) reduces to

$$\frac{\theta}{\phi} = 1 - \frac{1}{\phi}\left(\frac{b^E - b^D}{b^E - b^{D_\mathrm{d}}}\right)\left(1 - \left(\frac{h}{h_\mathrm{min}}\right)^{D-E}\right) \tag{4.50}$$

Second, as $D_\mathrm{d} = D$, the ratio of the number of drained pores to total pores at any iteration remains constant and equal to P_d. Therefore, Eq. (4.49) is simplified to

$$\frac{\theta}{\phi} = 1 - \frac{P_\mathrm{d}}{\phi}\left(1 - \left(\frac{h}{h_\mathrm{min}}\right)^{D-E}\right) \tag{4.51}$$

Equation (4.51) is similar to the Perrier et al. [51], Bird et al. [5], and Deinert et al. [17] soil water retention curve models. However, the interpretation of each model's

parameters is different; of these, only the Bird et al. [5] treatment is based on a three-phase model, whereas Deinert's [17] treatment is distinct from that of Perrier et al. [51] by their inclusion of the additional descriptor equal to the pore-volume fractal dimension.

4.4.8 Deinert et al. [17]

It was recently proposed [10] that tension head (or capillary pressure) should be related to fluid interfacial area rather than pore diameter (assumed in the Young-Laplace equation; $h = A/r$) under equilibrium conditions. Deinert et al. [16] also indicated that the variation in fluid interfacial area with fluid volume is a significant factor which determines equilibrium capillary pressure. Following Mandelbrot's relationship between surface area, A_s, and volume, V, of a fractal object, $A_s^3 \propto V^{D_s}$ [37] where D_s is surface fractal dimension, Deinert et al. [17] proposed the tension head (h) at equilibrium proportional to a power of the pore volume (V)

$$h \propto V^{(D_s-3)/3} \propto r^{D_s-3} \tag{4.52}$$

where r is the radius corresponding to the pore volume V. In the limiting case $D_s = 2$, Eq. (4.52) has the tension head inversely proportional to $V^{1/3}$ and r, analogous to the Young-Laplace equation.

Combining Eq. (4.52) with the Perrier et al. [51] model gives

$$\theta = \phi - \frac{V_{\max}}{V_t}\left[1 - \left(\frac{h}{h_{\min}}\right)^{\frac{D-3}{3-D_s}}\right] \tag{4.53}$$

in a 3D system. Note that Eq. (4.53) reduces to the Perrier et al. [51] model, Eq. (4.33), when $D_s = 2$, meaning that the pore-solid interface is smooth.

4.5 A General Fractal Model for the Soil Water Retention Curve

We consider a two phase (pore and solid) model with a continuous probability density function like Eq. (4.2) rather than using a discrete fractal approach such as the RS model. In such treatment, the power-law probability density function describing the pore sizes is written

$$f(r) = Cr^{-1-D_p}, \quad r_{\min} < r < r_{\max} \tag{4.54}$$

where C is a constant coefficient (a normalization factor), and $r_{\min}$ and $r_{\max}$ are the lower and upper limits of the (truncated) fractal distribution. As we mentioned previously, if we require the integral of Eq. (4.54) from $r_{\min}$ to $r_{\max}$ to be equal to 1, then the coefficient C takes the value $D/(l_{\min}^{-D_p} - l_{\max}^{-D_p})$.

The porosity of the medium (proportional to the total pore volume) may be found by integrating $r^3 f(r)$ between $r_{\min}$ and $r_{\max}$ to obtain

$$\phi = \int_{r_{\min}}^{r_{\max}} \xi r^3 f(r) dr = \frac{\xi C}{3 - D_p} \left[r_{\max}^{3-D_p} - r_{\min}^{3-D_p} \right] \tag{4.55}$$

where ξ is a normalization factor with units length^{-3}, and a numerical value that depends on the pore shape. The water content as a function of r can then be defined as

$$\theta = \int_{r_{\min}}^{r} \xi r^3 f(r) dr = \frac{\xi C}{3 - D_p} \left[r^{3-D_p} - r_{\min}^{3-D_p} \right] \tag{4.56}$$

Equations (4.55) and (4.56) differ only in the upper limit of the integral: porosity is scaled over all pore radii (from $r_{\min}$ to $r_{\max}$) in Eq. (4.55), while water content is defined as the cumulative pore volume from smallest pore radius ($r_{\min}$) to some arbitrary value of r. Note that this ignores accessibility (percolation) issues, and water held on the rough surfaces of pores with radii larger than r.

Combining Eqs. (4.55) and (4.56) with the capillary equation $h = A/r$ gives the soil water retention curve in terms of relative saturation

$$\begin{aligned} \theta &= \phi - \beta \left[1 - \left(\frac{h}{h_{\min}} \right)^{D_p - 3} \right] \quad h_{\min} < h < h_{\max} \\ S &\equiv \frac{\theta}{\phi} = 1 - \frac{\beta}{\phi} \left[1 - \left(\frac{h}{h_{\min}} \right)^{D_p - 3} \right] \quad h_{\min} < h < h_{\max} \end{aligned} \tag{4.57}$$

in which $\beta = \phi r_{\max}^{3-D_p} / (r_{\max}^{3-D_p} - r_{\min}^{3-D_p})$. The bounds on the tension are $h_{\min} = A/r_{\max}$, and $h_{\max} = A/r_{\min}$.

This general fractal model for the WRC (Eq. (4.57)) reduces to the Tyler and Wheatcraft [60] model for $\beta = \phi$, and to the RS model for $\beta = 1$. The increased generality of this model means that it is can address a wider range of media. Equation (4.57) is consistent with the model developed by Perrier et al. [51], except that in their model $\beta = V_{\max}/V_t$, where $V_{\max}$ is the upper bound on the total pore volume as $r_{\min}$ approaches 0, and V_t is the total volume of a soil sample.

Note that all WRC models discussed above (except Bird [4]) ignore water trapped on the rough surfaces of pores. While Bird [4] included the residual water content in his treatment, its contribution to the soil water retention curve model is as a fitting parameter rather than a physically interpreted factor. The approach of Toledo et al. [57] has some promise, but one should consider carefully before combining a surface wetting model with a model based on the strong wetting assumption.

4.6 Assumptions in WRC Measurement and Modeling

The preceding discussion tacitly assumes that the water retention data are good, but as with all measurement, there exist procedural trade-offs, assumptions, and

error. We refer back to Sect. 3.5, where many issues were raised; here we raise a few additional issues that will play into further discussions of the WRC in Chap. 8.

4.6.1 Finite-Size Effects at High Saturations

Larson and Morrow [35] indicated that the soil water retention curve depends not only on the geometrical and wetting properties of individual pores but also upon the pores' connections to the surface of the sample. Since pores' connections (accessibility) depend on the distance from the sample surface, the WRC must be sensitive to the sample size. In fact, pores that are close to the surface of a sample are accessible more than interior pores. It is possible in natural porous media that some large pore bodies might be connected to others via small pore throats. These pores are not drained until a sufficient large suction relevant to the largest pore throats is executed. Therefore, they are assigned to the small pore bodies (or large suction) part of the pore-size distribution incorrectly [35]. Dullien [18] also indicated that mercury intrusion method results in the entry pore-size distribution rather than the real one. One possible practical way to obtain a more real pore-size distribution is to reduce the fraction of less accessible interior pores by decreasing the sample size. Larson and Morrow [35] studied the sample thickness effect on soil water retention curve by experiments. Their results indicated that as the sample size decreased, the wet end of soil water retention curve became sharper which is consistent with the physical interpretation of air entry value where air starts effectively invading through the sample. Thus, the existence of such a disrupting point (air entry value) at the wet end of soil water retention curve questions the application of the continuous form proposed by van Genuchten [62].

4.6.2 Non-equilibrium Condition at the Dry End

It is theoretically assumed that soil water retention curve is measured under equilibrium conditions. However, in practice this assumption becomes more unrealistic as the soil dries [6, 29, 30]. This lack of equilibrium means that water that doesn't drain when it "should" is attributed to subsequent "equilibrium" pressures in the sequence—to pores smaller than those that actually held it, or to residual water in the case of the final pressure.

Bittelli and Flury [6] found errors in soil water retention curves measured with pressure plates, and reported large discrepancies between pressure plate and dew point meter measurements at matric potentials less than -100 kPa: water content at -1.5 MPa as determined from pressure plates was twice that measured by the dew point meter method. They also indicated that the MvG [42, 62] model underestimated unsaturated hydraulic conductivity determined from soil water retention curve measured with pressure plates for a silt loam soil sample.

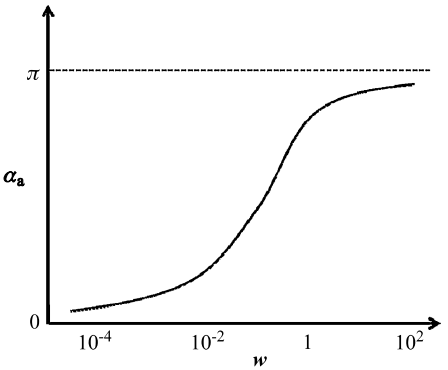

Fig. 4.11 Apparent contact angle α_a as a function of capillary number w for silicone oils (completely wetting $\alpha_e = 0$) experiments on a glass capillary (after Hoffman [26])

4.6.3 Contact Angle Assumptions

The contact angle of pure water on smooth clean mineral surfaces is generally zero, but where the surface is rough or the fluids are moving, the contact angle can be considerably greater than zero and may even exceed 90°. In an outstanding review paper, de Gennes [14] discusses static and dynamic wettings, and connects them to wettability, wetting transitions, long-range forces e.g., van der Waals, and fluid dynamics. For forced flow in a capillary (pipe), de Gennes considers the experiments of Hoffman [26], who measured velocities for two series of fluids e.g., silicone oils (completely wetting $\alpha_e = 0$; where α_e is the contact angle at equilibrium) and other oils and industrial products (partially wetting $\alpha_e > 0$) in a glass capillary of 2 mm in diameter. Hoffman [26] measured an apparent contact angle (α_a) by a photographic technique. Introducing a dimensionless parameter, the capillary number w ($w = u_L\eta/\rho g$; where u_L is the local velocity, η is fluid viscosity, ρ is fluid density, and g is gravitational acceleration), Hoffman [26] found a universal relation between w and α_a ($w = F(\alpha_a)$ where F denotes a function) shown in Fig. 4.11. As can be seen, Hoffman's experiments covered almost five orders of magnitude of capillary numbers (and velocities). Note that $\alpha_a(w)$ first increases, then levels off around $w = 1$, $\alpha_a \to \pi$.

Revisiting Hoffman's experiments, de Gennes [14] found that at low velocities ($w < 10^{-1}$), the Hoffman data can be represented in the form

$$w = \xi \alpha_a^m \tag{4.58}$$

where ξ is a constant coefficient, and $m = 3 \pm 0.5$. Later, de Gennes [15] derived Eq. (4.58) theoretically, with $m = 3$ for the case of a perfectly wetting fluid.

In a second series of experiments involving partially wetting fluids, Hoffman [26] could still express his data in terms of apparent contact angle α_a and equilibrium contact angle $\alpha_e > 0$, finding $w = F(\alpha_a) - F(\alpha_e)$. However, a more straightforward equation was not proposed. de Gennes [15] related the local velocity u_L to the macroscopic velocity u through the tortuosity parameter $\tau > 1$ ($u_L = \tau u$), and derived a dynamic capillary pressure for the imbibition process:

$$p_d \propto l_c w^{2/3} \tau^{5/3} \tag{4.59}$$

where p_d is the dynamic capillary pressure, l_c is the length of the contact line, and τ is the tortuosity parameter. When the randomness is weak in the porous medium, de Gennes [15] postulated that l_c would be independent of the capillary number, but inversely proportional to pore radius. Under this condition, the de Gennes [15] results agree with the empirical equation that Weitz et al. [63] proposed from experiments.

4.6.4 The Power-Law Form of the WRC

Although the same power-law form is presented for soil water retention curve by both de Gennes [13] and Tyler and Wheatcraft [60], the de Gennes model (Eq. (4.28)) features the surface fractal dimension, while the Tyler and Wheatcraft model (Eq. (4.31)) features the pore space fractal dimension. As we saw in Sect. 4.2, these different dimensions exert different influences on the WRC. The distinction becomes important when the goal is to predict the WRC from 2D or 3D soil images, where one can choose to measure the fractal dimension of the pore space, the solid matrix, and/or the pore-solid interface.

Crawford et al. [12] argued that the WRC "is a complicated function of both the pore-size distribution and the connectivity, and does not depend in a simple way on the spatial correlation of structure." They further concluded that the interpretation of the WRC is ambiguous because a power-law relationship between tension head and water content could be a consequence of a fractal pore space, a fractal solid matrix, a fractal pore-solid interface, or a non-fractal self-similar pore-solid interface. They measured fractal dimensions of both the pore space and the solid matrix from soil thin sections, and found that the fractal dimension of solid matrix was a better predictor of the exponent in the Tyler and Wheatcraft [60] model than the fractal dimension of pore space. However, they did not measure surface fractal dimension from 2D images, and it is not certain that the Tyler and Wheatcraft model is the best basis for comparison. Building on the Crawford et al. [12] results, Deinert et al. [17] found that the exponent of the soil water retention curve fractal model is produced not only when either the pore space or the pore-solid interface is fractal, but also when both are fractal. Thus the question whether surface fractal dimension determined from soil images could provide an accurate characterization of soil water retention curve remains unanswered.

4.7 Conclusions

In the previous chapter we raised the question of how best to model fluid movement in a porous medium. Of course the specific answer varies from process to process, and from medium to medium, but we argued that in general (1) a pore network model with a fixed grid was poorly suited to model a medium with a pore size distribution wider than (say) an order of magnitude, and (2) there are advantages to

having a closed-form or at least semi-analytical model. It was in that context that we devoted this chapter to fractal models of the porespace and the WRC.

It is obvious that fractal mathematics are a good match for porous materials whose fundamental parameters have fractal characteristics. And in fact, we saw that soil with a fractal particle size distribution seems to be well described by a very simple fractal porespace model such as RS. The description is good enough that at several points we questioned whether differences between model and measurement were due to model deficiencies or measurement issues! The excellent predictions of such simple models support further investigations into their utility.

Nonetheless, some differences between model and measurement must be due to the fractal models having (at this point) no percolation concepts built in. Models such as RS are in some sense no different from the capillary bundle model: they do not include accessibility, scale effects, or critical behaviors at thresholds. Additionally, the critical pore radius r_c, and the threshold water content θ_t, have not been clearly related to percolation concepts. We take up these issues in the following chapters.

References

1. Anderson, A.N., McBratney, A.B., Crawford, J.W.: Application of fractals to soil studies. Adv. Agron. **63**, 1–76 (1998)
2. Arya, L.A., Paris, J.F.: A physic-empirical model to predict the soil moisture characteristics from particle size distribution and bulk density data. Soil Sci. Soc. Am. J. **45**, 1023–1029 (1981)
3. Avnir, D., Biham, O., Lidar, D., Malcai, O.: Is the geometry of nature fractal? Science **279**, 38–40 (1998)
4. Bird, N.R.A.: Comment on "An improved fractal equation for the soil water retention curve" by E. Perfect et al. Water Resour. Res. **34**, 929 (1998)
5. Bird, N.R.A., Perrier, E., Rieu, M.: The water retention function for a model of soil structure with pore and solid fractal distributions. Eur. J. Soil Sci. **51**, 55–63 (2000)
6. Bittelli, M., Flury, M.: Errors in water retention curves determined with pressure plates. Soil Sci. Soc. Am. J. **73**, 1453–1460 (2009)
7. Brooks, R.H., Corey, A.T.: Hydraulic properties of porous media. Colorado State University, Hydrology Paper No. 3, 27 p. (1964)
8. Campbell, G.S.: A simple method for determining unsaturated hydraulic conductivity from moisture retention data. Soil Sci. **117**, 311–314 (1974)
9. Chen, Y., Zhang, C., Shi, M., Peterson, G.P.: Role of surface roughness characterized by fractal geometry on laminar flow in microchannels. Phys. Rev. E **80**, 026301 (2009)
10. Cheng, J.-T., Pyrak-Nolte, L.J., Nolte, D.D., Giordano, N.J.: Linking pressure and saturation through interfacial areas in porous media. Geophys. Res. Lett. **31**, L08502 (2004)
11. Cihan, A., Perfect, E., Tyner, J.S.: Water retention models for scale-variant and scale-invariant drainage of mass prefractal porous media. Vadose Zone J. **6**, 786–792 (2007)
12. Crawford, J.W., Matsui, N., Young, I.M.: The relation between the moisture-release curve and the structure of soil. Eur. J. Soil Sci. **46**, 369–375 (1995)
13. de Gennes, P.G.: Partial filling of a fractal structure by a wetting fluid. In: Adler, D., Fritzsche, H., Ovshinsky, S.R. (eds.) Physics of Disordered Materials, pp. 227–241. Plenum, New York (1985)
14. de Gennes, P.G.: Wetting: statics and dynamics. Rev. Mod. Phys. **57**(3), 827–863 (1985)

15. de Gennes, P.G.: Dynamic capillary pressure in porous media. Europhys. Lett. **5**, 689–691 (1988)
16. Deinert, M.R., Parlange, J.-Y., Cady, K.B.: Simplified thermodynamic model for equilibrium capillary pressure in a fractal porous medium. Phys. Rev. E **72**, 041203 (2005)
17. Deinert, M.R., Dathe, A., Parlange, J.-Y., Cady, K.B.: Capillary pressure in a porous medium with distinct pore surface and pore volume fractal dimensions. Phys. Rev. E **77**, 021203 (2008), pp. 3
18. Dullien, F.A.L.: New network permeability model of porous media. AIChE J. **21**, 299–307 (1975)
19. Filgueira, R.R., Pachepsky, Ya.A., Fournier, L.L., Sarli, G.O., Aragon, A.: Comparison of fractal dimensions estimated from aggregate mass-size distribution and water retention scaling. Soil Sci. **164**, 217–223 (1999)
20. Freeman, E.J.: Fractal geometries applied to particle size distributions and related moisture retention measurements at hanford. Washington, M.A. Thesis, University of Idaho, Moscow (1995)
21. Ghanbarian, B., Hunt, A.G., Ewing, R.P., Sahimi, M.: Tortuosity in porous media: a critical review. Soil Sci. Soc. Am. J. **77**, 1461–1477 (2013)
22. Ghanbarian-Alavijeh, B., Hunt, A.G.: Comments on "More general capillary pressure and relative permeability models from fractal geometry" by Kewen Li. J. Contam. Hydrol. **140–141**, 21–23 (2012)
23. Ghanbarian-Alavijeh, B., Millán, H., Huang, G.: A review of fractal, prefractal and pore-solid-fractal models for parameterizing the soil water retention curve. Can. J. Soil Sci. **91**, 1–14 (2011)
24. Ghanbarian-Alavijeh, B., Skinner, T.E., Hunt, A.G.: Saturation-dependence of dispersion in porous media. Phys. Rev. E **86**, 066316 (2012)
25. Gvirtzman, H., Roberts, P.V.: Pore scale spatial analysis of two immiscible fluids in porous media. Water Resour. Res. **27**, 1165–1176 (1991)
26. Hoffman, R.L.: A study of the advancing interface. I. Interface shape in liquid-gas systems. J. Colloid Interface Sci. **50**, 228–241 (1975)
27. Hunt, A.G.: Comments on "Fractal fragmentation, soil porosity, and soil water properties: I. Theory". Soil Sci. Soc. Am. J. **71**, 1418–1419 (2007)
28. Hunt, A.G., Gee, G.W.: Water-retention of fractal soil models using continuum percolation theory: tests of Hanford Site soils. Vadose Zone J. **1**, 252–260 (2002)
29. Hunt, A.G., Gee, G.W.: Wet-end deviations from scaling of the water retention characteristics of fractal porous media. Vadose Zone J. **2**, 759–765 (2003)
30. Hunt, A.G., Skinner, T.E.: Hydraulic conductivity limited equilibration: effect on water retention characteristics. Vadose Zone J. **4**, 145–150 (2005)
31. Hunt, A.G., Ghanbarian, B., Saville, K.C.: Unsaturated hydraulic conductivity modeling for porous media with two fractal regimes. Geoderma **207–208**, 268–278 (2013)
32. Jullien, R., Botet, R.: Aggregation and Fractal Aggregates. World Scientific, Singapore (1987)
33. Katz, A.J., Thompson, A.H.: Fractal sandstone pores: implications for conductivity and pore formation. Phys. Rev. Lett. **54**, 1325–1328 (1985)
34. Kosugi, K.: Three-parameter lognormal distribution model for soil water retention. Water Resour. Res. **30**, 891–901 (1994)
35. Larson, R.G., Morrow, N.R.: Effects of sample size on capillary pressures in porous media. Powder Technol. **30**, 123–138 (1981)
36. Madadi, M., Sahimi, M.: Lattice Boltzmann simulation of fluid flow in fracture networks with rough, self-affine surfaces. Phys. Rev. E **67**, 026309 (2003)
37. Mandelbrot, B.B.: The Fractal Geometry of Nature. Freeman, San Francisco (1982)
38. Millán, H., González-Posada, M.: Modelling soil water retention scaling: comparison of a classical fractal model with a piecewise approach. Geoderma **125**, 25–38 (2005)
39. Mitzenmacher, M.: A brief history of generative models for power law and lognormal distributions. Internet Math. **1**(2), 226–251 (2004)

40. Mourzenko, V.V., Thovert, J.-F., Adler, P.M.: Percolation and conductivity of self-affine fractures. Phys. Rev. E **59**, 4265–4284 (1999)
41. Mourzenko, V.V., Thovert, J.-F., Adler, P.M.: Permeability of self-affine fractures. Transp. Porous Media **45**, 89–103 (2001)
42. Mualem, Y.: A new model for predicting the hydraulic conductivity of unsaturated porous media. Water Resour. Res. **12**, 513–522 (1976)
43. Nigmatullin, R.R., Dissado, L.A., Soutougin, N.N.: A fractal pore model for Archie's law in sedimentary rocks. J. Phys. D, Appl. Phys. **25**, 32–37 (1992)
44. Ojeda, M., Perfect, E., Alcaniz, J.M., Ortiz, O.: Fractal analysis of soil water hysteresis as influenced by sewage sludge application. Geoderma **134**, 386–401 (2006)
45. Oron, A.P., Berkowitz, B.: Flow in rock fractures: the local cubic law assumption reexamined. Water Resour. Res. **34**, 2811–2825 (1998)
46. Perfect, E.: Estimating mass fractal dimensions from water retention curves. Geoderma **88**, 221–231 (1999)
47. Perfect, E.: Modeling the primary drainage curve of prefractal porous media. Vadose Zone J. **4**, 959–966 (2005)
48. Perfect, E., Rasiah, V., Kay, B.D.: Fractal dimensions of soil aggregate-size distributions calculated by number and mass. Soil Sci. Soc. Am. J. **56**, 1407–1409 (1992)
49. Perfect, E., Kenst, A.B., Díaz-Zorita, M., Grove, J.H.: Fractal analysis of soil water desorption data collected on disturbed samples with water activity meter. Soil Sci. Soc. Am. J. **68**, 1177–1184 (2004)
50. Perrier, E., Bird, N., Rieu, M.: Generalizing a fractal model of soil structure: the pore-solid fractal approach. Geoderma **88**, 137–164 (1999)
51. Perrier, E., Rieu, M., Sposito, G., de Marsily, G.: Models of the water retention curve for soils with a fractal pore size distribution. Water Resour. Res. **32**, 3025–3031 (1996)
52. Poon, C.Y., Sayles, R.S., Jones, T.A.: Surface measurement and fractal characterization of naturally fractured rocks. J. Phys. D, Appl. Phys. **25**, 1269–1275 (1992)
53. Rieu, M., Sposito, G.: Fractal fragmentation, soil porosity, and soil water properties: I. Theory, II. Applications. Soil Sci. Soc. Am. J. **55**, 1231–1244 (1991)
54. Rieu, M., Perrier, E.: Fractal models of fragmented and aggregated soils. In: Baveye, P., et al. (eds.) Fractals in Soil Science, pp. 169–201. CRC Press, Boca Raton (1997)
55. Sahimi, M.: Flow and Transport in Porous Media and Fractured Rock: From Classical Methods to Modern Approaches. Wiley-VCH, New York (2011). 709 pp.
56. Shirazi, M.A., Boersma, L., Hart, J.W.: A unifying quantitative analysis of soil texture: improvement of precision and extension of scale. Soil Sci. Soc. Am. J. **52**, 181–190 (1988)
57. Toledo, P.G., Novy, R.A., Davis, H.T., Scriven, L.E.: Hydraulic conductivity of porous media at low water content. Soil Sci. Soc. Am. J. **54**, 673–679 (1990)
58. Turcotte, D.L.: Fractals and fragmentation. J. Geophys. Res. **91**, 1921–1926 (1986)
59. Tyler, S.W., Wheatcraft, S.W.: Application of fractal mathematics to soil water retention estimation. Soil Sci. Soc. Am. J. **53**, 987–996 (1989)
60. Tyler, S.W., Wheatcraft, S.W.: Fractal processes in soil water retention. Water Resour. Res. **26**, 1047–1054 (1990)
61. Tyler, S.W., Wheatcraft, S.W.: Fractal scaling of soil particle size-distributions: analysis and limitations. Soil Sci. Soc. Am. J. **56**, 362–369 (1992)
62. van Genuchten, M.Th.: A closed-form equation for predicting the hydraulic conductivity of unsaturated soils. Soil Sci. Soc. Am. J. **44**, 892–898 (1980)
63. Weitz, D.A., Stokes, J.P., Ball, R.C., Kushnick, A.P.: Dynamic capillary pressure in porous media: origin of the viscous-fingering length scale. Phys. Rev. Lett. **59**, 2967–2970 (1987)
64. Zhang, X., Knackstedt, M.A., Sahimi, M.: Fluid flow across mass fractals and self-affine surfaces. Physica A **233**, 835–847 (1996)

Chapter 5
Specific Examples of Critical Path Analysis

At the end of Chap. 2, the general technique of critical path analysis was introduced within the framework of the electrical conductivity of disordered systems. In many systems the charges that move between these sites are electrons, but in other cases they are ions, or even protons. Critical path analysis forms the basis of much of the remainder of this book. However, there are some subtleties to the technique, and its application cannot be as easily generalized as is often assumed: to some extent every case or system must be evaluated separately.

In typical solid-state applications, conductances are connected between sites, which are located randomly in space (why?),[1] so the critical bond fractions from the lattice models of Chap. 1 are not directly applicable. Nevertheless, when transport is locally defined according to, say, the probability per unit time that an electron moves from one clearly defined site to another, then it is clear that the appropriate form of percolation theory to apply is bond percolation, even though one may not know from the results of Chap. 1 what an appropriate bond percolation threshold is. But in porous media it is not initially obvious even which form of percolation theory—bond, site, or continuum—should be used. Network models, which distinguish carefully between pore bodies and pore throats, and for which it is known that the chief limitation to flow comes through the pore throats, clearly require a bond percolation approach. But we contend that use of a continuous random fractal model requires application of continuum percolation theory. If continuum percolation is not used, one can make a good case for treating the wetting of a porous medium as a site percolation problem, and the drying of the same medium as a bond percolation problem [35]. In each of these cases, for which an important random component of the model is already linked with the topology of the connections, the critical percolation probability becomes a major issue, especially when the distribution of local flow (or transport) rates is very wide, because an important component of the analysis is determining the critical path.

[1] In solid-state physics applications, electronic transport is wave-like in ordered systems. Localization of electrons and hopping transport occur primarily in the presence of disorder.

A. Hunt et al., *Percolation Theory for Flow in Porous Media*,
Lecture Notes in Physics 880, DOI 10.1007/978-3-319-03771-4_5,

In the electrical conductivity in condensed matter systems described below (and, if our interpretation is correct, also in humid clay minerals, Sect. 7.4), transport occurs by the "hopping" of charges from site to site. The term "hopping" means that charges, which are located on specific sites most of the time, may jump to another site in a much shorter time. "Hopping" can be a classical process by which a particle jumps over an energy barrier to a neighboring site, or it can be a quantum mechanical process whereby the particle tunnels through an energy barrier.

Consider first the classical process. While the typical time taken to jump to another site is essentially zero, the time a charge spends "waiting" to jump is typically an exponential function of the energy barrier, E, between the sites, that is, $\tau = \nu_{\rm ph}^{-1} \exp(E/k_{\rm B}T)$. Here the quantity $\nu_{\rm ph}$ is a vibrational or "attempt" frequency, and $k_{\rm B}T$ is the product of the Boltzmann constant and the temperature. The subscript, ph, refers to a phonon, a quantized lattice vibration. The exponential dependence on energy, E, ultimately derives from the probability that the energy to transport the particle over the barrier can be absorbed by the particle from thermal fluctuations in the surroundings, and the probability that such thermal fluctuations, or "phonons," may be found is proportional to the Boltzmann factor, $\exp(-E/k_{\rm B}T)$. This "waiting" time may also be loosely referred to as a relaxation time, or a hopping time. In disordered systems, such energy barriers can vary widely from place to place, and the total time required to transport charges through the material (related to an effective velocity, or current) depends on all the waiting times along the particular path followed. For dc conduction in macroscopic natural systems, there is usually enough time, enough individual charges, and enough local heterogeneity that the dominant transport paths can be identified as those with the "least resistance," or with smallest transport times, that is, smallest activation energies.

In the quantum process, the transition rates are related through Fermi's "golden rule" (see any fundamental text on quantum mechanics) to the square of overlap matrix elements calculated between localized "hydrogenic" wave functions. The electrons are localized on sites due to disorder, and occasionally tunnel from site to site. This tunneling introduces an exponential factor with argument proportional to twice (from the operation of squaring the matrix element) the separation of sites.

5.1 r-Percolation

The first system investigated in terms of critical path analysis [1] was a slightly idealized representation of impurity conduction in crystalline semiconductors. This system is represented schematically in two dimensions in Fig. 5.1 and can be described as follows. Sites, i, are located randomly in three-dimensional space (their individual positions are uncorrelated) with a mean concentration, N_0. Resistances, R_{ij}, between each pair of sites, i, j, have the values [26],

$$R_{ij}^{-1} = \frac{e^2 \nu_{\rm ph}}{k_{\rm B}T} \exp\left[-\frac{E_0}{k_{\rm B}T}\right] \exp\left[-\frac{2r_{ij}}{a}\right] \equiv R_0^{-1} \exp\left[-\frac{2r_{ij}}{a}\right] \tag{5.1}$$

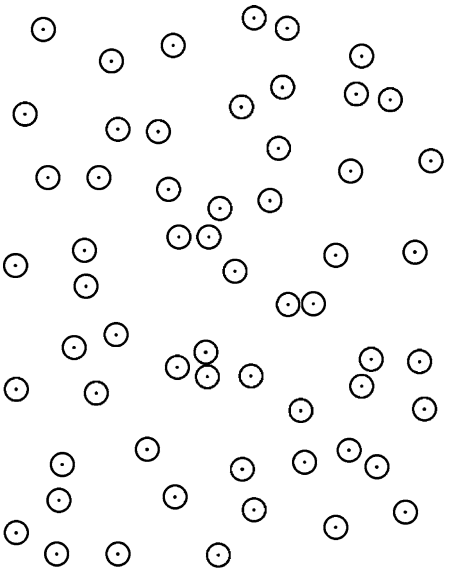

Fig. 5.1 A schematic (and two-dimensional) representation of the Ambegaokar site percolation treatment of r-percolation. If one draws spheres of a given radius, r, about every site on the network, when the radius of these spheres reaches r_c, an interconnected network of spheres of infinite size will appear. This r_c is the critical radius for percolation and defines the minimum possible value of the maximum resistance encountered by the current

In this expression for R_{ij} the only variable quantity is r_{ij}, the distance between sites i and j. The other quantities are the electronic charge, e, a fundamental vibrational frequency, $\nu_{ph} \approx 10^{12}$ Hz, the Boltzmann constant k_B, the temperature T, a uniform activation energy, E_0, and a fundamental length scale, a. The magnitude of a is a few nanometers and its origin is in its description of the radius of the hydrogenic wave function. Typical site separations, r_{ij}, may be 5 to 15 times larger. Equation (5.1) actually arises from consideration of equilibrium transition rates, w_{ij}, that describe the probability per unit time that an electron will jump from site i to site j. When $r_{ij}/a \gg 1$, w_{ij} is very small, and it is very difficult, and thus unlikely, for an electron on site i to jump to site j in a short time. In Sect. 7.4 we will revisit this subject when we consider a time-dependent (or frequency-dependent) electrical field.

Since in Eq. (5.1) all the quantities except r_{ij} are constant, it is convenient to express the individual resistances in terms of a constant prefactor, R_0 and the random variable r_{ij}. The resistances actually represent averages over local stochastic processes involving the sudden hopping motion of electrons from, e.g., site i to site j. Because the only variable in the resistances is the site separation, r, this system is also called r-percolation. Note that the origin of the exponential function in r_{ij}/a most simply relates to an overlap in electronic (hydrogenic) wave functions on sites i and j, and represents a tunneling probability. In the more complicated r–E percolation discussed in the following subsection, the physical interpretation of this function remains the same.

Let the mean concentration of sites be N_0. Since the placement of the sites is random, the probability density function $W(r)$, for finding a site j within dr of a distance r of site i, is proportional to the differential volume, $4\pi r^2 dr$:

$$W(r)dr = 4\pi r^2 N_0 dr \tag{5.2}$$

The mean number, $\langle N \rangle$, of sites j within a distance r of i is then,

$$\langle N \rangle = \frac{4}{3}\pi r^3 N_0 \tag{5.3}$$

When r is chosen so that $\langle N \rangle = 1$, r must be the typical site separation, b, i.e., $(4/3)\pi b^3 N_0 = 1$. A typical value of the quotient $r_{ij}/a = b/a$ may be 10 or larger, so a site which is twice as far from a given site as the typical nearest neighbor distance, b, will be connected to it with a resistance which is $e^{10} \approx 10^4$ larger than the typical value. Thus if one starts to connect appropriate resistors between neighboring sites in Fig. 5.1 the resistance values may be spread over 10–20 orders of magnitude or more. This exponential dependence of R_{ij} on the random variable r_{ij} makes the spread of R_{ij} values enormous, and promotes the value of percolation theory for finding the macroscopic transport coefficients.

We make use again of the probabilistic identity $W(r)dr = W(R)dR$, familiar from substitution of variables in integration, to transform Eq. (5.2) to

$$W(R) = \frac{\pi a^3 N_0}{2R} \ln^2\left(\frac{R}{R_o}\right) = \frac{3a^3}{8b^3 R} \ln^2\left(\frac{R}{R_o}\right) \tag{5.4}$$

Note the appearance of the factor R^{-1}, which is a result of the fact that the R_{ij} are exponential functions of the random variable, r_{ij}. Insofar as the R_{ij} are exponential functions of random variables, this power of -1 is universal.

For ill-condensed matter (impurity conduction systems, glasses, disordered ceramics, super-cooled liquids, etc.), this type of local transport (quantum mechanical tunneling and/or thermally activated hopping) is the rule rather than the exception, and the factor R^{-1} leads to a number of universal results, although these results are not discussed here. But for most applications in porous media, local resistances (whether electrical or hydraulic) will not be of this form, but are actually powers of random variables. This will lead to fundamental differences between the two systems. The logarithmic factor in Eq. (5.4) is also a product of the functional form of the resistances, but its specific form, $\ln^2(R/R_0)$, requires also that the pdf of the site separations, Eq. (5.2), be a power law with power 2. If the pdf of the site separations were an exponential function of the distance (as is the case for nearest-neighbor separations in a one-dimensional analogue to the present system), then the logarithmic factor would be replaced with a power. That power, in contrast to R^{-1}, is not universal, but depends on the specifics of the system, such as the ratio b/a.

Now that we have the expressions for the local resistance values in terms of site separations, and the pdf for those site separations, it is, in principle, a straightforward process to find the critical resistance of the system. What is missing is a reference to percolation. Clearly the problem under discussion is most fundamentally related to bond percolation, but in Chap. 1 there was no critical bond fraction given for a random lattice. In fact, computer simulations [37] for such random systems have shown that the percolation threshold is defined in terms of the average number of bonds, α, connected to an arbitrary site. When $\alpha \geq 2.7 \equiv \alpha_c$, then the network of interconnected bonds percolates. The percolation condition can now be satisfied by

setting the average number of sites within a distance r_c of an arbitrary site equal to the critical value, α_c:

$$\alpha_c = \int_0^{r_c} 4\pi r^2 N_0 dr = \int_0^{r_c} 3\frac{r^2}{b^3} dr \tag{5.5}$$

The meaning of Eq. (5.5) is that on the average, α_c bonds with lengths that do not exceed r_c can be connected to such an arbitrary site. That result implies that it is possible to connect an infinitely large network of connected bonds that do not individually exceed r_c in length. This means that the largest resistance in such a network is given by $R_c = R_0 \exp(2r_c/a)$.

The solution of Eq. (5.5) is

$$r_c = \alpha_c^{1/3} b \tag{5.6}$$

The critical resistance, R_c, is then

$$R_c = R_0 \exp\left[\frac{2\alpha_c^{1/3} b}{a}\right] \tag{5.7}$$

and is not obtainable by any procedure based on averaging. Furthermore, with $\alpha_c^{1/3} \approx 1.4$ and $b/a \approx 10$, $R_c \approx R_0 \exp(28) \approx R_0 10^{12}$, two things are apparent: (1) paths which allow a space between sites even twice the critical separation have resistances 12 orders of e larger, and (2) using a typical separation $2b/a$ in place of the critical separation underestimates the controlling resistance by four orders of magnitude. These are the reasons why predictions of transport processes that are not based on percolation theory will fail. Note that Eq. (5.7) can just as easily be derived if one considers the dimensionless variable, $\xi \equiv 2r/a$, such that $R = R_0 \exp \xi$. The integrand is then modified by the extra factor $(a/2)^3$ and the variable of integration becomes ξ instead of r, but the functional dependence is still ξ^2. Thus one finds $\xi_c = (2/a)\alpha_c^{1/3} b$, leaving unchanged the result that $R_c = R_0 \exp[(2/a)\alpha_c^{1/3} b]$. For r-percolation, such a change of variables seems needlessly complicated, but for r–E percolation, application of such a technique using a dimensionless variable proves to be very useful.

We can find the typical separations, d, of all resistances $R < R_c$ as follows:

$$\frac{(\frac{4\pi}{3})d^3}{(\frac{4\pi}{3})b^3}\left[\int_0^{r_c} 4\pi r^2 N_0 dr\right] = 1 \tag{5.8}$$

The solution of Eq. (5.8) is,

$$d = \alpha_c^{-\frac{1}{3}} b \tag{5.9}$$

This result, Eq. (5.9), allows the percolation condition to be expressed in a nice geometric form:

$$r_c = \alpha_c^{\frac{2}{3}} d \tag{5.10}$$

i.e., that the typical length of bonds, r_c, is proportional to their typical separation, d, with a proportionality constant $\alpha_c^{2/3}$. The interpretation is thus clear that a larger

value of α_c requires that the typical bond length be a larger fraction of the typical bond separation, making it increasingly difficult to connect the bonds into a percolating network.

Although we have treated the impurity conduction problem as a bond percolation problem, it can be easily represented in terms of site percolation through a geometrical construction. Ambegaokar et al. [1] presented this problem initially in terms of overlapping spheres (see the circles in Fig. 5.1). Their idea was that one could construct spheres of an arbitrary but uniform radius, r, about each site i, and increase r until at $r = r_c$ a path of touching or overlapping spheres could be found. Imagining these spheres to be metallic (and not bothering about the physical problems of their overlap) allows an obvious site percolation interpretation in terms of a connected conducting path. The largest resistances on that path, where the spheres just touch, is R_c, and this value (Eq. (5.7)) dominates current.

Proceeding with critical path analysis, we need to find a useful expression for $p - p_c$, in terms of which all other percolation variables are expressed. But we have expressed R_c not in terms of a critical bond probability, but rather in terms of the number of connected bonds, α_c. However, $p - p_c$ must be proportional to $\alpha - \alpha_c$. Thus the first step must be to express some arbitrary R, which for $R < R_c$ gives the maximum resistance on finite-sized clusters of interconnected resistors, and for $R > R_c$ gives the maximum resistance of the infinite cluster, in terms of an arbitrary α. This is done as follows:

$$\alpha = \int_0^r 3\frac{y^2}{b^3}dy \tag{5.11}$$

using y as a dummy (spatial) variable. Combining Eq. (5.5) and Eq. (5.7) gives

$$\alpha - \alpha_c = \frac{r^3 - r_c^3}{b^3} = \left(\frac{a}{2b}\right)^3 \left[\ln^3\left(\frac{R}{R_0}\right) - \ln^3\left(\frac{R_c}{R_0}\right)\right] \tag{5.12}$$

This expression is somewhat complicated. We factor $r^3 - r_c^3$ in keeping with the spirit of percolation theory, in which quantities are expanded to lowest order in $p - p_c$; thus $(r - r_c)(r^2 + rr_c + r_c^2) \approx (r - r_c)3r_c^2$. In the second factor, which contains only sums, r may be approximated as r_c. This result is identical to the first term in a Taylor series expansion of $r^3 - r_c^3$ evaluated at the point r_c. Then,

$$p - p_c \propto \alpha - \alpha_c = \frac{r^3 - r_c^3}{b^3} \approx \frac{3r_c^2}{b^3}(r - r_c) = \left(\frac{3a\alpha_c^{2/3}}{2b}\right)\ln\left(\frac{R}{R_c}\right) \tag{5.13}$$

From Chap. 1 we can write for the conductivity of a subnetwork defined by a maximal resistance R,

$$\sigma = \frac{l}{R\chi^{2\nu}} \tag{5.14}$$

where l is the typical separation of resistances R, and χ is the correlation length evaluated at a value of p corresponding to the chosen R. The point will be to opti-

mize the right-hand side of Eq. (5.14) in terms of system and percolation parameters. We can write χ as,

$$\chi \propto (p - p_c)^{-\nu} \propto \ln^{-\nu}\left(\frac{R}{R_c}\right) \tag{5.15}$$

To address the separation of the largest resistances in the subnetwork we must use a discretized distribution of resistance values rather than a continuous distribution, because otherwise it is impossible to define "the largest" resistance values. Since the resistances considered are exponential functions of a random variable, it makes sense to discretize the distribution in steps of the natural constant $e = 2.718$, i.e., $R = R_0 \exp(j)$, where j is an integer. Such a unit of resistance corresponds to an increment in r of magnitude $a/2$. Then it is possible to write the separation of the largest resistances, with length r, in terms of the separation, d, of all resistors with $R \leq R_c$,

$$l = d\left[\frac{\int_{r-a/2}^{r+a/2} 4\pi r^2 N_0 dr}{\int_0^r 4\pi r^2 N_0 dr}\right]^{-\frac{1}{3}} = d\left[\frac{3r}{a}\right]^{\frac{1}{3}} = b\left[\frac{3r}{\alpha_c a}\right]^{\frac{1}{3}} \tag{5.16}$$

Whether this value of l has any relationship with the typical separation of maximally valued resistances along the current-carrying paths on the infinite cluster is not yet clear, however. While the distribution of resistance values on the infinite cluster may be approximated as being the same as in the bulk (except terminated at R), it is clear that the dominant current-carrying path might avoid most of the larger resistances. Two widely different perspectives can be formulated for this problem. Stauffer (and others) use the "links-nodes-blobs" model to argue $l \propto \chi$. Certainly it makes no sense to choose $l > \chi$, because one would then be basing the calculation of l on a value of the controlling resistance smaller than the value used in Eq. (5.14). Hunt [13] has used Eq. (5.16), which can lead to $l \ll \chi$. While simulations clearly show that $l \propto L$ in two dimensions, comparison of analogous results with experiments on variable-range hopping systems in three dimensions [24, 25] has proved at least ambiguous [13]. Below we give a self-consistent argument for using Eq. (5.16) or slight modifications thereof.

l from Eq. (5.16) is not a function of the variable $p - p_c$ (or $r - r_c$), and its dependence on $r \propto \ln(R)$ is weak. So for the purpose of optimizing Eq. (5.14), the dependence of l on r may be neglected. Then one can write,

$$\sigma \propto \frac{1}{R} \ln^{2\nu}\left(\frac{R}{R_c}\right) \tag{5.17}$$

It is easy to optimize such an expression for the dependence of σ on R with respect to the arbitrary parameter R, so as to find the optimal value of the limiting resistance, R_{opt}. Note also that it is immaterial whether the optimization is formulated in terms of R_c or $g_c \equiv R_c^{-1}$. This equivalence is not preserved in typical problems in porous media, as will be seen. The result of optimizing Eq. (5.17) is,

$$R_{opt} = R_c \exp(2\nu) \tag{5.18}$$

a result which is independent of the details of the system. Note that if the Stauffer argument is used the power of 2ν on the logarithm is reduced to ν, and

$R_{opt} = R_c \exp(\nu)$. In two dimensions the power of the logarithm is reduced by ν in either perspective, so that the Stauffer argument yields $R_{opt} = R_c$, while a treatment analogous to Eq. (5.16) would yield $R_{opt} = R_c \exp(\nu)$. $R_{opt} = R_c$ appears to be confirmed in 2D simulations [14, 40].

How does one proceed further? The question which needs to be evaluated is, what fraction of the largest resistors on the connected path is shorted by smaller resistances? If $l \propto \chi$, the implication is that in the limit $p \to p_c$, all the largest resistances are shorted. This argument appears to be inconsistent, especially in the context of the optimization procedure, which in three dimensions leads to $R_{opt} > R_c$ (using either $R_c \exp(\nu)$ or $R_c \exp(2\nu)$), and suggests that it is only inclusion of resistances larger than the optimal value, R_{opt}, which does not change the conductivity. Such a result is consistent with the physical result that 100 % of the largest resistances are shorted only for the choice $R \geq R_{opt}$. If $R_{opt} > R_c$, then it is not logical to choose l as a singular function at R_c. If l is not singular at R_c, then l may be approximated as slowly varying in the immediate vicinity of R_c, and the result (in three dimensions) follows that $R_{opt} = R_c \exp(2\nu)$, generating the self-consistent result that the fraction of shorted maximal resistors is only 1 at this larger value of R.

However, the above argument leaves a loophole in 2D. If l is assumed to be a singular function of $p - p_c$ ($l \propto \xi$) in 2D, then the optimization procedure does not lead to $R_{opt} > R_c$, because of the cancellation of l/χ (in contrast to l/χ^2 in 3D). Of course one could also make the argument that l is not singular at R_c, and that result would also be self-consistent. If both possibilities, which are mutually exclusive, are self-consistent in 2D, it may imply that 2D systems allow different solutions depending on the details of the problem. It certainly appears likely that the optimization is fundamentally different in 2D than in 3D, since only the argument that l is not singular at p_c is self-consistent there. So we continue to use Eq. (5.16) (and the appropriate analogue for variable-range hopping systems) for l in 3D systems. Skaggs [39] and references cited therein discuss this subject in a detail beyond the scope of this book.

An especially important physical result is an evaluation of the correlation length at R_{opt}. To find this value of χ, simply substitute $R = R_c \exp(2\nu)$ into the expression (Eq. (5.13)) for $p - p_c$, and raise to the $-\nu$ power. The result is,

$$\chi(R_{opt}) = \left[\frac{b}{3a\nu\alpha_c^{2/3}} \right]^{\nu} \equiv L \tag{5.19}$$

This value, denoted L, is particularly important because it gives (to within a numerical constant) the structure of the optimal current-carrying paths. Thus the largest holes in the current-carrying paths are of approximate radius L, percolation calculations of all transport quantities require that the system size be considerably greater than L, or the effects of fluctuations will be large, etc. In the language of hydrology, L^3 would be the representative elementary volume (REV). Note that Berkowitz and Balberg [4] already pointed out that in the neighborhood of the percolation threshold, χ^3 gives the REV; our result for critical path analysis is in conformance with their analysis. Also analogous calculations of l and L for the hydraulic conductivity of network models of porous media were verified [13] to give the right dependence

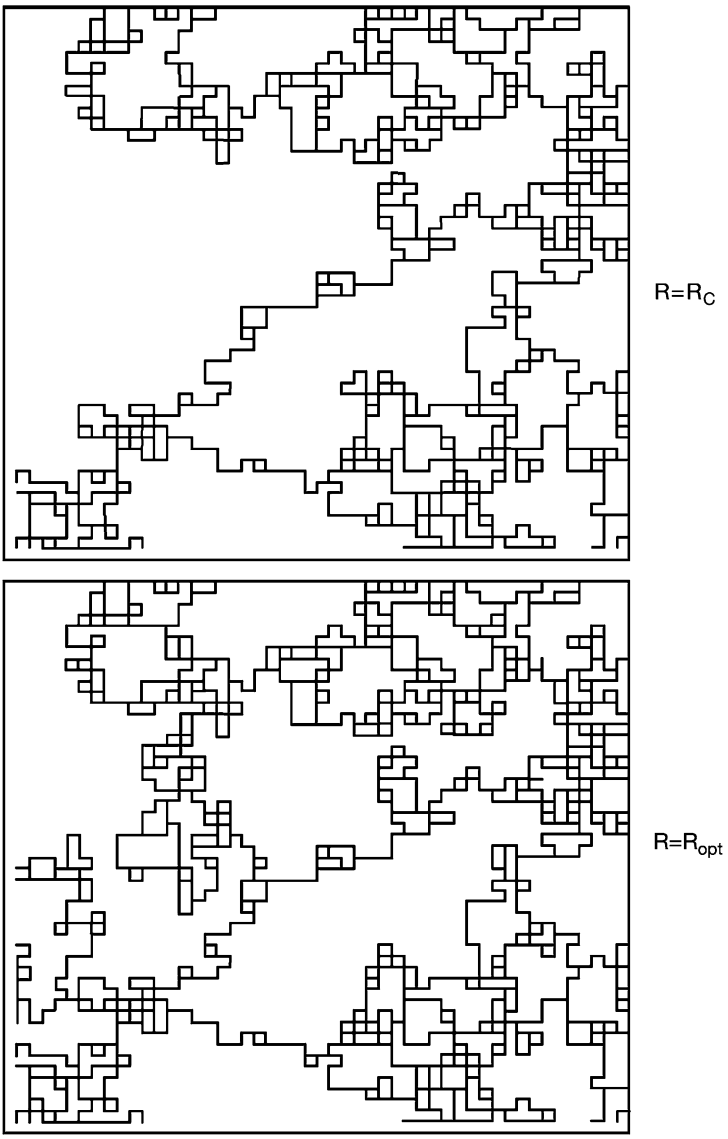

Fig. 5.2 A comparison of the backbone clusters for maximum R values R_c and R_{opt}. Note that in the first case the correlation length is infinite, and there is only one connected path across the (finite-sized) system. In an infinitely large system there would still be only one connected path. But for R_{opt} there are several connected paths (from Todd Skaggs, unpublished)

on system and distribution parameters, although the values from the simulations were typically 30–40 % smaller than predicted.

Figure 5.2 gives a comparison of the backbone cluster for the largest $R = R_c$ with the corresponding cluster for the largest $R = R_{max}$.

5.2 r–E-Percolation (Variable-Range Hopping)

Amorphous semiconductors represent the classic case for the application of critical path analysis. Here the energy is also a random variable, meaning that electrons can have a variety of energy values. At a temperature $T = 0$, the electrons occupy the lowest energy states and essentially do not move. At higher temperatures they can move and there is a non-zero electrical conductivity. The Fermi energy at $T = 0$ divides states occupied by electrons (with $E < E_f$) from those without electrons (with $E > E_f$). Since we will consider only continuous energy distributions, E_f is then the highest energy of any state occupied by electrons. In such systems, called r–E-percolation, the resistances between individual sites are functions of two random variables, energy and distance:

$$R_{ij}^{-1} = \left(\frac{e^2 \nu_{ph}}{k_B T}\right) \exp\left[-\frac{E_{ij}}{k_B T} - \frac{2r_{ij}}{a}\right] \tag{5.20}$$

T is the absolute temperature. The random energy, E_{ij}, is either the difference in energy from the initial, E_i, to the final, E_j, state (if this difference is positive and the sites are on opposite sides of the Fermi energy), or it is the larger of the absolute values of the two energies (measured with respect to the Fermi energy, E_f). The reason for this peculiar definition of E_{ij} is that the resistance is inversely proportional to the probability per unit time that an electron jumps from site i to site j. This probability is composed of the product of the conditional probability that an electron could jump from site i to site j, if it were on site i to begin with and site j were empty, with the probabilities that an electron resides on site i and that no electron resides on site j. The first probability brings in a factor of $\exp[-(E_j - E_i)/kT]$, if $E_j > E_i$, because of the need to find a phonon to deliver this energy to the electron. The second probability is the product of the Fermi function, $f(E_i)$ for electron occupation of a site at energy E_i, and $1 - f(E_j)$ for no electron occupation of site j. $f(E_i)$ for example is often approximated by a Boltzmann factor in the energy difference $E_i - E_f$. So the energy term in the exponent represents a composite of effects of site occupation and energy conservation.

The energies of the individual sites are considered to be distributed uniformly between $-W_0/2$ and $W_0/2$, so that the probability that a site has energy within dE of any given energy in that range is

$$W(E)dE = \frac{dE}{W_0} \tag{5.21}$$

One can now write for the density of states (per unit energy per unit volume) at the Fermi energy, E_f,

$$N(E_f) = \frac{1}{W_0 b^3} \tag{5.22}$$

where b is again the typical separation of sites. With two random variables, and with local correlations introduced by the fact that neighboring bonds share one common site (and its energy value), the application of critical path analysis is considerably

more complex. In analogy to Eq. (5.5), one would have to integrate over three spatial coordinates and one energy coordinate. Pollak [34] did this integration, obtaining the result that,

$$\sigma_{\mathrm{dc}} \propto \exp\left[-\left(\frac{T_0}{T}\right)^{\frac{1}{4}}\right] \tag{5.23}$$

with

$$k_{\mathrm{B}} T_0 \propto W_0 \left(\frac{b}{a}\right)^3 \tag{5.24}$$

The same result was obtained earlier by Mott [30], who however used an optimization procedure for individual resistances. In this procedure electrons can hop greater distances to relieve the energy increase, since there are more sites to attempt at larger distances. The competition between energy and distance tends to shift slowly towards a greater relevance of energy at lower temperatures (because of the ratio of $-E/k_{\mathrm{B}}T$ in the exponential function) so hops become longer and stay at energies nearer the Fermi energy with diminishing temperature.

Mott's procedure is not strictly valid, because it does not guarantee that the individual optimal resistances connect up to form a continuous path for current flow, but it is cited more often because of its simplicity. Here we present an equally simple percolation argument. The argument is based on a generalization of Eq. (5.10). If the maximum hopping energy allowed is E_{m} (when $r_{ij} = 0$), and the maximum hopping distance is r_{m} (when $E_{ij} = 0$), then we must have

$$\frac{E_{\mathrm{m}}}{kT} = \frac{2r_{\mathrm{m}}}{a} \tag{5.25}$$

This equation guarantees the existence of a maximum resistance, $R_{\mathrm{c}} = R_0 \exp E_{\mathrm{m}}/kT = R_0 \exp 2r_{\mathrm{m}}/a$. Connectivity is guaranteed if we relate the typical separation of the sites utilized for the transport equal to the appropriate fraction of the length of the individual resistors. To lowest order, the typical resistance length is

$$\langle r \rangle = \frac{\int_0^{r_{\mathrm{m}}} r(4\pi r^2)dr}{\int_0^{r_{\mathrm{m}}} (4\pi r^2)dr} = \left(\frac{3}{4}\right) r_{\mathrm{m}} \tag{5.26}$$

If one takes into account the fact that the occurrence of large hopping distances must be suppressed because the energy range of sites must be increasingly restricted with increasing r, the numerical coefficient (3/4) would be altered, so this factor cannot be considered accurate.[2] Choosing 1 for the numerical coefficient is therefore equally justified, though slightly less accurate, and it is best simply not to attach any importance to the factor (3/4).

[2] Getting that particular number was the motivation, in fact, for going beyond the particular calculation here to generate a fully consistent percolation calculation (Pollak, personal communication, 2005).

The typical separation between sites with low enough energies (less than E_m) is,

$$d = b\left(\frac{3}{4\pi}\right)^{\frac{1}{3}}\left[\frac{W_0}{E_m}\right]^{\frac{1}{3}} = \left(\frac{3}{4\pi}\right)^{\frac{1}{3}}\left[\frac{1}{N(E_f)E_m}\right]^{\frac{1}{3}} \tag{5.27}$$

Inserting the results of Eq. (5.26) and Eq. (5.27) into Eq. (5.10), and solving simultaneously with Eq. (5.25), yields

$$r_m = a\left(\frac{\alpha_c^2}{9\pi}\right)^{\frac{1}{4}}\left[\frac{1}{k_B T N(E_f) a^3}\right]^{\frac{1}{4}} \propto a\left[\frac{k_B T_0}{k_B T}\right]^{\frac{1}{4}} \propto a\left[\frac{W_0 (b/a)^3}{k_B T}\right]^{\frac{1}{4}} \tag{5.28}$$

This result is compatible with the prior results of Pollak [34] and Mott [30] since $r_m/a = (T_0/T)^{1/4}$, but it yields a slightly different numerical constant than their's. The numerical constants given here are not correct. Since, in order to connect sites with smaller energies, the hopping distance thus increases with diminishing temperature, this type of transport has become known as variable-range hopping. If the combination of variables $2r/a + E/kT$ is defined to be ξ, then one can represent the effects of the full percolation calculation in a form analogous to Eq. (5.5):

$$4\alpha_c \frac{T}{T_0}\int_0^{\xi_c} \xi^3 d\xi = \alpha_c \tag{5.29}$$

Instead of integrating over $\xi^2 d\xi$ as in r-percolation, here one must integrate over $\xi^3 d\xi$ because of the existence of three spatial dimensions (random variables) and one energy dimension (random variable). Clearly the result of the integral is $\xi_c = (T_0/T)^{1/4}$. The integral thus expresses that the resistance values required for percolation are spread through the interior of a four-dimensional volume. One can calculate the typical spatial separation of the resistances with the largest values in a similar way as for r-percolation, by noting that the largest resistance values are spread out over the surface of this four dimensional volume:

$$l = a\left(\frac{T_0}{T}\right)^{(1/4)}\left[\frac{\int_{\xi_c-1}^{\xi_c+1} \xi^3 d\xi}{\int_0^{\xi_c} \xi^3 d\xi}\right]^{-\frac{1}{3}} = a\left(\frac{T_0}{T}\right)^{\frac{1}{3}} \tag{5.30}$$

Thus the largest resistances are located with a unit variation in ξ from the surface, or percolating value, ξ_c. It is also possible to calculate the correlation length which describes the dc conduction. To calculate the correlation length, it is necessary first to find the fundamental length scale of the resistances. In the case of r–E percolation only a fraction of the sites actually take part in the conduction process, and their typical separation is $a(T_0/T)^{1/4}$, so that this fundamental scale is $a(T_0/T)^{1/4}$. Then we have,

$$\chi \propto a\left(\frac{T_0}{T}\right)^{\frac{1}{4}}(p - p_c)^{-\nu} = a\left(\frac{T_0}{T}\right)^{\frac{1}{4}}\left[kT\left(\xi^4 - \xi_c^4\right)\right]^{-\nu} \tag{5.31}$$

The substitution giving the second form on the right hand side was obtained by writing Eq. (5.29) also for an arbitrary ξ (and α) and making p and p_c proportional

to α and α_c. Linearization allows $\xi^4 - \xi_c^4$ to be expressed as roughly $\xi_c^3(\xi - \xi_c)$, and one finds

$$\chi \propto a\left(\frac{T_0}{T}\right)^{\frac{1}{4}}\left[\left(\frac{T_0}{T}\right)^{\frac{1}{4}}\ln\left(\frac{R}{R_c}\right)\right]^{\nu} = a\left(\frac{T_0}{T}\right)^{(1+\nu)(\frac{1}{4})}\ln^{\nu}\left(\frac{R}{R_c}\right) \tag{5.32}$$

Evaluated at $R = R_c \exp(2\nu)$, just as for r-percolation, this expression yields

$$\chi(R_{opt}) \equiv L \propto a\left(\frac{T_0}{T}\right)^{(\frac{1+\nu}{4})} \tag{5.33}$$

One can now write for the electrical conductivity,

$$\sigma = \frac{l}{L^2 R_{opt}} = \frac{a\left(\frac{T_0}{T}\right)^{1/3}}{\left[a\left(\frac{T_0}{T}\right)^{(\frac{1+\nu}{4})}\right]^2 R_0 \exp\left(\frac{T_0}{T}\right)^{1/4}} \tag{5.34}$$

Note that in the case of either r-percolation or r–E percolation systems, the uncertainty in the calculation of l has no effect on the exponent ($2\alpha_c^{1/3}b/a$ or $(T_0/T)^{1/4}$, respectively). The effect is thus on the pre-exponential, which is only a power of the temperature. Since the exponential function is a much more rapidly varying function of system parameters (and, in the case of variable range hopping, of the temperature), it was possible to use the percolation theoretical argument to predict the electrical conductivity over as much as 14 orders of magnitude of the conductivity with minimal discrepancy with experiment (though not in a-Si [25] rather with a-Si:H:Au [24]). While such accuracy is clearly a selling point in the theory it does not, except perhaps in the latter case, help to distinguish between theoretical treatments of l. The only reason why, in the latter case, it was possible to make any judgment as to the accuracy of a particular result for l was that experimental data were reported in the form of the ratio of the ac to the dc conductivity (which eliminated the exponential T dependence), but a detailed treatment of the ac conductivity is a topic beyond the present scope. In the case of the hydraulic conductivity, which has no equivalent separation of exponential and non-exponential contributions, this uncertainty in theory has reduced confidence somewhat in the validity of the percolation-based treatment and introduced some confusion.

An important point of this exercise is to demonstrate from basic physics how to calculate relevant length scales. The numerical values of these length scales are not well-defined, but their dependence on system parameters has been approximately verified both in comparison with experiment [13], and in numerical simulations [14]. As problems of hydrology are addressed, it will be important to have prior guidance for calculating these quantities.

5.3 Saturated Hydraulic Conductivity

One difference between hydrological and solid state applications of critical path analysis is that in the former case the sites take up a non-negligible volume. In

addition, in spite of the approximation of (probabilistic) fractal modeling, the coordination number of large pores is likely larger, on average, than of small pores. As a practical matter, we cannot put pores on a regular grid if their lengths and radii vary over more than an order of magnitude. For all of these reasons, it is better to base the critical path analysis on continuum percolation theory than to use the bond or site versions.

In continuum percolation, accurate application of critical path analysis requires an expression for the critical volume fraction for percolation, which we denote V_c. In contrast to the solid-state problems discussed above, this value is not known from simulations, but we will show in Chaps. 6 and 7 that it is approximately known empirically from experiments in unsaturated media involving solute diffusion [29], electrical conductivity, and air permeability. Balberg [2] (inspired by earlier work of Kogut and Straley [21]) already gave a detailed discussion of continuum percolation problems in porous media. In particular he demonstrated that in continuum percolation, transport exponents may be non-universal, but this topic is postponed until the next chapter. Finally, the local transport law (Poiseuille flow) is a power law in geometric quantities such as the pore radius and the pore length, rather than an exponential function. This difference will be important too, and the implications of this difference have not been completely appreciated [3, 20, 23] in existing critical path applications to the saturated hydraulic conductivity.

Let's assume low Reynolds number flows, meaning that for any given geometry the dependence of the flow through a pore can be written in terms of an effective pore length and pore radius. The appropriate way to relate these radii and lengths to physical lengths requires pore-scale treatments of the Navier-Stokes equation. For calculating the ratio of the hydraulic conductivity at an arbitrary saturation to its value at full saturation such complications are unimportant, as long as the fractal model of the pore-space is accurate, since these geometrical factors do not change with pore size. However, to calculate the hydraulic conductivity at full saturation, such a complication is important and can only be resolved exactly by detailed imaging and careful numerical work at the single pore scale, subjects not addressed in this book. Note that the proposed activity of calculating the hydraulic conductivity is called "upscaling" (at the pore scale) in the hydrology literature, but in the physics literature it would be referred to something like, "calculating an effective macroscopic transport parameter from its microscopic variability."

We have already given the pdf of the pore distribution in the previous chapter. Now we need to relate the pore dimensions to local conductances. Poiseuille flow implies that pores of radius r and length l have a hydraulic conductance

$$g^{\mathrm{h}} \propto \frac{r^4}{\mu l} \tag{5.35}$$

with μ the viscosity of the fluid, here assumed to be water. The reason for the form of Eq. (5.35) is that in the linear regime (assumed here) the total flow through such a pore is simultaneously proportional to g^{h}, and to the pressure difference across the pore, ΔP. The numerical constants are suppressed. If the medium is assumed to be

fractal, the aspect ratio (shape) of pores is, on the average, independent of their size, meaning that l must be taken as proportional to r. In this case, then,

$$g^{\mathrm{h}} \propto r^3 \tag{5.36}$$

To calculate the hydraulic conductivity accurately under conditions of saturation, one needs first to find a critical value of a conductance, g_{c}, from critical path analysis, then find expressions for l and χ, and finally optimize the result. The easy part is to find g_{c}. Under saturated conditions, r_{c} is given through [16]

$$\frac{3-D_{\mathrm{p}}}{r_{\mathrm{m}}^{3-D_{\mathrm{p}}}} \int_{r_{\mathrm{c}}}^{r_{\mathrm{m}}} r^3 r^{-1-D_{\mathrm{p}}} dr = V_{\mathrm{c}} \tag{5.37}$$

with the critical volume content for percolation, V_{c}. Solution of this equation yields,

$$r_{\mathrm{c}} = r_{\mathrm{m}}(1-V_{\mathrm{c}})^{\frac{1}{3-D_{\mathrm{p}}}} \tag{5.38}$$

Note that we can write for an arbitrary r,

$$r = r_{\mathrm{m}}(1-V)^{\frac{1}{3-D_{\mathrm{p}}}} \tag{5.39}$$

The critical conductance, $g_{\mathrm{c}}^{\mathrm{h}}$ must be of the form,

$$g_{\mathrm{c}}^{\mathrm{h}} \propto r_{\mathrm{m}}^3 (1-V_{\mathrm{c}})^{\frac{3}{3-D_{\mathrm{p}}}} = r_{\mathrm{c}}^3 \tag{5.40}$$

We assumed [16], as in [40] (as well as [3, 20, 23] that both l and χ are proportional to r_{c}, so that the saturated hydraulic conductivity, K_{S}, is represented by

$$K_{\mathrm{S}} \propto r_{\mathrm{c}}^2. \tag{5.41}$$

How does this arise?

First we linearize the difference $V - V_{\mathrm{c}}$:

$$V - V_{\mathrm{c}} = (3-D_{\mathrm{p}}) \left(\frac{r_{\mathrm{c}}}{r_{\mathrm{m}}}\right)^{3-D_{\mathrm{p}}} \left(\frac{r-r_{\mathrm{c}}}{r_{\mathrm{c}}}\right) \tag{5.42}$$

Then, for the case that $g_{\mathrm{c}} \propto r_{\mathrm{c}}^3$, we can write $V - V_{\mathrm{c}}$ in terms of the conductance difference:

$$V - V_{\mathrm{c}} = \left(\frac{3-D}{3}\right) \left(\frac{r_{\mathrm{c}}}{r_{\mathrm{m}}}\right)^{3-D_{\mathrm{p}}} \left(\frac{g-g_{\mathrm{c}}}{g_{\mathrm{c}}}\right) \tag{5.43}$$

For the optimization procedure, the material result is that $V - V_{\mathrm{c}} \propto g - g_{\mathrm{c}}$. The optimization

$$\frac{d}{dg}\left[g(g_{\mathrm{c}}-g)^{2\nu}\right] = 0 \tag{5.44}$$

yields

$$g_{\mathrm{opt}} = \frac{g_{\mathrm{c}}}{1+2\nu} \tag{5.45}$$

The factor $1 + 2\nu$ could be written (if ν were very small) as $\exp(2\nu)$. The reader may verify that repeating the procedure with respect to the resistance yields $R_{\mathrm{opt}} =$

$R_c/(1-2\nu)$ which, again if ν were very small, would yield $R_{opt} = R_c \exp(-2\nu)$, and the two methods would be consistent (as in the exponential case above). But $\nu = 0.88$ (in 3D), which is not small, and the optimization procedure with respect to the resistance yields a value which is outside the range of physical values. This means either that it is preferable to use the optimization procedure with respect to the conductance rather than the resistance, or that the optimization procedure is not reliable in the present context. We choose to consider the optimization procedure with respect to the conductance as reasonable, but to interpret the results with caution. There is a physical reason behind these results.

In the case where g is an exponential function of random variables (e.g., impurity conduction systems), a small change in g is associated with a very small change in p, because of the logarithmic dependence of p on g. When (as here) g is a power of a random variable, the result is that a small change in g makes a change of roughly the same magnitude in V (corresponding to p), which sweeps χ right out of the range where percolation theory gives an accurate estimation of the separation of dominant current-carrying paths. This means that for g very near g_c the separation of current-carrying paths can be very small, i.e., on the order of the separation of pores, which is the same order as r_c, and the same order as the separation of controlling resistances along the dominant paths. For a pictorial example of such a contrast between current-carrying paths for exponential and power law functions of random variables, refer to Fig. 5.3. Note that the exponential case is the same as in Fig. 5.2.

For these reasons we [16] decided to formulate K_S as proportional to

$$K_S \propto \frac{l r_c^3}{\chi^2} = \frac{r_c r_c^3}{r_c^2} = r_c^2 \tag{5.46}$$

However, it should be kept in mind that l and L could have been written as other pore length scales with different numerical constants, meaning that in some sense a proportionality to r_c^2 is a matter of convenience. Note that K_S proportional to the square of a pore radius is a result obtained by many other authors, including Katz and Thompson [20] (also Kozeny [22]-Carman [8], Johnson and Schwartz [19], Bernabé and Revil [6], and Torquato and Lu [42], none of whom used critical path analysis, but also Banavar and Johnson [3] and Le Doussal [23], who did). Katz and Thompson [20] also used the critical radius, r_c, and their critical path analysis yielded as well the same sort of result for the critical radius, r_c. However, there is considerable uncertainty in the numerical prefactors, probably reflecting the choice to make other pore length scales proportional to r_c^2. Nevertheless, the Katz and Thompson [20] and the Hunt and Gee [16] treatments of K_S are loosely equivalent. The focus here is not on K_S, for which one really needs additional information (pore shape, in particular). But it is essential to present the basic discussion of K_S. Also, although we anticipate that both percolation-based treatments could be improved, in a controlled test [5] of four methods to calculate K (Kozeny-Carman, a "stochastic" pore scale model due to Bernabé and Revil [6], and the Johnson and Schwartz [19] treatment being the other three) the Katz and Thompson [20] result came out on top. Notably, in the case of large variance the Kozeny-Carman results came in a distant last place, although all four results were equally accurate in the limit of low variance.

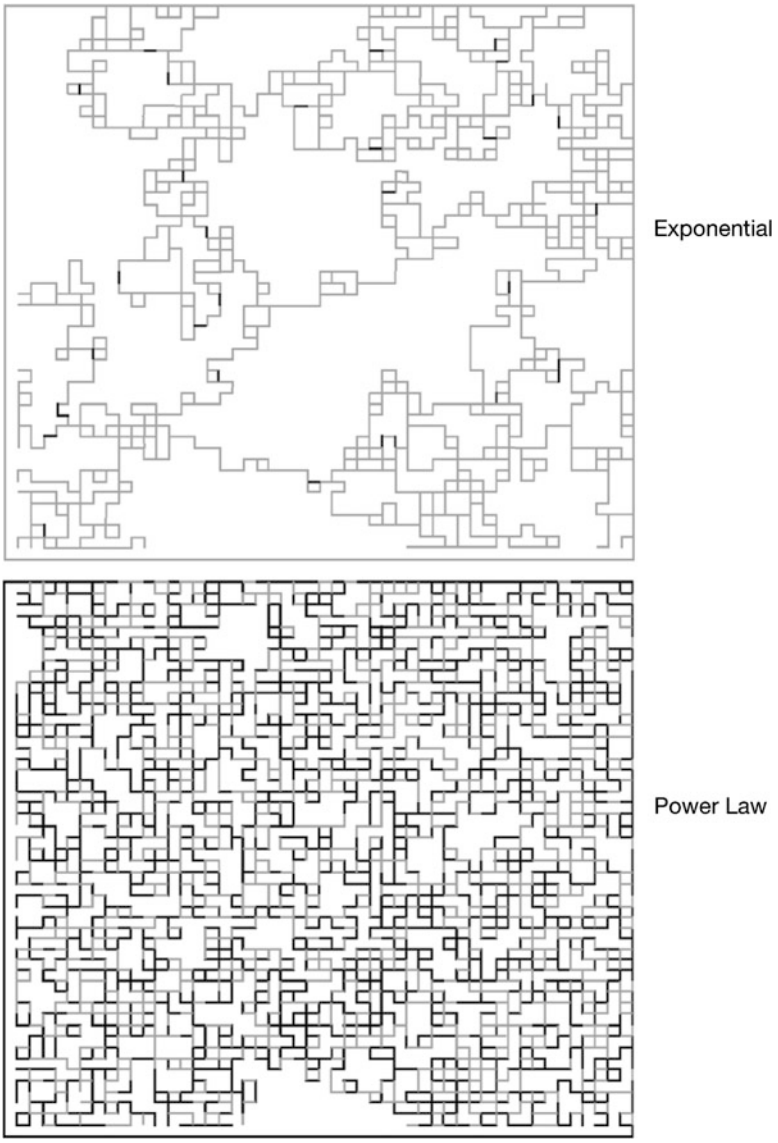

Fig. 5.3 A comparison of the backbone clusters for maximum $R = R_{opt}$ for the case that *top* the resistances of the bonds follow Eq. (5.1) or Eq. (5.20), and *bottom* the bond resistances follow Eq. (5.35), i.e., exponential vs. power law functions (from Todd Skaggs, unpublished)

5.4 Unsaturated Hydraulic Conductivity

Typical formulations [9, 27, 28, 31–33, 43] of the unsaturated hydraulic conductivity are in the form of a ratio with K_S. Reasons for this (discussed in previous chapters)

are chiefly the typical lack of direct information regarding the pore space, and the difficulty of formulating an accurate calculation of K_S without explicit information about pore sizes and shapes. However, in fractal systems, the particular pore shapes are the same for all radii, and thus this geometric factor cancels out in the ratio of $K(S)/K_S$. The formulation of the hydraulic conductivity in this ratio also greatly simplifies the application of critical path analysis.

The effects of partial saturation are treated using the premise that film flow permits [7, 41] the porous medium to adjust to removal of water by evacuating *all* pores with radii larger than some equilibrium value, which we call, $r_>$. Thus effects of neither hysteresis nor non-equilibrium are considered yet. The following is taken from Hunt and Gee [16]. The relative saturation is the quotient of the pore space volume in pores with $r < r_>$ and the total pore volume,

$$S = \left(\frac{1}{\phi}\right)\left(\frac{3-D_p}{r_m^{3-D_p}}\right)\int_{r_0}^{r_>} dr r^{2-D_p} = \frac{1}{\phi}\frac{[r_>^{3-D_p} - r_0^{3-D_p}]}{r_m^{3-D_p}} \tag{5.47}$$

Remember from Chap. 4 that r_0 and r_m are the lower and upper bounds of validity of the fractal description of the pore space. When $r_> = r_m$, Eq. (5.47) yields $S = 1$.

Next, the percolation condition relating the smallest (or critical) pore size to be traversed, to the critical volume fraction, V_c, when the largest pore filled with water has $r = r_>$, is

$$V_c = \left(\frac{3-D_p}{r_m^{3-D_p}}\right)\int_{r_c}^{r_>} dr r^{2-D_p} = \left(\frac{r_>}{r_m}\right)^{3-D_p} - \left(\frac{r_c(\theta)}{r_m}\right)^{3-D_p} \tag{5.48}$$

Equation (5.48) has the same form as Eq. (5.47), but the upper limit has been reduced from r_m to $r_>$, producing a related reduction in $r_c(\theta)$ (and requiring its representation as a function of θ), consistent with the effects of partial saturation. Since our goal here is to calculate the hydraulic conductivity as a function of moisture content we should consider using a threshold moisture content, θ_t, in place of the critical volume fraction, V_c. This turns out to be a good plan, since solute diffusion experiments demonstrate a vanishing of the diffusion constant at some moisture content, θ_t. Together, Eqs. (5.37), (5.47), and (5.48) (and using θ_t in place of V_c) allow r_c for unsaturated conditions to be expressed in terms of r_c for saturated conditions,

$$r_c(\theta) = r_c(\theta = \phi)\left[\frac{1-\phi+(\theta-\theta_t)}{1-\theta_t}\right]^{\frac{1}{3-D_p}} \tag{5.49}$$

The critical hydraulic conductance as a function of moisture content is now,

$$g_c(\theta) = g_c(\theta = \phi)\left[1 - \phi\frac{1-S}{1-\theta_t}\right]^{\frac{3}{3-D_p}} \tag{5.50}$$

Equation (5.50) implies a scaling of the same form for the ratio $K(S)/K_S$. The hydraulic conductivity of the medium is controlled by the hydraulic *conductance* of the rate-limiting pore throat, which is proportional to the *cube* of the critical radius. How does the vanishing of the correlation length (and therefore the minimum path separation) at the percolation threshold affect the critical path results for $K(S)/K_S$?

The answer is, not at all—at least to a very good approximation, over a fairly wide range of moisture contents. Why? The answer has two parts: (1) such topological complications only have a strong effect in the vicinity of the percolation threshold, and (2) the calculation of K_S takes into explicit account the competition between the effects of finding the minimum value of the blocking or bottleneck resistance and the infinite path separation. Thus in the calculation of $K(S) = K_S$ $(S = 1)$, the effects of the path separation are already included, and as long as the percolation threshold is not approached too closely, there is very little change in these effects. However, this perspective must be reevaluated for lower moisture contents, as the percolation threshold is approached [15]. Thus we can now write for the unsaturated hydraulic conductivity,

$$K(S) = K_S\left[1 - \phi\frac{1-S}{1-\theta_t}\right]^{\frac{3}{3-D_p}} \tag{5.51}$$

a result which can also be written

$$K(S) = K_S\left[\frac{1-\phi+(\theta-\theta_t)}{1-\theta_t}\right]^{\frac{3}{3-D_p}} \tag{5.52}$$

While the present evidence is that Eq. (5.52) is accurate for typical porous media over a wide range of moisture contents, it cannot be accurate [15] in the limit $\theta \to \theta_t$. In that limit, Eq. (5.52) yields

$$K(\theta_t) = K_S\left[\frac{1-\phi}{1-\theta_t}\right]^{\frac{3}{3-D}} \tag{5.53}$$

But $K(\theta_t)$ from Eq. (5.53) is *not* zero as required; it is the hydraulic conductivity associated with the limiting conductance of the smallest pore in the system. However, it is a requirement from percolation theory that the hydraulic conductivity vanish at the percolation threshold, unless an alternate conduction mechanism exists with a lower threshold value. Specifically, in this limit the hydraulic conductivity (like the electrical conductivity) must vanish according to

$$K(\theta) = K_1(\theta-\theta_t)^{\mu} \tag{5.54}$$

How these results are to be reconciled is the subject of the next chapter; the reconciliation illuminates the difference between the electrical and hydraulic conductivities of porous media, and also clarifies the role of some exact results for non-universal scaling of transport properties derived by Balberg [2].

5.5 Hydraulic Conductivity for Geologic Media: Parallel vs. Series

In this section we present a general result, which may be utilized to "upscale" the hydraulic conductivity in geologic media, that is to calculate an effective hydraulic conductivity, K_{eff}, when a wide distribution of individual K values exists. At the

beginning of this chapter we argued that one should carefully address the difficulties of each medium individually. We have also argued that the appropriate conceptual view of this problem is not even upscaling the *conductivity*, per se. One should characterize the dominant conduction paths in terms of their blocking resistance value, and then find the frequency of occurrence of such paths. A discussion in terms of the hydraulic conductivity implies already that the individual portions of the medium have uniform conduction properties. Nevertheless, as witnessed by the large number of such results for upscaling in use, there is a need to write a general result, which can be applied as a simple algorithm. We write such a result here. As yet it is untested in real situations, but it is clearly a conceptual advance over the results currently in use.

It is a typical argument in geology to consider a horizontally layered system and contrast the vertical flow properties with the horizontal flow properties. The effective hydraulic (or electric) conductivities under such conditions are given through the average resistance and average conductance values, respectively, since the respective configurations of the resistance values are in series and in parallel. We cast this discussion in the language of percolation theory and then seek the appropriate generalizations.

In one-dimensional systems, water (or current) must flow through every element of the system. In the thermodynamic limit of infinite system size, this means that every element of a distribution of resistance values must be present, with its occurrence described by the relevant probability density function of resistance values, $W(R)$. The equivalent resistance of such a one-dimensional system is given by the series combination of the individual resistances, which is the arithmetic sum of the resistance values. The conductivity, whether hydraulic or electrical, must be inversely proportional to the total resistance of the system, R_{tot}, which can be simply calculated as:

$$R_{\text{tot}} \propto \langle R \rangle = \int_0^\infty RW(R)dR \quad \text{or} \quad R_{\text{tot}} = \sum_i R_i \tag{5.55}$$

Thus,

$$K_{\text{eff}} \propto \left[\sum_i R_i\right]^{-1} \propto \left[\sum_i K_i^{-1}\right]^{-1} \tag{5.56}$$

If the individual elements are geometrically identical, then K_{eff} is equal to the second sum. Such a particular operation is often referred to as obtaining the harmonic mean of the conductivities. For the two versions of Eq. (5.56) to be equivalent, it is necessary that all individual elements have the same size and shape; otherwise the only valid sum is over the resistances, R_i.

The opposite extreme to the combination of all the resistances in series, as in a one-dimensional system, is the combination of all the resistances in parallel. In the case of a parallel combination the total conductance is the sum of the individual conductances, and the upscaled hydraulic conductivity, K_{eff}, is then given through,

$$K_{\text{eff}} \propto \left[\sum_i K_i^1\right]^1 \tag{5.57}$$

The same geometric restriction applies here, namely that the individual elements all be congruent (have the same size and shape); otherwise it will be necessary to include geometrical factors to transform the elements of the series to conductances. When the factors are all identical, the approximation (Eq. (5.57)) becomes an equality. As a consequence of the validity of these two extremes, Scheibe and Yabusaki [36] proposed the following formula

$$K \propto \left[\sum_i K_i^z\right]^z, \quad -1 \le z \le 1 \tag{5.58}$$

The problem with such power-law averaging [10, 11] is that it is conceptually incorrect. Comparison of percolation theoretical calculations with simulations [5, 37] consistently demonstrates that the importance of individual resistances to a medium's effective resistance is not a monotonically increasing or decreasing function of resistance. Rather, this importance is peaked. Specifically, the peak of importance of resistance values occurs at the critical resistance, R_c. Smaller resistances on the percolation path behave very much like shorts. Larger resistances are avoided. These critical resistances control the field of potential drops in the entire medium [5].

To a lowest order approximation (used as well by Balberg [2]) one can calculate the hydraulic conductivity of a medium, to which critical path analysis is to be applied, by including all the resistance values smaller than R_c on a one-dimensional path, and ignoring the remainder of the resistance distribution. While this is not completely accurate, it is an improvement over Eq. (5.58), and in more or less the same spirit, as we will show.

The two cases, parallel and series combinations of resistances, correspond in critical path analysis to the percolation probabilities, $p_c = 0$ and $p_c = 1$, respectively (Why?). The answer is because, in the first case, it is possible to find a path through the medium which utilizes a vanishingly small part of the resistance distribution. In the second case, it is impossible to find a path through the medium that excludes any portion of the resistance distribution. The first case requires that each individual resistor out of the entire distribution span the entire system, from one side to the other, consistent with a parallel configuration of the resistors. Such a topology is precisely what is imagined in pore scale models that rely on bundles of capillary tube approximations. That is, out of a continuum of possible values, the bundle of capillary tubes model chooses one end point, meaning that the conditions for which it is valid never occur. The second case, meanwhile, is equivalent to a series configuration. The latter can be obtained in a 1D system, while the former is a necessary result only of an infinite dimensional system (using the Vyssotsky et al. [44] formula, $Zp_c = d(d-1)$).

What we present here is a procedure which maintains the fundamental perspective of critical path analysis, but also reduces to the proper results in the respective limits $p_c = 0$ and $p_c = 1$.

$$K_{\text{eff}} = \langle K \rangle \left[\frac{\int_{K_c}^{K_{\max}} W(K) K^{-1} dK}{K_{\max}^{-1}}\right]^{-1} \tag{5.59}$$

In this expression the probability density function, $W(K)$, must be proportional to the distribution of K values in bulk, but normalized so that $\int W(K)dK$ between the limits K_c and K_{max} is 1. Further, we require the same geometric constraints as in Eq. (5.56) and Eq. (5.57). Note that when $p_c = 0$, Eq. (5.59) yields $\langle K \rangle$, since $K_c = K_{max}$, $W(K)$ becomes a delta function, $\delta(K - K_{max})$, and the integral then yields K_{max}^{-1}, which cancels the denominator. But when $p_c = 1$, the integral yields the harmonic mean conductivity, while the denominator, $(K_{max}^{-1})^{-1}$ approximately cancels $\langle K \rangle$, since for a wide distribution of hydraulic conductivity values, the arithmetic mean is dominated by the largest K value.

It is important here that Eq. (5.59) essentially represents an averaging procedure where the importance of K values is strongly peaked at the critical conductivity, K_c. For $p_c = 0$, this peak moves to K_{max}, while for $p_c = 1$, the peak moves to K_{min}. Thus, in the two extreme cases, Eq. (5.59) corresponds to the parallel and series combinations, and the importance of individual conductivity values is either monotonically increasing or monotonically decreasing. But in any other case (much more realistic values of p_c) this procedure yields an averaging procedure with importance peaked at K_c. Note however that Eq. (5.59) performs rather disappointingly when it is applied to a bimodal distribution [17, 18], appropriate for geological media composed of sands and muds. In particular, when the upper mode of the distribution (say sand fraction) is below the percolation threshold, Eq. (5.59) drastically underestimates K, although it otherwise does quite well. Further, Eq. (5.59) does generate a rapid increase in K when the upper mode just exceeds the percolation threshold, and percolation theoretical results are generally in accord with the sigmoidal shape of $\log[K]$ vs. sand fraction [17, 18]). Power-law averaging performs most poorly, never generating a point of inflection for any value z [17, 18].

The implication of this discussion is that the tendency of water (or electrical current) to follow the path of least resistance means that such a path is configured in parallel with other paths, whose resistances are much higher (and can be ignored), while the resistances on such an optimal path are configured in series. Power-law averaging [36] instead configures all the resistors equivalently, somewhere between series and parallel. While power-law averaging can yield any value for K_{eff} between the two limits, and thus any value that experiment can develop, the logic of cause and effect is missing and the exponent μ has neither predictive value nor experimental significance.

5.6 Summary

Several examples of the application of critical path analysis were given. The most difficult issue in these examples is the relationship between a critical, or rate-limiting, conductance and the effective electrical or hydraulic conductivity. In the first four calculations of the effective conductivity, we have chosen to apply a general technique of Friedman and Pollak [12] in making this transition. This technique develops the result in terms of the following length scales: (1) the separation of controlling resistances along a path and (2) the separation of dominant paths. In the fifth

calculation we developed an algorithmic procedure that offers greater simplicity, if not greater accuracy.

In well-connected three-dimensional systems with local conductances being exponential functions of random variables, the typical separation of controlling resistances appears not to be a critical function of percolation variables, but the opposite is likely in two-dimensional systems. In three-dimensional systems, critical path analysis requires an optimization of topological (current-carrying path separations) and geometrical (resistance magnitude), but in two-dimensional systems a simpler scaling argument becomes possible with the conductivity given merely by the critical conductance. If, however, local conductances are power functions of random variables, as is often the case in porous media, then even in the three-dimensional case it is difficult to separate the effects of topology and geometry, since both show up in factors relating to length scales of similar magnitudes. Nevertheless the calculations of the hydraulic conductivity at full saturation with the highest degree of accuracy are based on precisely this form of critical path analysis. Finally, it is possible even in the kind of messier problem that is prevalent in porous media to formulate conductivity ratios, which are given purely in terms of the geometry (though we will find that this formulation will generally break down as the percolation threshold is approached). When the relevant problem is formulated as a ratio of conductivities at two different saturations, even three-dimensional problems are equally tractable. But for the case of porous media we will find (next chapter) that not all conductivities are equivalent. Specifically, the electrical and thermal conductivity as functions of saturation behave quite differently from the hydraulic conductivity. Nevertheless, we also presented at the end of this chapter an upscaling result that should apply on geologic scales equally to the electrical and to the hydraulic conductivities.

Problems

5.1 Show that integration of Eq. (5.4) to find R_c directly yields the same value as Eq. (5.7) derived through the procedure of Eq. (5.5) and Eq. (5.6). This provides the link between the probabilistic identity $W(r)dr = W(R)dR$, and substitution of variables in integration.

5.2 Repeat the analysis of Eq. (5.35) through Eq. (5.41) for a log-normal distribution of pore radii. What additional assumptions must be made in order to complete the analysis? Constrain the pore-size distributions for the log-normal and the fractal case to be in some sense similar (define the similarity or equivalence) and then compare the results for the hydraulic conductivity. Give graphical representations of both the comparison between the two pore-size distributions, and the two results for the hydraulic conductivity.

5.3 Repeat the analysis of Eq. (5.42) through Eq. (5.45) for a log-uniform distribution of pore radii. Compare your results with those for r-percolation.

5.4 Assume for simplicity that, as r-percolation involves an integral over a three-dimensional spherical region of space, r–E percolation involves an integral

over the analogue to a sphere in four-dimensional space. In such a picture write an analogue to Eq. (5.16) for l. What length replaces d as the first factor? What is the dependence of l on T?

5.5 Find the temperature dependence of the correlation length for $R = R_{\text{opt}}$ in r–E percolation.

5.6 Show that variable-range hopping in d dimensions leads to the result

$$\sigma \propto \exp\left[-\left(\frac{T_0}{T}\right)^{\frac{1}{d+1}}\right]$$

5.7 Let the density of states, $N(E)$, be proportional to E^{n}. Show that VRH in d dimensions now leads to

$$\sigma \propto \exp\left[-\left(\frac{T_0}{T}\right)^{\frac{n+1}{n+d+1}}\right]$$

5.8 Suppose that a VRH system is long in two of its dimensions [38], y, but short in the third, x, i.e. $y \gg x$. Consider moreover that x may be shorter than the correlation length found in Problem 5.5, and that a potential difference is set up across one of the long axes of the system (longitudinal, rather than transverse, conduction). In this case the conduction path cannot develop fully in the third dimension, and conduction follows some intermediate dimensionality between 2 and 3. It is possible to constrain the conduction path to stay within the system by the trick of allowing conduction to proceed through larger resistances, and using a larger effective critical resistance, i.e.,

$$\chi = \chi_0(p - p_{\text{c}})^{-\nu} \leq x$$

Let the exponent $2r_{ij}/a + E_{ij}/kT = \xi$. First solve this equation for the correlation length for p, and then substitute this new value of p into a linearized version of the following equation (relating $\xi - \xi_{\text{c}}$ to $p - p_{\text{c}}$):

$$\xi_{\text{c}}^4\left[\frac{T}{T_0}\right] = 1$$

to find

$$\sigma \propto \exp\left[-\left(\frac{T_0}{T}\right)^{\frac{1}{4}}\right]\exp\left[-\left(\frac{T_0}{T}\right)^{\frac{1}{4}}\left(\frac{\chi_0}{x}\right)^{\frac{1}{\nu}}\right]$$

A more accurate calculation would replace χ_0 with the correlation length for the dc conductivity in 3D VRH (from Problem 5.5), but this is sufficiently accurate for the present purposes, and provides a preparation for material in Chap. 9.

References

1. Ambegaokar, V.N., Halperin, B.I., Langer, J.S.: Hopping conductivity in disordered systems. Phys. Rev. B **4**, 2612–2621 (1971)

2. Balberg, I.: Recent developments in continuum percolation. Philos. Mag. B **30**, 991–1003 (1987)
3. Banavar, J.R., Johnson, D.L.: Characteristic pore sizes and transport in porous media. Phys. Rev. B **35**, 7283–7286 (1987)
4. Berkowitz, B., Balberg, I.: Percolation theory and its application to groundwater hydrology. Water Resour. Res. **29**, 775–794 (1993)
5. Bernabé, Y., Bruderer, C.: Effect of the variance of pore size distribution on the transport properties of heterogeneous networks. J. Geophys. Res. **103**, 513 (1998)
6. Bernabé, Y., Revil, A.: Pore-scale heterogeneity, energy dissipation and the transport properties of rocks. Geophys. Res. Lett. **22**, 1529–1532 (1995)
7. Blunt, M.J., Scher, H.: Pore-level model of wetting. Phys. Rev. E **52**, 6387–6403 (1995)
8. Carman, P.C.: Flow of Gases Through Porous Media. Butterworths, London (1956)
9. Childs, E.C., Collis-George, N.: The permeability of porous materials. Proc. R. Soc. Lond., Ser. A **201**, 392–405 (1950)
10. Desbarats, A.: Spatial averaging of hydraulic conductivity in 3-dimensional heterogeneous porous-media. Math. Geol. **24**(3), 249–267 (1992)
11. Deutsch, C.V.: Calculating effective absolute permeability in sandstone/shale sequences. SPE Form. Eval. **4**(3), 343–348 (1989)
12. Friedman, L., Pollak, M.: The Hall effect in the variable-range hopping system. Philos. Mag. B **44**, 487–507 (1981)
13. Hunt, A.G.: AC hopping conduction: perspective from percolation theory. Philos. Mag. B **81**, 875–913 (2001)
14. Hunt, A.G.: Applications of percolation theory to porous media with distributed local conductances. Adv. Water Resour. **24**(3,4), 279–307 (2001)
15. Hunt, A.G.: Percolative transport and fractal porous media. Chaos Solitons Fractals **19**, 309–325 (2004)
16. Hunt, A.G., Gee, G.W.: Application of critical path analysis to fractal porous media: comparison with examples from the Hanford Site. Adv. Water Resour. **25**, 129–146 (2002)
17. Hunt, A.G., Idriss, B.: Percolation-based effective conductivity calculations for bimodal distributions of local conductances. Philos. Mag. **89**, 1989–2007 (2009)
18. Idriss, B.: Upscaling the hydraulic conductivity for a bimodal conductivity distribution. Master's thesis, Wright State University (2008)
19. Johnson, D.L., Schwartz, L.M.: Unified theory of geometric effects in transport properties of porous media. In: SPWLA, 30th Annual Logging Symposium, Soc. of Prof. Well Log Anal, Houston, TX (1989)
20. Katz, A.J., Thompson, A.H.: Quantitative prediction of permeability in porous rock. Phys. Rev. B **34**, 8179–8181 (1986)
21. Kogut, P.M., Straley, J.: Distribution-induced non-universality of the percolation conductivity exponents. J. Phys. C, Solid State Phys. **12**, 2151–2159 (1979)
22. Kozeny, J.: Über Kapillare Leitung des Wasssers im Boden. Sitzungsber. Adak. Wiss. Wien **136**, 271–306 (1927)
23. Le Doussal, P.: Permeability versus conductivity for porous media with wide distribution of pore sizes. Phys. Rev. B **39**, 4816–4819 (1989)
24. Long, A.R., Hansmann, L.: In: Pollak, M., Fritzsche, H. (eds.) Hopping and Related Phenomena, p. 309. World Scientific, Singapore (1990)
25. Long, A.R., McMillen, J., Balkan, N., Summerfield, S.: The application of the extended pair approximation to hopping conduction in rf sputtered amorphous silicon. Philos. Mag. B **58**, 153–169 (1988)
26. Miller, A., Abrahams, E.: Impurity conduction at low concentrations. Phys. Rev. **120**, 745–755 (1960)
27. Millington, R.J., Quirk, J.P.: Permeability of porous media. Nature (London) **183**, 387–388 (1959)
28. Millington, R.J., Quirk, J.P.: Permeability of porous solids. Trans. Faraday Soc. **57**, 1200–1206 (1961)

29. Moldrup, P., Oleson, T., Komatsu, T., Schjoning, P., Rolston, D.E.: Tortuosity, diffusivity, and permeability in the soil liquid and gaseous phases. Soil Sci. Soc. Am. J. **65**, 613–623 (2001)
30. Mott, N.F.: Conduction in non-crystalline materials 3. Localized states in a pseudogap and near extremities of conduction and valence bands. Philos. Mag. **19**, 835 (1969)
31. Mualem, Y.: A catalogue of the hydraulic properties of unsaturated soils. Res. Proj. No. 442, Technion, Israel Institute of Technology, Haifa (1976)
32. Mualem, Y.: Hysteretical models for prediction of hydraulic conductivity in unsaturated porous media. Water Resour. Res. **12**, 1248–1254 (1976)
33. Mualem, Y., Dagan, G.: Hydraulic conductivity of soils: unified approach to the statistical models. Soil Sci. Soc. Am. J. **42**, 392–395 (1978)
34. Pollak, M.: A percolation treatment of dc hopping conduction. J. Non-Cryst. Solids **11**, 1–24 (1972). doi:10.1016/0022-3093(72)90304-3
35. Sahimi, M.: Flow phenomena in rocks—from continuum models to fractals, percolation, cellular automata, and simulated annealing. Rev. Mod. Phys. **65**(4), 1393–1534 (1993)
36. Scheibe, T., Yabusaki, S.: Scaling of flow and transport behavior in heterogeneous groundwater systems. Adv. Water Resour. **22**, 223–238 (1998)
37. Seager, C.H., Pike, G.E.: Percolation and conductivity: a computer study II. Phys. Rev. B **10**, 1435–1446 (1974)
38. Shklovskii, B.I., Efros, A.L.: Electronic Properties of Doped Semiconductors. Springer, Heidelberg (1984)
39. Skaggs, T.H.: Effects of finite system size and finite heterogeneity on the conductivity of broadly distributed resistor networks. Physica B **338**, 266–269 (2003)
40. Stauffer, D., Aharony, A.: Introduction to Percolation Theory, 2nd edn. Taylor and Francis, London (1994)
41. Tokunaga, T., Wan, J.: Water film flow along fracture surfaces of porous rock. Water Resour. Res. **33**, 1287–1295 (1997)
42. Torquato, S., Lu, B.: Rigorous bounds on the fluid permeability: effect of polydispersivity in grain size. Phys. Fluids A **2**, 487–490 (1990)
43. van Genuchten, M.T.: A closed form equation for predicting the hydraulic conductivity of unsaturated soils. Soil Sci. Soc. Am. J. **44**, 892–898 (1980)
44. Vyssotsky, V.A., Gordon, S.B., Frisch, H.L., Hammersley, J.M.: Critical percolation probabilities (bond problem). Phys. Rev. **123**, 1566–1567 (1961)

Chapter 6
Hydraulic and Electrical Conductivity: Conductivity Exponents and Critical Path Analysis

This chapter describes how to estimate hydraulic and electrical conductivity, primarily as functions of saturation but, in a more limited fashion, also their dependence on porosity. Electrokinetic currents, because of their very close relationship with electrical and hydraulic conductivity, are discussed here too. Other properties, such as air permeability, solute and gas diffusion, and thermal conductivity are discussed in Chap. 7. The results are valid for generating sample scale properties from pore-scale variability. The theoretical development and the parameters obtained are consistent across the various properties, and the results predict experimentally measured values.

6.1 Background

For a long time a few results for the electrical and hydraulic conductivity have dominated the literature. These results are known as Archie's law [2] for the electrical conductivity, and the Kozeny-Carman equation for the hydraulic conductivity. Archie's law accounts for both the saturation and the porosity dependence, while the Kozeny [40]-Carman [14] equation is used only for saturated conditions. For the saturation-dependence of the hydraulic conductivity, there is less conformity in usage, but the Mualem [51, 52]-van Genuchten [71] type formulations have dominated in soil physics and achieved influence outside that subject area. The focus of this chapter is on the saturation dependence of these properties, but we find that one can, under some conditions, infer the porosity dependence as well, so that there is some point in addressing the suite of equations and properties together.

In turns out that both the Kozeny-Carman equation and Archie's law have some features in common with predictions from percolation theory. In particular, the idea that the hydraulic and electrical conductivity could each be proportional to a power of the porosity (or saturation) is consistent with percolation scaling on a continuum; the propensity for these powers to equal 2 in Archie's law is consistent with universal scaling results from percolation theory. But the effects of the local conductance distribution from the distribution of pore sizes must be properly accounted

A. Hunt et al., *Percolation Theory for Flow in Porous Media*,
Lecture Notes in Physics 880, DOI 10.1007/978-3-319-03771-4_6,

for; early work dating back to the 1970's already suggests that the universal scaling from percolation theory need not always be relevant.

What is novel in our method, and, in this book, new in this chapter, is the development of tests to distinguish when geometry (the pore size distribution) is important to the conductivity, and how to weight its influence relative to that of the topology of the flow paths. This technique combines critical path analysis (chiefly geometry) and percolation scaling (chiefly topology). As a result of such tests, we find that universal percolation scaling should explain a wide range of data; we can also predict under what conditions non-universal results may apply, and what form they should take, whether non-universal power laws or otherwise.

Our inquiries here into the electrical and hydraulic conductivities are based on applying concepts from critical path analysis and percolation theory to (mostly) the Rieu and Sposito truncated random fractal model (Rieu and Sposito [59]; henceforth RS). Critical path analysis isolates the effects of the pore-size distribution, while percolation scaling identifies the effects of the fluid connectivity, which are effectively assumed to override any special connectivity properties of the medium itself. While the connectivity properties of the medium are important, it is ordinarily possible to summarize their effects in a single parameter, the percolation threshold. For a relatively wide range of conditions, we find that the saturation dependence of the electrical conductivity follows universal scaling of percolation theory, but that the conditions for an equivalent result for the hydraulic conductivity are much more restrictive. Only when the saturation dependence of the conductivity (whether electrical or hydraulic) follows universal scaling between the limits of zero and full saturation, can one recover universal scaling for the porosity dependence. This appears to be a relatively rare occurrence in the hydraulic conductivity, but a rather common result for the electrical conductivity. The explanation lies in the much stronger pore-size dependence of local hydraulic, than electrical, conductances.

When the pore-size distribution dominates, which is usually true for the hydraulic conductivity, we argued in previous editions that critical path analysis would normally deliver a saturation dependence that is a more complicated function, and which could not be represented as a simple power law. This precludes the relevance of either universal or non-universal scaling results. However, at low enough saturation (whether electrical or hydraulic conductivity), we argued that the behavior should be dominated by the topology of the connections of the water-filled pores, allowing for universal scaling behavior (referred to a finite threshold moisture content). We also analyzed the limitations of this argument. But this discussion was based on the RS model, and our expansion of the models treated in this third edition requires a reevaluation of our results and a revision of the discussion. In fact it is possible that non-universal scaling behavior should be expected more often than we had suggested in earlier editions.

The RS model allows, in principle, a power-law dependence of pore sizes down to zero pore radius. Under such conditions, it is known that one can derive non-universal scaling of the conductivity. However, the RS model delivers porosity equal to one under such conditions as well as an infinite specific surface ratio. Since these limits are unphysical, earlier editions of this book, which relied exclusively on this

model of the pore space, did not devote a great deal of attention to the question of the relevance of non-universal behavior. We pointed out at the end of the chapter (and still do) that the effects of film flow at low saturations would confound our predictions for universal scaling with a finite threshold. This conclusion is required because film continuity can be maintained effectively down to an arbitrarily low moisture content associated with the presence of a few molecular thicknesses of water on each particle. Now we can argue that such a water presence, ignoring the roughness of the particles, should produce a non-universal scaling result proportional to the cube of the absolute moisture content. This is not the only complication, however. The Tyler and Wheatcraft [70] fractal model effectively allows pore sizes in the limit of zero radius with realistic values of the porosity and, possibly, no requirement that the specific surface area diverge. The Tyler and Wheatcraft [70] model and the RS model are endpoints of a more generalized model, treated in Chap. 4, and which is roughly equivalent to the pore-solid fractal model of Bird et al. [9]. Using that model, critical path analysis yields non-universal scaling for either the electrical or the hydraulic conductivity in the limit that the parameter $\beta = 1$. When we fit observed water retention curves with this generalized model, this limiting value of β turns up rather frequently. And in one case, the dependence of the hydraulic conductivity on saturation, as inferred from the scaling of the typical solute arrival time (Chap. 11), appears to be more or less in accord with this non-universal scaling result.

Overall, however, we find that, especially for the saturation-dependence of the electrical conductivity, experimental results are consistent with universal scaling, as our analysis predicts. Further, old results from Thompson et al. [67] indicate a strong clustering of the porosity dependence of the electrical conductivity around universal scaling. In the following chapter we show that both the air permeability and solute and gas diffusion are also consistent with universal scaling predictions from percolation theory.

It is of general importance to consider the limitations of our methods, and in what kinds of systems we might expect them to be incomplete. For example, one can imagine scenarios in which Archie's law follows universal scaling for saturation dependence but not for porosity dependence, consistent with phenomenological representations of Archie's law that allow for different dependences of the electrical conductivity on saturation and on porosity. An example of such a series of media is described in Sahimi [63]; sequences of media formed by cementing concentric chemical depositional layers around spherical particles (a model of diagenesis) can generate dependences on porosity distinct from universal scaling. Models of bioclogging could generate inward growth of bacterial films towards the center of a pore. Depending on the apportionment of bacteria within pores of different pore radii, it may be possible to generate a wide range of effective porosity dependences of the hydraulic conductivity. If this effect were independent of pore size, for example, the analyses presented here could be applied with little modification, since the pore that delivers the critical pore radius would remain the same, even if the radius did not. However, we have not expanded our treatment of the models of the pore space in this direction.

We have greatly expanded the number of experiments considered. This has forced us to address additional issues regarding potential failures of the assumption of Poiseuille flow, for example, as well as alternate means of water transport. There we have begun to address the issue of film flow, and its effects on the hydraulic conductivity.

We also can identify complications from experiment. In particular, when analysis leads us to expect universal scaling from percolation theory, but observations indicate otherwise, we find that factors other than non-universal exponents of percolation frequently influence experimental results. For example, we have seen evidence for experimental issues such as contact resistance, non-zero conductivity of the solid phase, misjudging the value of a critical moisture content, and dissolution of precipitated ions; these issues complicate the analysis and may, if not accounted for, appear to support non-universal exponents in the electrical conductivity. We analyze nearly 50 data sets for electrical conduction or diffusion (and summarize prior analysis of another 50 data sets), all of which appear consistent with universal scaling. Some of these data sets (e.g., [2]) had been interpreted differently in the past to support the relevance of non-universal exponents.

Since significant further evidence for the relevance of universal scaling emerges from analyses of the saturation dependence of the air permeability and of diffusion constants, both topics of the following chapter, we defer a final evaluation of the merits of universal scaling until the end of the next chapter.

6.2 Hydraulic and Electrical Conductivities, and Electrokinetic Coupling: Universal and Non-universal Exponents

The scaling difference between electrical and hydraulic conduction, though only a matter of the specific power of a pore radius, produces a huge difference in measurable properties. We start by contrasting electrical and hydraulic conductivity, with each expressed as a function of moisture content, and for completeness include electrokinetic and film flow effects as well. The discussion assumes Poiseuille flow, though some of the experimental evidence we discuss suggests that this assumption may be violated.

From Chap. 5 we had that the hydraulic conductance of a (roughly cylindrical) pore of radius r and length l filled with fluid of viscosity η is

$$g^{\mathrm{h}} \propto \frac{r^4}{\eta l} \tag{6.1}$$

The electrical conductance of the same pore is

$$g^{\mathrm{e}} \propto \sigma_{\mathrm{b}} \frac{r^2}{l} \tag{6.2}$$

where σ_{b} is the electrical conductivity of the water or brine filling the pore; σ_{b} is therefore proportional to the concentration of charge carriers. Equation (6.2) is

equivalent to stating that the resistance of a homogeneous wire of resistivity $\rho \equiv 1/\sigma$, length l, and cross-sectional area A is $\rho l/A$, a result familiar from elementary physics. Equation (6.2) implicitly assumes that conduction is uniform within a given pore, and would be relevant for the thermal conductivity of the medium as well, if it weren't for the fact that the solid medium typically has a higher thermal conductivity than the fluid-filled pore space.

Because electrokinetic effects (as opposed to thermal conduction) also relate chiefly to the water-filled pore space, we include them in this discussion. In this case the flux is only along the boundary of the pore, so that the total charge transport is confined to a cylindrical shell of circumference $2\pi r$ and thickness Δr, rather than a cylinder of cross-sectional area πr^2. Therefore the conductance g^{ek} (the coefficient of proportionality between electrokinetic current, J^{ek}, and the gradient of pore pressure) takes the form [35]

$$g^{\mathrm{ek}} \propto \frac{r}{l} \tag{6.3}$$

Similarly, for films of thickness Δr, the conductance would take the form

$$g^{\mathrm{ff}} \approx \Delta r^2 (r \Delta r)/l \tag{6.4}$$

In finding the controlling conductance in an infinitely large system, critical path analysis will yield the same critical radius r_{c} for electrical as for the hydraulic conductivity [22], and for that matter also for the electrokinetic current and film flow, since in all these cases a pore's conductance is a monotonically increasing function of r. Using a network model on a cubic grid, Friedman and Seaton [22] showed that the relationship between the saturated electrical conductivity σ_{S} and the saturated hydraulic conductivity K_{S} is $K_{\mathrm{S}} \propto r_{\mathrm{c}}^2 \sigma_{\mathrm{S}}$. Extending the relationship to include an electrokinetic conductance, g^{ek} would yield $g_{\mathrm{c}}^{\mathrm{e}} \propto r_{\mathrm{c}} g_{\mathrm{c}}^{\mathrm{ek}}$. The proportionality constant r_{c}^2 between K_{S} and σ_{S} is therefore system dependent rather than universal, even when both properties are determined by critical path analysis. We will see that the connection between the two properties is even less straightforward, and that there is little hope of deriving a rigorously predictive relationship between the two quantities—without knowing much more about the medium than one is likely to know if one's aim is simply to obtain K_{S} from σ_{S}.

Consider next the implications of treating a self-similar medium. If a medium is fractal, it is not possible to distinguish the size of a pore on the basis of its aspect ratio l/r. More generally, while all pore shapes of a given size need not be identical, self-similarity still requires that the distribution of pore shapes be independent of pore radius. Thus self-similarity implies $r \propto l$ in the mean.

In a medium in which the pore space is self-similar, we can summarize the scaling of various pore-scale conductances with r:

$$g^{\mathrm{h}} \propto r^3 \tag{6.5}$$

$$g^{\mathrm{e}} \propto r^1 \tag{6.6}$$

$$g^{\mathrm{ek}} \propto r^0 \tag{6.7}$$

$$g^{\mathrm{ff}} \approx r^0 \Delta r^3 \tag{6.8}$$

Of course the porous medium may be simulated using a network model with a fixed grid, such that all pore lengths are identical even while the pore radii vary. In such a case it would be necessary to increase by 1 the powers of r in Eqs. (6.5) through (6.8), giving the original values of 4, 2, 1, and 1, respectively. The particular results derived below would then no longer hold, but analogues to these results are treated in the problem sets.

Assume the RS model as a case consistent with $l \propto r$. Consider that if a pore has radius r with probability $W(r)$, it must have volume r^3, making the chance that a small volume chosen arbitrarily belongs to a pore of radius r proportional to $r^3 W(r)$. Thus, since $W(r) \propto r^{-1-D\mathrm{p}}$, we must have the probability of "landing on" a pore of radius r be $r^3 W(r) \propto r^{2-Dp}$. Combine Eq. (6.5) and Eq. (6.6) with the relationship

$$W(r)dr = W(g)dg \tag{6.9}$$

as well as $r^3 W(r) \propto r^{2-D\mathrm{p}}$, and the results

$$W\left(g^{\mathrm{h}}\right) \propto \left(g^{\mathrm{h}}\right)^{-\frac{D_{\mathrm{p}}}{3}} \tag{6.10}$$

and

$$W\left(g^{\mathrm{e}}\right) \propto \left(g^{\mathrm{e}}\right)^{2-D_{\mathrm{p}}} \tag{6.11}$$

follow. In Eq. (6.10) it is almost always true that $0 < D_{\mathrm{p}}/3 < 1$, while in Eq. (6.11) $-1 < 2 - D_{\mathrm{p}} < 0$ as long as $2 < D_{\mathrm{p}} < 3$, which is typically the case. Thus, under usual circumstances, the distributions of both the electrical and hydraulic conductances are power laws with exponents $-\alpha$ such that $0 < \alpha < 1$. But Balberg [3] determined that if

$$W(g) \propto g^{-\alpha} \quad 0 < \alpha < 1 \tag{6.12}$$

for a distribution that continued to $g = 0$, then the conductivity described by that distribution must obey

$$\sigma \propto (p - p_{\mathrm{c}})^{\frac{\alpha}{1-\alpha}} \tag{6.13}$$

Equations (6.10) and (6.11) give results that correspond to those treated by Balberg [3] as generating non-universal exponents of percolation theory, except that, as we will see, they cannot be extended to $g = 0$ as required for that derivation. In contrast, the distribution of electrokinetic (as well as film flow) conductances follows the form

$$W\left(g^{\mathrm{ek}}\right) \propto \delta(g - g_0) \tag{6.14}$$

(where δ is the Dirac delta function): all conductances have the same value, which we designate g_0. For film flow, this conductance value is proportional to Δr^3. Since each film has the same thickness, and since the total area of the pore boundaries is essentially given in terms of the specific surface area, it is possible to relate the specific water volume, θ, linearly to the individual film thicknesses, Δr. This makes each g^{ff} proportional to θ^3.

In a system with heterogeneous mineralogy, Eq. (6.14) would no longer hold for electrokinetic currents, because the streaming potential (which we do not discuss; see, e.g., [6]) would also vary. Similar arguments would hold in film flow. However, even in a heterogeneous network there could be no correlation between saturation and the conductance distribution, so arguments that the electrokinetic current (as a function of saturation) is governed by non-universal exponents would still not apply.

A network in which all conductances have the same value cannot generate a non-universal exponent for the saturation-dependence of the conductivity, unless, as in film flow above, each individual conductance contains a prefactor with a non-universal dependence on saturation. Further, application of critical path analysis to such a network cannot yield a saturation dependence of the electrokinetic current J^{ek}, since the critical conductance value will have no dependence on saturation. Thus the only saturation dependence available for J^{ek} is topologically based, and must be given by the universal scaling of percolation theory (also given in [66]). When the pore size distribution is irrelevant to conductivity, the universal exponents of percolation theory describe the behavior of the *saturation* dependence of the conductivity over the full range of saturations and J^{ek} must depend on saturation as

$$J^{\mathrm{ek}} \propto (\theta - \theta_{\mathrm{t}})^{\mu} \tag{6.15}$$

Normalization for $\theta = \phi$, or for $\phi = 1$ of such a property that depends only on surface properties is subtler than we wish to address, so this concludes our discussion of electrokinetic currents. However, we can still address the saturation dependence of film flow: Factoring out θ^3, common to each conductance, allows the total film flow hydraulic conductivity to be written as proportional to θ^3. This result has recently been obtained by Wang et al. [73], with some evidence to indicate that it corresponds to observations of the hydraulic conductivity under dry conditions.

From Chap. 5 the ratio of the (unsaturated) hydraulic conductivity $K(\theta)$ and its value K_{S} at saturation is

$$K(\theta) = K_{\mathrm{S}} \left[\frac{(1-\phi) + (\theta - \theta_{\mathrm{t}})}{1 - \theta_{\mathrm{t}}} \right]^{\frac{3}{3-D_{\mathrm{p}}}} \tag{6.16}$$

This equation was developed in critical path analysis as the cube of the ratio of the corresponding critical radii. In analogy with Eq. (6.16) for hydraulic conductivity, we can write for electrical conductivity [28]

$$\sigma(\theta) = \sigma_{\mathrm{S}} \left[\frac{(1-\phi) + (\theta - \theta_{\mathrm{t}})}{1 - \theta_{\mathrm{t}}} \right]^{\frac{1}{3-D_{\mathrm{p}}}} \tag{6.17}$$

The only difference between the forms of Eqs. (6.16) and (6.17) is that the power $3/(3 - D_{\mathrm{p}})$ in Eq. (6.16) is replaced by $1/(3 - D_{\mathrm{p}})$ in Eq. (6.17). This is done because the power of r for hydraulic conductivity (3 in Eq. (6.5)) is replaced by a different value in the electrical conductivity (1 in Eq. (6.6)). When both Eq. (6.16) and Eq. (6.17) hold, the hydraulic conductivity is proportional to the electrical conductivity to the third power.

Combination of Eq. (6.16) with Eq. (4.24) for moisture content as a function of hydraulic head h gives the following result for $K(h)$:

$$K(h) = K_S\left[1 - \frac{1 - (\frac{h_A}{h})^{3-D_p}}{1 - \theta_t}\right]^{\frac{3}{3-D_p}} \tag{6.18}$$

In the case $\theta_t \to 0$, Eq. (6.18) reduces to $K(h) = K_S(h_A/h)^3$ independent of pore-size distribution. Usual soil physics treatments imply the dependence h^{-2}. But for $\theta_t > 0$, $K(h)$ in Eq. (6.16) follows an approximate rather than an exact power law, and the approximate power is greater than 3. See the discussion following Eq. (6.21) for further details.

6.2.1 Balberg Non-universality

Balberg [3] demonstrated explicitly that distributions such as Eq. (6.10) or Eq. (6.11), if continued to $g = 0$ (which represents no mathematical problem, i.e., the distribution is normalizable), lead to non-universal exponents for conduction. That is, the conductivity vanishes according to some non-universal power of the difference between a volume fraction and its critical value. If we adapt Eq. (6.13), derived using continuum variable p, to the case that the fractional volume is a water content, we find

$$\sigma \propto (\theta - \theta_t)^{\frac{\alpha}{1-\alpha}} \tag{6.19}$$

Substituting the exponent from Eq. (6.10) [Eq. (6.11)] into Eq. (6.13) would yield the non-universal exponent $D_p/(3 - D_p)[(D_p - 2)/(3 - D_p)]$. However, the distributions given in Eq. (6.10) and Eq. (6.11) are truncated, both at a maximum g corresponding to r_m, and, more importantly, at a minimum g corresponding to r_0. The cut-off at the minimum g is required by physical constraints, not mathematical conditions: in the Rieu and Sposito (RS) model, a medium with $r_0 = 0$ would have porosity $\phi = 1$, zero solid volume, and infinite solid surface area in a finite volume (see Chap. 8). Because these are clearly unphysical results, we do not expect Balberg's prediction of non-universal exponents to be observed in the saturation dependence of hydraulic or electrical conductivity through water-filled pore space, at least if the RS model is preferred. On the other hand, the Balberg derivation will be seen below to be useful in the present analysis, because his results follow from Eq. (6.20) and Eq. (6.21) below in the limit $\phi \to 1$. This provides a mathematical check on the present results.

In this discussion we have identified the scaling of the bottleneck resistance as a function of moisture content with the scaling of the conductivity. In order to clarify the correspondence with the results of Balberg [3], we make the same assumption that was made there—that conduction on these paths is basically one-dimensional—then calculate the average resistance of the resulting paths. To do this, one integrates

over the bulk resistance distribution cut off at g_c^{-1}, with the result that $\langle g^{-1}\rangle^{-1}$ is given in each case by $g_c^{-\alpha}$. Instead of Eq. (6.16) and Eq. (6.17), the results are [32]

$$K(\theta) = K_S\left[\frac{(1-\phi)+(\theta-\theta_t)}{1-\theta_t}\right]^{\frac{D_p}{3-D_p}} \tag{6.20}$$

and

$$\sigma(\theta) = \sigma_S\left[\frac{(1-\phi)+(\theta-\theta_t)}{1-\theta_t}\right]^{\frac{D_p-2}{3-D_p}} \tag{6.21}$$

differing from Eq. (6.16) and Eq. (6.17) solely in the substitution of D_p for 3 in the numerator of the exponent. While these exponents are exactly $\alpha/(1-\alpha)$, as required by Balberg [3], the arguments of the powers in Eq. (6.20) and Eq. (6.21) are not simply $\theta - \theta_t$, as in his result. While it is already clear that Eq. (6.20) and Eq. (6.21) yield Eq. (6.19) (with $p - p_c \to \theta - \theta_t$) in the case $\phi = 1$, we still need to demonstrate under what range of moisture contents Eq. (6.20) and Eq. (6.21) are generally valid, before we can apply the condition $\phi = 1$.

Although Eq. (6.20) and Eq. (6.21) were derived to allow comparison with those of Balberg [3], they may have significance beyond that comparison. For example, derivation of Eq. (6.20) implies that Eq. (6.18) in the case $\theta_t = 0$ would reduce to the non-universal result $K(h) \propto h^{-D_p}$, rather than h^{-3}. Note that the observed scaling of K with h is usually according to a power between 2 and 3: typically closer to 3 than to 2, but not to precisely either 2 or 3 (Sposito, personal communication, 2002). Furthermore, $K(h)$ tends to drop more rapidly for coarser soils than for finer soils [25]. Such a result cannot be understood in terms of Eq. (6.18), which has no pore size information beyond h_A. But if D_p tends to be larger for sandy soils than for clayey soils [10], such a result is indicated, and is consistent with Eq. (6.20). Without analyzing a large number of additional media, these comments need not be conclusive to the typical physicist reading this passage, but they should have considerable significance to the typical soil physicist. If these considerations are indeed relevant, then the Balberg [3] treatment, *which uses the average resistance* along the critical path *rather than the largest resistance*, is a significant refinement to the simpler critical path treatment.

For typical values of the fractal dimensionality of soils (say 2.8; [74]), the difference between D_p and 3 in the numerator of the exponent (Eq. (6.16) versus Eq. (6.20), and Eq. (6.17) versus Eq. (6.21)), while small, may be detectable. However, there is some theory-based uncertainty as to whether using D_p is really more accurate than 3: as Mallory [47] pointed out, the distribution of resistances on the backbone clusters differs from the bulk distribution in more ways than the simple existence of a cut-off at the critical value. Larger resistors are shorted more often than smaller ones, so integration over the bulk distribution, even with the cut-off, is not strictly justifiable. Our comparisons with experiment have thus far used Eq. (6.16) rather than Eq. (6.20), and we continue to use that equation here for evaluation, but we emphasize that the issue of which exponent is more appropriate and accurate remains unresolved.

In order to complete our comparison with Balberg's [3] results, we need to discuss the relationship between critical path analysis and percolation scaling. This analysis leads to inferences regarding the Kozeny-Carman phenomenology and Archie's law as well.

6.2.2 *Transition from Critical Path Analysis to Percolation Scaling*

Regardless of whether the exponent's numerator contains 3 (Eqs. (6.16) and (6.17)) or D_p (Eqs. (6.20) and (6.21)), the critical path equations imply that when the moisture content $\theta \to \theta_t$, the conductivity (whether hydraulic or electrical) is governed by the smallest pore in the system. But this contradicts percolation scaling, according to which K and σ must both go to zero in the limit $\theta \to \theta_t$, even if the smallest pore $r_0 > 0$. In fact, if $r_0 > 0$, then one expects universal scaling to hold, and

$$\frac{K(\theta)}{K_0} = \frac{\sigma(\theta)}{\sigma_0} \propto (\theta - \theta_t)^{\mu} \tag{6.22}$$

with the constants K_0 and σ_0 having appropriate units and physical foundations. So we must address the issue of the dependence of $K(\theta)$ and $\sigma(\theta)$ in the limit $\theta \to \theta_t$, first considering hydraulic conductivity.

When θ is near θ_t, Eq. (6.22), which results from topology and percolation scaling, must replace Eq. (6.16), which describes $K(\theta)$ based on the size (geometry) of the bottleneck pore. Denote by θ_{xK} the moisture content at that cross-over or replacement point. The value of θ_{xK} can be determined [29] by setting equal the two dependences of $K(\theta)$, and also setting equal their derivatives, at some moisture content $\theta = \theta_{xK}$. The use of these two conditions, requiring continuity of both K and $dK/d\theta$, yields both θ_{xK} and the constant prefactor K_0 in Eq. (6.22). Notice that we must have $\theta_t \le \theta_{xK}$.

The practical consequence of the analysis for the cross-over moisture content is that for any θ, the appropriate equation for K is the one that gives the larger value of $|dK/d\theta|$. That is, the form to choose is the one most sensitive to changes in moisture content at the current moisture content. Equivalently, the less sensitive dependence is set equal to a constant. This procedure also permits us to find K_0, the prefactor of the hydraulic conductivity in the range of moisture contents where K is given by universal percolation scaling [29]. This is a valuable capability, as earlier recognized by Berkowitz and Balberg [5]: "One might suggest that, since the hydraulic conductivity can vary by orders of magnitude among rocks of the same porosity, the coefficients of equality in the power law relationship may be of greater significance than the critical exponent."

For ease of reference, Eq. (6.22) will be referred to as percolation scaling of K, while Eq. (6.16), derived from critical path analysis, will be referred to as fractal scaling. Although both ultimately derive from percolation theory, in Eq. (6.16) it is the fractal characteristics, through the power-law pore-size distribution, which make the dominant impact on K and show up in the exponent.

The result from the above analysis for θ_{xK} is [30],

$$\theta_{xK} = \theta_t + \left[\frac{\mu(1-\phi)}{\frac{3}{3-D_p} - \mu} \right] \tag{6.23}$$

Note that if consistency with the Balberg result for non-universal scaling is required, $3/(3-D_p)$ must be replaced by $D_p/(3-D_p)$. For $\mu = 2$ and typical soil values $\phi = 0.4$ and $D_p = 2.8$ [74], Eq. (6.23) leads to $\theta_{xK} - \theta_t \approx 0.09$, about 22 % of the range of moisture contents. In the more complicated model related to the pore-solid-fractal model, the only change to Eq. (6.23) is that $1-\phi$ is replaced by $\beta - \phi$.

6.2.3 Comparison with Experiment

We begin with Hunt and Gee [33], who compared the above results with data from the Hanford site, and continue with our recent [23] comparison to the much larger UNSODA data set from the USDA Salinity Laboratory, Riverside, California [44]. In 2002 we used the theoretical development given here, while in 2012 we applied a somewhat more complicated model related to the pore-solid fractal (PSF) model of Bird et al. [9]. The Bird et al. model has an additional parameter β, corresponding to its more complex partitioning of the space in the medium (described in greater detail in Chap. 4), and allows the smallest pore radius to approach zero without incurring $\phi \to 1$. Although our 2012 model is not precisely Bird et al.'s [9] PSF model, the analytical results for the water-retention curve are identical to those of the PSF model, and we will refer to it using this abbreviation. Also, like the PSF model, it is consistent with the Rieu and Sposito [59] model treated here in the case $\beta = 1$, while it is consistent with the Tyler and Wheatcraft [70] fractal model when $\beta = \phi$. In the (unphysical) limit $\phi \to 1$, all three models are indistinguishable. Besides the much larger data set and the more general model, the 2012 analysis, for which useful particle-size data were not available, simply fitted the PSF model water retention predictions to experiment and used the extracted parameters to predict the hydraulic conductivity. In 2002, we generated the water retention curves as well as the saturation dependence of the hydraulic conductivity from particle-size data.

Figure 6.1 demonstrates an example of the predictive capability of the critical path analysis-based techniques, including the relevance of the cross-over to universal scaling, for the values of D_p, ϕ, and θ_t from the McGee Ranch soil [32, 33], along with experimentally measured values of K. $D_p \approx 2.81$ was obtained via Eq. (3.16) from porosity and particle size data taken from various places on the surface, while θ_t was obtained by comparison with studies examining percolation scaling of the diffusion constant [34]. K_S was chosen as the largest measured K value. The solid line is the theoretical prediction using the mean value of D_p; dashed lines represent uncertainty in the measurement of D_p. Given that all the parameters were obtained from measurements of other properties, Fig. 6.1 represents a zero-parameter prediction. Note that the data for Fig. 6.1 [62] were obtained at different depths in the

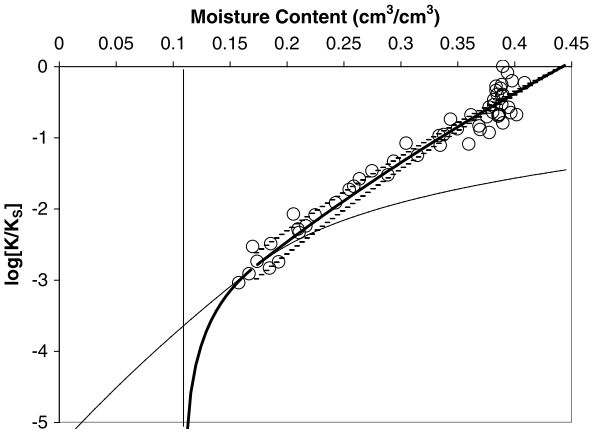

Fig. 6.1 The hydraulic conductivity of the McGee Ranch soil as a function of moisture content. Data from [62]. The *circles* are the experimental values. The *bold line* is the combined prediction of critical path analysis (Eq. (6.22)) and universal scaling near the percolation threshold (Eq. (6.16)). The *light line* at for $\theta > 0.15$ is Eq. (6.16), for $\theta < 0.15$, Eq. (6.22). The *dashed lines* on either side of the *bold line* represent the approximate uncertainty in the prediction due to the variability (9 samples) in the measured values of r_0 and r_m and the consequent uncertainty in D_p. The critical moisture content, 0.107, for percolation was obtained from the regression of Hanford site soils on the Moldrup relationship for the threshold moisture content for diffusion (Chap. 7), and is shown by the *vertical line*. K_S was chosen to be the largest K value measured. The porosity was 0.444. Note that the unsteady drainage (field) experiment did not attain moisture contents lower than approximately θ_{xK}, where K begins to drop precipitously

column in a field experiment (unsteady drainage), and stop at a moisture content approximately equal to θ_{xK}. Lower moisture contents are associated with very small values of K, and require much longer drainage times than attainable in experiment. Thus the question of equilibration becomes very important at moisture contents below θ_{xK}, a topic discussed in detail in Chap. 8.

Continuing, Fig. 6.2 shows predicted and observed $K(\theta)$ for a multi-modal pore-size distribution, addressed analytically by assuming that each mode of the distribution can be treated using the RS model. Using the soil particle size data, Hunt and Gee [33] were able to find the appropriate values of D_p in each mode of the distribution, meaning that the theoretical points in Fig. 6.2 again represent a zero-parameter prediction. An interesting aspect of a multi-modal pore size distribution is its effect on the representation of $K(h)$. While $K(h)$ tends to follow a power law in hydraulic head (either h^{-3} or h^{-D_p}) in the case of a simple power law pore-size distribution (with a positive curvature on a $\log[K]$ vs. h plot), when the distribution is bimodal this universal tendency is lost. Consider a case when the largest water-filled pore is in the upper mode of the pore-size distribution (say, with dimension D_u), but the critical pore radius is in the lower mode (say, D_l). Then the product of the two powers $3 - D_u$ and $3/(3 - D_l)$, relevant for $\theta_t \ll 1$, will not be 3, because the two values of D are not the same. (Use of the Balberg technique is a bit more complex here, but does not qualitatively change the conclusions.) If the lower mode

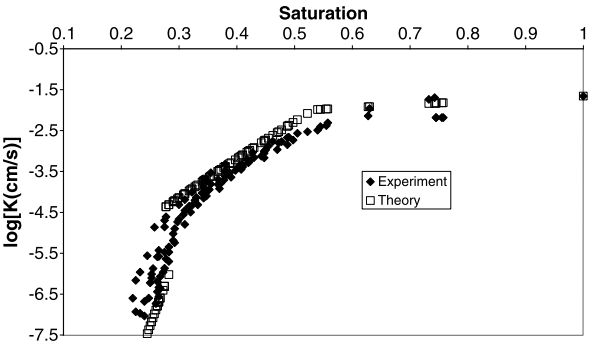

Fig. 6.2 The hydraulic conductivity of the North Caisson soil. The North Caisson soil had a multi-modal particle-size distribution. Like the McGee Ranch soil the theoretical comparison involves no uncertain parameters. Data from [62]

of the distribution has a very small associated porosity, such as a small silt fraction in a sandy soil, then the usual fractal analysis will generate a value of D_1 very close to 3, and $K(h)$ will have a cusp associated with a cross-over to a much more rapid drop in K with increasing h. Experimental data near the cusp may appear to have a negative curvature on the typical plot because of the experimental uncertainty, but it is actually positively curved everywhere except at the cross-over. Interestingly, the variability in K values increases rapidly below the cross-over, since there is typically considerable relative variability in the concentration of fine soil particles when the medium is rather coarse. So if (for example) silt and clay compose on average 5 % of a given soil, one is likely to encounter samples with concentrations from 2 % to 10 %; this variability can easily change $1/(3 - D_1)$ by a factor of 50 to 15, respectively [33].

In Ghanbarian-Alavijeh and Hunt [23], the water retention curve for the PSF model,

$$\theta = \phi - \beta\left[1 - \left(\frac{h_{\min}}{h}\right)^{3-D}\right], \quad h_{\min} < h < h_{\max} \tag{6.24}$$

was fitted to experimental data from the UNSODA data base to find the parameters D and β, while θ_t was identified with $\theta(h_{\max})$, effectively the lowest moisture content reached. These parameters were then inserted into the derived result for the hydraulic conductivity [23],

$$\frac{K(\theta)}{K_S} = \left[\frac{\beta - \phi + \theta - \theta_t}{\beta - \theta_t}\right]^{\frac{D}{3-D}} \quad \theta > \theta_{xh}, \tag{6.25}$$

where

$$\theta_{xh} = \theta_t + \left[\frac{\mu(\beta - \phi)}{\frac{D}{3-D} - \mu}\right] \tag{6.26}$$

or Eq. (6.22) and compared with experiments (Fig. 6.3) on 109 soils (1014 data points). This figure is plotted in the way usual in soil physics publications, with the observed values on the horizontal axis and the predicted ones on the vertical. Note that the standard procedure in soil physics is to use the van Genuchten formulation for the unsaturated hydraulic conductivity (Eq. (3.18)), shown in the second panel,

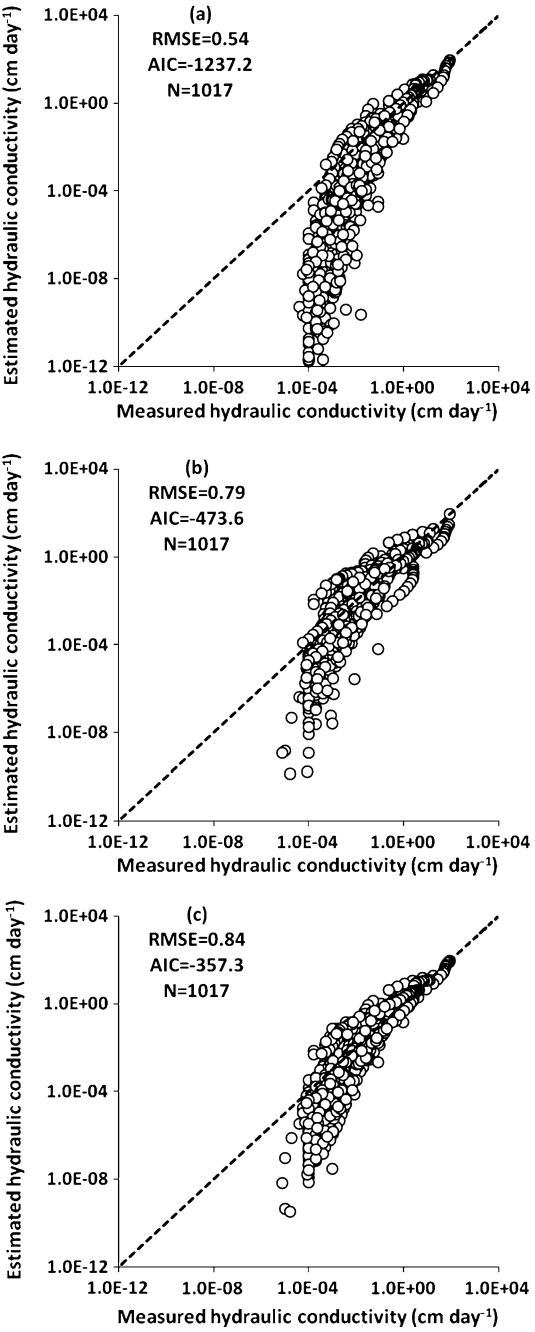

Fig. 6.3 Comparison of critical path analysis (CPA) based calculation of the saturation dependence of K with two other methods [23]. *First panel*, CPA; *second panel*, Mualem-van Genuchten, *third panel* Mualem method applied to PSF model. Two important results emerge: (1) CPA works much better at higher saturations, (2) CPA underestimates K by the greatest amount at low saturations. The latter result is due partly to the fact that in percolation theoretical methods there is no adjustable parameter in the "tortuosity-connectivity" factor, and that the added flexibility in the Mualem method is serving to hide its defects (Hunt et al. [36]—"What is wrong with soil physics?")

while the third panel shows what would happen if the Mualem-van Genuchten procedure were applied to the PSF model. At higher moisture contents (and higher observed K values), application of critical path analysis to the PSF clearly performs best. This is shown by comparing the values of Akaike's information criterion (AIC), which are -1273 (critical path) -478 (van Genuchten), and -357 (Mualem van Genuchten applied to PSF). Larger negative AIC values indicate more accurate predictions.

All methods underestimate K at small moisture contents, ours by the most, at least *on the average*. It is relevant, however, that hydraulic conductivity values smaller than about 10^{-9} cm/s (10^{-4} cm/day) are simply not measured. This particular value corresponds to less than an atomic distance of transport in a second; at such low water transport rates it is less than clear that equilibrium moisture contents have been reached, nor that Poiseuille flow in water-filled pores has any relevance. Thus applying any of the usual formulations for the hydraulic conductivity under conditions that they predict such low values of K is probably not supported. Simply "chopping off" the graphs horizontally at 10^{-4} cm/day allows the critical path analysis prediction to appear at its best.

One reason that Mualem-van Genuchten treatments lead to a smaller underestimation of K at low moisture contents is their use of an inappropriate tortuosity-connectivity correction factor whose exponent is too small, i.e., $1/2$ instead of 2. The fact that such small values of this exponent (including negative values when used as an adjustable parameter, which would imply vanishing path lengths!) work so well is indicative of systematic problems in all three formulations, most likely the neglect of alternative flow mechanisms. We have not yet checked whether we can eliminate the problems at low moisture contents by considering film flow contributions to the hydraulic conductivity, as claimed by Wang et al. [73]. Given that the cubic dependence of film flow conductivity on moisture content derived here is the same as in Wang et al. [73], it seems likely, however.

There are other important physical considerations, however. The most obvious is that it is known that the WRC does not always provide a reliable estimate of the pore-size distribution, as discussed in Chap. 3. Comparison with the experimental WRC sometimes appears to overestimate the parameter D (2.932 instead of 2.885) or underestimate β (0.3 instead of 0.315), as shown in Figs. 6.4 and 6.5, leading to significant underestimation of the hydraulic conductivity. Consider that in the two cases shown, errors of 2 % in D or 5 % in β can lead to errors of orders of magnitude in the conductivity. If our methods perform better than existing methods in spite of such sensitivity, we argue that the weak link is the inference that one can obtain the conductance distribution (i.e., the pore size distribution) from the WRC. More broadly, the accuracy of our theoretical calculations is such that it helps expose weaknesses in inferences regarding the pore space.

We have also conducted a more in-depth study [23] on 8 UNSODA systems included in Fig. 6.3, for which the WRC exhibited a pronounced cross-over in slope. Our goal was to check whether the agreement between theory and experiment could be improved if we allowed two separate fractal regimes in our model. The details

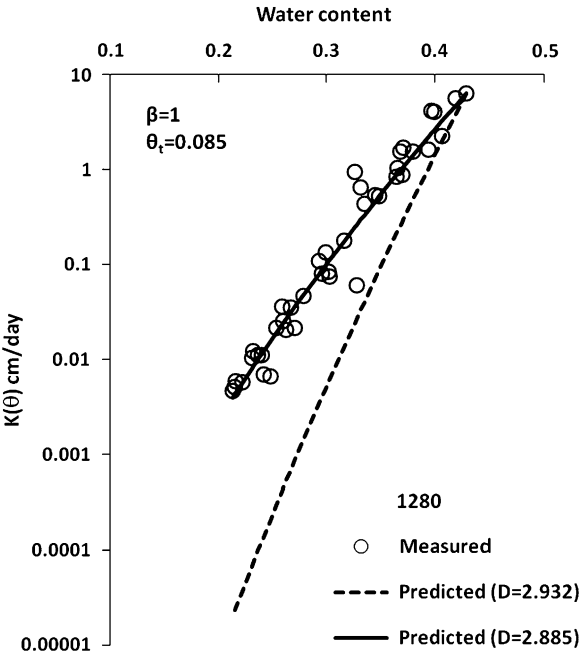

Fig. 6.4 Demonstration of the high sensitivity of CPA-based calculations to parameters extracted from the WRC. Here a slight error (2 %) in the determination of D leads to a two order of magnitude error in K at $S \approx 0.5$

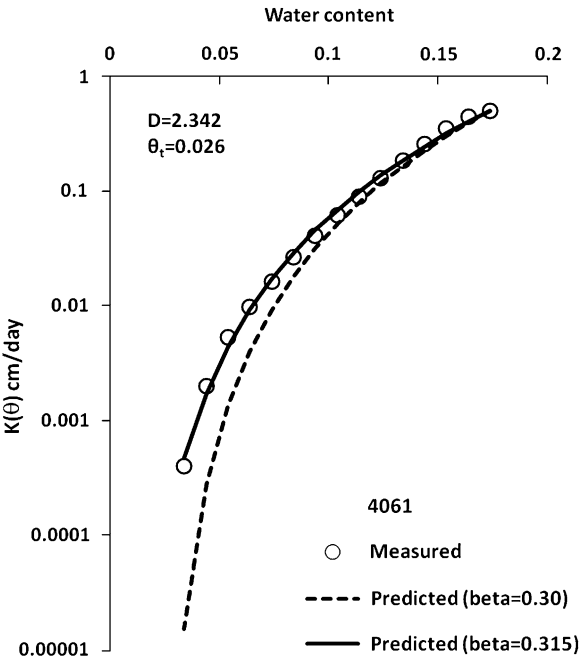

Fig. 6.5 Demonstration of high sensitivity of K as determined by CPA to the parameter β in the PSF model. An error of 5 % leads to an underestimation of K by one and a half orders of magnitude at $S \approx 0.3$

of the derivation are left to the Appendix; the process is time-consuming, but not difficult. We emphasize one point from this study: the fact that the observed change in slope occurred at the same moisture content in both the WRC and the hydraulic conductivity indicates that the relevant critical volume fraction is zero, at least for θ in the upper mode of the distribution.

To our surprise, we could not confirm that the more complicated model led to superior predictions. Consider Fig. 6.6, which compares the predictions derived from the monomodal and bimodal treatments with experiment. Qualitatively, our predictions for $K(\theta)$ matched the shape of the observed results better, but quantitative comparison did not hold up well. In particular, we typically predicted a much steeper reduction in K with diminishing moisture content than was actually observed.

In order to understand the discrepancy between theory and experiment, we investigated first the possibility that the fits to the WRC did not return the appropriate value of the fractal dimensionality. Thus we fitted Eq. (6.52) to the measured unsaturated hydraulic conductivity curves and determined D_1 and D_2. Figure 6.7 shows the fitted unsaturated conductivity model and the model capability for all soil samples. Clearly it is possible to fit both K and the WRC, but not with the same D values. The comparison of calculated fractal dimension of the first and second regimes (D_1, D_2) using the WRC and unsaturated hydraulic conductivity data given in Table 6.1 returned relative error values less than 4 %. Although the relative error values are small, Fig. 6.6 shows that a small discrepancy in fractal dimension may lead to even 8 orders of magnitude difference in the hydraulic conductivity at very low water contents (see samples 4033 and 4681). These results are generally consistent with those obtained in the monomodal case above, though the sensitivity to discrepancies in D is even greater. High sensitivity to model parameters might be regarded as a drawback, but it also has an advantage: it makes it possible to distinguish between the efficacies of different means to extract parameters from experimental data, by accentuating discrepancies between prediction and experiment. In particular, small changes in the value of D, if the value of D is near three, are consistent with large changes in a pore-size distribution.

Several possible explanations for the discrepancy must be considered.

In Chap. 8 we discuss the complication that at lower moisture contents a rapid drop in K can make it difficult to remove water from the medium, forcing tension values higher, and thus attributing the water remaining to smaller pores. This means that non-equilibrium conditions could confound our test, particularly at low moisture contents, where the problem appears most acute. The discrepancies might also be due to a failure of some common assumptions discussed in Chap. 3, e.g., of the existence of cylindrical soil pores that are perfectly wetting (ideal contact angle) in the Young-Laplace equation. In addition, changes in shapes of pores with diminishing pore size (due to changes in mineralogy) can lead to the relevance of different pore radii to different physical properties—a mean radius to water volume, but a bottleneck radius to flow, for example.

One possibility that deserves special attention is that Poiseuille's law may not always be valid in natural porous media. Under the condition that the threshold water content is zero (as appears by our analysis to be appropriate for each of these

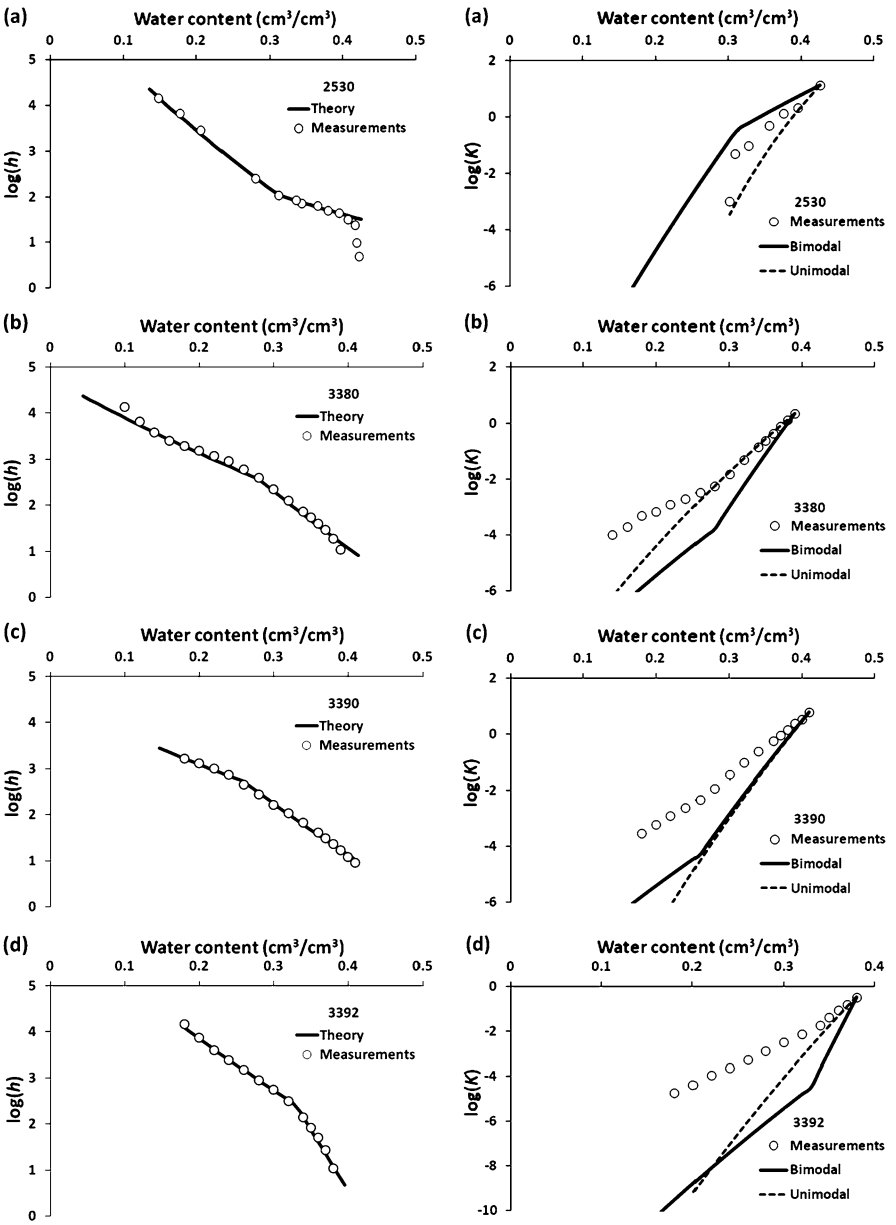

Fig. 6.6 Demonstration that parameters extracted from the WRC in the bimodal pore-size distribution frequently lead to severely inaccurate predictions of K, even though the shape of the predicted $K(S)$ curve qualitatively resembles that of the experimental data

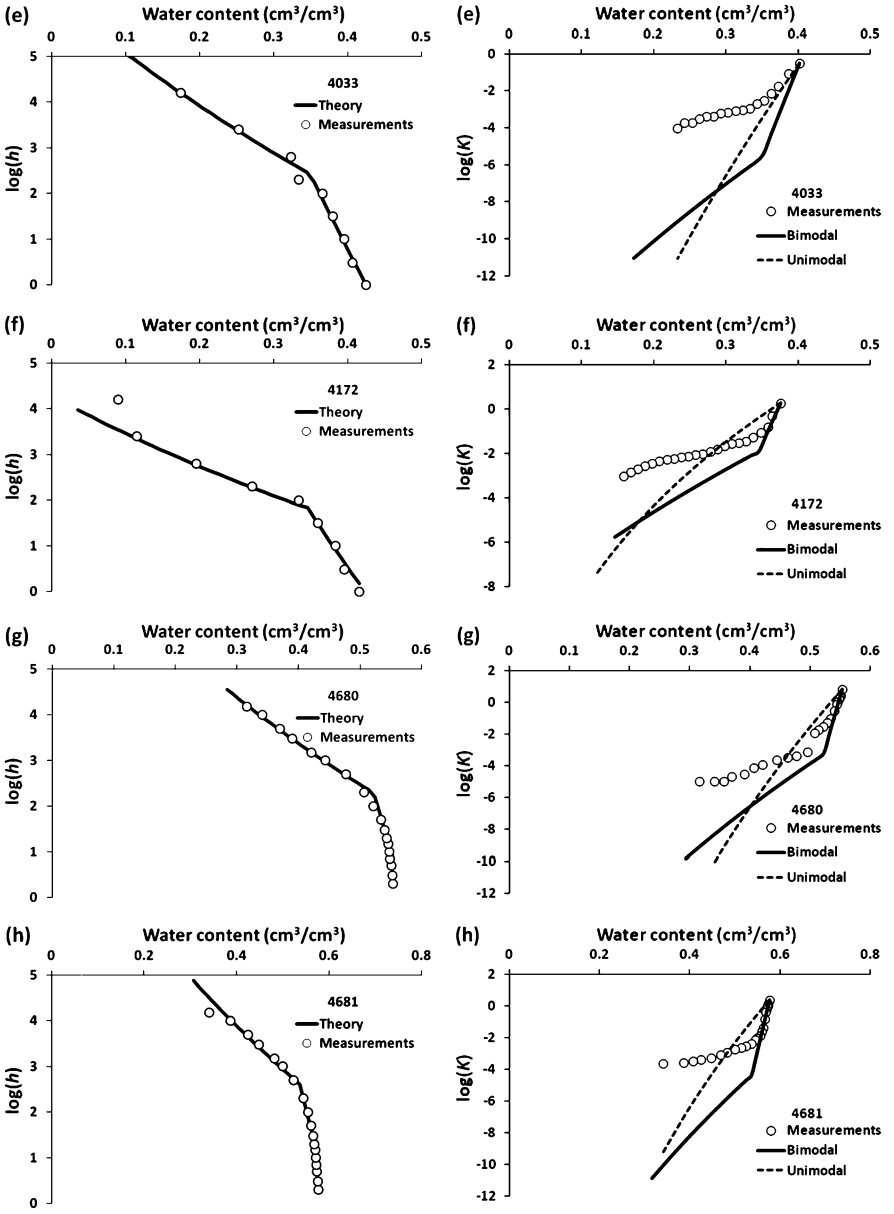

Fig. 6.6 (Continued)

soils), the saturation-dependence of the critical pore radius should track exactly the saturation dependence of the largest water-filled pore. This allows a rather precise comparison of the theoretical scaling of hydraulic conductivity with pore radius, if the WRC is a reliable representation of the pore space. As seen in Fig. 6.6, the

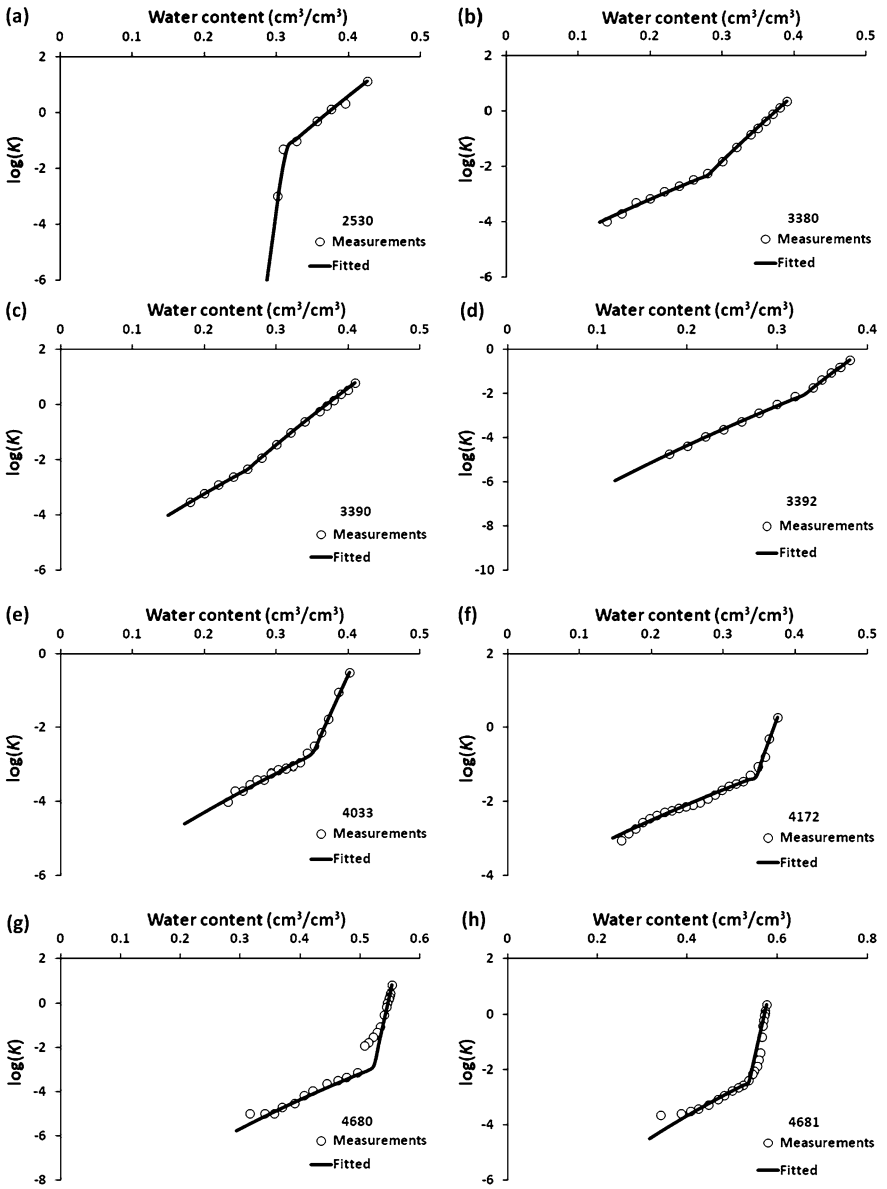

Fig. 6.7 Demonstration that only slight changes in the parameters extracted from the WRC could lead to $K(S)$ curves that match experiment very well. See discussion in text

pore size (tension head) ranges between 2 to 4 orders of magnitude, while the hydraulic conductivity typically changes by 3 to 6 orders in the same range of water content. But Poiseuille's law for self-similar fractal porous media makes $K(\theta) \propto r^3$ [23, 26], implying that if pore sizes change between 2 and 4 orders of magnitude,

Table 6.1 Values of fractal dimensionality in bimodal distribution as obtained by comparison from WRC and $K(\theta)$, respectively

Soil code	Water retention model	Unsaturated hydraulic conductivity	Relative error (%)	Water retention model	Unsaturated hydraulic conductivity	Relative error (%)
	D_1	D_1		D_2	D_2	
2530	2.900	2.935	1.2	2.964	2.993	1.0
3380	2.962	2.941	−0.7	2.935	2.875	−2.1
3390	2.958	2.932	−0.9	2.928	2.908	−0.7
3392	2.983	2.957	−0.9	2.958	2.921	−1.3
4033	2.986	2.968	−0.6	2.953	2.862	−3.2
4172	2.981	2.974	−0.2	2.925	2.825	−3.5
4680	2.990	2.989	0.0	2.948	2.880	−2.4
4681	2.989	2.982	−0.2	2.950	2.840	−3.9

the hydraulic conductivity should change between 6 and 12 orders, if the same radius r is relevant to both properties. Table 6.1 records the logarithms of the ratios of the largest to smallest pore sizes as well as the largest to smallest $K(\theta)$ values in each regime for each soil. We expect that the logarithms in columns 3 and 5 should be exactly three times those of columns 2 and 4. For non-zero values of θ_t this ratio can be different from 3. Note that both the Mualem-van Genuchten [71] and Burdine [12] formulations ultimately appeal to Miller-Miller similitude [49] and would be consistent with the power of 2, again in the case that a single value for a characteristic pore radius characterizes both flow and water retention. However, influences of both pore roughness and shape can confound this inference, and the actual relationship between the two scaling exponents depends on the means chosen to generate the representative pore radii. For flow the most important radius is a bottleneck in a plane perpendicular to the flow, whereas for water retention, a mean minimum radius is more nearly characteristic.

If pores could be considered self-similar, one would have a basis for asserting that these two different radii would at least have the same dependence on mean pore volume. But if pore shapes are irregular, there is no *a priori* reason to assume that all cross-sections will scale identically with changes in pore size. As a result, systematic pore shape changes with size would contradict our assumption of self-similarity. In fact, the data analyzed here imply that the ratio of the two scaling exponents is typically less than 2. Powers significantly greater than 2 would indicate the relevance of r^3 scaling of K, whereas powers less than 2 suggest the relevance of r^2 scaling to the hydraulic conductivity for $\theta_t = 0$. The result, that 3 of the 16 cases yield a value less than 2, is actually rather ambiguous, although at first sight would seem to imply that r^2 scaling of K is more likely. In this context we mention the results of Priesack and Durner [56], who found that the exponent 3 may work much better than 2. And the comparisons in Fig. 6.3 indicated that our entire theoretical framework, including the exponent of 3, was quite accurate. In any case, reflection

on the results summarized here leads to the conclusion that assumption of Poiseuille flow scaling may not always be justified.

6.2.4 Cross-over Moisture Content for the Electrical Conductivity

Repeating for the electrical conductivity the analysis that led to the hydraulic conductivity cross-over θ_{xK} from fractal to percolation scaling yields [31]

$$\theta_{x\sigma} = \theta_t + \left[\frac{\mu(1-\phi)}{\frac{1}{3-D} - \mu}\right] \tag{6.27}$$

(or, using Balberg's approach, $(D_p - 2)/(3 - D_p)$ rather than $1/(3 - D_p)$ in the denominator). Moreover, if the pore-solid fractal approach is used, Eq. (6.27) should be modified by replacing $1 - \phi$ with $\beta - \phi$. If the same values for $\theta_t = 0.04$, $\mu = 2$, $D_p = 2.8$, and $\phi = 0.4$ are substituted into Eq. (6.27) as into Eq. (6.23), one finds $\theta_{x\sigma} - \theta_t \approx 0.4$ for the electrical conductivity, rather than the value 0.09 found for the hydraulic conductivity. That is, in the case of electrical conductivity, it is percolation scaling which dominates over the entire range of water contents. Thus the saturation dependence of the electrical conductivity, in contrast to that of the hydraulic conductivity, may to a good approximation be written in the form of percolation scaling all the way to full saturation where $\theta = \phi$ [31]:

$$\sigma = \sigma_0(\phi - \theta_t)^{\mu} \tag{6.28}$$

K at saturation is typically determined through r_c, but σ is not. When K at saturation contains information from a significant portion of the distribution of pore sizes, but σ at saturation is independent of the pore size distribution, there is no possibility to infer the hydraulic conductivity from the electrical conductivity.

Further, Eq. (6.28), in its simplicity, should recall Archie's law, in which the conductivity is written as a power of the porosity.

6.2.5 Return to Balberg Non-universality

Equations (6.20) through (6.22) allow us to set a limit on the applicability of Balberg's results for non-universal scaling. Consider the limit $r_0 \to 0$, i.e. that fractal fragmentation has proceeded indefinitely (and the limit that the power law of the conductance distribution continues to zero conductance). From Eq. (4.19) it is seen that $\phi \to 1$. If $\phi = 1$, Eq. (6.20) yields

$$K = K_S\left(\frac{\theta - \theta_t}{\phi - \theta_t}\right)^{\frac{D_p}{3-D_p}} \tag{6.29}$$

and Eq. (6.21) yields

$$\sigma = \sigma_S \left(\frac{\theta - \theta_t}{\phi - \theta_t} \right)^{\frac{D_p - 2}{3 - D_p}} \tag{6.30}$$

Further, Eq. (6.26) and Eq. (6.27) both yield

$$\theta_x = \theta_t \tag{6.31}$$

Thus in the limit $r_0 \to 0$, the percolation scaling regime disappears, while the fractal scaling regime develops a dependence on the moisture content $(\theta - \theta_t)$ to a power, for which the value of the exponent is related to the specific characteristics of the fractal structure, and is thus non-universal [32]. The predicted powers are in exact agreement with the results of Balberg if the average pathway resistance (rather than the critical resistance) is used. In a formal sense, extending the Rieu and Sposito fractal pore space model to pores of zero radius is consistent with continuing the power law conductance distribution to zero conductance, which allows direct comparison of Eq. (6.29) and Eq. (6.30) with results of Balberg [3]. While Eq. (6.29) and Eq. (6.30) predict that the non-universal behavior is valid for the entire range of (conducting) moisture contents, i.e., $\theta_t < \theta < \phi$, the universal contribution to the power μ should also be added on at least in the vicinity of θ_t. Although we have been treating universal scaling effects separately, in the limit $\phi = 1$ the non-universal scaling results dominate over the entire range of moisture contents, and the additional contribution from universal scaling ($\mu = 2$) may simply be added on in the vicinity of the percolation threshold at θ_t. Note that for typical values of $D_p \approx 2.8$ in soils [74], the non-universal contributions to the power of Eq. (6.18) and Eq. (6.19) are 14 and 4 respectively, i.e., much larger than 2. However, such soils also typically have $\phi \approx 0.4$, and the argument of the power, $(1 - \phi) + \theta - \theta_t$ then becomes approximately $0.6 + \theta - \theta_t$. Such a function does not present as a power law when graphed logarithmically.

6.2.6 *Inferences on Porosity Dependences at Full Saturation: Archie's Law*

The equation for the crossover moisture content for electrical conductivity, Eq. (6.27), also allows further discussion of the electrical conductivity under saturated conditions. It has been shown [30] that for natural media with insignificant clay content, $\theta_t = p_c \phi$, with p_c a numerical constant independent of porosity. While that derivation was motivated by theory, experimental data discussed there and in many sections of this book provide additional confirmation. The basis for this proportionality is easily understood in terms of a network of identical tubes: when a fraction p_c of the tubes is filled with water, the water-filled tubes percolate and the moisture content is $p_c \phi$. This result can be generalized heuristically to an arbitrary network with unknown p_c. Such an argument is very much in the spirit of the first

continuum percolation calculation of a critical volume fraction [64]. Combining this proportionality with the experimentally obtained approximation $p_c \approx 0.1$ (further discussion in Chap. 8), Eq. (6.28) may be rewritten [28] as

$$\sigma \propto (\phi - 0.1\phi)^{\mu} = (0.9)^{\mu}\phi^{\mu} \tag{6.32}$$

Equation (6.32) is in the form of Archie's law, and the result implies that the observed power μ of the porosity should be 1.3 in 2D systems, and 2.0 in 3D. Berkowitz and Balberg [5] suggested that validity of Archie's law might result from a critical moisture content that is zero, but did not mention the possibility that it could also arise as a consequence of a proportionality of θ_t to ϕ. In fact we find experimental evidence for both cases.

Although we do not expect that non-universal scaling will commonly apply to the saturation dependence of conduction properties, there is nevertheless a possible relevance of non-universal scaling to the *porosity*-dependence of the conductivity (hydraulic or electrical) of saturated media. Such a topic relates to a wider range of models of porous media than those we have concentrated on so far, including diagenesis. Non-universal exponents can, however, also result from pore-size distribution effects, and may also implied by inappropriate analysis of experimental data.

Diagenesis is a physico-chemical process by which rock is altered at the grain scale. For example, after burial, sediments may be exposed to thermal, chemical, and pressure gradients that drive dissolution and precipitation of minerals. One can envision a precipitation process by which sand grains grow concentrically, except where they are already in contact with other grains. Such simplified models of diagenesis are discussed by Sahimi [63], and bear some resemblance to the Swiss cheese and cannonball rock models for generation of non-universal exponents of conduction. Certainly the progression to systems with smaller porosity is geometrically distinct from e.g. drying of a fractal medium. In the former case, pore shapes change continuously as the particles dilate, but in the latter, pore shapes must be independent of pore size; thus in the latter case both the largest water-filled pore and the critical pore radius have shapes independent of moisture content, and both the connectivity of the water-filled medium and the sizes of the water-filled pores (but not the porosity) change with saturation. In diagenesis, however, as the pore sizes are reduced, the connectivity of the medium remains constant (at early stages), but the porosity and geometry change.

An important aspect of models that account for diagenesis is that they allow different dependencies of the electrical conductivity on saturation and on porosity. Because the pore necks may diminish rapidly with diminishing porosity, it becomes possible to develop a non-universal dependence of the conductivity on porosity. This allows a more general phenomenological representation of Archie's law:

$$\sigma = \sigma_0 (S - S_c)^{\mu} \phi^{n} \tag{6.33}$$

with μ and n being different powers. We still expect μ to be 1.3 in 2D and 2.0 in 3D. However, n could respond to different influences, and variation in values of n could have different interpretations. What many models of diagenesis have in common (and also with the models of Feng et al. [20]) are (1) reliance on a

Table 6.2 Archie's law porosity exponents from 2D simulations [42]

System	m
Random	1.22
Random	1.21
Triangle grains	1.26
Triangle pores	1.35
Diamond grains	1.24
Diamond pores	1.38

specific pore geometry, and (2) dependence of the relevant pore radii on porosity. While this research direction is not incompatible with percolation theory (indeed, many of its papers have been developed within the framework of percolation theory and examination of non-universal exponents), it is not a necessary development of percolation theory. An extensive literature exists on this subject, but because we have often found that more mundane explanations exist for results that at first glance might appear to imply non-universal exponents, we will not explore the literature on diagenesis. For a good early review on diagenesis, the reader is referred to Sahimi [63]. But we will continue using μ for both powers (and μ^* for, e.g., pore-size induced deviations from 2) as well as the logical development of this subsection.

6.2.7 Universal Exponents Masquerading as Non-universal

Regarding the porosity dependence of electrical conductivity, we find a great deal of evidence to support the relevance of universal exponents of percolation theory. For simulations of 2D conduction, Kuentz [42] effectively found $\mu = 1.28 \pm 0.07$ (Table 6.2), while experiments on 3D systems compiled by Krohn and Thompson (1986) yield $\mu = 1.86 \pm 0.19$. Thompson et al. [67] give more than 40 values (Table 6.3), also with μ around 1.8. Balberg [3] and Krohn and Thompson [41] have two different perspectives on the wider range of μ values reported in the literature at that time; by constraining their results to systems that were consistent with each other, Krohn and Thompson [41] produced a much smaller variation in μ values. Nevertheless, the measured porosity exponent in Archie's law need not be precisely 2.0. We have already mentioned the potential relevance of diagenesis to series of related rocks with decreasing porosity. There exist also possible influences of pore-size variability. Analysis may be confounded by incorrect estimations of a relevant critical volume fraction, in the case that θ_t is not zero. We will later see that such effects can be detected already in the saturation dependence of σ.

While the effects of connectivity and tortuosity (represented by percolation scaling) appear to have the dominant effect on μ for electrical conductivity, the pore size distribution may introduce some variability. In particular, if $\theta_{x\sigma} < \phi$ (the cross-over for the electrical conductivity is less than the porosity), then the pore size distribution will modify somewhat the value of μ expected from experiment. In such a

Table 6.3 Archie's law porosity exponents from 3D rocks (mainly sandstones, from [67]). The minimum l value was a theoretical estimation of Thompson et al. [67], who determined the maximum l from mercury porosimetry. The D_p value calculated for the pore space is from Eq. (2.16)

Price river (depth)	D calculated	Porosity	Min l	Max l	m
67.5	2.975881	0.0828	0.02	0.72	1.78
93.8	2.975627	0.1265	0.02	5.14	1.81
93.2	2.975393	0.116	0.02	3	1.77
111.3	2.977919	0.1165	0.02	5.46	1.84
115	2.97452	0.1485	0.02	10.99	1.83
117	2.972552	0.1586	0.02	10.8	1.94
122.6		0.1282	0.02		1.84
125.4	2.976145	0.1192	0.02	4.09	1.87
128.1	2.977859	0.1275	0.02	9.47	1.88
130.3	2.974817	0.1095	0.02	2	1.85
132	2.974178	0.1242	0.02	3.4	1.9
137.3	2.974131	0.12	0.02	2.8	1.89
139.9	2.976272	0.1196	0.02	4.29	1.88
148.4	2.973592	0.1247	0.02	3.1	1.89
160.2	2.979283	0.1071	0.02	4.74	1.85
161.7	2.974569	0.1517	0.02	12.9	1.66
164.3	2.973942	0.1508	0.02	10.6	1.49
169.3	2.975546	0.1427	0.02	10.85	1.84
178.4	2.97544	0.1287	0.02	5.46	1.81
178.2	2.978037	0.1056	0.02	3.22	1.79
178.1	2.978725	0.0991	0.02	2.7	1.74
183.4	2.972752	0.1223	0.02	2.4	1.92
181.8	2.964996	0.123	0.02	0.85	1.88
189.1	2.974282	0.0922	0.02	0.86	1.77
197.1	2.971668	0.1044	0.02	0.98	1.77
199.7	2.979947	0.0848	0.02	1.66	1.78
203.8	2.977885	0.0656	0.02	0.43	1.69
210	2.981212	0.0359	0.02	0.14	1.57
224.8	2.971516	0.0751	0.02	0.31	1.78
233.1	2.972501	0.0726	0.02	0.31	1.79
265.8	2.978607	0.0526	0.02	0.25	1.77
607.3	2.97957	0.0943	0.02	2.55	1.81
626.2	2.984087	0.0691	0.02	1.8	1.72
637.8	2.984759	0.0658	0.02	1.74	2.24
652.9	2.981554	0.068	0.02	0.91	1.81
652.9	2.986981	0.042	0.02	0.54	1.66

Table 6.3 (Continued)

Price river (depth)	D calculated	Porosity	Min l	Max l	m
Boise Table 1	2.948788	0.35	0.02	90	2.12
Boise Marsing 1	2.961246	0.239	0.02	23	2.1
Boise Silver 1	2.98126	0.097	0.02	4.63	2.37
Berea	2.96568	0.205	0.02	16	1.76
Navajo	2.973338	0.178	0.02	31.18	1.71
Coconino	2.975293	0.099	0.02	1.36	1.86
Nugget	2.981648	0.109	0.02	10.77	1.87
St Peters	2.983855	0.093	0.02	8.45	1.73
Tennessee	2.978262	0.062	0.02	0.38	1.67
Red Navajo	2.963027	0.23	0.02	23.5	1.8
Layered Navajo	2.964098	0.2295	0.02	28.5	1.76
White Navajo	2.96259	0.2676	0.02	82.5	1.5
Carmel	2.969541	0.1161	0.02	1.15	1.66
Austin Chalk	2.934058	0.2881	0.02	3.46	2.22

case, the electrical conductivity at saturation should be larger than the value predicted from Eq. (6.20) by a factor F:

$$F = \left[1 - \left(\frac{\phi - \theta_{x\sigma}}{\phi - \theta_t}\right)\right]^{\mu} \left[\frac{1}{1 - (\frac{\phi - \theta_{x\sigma}}{1 - \theta_t})}\right]^{\frac{D_p - 2}{3 - D_p}} \tag{6.34}$$

Because $F \geq 1$, the saturation exponent can only increase. One might think that representing the electrical conductivity as a power of the porosity would thus also always yield a power $\mu^* \geq 2$ in a fully 3D medium. Accordingly, one might then also assume that since the exponent $(D_p - 2)/(3 - D_p)$ for the electrical conductivity would be replaced by $D_p/(3 - D_p)$ for the hydraulic conductivity, approximate powers for K should tend to be larger than for the electrical conductivity. These conclusions cannot be generally confirmed, however, since the actual result for the power of the porosity depends on the precise sequence of media considered. The value of a particular model is that one can directly analyze different sequences of media.

Consider: If one holds the ratio r_m/r_0 constant while changing the porosity, then D_p is a *diminishing* function of the porosity, making high-porosity media more nearly commensurate with universal scaling than lower-porosity media, and thus tending to produce a porosity exponent less than 2, not greater. If, on the other hand, one holds D_p constant (forcing an increase in r_m/r_0 with increasing ϕ), then there is a tendency for an effective μ^* to exceed 2 and to be larger for larger values of D_p. These tendencies can be shown graphically as well (similarly to Fig. 6.11). In this case larger values of D_p correspond to larger disorder (larger ratio r_m/r_0). For example, for $\phi = 0.4$, the effective (and approximate) μ^* rises rapidly from 2.3 to 8.3 as D_p increases from 2.9 to 2.97.

It would be useful to make a comparison with experimental data to make further tests of the present concepts. Because of the tendency for the exponents to be clustered near $\mu = 2$, the best published data set for such comparison might appear to be that of Thompson et al. [67]. But in order to make a comparison with the data compiled by Thompson et al. [67], it would be necessary to use values for D_p calculated from Eq. (4.19), in contradiction to the result used by Thompson et al. [67]: Eq. (4.20). Such a calculation is rendered unreliable since Thompson et al. [67] did not actually measure r_0; rather they assumed that r_0 was the same for all of their media. Because the comparison (presented in the first edition of this book) was more suggestive than conclusive, and because in the meantime we have obtained many additional data sets, we omit from the present edition the investigation of such variability of μ^* as may result from pore size distributions, noting only that the typically observed discrepancies of 10–15 % would not be unusual.

We now pose the question: which porous media have the appropriate structure to make a simple scaling result like Eq. (6.22) a valid predictor of the hydraulic or electrical conductivity under conditions of full saturation? Models for the hydraulic conductivity along these lines are known as Kozeny-Carman, just as they are known as Archie's law for the electrical conductivity. The analysis will be appropriate for porous media which are well described by fractal models, but it may be approximately valid for other media to the extent that they can be approximated by the fractal model. Also it is assumed that the conduction in these systems is 3D; a simple alteration extends the derivation to 2D.

6.2.8 Regions of Applicability

Of the three parameters (r_m/r_0, D_p, and ϕ) which describe a fractal pore-space in the RS model, only two are independent, so we represent the entire range of accessible parameters in a 2D parameter space of porosity and fractal dimensionality. If Eq. (6.21) and Eq. (6.22) are solved for $\theta_x = \phi\ (1 - 0.1)$, each solution represents a distinct curve in this space (we used 0.1 mainly because field soils rarely saturate above 90 %. Two sets of curves (Fig. 6.3) divide the parameter space into three regions. For the leftmost region both the hydraulic and electrical conductivity can be represented as proportional to ϕ^2, and they are thus proportional to each other. While this region is large, it represents relatively ordered media, and few natural media are found there (though many artificial media are because of their near uniformity). *This represents a crucial difference between natural and artificial media, and means that conclusions reached by studying artificial media will typically be unsuitable for natural media*. In the middle region it is still reasonable to represent the electrical conductivity in the simple scaling form, but the hydraulic conductivity develops a more complicated dependence on ϕ, so there is no simple relationship between the two. In the rightmost region, neither property is a simple power of ϕ and $K \propto \sigma r_c^2$, just as in Friedman and Seaton [22] (the reader should check that this conclusion is independent of the assumption of self-similarity). Of course, if

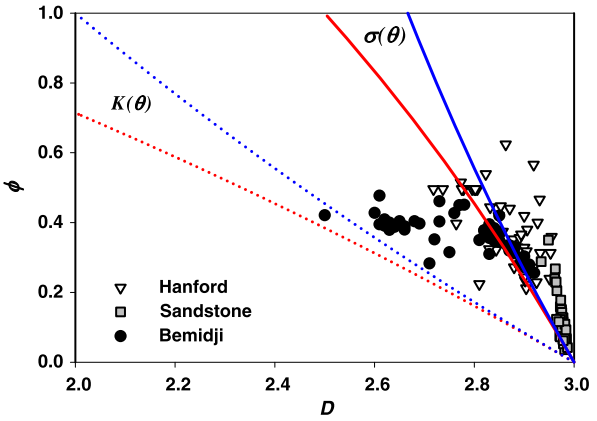

Fig. 6.8 Plot of the ϕ–D_p (porosity–fractal dimension) plane showing regions of validity for percolation scaling. Below the electrical conductivity lines, scaling is valid for electrical conductivity; below the hydraulic conductivity lines, scaling is valid for the hydraulic conductivity. The *upper lines* represent solutions of Eqs. (6.23) and (6.27) under the conditions that θ_{xK} and $\theta_{x\sigma}$, respectively, are equal to 0.9ϕ. The *lower lines* represent the solutions of the equivalent equations generated by the Balberg [3] theoretical framework. Bemidji refers to unpublished data provided by William Herkelrath, which are found mostly in the range where the saturated hydraulic conductivity follows an approximate power of the porosity with exponent larger than 2 and the electrical conductivity would be consistent with a power 2

the fundamental parameters of a porous medium are not known, one cannot predict which of the three regions a system will be found in, nor would it be possible to determine r_c^2, even if it could be guessed that the rightmost region were appropriate.

For porosities just above the relevant cross-over, each conductivity may be approximated as a non-universal power of ϕ, with $\mu^* > 2$ for the case that D_p is held constant. An equivalent result is obtained by holding the porosity constant and increasing D_p past its cross-over. So crossing the parameter space from bottom to top (or equivalently, from left to right), each conductivity solution moves from the universal scaling region, through a region in which the conductivity can be approximated by a non-universal scaling power, before entering a region where it is clearly inappropriate to use simple scaling results. This process sets on at smaller values of D_p in the hydraulic conductivity than in the electrical conductivity. Note also that smaller values of D_p for a given ϕ are associated with narrower pore-size distributions, supporting (and allowing testing of) the common perception that larger exponents for the saturation dependence of the electrical conductivity arise from wider distributions.

In Fig. 6.8, the Hanford Site soils (Table 6.4) are well out of the regime of validity of Eq. (6.22) for K, but tend to cluster about the boundary for the validity of Eq. (6.22) for σ. For small porosities, such as in rock, the region of validity of Eq. (6.22) for K may approach actual conditions. Thus there appears to be a greater justification for representing K as a power of ϕ in rocks than in soils, though for K the power is likely to be larger than 2, in contrast to the result for σ. This is

Table 6.4 (From [33]). Physical characteristics of Hanford site soils. Except for the soil texture and K_S (from [38]), all the primary data came from [21]

Soil	D_p	D_s	ϕ	θ_d	Texture	K_S	h_A
VOC 3-0647	2.773	2.8	0.515	0.134	loamy sand	0.0002	85
VOC 3-0649	2.823	2.898	0.539	<0.12	loam	ng	530
VOC 3-0650	2.863	2.917	0.624	0.37§	sandy loam	2.6E-07	51.5
VOC 3-0651	2.857?	2.87	0.374	0.126	loamy sand	0.0094	25
VOC 3-0652	2.878	2.56	0.352	0.11	sand	0.00037	58
VOC 3-0653	2.9?	2.874	0.419	0.12	sandy loam	5.8E-06	55
VOC 3-0654	2.931	2.916	0.466	<0.18	sandy gravel	0.00027	40
VOC 3-0654-2	2.849		0.419	0.11	sandy gravel	0.0136	3
VOC 3-0655	2.927		0.4	<0.15	silty,sandy gravel	0.000158	13
VOC 3-0657	2.955		0.359	<0.1	gravelly sand	0.0136	30
ERDF 4-1011	2.871	2.816	0.44	0.125	loamy sand	0.00001	56
ERDF 4-0644	2.906	2.81	0.38	0.115	loamy sand	5.7E-06	100.5
B8814-135	2.891	2.727	0.356	0.14	silty sand	1.36E-06	135
B8814-130B	2.886	2.682	0.329	0.11	loamy sand	4.1E-07	46
FLTF D02-10	2.778	2.776	0.496	0.2	silt loam	0.00012	100
FLTF D02-16	2.718	2.71	0.496	0.18	silt loam	0.00012	150
FLTF D04-04	2.806	2.804	0.496	0.2	silt loam	0.00012	100
FLTF D04-10	2.778	2.773	0.496	0.19	loam	0.00024	100
FLTF D05-03	2.737	2.735	0.496	0.205	loam	0.00029	130
FLTF D07-04	2.796	2.791	0.496	0.198	silt loam	0.00012	98
FLTF D09-05	2.8	2.83	0.496	0.19	loam	0.00029	72
FLTF D10-04	2.775	2.769	0.496	0.21	silt loam	0.00012	90
FLTF D11-06	2.803	2.798	0.496	0.2	silt loam	0.00012	76
FLTF D11-08	2.802	2.797	0.496	0.22	silt loam	0.00012	80
Inj. Test Site 1-1417	2.919	2.876	0.566	0.088	sand	0.00014	35
Inj. Test Site 1-1418	2.953	2.762	0.313	0.08	gravelly sand	0.00014	2
Inj. Test Site 2-1417	2.9	2.719	0.328	0.033	sand	0.00014	20
Inj. Test Site 2-1637	2.932	2.708	0.313	0.07	sand	0.0042	11
Inj. Test Site 2-1639	2.951	2.654	0.239	0.06	sand	0.0012	5
Inj. Test Site 2-2225	2.844	2.548	0.322	0.06	sand	0.0055	15
Inj. Test Site 2-2226	2.925	2.573	0.229	0.06	sand	0.015	7
Inj. Test Site 2-2227	2.919	2.666	0.271	0.056	sand	0.0087	5.4
Inj. Test Site 2-2228	2.904	2.376	0.212	0.047	sand	0.021	10
Inj. Test Site 2-2229	2.902	2.465	0.234	0.069	sand	0.0064	11
Inj. Test Site 2-2230	2.853	2.8	0.447	0.11	sand	0.00023	40
Inj. Test Site 2-2231	2.905	2.716	0.318	0.13	gravelly sand	0.0075	70
Inj. Test Site 2-2232	2.88	2.508	0.272	0.08	sand	0.041	14

Table 6.4 (Continued)

Soil	D_p	D_s	ϕ	θ_d	Texture	K_S	h_A
Inj. Test Site 2-2233	2.9	2.492	0.243	0.075	sand	0.017	11
Inj. Test Site 2-2234	2.81	<2	0.224	0.025	sand	0.021	80
US Ecology MW10-45	2.859	2.634	0.34	0.066	sand	0.00531	15.2
US Ecology MW10-86	2.764	2.569	0.397	0.069	sand	0.0197	20
US Ecology MW10-165	2.8299	2.511	0.324	0.058	sand	0.00663	22
218 W-5-0005	2.894	2.765	0.366	0.12	sandy loam	0.000067	35
North Caisson	2.806			0.08	sand	0.02	5
McGee Ranch	2.832			0.107	silt loam	0.001	45

why we plot the sandstone data from Thompson et al. [67] on the same figure. Interestingly, if the correct expression relating porosity and the fractal dimensionality (Eq. (4.19)) is used, the data compiled by Thompson et al. [67] follow the same trend as the Hanford Site soils, near the margin of the validity of Archie's law for the electrical conductivity, meaning that their exponents might well differ slightly from 2 (as they indeed do). But if the Thompson et al. [67] result for D_p is used, the rock samples fall along a curve connecting the origin to the lowest porosity value of the Hanford site soils, clearly a quite different tendency. This supports our contention that the Thompson et al. [67] calculation of D_p is incorrect. It also suggests an intriguing possible connection between transport and structure: some aspect of transport during depositional processes may prevent too large a value of the fractal dimensionality, i.e., too great a disorder.

We note in conclusion some potentially relevant work based on the Effective-Medium Approximation and a related paper using percolation theory. Sahimi [63] gave a derivation of the Effective-Medium Approximation (EMA) to produce Archie's law. The exponent he used, $\mu^* = z/(z-2)$, is appropriate for spherical particles but should be larger for flatter particles, such as clay grains [48]. Bussian [13] generalized the self-similar EMA to include finite rock conductivity. He found $\mu^* > 3/2$ in almost all cases, arguing that it was due to the finite rock conductivity resulting from clay particles. Hilfer [24] also used percolation theory to find $\mu^* \geq \mu$. Sahimi [63] criticized this result on the basis of its quasi-universality (and his understanding of the larger variability of μ^*). Clearly there is some variability in the exponent, but not a great deal, and it appears that Hilfer's result is more general and more relevant than Sahimi indicated. In any case, Hilfer's work is related to the present treatment.

6.3 Electrical Conductivity as a Function of Saturation: Trends and Potential Complications in Experimental Data

If the percolation interpretation of Archie's law is correct at full saturation, then the electrical conductivity must follow Eq. (6.22) as a function of saturation. In the

next section, we examine data relating to electrical conductivity as a function of saturation.

Electrical conductivity is frequently analyzed in terms of a "formation factor." We avoid this analysis because it is rooted in assumptions (which we have shown to be unjustified) regarding a universal relationship between the electrical and hydraulic conductivity. We will continue use of the concept of tortuosity, despite some uncertainty in its definition far from the percolation threshold, and despite possible confounding influence of other factors, such as a non-zero critical volume fraction for percolation.

We performed extensive analysis of eleven data sets for the electrical conductivity as a function of saturation, $\sigma(\theta)$ [19]. This analysis (1) showed that the typical formula used in the soil physics community for the saturation dependence of the electrical conductivity is inferior in description of the data to percolation scaling, even for the data set it was originally developed for (and has a less satisfying physical basis), (2) identified several errors in analysis which could lead to a false estimate for the actual experimental power on $\sigma(\theta)$, and (3) identified several physical complications which can make experimental data appear to have a lower degree of universality than implied by percolation scaling. One such complication involves overlooking effects of contact resistance, which can prevent the data from obeying a power law even though the data approach the appropriate power law asymptotically in the large resistance (low moisture content) limit. Another complication is overlooking effects of "residual" salinity, i.e., cases where the salinity of the injected fluid is less than the salinity *in situ*. This can arise from dissolution of ions in the solid medium, and is most important in the case where the injected fluid has low conductivity. Such an influence introduces an additional saturation dependence, though it is easily modeled.

In both petroleum engineering and soil science, it is frequently assumed that the electrical conductivity has contributions from both the solid and liquid phases [16, 54, 58]. A widely used relationship in soil science is

$$\sigma(\theta) = \sigma_s + \sigma_b \theta (a\theta + b) \tag{6.35}$$

where the σ_s term denotes a "surface" or "solid" term [16, 58]. Interpreted as the contribution of hydrated clay minerals, this term is considered independent of moisture content except under extremely dry conditions (discussed in Sect. 7.4). The second term, attributed to conducting fluid in the pore space, is the product of the conductivity of the liquid phase, the water content, and a "transmission coefficient" (a fudge factor) which is itself a linear function of the water content [58]. Over a limited range of moisture values, $\theta(a\theta + b)$ can present as $(\theta - \theta_c)^\mu$ for $\mu = 2.0$ (as can be seen in Fig. 6.9), so this traditional phenomenology may mask a universal dependence compatible with Archie's law.

Because the solid phase is always well above the percolation threshold, a "surface" or "solid" conductivity term might be taken to be independent of saturation. In Sect. 7.4 we discuss data that show a pronounced dependence of the clay conductivity on water contents: at sufficiently low water contents it may be necessary to expand the analysis, depending on the mineralogy of the medium. The solid phase

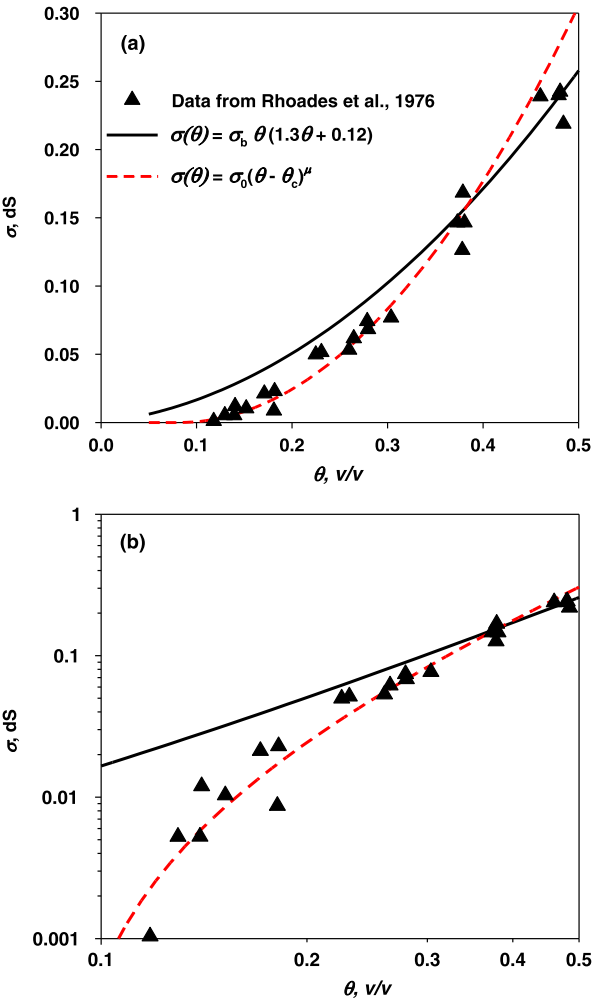

Fig. 6.9 Analysis of data by Rhoades et al. [58], data for the saturation dependence of the electrical conductivity. The percolation scaling result (Eq. (6.28)) is compared with the phenomenology (Eq. (6.35)) of Rhoades et al. [58]. (**a**) Linear plot, (**b**) logarithmic representation. Note that (**b**) clearly shows the superiority of Eq. (6.28)

conductivity becomes more important as the water content is reduced [17, 45], approaching the (water) percolation threshold from above. So while surface conductivity is typically neglected, it may dominate the system conductivity if the solution electrical conductivity is low, the medium has low porosity or a low degree of saturation, and/or the medium has a high specific surface area [39].

Universal formulations of the electrical conductivity were derived for a conductivity ratio σ_b/σ_s that is very large or infinite. Complications arise if this ratio is small. In a number of the media we analyzed, there is evidence of a significant contribution of the solid medium to the electrical conductivity, implying that the conductivity ratio is not particularly large. In such cases, individual conducting pathways will tend to include both phases. We see therefore three approximations in order of increasing complexity:

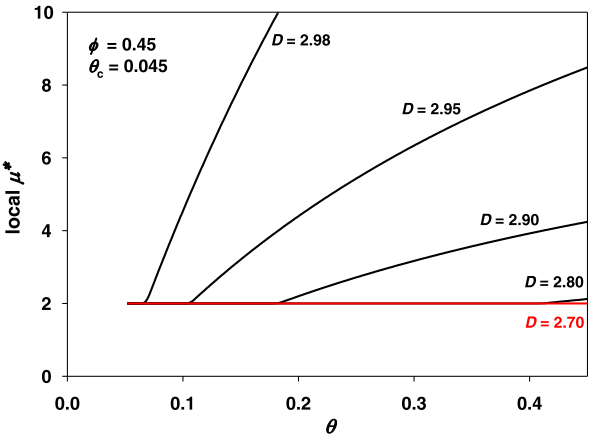

Fig. 6.10 Values of the apparent conductivity exponent (logarithmic derivative) μ^* calculated across a moving range of water contents $\Delta\theta = 0.01$ for the given porosity and several values of D_p. Data following some of these curves could be interpreted as having a non-universal value of the conductivity exponent

1. The solid phase is assumed to have zero conductivity, so current flows only through the liquid phase (Eq. (6.22)).
2. The solid and liquid phases are assumed to conduct strictly in parallel, and so a constant solid phase conductivity σ_s is added to Eq. (6.22):

$$\sigma(\theta) = \sigma_s + a\sigma_b(\theta - \theta_t)^{\mu} \tag{6.36}$$

   This parallel approach is quite common, and yet it is most appropriate for $\sigma_s \ll \sigma_b$ in which only a negligible quantity of current flows from one phase to another.
3. If the solid and fluid conductivities do not have a large contrast, then an optimized path of conduction will sometimes go through the solid phase in order to bypass a more tortuous path through the liquid, and sometimes through liquid to bypass a higher resistance solid path. In other words, the two phases will not conduct strictly in parallel; in fact, the degree of interaction in the conducting pathways will vary with the relative conductivities of the two phases, as well as with the liquid content. There is no universally agreed-upon mathematical formulation for this interaction, which has been an active area of research for decades. We conjecture that such a phenomenon would reduce the value of μ by the tortuosity contribution to the conductivity exponent [65]. This could reduce the exponent on χ to $2\nu = 1.76$ when there is little contrast between solid and liquid conductivities.

When D_p increases slightly past the limit of validity of Eq. (4.20), electrical conductivity is under-predicted by percolation scaling [28]; with further increases in D_p, percolation scaling is no longer a useful framework for analysis. For some combinations of ϕ and D_p the difference is subtle (Fig. 6.10), and data may indicate percolation scaling (Eq. (6.20)) with an exponent $\mu^* > \mu$. We have done no analysis to test this suggestion.

When data are within the range of validity of percolation scaling, and yet indicate a non-universal value μ^*, caution is still advisable. For example, incorrect estimates

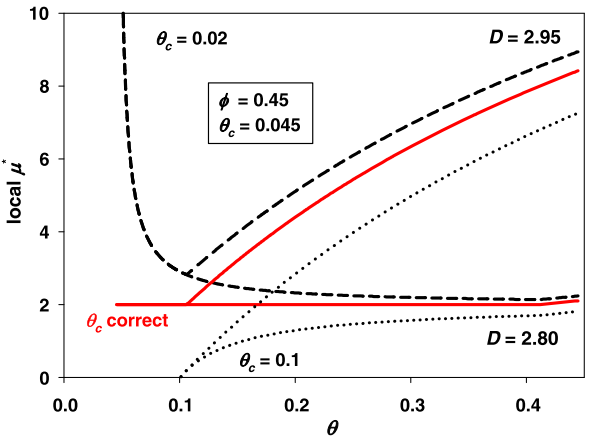

Fig. 6.11 Values of the apparent conductivity exponent (logarithmic derivative) μ^* calculated across a moving range of water contents $\Delta\theta = 0.01$ for the given porosity and two values of D_p for cases where the critical water content is underestimated, correct, and overestimated

of θ_t can produce apparently non-universal values for μ^*. Hence simultaneous fitting for both θ_t and μ has built-in pitfalls: under-estimation of θ_t can result in apparent values of $\mu^* > \mu$, while over-estimation of θ_t can produce values of $\mu^* < \mu$ (Fig. 6.11). As a practical matter, it is best to start with the assumption that universality is observed, and only resort to non-universal exponents when other, more mundane explanations have been exhausted. We try to minimize effects of incorrect estimations of θ_t, including exclusion of the possibility of its existence, probably contributing to our tendency to generate universal scaling where others do not.

6.3.1 Comparison with Experiment

Here we apply the percolation scaling framework to analysis of experimental data. To the best of our knowledge, all of these data are from water-wet media, and hysteresis (if present) is ignored. The datasets examined (Table 6.5) represent both coarse and fine soils, and both igneous and clastic sedimentary rock. We discuss some of these datasets, with the presentation proceeding from simpler to more complex cases. The complex cases illustrate how a sound theoretical footing can help handle potentially confounding issues.

The data of Rhoades et al. [58] (Fig. 6.9a) were originally plotted in a form that subtracted out any surface or solid conductivity σ_s, so our analysis simply involved fitting values for a and θ_t. Our Eq. (6.31) yields the same R^2 as Rhoades et al.'s Eq. (6), but where their a and b are meaningless fitting parameters, our parameters a and θ_t have physical significance: a gives the medium's tortuosity at saturation, while θ_t is the critical volume for percolation. For the Indio soil represented here, we have a tortuosity at saturation of 1.23, and a critical volume fraction $\theta_t = 0.073$. Plotting the same data in logarithmic coordinates (Fig. 6.9b) highlights the percolation scaling formulation's superiority at low water contents.

Table 6.5 Sources of electrical conductivity data examined. All data except Ren's [57] were obtained by digitizing published figures

Source	Medium	Parameters fit[a]	Slope	Intercept	R^2	Comments
Archie [2]	Gulf coast sandstones	$\phi_c = 0.020$, $a = 1.591$	1.000	0.0023	0.746	No units given in figure
	Nacatoch sand	$\phi_c = 0.010$, $a = 1.067$	1.000	0.0019	0.852	
Rhoades et al. [58]	Indio vfsl	$\theta_c = 0.073$, $a = 1.232$	1.000	−0.0053	0.982	Surface contribution (if any) removed in figure
Abu-Hassanein et al. [1]	soil A: 7 % S, 40 % c	$\theta_c = 0.011$, $\sigma_r = 0.725$	0.991	0.0011	0.973	Each soil tested at 3 bulk densities; all densities lumped together in our analysis
	soil B: 7 % S, 53 % c	$\theta_c = 0.064$, $\sigma_r = 0.787$	0.843	0.0210	0.823	
	soil C: 38 % S, 40 % c	$\theta_c = 0.020$, $\sigma_r = 0.112$	0.919	0.0023	0.880	
	soil D: 35 % S, 20 % c	$\theta_c = 0.000$, $\sigma_r = 0.239$	0.900	0.0038	0.865	
Roberts and Lin [61]	Tuff: Distilled water	$\theta_c = 0.0024$, $\sigma_r = 0.0039$ (both)	0.715	0.0000	0.962	$\sigma_b = 0.0$ (DW),
	J-13 water		1.215	−0.0000	0.916	$\sigma_b = 0.0256$ (J-13)[b]
Ren [57]	Silica sand	$\theta_c = 0.066$, $a = 2.703$ ($\sigma_s = 0.396$)	0.972	0.0143	0.948	Conductive solid phase, 6 solution concentrations[b]
Binley et al. [7, 8]	Sandstone	($\theta_c = 0.000$) $a\sigma_b = 0.1466$, $\sigma_s = 0.0020$	1.000	−0.0004	0.965	Cassiani et al. [15] give $a\sigma_b = 0.143$, $\sigma_s = 0.0156$
Rinaldi and Cuestas [60]	Loess, 16 % clay	$\theta_c = 0.040$, $a = 2.132$, $\sigma_r = 0.085$	1.028	−0.0032	0.980	4 solution concentrations

Archie's [2] seminal paper presented electrical resistivity data for a number of saturated consolidated Gulf Coast sandstones, and for samples of saturated unconsolidated Nacatoch sand. Fitting Eq. (6.23) to his sandstone and sand data, we obtain correlation slopes of almost precisely one and intercepts near zero, in contrast to his slopes of 0.66 (sandstone) and 1.55 (sand) (Table 6.5). As expected, tortuosity is

Table 6.5 (Continued)

Source	Medium	Parameters fit[a]	Slope	Intercept	R^2	Comments
Kechavarzi and Soga [37]	Clean sand	$\theta_c = 0.000$, $a\sigma_b = 20.67$, and $c\rho_c = 0.792$ (Test 1), 0.705 (Test 2), and 0.702 (Test 3)	0.980	0.0114	0.980	3 replications.[c] Miniature resistivity probe appears to have contact resistance
Mori et al. [50]	Tottori dune sand	$\theta_c = 0.000$, $a = 1.417$	1.060	−0.0739	0.982	3 solution concentrations
Tuli and Hopmans [69]	Oso flaco fine sand	$\theta_c = 0.065$, $a = 1.637$, $\sigma_r = 0.384$ ($\sigma_s = 0.0725$)	1.002	−0.0011	0.984	σ_s value given. 4 solution concentrations

[a]Values in parentheses were given rather than fit. Units omitted from table for simplicity; see corresponding figures for actual units

[b]Where different solution concentrations were used, only σ_b varied: other parameters were held constant across all concentrations

[c]Fitting allowed a different value of ρ_c for each replication, but kept other parameters constant across all replications

lower in sand than in sandstone. The critical volume for percolation in the sand is just 1 % of porosity; that in the sandstone (2 % of porosity) would presumably be higher if the sandstones were strongly cemented.

Binley et al. [7] use their data to make inferences regarding moisture content and are content with a simple calibration to Archie's law. A second set of data from the same sandstone ($\phi = 9.3$ %) was published in 2002. Cassiani et al. [15] tested their own model using the data from Binley et al. [7], and found a constant solid contribution to the electrical conductivity of $\sigma_s = 0.00143\ \mathrm{S\,m^{-1}}$ added to the $0.0156\ \mathrm{S\,m^{-1}}$ electrical conductivity of the fully saturated pore space. However, the Cassiani et al. [15] analysis implies a relatively weak θ-dependent contribution (Fig. 6.12). Using Cassiani et al.'s numerical values, and the common assumption that at typical experimental frequencies the solid and solution conductions operate in parallel, we have $\sigma(\theta) = 0.00143 + 0.0156(\theta - \theta_t)^{2.0}\ \mathrm{S\,m^{-1}}$ as a specific instance of Eq. (6.36). We have no independent basis upon which to choose a value of θ_t in these sandstones. We could assume $\theta_t = 0.1\phi$, but $\theta_t = 0$ is more likely in a medium with significant solid conductivity. As in the case of conducting spheres with pendular bridges (see Sect. 7.2), any water at all should increase conductivity. Using the numerical values from Cassiani et al. [15] and assuming $\theta_t = 0$ gives a no-parameter fit that is clearly superior to Cassiani et al.'s [15] fit (Fig. 6.12). Fitting gives values slightly different from Cassiani et al.'s [15], and yields a slope of 1.00 and an intercept of −0.0004 for regressing predicted against observed values. Notice that if the solid contribution (σ_s in Eq. (6.36)) had been underestimated, the prefactor $\sigma_b = 0.0156$

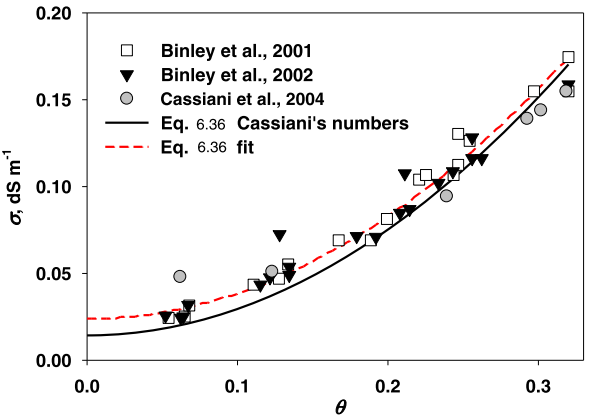

Fig. 6.12 Comparison of data for electrical conductivity, σ, as a function of water content, θ from Binley et al. [7, 8] with Eq. (6.28) and model results of Cassiani et al. [15]

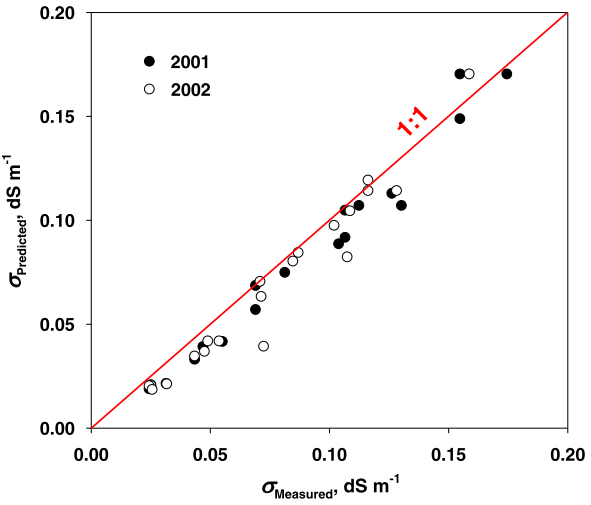

Fig. 6.13 Direct comparison of measured and predicted electrical conductivity values for the data of Fig. 6.12

would be overestimated. That is, if we had optimized for θ_t alone, our value would be dependent on the accuracy of the estimated σ_s.

Our predicted values compare well with Binley et al.'s [7, 8] observations (Figs. 6.12 and 6.13). For both datasets (2001 and 2002), individually as well as combined, Eq. (6.36) with $\theta_t = 0$ matches the data with slope near one, intercept near zero, and a high correlation coefficient (Table 6.5). In support of our conjecture about the exponent μ taking on smaller values for systems with conducting solids, we find $\mu^* = 1.88$ fits the data just as well as $\mu = 2.0$.

A greater solid phase conductivity is seen (Fig. 6.14) in silica sand data (personal communication; described in Ren et al. [57]). Here it is clear that the solid phase makes a constant contribution to the overall conductivity—again suggesting $\theta_t = 0$—with the remaining conductivity varying with the conductivity and volume fraction of the solution. When we subtract the solid contribution, estimated as the mean conductivity for the $\sigma_b = 0$ solution, the data fall on lines of $\mu = 2$ in logarith-

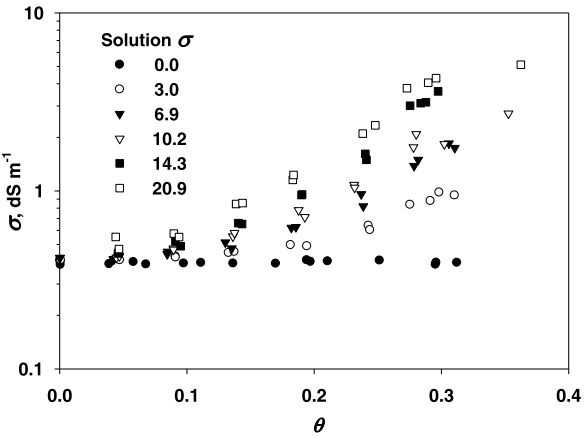

Fig. 6.14 Electrical conductivity of unsaturated silica sand at different solution contents and conductivities. Data from Ren et al. [57]

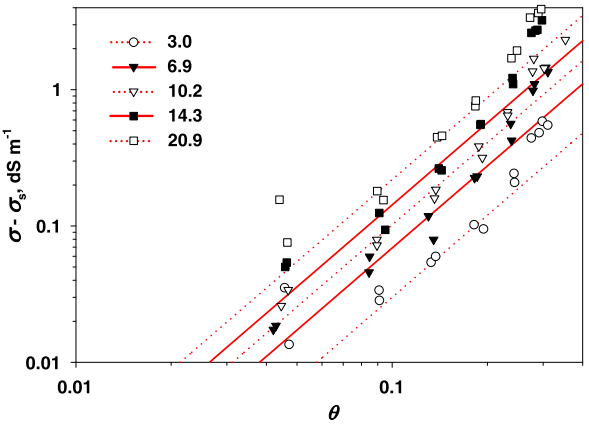

Fig. 6.15 Comparison of data with zero-parameter predictions of electrical conductivity of silica sand after subtracting the solid-phase electrical conductivity (Data from Fig. 6.14)

mic space (Fig. 6.15). Because each datum is from a separate packed core, the data as a whole are somewhat noisy, but the figure shows reasonable prediction of total conductivity from only the known values σ_b and θ, the assumed $\theta_t = 0$, and the estimated value of σ_s. A slight improvement is given by optimizing for a and θ_t. The lower slopes at low water contents, as suggested by the data, are consistent with our conjecture that a somewhat smaller value of μ may be more appropriate for media with similar solid and liquid phase conductivities. Thus, at low saturations, the current does not have to avoid the solid phase, and the topology of the current path is not coincident with the topology near the percolation threshold, so that the conductivity does not quite follow the percolation prediction.

Residual salt in soil, whether precipitated or in the form of exchangeable cations, may contribute a significant fraction of the liquid-phase conductivity. Making the assumption that any residual salinity dissolves completely at any non-zero water

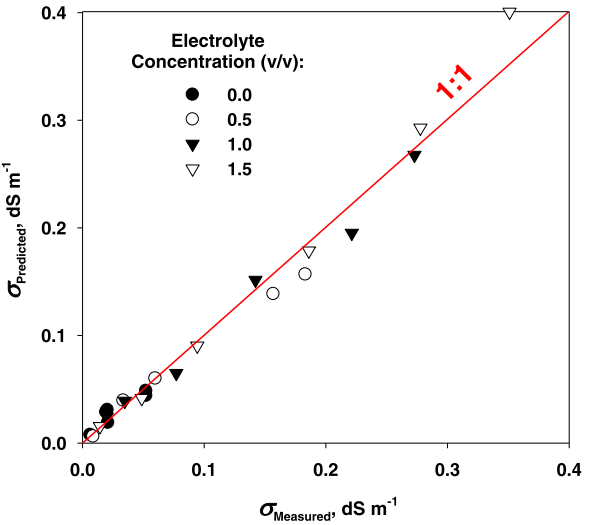

Fig. 6.16 Comparison of predicted (Eq. (6.28)) with measured electrical conductivity in loessial soils (data from Rinaldi and Cuestas [60])

content, we adapted Eq. (6.36) to account for residual salinity:

$$\sigma(\theta) = \frac{a(\sigma_b\theta + \sigma_r)}{\theta(1-\theta_t)^{\mu}}(\theta - \theta_t)^{\mu} \tag{6.37}$$

where σ_r is the residual salinity's contribution to electrical conductivity. The factor $(\sigma_b\theta + \sigma_r)/\theta$ therefore accounts for both solution and residual salinity contributions. Note that Eq. (6.37) is consistent with an apparent $\mu^* = \mu - \sigma_r(\theta - \theta_t)/[((\sigma_b\theta + \sigma_r)\theta)]$, and approaches μ if either $\theta \to \theta_t$ or $\sigma_r \to 0$. We apply the analysis of Eq. (6.37) to the data of Rinaldi and Cuestas (2002), who packed loess soils with known volume fractions of NaCl solution, and measured electrical conductivity at different water contents (their Fig. 12). In the zero-electrolyte treatment, the increase in electrical conductivity with water content can reasonably be attributed to residual salts in the soil. Fitting Eq. (6.32) to their data provides an excellent fit (Fig. 6.16), with $R^2 = 0.98$. The optimized value for the residual salt equivalent conductivity is 0.085 S m^{-1}. If the relative concentration of the various cations were known, their absolute concentrations could also be determined.

The data of Abu-Hassanein et al. [1] provide another example of the importance of accounting for residual salt. They present data on four soils differing in texture and clay mineralogy; each soil was also tested at three different degrees of compaction. Tap water ($\sigma_b = 9.5 \times 10^{-3}$ S m^{-1}) was used throughout. Because we didn't know *a priori* whether any given soil will have residual salt and/or solid phase conductivity, we added a solid phase conductivity to Eq. (6.37). As it turned out, the solid contribution was zero for all but soil *D*, which had a negligible value of $\sigma_s = 6.6 \times 10^{-5}$ S m^{-1}, so this was dropped from the analysis. Fitting each soil in turn, we obtain R^2 between 0.82 and 0.97 (Fig. 6.17). Residual salt accounts for 92–99 % of the saturated conductivity. Note that in Fig. 6.20, when all data sets for $\sigma(\theta)$ are plotted simultaneously, these data lie conspicuously above the universal line. Consistent with expectations, higher-clay soils had higher percentages of their

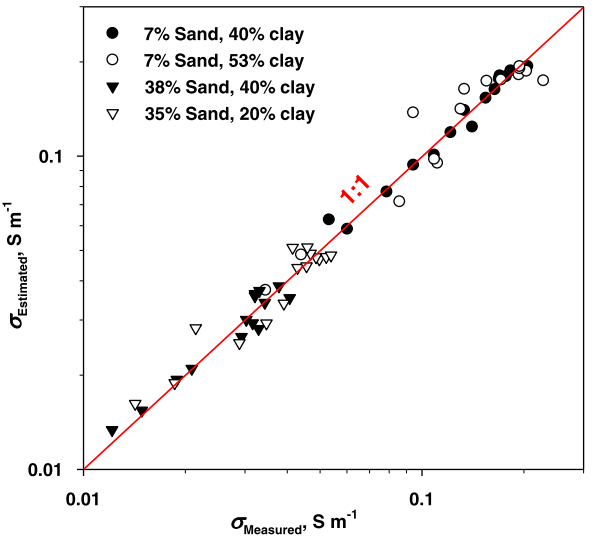

Fig. 6.17 Comparison of predicted (Eq. (6.37)) with measured electrical conductivity in four soils (data from Abu-Hassanein et al. [1])

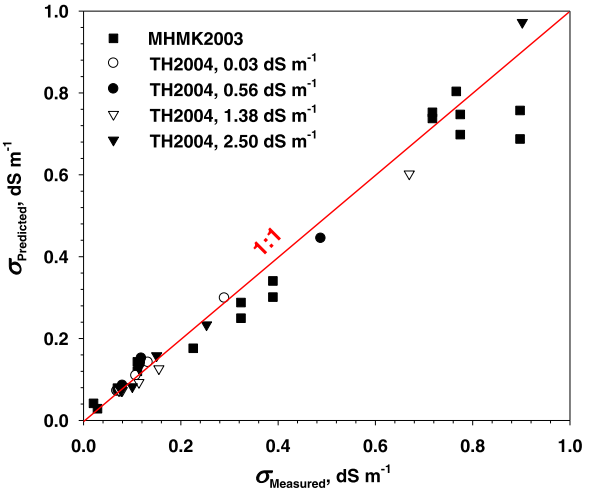

Fig. 6.18 Comparison of predicted and measured electrical conductivity in soils presented by Mori et al. [50] labeled as MHMK2003 and Tuli and Hopmans [69], labeled as TH2004

conductivity contributed by residual salinity, and also had higher critical volumes for percolation.

The datasets from Mori et al. [50] and Tuli and Hopmans [69] are somewhat similar, so we present them together (Fig. 6.18). We obtain $R^2 = 0.98$ fitting Eq. (6.36) to Mori et al.'s data, slightly lower than their 0.99 using the Rhoades equation (Eq. (6.35)), but we learn that $\theta_c = 0.0$ and $a = 1.417$. Tuli and Hopmans [69] give $\sigma_s = 0.0725\ \mathrm{dS\,m^{-1}}$ for Oso Flaco sand; this is the only medium we encountered that combined non-negligible solid conductivity with a non-zero critical volume for percolation. Our fit yields a mean absolute residual of only 0.02, compared with their value of 0.08.

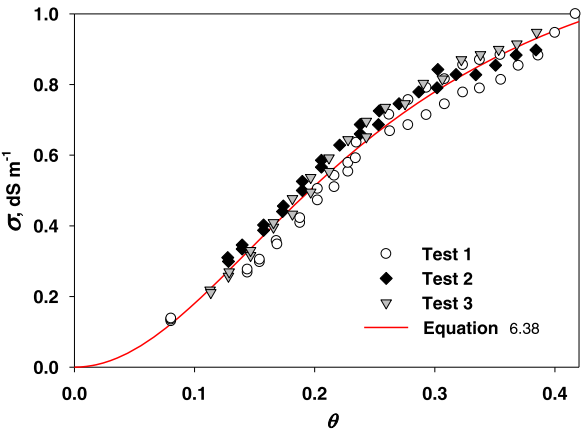

Fig. 6.19 Comparison of electrical conductivity as a function of water content with Eq. (6.38), including effects of a contact resistance that is independent of water content (Data from Kechavarzi and Soga [37])

Last, we examine an unexpected complication in the data published by Kechavarzi and Soga [37]. They present triplicate calibration curves for their miniature resistivity probes, and report that fitting Archie's law to the data gives $R^2 = 0.91$, a disappointing value for a calibration curve. A plot of the raw data (Fig. 6.19) shows a marked decrease in the slope of the $\sigma(\theta)$ curve; this, combined with the unknown characteristics of the miniature probe, raised the possibility that there was some contact resistance in their experimental setup. The washed sand was unlikely to have residual salinity, and solid conductivity would curve the slope up rather than down. We accordingly allowed for contact resistance ρ_c in the $\sigma(\theta)$ relationship through a modification of Eq. (6.36) (with zero solid conductivity), giving

$$\sigma(\theta) = \frac{1}{c\rho_c + \frac{1}{a\sigma_b(\theta-\theta_t)^\mu}} \tag{6.38}$$

where the constant c allows for unknown geometric factors specific to their experimental setup. Equation (6.38) yields $\mu^* = \mu/[1 + a\sigma_b c\rho_c(\theta - \theta_t)]$, which coincides with μ if any of the constants are 0 as well as in the limit $\theta \to \theta_t$. This new equation fits the data quite well (Fig. 6.19), with $R^2 = 0.97$.

The analyses of the saturation dependence of the electrical conductivity are summarized in Table 6.5. Our examination of the datasets discussed above found critical volume fractions for percolation ranging from 0.0 to 0.073, reasonably in line with Hunt's [29] observed range. Values of a, which we interpret as the electrical tortuosity at saturation, ranged from 1.07 to 2.73, a relatively small variation. These results are roughly compatible with reported literature values of $1/a$ in the range 0.56 to 0.8 (see Sect. 10.1), which would give a range of a values of 1.25 to 1.9 [4].

In two cases the brine conductivity σ_b was not given, forcing us to lump $a\sigma_b$ into a single parameter; when this is done, the value of the lumped parameter cannot yield useful information about its component parts. Conductivity attributable to residual salinity was encountered in tuff and several of the soils, but in only one sand and none of the sandstones. In Fig. 6.20 we represent all the saturation dependent electrical conductivity from Table 6.5 together. As predicted, all the data

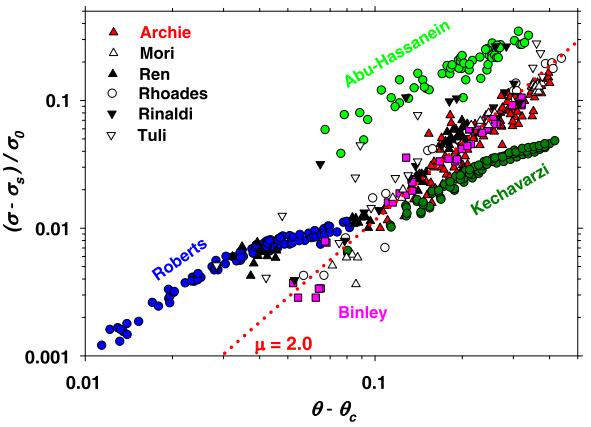

Fig. 6.20 Summary plot of all the data sets presented in Table 6.5 showing constant adherence to the predicted universal behavior. For all data sets, the water content was normalized by subtracting the critical value, and the electrical conductivity was normalized by subtracting the solid phase contribution, then dividing by the brine conductivity value. Data are parallel to the line given by the universal conductivity exponent, $\mu = 2$. Those data sets that lie above the universal line were analyzed as having residual salinity, those that curved downward away from the universal line, as having a contact resistance

indicate an exponent $\mu = 2.0$ (Fig. 6.20), with deviations below the line indicating contact resistance (e.g., [37]), and deviations above the line indicating the effect of residual salinity (e.g., [1, 61]). Deviations attributable to residual salinity are most pronounced for low-conductivity solutions and/or low water contents (e.g., [57]). Further, as predicted, the apparent power μ^* increases to 2 in the limit $\theta \to \theta_t$ for data sets with either contact resistance (e.g., [37]) or with residual salinity (e.g., [1]).

In subsequent analysis, we plotted critical volume fractions vs. porosity to examine the possibility that a linear relationship exists between them. The result (Fig. 6.21) is consistent with our conjecture that $\theta_t \propto \phi$, and finds a similar coefficient (0.12 rather than 0.1). In this analysis the regression line was forced through the origin, and we did not include cases for which $\theta_t = 0$. Note that almost all cases with $\theta_t = 0$ had large solid conductivities; in such cases the simple percolation argument that $\theta_t = p_c\phi$ will not hold. However, plotting $1/a$ against $(1 - \theta_t)^2$ shows no relationship as might have been expected from arguments leading to Eq. (6.32). This indicates that a may indeed be best interpreted as the tortuosity of the conducting pathways in the limit of full saturation.

6.4 Effects of Arbitrary Pore-Size Distributions

This calculation of $K(\theta)$ follows the same procedure as in Chap. 5, but here we assume no particular form for the pore size distribution. However, we do assume that there are minimum and maximum pore sizes, so the pdf for $W(r)$ should still

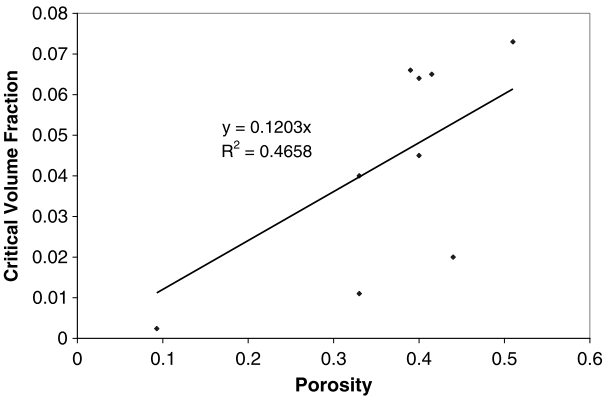

Fig. 6.21 Plot of the (non-zero) critical volume fractions from Fig. 6.20 vs. porosity. Although the plot is quite noisy, it generates $\theta_t \propto \phi$. The proportionality constant is approximately 1/8 when the fit is constrained to pass through origin

be valid between the limits r_0 and r_m. Thus the same integral provides the basis for all the calculations of equilibrium quantities, regardless of the actual form of $W(r)$ appropriate for a given soil:

$$\int_{r_1}^{r_2} r^3 W(r) dr \tag{6.39}$$

When $r_2 = r_m$ and $r_1 = r_0$—that is, when we are integrating from the smallest to the largest pore in the system—Eq. (6.39) yields a numerical constant of order unity times the porosity ϕ. As we saw in the fractal treatment, it is possible to define a suitable normalization constant to generate precisely the porosity; here this is also of no real concern since we will be using proxy data from the cumulative soil particle size distribution. Such a choice guarantees normalization as well. When $r_2 = A/h$ (as long as this value is less than $<r_m$) and $r_1 = r_0$, Eq. (6.39) defines the moisture content θ. When $r_2 = r_m$ and $r_1 = r_c$, Eq. (6.39) yields the critical moisture content for percolation θ_t; if θ_t is known we can thereby deduce the bottleneck pore radius r_c under saturated conditions. When $r_2 = A/h$ and $r_1 = r_c$, Eq. (6.39) again yields θ_t, and can be used to deduce the bottleneck pore radius $r_c(\theta)$ for any moisture content $\theta > \theta_t$.

If one assumes that distributions of pore aspect ratios are independent of pore size, the ratio $[r_c(\theta)/r_c|_{\theta=\phi}]^3$ again yields $K(\theta)/K_S$, as long as $\theta > \theta_{xK}$. Building in this assumption deprives the procedure of some generality, but the assumption is not unreasonable for many natural media, and allows the procedure to generate the known appropriate $K(\theta)/K_S$ when the medium is well described by a fractal model. Thus the present formulation allows comparison of the present prediction with analytical results for media presumed compatible with the fractal model.

The cross-over moisture content θ_{xK} is found as follows. Instead of using Eq. (6.16) as the functional form for the hydraulic conductivity (a result specific to fractal geometry), K is set to the unspecified (and thus general) form $K(\theta)$. Com-

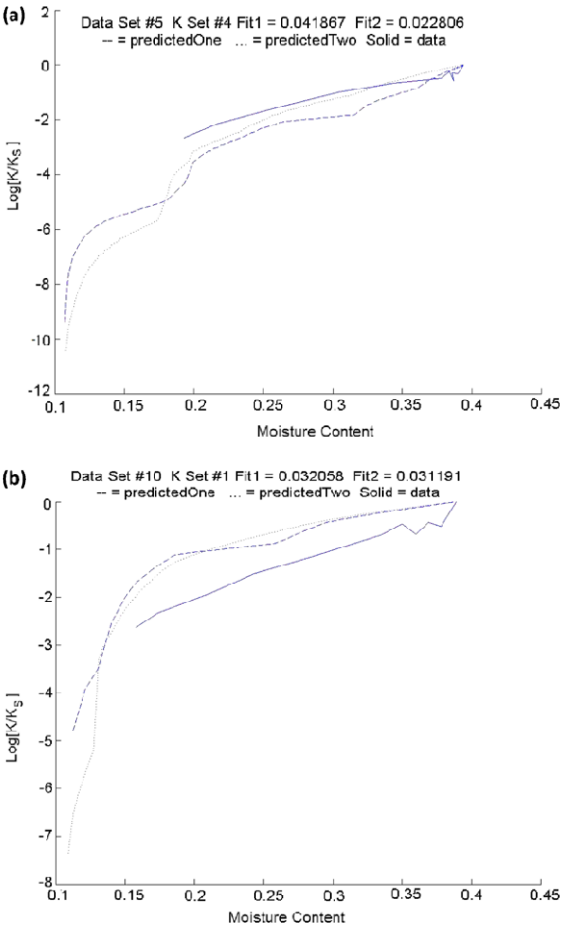

Fig. 6.22 Use of numerical model to predict K for arbitrary soil pore space distribution and comparison with saturation dependence of K for McGee Ranch soils (used in Fig. 6.1). Note that there were 11 different particle size distributions taken from surface soils from which to generate a pore size distribution, and that K was measured at 5 different depths. This leaves as many as 55 possible comparisons, of which we present 2. Note that these two presented had the lowest R^2 values of all 55 comparisons. The larger discrepancy than in Fig. 6.1 may be because the particle size data chosen was not representative of the pore-size distribution at the particular depth. In any case comparing a numerical result with an analytical result for a fractal model and experimental data can clarify the relevance of the fractal model

bining this K with Eq. (6.20), and setting $K(\theta)$ and $dK/d\theta$ equal for each equation when $\theta = \theta_{xK}$ yields

$$\theta_{xK} = \theta_t + \frac{2K(\theta_{xK})}{\frac{dK}{d\theta}\big|_{\theta=\theta_{xK}}} \tag{6.40}$$

This is the fundamental analytical result employed by Blank et al. (2008) to make comparisons between theoretical and experimental results for $K(\theta)$. The factor 2 is from the percolation exponent μ.

The pore-size distribution for field samples is seldom, if ever, known. But one often has access to the cumulative particle-size distribution, which can be used as a proxy for the cumulative pore-size distribution (with the usual uncertainties relating pore and particle sizes). Evaluating Eq. (6.39) between any two limits is thus equivalent to taking differences in the cumulative particle size distribution evaluated at two corresponding limits. Comparison with experiment is shown in Fig. 6.22a,b. The comparisons are drawn from the same soils as in Fig. 6.1, but here no assump-

tions have been made regarding the form of the pore size distribution. Given results from both experiment and an analytical model of flow on a random fractal, the numerical procedure could serve as a test of the validity of the fractal model. But note that in the present case there were 11 different particle size distributions to choose from (all taken at the surface), while the hydraulic conductivity was determined at 5 different depths. We have chosen the two comparisons with the lowest R^2 values. We believe that this means that the two particle size distributions chosen were the least suitable for the hydraulic conductivity shown, though this is not the only possible interpretation. Thus, if we chose to fit the fractal model to the same particle size distributions, and use those to predict the same two hydraulic conductivity functions, we would also presumably have similar discrepancies. The meaning of the discrepancies would indeed be that the model was not appropriate for the data, but we think that in such a case the message would simply be that the parameters were inappropriate, not the choice of model. Figure 6.1 did indicate that for this particular suite of soils, the fractal model was appropriate.

6.5 Water Film Issues

As saturation is reduced and pathways through water-filled pore space lose connectivity, other modes of water transport become more prominent. Two such modes are film flow and vapor phase flow. We do not discuss the latter. Film flow will be governed by the roughness of grain surfaces, with surface fractal dimension D_s. It has been argued [18, 68] that such conduction will follow

$$K \propto S^{\frac{3}{m(3-D_s)}} \tag{6.41}$$

For discussion of the physical interpretation of the parameter m, see the original articles. Equation (6.41) is reminiscent of Eq. (6.16), and clearly has a similar origin. But a quasi-universal film-flow conductivity, proportional to the cube of the saturation, may be derived rather easily. The treatment starts with an expression for medium saturation when all water is present as films, that is when the film thickness Δr is smaller than the smallest pore radius, itself smaller than the smallest particle radius, r_0:

$$S = \frac{\int_{r_0}^{r_m} r^2 \Delta r W(r) dr}{\int_{r_0}^{r_m} r^3 W(r) dr} = \frac{\int_{r_0}^{r_m} dr \Delta r r^{1-D} \frac{2-D}{r_m^{3-D}}}{\int_{r_0}^{r_m} dr r^{2-D} \frac{3-D}{r_m^{3-D}}} = \left(\frac{A}{V}\right) \Delta r \tag{6.42}$$

In this expression the fractal dimensionality, D, refers to the distribution of particle radii. When film thicknesses Δr exceed r_0, then the saturation must be written differently to include some water-filled pores:

$$S = \frac{\int_{\Delta r}^{r_m} r^3 W(r) dr + \int_{r_0}^{\Delta r} r^2 \Delta r W(r) dr}{\int_{r_0}^{r_m} r^3 W(r) dr} \quad \Delta r > r_0 \tag{6.43}$$

After considerable simplification,

$$S = \frac{\Delta r A}{v} - \left(1 - \frac{1}{\phi}\right)\left[1 - \frac{1}{2-D}\left(\frac{\Delta r}{r_0}\right)^{3-D} + \left(\frac{3-D}{2-D}\right)\left(\frac{\Delta r}{r_0}\right)\right] \tag{6.44}$$

Consider the case Eq. (6.42) when the film thickness is small compared to the smallest pore size. This temporarily permits us to avoid the difficulties associated with combined film and capillary flow. The conductance of the film in each pore, if all pores had the same shape (which would have to be true in the mean at least if the medium were a random fractal), would be proportional to:

$$g \propto \frac{r\Delta r}{l}(\Delta r)^2 \tag{6.45}$$

Equation (6.45) always yields a conductance proportional to the cube of the film thickness. When the pore length l is proportional to the pore radius r, then Eq. (5.45) yields

$$g \propto (\Delta r)^3 \approx S^3 \tag{6.46}$$

independent of pore size. If all conductances have approximately the same value, and that value is proportional to S^3, then the hydraulic conductivity must also be proportional to S^3. Even if the condition on the proportionality of pore length and radius is not fulfilled, critical path analysis would still identify a bottleneck conductance g, among a distribution of conductances, whose dependence on saturation would control the system response. It is easily seen that the proportionality of each individual g to S^3 would still guarantee that the hydraulic conductivity be proportional to S^3. In this lowest level approximation, there is no threshold moisture content, since water flow can occur as soon as the water films begin to form, since they form everywhere. However, see Chap. 7 for a discussion of complications that can become relevant at molecular scales.

In natural porous media, especially those in which the pore size distribution covers at least two orders of magnitude, we don't expect to see Eq. (6.41) or Eq. (6.46) easily verified. In such media the pore size distribution itself is sufficient to cause a variation in K of 6 or more orders of magnitude if $r^4/l \approx r^3$ scaling governs the hydraulic conductivity. When $\theta < \theta_{xK}$, percolation scaling will cause a further drop before film flow can prevent K from disappearing altogether. For example, if $K_S = 10^{-2}$ cm/s, then values well below 10^{-8} cm/s would still be dominated by capillary flow through water-filled pores. Values of K much lower than 10^{-8} cm/s are seldom measured, because experiments under typical conditions would have to last several years. On the other hand, monosized sphere packs (e.g., glass beads) may have a ratio of the maximum to the minimum pore size as small as 2, so their hydraulic conductivity may vary by as little as $2^3 = 8$ before other flow mechanisms become more important.

To see more clearly how an alternate means to transport water might show up in experimental data, consider Fig. 6.23, which shows data for $K(S)$ from Dr. M. Ioannidis (personal communication, 2006) for a medium of nearly monodisperse glass beads. The porosity of the medium is 0.3, noticeably smaller than appropriate

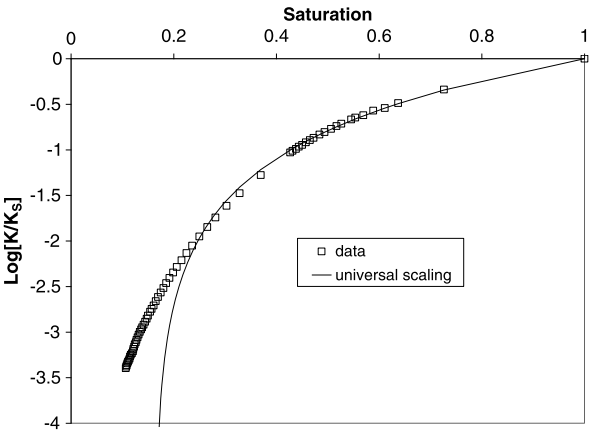

Fig. 6.23 Semi-log comparison of universal scaling with data from Dr. Ioannidis on the saturation dependence of the hydraulic conductivity of comparatively ordered granular media. The media should be considered to have pore radii that vary over less than a factor 2

for a cubic packing, and more nearly appropriate for a random close packed structure. To a first approximation, one can consider the experimental medium to have no variability in pore size (Ioannidis, personal communication, 2007). The theoretical formulation of this chapter would therefore require that the hydraulic conductivity should exactly follow the universal scaling of Eq. (5.21). Clearly it does not, at least not over the full range of saturations.

Our single fit parameter is a critical volume fraction (or moisture content) for percolation. The value obtained is $\theta_t = 0.049$. This corresponds to a critical fraction of the porosity of 0.049/0.3, about 16 %, a very common result for continuum percolation noted first by Scher and Zallen [64]. Over almost two orders of magnitude, K via Eq. (6.22) is in good agreement with the experimental data; only at lower saturations do the experimental data exceed the prediction. This discrepancy has two obvious potential interpretations. One possibility is that a different mechanism for water transport, such as film flow, becomes important as the saturation nears 20 %. The second is that universal scaling of the hydraulic conductivity is not valid, and that both the exponent μ^* and the critical volume fraction θ_t should be considered fitting parameters. This possibility is shown in Fig. 6.24; then in Fig. 6.26 we show that $\log(K)$ vs. $\log(\theta)$ is rather well described as a non-universal power with $\mu^* = 2.81$ and $\theta_t = 0.0145$, rather than $\mu = 2.0$ and $\theta_t = 0.049$.

How should one interpret these results? We will consider this problem from two perspectives. First we re-visit Buckingham's paper [11] of a century ago and its continuing influence. Consider Fig. 6.25, Buckingham's schematic understanding of the dependence of hydraulic conductivity (denoted by Buckingham as λ) as a function of moisture content. As reported by Narasimhan [53],

> Buckingham was led to the conclusion 'that the capillary conductivity, λ, will be a strong function of water content, θ, in a soil.' He conjectured that the relation would have the shape indicated schematically in Fig. 6.25. Between A and B, flow occurs dominantly through saturated capillaries. Between B and C, capillary and film flow coexist. Between C and D flow is exclusively through films. Between D and F films progressively break up.

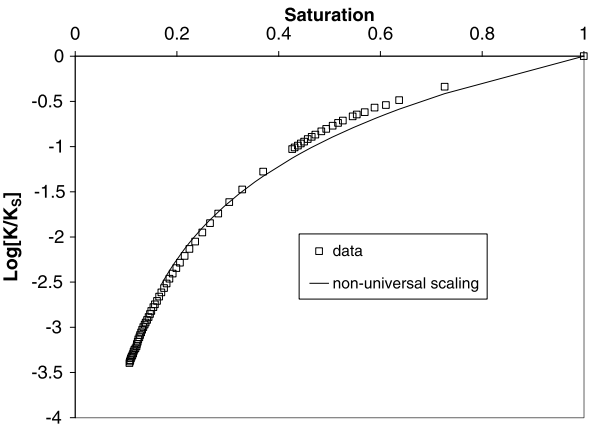

Fig. 6.24 Semi-log comparison of non-universal scaling with the same data as in Fig. 6.23 and with choice of an optimal value of the exponent, μ^*

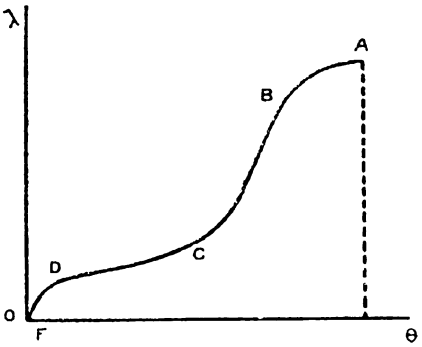

Fig. 6.25 Buckingham's [11] schematic interpretation of the various regimes of hydraulic conductivity

Based on our quantitative theory of K, we broadly agree with this interpretation of Fig. 6.25. Capillary flow will dominate from A to B, but also for much of the range from B to C, where the steep slope is related to the approach to the percolation threshold for the water-filled pores. Although film flow will become important well before C, it is not film flow in parallel that is so important (and seemingly implied by Narasimhan [53]), but film flow in series with capillary flow, preventing the mean separation of water flow paths from diverging as the percolation threshold is approached. Even as the percolation threshold is approached, water need flow only a microscopic distance through thin films to incorporate finite-sized clusters into the flow and thus avoid divergence in flow path separation [28].

From C onward we generally agree with Buckingham: film flow can maintain higher values of K than predicted by theory as the percolation threshold is approached. As the saturation drops further, in the vicinity of C, Fig. 6.20 shows qualitatively what one would expect if an alternate mode of conduction were to act in parallel to the mechanism of capillary flow treated theoretically. Narashimhan [53] continues, "Voluminous soil hydraulic conductivity data now exist not only confirming Buckingham's conjecture of the form of the functional dependence but also showing that the λ vs. θ relation is strongly hysteretic [51]." Linear plots of the uni-

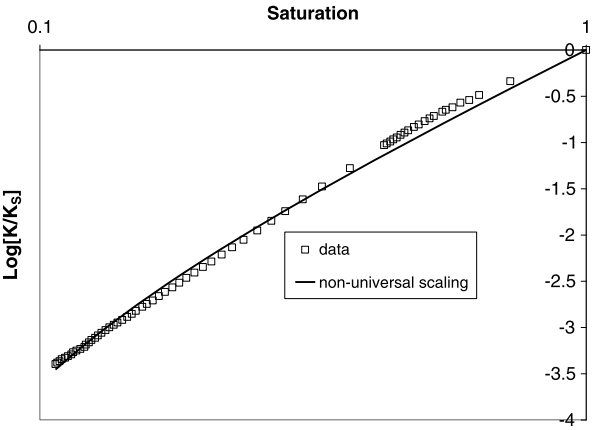

Fig. 6.26 The same comparison as in Fig. 6.24, except represented on a log-log plot

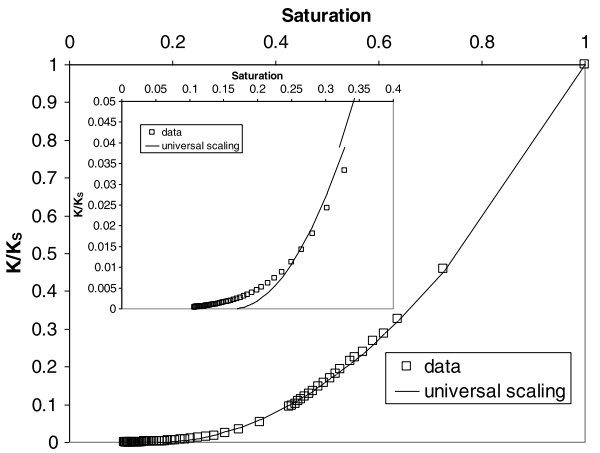

Fig. 6.27 The same comparison as in Fig. 6.23, but shown on a linear plot to make a graphical correspondence with the schematic drawing of Buckingham [11]

versal curve, together with $K(\theta)$ from Ioannidis as a function of moisture content (Figs. 6.24 and 6.27), are in general accord with Buckingham's sketch (Fig. 6.25). Buckingham's proposed mechanism appears generally consistent with the discrepancy between data and universal scaling of percolation theory.

Secondly, we consider the actual values of the fitting parameter θ_t. To estimate the critical volume fraction in Ioannidis' glass bead medium, one can apply the Vyssotsky et al. [72] bond percolation result. In a hexagonal close-packed system (similar to random close-packed) there are two types of sites: one with coordination number 4, the other with coordination number 8. In hexagonal packing there are 2 tetrahedra for every octahedron; the mean is therefore ~5.3, giving $p_c \approx 0.283$. If half of the pore space is found in the bonds, then a water volume fraction $\theta = (0.5)(0.28)\phi = 0.0425$ should suffice for percolation. The critical volume fraction found using the universal value $\mu = 2.0$ ($\theta_t = 0.049$) is considerably closer to $\theta_t = 0.0425$ than is the value $\theta_t = 0.0149$ fitted using a non-universal exponent. The critical volume fraction fitted using a non-universal exponent requires

closer to $1/6$ of the pore space to be in the bonds. Moreover, $\theta_t = 0.049$ is consistent with the critical volume fractions extracted from a wide range of experiments [19, 30].

We conclude that the discrepancy between the prediction of universal scaling of the hydraulic conductivity and experiment shown in Fig. 6.18 does not imply relevance of a non-uniform conductivity exponent. It more likely represents a cross-over from K dominated by flow through water-filled pores, to the less conductive film flow. At higher saturations, film flow operates in parallel with capillary flow but is negligible in comparison; when the continuity of capillary flow is interrupted, film flow operates in series with capillary flow through finite clusters.

How do the data from Ioannidis fit in with the themes of this chapter? Practically speaking, Buckingham's conclusions are most relevant for granular media with narrow grain size distributions. Even in Ioannidis' artificial medium, we detect only the onset of film flow. In natural media with much broader pore size distributions, the hydraulic conductivity variation attributable to the pore size variability is already several orders of magnitude; effects of percolation scaling extend a couple of orders of magnitude below that. Thus, if the saturated hydraulic conductivity is 10^{-2} cm/s, our percolation approach may account for values down to 10^{-7} cm/s to 10^{-11} cm/s, and values in this range are rarely measured. So while Buckingham's thesis has supposedly been amply verified [53], we doubt that it has been verified often. Recall that the difference between two nearly equal values may easily vary over several orders of magnitude. Rigorous comparisons between theory and experiment for this capillary/film flow cross-over issue therefore require exacting methods, and may still be inconclusive. Nonetheless, we believe our interpretation of alternate water transport modes operating in concert with capillary flow is consistent with both theory and observations.

The above discussion simultaneously addresses two common but apparently unrelated questions: (1) what properties or mechanisms could result in a non-universal conductivity exponent? and (2) why is the critical volume fraction so small? As seen here, both questions may be resolved by considering a parallel conduction mechanism.

How would Narasimhan view our above approach? We assume that he would be skeptical, in view of the following quotes from the same paper [53]:

> Philosophically, Buckingham's skepticism raises the issue of the role of mathematics in the earth sciences. Milton Whitney, who led the Bureau of Soils and who had the vision to bring in talented physicists such as Briggs and Buckingham, believed that soil physics problems were so complex that they should not be handled strictly mathematically [43].

It is appropriate to conclude this section with a thoughtful remark attributed to Ansel Adams, the renowned landscape photographer and conservationist: 'There is nothing more disturbing than a sharp image of a fuzzy concept.' It is our belief, however, that with improvements in both the resolution and quantitative analysis of experiments, fuzzy concepts lose their validity if they do not become clearer.

6.6 Electrical Conductivity for $\theta < \theta_t$

We now present a suggestion for the means to calculate the electrical conductivity for $\theta < \theta_t$. Below the percolation threshold, electrical conduction must utilize a portion of the medium with a smaller electrical conductivity, σ_s, than whatever conducting fluid (with $\sigma = \sigma_0$) is filling the pore space. Clearly, however, the system conductivity is maximized by minimizing the path length in the lower-conducting medium.

The present calculations simply seek an optimal path length. An optimal path will utilize many finite clusters in addition to the infinite cluster. Such a path was shown [28] to scale with $p - p_c$ exactly as the correlation length χ. This was the basis of our earlier argument regarding liquid-phase diffusion: the total distance that water must flow through liquid films above the percolation threshold is not a critical function of percolation. Rather, both the separation between the connected water carrying paths and the total distance through the disconnected finite clusters scale the same way, and the distance through film flow is the difference between the two. Of course it is not necessary that the difference between two divergent quantities cancel; only that their ratio do so. However, if it is the optimal path that is sought, then the difference should be as small as possible, and thus not diverge. Thus the total distance that the electrical current travels through the liquid should scale as the correlation length for $\theta < \theta_t$, and the distance through the solid medium must be the size of the system, x, less the correlation length χ. This suggests that the conductivity should have the form

$$\sigma(\theta) = \frac{x}{\frac{\chi}{\sigma_0} + \frac{x-\chi}{\sigma_s}} = \frac{x}{\frac{\chi_0(\theta_t-\theta)^{-\nu}}{\sigma_0} + \frac{x-\chi_0(\theta_t-\theta)^{-\nu}}{\sigma_s}} \tag{6.47}$$

proportional to the inverse of the sum of the resistances along 1D paths which minimize the total resistance. Such a power-law rapidly reduces the conductivity below the percolation threshold to the solid or surface conductivity.

The above calculation can equally apply to finding an optimal flow path (and associated K) through a system of muds and sands for which the sand portion does not percolate. The Stanley group has long addressed the problem of finding distributions of such path lengths and transit times; see for example Lopez et al. [46].

Because Chaps. 6 and 7 are very closely related, a summary of Chap. 6 is combined with the summary of Chap. 7, and given at the end of Chap. 7.

Problems

6.1 Prove that r_c is the same for electrical and hydraulic conductivities and draw an analogy to Problem 3.1 in Chap. 3, which asked to show that the value obtained for R_c was independent of whether one obtained r_c first and substituted into the equation for $R(r)$, or whether one integrated over R directly.

6.2 Consider a log-normal distribution of pore sizes, but assume as in a fractal model that all pores have the same shapes (this is a necessary assumption in a fractal model, but only an assumption of convenience, otherwise). Derive equivalent expressions for the saturation dependence of the hydraulic and electrical conductivity using critical path analysis and find the moisture contents at which the critical path analysis must be replaced by percolation scaling. These exercises may be performed numerically. Compare the ranges of parameter space (D_p, ϕ), for which Archie's law may be reasonably derived from percolation theory determined from the log-normal and the power-law distributions. Does a log-normal distribution tend to make Archie's law more or less widely applicable than is the case for a power-law distribution of pore sizes?

6.3 Graphically represent the apparent power $\mu^*(\phi)$ of the porosity in Archie's law when the pore size distribution modifies its value from 2 in the cases that (a) the ratio r_0/r_m is held constant and (b) the fractal dimensionality is held constant. You will need to keep in mind that in either case μ^* is $d\ln(\sigma)/d\ln(\phi) = (\phi/\sigma)d\sigma/d\phi$.

Appendix: Calculation of Water Retention and Unsaturated Hydraulic Conductivity for Pore-Solid Fractal Model with Two Fractal Regimes

Water Retention Curve

We assume that the pore-size distribution of soils follows the pore-solid fractal (PSF) approach proposed by Perrier et al. [55]. This model combined with percolation theory has been successfully applied to model unsaturated hydraulic conductivity of soils with different textures [23]. The continuous probability density function, $W(r)$, of pores consistent with the Hunt and Gee [33] analogy would be:

$$W(r) = \beta \frac{3-D}{r_{max}^{3-D}} r^{-1-D}, \quad r_{min} < r < r_{max} \tag{6.48}$$

where $\beta = p/(p+s)$ in which p and s are the pore and solid fractions [55], respectively, D is the pore-solid interface fractal dimension, r is the pore radius ($r \propto 1/h$ where h is the tension head), and r_{min} and r_{max} are the smallest and largest pore radii, respectively.

Figure 6.28 shows a schematic of a soil water retention curve with two fractal regimes. The first regime covers mostly the large (frequently structural) pores, and the second regime includes the small (textural) pores. The water content at the crossover point is denoted by θ_x which is equal to the porosity of the second regime ϕ_2.

In a porous medium having a probability density function that scales differently in two different regimes, e.g., D_1 and D_2 (Fig. 6.28), the total porosity may be found by integrating $r^3 W(r)$ between r_{min} and r_{max} to obtain

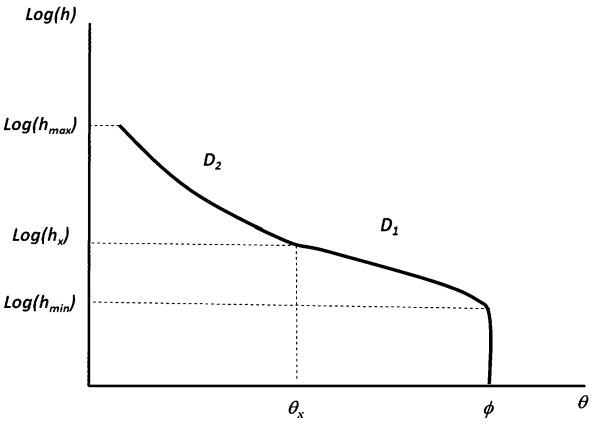

Fig. 6.28 Depiction of two separate fractal regimes in a soil water retention curve and corresponding definitions

$$\phi = \phi_1 + \phi_2 = \beta_1 \frac{3 - D_1}{r_{\max}^{3-D_1}} \int_{r_x}^{r_{\max}} r^3 r^{-1-D_1} dr + \beta_2 \frac{3 - D_2}{r_x^{3-D_2}} \int_{r_{\min}}^{r_x} r^3 r^{-1-D_2} dr$$
$$= \beta_1 \left[1 - \left(\frac{r_x}{r_{\max}} \right)^{3-D_1} \right] + \beta_2 \left[1 - \left(\frac{r_{\min}}{r_x} \right)^{3-D_2} \right] \tag{6.49}$$

where r_x is the pore radius at the cross-over point where the fractal behavior of the medium changes from regime 1 to regime 2, and D_1 and D_2 are the pore-solid interface fractal dimension of the first and second regimes, respectively.

The water content of pores with radii less than or equal to r in the second regime ($h_x < h < h_{\max}$) is determined as follows ($r < r_x$):

$$\theta = \beta_2 \frac{3 - D_2}{r_x^{3-D_2}} \int_{r_{\min}}^{r} r^3 r^{-1-D_2} dr = \beta_2 \left[\left(\frac{r}{r_x} \right)^{3-D_2} - \left(\frac{r_{\min}}{r_x} \right)^{3-D_2} \right] \tag{6.50}$$

Likewise, the water content of pores with radii less than or equal to r in the first regime ($h_{\min} < h < h_x$) would be ($r > r_x$):

$$\theta = \beta_1 \frac{3 - D_1}{r_{\max}^{3-D_1}} \int_{r_x}^{r} r^3 r^{-1-D_1} dr + \beta_2 \frac{3 - D_2}{r_x^{3-D_2}} \int_{r_{\min}}^{r_x} r^3 r^{-1-D_2} dr$$
$$= \phi_2 + \beta_1 \left[\left(\frac{r}{r_{\max}} \right)^{3-D_1} - \left(\frac{r_x}{r_{\max}} \right)^{3-D_1} \right] \tag{6.51}$$

Combining Eqs. (6.50) and (6.51) with the capillary equation gives the following piecewise soil water retention curve model:

$$\theta = \begin{cases} \phi \quad h < h_{\min} \\ \phi_2 + \beta_1 \left[\left(\frac{h}{h_{\min}} \right)^{D_1-3} - \left(\frac{h_x}{h_{\min}} \right)^{D_1-3} \right] = \phi - \beta_1 \left[1 - \left(\frac{h}{h_{\min}} \right)^{D_1-3} \right] \\ \quad h_{\min} < h < h_x \\ \beta_2 \left[\left(\frac{h}{h_x} \right)^{D_2-3} - \left(\frac{h_{\min}}{h_x} \right)^{D_2-3} \right] = \phi_2 - \beta_2 \left[1 - \left(\frac{h}{h_x} \right)^{D_2-3} \right] \quad h_x < h < h_{\max} \end{cases} \tag{6.52}$$

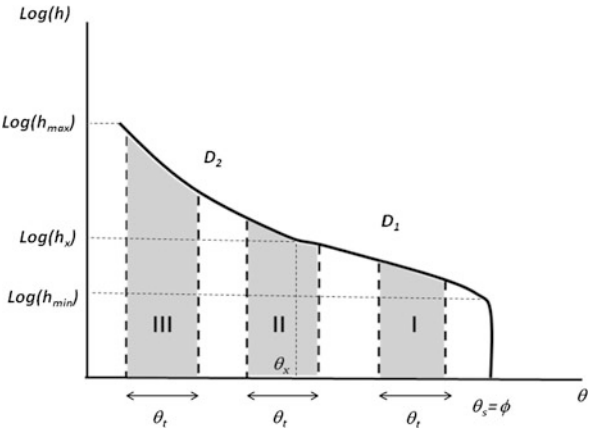

Fig. 6.29 Three distinct ranges of moisture content that control the determination of r_c when θ_t is less than either partial porosity

Unsaturated Hydraulic Conductivity

Following Ghanbarian-Alavijeh and Hunt [23], we use critical path analysis combined with the PSF model to find the critical pore radius for percolation for saturated and unsaturated conditions. Generally, there are two possibilities.

Possibility 1: $\theta_t < \phi_1$

Using the pore-solid fractal approach, we define the critical volume content of percolation θ_t from critical path analysis for saturated conditions ($\theta = \phi$) as follows:

$$\theta_t = \frac{p_1}{p_1 + s_1} \frac{3 - D_1}{r_{max}^{3-D_1}} \int_{r_c(\theta=\phi)}^{r_{max}} r^3 r^{-1-D_1} dr = \beta_1 \left[1 - \left(\frac{r_c(\theta = \phi)}{r_{max}} \right)^{3-D_1} \right] \quad (6.53)$$

Solution of Eq. (6.53) combined with Eq. (6.52) for $r_c(\theta = \phi)$ gives

$$r_c(\theta = \phi) = r_{max} \left[\frac{\beta_1 - \theta_t}{\beta_1} \right]^{\frac{1}{3-D_1}}, \quad \theta_t < \phi_1 \quad (6.54)$$

For unsaturated condition as we show in Fig. 6.29, three cases are possible:

(I) $\theta - \theta_t > \phi_2$ and $\theta > \phi_2$ (see Fig. 6.29)

The critical water content for percolation θ_t would be

$$\theta_t = \beta_1 \frac{3 - D_1}{r_{max}^{3-D_1}} \int_{r_c(\theta)}^{r} r^3 r^{-1-D_1} dr = \beta_1 \left[\left(\frac{r}{r_{max}} \right)^{3-D_1} - \left(\frac{r_c(\theta)}{r_{max}} \right)^{3-D_1} \right] \quad (6.55)$$

Rewriting Eq. (6.55) combined with Eq. (6.52) for $r_c(\theta)$ yields

$$r_c(\theta) = r_{max} \left[\frac{\beta_1 - \phi + \theta - \theta_t}{\beta_1} \right]^{\frac{1}{3-D_1}} \quad (6.56)$$

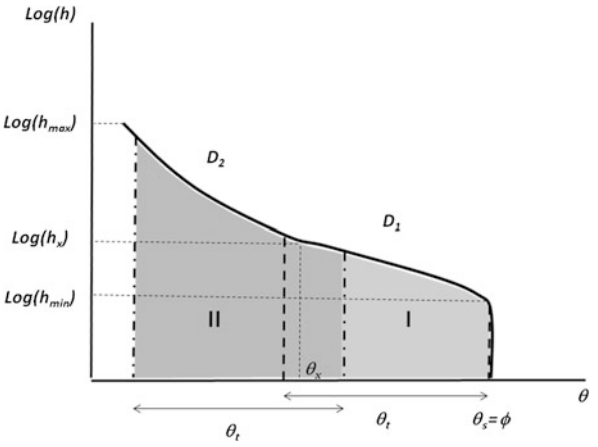

Fig. 6.30 Two separate distinct ranges of moisture contents that guide determination of r_c when θ_t is larger than the porosity associated with the upper fractal regime

(II) $\theta - \theta_t < \phi_2$ and $\theta > \phi_2$ (see Fig. 6.29)

$$\theta_t = \beta_2\left[1 - \left(\frac{r_c(\theta)}{r_x}\right)^{3-D_2}\right] + \beta_1\left[\left(\frac{r}{r_{max}}\right)^{3-D_1} - \left(\frac{r_x}{r_{max}}\right)^{3-D_1}\right] \tag{6.57}$$

Solving Eq. (6.57) combined with Eq. (6.52) for $r_c(\theta)$ results

$$r_c(\theta) = r_x\left[\frac{\beta_2 - \phi_2 + \theta - \theta_t}{\beta_2}\right]^{\frac{1}{3-D_2}} \tag{6.58}$$

in which $r_x = r_{max}[\frac{\beta_1-\phi_1}{\beta_1}]^{1/(3-D_1)}$.

(III) $\theta - \theta_t < \phi_2$ and $\theta < \phi_2$ (see Fig. 6.29)

$$\theta_t = \beta_2\left[\left(\frac{r}{r_x}\right)^{3-D_2} - \left(\frac{r_c(\theta)}{r_x}\right)^{3-D_2}\right] \tag{6.59}$$

Solution of Eq. (6.59) combined with Eq. (6.52) for $r_c(\theta)$ gives

$$r_c(\theta) = r_x\left[\frac{\beta_2 - \phi_2 + \theta - \theta_t}{\beta_2}\right]^{\frac{1}{3-D_2}} \tag{6.60}$$

Possibility 2: $\theta_t > \phi_1$

In this case, the critical water content for percolation θ_t at saturation ($\theta = \phi$) is

$$\theta_t = \beta_2\left[1 - \left(\frac{r_c(\theta = \phi)}{r_x}\right)^{3-D_2}\right] + \phi_1 \tag{6.61}$$

Rewriting Eq. (6.61) combined with Eq. (5.5) for $r_c(\theta = \phi)$ gives

$$r_c(\theta = \phi) = r_x\left[\frac{\beta_2 - \theta_t + \phi_1}{\beta_2}\right]^{\frac{1}{3-D_2}}, \quad \theta_t > \phi_1 \tag{6.62}$$

As we show in Fig. 6.30, there are two cases possible for the unsaturated condition:

(I) $\theta - \theta_t < \phi_2$ and $\theta > \phi_2$ (see Fig. 6.30)

$$\theta_t = \beta_2 \left[1 - \left(\frac{r_c(\theta)}{r_x} \right)^{3-D_2} \right] + \theta - \phi_2 \tag{6.63}$$

Solution of Eq. (6.63) for $r_c(\theta)$ gives

$$r_c(\theta) = r_x \left[\frac{\beta_2 - \phi_2 + \theta - \theta_t}{\beta_2} \right]^{\frac{1}{3-D_2}} \tag{6.64}$$

(II) $\theta - \theta_t < \phi_2$ and $\theta < \phi_2$ (see Fig. 6.30)

$$\theta_t = \beta_2 \left[\left(\frac{r}{r_x} \right)^{3-D_2} - \left(\frac{r_c(\theta)}{r_x} \right)^{3-D_2} \right] \tag{6.65}$$

Solution of Eq. (6.65) for $r_c(\theta)$ yields

$$r_c(\theta) = r_x \left[\frac{\beta_2 - \phi_2 + \theta - \theta_t}{\beta_2} \right]^{\frac{1}{3-D_2}} \tag{6.66}$$

In fact, when $\theta_t > \phi_1$, $r_c(\theta)$ follows the same function of water content (Eqs. (6.64) and (6.66)) for both $\theta > \phi_2$ and $\theta < \phi_2$.

To model unsaturated hydraulic conductivity, we invoke Poiseuille's law for self-similar fractal porous media in which the hydraulic conductance g of a given pore is proportional to r^4 and the inverse of the pore length (l), also assumed to be proportional to $r (l \propto r)$. Therefore, g is a function of pore radius cubed, r^3 [23, 27]. Since the hydraulic conductivity $K(\theta)$ is directly proportional to the critical hydraulic conductance g_c, the unsaturated hydraulic conductivity normalized with the saturated hydraulic conductivity (as the reference point) is given by

$$\frac{K(\theta)}{K_s} = \frac{g_c(\theta)}{g_c(\theta = \phi)} = \frac{r_c^3(\theta)}{r_c^3(\theta = \phi)} \tag{6.67}$$

Thus, the new piecewise unsaturated hydraulic conductivity model for the two possibilities outlines above would be

Possibility 1: $\theta_t < \phi_1$

$$\frac{K(\theta)}{K_s} = \begin{cases} \left[\frac{\beta_1 - \phi + \theta - \theta_t}{\beta_1 - \theta_t} \right]^{3/(3-D_1)}, & \theta - \theta_t > \phi_2, \theta > \phi_2 \\ \left(\frac{\beta_1^{3/(3-D_1)}}{\beta_2^{3/(3-D_2)}} \right) \left(\frac{\beta_1 - \phi_1}{\beta_1} \right)^{3/(3-D_1)} \frac{[\beta_2 - \phi_2 + \theta - \theta_t]^{3/(3-D_2)}}{[\beta_1 - \theta_t]^{3/(3-D_1)}}, & \\ \theta - \theta_t < \phi_2, \theta > \phi_2, \theta < \phi_2 \end{cases} \tag{6.68}$$

Possibility 2: $\theta_t > \phi_1$

$$\frac{K(\theta)}{K_s} = \left[\frac{\beta_2 - \phi_2 + \theta - \theta_t}{\beta_2 + \phi_1 - \theta_t}\right]^{3/(3-D_2)} \tag{6.69}$$

If one assumes that the percolation threshold is equal to 0, the unsaturated hydraulic conductivity model proposed above (Eqs. (6.68) and (6.69)) is simplified to

$$\frac{K(\theta)}{K_s} = \begin{cases} \left[\frac{\beta_1 - \phi + \theta}{\beta_1}\right]^{3/(3-D_1)}, & \theta > \phi_2 \\ \left(\frac{\beta_1^{3/(3-D_1)}}{\beta_2^{3/(3-D_2)}}\right)\left(\frac{\beta_1 - \phi_1}{\beta_1}\right)^{3/(3-D_1)} \frac{[\beta_2 - \phi_2 + \theta]^{3/(3-D_2)}}{\beta_1^{3/(3-D_1)}}, & \theta < \phi_2 \end{cases} \tag{6.70}$$

In all comparisons that we have made with experiment, we have found that $\theta_t = 0$ was appropriate, for reasons that we explain in the text. Nonetheless, in principle one should refer to Eqs. (6.68) and (6.69) for more general results. As long as both regimes are associated with textural pores, the simplest assumption should be used, namely that θ_t is independent of moisture content. In this case one would normally expect θ_t to be finite. But in the case that structural and textural pores are present, it must be considered possible that θ_t takes on a different value for the two types of pores. If θ_t is large, it is important that the results we obtain here would not extend to low saturations, where universal scaling of the hydraulic conductivity would be expected. But when the percolation threshold occurs at zero moisture content, the range of moisture contents at which universal scaling should be observed will typically be $0 < \theta < 0.1$, and is often even more restricted. In the case that $\theta_t = 0$ we could neglect this complication, since the experimenters never explored moisture contents sufficiently low that universal scaling of the hydraulic conductivity would be encountered.

References

1. Abu-Hassanein, Z.S., Benson, C.H., Blotz, L.R.: Electrical resistivity of compacted clays. J. Geotech. Eng. **122**, 397–406 (1996)
2. Archie, G.E.: The electrical resistivity log as an aid in determining some reservoir characteristics. Trans. Am. Inst. Mech. Eng. **146**, 54–61 (1942)
3. Balberg, I.: Recent developments in continuum percolation. Philos. Mag. B **30**, 991–1003 (1987)
4. Bear, J.: Dynamics of Fluids in Porous Media. Elsevier, New York (1972)
5. Berkowitz, B., Balberg, I.: Percolation theory and its application to groundwater hydrology. Water Resour. Res. **29**, 775–794 (1993)
6. Bernabé, Y.: Streaming potential in heterogeneous network. J. Geophys. Res. **103**, 20827–20841 (1998)
7. Binley, A., Winship, P., Middleton, R., Pokar, M., West, J.L.: Observation of seasonal dynamics in the vadose zone using borehole radar and resistivity. In: Proceedings of the Symposium on the Application of Geophysics to Environmental and Engineering Problems, SAGEEP, March 4–7, 2001
8. Binley, A., Winship, P., West, L.J., Pokar, M., Middleton, R.: Seasonal variation of moisture content in unsaturated sandstone inferred for borehole radar and resistivity profiles. J. Hydrol. **267**, 160–172 (2002)

9. Bird, N.R.A., Perrier, E., Rieu, M.: The water retention function for a model of soil structure with pore and solid fractal distributions. Eur. J. Soil Sci. **51**, 55–63 (2000)
10. Bittelli, M., Campbell, G.S., Flury, M.: Characterization of particle-size distribution in soils with a fragmentation model. Soil Sci. Soc. Am. J. **63**, 782–788 (1999)
11. Buckingham, E.: Studies on the movement of soil moisture. Bul. No. 38, Bureau of Soils, USDA, Washington, D.C. (1907)
12. Burdine, N.T.: Relative permeability calculations from pore-size distribution data. Petrol. Trans. Am. Inst. Min. Eng. **198**, 71–77 (1953)
13. Bussian, A.E.: Electrical conductance in a porous medium. Geophysics **48**, 1258–1268 (1983)
14. Carman, P.C.: Flow of Gases Through Porous Media. Butterworths, London (1956)
15. Cassiani, G., Dalla, E., Brovelli, A., Pitea, D.: Pore-scale modeling of electrical conductivity in unsaturated sandstones. In: Computational Methods in Water Resources: Proceedings of the XVth International Conference, Chapel Hill, NC, USA, June 13–17, 2004, pp. 235–246 (2004)
16. Cremers, A., Laudelout, H.: Note on the "isoconductivity value" of clay gels. Soil Sci. **100**, 298–299 (1965)
17. Cremers, A., van Loon, J., Laudelout, H.: Geometry effects for specific electrical conductance in clays and soils. In: Proc. Internat. Conf. Clays Clay Miner 14th, Ghent, Belgium, pp. 149–162 (1966)
18. Davis H.T., Novy, R.A., Scriven, L.E., Toledo, P.G.: Fluid distribution and transport in porous media at low wetting phase saturations. J. Phys. Condens. Matter **2**, SA457–SA464 (1990)
19. Ewing, R.P., Hunt, A.G.: Dependence of the electrical conductivity on saturation in real porous media. Vadose Zone J. **5**, 731–741 (2006)
20. Feng, S., Halperin, B.I., Sen, P.N.: Transport properties of continuum systems near the percolation threshold. Phys. Rev. B **35**, 197 (1987)
21. Freeman, E.J.: Fractal geometries applied to particle size distributions and related moisture retention measurements at Hanford, Washington. M.A. Thesis, University of Idaho (1995)
22. Friedman, S.P., Seaton, N.A.: Critical path analysis of the relationship between permeability and electrical conductivity of three-dimensional pore networks. Water Resour. Res. **34**, 1703 (1998)
23. Ghanbarian-Alavijeh, B., Hunt, A.G.: Unsaturated hydraulic conductivity in porous media: percolation theory. Geoderma **187–188**, 77–84 (2012)
24. Hilfer, R.: Geometric and dielectric characterization of porous media. Phys. Rev. **44**, 60–75 (1991)
25. Hillel, D.: Environmental Soil Physics. Academic Press, San Diego (1998)
26. Hunt, A.G.: AC hopping conduction: perspective from percolation theory. Philos. Mag. B **81**, 875–913 (2001)
27. Hunt, A.G.: Applications of percolation theory to porous media with distributed local conductances. Adv. Water Resour. **24**(3,4), 279–307 (2001)
28. Hunt, A.G.: Continuum percolation theory and Archie's law. Geophys. Res. Lett. **31**(19), L19503 (2004)
29. Hunt, A.G.: Percolative transport and fractal porous media. Chaos Solitons Fractals **19**, 309–325 (2004)
30. Hunt, A.G.: Continuum percolation theory for water retention and hydraulic conductivity of fractal soils: 1. Estimation of the critical volume fraction for percolation. Adv. Water Resour. **27**, 175–183 (2004)
31. Hunt, A.G.: A note comparing van Genuchten and percolation theoretical formulations of the hydraulic properties of unsaturated media. Vadose Zone J. **3**, 1483–1488 (2004)
32. Hunt, A.G.: Continuum percolation theory for transport properties in porous media. Philos. Mag. **85**, 3409–3434 (2005)
33. Hunt, A.G., Gee, G.W.: Application of critical path analysis to fractal porous media: comparison with examples from the Hanford Site. Adv. Water Resour. **25**, 129–146 (2002)
34. Hunt, A.G., Gee, G.W.: Water retention of fractal soil models using continuum percolation theory: tests of hanford site soils. Vadose Zone J. **1**, 252–260 (2002)

35. Hunt, A., Gershenzon, N., Bambakidis, G.: Pre-seismic electromagnetic phenomena in the framework of percolation and fractal theories. Tectonophysics **431**, 23–32 (2007)
36. Hunt, A.G., Ewing, R.P., Horton, R.: What's wrong with soil physics. Soil Sci. Soc. Am. J. (2013). doi:10.2136/sssaj2013.01.0020
37. Kechavarzi, C., Soga, K.: Determination of water saturation using miniature resistivity probes during intermediate scale and centrifuge multiphase flow laboratory experiments. Geotech. Test. J. **25**, 95–103 (2002)
38. Khaleel, R., Freeman, E.J.: Variability and scaling of hydraulic properties for 200 area soils. Hanford Site, Westinghouse Hanford Company Report WHC-EP-0883 (1995)
39. Klein, K.A., Santamarina, J.C.: Electrical conductivity in soils: underlying phenomena. J. Envir. Eng. Geophys. **8**, 263–273 (2003)
40. Kozeny, J.: Über Kapillare Leitung des Wasssers im Boden. Sitzungsber. Adak. Wiss. Wien **136**, 271–306 (1927)
41. Krohn, C.E., Thompson, A.H.: Fractal sandstone pores: automated measurements using scanning-electron-microscope images. Phys. Rev. B **33**, 6366–6374 (1986)
42. Kuentz, M., Mareschal, J.C., Lavallee, P.: Numerical estimation of electrical conductivity in saturated porous media with a 2-D lattice gas. Geophysics **65**, 766–772 (2000)
43. Landa, E.R., Nimmo, J.R.: The life and scientific contributions of Lyman J. Briggs. Soil Sci. Soc. Am. J. **67**, 681–693 (2003)
44. Leij, F.J., Alves, W.J., van Genuchten, Th. Williams J. R, M.: Unsaturated Soil Hydraulic Database, UNSODA 1.0 user's manual. Rep. EPA/600/R96/095, USEPA, Ada, OK (1996)
45. Letey, J., Klute, A.: Apparent mobility of potassium and chloride ions in soil and clay pastes. Soil Sci. **90**, 259–265 (1960)
46. Lopez, E., Buldyrev, S.V., Dokholyan, N.V., Goldmakher, L., Havlin, S., King, P.R., Stanley, H.E.: Postbreakthrough behavior in flow through porous media. Phys. Rev. E **67**, 056314 (2003), 16 pp.
47. Mallory, K.: Active subclusters in percolative hopping transport. Phys. Rev. B **47**, 7819–7826 (1993)
48. Mendelson, K.S., Cohen, M.H.: The effect of grain anisotropy on the electrical properties of sedimentary rocks. Geophysics **47**, 257–262 (1982)
49. Miller, E.E., Miller, R.W.: Physical theory for capillary flow phenomena. J. Appl. Phys. **27**, 324–332 (1956)
50. Mori, Y., Hopmans, J.W., Mortensen, A.P., Kluitenberg, G.J.: Multi-functional heat pulse probe for the simultaneous measurement of soil water content, solute concentration, and heat transport parameters. Vadose Zone J. **2**, 561–571 (2003)
51. Mualem, Y.: A Catalogue of the Hydraulic Properties of Unsaturated Soils. Res. Proj. No. 442, Technion, Israel Institute of Technology, Haifa (1976)
52. Mualem, Y.: Hysteretical models for prediction of hydraulic conductivity in unsaturated porous media. Water Resour. Res. **12**, 1248–1254 (1976)
53. Narasimhan, T.N.: Central ideas of Buckingham, 1906: a century later. Vadose Zone J. **6**, 687–693 (2007)
54. Patnode, H.W., Wyllie, M.R.J.: The presence of conductive solids in reservoir rocks as a factor in electric log interpretation. Trans. AIME **189**, 47–52 (1950)
55. Perrier, E., Bird, N., Rieu, M.: Generalizing the fractal model of soil structure: the pore-solid fractal approach. Geoderma **88**, 137–164 (1999)
56. Priesack, K., Durner, W.: Closed-form expression for the multi-modal unsaturated conductivity function. Vadose Zone J. **5**, 121–124 (2006)
57. Ren, T., et al.: unpublished data (1999)
58. Rhoades, J.D., Raats, P.A.C., Prather, R.J.: Effects of liquid-phase electric conductivity, water content, and surface conductivity on bulk soil electrical conductivity. Soil Sci. Soc. Am. J. **40**, 651–655 (1976)
59. Rieu, M., Sposito, G.: Fractal fragmentation, soil porosity, and soil water properties I. Theory. Soil Sci. Soc. Am. J. **55**, 1231 (1991)

60. Rinaldi, V.A., Cuestas, G.A.: Ohmic conductivity of a compacted silty clay. J. Geotech. Geoenviron. Eng. **128**, 824–835 (2002)
61. Roberts, J.J., Lin, W.: Electrical properties of partially saturated Topopah Spring tuff. Water distribution as a function of saturation. Water Resour. Res. **33**, 577–587 (1997)
62. Rockhold, M.L., Fayer, M.J., Gee, G.W.: Characterization of unsaturated hydraulic conductivity at the Hanford Site. PNL 6488, Pacific Northwest National Laboratory, Richland, WA 99352 (1988)
63. Sahimi, M.: Flow phenomena in rocks—from continuum models to fractals, percolation, cellular automata, and simulated annealing. Rev. Mod. Phys. **65**(4), 1393–1534 (1993)
64. Scher, H., Zallen, R.: Critical density in percolation processes. J. Chem. Phys. **53**, 3759 (1970)
65. Stauffer, D., Aharony, A.: Introduction to Percolation Theory, 2nd edn. Taylor and Francis, London (1994)
66. Surkov, V.V., Tanaka, H.: Electrokinetic effect in fractal pore media as seismoelectric phenomena. In: Dimri, V.P. (ed.) Fractal Behavior of the Earth System. Springer, Heidelberg (2005)
67. Thompson, A.H., Katz, A.J., Krohn, C.E.: Microgeometry and transport in sedimentary rock. Adv. Phys. **36**, 625 (1987)
68. Toledo, P.G., Novy, R.A., Davis, H.T., Scriven, L.E.: On the transport properties of porous media at low water content. In: Van Genuchten, M.T., Leij, F.J., Lund, L.J. (eds.) Indirect Methods for Estimating the Hydraulic Properties of Unsaturated Soils, University of California, Riverside (1992)
69. Tuli, A., Hopmans, J.W.: Effect of degree of saturation on transport coefficients in disturbed soils. Eur. J. Soil Sci. **55**, 147–164 (2004)
70. Tyler, S.W., Wheatcraft, S.W.: Fractal processes in soil water retention. Water Resour. Res. **26**, 1045–1054 (1990)
71. van Genuchten, M.T.: A closed form equation for predicting the hydraulic conductivity of unsaturated soils. Soil Sci. Soc. Am. J. **44**, 892–898 (1980)
72. Vyssotsky, V.A., Gordon, S.B., Frisch, H.L., Hammersley, J.M.: Critical percolation probabilities (bond problem). Phys. Rev. **123**, 1566–1567 (1961)
73. Wang, Y., Ma, J., Zhang, Y., Zhao, M., Edmonds, W.M.: A new theoretical model accounting for film flow in unsaturated porous media. Water Resour. Res. (2013). doi:10.1002/wrcr.20390
74. Wu, Q., Borkovec, M., Sticher, H.: On particle-size distributions in soils. Soil Sci. Soc. Am. J. **57**, 883–890 (1993)

Chapter 7
Other Transport Properties of Porous Media

In this chapter we discuss air (non-wetting phase) permeability, thermal conductivity, and diffusion in both liquid and gas phases. The saturation dependence of thermal conductivity serves to illustrate some interesting limitations and complications of a percolation-based approach. Then we summarize a treatment of the frequency-dependent electrical conductivity in hydrated smectite clay minerals. We interpret these experimental results using critical path analysis for interacting hopping charges (a topic of Chap. 5) through surface water between and on the outside surfaces of sheet silicates, which also brings in the subject of the continuity of water paths. We then address the particle size dependence of the ac conductivity. While we argued in Chap. 5 that the hydraulic conductivity cannot be predicted from the dc electrical conductivity (because dc electrical conductivity mostly follows the universal scaling of percolation), ac conductivity does appear to have utility for predicting the hydraulic conductivity. Finally we briefly present potential applications to electroseismic phenomena, and give a combined summary for Chaps. 6 and 7.

By contrasting the predicted behaviors of the various properties, and comparing those predictions with experiment, we generate a deeper understanding of the relative roles of geometry (pore size) and topology (pore connectivity). These relative roles are different for different properties. When we learn (for example) that solute diffusion *in finite systems* also follows universal scaling, this result strengthens the conclusion from the previous chapter that the saturation-dependence of electrical conductivity is given by universal scaling. We also discover which property is most sensitive to the particular way water is apportioned in the pore space (thermal conductivity).

7.1 Air Permeability

Air flow in partially saturated porous media is of roughly equal relevance to the hydraulic conductivity. Richards' equation, as often applied, accounts only for water flow, but in fact it should be written for both air and water flow; if water leaves a

A. Hunt et al., *Percolation Theory for Flow in Porous Media*,
Lecture Notes in Physics 880, DOI 10.1007/978-3-319-03771-4_7,

pore, air must enter it, and accessibility issues may hinder the air entrance more than the water departure. For example, in heap leaching of mined ore, it is important to be able to predict simultaneously the air and water flow. Similarly, the preferred locations of bacteria depend on their particular metabolism, but as a rule, bacterial colonies tend to be found along phase interfaces, particularly where air, water and solid phases are found together. Thus the growth characteristics of these colonies may depend sensitively on both air and water flow.

Unlike the electrical and hydraulic conductivities, the air permeability k_a as a function of the air-filled porosity ε is relatively simple to predict. Recall that if water and air are the only two fluids, they must occupy the entire void volume: $\varepsilon + \theta = \phi$. For an arbitrary fluid the permeability is obtained from the conductivity by multiplying by the kinematic viscosity. This adjustment allows direct comparison between permeabilities of different fluids, as long as (1) they wet the surface similarly, and (2) their critical volume fractions for percolation are the same.

We will wish to scale the air permeability to its value under perfectly dry conditions, $k_a(\varepsilon = \phi)$, similarly to the scaling of the (water) permeability to its value under conditions of complete saturation, $k_w(\theta = \phi)$. The latter should scale with saturation in the same fashion as the unsaturated hydraulic conductivity (Chap. 6). This brings up first the subject of whether $k_a(\varepsilon = \phi) = k_w(\theta = \phi)$. To the extent that the critical volume fraction for percolation (ε_t for air and θ_t for water) is independent of the fluid, the air permeability of a completely dry porous medium should equal the water permeability of the same medium when water saturated. However, this will not generally be true.

A key difference between air and water in soil is that water is a wetting fluid, while air is not. This difference is accentuated by clay minerals, which have high specific surface area, and whose surfaces are often electrostatically charged; both of these properties cause clay to adsorb water. A wetting fluid has a no-slip condition (zero velocity) at the solid surface, and the presence of the electrical double layer, with dissolved cations interacting with negative charges at the mineral surface, provides additional near-surface viscous drag. In contrast, a non-wetting fluid has some slip at the surface, such that the extrapolated point at which there would be no slip is actually below the solid surface [93]. Additionally, air being less dense than water decreases the molecular interactions. So while air and water appear to have similar permeabilities (after adjustment for viscosity) in coarse materials like sand, in finer and higher-surface area materials, the distinction between wetting and non-wetting fluid (and especially between water and air) becomes important.

It can be convenient to think of this contrast as effectively increasing the pore sizes for air, and reducing them for water, because this would have the effect of reducing r_c for water below that for air. And in fact, in high-clay soils we do observe that $\varepsilon_t < \theta_t$, while in low-clay soils water sorption can sometimes be neglected and we expect $\varepsilon_t \approx \theta_t$. In such cases ε_t, like θ_t, should be on the order of 0.1ϕ. Our analysis of nearly 40 soils below will be seen to be consistent with this proportionality *in the mean*, but it turns out not to be useful as a prediction.

Consider now the saturation dependence of the air permeability. Because water is the wetting fluid, at any intermediate water content $0 < \theta < \phi$ the water occupies

the smaller pores, while air occupies the larger. Consequently, adding water to a dry medium does not change the bottleneck radius r_c for air flow, even while it increases the r_c for water flow. This holds for all air-filled porosity values $\varepsilon \geq \varepsilon_t$. Because there are no *geometrical* effects via a bottleneck pore radius, permeability must be controlled by the *topological* effects. It is precisely these topological effects that are accounted for by universal percolation scaling, so air permeability $k_a(\varepsilon)$ must follow [44]

$$k_a(\varepsilon) \propto k_a|_{\varepsilon=\phi}(\varepsilon - \varepsilon_t)^{\mu} \tag{7.1}$$

over the entire range of air-filled porosity values. This result, like all percolation results, becomes approximate far from the percolation threshold because percolation theory is approximate far from the threshold, but clearly there is virtually no additional dependence related to the pore size distribution. The conclusion of Hazlett and Furr [37] is essentially equivalent to this result. Since we have shown that the pore size distribution is not relevant to the saturation-dependence of the air permeability, it should be obvious that non-universal scaling is not an issue here. However, we can add the following comment: approach to the threshold value of air-filled porosity for percolation does not correspond to an approach to zero conductance. Rather, this limit corresponds to a finite conductance, and there is no *a priori* reason to expect any singular behavior in the pore size distribution at a finite conductance. In other words, we do not expect such strong correlation between the structural constraints on the particles that organize the pore space with the energetic constraints on the fluids within the pore-space, which are a function of the interfacial tension and any electrostatic attraction to the solid boundary.

Equation (7.1) is clear in its implications for theory, but it is not useful for comparison with experiment. One would like to use the results for completely dry materials, as far as possible from the percolation threshold, to predict the behavior of media with the approach to the percolation threshold where measurements are more problematic. On the other hand, the exponent 2 is valid asymptotically in the approach to the percolation threshold, with any deviation from exact scaling increasing with distance from the threshold, meaning that the numerical prefactor ought best be fixed by comparisons near the percolation threshold. Thus the perspectives of utility and theory are opposite. But fortunately, proportionality (7.1) appears to give an accurate prediction in the majority of soils all the way from the threshold to completely dry conditions (as we show below). That means that one can write the more useful

$$k_a(\varepsilon) = k_a|_{\varepsilon=\phi}\left[\frac{\varepsilon - \varepsilon_t}{\phi - \varepsilon_t}\right]^{\mu} \tag{7.2}$$

with 3 parameters: porosity (which we generally know), the reference permeability for the dry medium $k_a(\varepsilon = \phi)$, and the threshold air content ε_t. The tricky part of this prediction problem is generating a value of ε_t without conducting experiments in air permeability, an issue we return to below.

As always we have the complication that for 2D systems the exponent μ should be 1.3, rather than 2.0 in 3D. For experiments which were essentially 2D in nature

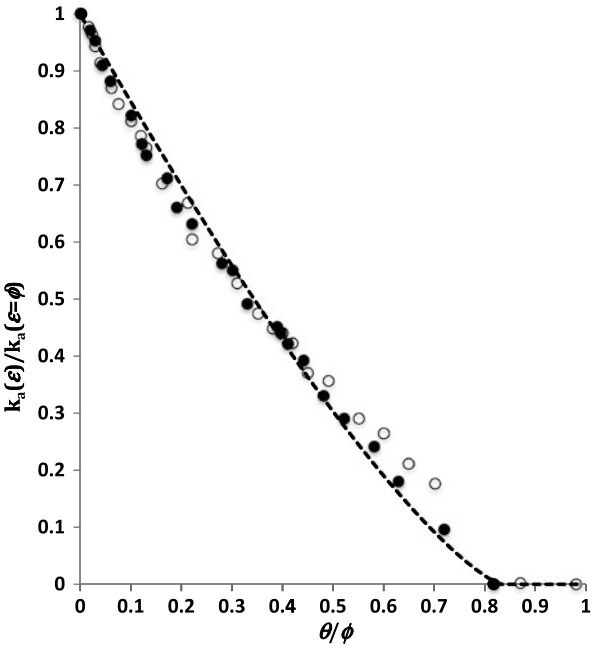

Fig. 7.1 Plots of the air-phase permeability as a function of wetting phase saturation. The *solid dots* are actual measurements with two phases present; the *open circles* are measurements of single phase flow. Data from Steriotis et al. [98]. The experimental conditions were appropriate for 2D flow. The exponent, m, was chosen to be 1.27 (not updated to 1.3). The theoretical prediction (*dashed curve*) from Eq. (7.1) uses one parameter, the critical air fraction for percolation, equal to 0.16. Only the *solid circles* represent a direct measurement; the *open circles* are from a proxy, which Steriotis et al. [98] wished to show were a reasonable approximation to the actual values

(the dimension transverse to flow smaller by a factor of ca. 1000 than the other two dimensions), Steriotis et al. [98] reported the non-wetting phase relative permeability shown in Fig. 7.1. These experimental results are compared with the prediction of Eq. (7.1), using the 2D value $\mu = 1.3$ [44]. This comparison required one adjustable parameter, $\varepsilon_t = 0.16\phi$.

Unsal et al. [106] present data for air permeability which compare well with universal scaling (Eq. (7.1)), as seen in Figs. 7.2 and 7.3. Interestingly, Unsal et al. [106] asserted that they could extract the pore-size distribution from their data, an assertion at odds with the strictly topological control of permeability given in Eq. (7.1).

Since examining Unsal's data, we have found nearly forty additional experimental datasets [8, 14, 20, 24, 96, 99, 104, 105], many of which are reproduced in Figs. 7.4–7.6. The characteristics of each medium are listed in Table 7.1. For each medium we sought an exponent near 2 by varying ε_t to maximize the correlation coefficient. As shown below, the values of ε_t we obtained could be predicted by analysis of the water retention curve (WRC). Figures 7.4 and 7.5 show that the R^2 values obtained in this procedure often exceeded 0.99, sometimes even 0.999. In

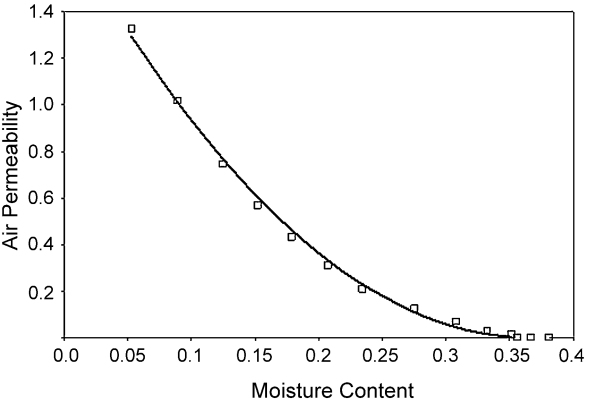

Fig. 7.2 Comparison of air permeability with universal percolation scaling (Eq. (7.1)). Data from Unsal et al. [106]

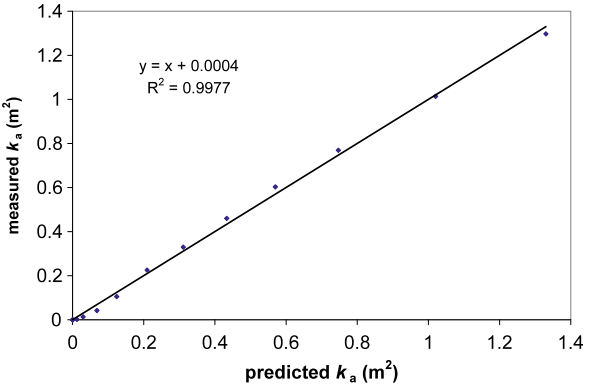

Fig. 7.3 Direct comparison of predicted and observed values of the air permeability (data from Fig. 7.2). Note that the slope is 1, $R^2 = 0.998$, and the value of the intercept is about 1/1000 of the typical permeability values

these cases the data had little noise, and covered most of the possible range of relative saturations without large gaps.

We also investigated a large dataset of Tang et al. [100], which contains some samples for which the data were incomplete (Fig. 7.6). In this second dataset, six materials yielded values of the exponent well under 2 (Table 7.2). We therefore examined whether there were correlations between the exponent obtained and the number of data points or the range of saturations tested. Smaller exponents were indeed correlated with datasets that covered a smaller range of porosity (Fig. 7.7), contained fewer measurements (Fig. 7.8), or had both drawbacks. In particular, no experiment that yielded an exponent less than 2 covered more than 40 % of the available saturation range. As can be seen, reducing the range of accessed porosity values to 40 % by dropping the data points at lower air contents (Fig. 7.9) can reduce the value of the extracted exponent from 2 to 1.63, a value similar to two of the individual results from [100].

After these individual comparisons we investigated the general applicability of Eq. (7.2) by normalizing both ordinate and abscissa. Excluding the Tang et al. [100] dataset yields an exponent of 2.03 ± 0.03, a proportionality constant of 0.96 and an R^2 value of 0.97 (Fig. 7.10). (An ideal result would be an exponent of 2,

Table 7.1 Air permeability measurement characteristics in dataset 1

Reference	Medium type	# Data points	Porosity	Exponent	ε_t	R^2	Condition
Collis-George [14]	Cambridge sand	31	0.380	2.042	0.050	0.991	Disturbed
Brooks & Corey [8]	Volcanic sand	8	0.351	2.073	0.019	0.997	Unconsolidated
Brooks & Corey [8]	Glass beads	12	0.370	2.001	0.001	0.971	Unconsolidated
Brooks & Corey [8]	Fine sand	14	0.377	2.064	0.012	0.987	Unconsolidated
Brooks & Corey [8]	Touchet silt loam	9	0.485	2.054	0.020	0.924	Unconsolidated
Brooks & Corey [8]	Fragmented mixture	6	0.443	2.054	0.019	0.999	Unconsolidated
Brooks & Corey [8]	Fragmented Fox Hill	11	0.470	2.056	0.013	0.996	Unconsolidated
Brooks & Corey [8]	Berea sandstone	14	0.206	1.995	0.063	0.974	Consolidated
Brooks & Corey [8]	Hygiene sandstone	10	0.250	2.006	0.014	0.998	Consolidated
Touma & Vauclin [104]	Grenoble sand	12	0.312	2.021	0.213	0.966	Disturbed
Stonestorm [99]	Oakley sand	10	0.314	2.006	0.110	0.997	Disturbed
Dury [24]	Mixed sand	13	0.285	2.016	0.130	0.986	Disturbed
Springer et al. [96]	Silty sand	9	0.431	2.055	0.045	0.908	Disturbed
Tuli & Hopmans [105]	Columbia sandy loam	17	0.427	2.000	0.074	0.925	Disturbed
Tuli & Hopmans [105]	Oso Flaco sand	21	0.407	1.999	0.010	0.908	Disturbed
Dane et al. [20]	Mixture sand	15	0.364	2.000	0.055	0.982	Disturbed
Average		13	0.367	2.028	0.053	0.969	
Standard deviation		6	0.078	0.028	0.057	0.033	

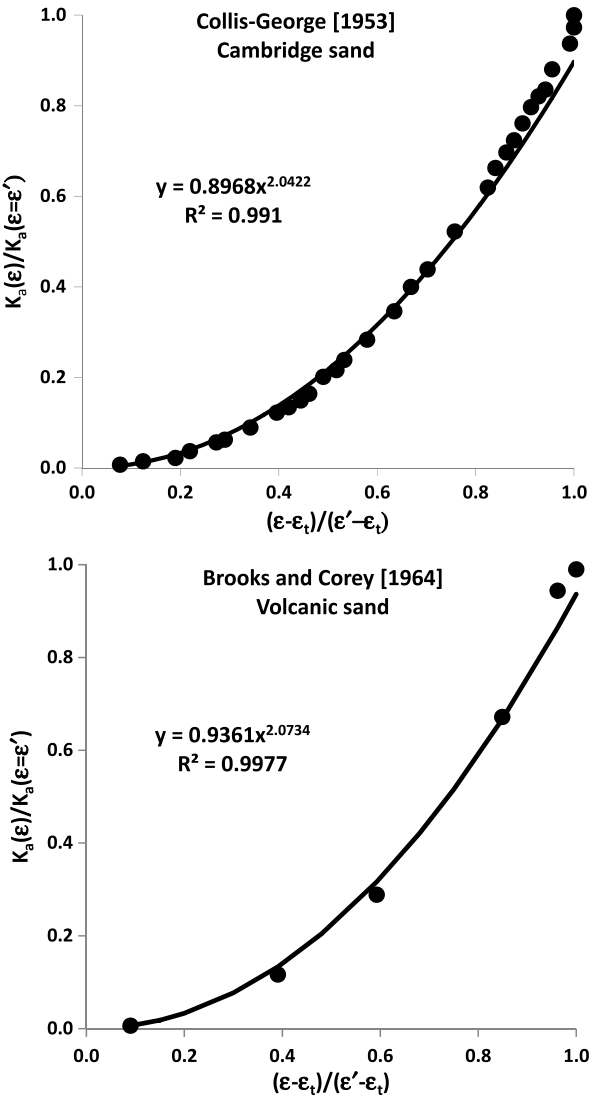

Fig. 7.4 Comparison of the normalized universal scaling of the air permeability with four classic data sets. The threshold ε_t was chosen to produce a power near 2 with a high value of R^2

and both proportionality constant and R^2 values equal to 1.) Treating the Tang et al. [100] dataset separately leads to the comparison in Fig. 7.11. If their six experiments with unexpectedly small values of the extracted exponent are dropped from consideration—a choice which might not be justified—the rest of the Tang dataset yields exactly the same relationship for the exponent as the remaining media, namely, 2.03 ± 0.03. It appears that the exponent $\mu = 2$ holds generally, and exceptions are due to incomplete data.

We return to the question of predicting ε_t. It should perhaps not be a surprise that the average value of ε_t was equal to 10 % of the average value of the porosity.

Fig. 7.4 (Continued)

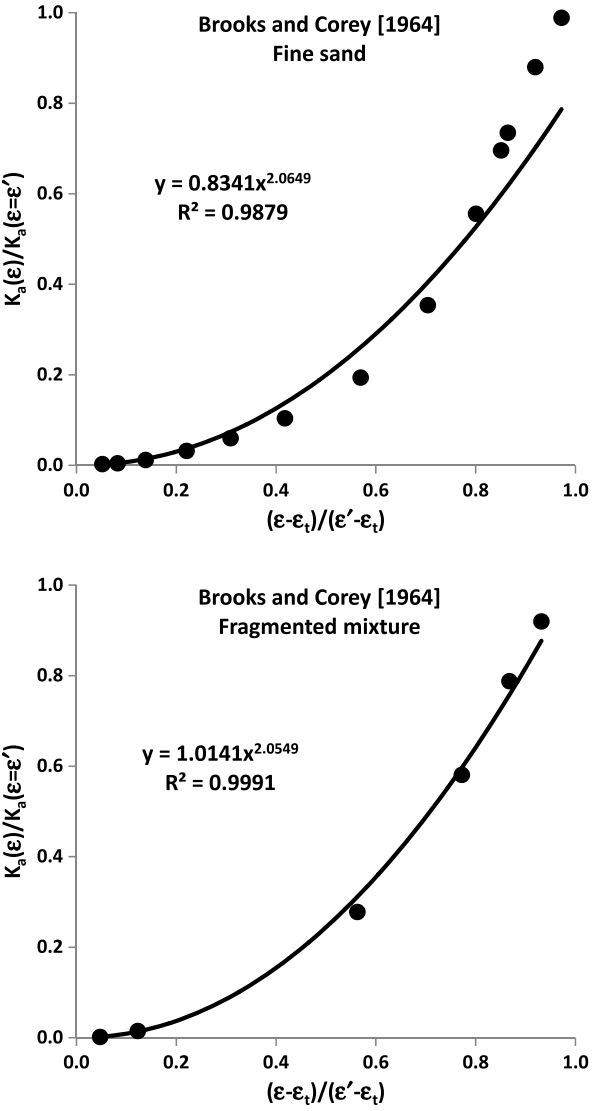

However, the variability of ε_t within the datasets could not usefully be predicted by this relationship. Values of ε_t were correlated with the air content at high moisture contents where the WRC deviated from fractal scaling, a result completely in accord with what is known about water retention curves (see Chap. 8).

We found a crossover point θ_i in which the slope of moisture content changes as shown in Fig. 7.12. At this crossover point, θ_i, air starts percolating into the porous medium. Subtracting this value from the moisture content at saturation ($\phi - \theta_i$) gives an estimate of the air-filled porosity threshold for percolation. Our results obtained from dataset 1 are given in Fig. 6.13. The *Touma and Vauclin* [104] data, whose

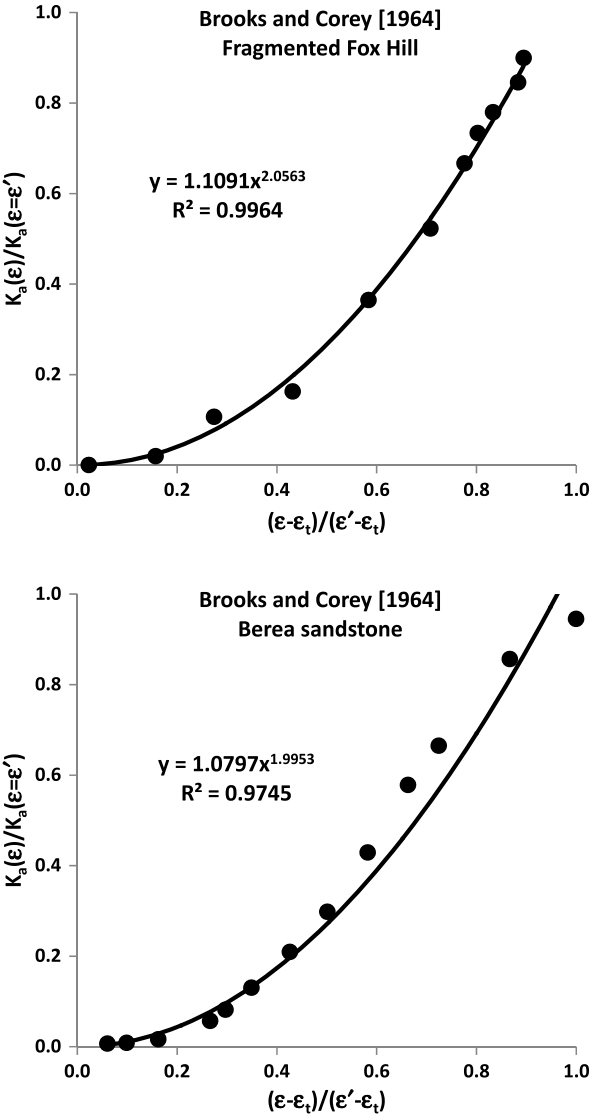

Fig. 7.5 Comparison of the normalized universal scaling of the air permeability with four additional datasets. The threshold ε_t was chosen to produce a power near 2 with a high value of R^2

ε_t value is almost 70 % of the porosity, was excluded from Fig. 6.13. The paired-samples t-test indicated that there is no significant difference ($p > 0.05$) between the ε_t values calculated from the measured air permeability data and those estimated as $\phi - \theta_i$ from the wet end of WRC. Unfortunately, accurate estimation of ε_t using the proposed approach requires accurate measurements of the WRC at the wet end, especially near saturation, so this method may not be reliable for small ε_t values (<0.035).

Fig. 7.5 (Continued)

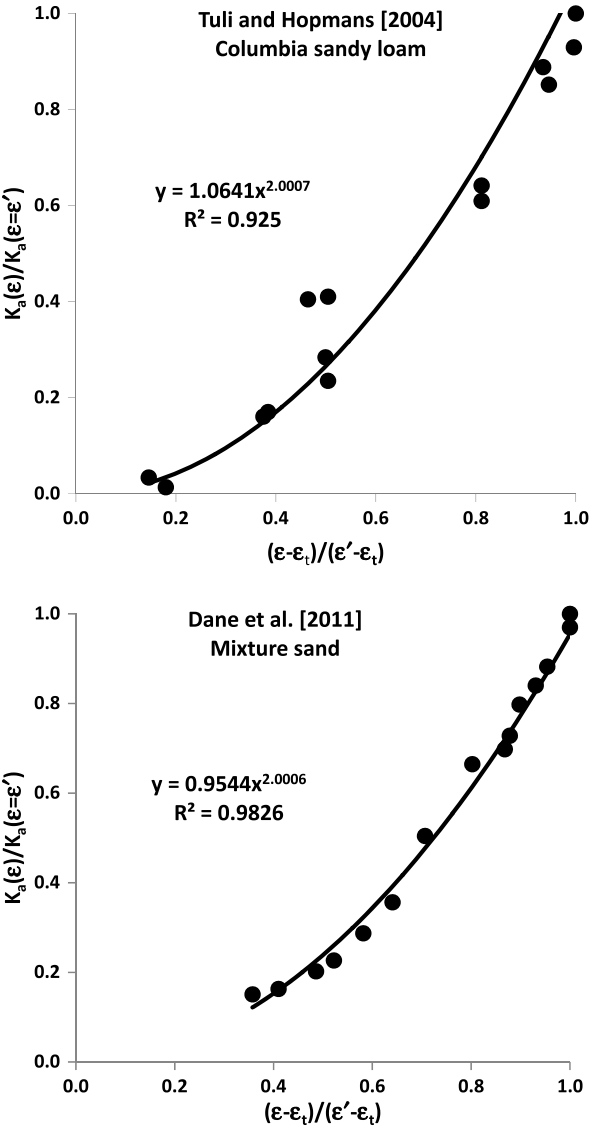

Although we could do a reasonably good job of predicting ε_t from the WRC, our skill at estimating this parameter was also small when its value was on the order of 10 % of the porosity or less (Fig. 7.13). This difficulty is likely traceable to the number of complications in the WRC at high moisture contents discussed in Chaps. 3 and 4, including edge effects (larger for small systems), and gravity (larger for tall systems).

Figures 7.14 and 7.15 present additional comparisons of theory and experiment. In Fig. 7.14 an ideal result would be $y = x$ with an R^2 of 1: the regression line

Table 7.2 Air permeability measurement characteristics in dataset 2

Reference	Soil type/ USDA textural class	# Data point	Porosity	Exponent	ε_t	R^2	Condition
K01 Tang et al. [100]	Epernay/ Clay	6	0.512	2.065	0.132	0.987	Undisturbed
K03 Tang et al. [100]	Epernay/ Clay	6	0.634	1.996	0.022	0.882	Remolded
K05 Tang et al. [100]	Epernay/ Clay	4	0.614	2.062	0.082	0.994	Remolded
K06 Tang et al. [100]	Epernay/ Clay	4	0.556	1.995	0.071	0.999	Remolded
K09 Tang et al. [100]	Epernay/ Clay	5	0.451	0.498	0	0.850	Remolded
K10 Tang et al. [100]	Epernay/ Clay	6	0.479	1.236	0	0.923	Remolded
K11 Tang et al. [100]	Le Breuil/ Sandy loam	7	0.531	2.008	0.0015	0.986	Undisturbed
K12 Tang et al. [100]	Epernay/ Clay	5	0.550	1.114	0	0.983	Undisturbed
K13 Tang et al. [100]	Avignon/ Silty clay loam	7	0.387	2.041	0.0255	0.993	Undisturbed
K14 Tang et al. [100]	Le Breuil/ Sandy loam	7	0.495	1.995	0.0075	0.984	Undisturbed
K15 Tang et al. [100]	Le Breuil/ Sandy loam	8	0.537	2.047	0.135	0.868	Undisturbed
K16 Tang et al. [100]	Avignon/ Silty clay loam	6	0.394	1.991	0.0038	0.972	Undisturbed
K17 Tang et al. [100]	Le Breuil/ Sandy loam	8	0.582	1.671	0	0.942	Remolded
K18 Tang et al. [100]	Le Breuil/ Sandy loam	8	0.522	1.997	0.059	0.960	Remolded
K19 Tang et al. [100]	Le Breuil/ Sandy loam	8	0.492	1.993	0.003	0.932	Remolded
K20 Tang et al. [100]	Le Breuil/ Sandy loam	8	0.582	2.005	0.040	0.955	Remolded
K21 Tang et al. [100]	Le Breuil/ Sandy loam	8	0.512	1.950	0	0.870	Remolded
K22 Tang et al. [100]	Le Breuil/ Sandy loam	8	0.482	1.471	0	0.880	Remolded
K23 Tang et al. [100]	Le Breuil/ Sandy loam	8	0.571	2.020	0.020	0.974	Remolded
K24 Tang et al. [100]	Le Breuil/ Sandy loam	8	0.507	1.564	0	0.965	Remolded
K25 Tang et al. [100]	Le Breuil/ Sandy loam	8	0.474	1.995	0.015	0.0964	Remolded
K26 Tang et al. [100]	Avignon/ Silty clay loam	5	0.429	2.006	0.0223	0.995	Undisturbed
K27 Tang et al. [100]	Avignon/ Silty clay loam	5	0.432	1.998	0.037	0.996	Undisturbed
Average		7	0.510	1.814	0.029	0.912	
Standard deviation		1	0.064	0.386	0.040	0.180	

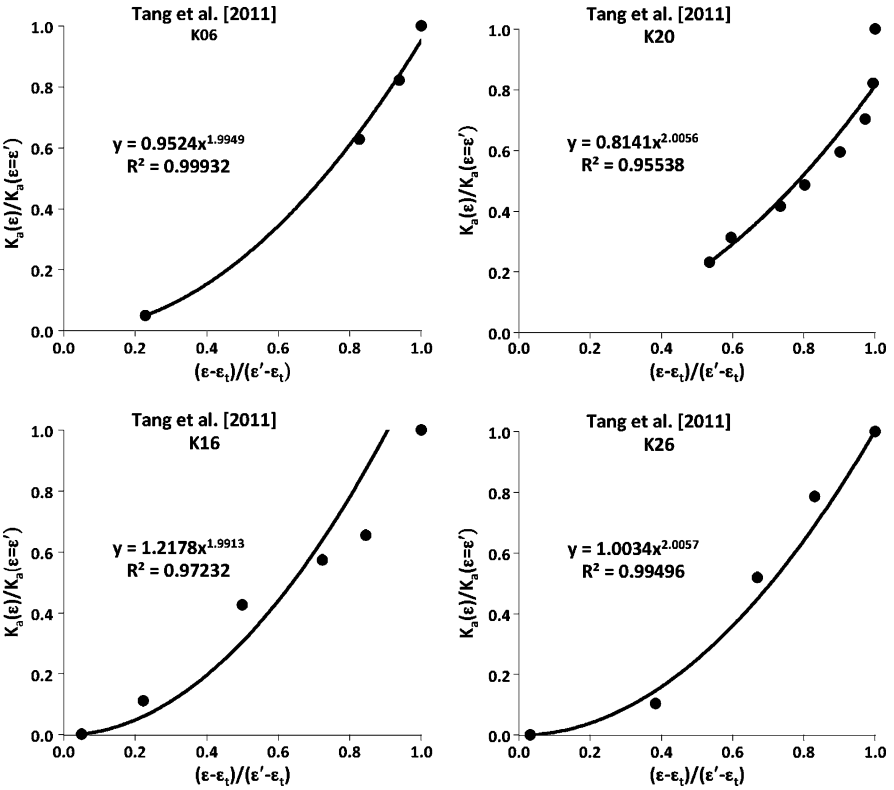

Fig. 7.6 Representative data from Tang et al. [100] compared with normalized form of universal scaling. Note the poorer coverage and greater fluctuations in the data than in Figs. 7.4 and 7.5

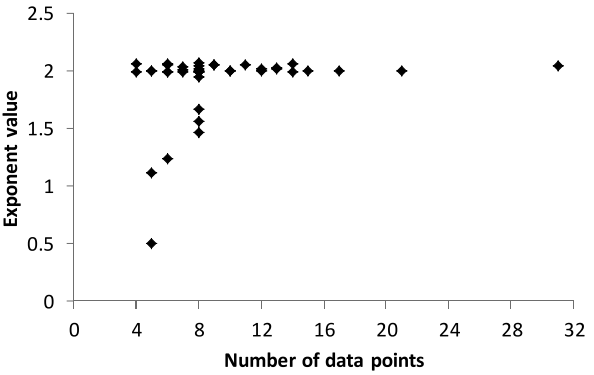

Fig. 7.7 Indication that for the Tang et al. [100] dataset that it was only in cases where the number of data points was relatively small that it was not possible to extract the universal power

should lie precisely on the 1:1 line. Our comparison yields $y = 0.95x + 0.04$, indicating a systematic discrepancy of less than 4 % over half the range of air permeability values, and an RMSE of 0.07, indicating a random error of about 7 %. The

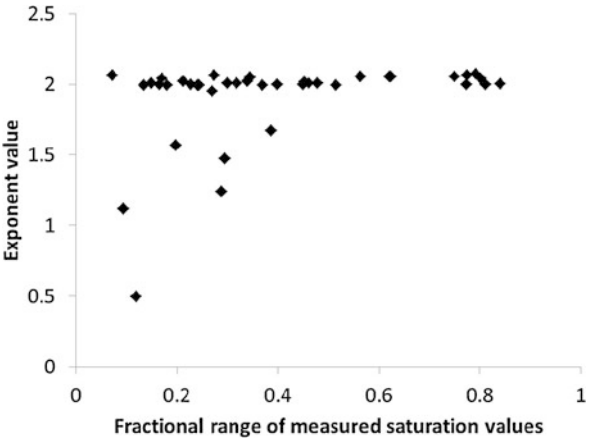

Fig. 7.8 Indication for the Tang et al. [100] data set that, only in cases where the measured range of saturation values was less than 40 % of the total accessible, was it not possible to match the universal exponent value of 2.0

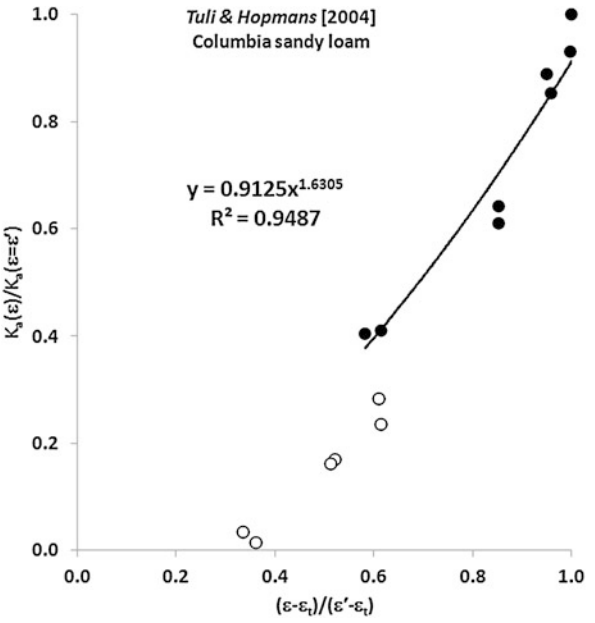

Fig. 7.9 Demonstration that failure to measure the six lowest saturations would also prevent detecting the universal behavior already found for the Columbia sandy loam, and generate (smaller) values of the exponent similar to those found in six soils of the Tang dataset

largest source of random error is probably experimental error, while the systematic bias presumably arises from our assumption that the percolation scaling results are accurate arbitrarily far from the threshold, at which moisture content our choice of normalization pins the theoretical value. That this is so can be easily seen by simply comparing the regression line with the 1:1 line and contrasting that discrepancy with the spread of data points around the two lines. Such a contrast indicates that, even under ideal experimental circumstances (dataset 1), the experimental uncertainty is likely greater than the error in theory. Our contention is therefore that appeal to experiments with (a) a restricted range of investigated saturations, or (b) measure-

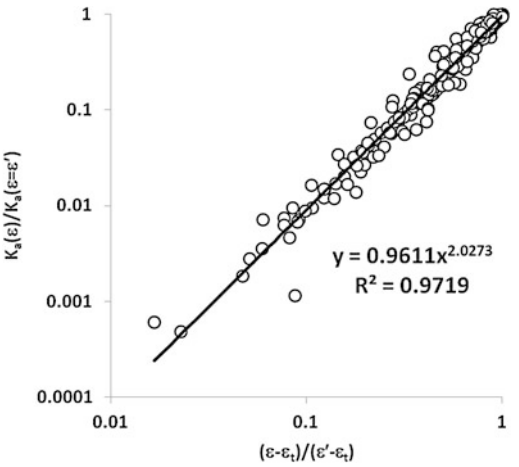

Fig. 7.10 Demonstration that all the data from the first dataset fit well to the normalized equation from universal scaling

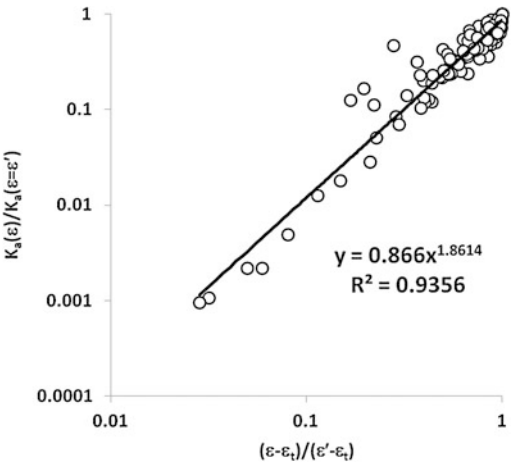

Fig. 7.11 Analogous plot for the Tang et al. [100] dataset. Although the predictive value of universal scaling appears lower in this data set, removal of the six samples discussed in the text (and considered in Figs. 7.7 and 7.8) would yield exactly the same result as in Fig. 7.10

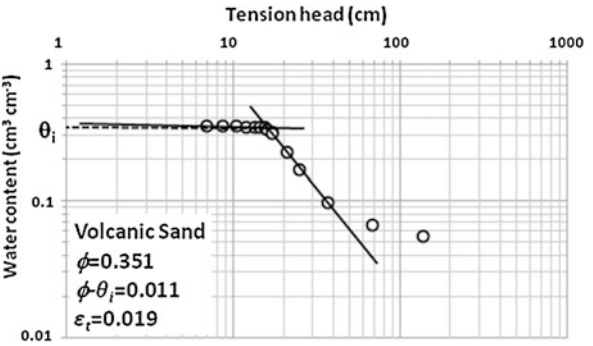

Fig. 7.12 Demonstration of the determination of ε_t from a soil water retention curve as the difference between the porosity and the moisture content at the intersection of the two lines in the construction

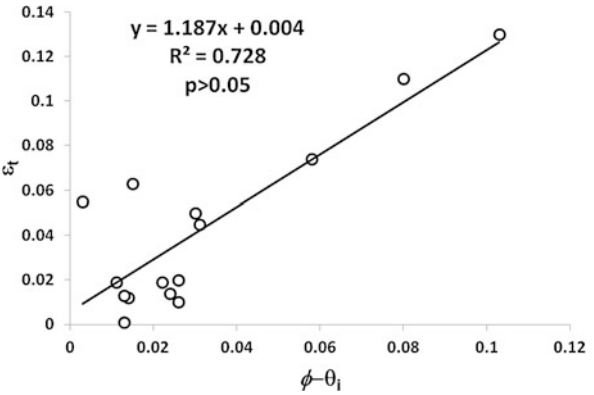

Fig. 7.13 Showing the correlation between ε_t as determined from the WRC and as determined by optimizing the fit to universal scaling

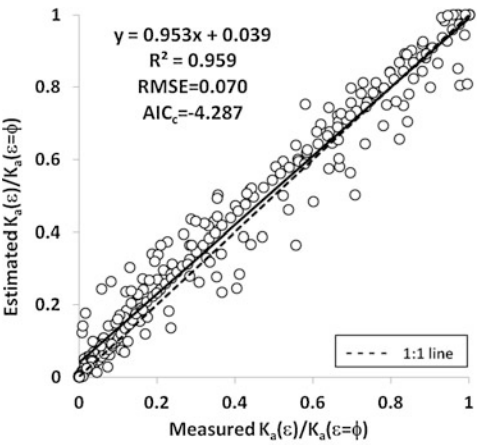

Fig. 7.14 Direct comparison of theoretical and experimental values for the normalized air permeability

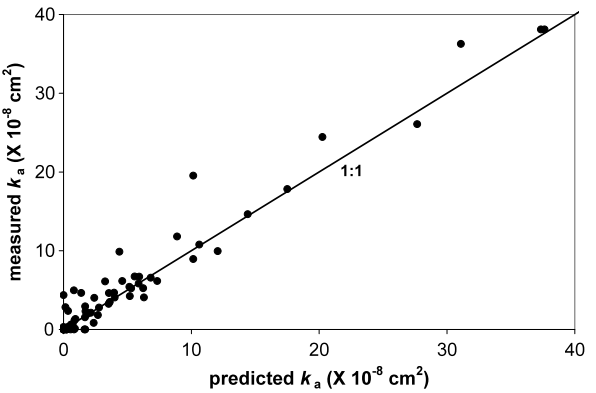

Fig. 7.15 Comparison of theoretical and experimental values of the air permeability

ments at saturation values that are too widely separated, will lead to worse estimates of the air permeability than could be obtained from a single measured value under dry conditions (provided the conditions of that single experiment are ideal), use of Eq. (7.2), and the water retention curve for estimating ε_t.

In conclusion, not only is there essentially no doubt that the air permeability is described by universal scaling from percolation theory, but furthermore the universal scaling, normalized to the air permeability under perfectly dry conditions, is such a good means to predict the air permeability that its accuracy may exceed that of the experiments themselves.

7.2 Thermal Conductivity

7.2.1 General Comments on the Saturation Dependence of Thermal Conductivity

The saturation dependence of thermal conductivity, $\lambda(\theta)$, is difficult to analyze within the context of percolation theory. First, all three phases in a typical unsaturated geological medium (water, air, solid) have non-zero thermal conductivities, though the thermal conductivity of air λ_a is typically sufficiently small to ignore. Second, the thermal conductivity of the water and solid phases is not a simple or universal ratio. The solid phase conductivity λ_s may be only half that of water, λ_w, (organic soils), or as much as 15 times greater (high quartz soil), with more typical ratios (5 to 10) depending on mineralogy; other ratios will obtain in artificial media. Third, the ratio of the thermal conductivity of a saturated soil to its value in the same soil when dry is typically less than 10. This implies that the kind of critical path analysis arguments that we have been employing, which can contain uncertainty regarding factors of 2 (in order to get tendencies of many orders of magnitude correct), will tend to contain too high a level of uncertainty. Also, because of the typically higher conductivity of the solid phase, even under dry conditions the medium is well above the percolation threshold. This introduces considerable uncertainty into percolation scaling arguments.

To summarize: even when the medium is dry it is well above the percolation threshold (which is never reached); when it is saturated, the volume fraction of conducting material is 1, as far from the percolation threshold as it is possible to get. This is the worst possible condition to handle with percolation theory! An additional complication arises from the physical arrangement of the solids. While water at all saturations tends to enhance the connectivity of the pathways, in granular media at fairly low saturations the most important effect of water is to enhance the conduction between adjacent grains. A simultaneous solution, rather than a separation, of all these problems is required because the total range of thermal conductivity values from dry conditions to saturation is seldom much more than an order of magnitude, mixing all these effects together. This places a high degree of importance on an accurate description of the geometry (a very difficult problem) for a property that

does not really exhibit a wide range of values. Under such conditions it is difficult to attack the problem logically and quantitatively. Our attempt here should be understood within the context of developing a unified picture of all conduction and transport properties in one place.

Theoretical Construction

We approach the problem from two opposite directions. First we look at geometrical influences under ideal conditions to make geometry dominant; then we look at percolation scaling under ideal conditions to make scaling simple. Then we combine the two approaches to see whether the resulting expression is compatible with experiment over all saturations and mineralogies, so as to include realistic non-ideal conditions.

Consider a medium composed of solid spheres. Ignoring deformation, contact between two spheres is simply a point, leading to an infinite contact resistance between each osculating pair. When water enters such a medium it tends to form pendular (ring) structures at the contact points. Because the pendular structures are much wider than they are long, for a small increase in water content one gains a large increase in conductivity [87]. The resulting conduction problem has never been solved analytically. However, for a cubic lattice of spheres with water occurring only in pendular rings, the conductivity is approximately [29]

$$\lambda(\theta) \approx \lambda|_{\theta=0} + a\theta^b \tag{7.3}$$

with $a \approx (\lambda_s/\lambda_w)^{3/2}$ and $b \approx 0.1 + 1.75(\lambda_w/\lambda_s)$. Commonly b appears to take on a value near $1/4$. This approximate power-law form of $\lambda(\theta)$, with a sublinear power at typical values of λ_s/λ_w, is consistent with measurements of $\lambda(\theta)$ in granular media at low water contents. The form of Eq. (7.3) also holds for deformed spheres with area rather than point contact [29], so the behavior (if not the actual value of the exponent) applies beyond perfect spheres in a cubic lattice. Equation (7.3) also holds, under some rather restrictive assumptions (needed for calculation), for spherical particles with a range of sizes, though the expressions for the parameters are not identical [29]. At higher water contents, as menisci coalesce and fill pores, resistance to heat flow is mainly due to air inclusions, probably well described by simplistic treatments of tortuosity. In the wet regime $\lambda(\theta)$ is often predicted by a simple linear mixing model.

We construct the following percolation theoretical argument for the thermal conductivity of natural porous media under the conditions that $\lambda_a = 0$, and $\lambda_w = \lambda_s$, and that geometrical effects of pendular structures can be ignored. Under such conditions, ignoring everything except the bulk fraction of the medium which is either solid or water, one can represent thermal conductivity via universal scaling as

$$\lambda(\theta) \propto (1 - \phi + \theta)^2 \tag{7.4}$$

Note that, even in the case $\phi \to 1$, the solid portion of the medium percolates by construction: any medium must be "grain-supported" or it would collapse, and the

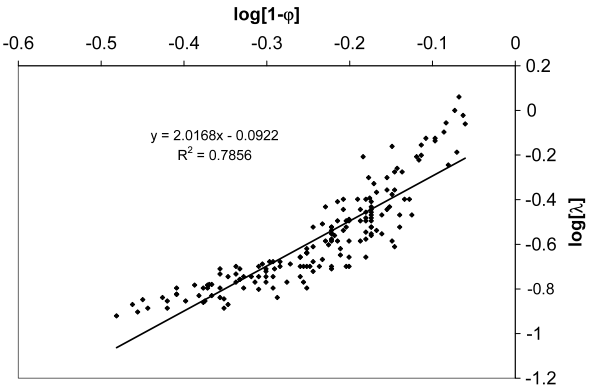

Fig. 7.16 Comparison of Eq. (7.4) for $\theta = 0$ (dry soils) with all the relevant data collected by Côté and Konrad [17]. While considerable curvature exists, the slope picked by Excel on a logarithmic plot is 2.017, less than 1 % different from the slope predicted

porosity would change. Thus there should be no need to include a critical solid fraction for percolation.

An expression such as Eq. (7.4) cannot be quantitatively accurate, because the percolation threshold is not approached even at $\theta = 0$. Further, in the limit $\theta \to \phi$ (effectively $p = p_c = 1$) it predicts $d(\log \lambda)/d(\log \theta) = 2$, instead of 1. On the other hand, Eq. (7.4) does reproduce an observed proportionality of the thermal conductivity of dry soils ($\theta = 0$) to a non-linear power of the density $(1 - \phi)^n$ [10], with Campbell [9] choosing $n = 2$. In fact, Campbell's result for the thermal conductivity of dry soils, considered by some to be predictive, is $\lambda = 0.03 + 0.7(1 - \phi)^2$, a relationship similar to Archie's law. To investigate further, we digitized 168 data points for thermal conductivity of dry rocks and soils from Côté and Konrad [17], and present $\log[\lambda]$ vs. $\log[1 - \phi]$ to investigate Eq. (7.4) in the limit $\theta \to 0$. The extracted power is 2.017, less than 1 % different from the predicted value, but considerable curvature exists (Fig. 7.16). Note that analysis of rocks separately leads to a larger slope (2.47) and soils separately to a smaller slope (1.43), while each of those individual graphs also contains noticeable curvature (not shown). Including 18 additional soil data points from Lu et al. [64] would make no visible change in the curvature, but would reduce the power to 1.98. Given that the thermal conductivity of dry soils and rocks is sensitive to the exact mineralogy, our preliminary comparison, lumping all types together, is suggestive but not conclusive.

By itself Eq. (7.4) bears little resemblance to experimental results for the saturation-dependence of the thermal conductivity. So we return to the approximate result (Eq. (7.3)) of Ewing and Horton [29] and the fact that it appears to have relevance also in media with a wider range of particle sizes. This allows an interpretation of Eq. (7.3) in terms of critical path analysis, namely that it generates the appropriate expression for the dependence of the critical (most highly resistive) pendular ring on a percolating path. If this is true, then we could postulate the following formula for the thermal conductivity,

$$\lambda(\theta) \propto (1 + \theta - \phi)^2 (a + c\theta)^{1/4} \tag{7.5}$$

which includes simultaneously effects of the saturation dependence of the topology of the connected network (the first factor) and the resistance of the most resistive

elements (the second factor). These factors affect the thermal conductivity simultaneously (think back on the elementary physics formula, $R = \rho l/A$, discussed in the Chap. 5) and thus should appear in a product. Of course in the limit $\theta \to \phi$, topology and percolation scaling no longer have a significant effect and the contribution from Eq. (7.4) should be replaced by a function that asymptotically approaches a constant value. Further, the resistance of the critical conductance only begins to fall after a volume of water roughly equal to the surface film contribution to θ_t (see Chap. 6) has been adsorbed. Finally, at higher saturations menisci start to coalesce, water fills pores, and the pendular rings cease to grow as individual structures [29]. Thus, c in Eq. (7.5) must be zero for very small saturations and jump to a geometrically dependent non-zero value at some saturation. At the moisture content at which pendular structures cease to grow, the term $c\theta^{1/4}$ should remain constant. Finally, note that, according to the interpretation, the term a in Eq. (7.5) ultimately represents the contact area in the absence of water. Together, this generates four parameters.

In the context of this book, Eq. (7.5) is rather disappointing: it has more parameters and less simplicity than corresponding equations for the hydraulic and electrical conductivities! Further, as we will see, it only describes data for the thermal conductivity up to a fairly low water content; at higher saturations Eq. (7.5) uniformly overestimates λ; seriously so in the case of sandy soils. The reason for this is, of course, that the topological description near the percolation threshold cannot hold in the vicinity of $p = 1$. Once the correlation length diminishes to a typical grain spacing, it cannot diminish further, and the conductivity cannot rise further, although Eq. (7.5) does describe *almost* the entire saturation dependence of λ for some clay-rich soils (Fig. 7.17a). So, from an analytical perspective, one would simply have to stop at Eq. (7.5), and ignore more saturated conditions. Such a course, however, is not satisfying.

It turns out that a small modification of Eq. (7.5) makes it perform well over the entire range of saturations for all soils investigated. These include thermal conductivity data of Lu et al. [64], and the saturation-dependent phenomenology of Campbell [6], for which the dry limit was mentioned below Eq. (7.4). The latter, being an empirical prediction, represents a smoothing of experimental error and may not be as reliable a comparison, though it simultaneously implies a much wider relevance of the present results. The specific modification of Eq. (7.5) is to reduce the power of the factor $(1 - \phi + \theta)$ from 2 to 1, making it a linear function. This modification should not be applied over the entire range of saturations; moreover it would ruin the approximate correlation of the thermal conductivity under purely dry conditions with the square of the density. However, as noted in Chap. 2, precisely this function should be adopted at values of $p > 0.8$, which in Fig. 7.17b, occurs at $\theta = 0.25$, but in Fig. 7.17a occurs at moisture contents between 0.2 and 0.28.

Perhaps because of the dominant role of pendular structures over most of the range where the quadratic result would be preferred, the linear result describes the thermal conductivity well (Fig. 7.17b) over the entire range of moisture contents, and the fitted parameters are as physically meaningful as those extracted from a comparison with Eq. (7.5) (Table 7.3). The one exception is the total amount of water in pendular structures, which should not exceed 10 % of the porosity. But

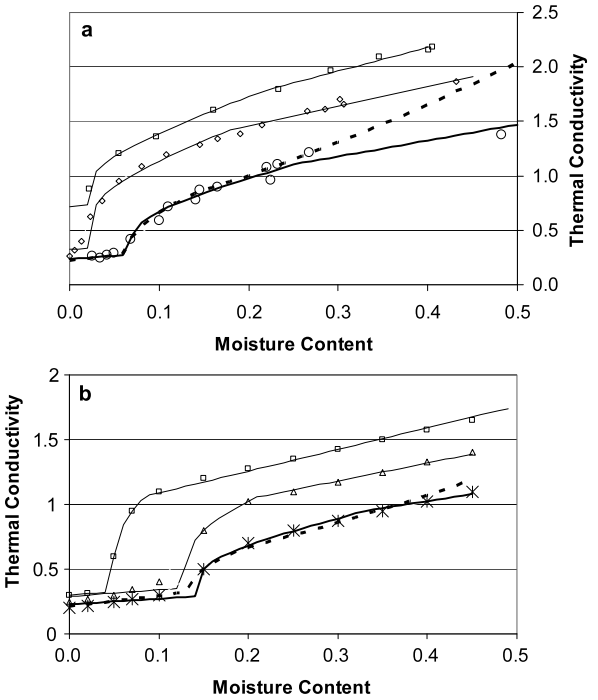

Fig. 7.17 (**a**) Comparison of experimental data for the thermal conductivity from Lu et al. [64], with predictions from Eq. (7.5) and its modification. Experimental data are the various symbols, while Eq. (7.5) is the *dashed line*, and Eq. (7.5) with a substitution of the linear power is represented by the *solid lines*. Note that in the particular soil with contrasting theoretical expressions, the superiority of the linear model is confined to a single data point, but typically the divergence between experiment and Eq. (7.4) becomes clear for data above $\theta = 0.25$, or even $\theta = 0.2$. Soils with higher thermal conductivity have higher sand contents. (**b**) Comparison of phenomenological data (equation from Campbell plotted by Bristow) with theoretical predictions from Eq. (7.5) and its modification. Different symbols were chosen for different soil types: *squares* for a sand, *triangles* for a silt loam and *crosses* for a clay loam. Again the discrepancy between experiment and Eq. (7.5) is smallest in the finest soil and it is this case that is compared with both Eq. (7.5) (*dashed line*) and the modification with a linear power (*solid line*). In the other two cases, Eq. (7.5) would become inaccurate already by $\theta = 0.20$ and $\theta = 0.35$, respectively

when we use the linear dependence, we may find fitted values giving, up to 40 % of the porosity occupied by pendular structures. However, this may not be as serious as it seems; the 1/4 power factor from the pendular structures rises very rapidly at first and more slowly at higher moisture contents, making its contribution nearly constant. That is, the fit is not very sensitive to the value of θ chosen at which the pendular structures no longer increase in size, so one can impose a physically sensible ceiling with minimal loss of agreement with experiment. In other cases the ratios of the parameters are consistent and not too different from Eq. (7.5) (Table 7.3). The threshold water fraction is likely largely stored in films. The sum of the threshold water fraction and the amount in pendular structures is 0.09 (silty clay loam) and

Table 7.3 Thermal conductivity parameters and statistical quantities

	cl (Bristow)	sl (Bristow)	sand (Bristow)	scl (Lu)	sl (Lu)	sand (Lu)
Equation (7.5)						
Dry soil conductivity	0.21	0.25	0.3	0.25	0.221	
Pendular contribution	0.305	0.5	1.02	0.42	0.56	
Threshold	0.14	0.12	0.04	0.06	0.068	
Pendular water fraction	0.06	0.07	0.03	0.03	0.07	
Slope	1.1	1.19	1.5	1.2	1.19	
Intercept	−0.03	−0.09	−0.27	−0.12	−0.09	
R^2	0.993	0.97	0.92	0.91	0.924	
Modified Eq. (7.5)						
Dry soil conductivity	0.13	0.16	0.16	0.144	0.12	0.43
Pendular contribution	0.3	0.49	0.79	0.29	0.38	0.54
Threshold	0.14	0.13	0.049	0.11	0.068	0.02
Pendular water fraction	0.19	0.077	0.036	0.18	0.18	0.2
Slope	0.994	0.992	1.007	0.998	0.988	0.998
Intercept	0.004	0.007	−0.009	0	0.008	0.004
R^2	0.997	0.997	0.999	0.989	0.985	0.998
Ratio linear/quadratic						
Dry soil conductivity	0.61904762	0.64	0.533333333	0.576	0.542986	
Pendular contribution	0.98360656	0.98	0.774509804	0.6904762	0.678571	
Threshold	1	1.0833333	1.225	1.8333333	1	
Pendular water fraction	3.16666667	1.1	1.2	6	2.571429	

Abbreviations: cl = clay loam, sl = silt loam, scl = silty clay loam

0.14 (silt loam) in the fits of the data of Ren using Eq. (7.5). These values are similar to the critical volume fraction, 0.11, in a Hanford Site silt loam, and to thresholds for diffusion in Moldrup's silt loams, 0.12 [73]. The linear fit leads to 0.29 and 0.25 for the water fractions of the silty clay loam and the silt loam, respectively. These values are upwards of 50 % of the porosity. Statistical comparisons always favor the linear version of the topological factor, because the quadratic version overestimates λ as saturation is approached. However, conceptually we should imagine a crossover from a quadratic dependence for $1 - \phi + \theta < 0.8$ to a linear dependence near saturation.

The theoretical objection is that using a linear power of the percolation argument makes that factor similar to a mixing model result. Mixing models derive ultimately from effects of volume averaging in heterogeneous media for which distinct constituents have differing conductivities. But we are already isolating the chief effect of the saturation dependence of the individual conductances when we concentrate on the effects of the critical pendular structures. We may multiply a topological effect on conductivity by a geometrical effect (Eq. (7.5)), as long as the two are independent. But the product of two geometrical effects could only make sense in a one-dimensional system where conductances add reciprocally. We conclude that so much of the regime of interest in the thermal conductivity is so far from the percolation threshold that the asymptotic results from percolation theory cannot be applied. Still, speaking practically rather than theoretically, the effective power of the percolation argument drops from 2 towards zero as $p = 1$ is approached, and using an effective $\mu = 1$ over the whole range of saturations give fair results.

If we consider thermal conductivity only in dry soils, we note a similarity to the electrical conductivity of saturated soils (main contribution from fluid phase): both appear proportional to the square of the relevant volume fraction. While Eq. (7.5) is much less accurate than corresponding equations for the electrical conductivity in terms of saturation (Chap. 6), in order to generate the corresponding property dependence under dry conditions, it must be evaluated in a limit that is as close to the percolation threshold as it is possible to reach, and under conditions that make its chief defects negligible. Equation (6.22) for the electrical conductivity, on the other hand, while much more accurate, must be evaluated at the limit furthest from the percolation threshold (Eq. (6.28)), and these two cases appear to have similar uncertainties.

To summarize: the percolation scaling result (Eq. (7.4)) requires a near coincidence of solid and wetting phase conductivities, it can only be extended to wet conditions by using an effective-medium result, and it neglects effects of pendular structures. Meanwhile, the sublinear power result (Eq. (7.2)) requires solid particles that can be represented as (intact or deformed) spheres. So there appears to be no simple and general analysis of the thermal conductivity that would be useful for prediction. In the 2nd edition of this book we were not hopeful about finding a straightforward conceptual resolution of the problems presented here. Now, however, it appears that the problem has a conceptual basis for understanding, and simply awaits further quantitative analysis before we can consider it fully understood.

It turns out that a very small modification of Eq. (7.5) makes it perform very well indeed over the entire range of saturations for all soils investigated. These

include thermal conductivity data of Lu et al. [64], and the saturation-dependent phenomenology of Campbell [6], for which the dry limit was mentioned below Eq. (7.4). It should be noted that the latter represents a smoothing of experimental error, and may not be as reliable a comparison, though it simultaneously implies a much wider relevance of the present results. The specific modification of Eq. (7.5) is to reduce the power of the factor $(1 - \phi + \theta)$ from 2 to 1 (making it a linear function). This modification should not really be applied over the entire range of saturations; moreover it would ruin the approximate correlation of the thermal conductivity under purely dry conditions with the square of the density. However, as noted in Chap. 2, precisely this function should be adopted at values of $p > 0.8$, which, in Fig. 7.17b, occurs at $\theta = 0.25$, but in Fig. 7.17a occurs at moisture contents between 0.2 and 0.28. In fact, probably because of the dominant role of the pendular structures over most of the range where the quadratic result would be preferred, the linear result describes the thermal conductivity well (Fig. 7.17b) over the entire range of moisture contents, and the parameters extracted mostly make as much sense as those extracted from a comparison with Eq. (7.5) (Table 7.3). The one exception is the total amount of water in pendular structures which typically yields about 10 % of the porosity or less. But in the case that the quadratic dependence is replaced by the linear dependence, this parameter on some occasions takes on much larger values, up to 40 % of the porosity. However, this may not be as serious as it seems; the $1/4$ power factor from the pendular structures rises very rapidly at first and more slowly at higher moisture contents, making its contribution nearly constant. Thus the fit does not depend sensitively on the value of θ chosen at which the pendular structures no longer increase in size, making it possible to decrease the agreement with experiment rather minimally at the cost of a significant decrease in pendular water. In other cases the ratios of the parameters are consistent and not too different from Eq. (7.5) (Table 7.3). The threshold water fraction is likely largely stored in films. The sum of the threshold water fraction and the amount in pendular structures is 0.09 (silty clay loam) and 0.14 (silt loam) in the fits of the data of Ren using Eq. (7.5). These values are similar to the critical volume fraction, 0.11, in a silt loam in the Hanford site as well as to characteristic values for the threshold for diffusion in silt loams of 0.12 [73]. The linear fit leads to 0.29 and 0.25 for the water fractions of the silty clay loam and the silt loam, respectively. These values are upwards of 50 % of the porosity. Statistical comparisons always favor the linear version of the topological factor, because the quadratic version overestimates λ as saturation is approached. However, conceptually we should imagine a crossover from a quadratic dependence for $1 - \phi + \theta < 0.8$ to a linear dependence near saturation.

Since the percolation scaling result (Eq. (7.4)) assumes a near coincidence of solid and wetting phase conductivities, can only be extended to saturated conditions by using an effective-medium result, and neglects possible effects of pendular structures, while reliability of the sublinear power result (Eq. (7.5)) requires existence of particles that can at least be represented as deformed spheres, we originally (in the second edition of this book) were not particularly hopeful about finding a relatively straightforward conceptual resolution of the problems presented here. Now,

however, it looks as though the problem has at least a firm conceptual basis for understanding, and is, at most, awaiting some advances in quantitative analysis before we can consider it fully understood.

7.3 Solute and Gas Diffusion

This section is greatly altered from earlier editions. Previously we stated that data from solute and gas diffusion did not obey the precise forms of the percolation formulations in Chap. 2. Since then we have expanded the discussion in Chap. 2 along the lines of Havlin and ben-Avraham [35], and analyzed much more data. The result is that it appears that the predicted universal scaling is generally observed, although we cannot simply ignore the data originally presented.

Our earlier theoretical discussion was largely based on numerical simulations of Ewing and Horton [28], plus some unpublished simulations. These simulations were organized according to the practices in soil physics. A simple cubic network model was employed, and saturated conditions with a variable pore connectivity assumed. Pruning (cutting) bonds reduced the porosity. The diffusion coefficient was found through particle tracking: random walkers were released on one side of a system of linear dimension x, and removed upon arrival at the other side, with their time of passage recorded. For any given porosity the effective diffusion coefficient was measured as a function of length, and finite-size scaling techniques were then applied to find the dependence on porosity. The authors expressed the diffusion coefficient D_{pm} of an inert conservative solute in the porous medium in terms of its value D_{w} in water:

$$\frac{D_{\mathrm{pm}}}{D_{\mathrm{w}}\phi} \equiv \Gamma^{-1} \tag{7.6}$$

and used the simulations to evaluate the quotient Γ^{-1}, known in the porous media community as the tortuosity. The authors found that this tortuosity had length dependence

$$\Gamma \propto x^{1.11} \tag{7.7}$$

Hunt and Ewing [45] then used the physical arguments from Sect. 2.4 to deduce that

$$\Gamma \propto (p - p_{\mathrm{c}})^{-1.11\nu}, \tag{7.8}$$

the result that would obtain from finite-size scaling. For continuum percolation problems which use moisture content θ rather than p as the fundamental variable, make the substitution $(p - p_{\mathrm{c}}) \rightarrow (\theta - \theta_{\mathrm{t}})$.

Consider the factor ϕ in the denominator of the left-hand side of Eq. (7.6). Hunt and Ewing [45] argued that, for unsaturated problems, ϕ should be replaced by θ. With these substitutions, one has

$$\frac{D_{\mathrm{pm}}}{D_{\mathrm{w}}} = \theta(\theta - \theta_{\mathrm{t}})^{0.98} \tag{7.9}$$

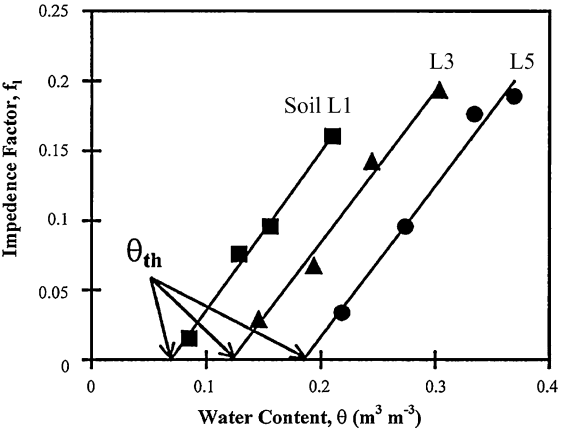

Fig. 7.18 Reprinted with permission from Moldrup et al. [73]. The ratio $D_{pm}/D_w\theta$ is plotted as a function of moisture content. Note from the experimental results for different soils that this ratio gives parallel lines of slope 1; the intercepts yield the critical moisture content for percolation, θ_t

This equation was also reported by Moldrup et al. [73] (Fig. 7.18), except that the reported power was 1 instead of 0.98, and a numerical prefactor of 1.1 was given. Note that what Ewing and Horton [28] called tortuosity is called "impedance factor" by Moldrup et al. [73], in which paper Fig. 7.18 first appeared. Because the values of θ_t (the threshold moisture content) obtained from the fit to Eq. (7.9) had a systematic dependence on the soil's specific surface area, and because that dependence could be understood in terms of the presence of water films (see Chap. 8), we leant greater credence to this analysis than it deserved. It was noted in previous editions that such a conclusion does lead to problems in the details of understanding the processes of solute and gas diffusion vis-à-vis electrical conduction. However, it turns out that Eq. (7.9) is, under typical conditions, virtually indistinguishable from the most useful form of a percolation prediction; this means that we can change our perspective without losing the specific advantages of the previous analyses.

Universal scaling of the diffusion constant can be written in the following forms, depending on whether solutes in water, or gases in air are considered:

$$\frac{D_{pm}}{D_w} = \left[\frac{\theta - \theta_t}{1 - \theta_t}\right]^{\mu} \quad \text{or} \quad \frac{D_{pm}}{D_g} = \left[\frac{\varepsilon - \varepsilon_t}{1 - \varepsilon_t}\right]^{\mu} \tag{7.10}$$

This particular normalization is chosen because it forces compatibility of the right-hand side of the equation with the left-hand side in the limit $\phi \to 1, \theta \to \phi, (\varepsilon \to \phi)$, for which the diffusion constant is measured relative to a medium that has no solid volume fraction neglecting the cross-over to linear behavior of effective-medium theory. The advantage of using this normalization is that knowledge of a single system-specific parameter (θ_t or ε_t), plus a single measurement at the wet (or dry) end, allows prediction of the relevant diffusion constant over the entire range of saturations.

Now compare Eq. (7.10) with form of Eq. (7.9) appropriate for solute diffusion. When the threshold moisture content is 10 % of the porosity (as is frequently the case) and for a typical value of the porosity ($\phi = 0.4$), Eq. (7.10) reduces to

$$\frac{D_{pm}}{D_w} = 1.09\theta\left(\theta - \theta_t'\right) + 0.0017$$

provided the given substitutions are made only in the normalization constant and in the term θ_t^2. $\theta_t' = 2\theta_t$ here should be understood to have the numerical value of θ_t in Eq. (7.9), but to equal twice the actual threshold moisture content. Moldrup et al. [73] reported θ_t' values as high as 0.24, so dividing them by 2 gives much more reasonable values. Since the numerical prefactor differs only by 1 % from the experimental phenomenology (Eq. (7.9) with prefactor 1.1), and the additive constant is close to zero, we can see that the Moldrup equation (our Eq. (7.9)) expresses to a very good approximation the result from universal scaling. Reanalysis of the data in Fig. 7.18 would show that it is consistent with Eq. (7.10) as well. The apparent threshold moisture content would still have the same dependence on specific surface area as the published result, but its numerical prefactor would be reduced by a factor 2.

When we examine data for gas diffusion, we find that they also follow universal scaling. As noted in Chap. 2, universal scaling of the diffusion constant is expected in finite-sized systems, for which restriction of the diffusing solute (gas) to the infinite cluster of water-filled (air-filled) pores is not required. Because Eq. (7.9) is so close to universal scaling, and because the gas diffusion appears to follow universal scaling, we argue that the better choice for solute diffusion is likely also to be universal scaling. For this reason it was necessary to change our presentation of diffusion properties in porous media.

Several experiments [11, 12, 15, 16] are summarized in Fig. 7.19, taken from Hu et al. [39]. Obviously for $\theta \gg \theta_t$, Eq. (7.9) and universal scaling (Eq. (7.10)) both approach $D_{pm}/D_w \approx \theta^2$. Additionally, some data sets diminish much more rapidly than θ^2 at small values of θ, consistent with either the critical behavior of Eq. (7.8) or universal scaling near θ_t. Figure 7.20 shows a set of data reported in Hu and Wang [38], most of which are compatible with the θ^2 behavior, although the "silica sand" shows clear evidence of a finite threshold. The "crushed tuff duplicate," on the other hand, suggests an approach to a non-zero background diffusion constant, which might represent the ability of solute diffusion through water films to give an alternate diffusion mechanism. These data do not show evidence of a non-zero θ_t, but are clearly consistent with θ^2 as the dependence on the moisture content. Figure 7.21 (which includes data from Hu and Wang [38] not published in Fig. 7.20, but appearing in Fig. 7.19) allows a simple power-law fit of the data from nearly 50 years of experiments including 606 individual measurements [2, 3, 11, 15, 16, 34, 50, 54, 66, 80, 81, 85, 86, 88, 89, 91, 94, 108]. The fitted exponent of 1.97 compares well with the universal scaling value of 2. Seven individual measurements showed evidence of a finite threshold with significant deviations below the regression, but these data had little effect on the regression.

In the case of gas diffusion, previous editions of this book had reference only to the data of Werner et al. [109], who analyzed 81 published measurements of gas-phase diffusion, both *in situ* and in laboratory measurements, for which the air filled porosity and the total porosity were available. The data were compared with several formulations in the literature, including Millington and Quirk [68], Currie [19], Sallam et al. [90], and Moldrup et al. [71], using standard RMSE. Werner et al. [109] stated, "The Moldrup relationship, $D_{pm}/D_g = \varepsilon^{2.5}/\phi$, originally proposed

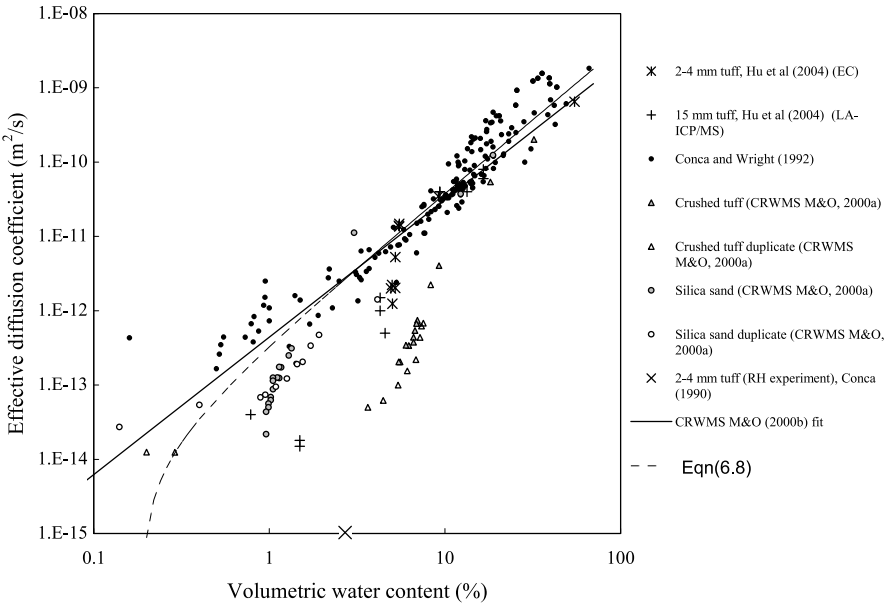

Fig. 7.19 After Hu et al. [39]. The first two data sets are from that work. Note that several of the data sets drop rapidly between 1 % and 10 % saturation, consistent with a critical saturation in that range of values. For large θ, Eq. (6.8) (now Eq. (7.10)) yields the asymptotic limit $\theta^{1.98} \approx \theta^2$. The CRWMS fit has a slope of 1.9. CRWMS refers to Civilian Radioactive Waste Management Systems

for sieved and repacked soils, gave the best predictions of several porosity-based relationships, but the relative deviation between observed and predicted D_{pm} can be substantial." In previous editions we adapted Eq. (7.9) to generate a similar result to "the Moldrup relationship." We now believe that Eq. (7.9) was the incorrect starting point and that universal scaling, including a threshold air content, is appropriate. In that case it is logical to assume that the fundamental information missing in this data set is ε_{t}, and that knowledge of the variability of ε_{t} would allow a much more accurate prediction of D_{pm}. Omitting the threshold tends to raise the value of the fitted exponent, because the increase in slope with the approach to the threshold air content is interpreted as a larger power. The conclusions of Werner et al. [109] therefore cannot be used to exclude the relevance of universal percolation.

More importantly, we now have analyzed the following data sets from publications of the Moldrup group, Moldrup et al. [71, 72, 74–78], which include roughly a factor 10 more data points than Werner et al. [109]. We analyzed these data in exactly the same way as with the air permeability (e.g., Fig. 7.10). In particular, we tested the validity of Eq. (6.9) by seeking a value of the critical air fraction for percolation which generated a high quality fit with a power near 2. Eight of the better fits to Eq. (7.10) are shown in Fig. 7.22. Here the ideal result would of course be $y = x^2$ with an R^2 of 1. Many of the individual data sets come very close to this result. In fact, that so many individual experiments yield a numerical prefactor

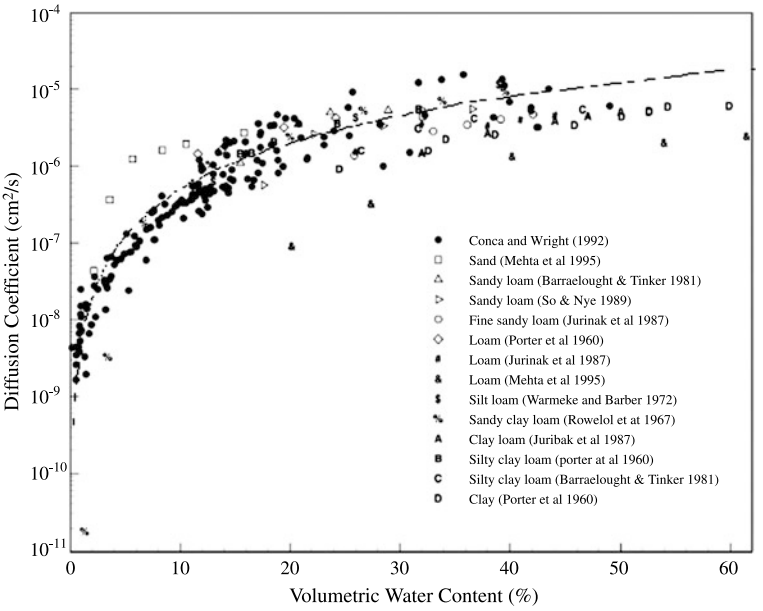

Fig. 7.20 After Hu and Wang [38]. Here the comparison with Eq. (7.9) (the *dashed line*) is given under the assumption that $\theta_t = 0$, which makes the predictions from Eq. (7.9) virtually indistinguishable from those of Eq. (7.10)

so close to 1, is remarkable, as once again we would not have expected such close agreement with percolation scaling so far from the threshold (at $\phi = 1$[!], which is even further away from the threshold than for the air permeability, where the normalization was taken at $\varepsilon = \phi$). After analysis of the individual data sets we plotted all the data on normalized axes (Fig. 7.23). Whereas the analysis of the air permeability generated $y = 0.96x^{2.03}$ with an R^2 of 0.97, the set of all the gas diffusion data yields $y = 1.35x^{2.01}$ with an R^2 value of 0.95. Although the numerical prefactor, 1.35, is quite large relative to our naïve expectations, we can show that this value is nearly what we anticipate. Consider again Fig. 2.2, which employs a critical volume fraction of 0.1ϕ for the case $\phi = 1$. Now we substitute the linear dependence of Eq. (2.20) for our quadratic dependence in Eq. (7.10). Forcing the quadratic universal dependence near the threshold to be compatible with the linear dependence near $p = 1$ would cause the continuation of the quadratic dependence to that limit to produce too large an air permeability value by a factor 1.29. Thus, normalization to the actual air permeability, which is a factor 1.29 smaller, makes the experimental values exceed the predicted ones by the same factor. It should also be kept in mind that the portion of the curve with $\varepsilon > 0.8$ is, as far as we know, never seen. In fact, the extracted numerical constant is 1.35, ca. 5 % larger than our prediction. Consequently, analysis of scaling far from the percolation threshold will allow predictions for gas diffusion to be just as accurate as those for the air permeability.

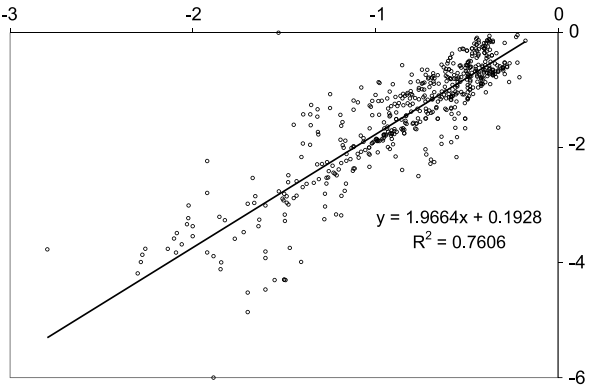

Fig. 7.21 Compilation of data (including sources not published in Figs. 7.19 and 7.20) from Hu and Wang [38] and Hu et al. [39]. Fitted slope of 1.97 compares to 2.0 predicted by Eq. (7.10) with $\theta_t = 0$. The data from Conca and Wright [16] were not given in a form normalized to water, so their data were graphically extrapolated to 100 % water content with the intercept fitted, which was then used to normalize that data. Then the normalized data from Conca and Wright [16] were incorporated with the following sets: Patil et al. [81], Graham-Bryce [34], Römkens and Bruce [86], Warncke and Barber [108], Sadeghi et al. [89], Barraclough and Nye [2], Mehta et al. [66], Barraclough and Tinker [3], Porter et al. [85], Jurinak et al. [50], Rowell et al. [88], So and Nye [94], Olesen and Kemper [80], Conca [15]; Olesen et al. [80], Schaefer et al. [91], and Klute and Letey [54]. The CRWMS and Hu data sets are not included because they show signs of non-zero θ_t (see Fig. 7.19) as well as not being normalized to diffusion in water

The value of this analysis is that, if it is possible to predict the threshold air content, one can predict the entire range of gas diffusion values without any measurement of the gas diffusion constant within the porous medium. Since we showed that one can predict the air permeability threshold reasonably well from the SWRC, and since the values of this threshold for gas diffusion are obviously also very small fractions of the porosity, we predict that the two threshold values will be the same for any given soil (the loss of air-phase connectivity should eliminate gas diffusion and gas flow at the same air-filled porosity value), and suggest reliance on the SWRC for estimating the threshold. This means that measurement of the SWRC, together with a single measurement of the air permeability, will be sufficient to predict not only the saturation dependence of the air permeability, but that of gas diffusion as well.

For perfectly dry conditions and in the case that the threshold air content is very small, Eq. (7.10) for the gas diffusion yields a proportionality to ϕ^2. Verboven et al. [107] report results for the mean gas diffusion constants of apples and pears as well as their mean porosities. These data are generally compatible with a quadratic dependence of the gas diffusion constant on porosity. It is not really significant to determine the exact behavior from the published data, because they consist only of mean values and standard deviations of porosity and diffusion constants. We have tried to analyze the unpublished data (thanks to Dr. Verboven for sharing it), but we reached no definite conclusions. Apparently the samples from which the poros-

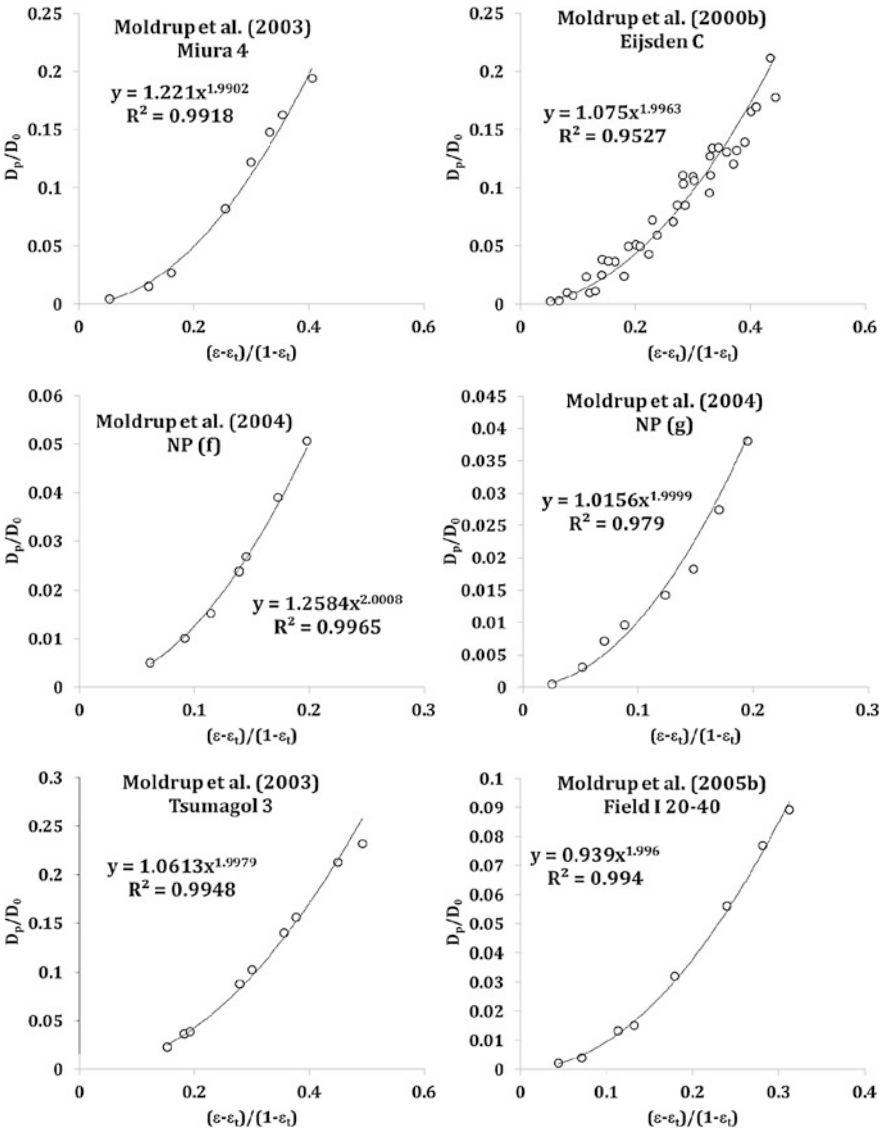

Fig. 7.22 Comparisons of gas diffusion data from various Moldrup data sets with the prediction from Eq. (7.10), a normalized universal scaling result. While R^2 values and the values of the exponent were individually as close to 1 and to 2, respectively, as for the air permeability, the numerical prefactor tended to deviate more from the ideal value of 1 than it did for the air permeability. This greater discrepancy is a result of the normalization criterion, which is applied at $\phi = 1$, rather than at the porosity of the particular material, and thus requires the validity of the percolation formulation at a considerably greater distance from the percolation threshold

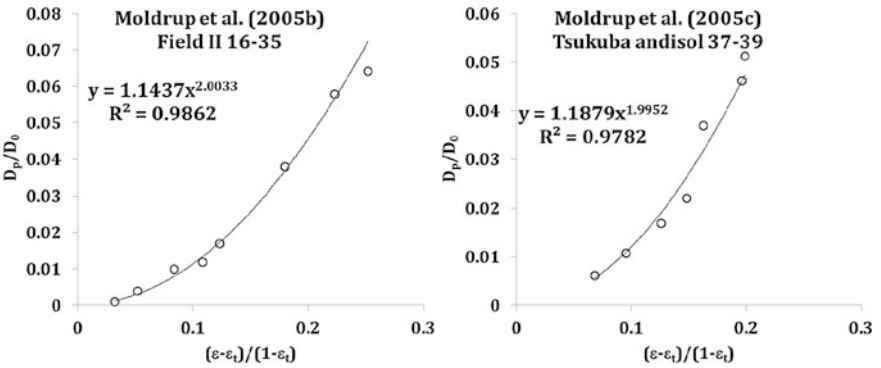

Fig. 7.22 (Continued)

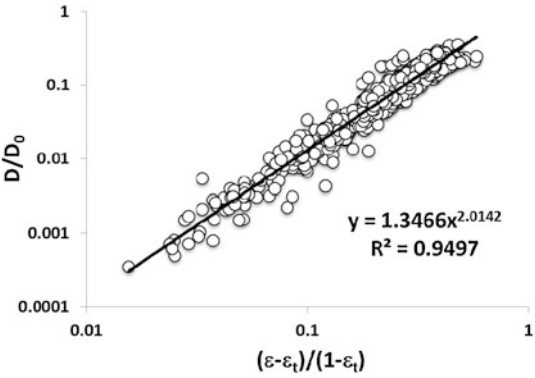

Fig. 7.23 Compilation of all the gas diffusion data from the 8 Moldrup data sets, clearly showing the consistency with universal scaling

ity values were extracted are not generally the same samples as those on which the diffusion constant was measured,so no unique relationship between porosity and diffusion can be extracted. Nevertheless we tried two different schemes to associate the porosity values with the diffusion data: scheme (1) generated a power law relationship of $D_g \propto \phi^{2.05}$, while scheme (2) generated $D_g \propto \phi^{2.26}$; both had R^2 values of about 0.85. Thus there is a tantalizing suggestion that the same simple scaling behavior for diffusion describes gas diffusion data from living organisms as well as solute diffusion data from soils.

7.4 Electrical Conductivity of Hydrated Clay Minerals

This section applies the techniques of critical path analysis for hopping conduction to the electrical conductivity σ of hydrated clay minerals. Most publications on the subject treat only the dc conductivity; experimental measurements of that quantity are made at frequencies ω that are assumed low enough to exclude ac conduction processes. This assumption may not be valid in practice. The ac conduction pro-

cesses are also typically considered to have a different source from the dc conduction, another assumption that appears to be invalid in light of the evidence presented in Hunt et al. [46]. The following discussion aims to clarify these topics.

The dc electrical conductivity of a porous medium is usually considered related to its water content through two terms. Equation (6.35) is the form traditionally used in soil science, but we will use Eq. (6.36) because of its superior physical interpretation. The first term, σ_s, gives a surface or solid contribution, and the second term represents the contribution of water in the pore space. The solid contribution may dominate the medium's bulk electrical conductivity at low water contents [18, 61]. The solid contribution arises especially from water associated with clay surfaces, and the specific physical processes giving rise to this electrical conductivity is an interesting and long-standing problem. There is as yet no consensus even as to what charge carriers give rise to the conductivity, even though it is clear that the conduction proceeds through the near-surface water phase. Both ionic conduction and proton transfer have been suggested. Conductivity diminishes with increasing cation charge, suggesting that the conducting entities are actually protons [46], because the greater Coulomb repulsion impedes the charge transport more. This argument would be qualitatively similar even if the moving charges were the ions, but the coupling of the charge and the applied field would have the opposite tendency because larger charges lead to larger changes in electric field potential energy, and thus larger currents. Nevertheless, the increase in conductivity due to the coupling with the field is linear in the charge, whereas the linear increase in Coulomb repulsion energy appears in an exponential (as an activation energy), so it is not *a priori* obvious whether ionic transport should yield a conductivity which increases with ionic charge.

The electrical conductivity of clay minerals is frequency-dependent down to rather low frequencies. This frequency dependence suggests the important role of disorder: the electrical conductivity of an *ordered* system is frequency-independent at frequencies as high as 10^{12} Hz and as low as 10^{-2} Hz or lower. The subject of the ac conductivity of non-crystalline materials, however, is part of a much broader discussion, in which critical path analysis also plays a part.

In the 1970s Andrew Jonscher wrote several articles (e.g., Jonscher [49]) pointing out the quasi-universal behavior of the ac electrical conductivity $\sigma(\omega)$ of non-crystalline solids. The substances included β-alumina, amorphous semiconductors, cellulose, humidified clays, and many others. In most of these systems, $\sigma(\omega)$ appeared to follow a sublinear power law $\sigma(\omega) \propto \omega^s$ (with $0 < s < 1$) over many decades of frequency. The existence of so many similar power laws triggered many investigations. Some key questions were asked: Is the behavior truly universal? If so, how is it best described? What could cause the same behavior in so many different systems? If the behavior is not universal, what underlying physical tendencies producing similar behavior could be found in so many systems? The discussion continues today with no sign of a consensus emerging.

For convenience we separate physical treatments of ac conduction in non-crystalline solids into three classes: (1) effects of energy and spatial disorder on hopping conduction, (2) effects of "dynamic" Coulomb interactions on hopping conduction, and (3) hopping conduction on fractal structures. The first class is treated

using critical path analysis or effective medium theories, and the third is often related to percolation scaling ideas. The second class will not be treated here, as its integration into the present discussion would require considerable background not yet presented here. We will concentrate on the first class, because it seems implausible that fractal structures are causative in so many cases, especially as most systems do not appear to be near a structural percolation threshold. Moreover, in Chap. 5 we showed how to calculate the dc conductivity of disordered systems using critical path analysis, and calculations of the ac conductivity have an analogous basis. Finally, one of us (AGH) has published on the ac conductivity of clay minerals, including a detailed analysis in terms of critical path analysis [46].

Even within the first class (effects of energy and spatial disorder on hopping conduction), there is still uncertainty. The effects of Coulomb interactions between hopping charges cannot be completely neglected in the model we developed. Although theory is relatively mature for "non-interacting" systems, controversy remains in cases where the hopping motions of the individual charge carriers are strongly correlated [32, 49]. In Hunt et al. [46] such interactions were treated in a somewhat heuristic way. Also, while the dependence of $\sigma(\omega)$ on frequency ω is classical percolation [43], the amplitude of the variability is only about two orders of magnitude. This smaller amplitude means that analysis in terms of effective medium theories or even mixing theories could also be useful, at least for the typical temperatures investigated.

The ac conductivity is related to the time dependence of the time derivative of the electrical polarization of a system. This is because a temporally changing dipole moment (such as produced by a spatial rotation) is equivalent to charge transport. However, charge transport in a capacitive medium (hopping conduction) over sufficiently small time and space intervals is considerably enhanced over steady-state current: thus ac conductivity is distinct from dc. The polarizability of a medium is described using the frequency-dependent dielectric permittivity $\varepsilon(\omega)$. As a consequence of the physical relationship between a time-changing polarization and the electrical current, $\sigma(\omega)$ in Fourier space is given by the sum of $i\omega\varepsilon(\omega)$ (where $i = \sqrt{-1}$) and the dc conductivity $\sigma(0)$. Thus the ac conductivity relates to a quantity, the polarization, which may be non-zero even in the absence of mobile charges. This explains the claim of many researchers (e.g., [95]) that the only process which can produce a non-vanishing ac conductivity is the rotation of a molecular dipole. But this is not the only such physical process! In fact, charges hopping through a disordered landscape (either r-percolation, E-percolation, or r–E percolation; Chap. 5) produce a time-dependent polarization, yielding the kind of $\sigma(\omega)$ behavior that is actually observed.

Before addressing the physics, we caution the reader that many phenomenological approaches have been used to fit the data, and arguments continue over which is the most nearly appropriate. The most commonly used phenomenology for ac conductivity is a power law. For dielectric relaxation one finds a large number of phenomenologies (Cole-Cole, Cole-Davidson, Havriliak-Negami, Kohlrausch-Williams-Watts; see references at Cole [13], Davidson [21], Havriliak and Negami [36], Kohlrausch [55, 56], Williams [110]), but none of these phenomenologies

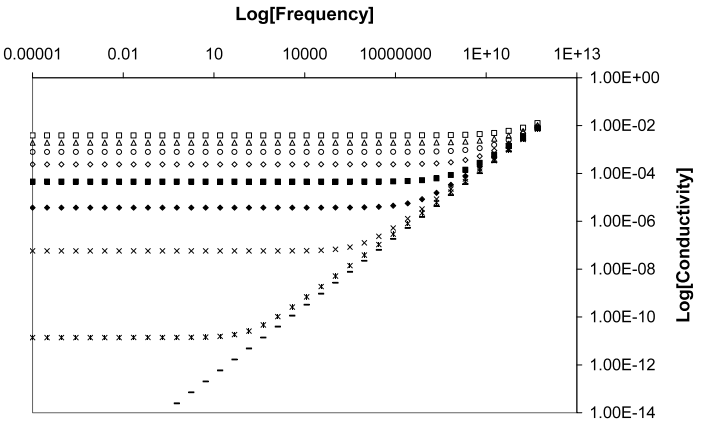

Fig. 7.24 Percolation theoretical calculations of ac electrical conductivity for disordered media at 9 different temperatures. Note that (1) the dc conductivity is a strong function of temperature, (2) the high frequency ac conductivity is nearly independent of temperature, (3) the ac conductivity is approximately a sublinear power of the frequency

works for the entire frequency range (as wide as 10^{-2} Hz to 10^{12} Hz) in any material (e.g., [23]). So perhaps it is not productive to try to derive such a "universal" result. We suggest that it is more important to derive a result which produces something similar to the apparent power-law behavior observed [49], as well as the dc conductivity and a characteristic time scale. Figure 7.24 shows a typical temperature and frequency dependence of the conductivity when it is described in percolation theory.

7.4.1 r-Percolation and E-Percolation

Hunt [40] derived a result for the ac conductivity of disordered materials, using what could be called E-percolation in analogy with the terminology of Chap. 5. Here the energy barriers between sites are random variables, but there is no relevant disorder in site separation: either the sites have equal separation, or the equivalent resistances between sites have insignificant dependence on that variable:

$$\sigma(\omega) - \sigma(0) \approx \sigma(0)\left[\frac{\omega}{\omega_c}\right]^s \quad \omega > \omega_c \tag{7.11}$$

where

$$\sigma(0) \propto \omega_c \propto \exp\left[-\frac{E_a}{k_B T}\right] \quad \text{and} \quad 1 - s \propto \frac{kT}{E_a} \tag{7.12}$$

In these equations k_B is the Boltzmann constant, T the absolute temperature, $\sigma(0)$ the electrical conductivity at zero frequency (i.e., the dc conductivity), and $\omega_c = \nu_{ph} \exp(-E_a/k_B T)$ is the critical frequency. ν_{ph}, called the phonon frequency, is a vibrational frequency, and E_a is an activation energy. Specifically, E_a is the smallest possible value of the largest activation energy on the transport path, the highest

unavoidable activation energy barrier [26]; it thus plays the part of a bottleneck resistance. General features of Eq. (7.11) and Eq. (7.12) have been verified in a wide variety of systems.

The dc conductivity given by Eq. (7.12) varies strongly with T. According to theory, as T diminishes the dc conductivity diminishes exponentially, but the high frequency ac conductivity scarcely changes. The relationship $1 - s \propto kT/E_a$ (Eq. (7.12)) arises from the requirement that in the high frequency limit, the results for different temperatures must approach the same limiting conductivity value (Fig. 7.13). The same results are obtained for increasing E_a at a constant temperature, which is compatible with the physical experiments on smectite clays that were performed on systems with diminishing water content. Such curves are shown for Mg-otay smectite clay in Fig. 7.14 [62, 63]. Similar frequency-dependent conductivity was also seen in Ca-, Mg-, K-, and Na-saturated hectorite, otay, SPV, and IMV smectites [62, 63], and also in Na- and Li-saturated smectites [4], so the results of Fig. 7.14 are rather general. Notice the strong similarity between Figs. 7.13 and 7.14.

Here we discuss the general physics behind Eq. (7.11) and Eq. (7.12), though without deriving them. We also present experimental data supporting the validity of these equations. We see that E_a calculated from critical path analysis appears reasonable for most of the systems investigated.

To better understand ac conduction, consider the r-percolation system described in Sect. 5.1. This r-percolation is analogous to the E-percolation described above. Electrons sit at sites which all have the same energy, but are separated by varying distances. Even in the absence of an electric field, electrons occasionally hop from one site to another. The rate at which an electron may hop from site i to site j is $\Gamma_{ij} = \nu_{ph} \exp[-2r_{ij}/a] \approx \tau_{ij}^{-1}$, where the relaxation time representation, τ_{ij}, makes explicit contact with Chap. 5 notation Here the phonon frequency, ν_{ph}, is often around 10^{12} Hz, but closer to 10^8 Hz in smectites; this rate expression is a chief input into the resistance value R_{ij} given in Chaps. 2 and 5. Now impose an electric field in (say) the positive x direction. Electrons will now tend to hop more frequently in the negative x direction than in any other direction, because that reduces their electrical potential energy. As long as the electric field is small, that tendency is slight, and the system is said to be in the Ohmic regime: the response to the field is linearly proportional to the strength of the field. But suppose that the electric field has been in this orientation only a very short time $t \propto \nu_{ph}^{-1} = \omega^{-1}$: which electrons will respond? Clearly those for which the typical hopping time (the inverse of the transition rate) is not greater than the time that the electric field has been in its new orientation (making $r_{ij} \approx a$). Causality (the fundamental precept that causes precede effects) allows a proof that in fact the electrons that contribute to the in-phase (real) part of the complex conductivity have response times approximately equal to the inverse of the frequency of the applied field, while those that respond much more rapidly contribute chiefly to the imaginary part. The electrons responding in phase with the field have a velocity $v = a/t$, or $v = a\nu_{ph}$. This velocity value is independent of the temperature, and because electrical conductivity is $nqev/\Xi$ (for n the volume concentration of mobile charges, qe their charge, v their velocity, and Ξ

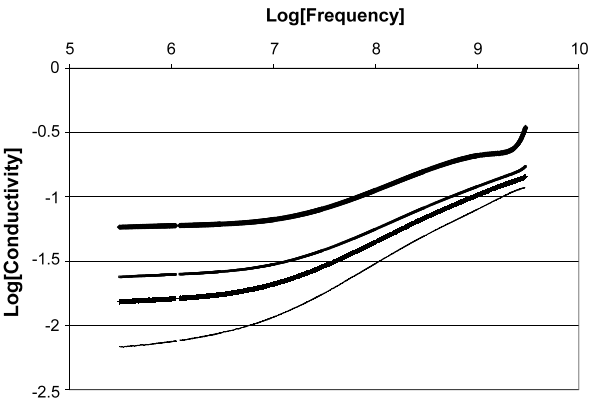

Fig. 7.25 AC conductivity of smectite clay minerals. In this figure, the dc conductivity increases more rapidly with increasing water content than does the high frequency ac conductivity (Data from [62, 63])

the electric field), this velocity tends to fix the ac conductivity in the high frequency limit.

Now consider the ac conductivity as a function of frequency, ω. A direct analogy exists between ω and p: there is a critical frequency ω_c analogous to p_c. In particular, changing the frequency can effectively sweep a system through a percolation transition.

The electron jumps that dominate are those with characteristic times t approximately equal to the time the electrical field has been in place, however, $t \approx \omega^{-1}$ and $v \approx r_{ij}\omega$. The exponential dependence of Γ_{ij} on r_{ij} makes the dependence of r_{ij} on ω logarithmic, justifying the statement that the typical distance r_{ij} increases only slightly with diminishing frequency. Thus the velocity of the hopping charges becomes, in r-percolation, a sublinear function of the frequency. While the hopping distances vary only slightly with frequency in r-percolation, they do not vary at all in E-percolation. In E-percolation, $v = \langle r \rangle \omega$, where $\langle r \rangle$ is a typical hopping distance. However, the number of electrons that can respond in time with the field is almost always a diminishing function of frequency, making the conductivity a sublinear function of the frequency. Meanwhile, because it is based on dividing the complex conductivity by i, it is the imaginary (out of phase) part of the dielectric permittivity at frequency ω which is dominantly influenced by hopping transitions with that characteristic rate. This completes an understanding that is based on the treatment of individual electrons, independent of each other [82, 83].

For high frequencies, only the fastest-responding electrons can adjust their positions (and thus their potential energies with respect to the external field) fast enough to hop. As the frequency decreases, more electrons can respond, and the responding electrons begin to cover overlapping paths. When the frequency is dropped sufficiently that the overlapping paths percolate, the ac conductivity is dominated by the same resistive process that controls the dc conductivity: no connections are through pairs with slower rates than this particular Γ. The critical frequency, $\omega_c = \nu_{ph} \exp[-E_{ac}/kT]$, is proportional to the critical rate Γ_c, and the critical resistance is proportional to the inverse of this critical rate. As a result, the ac conductivity at a frequency proportional to the dc conductivity is approximately equal to the

dc conductivity. This argument is based on the relevance of critical path analysis to hopping conduction in a disordered system. If the ac conductivity can be approximated by a power law in frequency, Eq. (7.11) and Eq. (7.12) must follow. In the case of hopping conduction in clay minerals, critical path analysis implies that both the dc and the ac conductivity should be controlled by the same rate-limiting process; thus $\sigma(0) \propto \omega_c$ and both of these quantities have the same activation energy E_a. In fact this is what is observed, *and it is incompatible with conduction via rotating dipoles*: there is no reason why the hopping conduction energy barriers (if they were associated with rotational motion) would have the same value as those encountered by particles in translational motion.

7.4.2 Percolation Calculation of E_a

Here we show that a percolation calculation of E_a leads to reasonable results without use of adjustable parameters.

Hunt et al. [46] used percolation theory at the molecular level to find the principal energy barrier limiting charge transport, and hence the dc conductivity in humified mono-ionic smectite clays. The activation energy was assumed due to Coulomb energy barriers from counterions in the vicinity of the path of the hopping charges, themselves believed to be protons. The measured electrical conductivities were consistent with proton hopping in a maximum interlayer spacing above a threshold water content, plus a constant term apparently due to hopping along external clay surfaces. The basic physical interpretations were that (1) a minimum water layer thickness is required for protons hopping along internal surfaces to effectively avoid the vicinity of such counterions, and (2) it takes considerably less water along external surfaces than along internal surfaces for protons to avoid the clay counterions. This interpretation is consistent with previous conclusions of Laird [59] that water along external surfaces tends to be concentrated in the vicinity of counterions.

Consider the possible charge pathways through the humified smectite clay (Fig. 7.26). Assume that proton hopping is the mechanism by which water transfers charge. This may initially seem implausible, because in neutral water at chemical equilibrium the concentration of protons (H^+ ions) is 10^{-7} M, too small to produce the conductivity observed. But chemical equilibrium can be compatible with a high conductivity if individual proton hops are highly correlated, such that as one proton vacates a given site, another proton moves into the now-vacant position. This interpretation allows transport to involve more protons than are actually free at any given moment, and applies equally to water in smectite clays. In such an interpretation the reduction in conductivity with decreasing number of the water layers relates to the presence of Coulombic energy barriers produced by counterions near the interior clay surfaces. These counterions produce a rough electrical potential with fluctuations that diminish with increasing distance from the surface. Closer to the surface, the higher potential energy barriers generate a greater resistance to proton hopping.

We thus have a problem of correlated proton hopping in a relatively slowly varying Coulombic potential (because the typical charge separation is greater than the

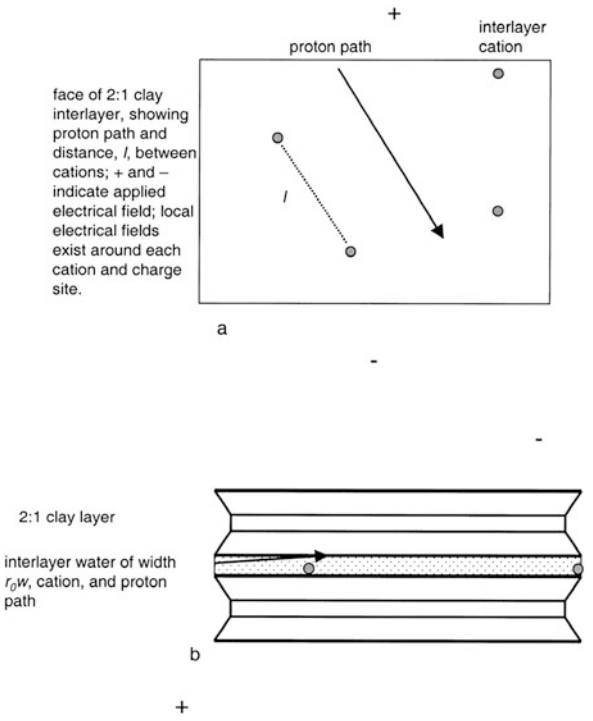

Fig. 7.26 Possible pathways for charge transport in smectite clay minerals (from [46])

separation of the water molecules). But the rate-limiting location on any given path is the one which is slowest (i.e., has the highest energy barrier; [25]), while the most important pathways are those with the fastest effective hopping rate—that is, the pathways along which the greatest energy barrier is small.

Dyre [25] expressed the idea of a limiting barrier height in terms of an effective-medium theoretical description, but the concept was formulated in the context of percolation theory. Start with the activation energy of the dc conductivity. Assume that the negative charge on the basal surfaces of a 2:1 phyllosilicate (e.g., smectite) is located in basal oxygen atoms that are proximal to sites of isomorphic substitution. The counter positive charges are associated with the exchangeable cations in the interlayers. Although these exchangeable cations are mobile, at any given instant they tend to be located as close as possible to the negative surface charge sites, and as far as possible from each other. Thus the spatial distribution of the interlayer cations is determined by the distribution of negative surface charges. The charge of the cations is qe (for q the valance of an individual cation, and e the protonic charge). The charge sites due to interlayer cations are separated on the clay layer surface by some typical distance, denoted l (see Fig. 7.26). Within the water, the potential due to a single cation is not a "naked" potential; it is reduced through the dielectric properties of the water. The energy of interaction of a charge e (the

protonic charge) and a single cation charge qe, separated by a distance r, is then

$$E = \frac{e^2 q}{4\pi\varepsilon_0\varepsilon_w r} \tag{7.13}$$

This energy of interaction is related to the activation energy of the hopping conduction, E_a, as will be shown. Consider a problem in two dimensions (2d) with no significant water thickness (Fig. 7.26a). A hopping charge must normally be brought within a distance $d = l/2$ of a cation of charge qe in order to find a path through the system. In three dimensions (represented in cross-sections in Fig. 7.26a and Fig. 7.26b), with water thickness wr_0 (for w the number of water layers, and $r_0 \approx 0.25$ nm the thickness of one water layer), this distance becomes $d = [(l/2)^2 + w^2 r_0^2]^{1/2}$. However, for smectites dominated by octahedral charges at high water contents, the distance may become $d = [(l/2)^2 + 1/4(w^2 r_0^2)]^{1/2}$, especially around divalent cations. We ignore this alternative, which would result in an increasing (rather than a decreasing) activation energy with increasing water content. In a neutral medium with some disorder in the position of the charges, the average interaction energy of a charge is zero. If, on average, a proton starts at zero energy, then at closest approach to a counterion its total energy has increased by an amount

$$E_{ac} = \frac{qe^2}{4\pi\varepsilon_0\varepsilon_w\sqrt{\frac{l^2}{4} + w^2 r_0^2}} \tag{7.14}$$

Now we must consider how l depends on the concentration of cation charges, N. In a 3D system we have $l \propto N^{-1/3}$; the 2D result ($l \propto N^{-1/2}$) may be more appropriate in platy systems, but it turns that the choice does not matter. Here we ignore orientation of the clay plates, which introduces a numerical factor $1/3$ for random orientations. We find

$$E_{ac} = \frac{2qe^2 N^{1/3}}{4\pi\varepsilon_0\varepsilon_w\sqrt{1 + 4N^{2/3} w^2 r_0^2}} \tag{7.15}$$

This E_{ac} was our first estimate of the activation energy for the dc conductivity due to the Coulombic repulsion of the counterions. Comparison with experimental data (not shown), which show a strong dependence of charge mobility on water layer thickness, indicated that Eq. (7.15) was incorrect. A Taylor series expansion in the quantity $N^{2/3} r_0^2 w^2$ of Eq. (7.15) shows why: the calculated E_{ac} is almost independent of $r_0 w$ for $r_0 w < l$, producing a conductivity independent of water content. For agreement with experiment it was necessary to modify Eq. (7.15) by dropping the first term in the square root. Apparently (if the proposed mechanism of transport is correct) the hopping protons cannot avoid the counterions in the plate parallel direction, but they can in the perpendicular direction. Then we have

$$\exp\left[\frac{-E_{ac}}{kT}\right] = \exp\left[\frac{-qe^2}{4\pi\varepsilon_0\varepsilon_w w r_0 kT}\right] = \exp\left[\frac{-0.707q}{w}\right] \tag{7.16}$$

This last expression was written in anticipation of comparison with experiments conducted at $T = 298$ K. Although using $\varepsilon_w = 80$ may underestimate E_{ac}, consider

the case for $w = 1$. The proposed mechanism of highly correlated hopping motions would be unlikely, during any individual hop, to change the number of protons on the water molecule nearest the counterion. One proton would simply replace another at a given location. But the conduction process would require a proton to jump between that site and a neighboring site. This means that, for the purpose of calculating a barrier height, the nearest distance of approach would be somewhat larger than wr_0, and the energy somewhat smaller. To estimate this effect, consider that the highest energy that the proton experiences (including the Coulombic attraction to the water molecules) is likely to occur at about half the water molecule spacing. At this distance, the Coulombic effects due to the counterion will be reduced to somewhere between $(4/5)^{1/2}$ and $2/3$—by 11 % to 33 %, depending on orientation. This numerical uncertainty is the same magnitude that would arise from using a dielectric permittivity of (say) 50 rather than 80, which would increase the Coulomb interaction strength by 38 %. As a consequence we ignore these complications and use the numerical factor of Eq. (7.16).

The pre-exponential for the conductivity was estimated from the perspective of a 3D random resistor network (disordered medium). In such a network, the dc conductivity $\sigma(0)$ is given by [31, 42, 43]

$$\sigma(0) = \frac{l_0}{L^2 R_c} \tag{7.17}$$

where $R_c = [(e^2/kT)\nu_{ph} \exp(-E_{ac}/kT)]^{-1}$, l_0 is the linear separation of critical (bottleneck) resistances on a critical path, and L is the linear separation of such paths. This makes L^{-2} the number of current-carrying paths per given cross-sectional area; in d dimensions L^{-2} is replaced by $L^{-(d-1)}$. Right at critical percolation $L \to \infty$ [97], but when critical path analysis [31] is used to develop σ_{dc}, the bottleneck resistance value is slightly larger than the critical value, and the value of L is more nearly the molecular separation, as found by the optimization procedure discussed in detail in Chap. 5. Thus L can be taken to be r_0 times some numerical constant; Hunt [43] found values between 5 and 15. In our problem, however, these considerations do not strictly apply. The L^2 is related to the dimensionality of the optimization procedure, and would be replaced by L if the optimization were performed in 2D. This is consistent with structural constraints for the 3D in the clay, for example, a distance between proton carrying paths of $(4 + w)r_0$, where $4 + w$ is the thickness (in units of water molecule size) of a simple clay sheet. It may be that in the plate parallel direction (Fig. 7.26) the path separation is structurally controlled, and is approximately equal to l. The largest resistance values, however, will be separated by $l_0 = l$, when protons come into the vicinity of a counterion. Thus the length scales in the pre-exponential are all multiples of r_0 with numerical values greater than 1. Altogether we have

$$\sigma_{dc} = \frac{e^2 l \nu_{ph}}{kT L r_0 (4 + w)} \exp\left[\frac{-E_{ac}}{kT}\right] \propto \frac{e^2 \nu_{ph}}{kT r_0 (4 + w)} \exp\left[\frac{-E_{ac}}{kT}\right] \tag{7.18}$$

The factor $\exp[-E_{ac}/(kT)]$ is given in Eq. (7.17). The predicted dc conductivity is compared with experimental values in Fig. 7.27.

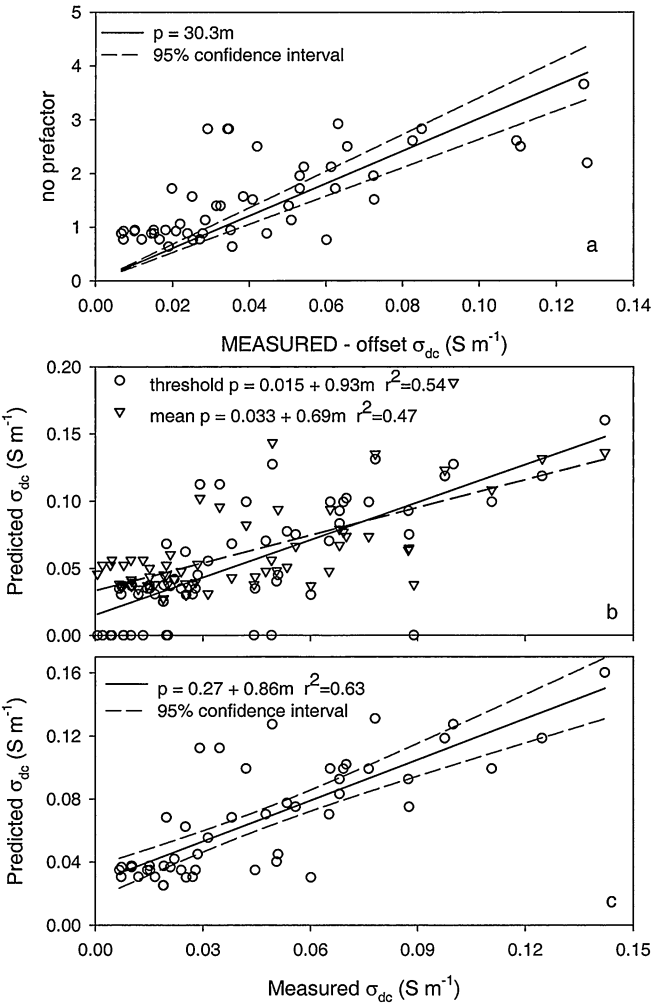

Fig. 7.27 Comparison of predicted and observed dc conductivity of smectite clay minerals. The various data correspond to 4 different mineralogies, 4 different cations, and 4 different moisture contents (from [46])

In predicting the dc conductivity $\sigma(0)$, we did not assume a continuous increase in water thickness w with θ. Rather, we assumed that the equivalent thickness of the water layer increased by r_0 every time the water content increased by a given fraction. This is in the spirit of continuum percolation theory: until there is sufficient water in a given layer, it does not form a continuous layer. This discretized thickness means that protons in a given water layer cannot avoid the layer below (with its greater proximity to counterions) until the given water layer is continuous. Since the water tends to collect preferentially in the vicinity of counterions, the apparent inability of protons to avoid counterions in a given water layer seems reasonable.

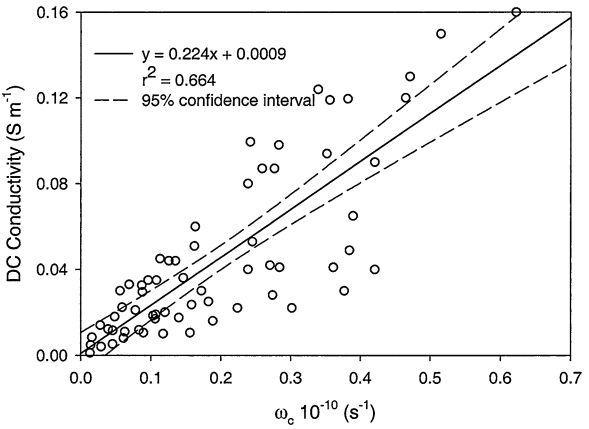

Fig. 7.28 Comparison of dc conductivity and critical frequency for the same systems as in Fig. 7.27 (from Hunt et al. [46])

A major subject of the analysis in Hunt et al. [46] relates to ac conductivity $\sigma(\omega)$ measurements performed by Logsdon and Laird. The advantage here is that the frequency-dependent analysis provides a second means to check that the predicted exponential dependence of $\sigma(0)$ on temperature is obeyed. We tried fitting Eq. (7.11) and Eq. (7.12) to the experimental data by using s, ω_c and $\sigma(0)$ as fitting parameters. Figure 7.28 shows a comparison of $\sigma(0)$ and ω_c, with the result that these two quantities appear to have the same temperature dependence. Further analysis also allowed a better check on the actual value of the phonon frequency, ν_{ph}. We found that $\nu_{ph} \approx 10^8$ Hz in contrast to the usual assumption of 10^{12} Hz. Since $\nu_{ph} \approx (k/m)^{1/2}$, with k an atomic (or molecular) spring constant and m a corresponding mass, this result implies that the binding in hydrated clay minerals is about 8 orders of magnitude weaker than in, say, quartz, which seems to be a very large contrast.

The more common use of ac conductivity measurements regards inferences of the pore size distribution through determinations of the power s using results from the critical frequency to infer the mechanism of conduction. It is known that, in addition to the temperature, the size of the particles in a medium can also influence the value of the critical frequency, which translates into an influence on a relaxation time. Thus, a range of particle sizes in a medium would have an influence on the power s as well. Information regarding the particle size distribution, obtainable in principle using non-destructive techniques, could help predict the hydraulic conductivity. Although we have shown that it is essentially impossible to generate information regarding the pore-size distribution from the dc electrical conductivity, the application of the ac conductivity to this purpose has some promise. Nevertheless, there is a significant uncertainty to be overcome before the ac conductivity may be used unambiguously to this purpose. Heretofore, most investigations have assumed that the dependence of the ac conductivity on medium geometry is controlled by diffusion in double layers near the surfaces of the particles. However, the above treatment of the ac conductivity of single particles is more nearly in accord with a surface conduction mechanism. The difference between the two treatments lies in the dependence of the critical frequency on particle size: in the first case

it is assumed to be proportional to the square of the particle radius, while in the second, by virtue of its proportionality to a surface resistance value, it is proportional to the first power of the particle radius. Equation (7.15), which formulates the dc conductivity in terms of a resistance of surface water films, gives the resistance as inversely proportional to the separation of maximally valued (controlling) resistances.

Consider equidimensional particles with all sides of approximately equal length r and a surface layer of higher conductivity of thickness Δr. Along this surface the number of maximally valued resistances would be proportional to its linear dimension, r, as would the equivalent resistance. The resistance, R, would also be inversely proportional to both the surface thickness, Δr, and its width, r, generating $R \approx 1/\Delta r$. The capacitance, C, would be proportional to $A/r = r^2/r = r$. Then it is possible, by using $\tau = RC \approx r/\Delta r$ ([48], based on theoretical work of Pollak and Pohl [84], and O'Konski [79]), to generate the linear dependence of relaxation times on particle size.

Analysis reveals no universality in experimental results; relaxation times are often proportional to the particle size, but may be proportional to a wide range of other powers of the particle size as well, including the quadratic dependence mentioned as due to diffusion in double layers. The conclusion of Hunt et al. [48] was that, in natural media at least, there was a reason to favor the surface conduction model that traces back to O'Konski [79], at least if one allows its possible generalization to fractal surfaces. The case of fractal surfaces would allow, in principle, the existence of a wider range of exponent values.

In Hunt et al. [48], it was demonstrated that the ac conductivity would be proportional to

$$\omega^{D-2} \tag{7.19}$$

for geometrical control (linear dependence on particle size) whereas the dependence on frequency would be

$$\omega^{\frac{D-1}{2}} \tag{7.20}$$

in the case of diffusion control (the quadratic dependence on particle size). One can immediately see that a power of $1/2$ requires a D value of 2.5 in the first case, but 2 in the second. Interestingly, using result (7.20), Lesmes and Morgan [60] obtained different results for the fractal dimensionality of the Berea sandstone than those obtained by optical measurements [22, 57, 101]. Lesmes and Morgan [60] obtained 2.02 ± 0.03, while the optical measurements returned values from 2.55 to 2.86. However, use of result (7.19), would have returned the fractal dimensionality 2.51 ± 0.02, near the lower limit of optically determined values, probably eliminating the perceived discrepancy.

We conclude with Figs. 7.29–7.33 that depict results from the literature illustrating the various dependences of the relaxation time on particle size. In addition to those shown, Klein and Sill [53] reported a linear dependence.

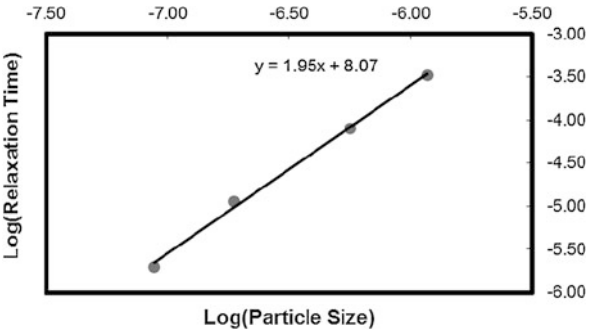

Fig. 7.29 The dependence of the inverse of the relaxation peak frequency (the relaxation time) as a function of the radius of the particles, showing a quadratic dependence. Data from [92]. The porous medium was composed of a dilute suspension of polystyrene particles

It is important that the data from Fig. 7.33 need not be interpreted as supporting a linear dependence of relaxation time on maximum water-filled pore radius. They can also be understood as supporting a cross-over from a sub-linear to a superlinear dependence. Given the difficulties in relating a water-retention curve to pore geometry, we make no definitive claims at this time, but suggest that there is sufficient evidence to consider the linear dependence as a viable interpretation.

7.5 Geophysical Applications

We now address two geophysical applications relating to seismic precursors in seismoelectric phenomena. These applications do not address whether seismic precursors could be used to predict earthquakes. Rather, our incursion into the realm of geophysics examines the implication that specific processes could explain data which has been argued to be related to seismic processes. In each case, the ultimate

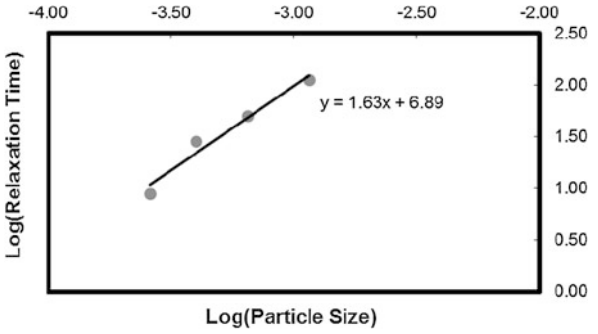

Fig. 7.30 The dependence of relaxation time on particle size. Data for soils from Titov et al. [103]. These results show a somewhat smaller power than quadratic. The data can alternatively [48] but without much conviction (on account of the small number of data points) be interpreted as showing a cross-over from a power of 2 at small sizes to a power of 1 at larger particle sizes

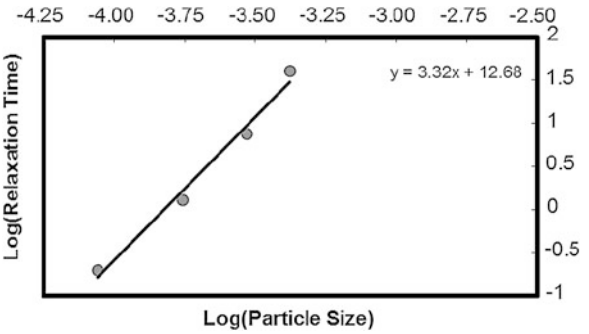

Fig. 7.31 Data from Kemma et al. [51], showing a more rapid increase in relaxation time with particle size than either linear or quadratic

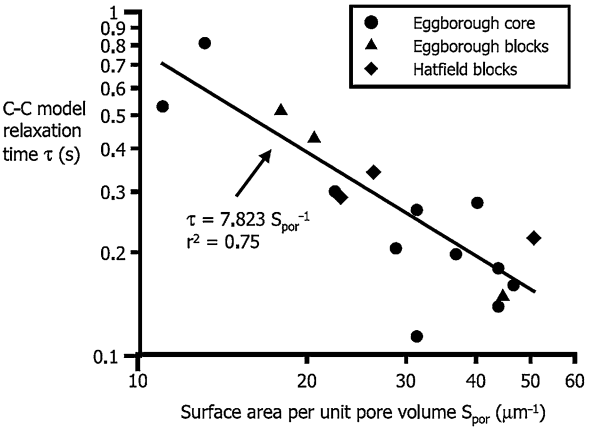

Fig. 7.32 Data from Binley et al. [5] showing a linear dependence of relaxation time on particle size. The specific surface area serves as a proxy for an inverse pore radius. Note that the relaxation time is determined by a fit to a "Cole-Cole" relaxation function, which is a generalization of Debye's exponential relaxation, though without any consistent physical interpretation

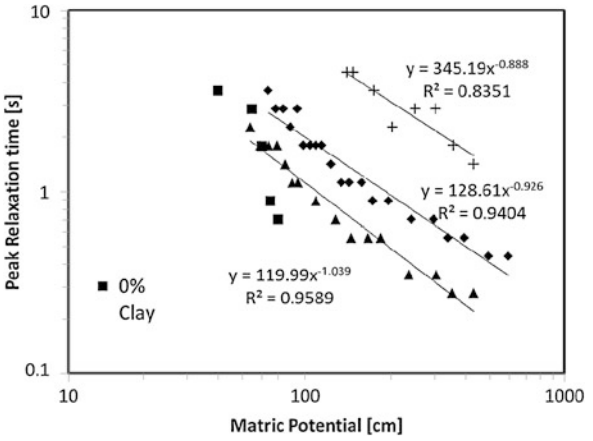

Fig. 7.33 Data from Breede [7]. Note that the independent variable here is the tension, related to the inverse of the largest water-filled pore size by the capillary equation

question is whether the magnitude of the apparent precursors can be explained in a manner consistent with theory. These examples thus hint at further possible ramifications of the present work.

Merzer and Klemperer [67] examined the sudden increase in the low-frequency contribution to the magnetic field 7 km from the Loma Prieta epicenter, three hours before the earthquake. This increase was superimposed upon other changes in the low-frequency magnetic field during the previous weeks. The authors suggested that a plausible explanation for the increase in the magnetic field strength could be a 15-fold increase in the electrical conductivity under saturated conditions. They gave three possible mechanisms for such an increase: (1) an increase in the salinity of the fluids occupying the fault zone, (2) an increase in the porosity, and (3) the exponent m of Archie's law ($\sigma(\phi) \propto \phi^m$; Archie [1]) changing from 2 to 1. In the context of percolation theory, it may be possible to find a physical basis for the third mechanism. In fact, a change in Archie's exponent from 2 to 1.3 would be expected if the random connectivity of the pore space were to change from 3D to 2D. Such a change would be consistent with the development of an interconnected network of micro-fractures along or parallel to the fault plane. It is difficult to say by how long the development of such an interconnected network could precede an actual earthquake, but one would expect that an earthquake would follow relatively quickly thereafter (e.g., [33]). The general mechanism proposed [67] has been criticized on the basis that the mutual inductance between the fault zone and the crust may mitigate the effects of the increased conductivity [27].

Another potential application regards the ability of the electrokinetic effect to generate sufficient charge separation to produce a measurable electric field. The question ultimately relates to the ability of the separated charge to recombine under the influence of the induced electric field. In a homogeneous medium the means to generate an electric field are not present, but the earth's crust is extremely heterogeneous. Here we consider partially saturated conditions. It is relatively easy to show that any electric field produced will be on the order of $J^{\mathrm{ek}}/J^{\mathrm{e}}$, where J^{e} is the electric current (proportional to the electrical conductivity). Note that (as shown in Sect. 5.1) J^{e} and J^{ek} are expected to have the same dependence on the moisture content (universal scaling), meaning that no electric field can be generated when both the electrokinetic and the return current are generated in the same medium, even if it is not homogeneous. However, if the electrokinetic current is generated in the vicinity of a fault, a large portion of the return current, which generally requires the entire medium, might need to flow in a different medium—for example, on the opposite side of the fault plane. If the first medium had a moisture content above the percolation threshold but the second was below the threshold, the possibility may exist to generate a large electric field.

The question of whether charges can percolate before crack networks do, which may be relevant for the possible existence of electromagnetic precursors to earthquakes [30, 47], has been addressed as long ago as 1983 [65]. In that article "Microcrack connectivity in rocks: a renormalization group approach to the critical phenomena of conduction and failure in crystalline rocks," Madden argued that percolation of charge is generally easier than percolation of cracks. This argument was made independently in the context of the glass transition by Hunt [41], who explained, using critical path analysis arguments, that the macroscopic transport of charge was easier (lower activation energy and smaller p_{c}) in viscous liquids than

mechanical response. This argument was based on the dimensionality of the transport process: steady-state electrical transport requires only the connection of a quasi-one-dimensional path, whereas viscosity experiments measure the transport of one entire surface relative to another. Miyazima [69] and Miyazima and Yamamoto [70] are currently putting this concept on a sounder footing. We quote the perspective of Freund and Sornette [30]:

> We conjecture that the intermittent and erratic occurrences of EM signals are a consequence of the progressive build-up of the battery charges (from plastic deformations of peroxy bonds in silicates) in the Earth crust and of their release when crack networks percolate through the stressed rock volumes.

Note that the relative ease of percolation of charge carriers relative to that of cracks is cited in both the change of Archie's law exponent from 2 to 1.3 (when the crack network finally percolates, a higher degree of continuity of charge pathways increases the electrical conductivity) and in the explicit arguments quoted in the previous paragraph, although details of the two arguments are distinct.

The point of this discussion is not to address the question of whether earthquake precursors may exist, but rather to show that a solid theoretical development of the fundamental conduction processes may inform the discussion of the potential relevance of earthquake precursors.

7.6 Summary

We have not described the wide range of phenomenological descriptions of the saturation dependence of transport properties in porous media that is in use. The confusion has developed largely from a denial of the relevance of percolation theory, but wide discussion of the potential relevance of non-universal scaling in continuum percolation theory has added grist to the mill. In fact, however, experiment reveals extraordinary simplicity and the universal conductivity exponent value of 2 shows up almost everywhere.

We find that the saturation dependences of the air permeability and the electrokinetic current are influenced only by topological effects described in percolation theory and thus follow universal scaling. We find that the hydraulic conductivity $K(\theta)$ is determined primarily by the pore-size distribution, while the electrical conductivity $\sigma(\theta)$ is mostly independent of the pore-size distribution. Since the saturation dependence of the electrical conductivity is mostly unaffected by the pore size distribution, so are those of solute and gas diffusion. Even the thermal conductivity follows universal scaling, though measurements of the thermal conductivity are made so far from the percolation threshold that a cross-over to a linear (rather than quadratic) dependence on saturation is seen. This cross-over is partially hidden by geometrical effects of pendular fluid structures.

In both $K(\theta)$ and $\sigma(\theta)$ the influence of pore sizes increases as one moves away from the percolation threshold. Combining percolation with a random fractal model of porous media, allows us to assess the ranges of moisture content where the individual influences dominate in the electrical and hydraulic conductivities. Assessment of the relative importance of the pore size distribution contribution vis-à-vis

topology can be accomplished by comparing critical path analysis with percolation scaling results, and the accessible saturation range is divided into two separate regimes. A similar division is useful for the electrical conductivity, though in the case that the pore-size distribution is not too wide, the critical path analysis is never needed and the relevance of percolation scaling extends through the entire range of saturations. Both the air permeability of dry soils and the hydraulic conductivity of saturated soils must be calculated by essentially the same optimization procedure that combines effects of topology (percolation scaling) and pore size distribution (using critical path analysis from percolation theory).

The minimal influence of the pore size distribution on the electrical conductivity justifies the application Archie's law to the saturation-dependence of the electrical conductivity with exponent 2. It also tends to restrict the porosity exponent to values near 2. At the dry end of the spectrum, the quadratic dependence of the thermal conductivity on density $\lambda \propto \rho^2$ has the same justification in percolation scaling, providing a nice symmetry.

If there is virtually no distribution of pore sizes (in artificial media), one may easily detect effects of film flow since the hydraulic conductivity follows universal scaling over only approximately two orders of magnitude of its variation. In natural media, where pore-size influences are much greater, the relevance of film flow is inferred from the failure of the hydraulic conductivity to vanish at the percolation threshold for capillary flow. In the case of the thermal conductivity, the pore size distribution is not relevant, as the thermal conductivity of each fluid in the pore space is typically less than that of the solid portion of the medium. Since the solid phase has a large conductivity, effects of pendular water structures at low water contents, which eliminate a large contact resistance between grains, can be seen.

The fact that the upper range of the percolation variable p is investigated in the thermal conductivity allows additional conclusions to be made. For $p > 0.8$, Kirkpatrick [52] found that the quadratic scaling from percolation theory is better replaced by the linear scaling from effective medium theory. Effects of this crossover are directly seen in the thermal conductivity, where the thermal conductivity of dry soils follows percolation scaling (in the density), but the saturation dependence is better described by the linear function. Finding this dependence in the thermal conductivity led us to the explanation of why the regression of the gas diffusion on the percolation scaling prediction yielded a proportionality factor of 1.35 instead of nearly 1, as in the case of the air permeability. The cause is that the factor used to normalize the gas diffusion is its value in air, i.e., for $\phi = p = 1$, rather than its value under dry conditions ($\varepsilon = p = \phi \approx 0.4$). Consequently, for gas diffusion, it is necessary to use the full scaling prediction, including the linear regime, in order to capture the correct normalization.

These and related results are summarized below in Table 7.4. In the case of the first four properties, the specific results of the random fractal model under typical conditions are used, while for the thermal conductivity the case that the solid and liquid portions of the medium have approximately the same thermal conductivities has been assumed. In the table (except for the thermal conductivity), "topology" implies that the predominant contribution to conduction comes from connectivity/tortuosity,

Table 7.4 Dominant influences on various conduction or flow properties, describable using percolation theory, depending on saturation. *Topology* means that universal percolation scaling applies, *geometry* means that a bottleneck pore (or pendular structure) radius is relevant as found in critical path analysis, and *competition* implies that a standard method, in which both influences are important, is required (described in Chap. 5. The difference between "small" and "large" values of saturation, S, depends on the property considered, so is not quantitatively defined. The entry— means that the value of the transport coefficient is normally zero. No entry means that the response cannot realistically be calculated using percolation theory, except for the case of the electrical conductivity at zero saturation. In this particular case, the distinction between media in which the solid fraction conducts or does not conduct is too great to allow such a simple classification. The subscript ek stands for electrokinetic current

Property	$S = 0$	Small S	Large S	$S = 1$
K	–	topology	geometry	competition
k_a	competition	topology	topology	–
σ_e		topology	topology	variable
σ_{ek}	–	topology	topology	topology
λ	topology	geometry		

so universal percolation scaling best describes the saturation dependence. In the case of the thermal conductivity, "topology" represents mostly the linear prediction from effective medium theory. "Geometry" refers to the relevance of the radii of the water inclusions, whether pore size dominated or in pendular structures, while "competition" means that the best expression is derived using a competition between the two methods (referred to by some authors such as Stauffer and Sahimi as critical path analysis). Entries for which the property in question does not have a non-zero contribution, or for which percolation concepts have no use that we can determine, are left blank. We expect that the nearly universal relevance of percolation theory to these properties will allow simultaneous representation of the saturation dependences of the electrical and thermal conductivity, solute and gas diffusion, as well as the air permeability on the same universal curve. Probably one will be able to see the effects of the pendular structures on the thermal conductivity in a slight bump.

Our conclusions are based on the following results. Our pore-size dominated results for the hydraulic conductivity performed best among commonly used phenomenologies, including a comparison with approximately 1200 individual data points from over 110 soils. Clear evidence for the relevance of universal scaling from percolation theory is seen in the saturation dependence of the air permeability (exponent value 2.03 extracted from 325 measurements) and gas diffusion (exponent of 2.01 extracted from 632 measurements) as well as in the electrical conductivity (612 experiments) and solute diffusion (exponent of 1.97 extracted from 605 experiments plus 11 more experiments on Fig. 7.18 [73] which are now also understood as following universal scaling. Additional evidence to support the relevance of universal scaling is found in the density dependence of the thermal conductivity (exponent of 2.02 extracted from almost 200 experiments), and the porosity dependence of the electrical conductivity (1.86 ± 0.19 from 50 different systems [102]). Altogether the analysis of those properties exhibiting universal scaling has extended to over 2400

individual experiments reported in ca. 100 publications. If the powers of the meta-data sets are averaged and a standard deviation taken, one finds 1.98 ± 0.07. If the porosity dependence of the electrical conductivity is excluded, the corresponding result is 2.01 ± 0.03. We also found two cases of two dimensional systems (simulations by Kuentz et al. [58] and experiments by Steriotis et al. [98]) for which the conductivity (or air permeability) follows universal scaling with the appropriate exponent from 2-D percolation, namely 1.3. Evidence for a change in the conductivity exponent μ from 2 to 1.3 was inferred from analysis of the increase in low frequency magnetic field strength three hours before the Loma Prieta earthquake. Otherwise little evidence for two dimensional values of μ was found.

We will see in Chap. 11 that measurements and simulations of the tortuosity also follow universal scaling formulations of percolation theory, further evidence for the utility of percolation theory in understanding flow and transport properties of porous media.

Since the agreement between theory and experiments is obscured by less scatter in many of the classic experiments [8, 14], for example) than in the more recent experiments [100], we suggest that an additional reason for the confusion of proliferating phenomenologies is a sloppier experimental technique in modern experiments.

References

1. Archie, G.E.: The electrical resistivity log as an aid in determining some reservoir characteristics. Trans. Am. Inst. Mech. Eng. **146**, 54–61 (1942)
2. Barraclough, D., Nye, P.H.: The effect of molecular size on diffusion characteristics in soil. J. Soil Sci. **30**, 29 (1979)
3. Barraclough, D., Tinker, P.B.: The determination of ionic diffusion coefficients in field soils. I. Diffusion coefficients in sieved soils in relation to water content and bulk density. J. Soil Sci. **32**, 225 (1981)
4. Bidadi, H., Schroeder, P.A., Pinnavaia, T.J.: Dielectric properties of montmorillonite clay films. Effects of water and layer charge reduction. J. Phys. Chem. Solids **49**, 1435–1440 (1988)
5. Binley, A., Slater, L.D., Fukes, M., Cassiani, G.: Relationship between spectral induced polarization and hydraulic properties of saturated and unsaturated sandstone. Water Resour. Res. **41**, W12417 (2005)
6. Bristow, K.L.: Thermal conductivity. In: Dane, J.H., Topp, C. (eds.) Methods of Soil Analysis. Part 4: Physical Methods, pp. 1209–1232. Soil Science Society of America, Madison (2002)
7. Breede, K.: Characterization of effective hydraulic properties of unsaturated porous media using spectral induced polarization (SIP). Schriften des Forschungszentrums Jülich. Reihe Energy & Environment 175, 72 S., 2013, ISBN 978-3-89336-875-4
8. Brooks, R.H., Corey, A.T.: Hydraulic properties of porous media. Colorado State Univ. Hydrology Paper 3 (1964)
9. Campbell, G.S.: Soil Physics with BASIC. Elsevier, New York (1985)
10. Chaudhary, D.R., Bhandari, R.C.: Thermal conductivity of two-phase porous materials: dry soils. Brit. J. Appl. Phys. (J. Phys. D) **2**, 609–610 (1969)
11. Civilian Radioactive Waste Management System Management and Operating Contractor (CRWMS M&O): The determination of diffusion coefficient of invert materials. TDR-EBS-MD-000002 REV 00.CRWMS M&O Las Vegas, NV (2000)

12. Civilian Radioactive Waste Management System Management and Operating Contractor (CRWMS M&O), Invert diffusion properties model. ANL-EBS-MD-000031 REV 01.CRWMS M&O Las Vegas, NV (2000)
13. Cole, K.S.: Dispersion and absorption in dielectrics I. Alternating current characteristics. J. Chem. Phys. **9**, 341 (1941)
14. Collis-George, N.: Relationship between air and water permeabilities in porous media. Soil Sci. **76**(4), 239–250 (1953)
15. Conca, J.L.: Diffusion barrier transport properties of unsaturated paintbrush tuff rubble backfill. In: Proc. First Int'l. High-Level Radioactive Waste Management Conf, pp. 394–401. ASCE and American Nuclear Society, Las Vegas (1990)
16. Conca, J.L., Wright, J.: Diffusion and flow in gravel, soil, and whole rock. Appl. Hydrogeol. **1**, 5–24 (1992)
17. Côté, J., Konrad, J.-M.: A generalized thermal conductivity model for soils and construction materials. Can. Geotech. J. **42**, 443–458 (2005)
18. Cremers, A., van Loon, J., Laudelout, H.: Geometry effects for specific electrical conductance in clays and soils. In: Proc. 14th Int'l. Conf. Clays Clay Miner., Ghent, Belgium, pp. 149–162 (1966)
19. Currie, J.A.: Movement of gases in soil respiration. In: Sorption and Transport Processes in Soils. Monogr. Soc. Chem. Ind., vol. 37, pp. 152–171 (1970)
20. Dane, J., Vrugt, J.A., Unsal, E.: Soil hydraulic functions determined from measurements of air permeability, capillary modeling, and high-dimensional parameter estimation. Vadose Zone J. **10**(1), 459–465 (2011). doi:10.2136/vzj2010.0053
21. Davidson, D.W.: Dielectric relaxation in glycerol, propylene glycol, and normal-propanol. J. Chem. Phys. **19**, 1484 (1951)
22. Davis, H.T.: On the fractal character of the porosity of natural sandstone. Europhys. Lett. **8**, 629–632 (1989)
23. Dixon, P.K., Wu, L., Nagel, S.R., Williams, B.D., Carini, J.P.: Scaling in the relaxation of super-cooled liquids. Phys. Rev. Lett. **65**, 1108 (1990)
24. Dury, O.: Organic pollutants in unsaturated soils: Effect of butanol as a model contaminant on phase saturation and flow characteristics of a quartz sand packing. Ph.D. thesis, Swiss Fed. Inst. of Technol, Zürich, Switzerland (1997)
25. Dyre, J.C.: Some remarks on ac conduction in disordered solids. J. Non-Cryst. Solids **135**, 219 (1991)
26. Dyre, J.C., Schroeder, T.B.: Universality of ac conduction in disordered solids. Rev. Mod. Phys. **72**, 873–892 (2000)
27. Egbert, G.D.: On the generation of ULF magnetic variations by conductivity fluctuations in a fault zone. Pure Appl. Geophys. **159**, 1205–1227 (2002)
28. Ewing, R.P., Horton, R.: Scaling in diffusive transport. In: Pachepsky, Ya. (ed.) Scaling Methods in Soil Physics, pp. 49–61. CRC Press, Boca Raton (2003)
29. Ewing, R.P., Horton, R.: Thermal conductivity of a cubic lattice of spheres with capillary bridges. J. Phys. D, Appl. Phys. **40**, 4959–4965 (2007)
30. Freund, F., Sornette, D.: Electromagnetic earthquake bursts and critical rupture of peroxy bond networks in rocks. Tectonophysics **431**, 33–47 (2007)
31. Friedman, L., Pollak, M.: The Hall effect in the variable-range hopping system. Philos. Mag. B **44**, 487–507 (1981)
32. Funke, K.: Ion transport and relaxation studied by high frequency conductivity and quasielastic neutron scattering. Philos. Mag. A **64**, 1025–1034 (1991)
33. Gao, Y., Crampin, S.: Observations of stress relaxation before earthquakes. Geophys. J. Int. **157**(2), 578–582 (2004)
34. Graham-Bryce, I.J.: Effect of moisture content and soil type on self diffusion of ^{86}Rubidium in soils. J. Agric. Sci. **60**, 239 (1963)
35. Havlin, S., ben-Avraham, D.: Diffusion in disordered media. Adv. Phys. **36**(6), 695–798 (1987)

36. Havriliak, S., Negami, S.: A complex plane analysis of α-dispersion in some polymer systems. J. Polym. Sci. C **14**, 99–117 (1966)
37. Hazlett, R.D., Furr, M.J.: Percolation model for permeability reduction in porous media by continuous-gas foams. Ind. Eng. Chem. Res. **39**, 2709–2716 (2000)
38. Hu, Q., Wang, J.: Aqueous phase diffusion in unsaturated geologic media: a review. Crit. Rev. Environ. Sci. Technol. **33**, 275–297 (2003)
39. Hu, Q., Kneafsey, T.J., Roberts, J.J., Tomutsa, L., Wang, J.S.Y.: Characterizing unsaturated diffusion in porous tuff gravel. Vadose Zone J. **3**, 1425–1438 (2004)
40. Hunt, A.: Transport in ionic conducting glasses. J. Phys. Condens. Matter **3**(40), 7831–7842 (1991)
41. Hunt, A.: Dielectric and mechanical relaxation in liquids and glasses: transition from effective medium to percolation theories. Solid State Commun. **84**(7), 701–704 (1992)
42. Hunt, A.G.: AC hopping conduction: perspective from percolation theory. Philos. Mag. B **81**, 875–913 (2001)
43. Hunt, A.G.: Applications of percolation theory to porous media with distributed local conductances. Adv. Water Resour. **24**(3,4), 279–307 (2001)
44. Hunt, A.G.: Continuum percolation theory for saturation dependence of air permeability. Vadose Zone J. **4**, 134–138 (2005)
45. Hunt, A.G., Ewing, R.P.: On the vanishing of solute diffusion in porous media at a threshold moisture content. Soil Sci. Soc. Am. J. **67**, 1701–1702 (2003)
46. Hunt, A.G., Logsdon, S.D., Laird, D.A.: Percolation treatment of charge transfer in humidified smectite clays. Soil Sci. Soc. Am. J. **70**, 14–23 (2006)
47. Hunt, A., Gershenzon, N., Bambakidis, G.: Pre-seismic electromagnetic phenomena in the framework of percolation and fractal theories. Tectonophysics **431**, 23–32 (2007)
48. Hunt, A.G., Huisman, J.A., Vereecken, H.: On the origin of slow processes of charge transport in porous media. Philos. Mag. **92**(36), 4628–4648 (2012)
49. Jonscher, A.K.: The "universal" dielectric response. Nature (London) **267**, 673–679 (1977)
50. Jurinak, J.J., Sandhu, S.S., Dudley, L.M.: Ionic diffusion coefficients as predicted by conductometric techniques. Proc., Soil Sci. Soc. Am. **51**, 626 (1987)
51. Kemna, A., Münch, H.-M., Titov, K., Zimmermann, E., Vereecken, H.: Relation of SIP relaxation time of sands to salinity, grain size and hydraulic conductivity. In: 11th Eur. Mtng. Environ. Eng. Geophys., Palermo, Italy (2005). P054
52. Kirkpatrick, S.: Percolation and conduction. Rev. Mod. Phys. **45**, 574–588 (1973)
53. Klein, J.D., Sill, W.R.: Electrical properties of artificial claybearing sandstone. Geophysics **47**, 1593–1602 (1982)
54. Klute, A., Letey, J.: The dependence of ionic diffusion on the moisture content of nonsorbing porous media. Proc., Soil Sci. Soc. Am. **22**, 213 (1958)
55. Kohlrausch, R.: Ann. Phys. (Leipz.) **12**, 393 (1847)
56. Kohlrausch, R.: Pogg. Ann. Phys. Chem. **91**, 179 (1854)
57. Krohn, C.J.: Fractal measurements of sandstones, shales, and carbonates. J. Geophys. Res., Solid Earth **93**(B4), 3297–3305 (1988)
58. Kuentz, M., Mareschal, J.C., Lavallee, P.: Numerical estimation of electrical conductivity in saturated porous media with a 2-D lattice gas. Geophysics **65**, 766–772 (2000)
59. Laird, D.A.: Layer charge influences on the hydration of expandable 2:1 phyllosilicates. Clays Clay Miner. **47**, 630–636 (1999)
60. Lesmes, D.P., Morgan, F.D.: Dielectric spectroscopy of sedimentary rocks. J. Geophys. Res. **106**(B7), 13,329–13,346 (2001)
61. Letey, J., Klute, A.: Apparent mobility of potassium and chloride ions in soil and clay pastes. Soil Sci. **90**, 259–265 (1960)
62. Logsdon, S.D., Laird, D.A.: Electrical conductivity spectra of smectites as influenced by saturating cation and humidity. Clays Clay Miner. **52**, 411–420 (2004)
63. Logsdon, S.D., Laird, D.A.: Cation and water content effects on dipole rotation activation energy of smectites. Soil Sci. Soc. Am. J. **68**, 1586–1591 (2004)

64. Lu, S., Ren, T., Gong, Y., Horton, R.: An improved model for predicting soil thermal conductivity from water content at room temperature. Soil Sci. Soc. Am. J. **71**, 8–14 (2007)
65. Madden, T.R.: Microcrack connectivity in rocks: a renormalization group approach to the critical phenomena of conduction and failure in crystalline rocks. J. Geophys. Res. **88**, 585–592 (1983)
66. Mehta, B.K., Shiozawa, S., Nakano, M.: Measurement of molecular diffusion of salt in unsaturated soils. Soil Sci. **159**, 115 (1995)
67. Merzer, M., Klemperer, S.L.: Modeling low-frequency magnetic-field precursors to the Loma Prieta Earthquake with a precursory increase in fault-zone conductivity. Pure Appl. Geophys. **150**, 217–248 (1997)
68. Millington, R.J., Quirk, J.P.: Permeability of porous solids. Trans. Faraday Soc. **57**, 1200–1206 (1961)
69. Miyazima, S.: A new percolation model with two threshold points. Prog. Theor. Phys. Suppl. **157**, 152–155 (2005)
70. Miyazima, S., Yamamoto, K.: Site- and bond-percolation problems for formation of macroscopic surface in a cubic lattice. J. Res. Inst. Sci. Technol. **18**, 101–106 (2006)
71. Moldrup, P., Olesen, T., Gamst, J., Schjønning, P., Yamaguchi, T., Rolston, D.E.: Predicting the gas diffusion coefficient in repacked soil: water-induced linear reduction model. Soil Sci. Soc. Am. J. **64**, 1588–1594 (2000)
72. Moldrup, P., Olesen, T., Schjønning, P., Yamaguchi, T., Rolston, D.E.: Predicting the gas diffusion coefficient in undisturbed soil from soil water characteristics. Soil Sci. Soc. Am. J. **64**, 94–100 (2000)
73. Moldrup, P., Oleson, T., Komatsu, T., Schjoning, P., Rolston, D.E.: Tortuosity, diffusivity, and permeability in the soil liquid and gaseous phases. Soil Sci. Soc. Am. J. **65**, 613–623 (2001)
74. Moldrup, P., Yoshikawa, S., Olesen, T., Komatsu, T., Rolston, D.E.: Gas diffusivity in undisturbed volcanic ash soils: test of soil-water-characteristic-based prediction models. Soil Sci. Soc. Am. J. **67**, 41–51 (2003)
75. Moldrup, P., Olesen, T., Yoshikawa, S., Komatsu, T., Rolston, D.E.: Three-porosity model for predicting the gas diffusion coefficient in undisturbed soil. Soil Sci. Soc. Am. J. **68**, 750–759 (2004)
76. Moldrup, P., Olesen, T., Yoshikawa, S., Komatsu, T., Rolston, D.E.: Predictive-descriptive models for gas and solute diffusion coefficients in variably saturated porous media coupled to pore-size distribution: I. Gas diffusivity in repacked soil. Soil Sci. **170**, 843–853 (2005)
77. Moldrup, P., Olesen, T., Yoshikawa, S., Komatsu, T., Rolston, D.E.: Predictive-descriptive models for gas and solute diffusion coefficients in variably saturated porous media coupled to pore-size distribution: II. Gas diffusivity in undisturbed soil. Soil Sci. **170**, 854–866 (2005)
78. Moldrup, P., Olesen, T., Yoshikawa, S., Komatsu, T., McDonald, A.M., Rolston, D.E.: Predictive-descriptive models for gas and solute diffusion coefficients in variably saturated porous media coupled to pore-size distribution: III. Inactive pore space interpretations of gas diffusivity. Soil Sci. **170**, 867–880 (2005)
79. O'Konski, C.T.: Electrical properties of macromolecules. V. Theory of ionic polarization in polyelectrolytes. J. Chem. Phys. **64**(5), 605–619 (1960)
80. Olesen, S.R., Kemper, W.D.: Movement of nutrients to plant roots. In: Adv. Agronomy, vol. 30, p. 91. Academic Press, New York (1968)
81. Patil, A.S., King, K.M., Miller, M.H.: Self-diffusion of rubidium as influenced by soil moisture tension. Can. J. Soil Sci. **43**, 44 (1963)
82. Pollak, M., Geballe, T.H.: Low-frequency conductivity due to hopping processes in silicon. Phys. Rev. **122**, 1742–1753 (1961)
83. Pollak, M., Pike, G.E.: AC conductivity of glasses. Phys. Rev. Lett. **28**, 1449–1451 (1972)
84. Pollak, M., Pohl, H.A.: Dielectric dispersion in some polymers and polyelectrolytes: a model. J. Chem. Phys. **63**(7), 2980–2987 (1975)
85. Porter, L.K., Kemper, W.D., Jackson, R.D., Stewart, B.A.: Chloride diffusion in soils as influenced by moisture content. Proc., Soil Sci. Soc. Am. **24**, 460 (1960)

86. Römkens, M.J.M., Bruce, R.R.: Nitrate diffusivity in relation to moisture content of non-adsorbing porous media. Soil Sci. **98**, 332 (1964)
87. Rose, W.: Volumes and surface areas of pendular rings. J. Appl. Phys. **29**(4), 687–691 (1958)
88. Rowell, D.L., Martin, M.W., Nye, P.H.: The measurement and mechanism of ion diffusion in soil. III. The effect of moisture content and soil solution concentration on the self-diffusion of ions in soils. J. Soil Sci. **18**, 204 (1967)
89. Sadeghi, A.M., Kissel, D.E., Cabrerra, M.L.: Estimating molecular diffusion coefficients of urea in unsaturated soil. Soil Sci. Soc. Am. J. **53**, 15 (1989)
90. Sallam, A., Jury, W.A., Letey, J.: Measurement of gas diffusion coefficient under relatively low air-filled porosity. Soil Sci. Soc. Am. J. **48**, 3–6 (1984)
91. Schaefer, C.E., Arands, R.R., van der Sloot, H.A., Kosson, D.S.: Prediction and experimental validation of liquid-phase diffusion resistance in unsaturated soils. J. Contam. Hydrol. **20**, 145 (1995)
92. Schwartz, G.: A theory of the low-frequency dielectric dispersion of colloidal particles in electrolyte solution. Presented before the division of Physical Chemistry of the American Chemical Society, 140th National Meeting, Chicago IL, Sept. 1961
93. Sendner, C., Horinek, D., Bocquet, L., Netz, R.R.: Interfacial water at hydrophobic and hydrophilic surfaces: slip, viscosity, and diffusion. Langmuir **25**(18), 10,768–10,781 (2009)
94. So, H.B., Nye, P.H.: The effect of bulk density, water content and soil type on the diffusion of chloride in soil. J. Soil Sci. **40**, 743 (1989)
95. Sposito, G., Prost, R.: Structure of water adsorbed on smectites. Chem. Rev. **82**, 553–573 (1982)
96. Springer, D.S., Loaiciga, H.A., Cullen, S.J., Everett, L.G.: Air permeability of porous materials under controlled laboratory conditions. Ground Water **36**(4), 558–565 (1998)
97. Stauffer, D.: Scaling theory of percolation clusters. Phys. Rep. **54**, 1–74 (1979)
98. Steriotis, T.A., Katsaros, F.K., Stubos, A.K., Mitropoulos, A.Ch., Kanellopoulos, N.K.: A novel experimental technique for the measurement of the single-phase gas relative permeability of porous solids. Meas. Sci. Technol. **8**, 168–173 (1997)
99. Stonestrom, D.A.: Co-determination and comparison of hysteresis affected, parametric functions of unsaturated soils: Water content dependence of matric pressure, air trapping, and fluid permeabilities in a non-swelling soil. Ph.D. thesis, Stanford Univ, Stanford, Calif (1987)
100. Tang, A.M., Cui, Y.-J., Richard, G., Défossez, P.: A study on the air permeability as affected by compression of three French soils. Geoderma **162**, 171–181 (2011)
101. Thompson, A.: Fractals in rock physics. Annu. Rev. Earth Planet. Sci. **19**, 237–262 (1991)
102. Thompson, A.H., Katz, A.J., Krohn, C.E.: Microgeometry and transport in sedimentary rock. Adv. Phys. **36**, 625 (1987)
103. Titov, K., Komarov, V., Tarasov, V., Levitski, A.: Theoretical and experimental study of time domain induced polarization in water-saturated sands. J. Appl. Geophys. **50**, 417–433 (2002)
104. Touma, J., Vauclin, M.: Experimental and numerical analysis of two-phase infiltration in a partially saturated soil. Transp. Porous Media **1**, 27–55 (1986)
105. Tuli, A., Hopmans, J.W.: Effect of degree of fluid saturation on transport coefficients in disturbed soils. Eur. J. Soil Sci. **55**(1), 147–164 (2004)
106. Unsal, E., Dane, J.H., Dozier, G.V.: A genetic algorithm for predicting pore geometry based on air permeability measurements. Vadose Zone J. **4**, 389–397 (2005)
107. Verboven, P., Kerkhofs, G., Mebatsion, H.K., Ho, Q.T., Temst, K., Wevers, M., Cloetens, P., Nicolaï, B.M.: Three-dimensional gas exchange pathways in pome fruit characterized by synchrotron X-ray computed tomography. Plant Physiol. **147**, 518–527 (2008)
108. Warncke, D.D., Barber, S.A.: Diffusion of zinc in soil I. The influence of soil moisture. Soil Sci. Soc. Am. J. **36**, 39 (1972)
109. Werner, D., Grathwohl, P., Hoehener, P.: Review of field methods for the determination of the tortuosity and effective gas-phase diffusivity in the vadose zone. Vadose Zone J. **3**, 1240–1248 (2004)
110. Williams, G.: Non-symmetrical dielectric relaxation behaviour arising from a simple empirical decay function. Trans. Faraday Soc. **66**, 80 (1970)

Chapter 8
Pressure Saturation Curves and the Critical Volume Fraction for Percolation: Accessibility Function of Percolation Theory

The pressure-saturation curves of porous media give fundamental information about the pore space. In equilibrium, ignoring effects due to hysteresis and pore accessibility, it should be possible to extract a pore-size distribution from $h(\theta)$ data, as described in Chap. 4. However, a number of percolation effects complicate the analysis and make such a simple inference impossible. The pressure-saturation relation is affected by both the lack of continuity of the air phase near saturation, and by a similar lack of continuity of the water phase near the dry end. Given that these effects are due to phase transitions (in the percolation sense), small changes in experimental conditions can produce major (and sometimes puzzling) changes in the results. Further, since the correlation length diverges near these transitions, numerical simulations under both wet and dry conditions are amenable to finite-size scaling analysis. Since the critical volume fractions for percolation of air and water are critical to the discussion, experimental evidence regarding these values is presented toward the end of this chapter.

When a porous medium is dried from near saturation, the wetting phase becomes discontinuous below the percolation transition. This forces a change in the mode of water transport from capillary flow to either film flow or vapor-phase flow. These new modes of transport could be safely ignored at high moisture contents, because they involve coefficients that are orders of magnitude lower than typical hydraulic conductivities from capillary flow. But if these new modes are not effective in a given situation, it will prove difficult to reduce θ to values less than the critical volume fraction θ_t for percolation. In fact, just reducing θ to θ_t is difficult because the hydraulic conductivity value for capillary flow vanishes rapidly as θ_t is approached. A related possibility, that even above the critical moisture content some water-filled pores could lose access to the infinite cluster and fail to drain, was discussed in [11], where it was pointed out that the phenomenon could explain the results of experiments with rapid drainage. As Gist et al. [7] point out: "The subset of pores occupied by mercury at the [percolation] threshold diameter has been directly visualized by injecting a porous medium with molten metal, then solidifying the metal. Examined opti-

A. Hunt et al., *Percolation Theory for Flow in Porous Media*,
Lecture Notes in Physics 880, DOI 10.1007/978-3-319-03771-4_8,

cally, the resulting structure has the fractal dimension expected from percolation theory [5]."

8.1 Structural Hysteresis

The role of percolation in hysteresis in wetting and drying of porous media has been appreciated in the physics community for nearly thirty years [30], but much less so in the porous media community. A basic consideration of hysteresis in wetting and drying should suggest that changes in the water content will be limited by the continuity of the air phase near saturation, and by continuity of the water phase at the dry end. That is, a porous medium that wets and dries will typically pass through two distinct percolation transitions. What this means is that, neglecting edge effects, water (air) may be trapped in isolated clusters during drying (wetting), while water (air) cannot enter in arbitrarily small quantities [less than the critical volume fraction] during wetting (drying). In a two-dimensional medium these two phase transitions would occur at the same moisture content, but in three-dimensional media they are generally separated by a wide range of moisture contents where both phases percolate.

A second important contributor to hysteresis, the so-called "ink-bottle effect," is well known to the porous media community [21, 22]. According to the capillary relationship (Eq. (3.12)), when an air-water-solid system is at equilibrium, a given pore can be filled with water only if its radius is less than some value: $r < A/h$. Water is "allowed" in these pores. But according to the pore-body, pore-throat picture of porous media, the tension required to remove water from such a pore is higher than that which allows water in: in the removal process (drainage) the meniscus must "fit" through a pore throat, while in the filling process (imbibition) the meniscus must span the pore body. This fundamental asymmetry in the wetting and drying processes means that, at a given water content, the pressure in a drying curve should be higher than in a wetting curve. This factor relates to the geometry of an individual pore, but in a system with self-similar properties it relates to every pore.

Consider imbibition under a high tension (negative water pressure) into an initially dry medium. Water cannot access most pores that are allowed, because the paths to those pores pass through other pores that are not small enough to allow water [8]. This problem is obviously related to percolation theory, but it was originally thought that traditional percolation theory was not adequate to treat this problem. In the 1980s considerable literature arose in the physics community regarding a special form of percolation theory called "invasion" percolation [31]. From our standpoint, invasion percolation deals with the movement of the wetting or drying front, and therefore (in principle) with spatial gradients of percolation quantities. By the end of the 1980s it was accepted that, at least with respect to hysteresis, the difference between traditional percolation theory (discussed here) and invasion percolation was minimal [27]—though at least one key investigation [30] had a significant inconsistency which will be revisited below.

In traditional percolation theory, the fraction of accessible sites is that fraction P that is part of the infinite cluster. During drying, all of the water-allowed sites are accessible to water. But in wetting the fraction of water-allowed sites that are also accessible to water is reduced by P. P is known to behave in 3D as

$$P \propto (p - p_c)^{\beta} = (\theta - \theta_t)^{0.4} \tag{8.1}$$

where the equality follows from the application to continuum percolation with the moisture content playing the role of p. An obvious problem in applying this concept is that our expression for P is a proportionality, not an equality. Clearly P should be constrained to equal 1 at or above some moisture content; a reasonable choice is to require $P = 1$ at $\theta = \phi$. For this case we can write [11]

$$P = \left(\frac{\theta - \theta_t}{\phi - \theta_t} \right)^{0.4} \tag{8.2}$$

The implication of this particular normalization factor is that, during wetting, it is certain only at saturation that all water-allowable pores are also water-accessible. For practical purposes the condition $P = 1$ is likely reached at much lower water contents.

It is possible to express the actual moisture content as the product $\theta \cdot P(\theta)$, as long as θ in this product refers to the *equilibrium* moisture content, that is, the volume of the allowable pore space. This notational complication can be easily removed by expressing both factors in terms of the tension h. Referring water content to pressure requires reference of the critical water content to a critical pressure h_c, which can be defined via [11]

$$\theta_t = \left[\frac{3 - D}{r_m^{3-D}} \right] \int_{r_0}^{A/h_c} r^{2-D} dr \tag{8.3}$$

Thus, starting from dry conditions with a very large value of $h \geq A/r_0$, reduction of h produces an increasing fraction of water-allowable pore space (but, ignoring edge effects, no increase in water-accessible pores or water content) until, at the value $h = h_c$, the water-allowable pore space percolates. Proceeding from this point we have [11]

$$\theta(h) = \frac{3 - D}{r_m^{3-D}} \left[\frac{\left(\frac{A}{h}\right)^{3-D} - \left(\frac{A}{h_c}\right)^{3-D}}{\left(\frac{A}{h_A}\right)^{3-D} - \left(\frac{A}{h_c}\right)^{3-D}} \right]^{0.4} \int_{r_0}^{A/h} r^{2-D} dr \tag{8.4}$$

We emphasize again that this approach neglects the effects of finite clusters of water-allowed pores which are accessible from the edges of the system. The effects of such pores can be incorporated into the treatment via finite-size scaling, but we will not do that here. The present approach also neglects water that would fill "pores" on rough (fractal) surfaces of individual grains, at least insofar as this contribution to the pore space is described by a separate surface fractal dimensionality. Such a contribution could theoretically lead to a change in slope of the pressure-saturation curves at low moisture contents.

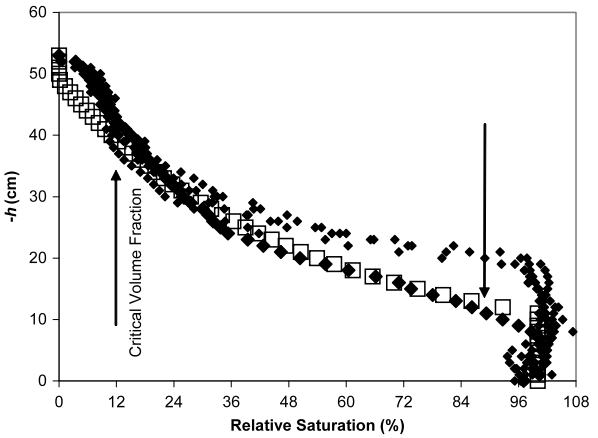

Fig. 8.1 Drainage data from Bauters et al. [1] for a collection of sands with differing fractions (the *smaller diamonds*) of hydrophobic particles, with the fraction being zero for the *large diamonds*. The theoretical curve was obtained by using the particle-size data to find the fractal dimensionality of the pore space while the air entry pressure, h_A, was used as an adjustable parameter. The critical moisture content for percolation (0.048) is designated by the *arrows*; in a soil with only sand particles these values are assumed identical for air and water

With these caveats we compare Eq. (4.24) with experimental measurements (Fig. 8.1) of the drying of blasting sand with various fractions of particles treated to be water-repellent [1]. Each different fraction of water-repellent particles gave a different curve, but displaying them all together shows that the critical moisture content for percolation is the same in each case. As in earlier chapters, particle-size data were used to find the ratio r_0/r_m, after which ϕ and the ratio r_0/r_m are combined to give D. A single air-entry pressure h_c was adjusted to produce the best fit with experiment over the range of intermediate saturations. The value of the critical volume fraction for percolation, $\theta_t = 0.048$, was chosen as the point below which theory and experiment deviated (due to non-equilibrium, discussed below).

It is clear from the data that the appropriate value of the characteristic pressure for imbibition could not be the same as for drainage. This is due to the "ink-bottle" effect mentioned earlier in this chapter. Lenhard [21] and co-workers [22] investigated this effect for a number of soils and found that the typical ratio of characteristic pressures for drainage and imbibition is 2, indicating that pore bodies characteristically have radii twice that of pore throats. Using Eq. (4.24) (derived for drainage) for imbibition, but with the characteristic pressure reduced by a factor 2 as per Lenhard et al. [22], does not suffice to transform a drainage curve into an imbibition curve [11]: the curve intersects reality only near saturation (Fig. 8.2). But when the accessibility effects of percolation are included by using Eq. (8.4) (without additional unknown parameters), the match between experiment and theory is quite good. Figure 8.2 provides an additional check on the estimate of the critical volume fraction: deviations from prediction set in at a moisture content $\phi - \theta_t$ (still with $\theta_t = 0.048$).

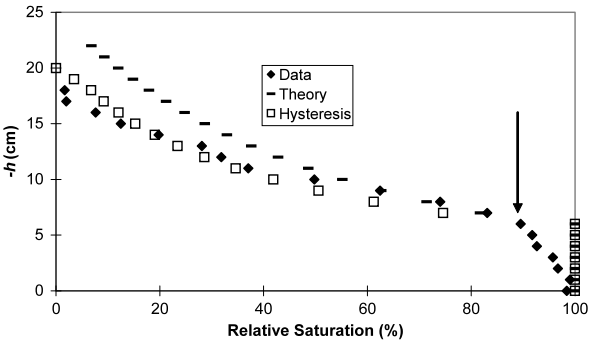

Fig. 8.2 The imbibition curve for the hydrophilic sand of Fig. 8.1. "Theory" uses Eq. (4.24) with a characteristic pressure half of h_A in Fig. 8.1. "Hysteresis" uses the prediction of Eq. (8.4). There are no other adjustable parameters here; the critical volume fraction comes from Fig. 8.1, and the fractal dimensionality from the particle size distribution. Here the critical air content for percolation is clearly also very close to 0.05

These deviations arise from "entrapped" air, and become apparent as the volume of air-filled pore space reaches the percolation threshold.

The general idea of allowable vs. accessible pores in the context of percolation theory was introduced by Heiba et al. [8] in a publication treating a Bethe lattice model. Publications of Wilkinson (e.g., [30]) later in the 1980s developed this framework further, accounting for the connectivity of water films during drying, and their absence during wetting. This led to different treatments for air entrapment during wetting (residual air) and residual water during drying. In that respect his treatment was more careful and general than the present treatment. However, Wilkinson treated the pressure as the fundamental percolation variable—which was reasonable for the bond percolation problem he was addressing with a network model—and then expressed the moisture content in terms of a *sublinear* power of h, rather than using the moisture content as the fundamental variable (in continuum percolation) and expressing the pressure as a *superlinear* power of θ. This reversal of the roles of the variables calls his conclusions into question, because those conclusions depend on the *sublinearity* of the powers.[1] In addition, his comparison with experiment was schematic, without specific data; a detailed comparison between his analysis and experimental data (for example, the results given here) has yet to be made. Wilkinson also did not consider various experimental difficulties, which include lack of equilibration due to low values of the hydraulic conductivity (or rapid drainage), nor the differences in media, some of which may be structured. Any one of these

[1] In particular, Wilkinson addressed the curvature of the pressure saturation curve, $\log[-h]$ vs. θ, at large moisture contents and determined that the typically observed negative curvature was appropriate from percolation theory. However, we find that a positive curvature is appropriate (and indeed observed for sandy media). The opposite curvature, which is also frequently observed, is actually a result of finite-size complications. See Sect. 8.4 for additional quantitative evidence supporting our interpretation.

factors can influence the shape of the drainage and imbibition curves. The first of these questions will be treated next; effects of the structure of a medium will be addressed in Chap. 12.

8.2 Hydraulic Conductivity-Limited Equilibration, and Dry-End Deviations from Fractal Scaling

Chapter 6 discussed the limits of validity of an equation for hydraulic conductivity,

$$K_{\mathrm{f}}(\theta) = K_{\mathrm{S}}\left[\frac{1-\phi+(\theta-\theta_{\mathrm{t}})}{1-\theta_{\mathrm{t}}}\right]^{\frac{3}{3-D_{\mathrm{p}}}} \tag{8.5}$$

and the fact that it must be replaced by

$$K_{\mathrm{p}}(\theta) \propto (\theta-\theta_{\mathrm{t}})^2 \tag{8.6}$$

in the vicinity of θ_{t}. For the sake of clarity, K calculated by Eq. (8.5) is fractal scaling, denoted K_{f}, while K according to Eq. (8.6) is percolation scaling, denoted K_{p}.

Standard methods of producing pressure-saturation curves use drainage across a porous ceramic plate. A positive air pressure is applied to the sample, and its effect on pore water-allowability is assumed equivalent to that of an equivalent tension applied to the water phase. These measurements typically require long equilibration times, because at low water contents, hydraulic conductivity values can be extremely low. For example, suppose we have a partially drained 10 cm high column of soil with porosity $\phi = 0.5$, and we subject it to a pressure $h = 1$ m. If $K(\theta) = 10^{-8}$ cm/s (a reasonable value), then removing water equivalent to a 1 mm thick layer, i.e. decreasing θ by 0.02, will take over 500 days. As long as measured values of K diminish in a regular way according to Eq. (8.5), one can extrapolate the equilibration time for the next step of an experiment. But the two relationships for K (K_{p} in Eq. (8.5) and K_{f} in Eq. (8.6)) raise a new complication: if θ drops below the cross-over moisture content $\theta_{K\mathrm{x}}$, then K decreases much more rapidly (see Fig. 8.3)). The equilibration times required by Eq. (8.6) are therefore much greater [16]. If this marked increase in equilibration time is not anticipated, then the ratio of the allowed time to the required time would equal the ratio $K_{\mathrm{p}}/K_{\mathrm{f}}$; the observed reduction in water content would likewise be too small, on the order of $K_{\mathrm{p}}/K_{\mathrm{f}}$. Specifically, on a fractal soil which at pressure h_i equilibrates to a moisture content $\theta = \theta_{\mathrm{xK}}$, then when the pressure is increased to h_{i+1} the water content will be reduced by only

$$\Delta\theta = \frac{K_{\mathrm{p}}}{K_{\mathrm{f}}}\phi\left[\left(\frac{h_{\mathrm{A}}}{h_{i+1}}\right)^{3-D} - \left(\frac{h_{\mathrm{A}}}{h_i}\right)^{3-D}\right] \tag{8.7}$$

within the allowed time: with too little drainage time, the moisture content will not drop as rapidly as predicted by the fractal model.

We have developed an algorithm for predicting the non-equilibrium moisture content of a medium. The algorithm is based on Eq. (8.7); that is, it assumes

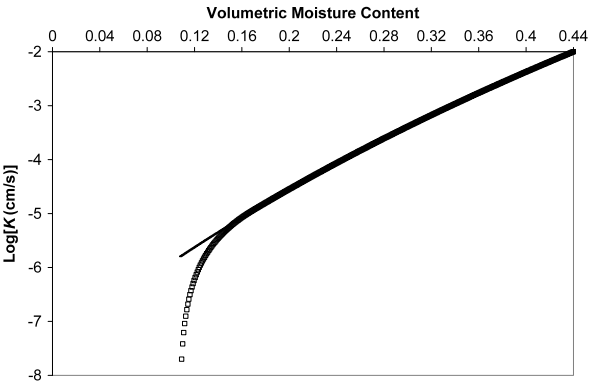

Fig. 8.3 A generic hydraulic conductivity as a function of saturation, but similar to that of the McGee Ranch soil (Fig. 6.1). This figure shows the deviation from fractal scaling of the conductivity at low moisture contents associated with the cross-over to percolation scaling

that the allowed drainage time at any given tension is calculated by extrapolating K_f (Eq. (8.5)) to ever-drier conditions. The algorithm assumes differentially small changes in tension, and relates a geometrical water loss to an actual water loss:

$$d\theta_a = \left[\frac{K_p(\theta_a)}{K_f(\theta_a)}\right] d\theta \tag{8.8}$$

where the subscript a denotes actual. Now integrate (over the dummy variable, θ') to obtain

$$\int_{\theta_{xK}}^{\theta} d\theta' = \int_{\theta_{xK}}^{\theta_a} d\theta' \frac{K_f(\theta')}{K_p(\theta')} \tag{8.9}$$

The right hand integral is given in terms of the Gauss hypergeometric function ${}_2F_1$. By defining

$$G(x) \equiv \frac{K_S}{(1-t)K_0}\left[\frac{1-\phi}{1-\theta_t}\right]^{\frac{3}{3-D}} (x-\theta_t)^{1-t}\, {}_2F_1\left[1-t, \frac{3}{3-D}, 2-t, \frac{\theta_t - x}{1-\phi}\right] \tag{8.10}$$

we can write an implicit relationship for θ_a:

$$\theta - \theta_{xK} = G(\theta_a) - G(\theta_{xK}) \tag{8.11}$$

that maps $\theta_t \le \theta_a \le \theta_{xK}$ to $0 \le \theta \le \theta_{xK}$. The original, or presumed water retention function, $h(\theta)$, is then mapped to $h(G(\theta_a))$. Note that since K vanishes at θ_t, the moisture content θ_t is never reached with this procedure. Figure 8.4 shows the effects of incomplete equilibration on the apparent water-retention curve, as predicted by this algorithm, for the same system shown in Fig. 8.3. Although the algorithm is simple, the results are robust. The procedure was also performed algorithmically for finite pressure steps Δh. Over the relatively wide range of Δh values investigated, the resulting non-equilibrium portion of the water retention curve (not shown) was identical to that predicted by Eq. (8.11), generated by changing the pressure in infinitesimal steps. An interesting aspect of these results is the quasi-universality of the shape of the water-retention curve in the vicinity of θ_t.

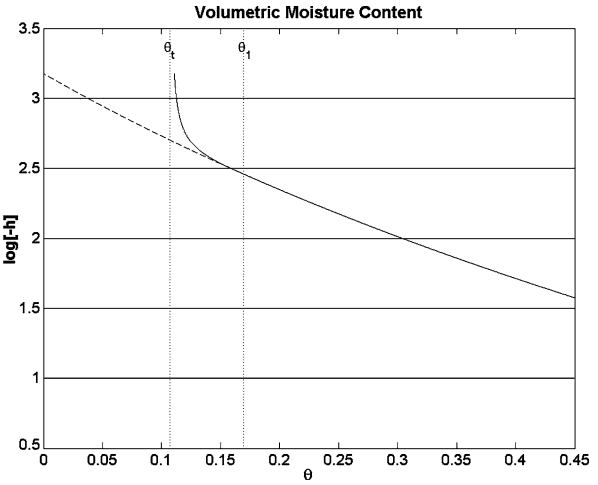

Fig. 8.4 The non-equilibrium water retention curve expected for the medium with K represented in Fig. 8.3. Here the threshold water content is given as θ_t, while the cross-over moisture content is given as θ_{xK} (changed from Hunt and Skinner [16]). Equations (8.10) and (8.11) were used to make this figure

The above is a somewhat oversimplified picture as well as an oversimplified calculation: both the actual value of K and its extrapolated value change over the time the water is draining. Nonetheless, it gives accurate predictions of experimental data, as shown in Figs. 8.5–8.6 (from Hunt and Skinner [16]). To generate these predictions, particle-size data were used to find the ratio r_0/r_m, the porosity ϕ and ratio r_0/r_m were combined to give D_p, then h_A was used as an adjustable parameter to generate the equilibrium moisture contents. θ_t was taken as the lowest water content obtained in the experiment, and θ_{xK} was calculated from Eq. (6.23); then for

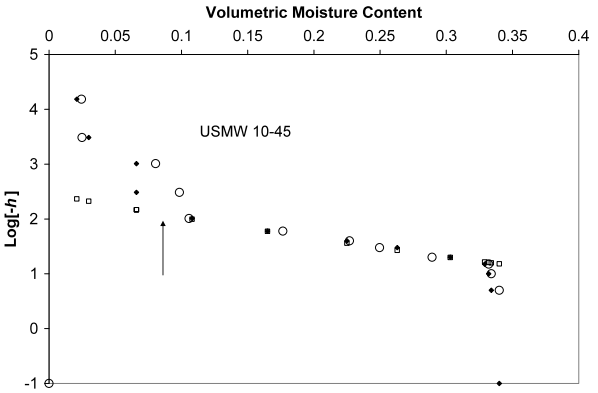

Fig. 8.5 A reevaluation of the deviation of experimental water-retention curves from the fractal scaling (Eq. (4.24)) at low moisture contents. The *solid diamonds* are experimental data for the USMW 10–45 soil from the Hanford site [6], while the open squares are the predictions from Eq. (4.24). The *open circles* are obtained from the algorithm described in the text, which reduces the actual moisture lost by the ratio of Eq. (8.6) to Eq. (8.5). This algorithm is only appropriate for $\theta < \theta_x$, which was obtained using Eq. (6.26) and the lowest moisture content attained by experiment for θ_t

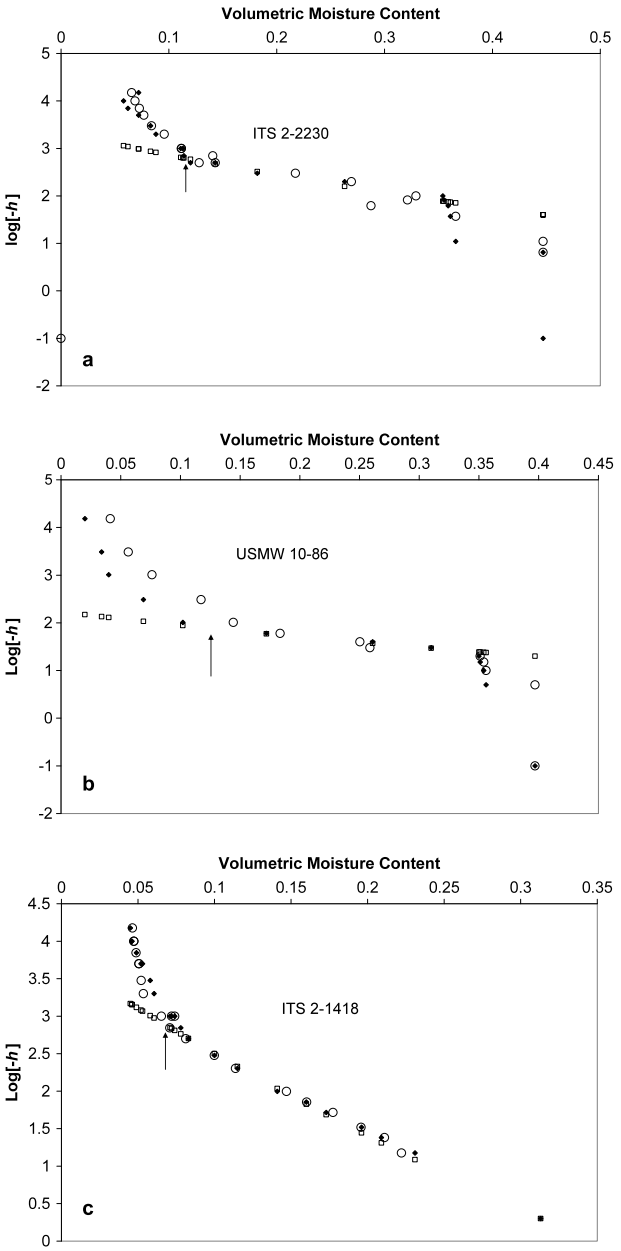

Fig. 8.6 The same demonstrations for 6 other Hanford site soils

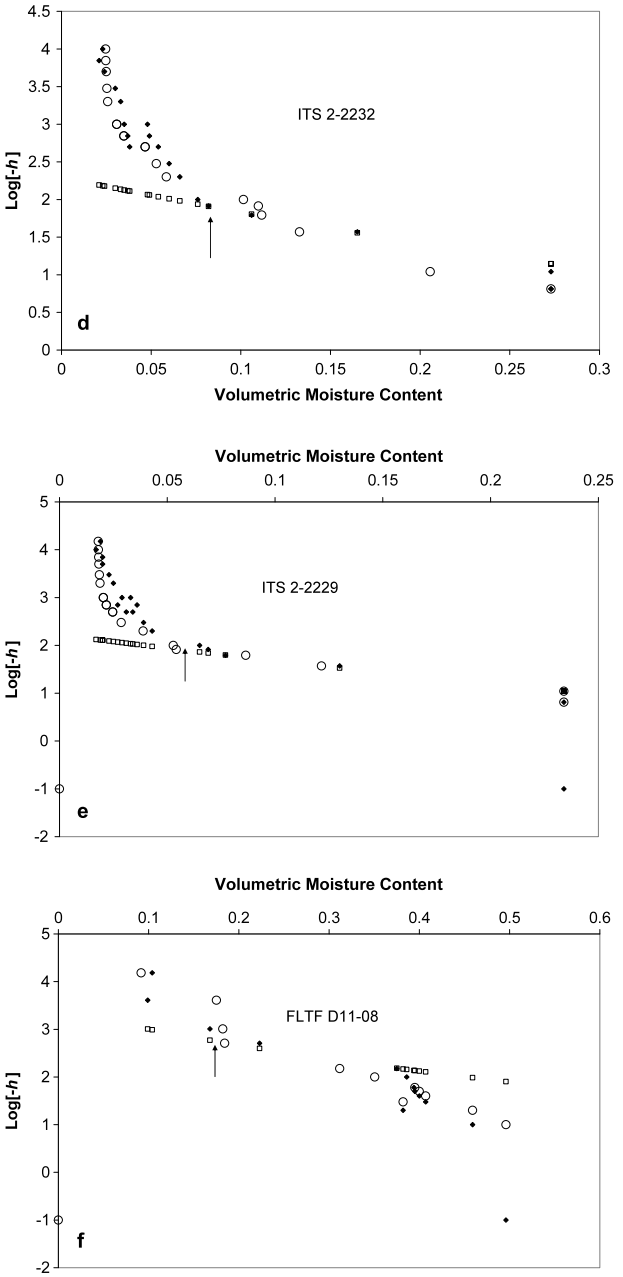

Fig. 8.6 (Continued)

all values of h corresponding to $\theta < \theta_{xK}$, the magnitude of $\Delta\theta$ was reduced by the ratio K_p/K_f as in Eq. (8.7). However, this procedure still yielded a predicted moisture content lower than the observed value. In order to match the observed moisture contents, it was necessary to take the ratio of the actual value of K and the value of K assumed to be accurate for a moisture content *two time steps prior*. This suggests that the value of K from a previous measurement was used as a guide for a subsequent measurement, which would imply that the authors of the study were not anticipating any reduction in K, even according to a result compatible with Eq. (8.5). Applying this connection to K two measurements earlier is equivalent to using an adjustable parameter; on the other hand the same value of this parameter was used for all seven of the cases investigated and presented here. Given this restriction on flexibility, the predictions appear to be quite accurate.

The results presented here suggest that widely-observed deviations from fractal scaling of pressure-saturation curves at low saturations are not a defect of the fractal model itself. On the contrary, because parameters derived from the use of fractal models (in particular, θ_t) can then be used to predict hysteresis in drainage and imbibition, or ($\theta_{x,k}$) the shape of the water retention curve in the vicinity of the percolation threshold, the case for fractal treatments is actually strengthened. It is not unreasonable to speculate that a large number of natural soils may be best described by the Rieu and Sposito [26] fractal model.

In addition to the 12 soils analyzed for dry-end deviations caused by non-equilibration (of which 7 are shown in this chapter), we have also analyzed soils for which neither the particle-size data nor the water-retention curves is consistent with the relatively simple Rieu and Sposito model [3]. Rather, in these soils there is considerable complexity at relatively high water contents. These results are described in Chap. 12 in another context.

We (Dr. Skinner and Dr. Hunt) were engaged in a project which reverses the procedure described here. Rather than predicting the (non-equilibrium) water retention curve from a given pore size distribution, we estimate the actual pore size distribution from the (non-equilibrium) water retention curve. The procedure involves inverting Eq. (8.8), solving for $0 < \theta < \theta_{xK}$ in terms of $\theta_t < \theta_a < \theta_{xK}$. For a fractal model then, the equilibrium water loss would be given by multiplying the non-equilibrium water loss by K_f/K_p. In the general case, K_f, is replaced by a general result from critical path analysis. The inverse problem is made more complex as a consequence of the lack of sufficient pore size data to apply critical path analysis for values of $\theta < \theta_{xK} + \theta_t$. Any solution must then be tested for self-consistency. We estimated first θ_t as the lowest moisture content reached. We estimated θ_{xK} as the point where the water retention curve appears to develop a positive deviation (in h). If θ_t was chosen to be too large, we generated negative moisture contents and chose a smaller value for θ_t. In order to constrain the values of θ_{xK} we required the ratio of conductivities to be a monotonically increasing function.

We found that using critical path analysis to generate an extrapolation of the numerical results for K to moisture contents $\theta < \theta_{xK} + \theta_t$ gives a good trial solution; when $K(\theta)$ so obtained is substituted into Eq. (6.35), we found that, for the case shown, our initial estimate of θ_{xK} was within 1 % of the solution from Eq. (6.35),

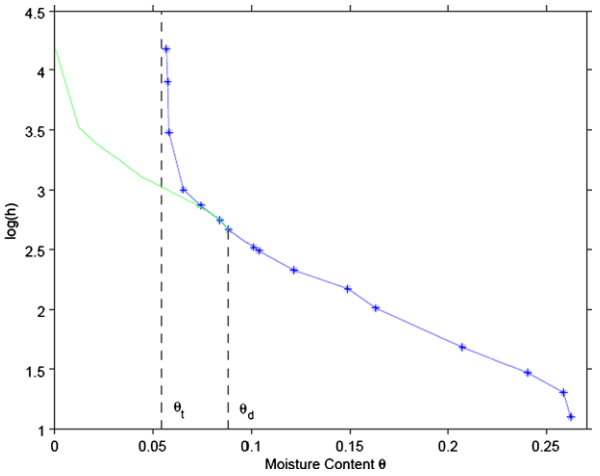

Fig. 8.7 The crosses and the associated curve show initial water-retention data (from [28]). The critical moisture content for percolation, θ_t, and the point at which the water retention curve begins to deviate from the equilibrium pore-size statistics, $\theta_d = \theta_{xK}$, are clearly indicated. Our procedure generated the green curve as the equilibrium water-retention curve, implying that a pore-size distribution extracted from the raw data would put a great deal more water into smaller pores than is justified. This result, if verified generally, would imply that many conclusions based on the importance of surface water and water in pits or fractures of individual particles have been overstated

which we considered to be acceptable. The results of our procedure are shown in Fig. 8.7. Such final results could then be used to recalculate any properties that were estimated originally from the pore size distribution implied by the water retention curve. If the results of Fig. 8.7 prove reliable, they will indicate that a much larger fraction than is typically assumed is contained in water-filled pores and that the amount of water on surfaces or in pits of grains is relatively small (<5 %). Note that this conclusion is generally compatible with other results that imply small critical moisture contents for percolation, and small water contents in pendular structures (thermal conductivity). But we found that the bootstrap inversion process to find the actual pore-size distribution was quite unstable and often yielded unphysical results. Only about 20 % of the time did we generate results that we deemed reliable.

This discussion ultimately leads to the question: Which is more useful in determining the pore size distribution: the water-retention curve, or the particle-size distribution? The reader will have to answer that question for him- or herself, but our contention is that, due to complications from phase continuity of the fluids (residual water, air entrapment, inaccessible allowed pores) and from fluid flow properties (non-equilibration), the water retention curve is quite inadequate by itself. Of course the particle-size distribution is also inadequate, lacking direct information on pore sizes as well as pore structure. From a pragmatic perspective, one uses the information that is available, and particle-size data are far more widely available than water retention data. We hope that future work will allow us to make use of both together, such that each can overcome deficiencies in the other.

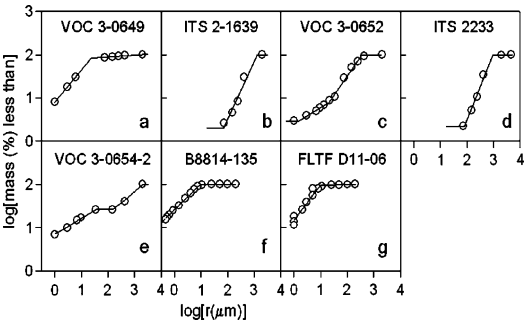

Fig. 8.8 Particle-size data for 7 Hanford site soils, all different from Figs. 8.4–8.6 (from [14]). The flat portions of the curve intersect the fractal scaling region at the radii r_0 and r_m

8.3 Analysis of Water-Retention Curves in Terms of the Critical Moisture Content for Percolation

The possibility that the dry end percolation transition might somehow produce deviations from the fractal scaling prediction motivated an earlier investigation into dry-end deviations in water retention curves [14]. While it was suspected that the lack of phase continuity could interfere with the removal of water, we did not think that the small magnitude of the hydraulic conductivity would produce the effect directly. Thus the values that were compiled were simply the moisture contents,[2] θ_d, at which the deviation from scaling set on. These moisture contents were then compared with the critical volume fractions for percolation from the solute diffusion experiments of Moldrup et al. [25].

The procedure followed was to use the particle size information from each of Freeman's [6] soils to find r_0/r_m, and thus determine the fractal dimensionality of the pore space from Eq. (4.19. Particle size data from seven of the soils are shown in Fig. 8.8). h_A was then adjusted to produce the best visual fit with the experimental data for the water-retention relationship (Eq. (4.24)), concentrating on the middle range of saturations. The value of θ_d was then determined by inspection (Fig. 8.9). Meanwhile, θ_t was also predicted using the relationship of Moldrup et al. [25], $\theta_t = 0.039(A/V)^{0.52}$, where A/V is the specific surface area. Application of this relationship normally relies on experimentally determined values of A/V, but that information was not available for Hanford site soils. The alternative was to calculate the dependence of the surface area on such quantities as r_0/r_m, and the fractal dimensionality of the solid medium, D_s, obtained from Eq. (4.20). We estimated A/V using the ratio implied by the RS model,

$$\frac{A}{V} \propto \frac{\int_{r_0}^{r_m} r^2 (r^{-1-D_s}) dr}{\int_{r_0}^{r_m} r^3 (r^{-1-D_s}) dr} \tag{8.12}$$

implicitly assuming that the geometrical factors relating particle volume and particle surface area were both scale-invariant, and also the same for all of our soils. This

[2] Although it became clear that the experimentally determined θ_d could be identified with the theoretical θ_{xK}, it is useful to continue referring to θ_d in the context of these experiments.

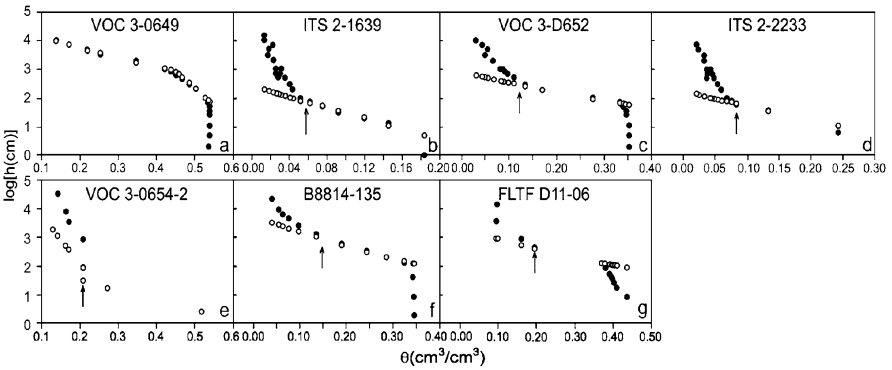

Fig. 8.9 The predicted and observed water retention curves for the same 7 Hanford site soils as in Fig. 8.8 (from [14]). h_A was again used as an adjustable parameter. In each case the arrow shows the value chosen for θ_d

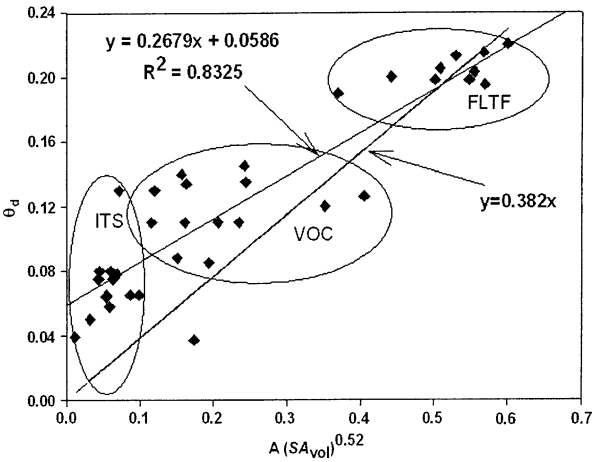

Fig. 8.10 Regression of θ_d on calculated θ_t, using the Moldrup relation for θ_t in terms of the specific surface area and using the Moldrup notation, SA_{vol} for A/V (from [14])

last (necessary) assumption is clearly incorrect, and introduced some random error into the comparison.

We could now compare the measured θ_d with the value of θ_t from the Moldrup relationship. There was clearly a proportionality constant that we had not estimated, but the important result [14] was that $\theta_d = C\theta_t + 0.06$ for some numerical constant C (Fig. 8.10); meanings of the abbreviations for the various soils are given in Hunt and Gee [14]. The value of R^2 for the regression was 0.83. At the time of the study the result that there was a positive intercept was not understood since the further development of the theoretical description [13] to include the cross-over from Eq. (8.5) to Eq. (8.6) had not been made. Thus several attempts were made to try to find some complicating factor in the analysis.

In the most important analysis, a subset of soils was excluded from consideration because in these soils the hydraulic conductivity could be deduced to fall to very low

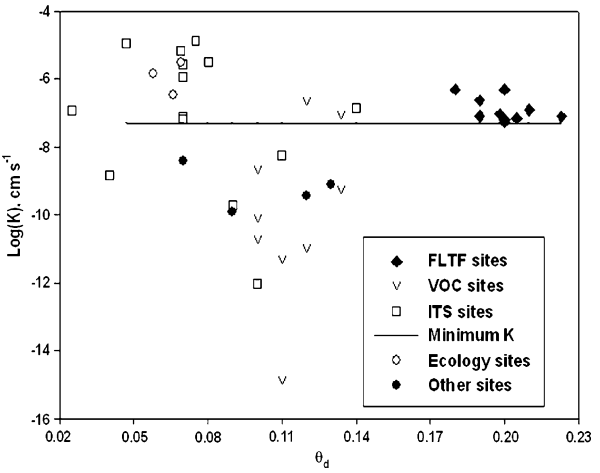

Fig. 8.11 From [14]. Representation of $\log(K)$ at θ_d vs. θ_d for 40 Hanford site soils. The *horizontal line* depicts the minimum value of $K = 5 \times 10^{-8}$ cm/s [14], for which equilibrium moisture contents were measurable under the stated experimental conditions [19]. The 15 soils with $K(\theta_d) < 5 \times 10^{-8}$ cm/s were excluded from subsequent analysis in terms of percolation theory; their deviation from fractal scaling was determined by other factors (see text)

values at moisture contents well above θ_t on account of either small K_S values or D_p values near 3. For values of the hydraulic conductivity less than approximately 5×10^{-8} cm/s, the experimental procedure used to gather the data, [19] could be shown [14] using Eq. (8.15) to be inadequate to drain the soils to equilibrium on account of their experimental time limit of six weeks. The prediction was based on the use of Eq. (8.5) to calculate $K(S)$ from porosity, fractal dimensionality and the saturated value of the hydraulic conductivity [18]. Figure 8.11 shows the values of K at θ_d from this calculation for soils of various areas on the Hanford site. Note that the lowest K values were obtained for the VOC (Volatile Organic Carbon) soils, and it is apparent from Fig. 8.10 that these soils also exhibited the largest values of θ_d relative to the regression equation. Although R^2 for the correlation between θ_d and θ_t rose to 0.94 after soils with low K values were excluded from the analysis, for reasons other than the proximity to the percolation transition, the intercept remained unchanged at 0.06. After the development of Eq. (6.23) for the relationship between θ_{xK} and θ_t [11], we could interpret θ_d as θ_{xK}. Indeed it turns out that if the mean values $D_p = 2.857$ and $\phi = 0.394$ for the Hanford site soils are inserted into Eq. (6.21), one finds $\theta_{xK} - \theta_t = 0.06$ [12]. The equivalence of these two numerical values implies that the conclusions for the subset of soils investigated in Sect. 8.2 are likely to apply to most of the data set of 43 soils.

The implication of the study as a whole was that *all of the deviations from fractal scaling* of the water retention curve could be attributed to lack of equilibration, i.e. values of $K(S)$ which were too low to allow the equilibrium change in water content actually to occur. Not all soils had low values of $K(S)$ for the same reason, but for

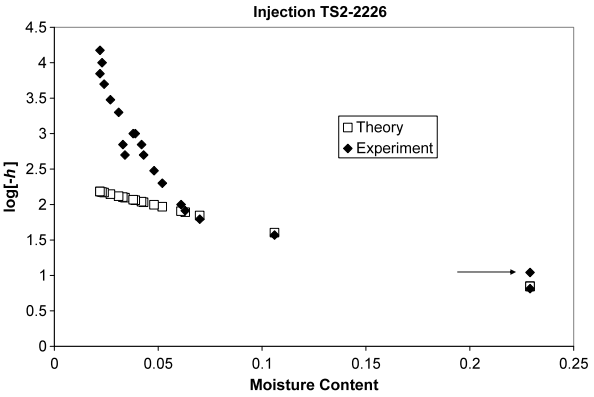

Fig. 8.12 An example of a wet-end deviation to higher moisture contents than predicted from fractal scaling. The *solid diamonds* are again data from Freeman [6], while the open squares are from Eq. (4.24). This deviation is predicted by percolation theory from the inability of air to enter the system until the air-allowable pore space percolates

a large number of the soils the cause was the approach to the percolation transition. This question is further discussed in the last portion of this chapter.

The development of this regression of θ_d on θ_t had an added benefit. It was now possible to calculate A/V from Eq. (8.12) for the McGee Ranch soil and North Caisson soils [13], and to use the same regression to predict their values of θ_t. Using the values of θ_t it became possible to predict the hydraulic properties of those two soils without use of adjustable parameters (Figs. 6.1 and 6.2). Of course the same regression could have been used for any of the individual soils in this study for the same purpose (and was), but there was a limited use for those predictions since the data for the hydraulic conductivity as a function of saturation for the remaining 43 soils was not made available to us. Nevertheless, those calculations were then used to predict $K(\theta_d)$ above and exclude soils from the analysis, for which $K(\theta_d) < 5 \times 10^{-8}$ cm/s.

Some important additional comments need to be made. The fact that the critical moisture content for percolation of the Hanford site soils (usually small clay contents) correlated quite well with the value from the Danish soils [25] and their often rather high clay contents will have several consequences for further analysis of the predictability of θ_t. It may be important, however, that the Hanford site soils often had 3–5 % clay sized particles and, though not often, sometimes up to 10 % or so.

8.4 Wet-End Deviations from Fractal Scaling of Water-Retention Curves, and Discussion of the Critical Volume Fraction for Percolation

In most cases the fractal predictions of water-retention curves also deviate from experiment at water contents near saturation. These deviations involve predictions of the water content that can be either too high (Fig. 8.12) or too low (Fig. 8.13). Understanding of these deviations is at present inferior to that of the deviations at low moisture contents, although it appears that on the whole such discrepancies

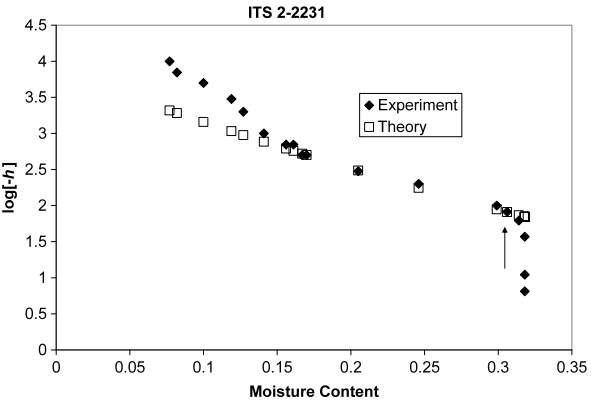

Fig. 8.13 An example of a wet-end deviation to lower moisture contents than predicted from fractal scaling. This deviation is related to finite-size effects, described in percolation theory [20]

relate to lack of percolation of the air phase. In Fig. 8.14 the determination of the wet-end moisture contents, θ_w, at which deviations from fractal scaling occurred, is shown. Hunt and Gee [15] showed that, for a suite of approximately 40 Hanford site soils θ_t was nearly the same as $\phi - \theta_w$, though perhaps slightly larger (Fig. 8.15). The case where a higher tension must be reached then h_A before air actually begins to enter the soil, with consequent upward curvature of the water-retention curve

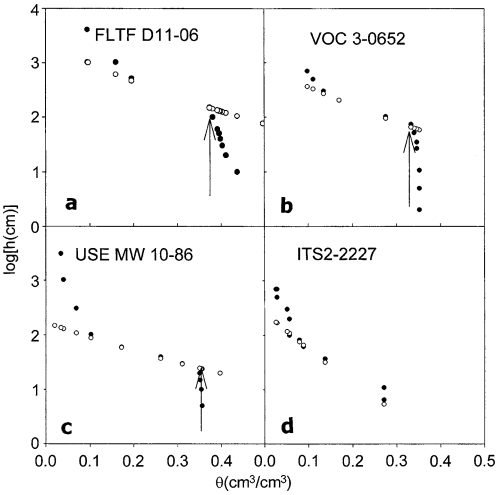

Fig. 8.14 From Hunt and Gee [15]. Determinations of wet-end moisture contents θ_w at which deviation from fractal scaling of water retention occurs for four soils. The open circles are theory (from Eq. (4.24)), the solid circles experiment. The fractal dimensionality for the pore space was determined in Hunt and Gee [14] from the particle-size distribution and the porosity, and the air-entry head (h_A) was used as an adjustable parameter. The wet-end deviations from fractal scaling are indicated with *arrows*. Two soils from Hunt and Gee [14] are used for which the wet-end deviation could clearly be seen, FLTF D11-06 (**a**) and VOC 3-0652 (**b**). For a number of the ITS soils, such as 2-2227 shown here, θ_w was better determined from the bubbling pressure by the method of Problem 8.1

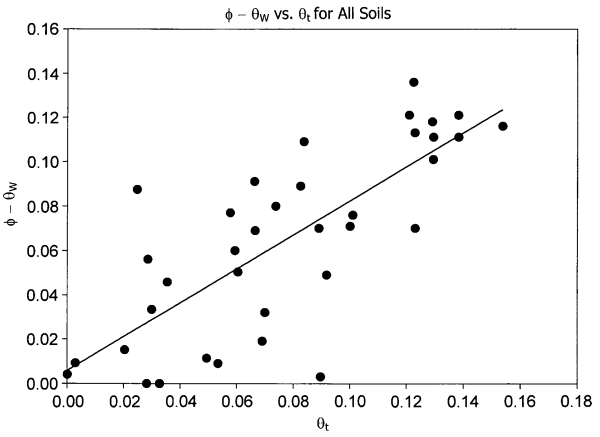

Fig. 8.15 Comparison for the Hanford site soils of θ_t, determined from θ_d using Eq. (6.23) with $\phi - \theta_w$, the wet end deviation from fractal scaling. θ_w determined as in Figs. 8.12–8.14

exceeding the prediction from fractal scaling, could be reasonably interpreted using percolation concepts. In some of these soils the actual value of θ_w could not be determined directly but was calculated by the method presented in Problem 8.1. But the case where air entered at lower tensions than expected seemed less easy to interpret. Now, however, we can refer to Larson and Morrow [20] who showed that the downward curvature is an artifact of finite size effects and disappears in the limit of infinite systems. Consequently we postulate the following understanding: If the system size is held constant, the variation in the wet-end deviation from fractal scaling with medium characteristics, even if associated with a downward curvature, does reflect a change in a critical air threshold.

The result that $\phi - \theta_w$ for the Hanford site soils is very nearly the same as θ_t raises the question of whether one should actually expect the critical volume fraction to have the same value for air as for water. If the effects of wetting of surfaces are neglected then it is possible for the two critical volume fractions to be the same. But this is not a sufficient condition for equality. One must also have that the critical moisture content for percolation be independent of the moisture content. While this is not by any means guaranteed by theory, experiment appears to confirm that θ_t is a constant, independent of moisture content (see the results for solute diffusion in Chap. 7). The effects of water adsorbed to surfaces would be minimized when the surface area to volume ratio of the soil is minimized, which would be the case for porous media composed mainly of large particles. Clay minerals, due to their lack of charge neutrality, are known to adsorb an especially large amount of water. Practically speaking, media with very low or zero clay content (sand and silt only) have relatively small surface area to volume ratios and in these media the fraction of the water adsorbed on surfaces can be neglected. So the result that θ_w for the Hanford site soils is very nearly the same as $\phi - \theta_t$ is consistent for media with low clay content, but the results of Moldrup et al. [25] for θ_t are interpreted in terms of the adsorption of water on clay mineral surfaces, providing an apparent conflict. An explanation for this puzzle may be given by a combination of the following argument for θ_t and the results that R^2 varied between 0.6 and 0.8 for the various correlations (and the fact that the Hanford sites do contain some clay).

How would one estimate the critical volume fraction for percolation in a porous medium with insignificant adsorption of water to solid surfaces? Consider first a network of tubes of uniform diameter and length placed on a lattice. The space between the tubes can be considered the solid portion of the medium. In such a case one can immediately deduce that the critical volume fraction for percolation must be

$$V_c = p_c \phi \tag{8.13}$$

and the critical volume fraction for percolation is a fraction of the porosity. Experimentally obtained values for very coarse soils [13] suggest that p_c in three dimensions is typically on the order of 0.1, and one finds $V_c = \theta_t \approx 0.1\phi$. For the proportionality constant to be so small requires a rather large coordination number for the pores, and it is also important that the pore space itself be well connected. There is some evidence of this; Manwart et al. [24] report that 97.2 % of the pore space in the Berea sandstone, and 99.4 % in the Fountainebleau sandstone belong to the percolating cluster. In soils we expect these values to be higher. With increasing clay content, however, a simple proportionality between V_c and ϕ becomes inadequate [13]; either the proportionality constant p_c tends to increase, or another contribution to V_c must exist. Continued use of Eq. (8.13) with an increasing value of V_c is not preferred for several reasons [13]. A second contribution to V_c comes from water adsorbed on the surface of particles; this is a water content, which will be present, but which does not contribute to capillary flow. It is this contribution to $V_c (= \theta_t)$, which appears to have been detected in the diffusion experiments that established the relationship $D_{pm}/(D_w\theta) = 1.1(\theta - \theta_t)$. Analysis of the experimental relationship $\theta_t = 0.039(A/V)^{0.52}$ showed [13] that this could be interpreted as a surface water contribution on clay minerals as long as $3 - D \approx 0.5$. $D = 2.5$ is a rather small value from the present perspective, although it has been stated [2] that D values for clayey soils are typically in the range 2.5–2.6 (in contrast to coarser soils).

On the basis of the above analysis it was concluded that a general expression for θ_t should probably contain both contributions and look something like

$$\theta_t - 0.1\phi \propto \left(\frac{A}{V}\right)^{3-D} \tag{8.14}$$

Theoretical development does not really permit an accurate estimation of the proportionality constant at present; one can also not use the experimental value from Moldrup et al. [25] since that experimental regression did not include a term independent of surface area. Thus it is best to leave the result (8.14) in terms of a proportionality. It is worthy of note that it is common in the porous media community to speak of a "residual" water content, present after normal drainage of a soil. Quoting Luckner et al. [23] by way of van Genuchten et al. [29] "The residual water content, θ_r, specifies the maximum amount of water in a soil that will not contribute to liquid flow because of blockage from the flow paths or strong adsorption onto the solid phase." Equation (8.14), with further developing and testing to clarify the values of the constants, should prove a general means to estimate both contributions

to θ_t. It is very important, however, that only the term $p_c\phi$ would contribute to the critical air fraction for percolation, since air is not wetting and does not adsorb to the surface of any particles. Thus, except for very coarse soils, one should expect that the critical air fraction for percolation should be much smaller than the critical moisture content. But for coarse soils these two values should usually be very similar if not identical, as appears to be the case in Fig. 8.15.

Such a small value of $p_c \approx 0.1$ for a lattice model in three dimensions would imply that the effective coordination number, Z, is 15 (using $Zp_c = d/(d-1)$). Even a face-centered cubic system has a value of Z of only 12, so this large value of Z suggests that the typical coordination number is quite large. In fact, Jerauld et al. [17] give a reasonable explanation for such a large Z value. In networks generated by Voronoi tessellation these authors do find $Z \approx 15$, making $p_c \approx 0.1$ a reasonable choice for media with relatively small clay content.

Overall, $p_c \approx 0.1$ appears in so many different contexts in this book that there is a motivation for understanding it.

8.5 General Formulation for Equilibrium and Analogy to Ideal Glass Transition

Sections 8.2 and 8.3 demonstrate that reduction of the moisture content to values near the threshold moisture content for percolation can easily cause experiments involving changes in moisture content in porous media to fall out of equilibrium. This process can also be called a kinetic transition, because on one side of the transition, the system obeys the ergodic hypothesis, but on the other side it does not, whereas the transition point is not precisely defined on account of its dependence on the rate of change of system parameters, and thus on experimental conditions. A similar situation exists in the case of the glass transition in viscous liquids. As the temperature of viscous liquids is reduced, the temperature dependent transport properties slow down so much that it may be impossible for the liquids to attain equilibrium with further reduction in temperature (on experimental time scales). All geologists are probably familiar with the argument that window glass will flow if given enough time (although the examples cited may not actually be evidence of this). Many investigators have sought to relate the glass transition in viscous liquids to a phase transition. What can be gained from a comparison between these systems and concepts?

In an ideal glass transition a kinetic transition is underlain by a structural phase transition, but the structural phase transition is never directly observed because the system falls out of equilibrium first. Since the result is never directly observed, one cannot measure directly a transport quantity that is approaching zero. Thus people look for some length scale, which seems to be diverging in the vicinity (but slightly below) the kinetic transition. Exactly this kind of result, Eq. (6.23) and the accompanying physics of a diverging correlation length, has now been obtained for porous media, and the accompanying predictions regarding lack of equilibration apparently

verified. Although similar evidence has been sought regarding the glass transition in viscous liquids, it has never been found, and so it must be concluded that the glass transition in viscous liquids is not an example of an ideal glass transition [10]. Nevertheless there is some benefit in a comparison, particularly in the matter of the calculation of such a kinetic transition point. The transition point corresponds to a temperature in the case of the glass transition, and a moisture content for porous media.

The "kinetic" transition in viscous liquids is basically a case where the system falls out of equilibrium and the ergodic hypothesis fails. The kinetic transition has been defined to result when the time for mechanical relaxation exceeds 100 seconds [10]. This is an imprecise definition and cannot be appropriate for all experiments. The mechanical relaxation time is an exponential function of the temperature, and relaxation times can thus increase very rapidly when the temperature is lowered, if it is low relative to the fundamental scale of the exponential function to begin with. In fact such an exponential dependence of the mechanical relaxation time on temperature allows for a definition of the transition temperature.

In experiments on the glass transition the system is cooled at a constant rate and at a given temperature, called the glass transition temperature, T_g, there is a sudden drop in the heat capacity of the system. For the calculation of T_g [9] a constant cooling rate was represented as a staircase function with finite changes in temperature ΔT in times Δt. The average slope $\Delta T/\Delta t$ was constrained to equal the actual dT/dt. The glass temperature was found by relating the temperature steps ΔT to the time steps Δt through the condition that the relaxation time of the system increases by Δt over the temperature range ΔT. The solution of this equation could be obtained by numerical methods if the dependence of the relaxation time (α-relaxation peak) on the temperature was known. The result could be verified to give the correct dependence of T_g on the cooling rate, even though this dependence was very weak (logarithmic). Thus, even in the absence of an assumption of a special value of T, for which motion was essentially frozen, the rapid slowing down of systems represented by the exponential function was sufficient to define a kinetic transition temperature, T_g.

In the actual calculation of the transition moisture content we approximate a discontinuous function, the discrete changes, Δh, in tension over discrete time intervals, Δt, by a continuous function [11], exactly the reverse of the situation for the glass transition. This approximation allows a simple application of the chain rule to relate theoretical and experimental quantities. Consider an experiment on a column of height z. If the required value of $d\theta/dt$ is larger than the ratio of $K(h)$ to z ((cm/s)/cm), the column moisture content cannot change rapidly enough to adjust. But the required value of $d\theta/dt$ is related to experimental quantities as follows [11]:

$$\frac{d\theta}{dt} = \frac{dh/dt}{dh/d\theta} \equiv \frac{\Delta h/\Delta t}{dh/d\theta} = \frac{K(h)}{z} \tag{8.15}$$

If, through a procedure during which the tension h is increased episodically by Δh and a subsequent time interval Δt is allowed for drainage, $K(h)$ has finally diminished to the extent that the right hand side can no longer exceed the left hand

side of Eq. (8.15), then the time scale of the experiment must be increased, or the system will fall out of equilibrium. Equation (8.15) can easily be solved for the time interval, Δt, as a function of $K(h)$, z, and the derivative $dh/d\theta$ while $dh/d\theta$ can be obtained from the appropriate equilibrium water retention function.

It may be of interest that while the glass transition in viscous liquids is apparently not an example of an ideal glass transition, the drying of porous media is.

8.6 Oil Residuals

In the early 1980s Chandler et al. [4] produced a very nice analysis of 2D simulations of residual oil ganglia remaining after flooding with water. The total oil remaining was a function of the width, y, of the channel flooded. We believe that it is a valuable exercise to bring up these results again and discuss them from a different perspective. In an infinite system the oil remaining would be equal to the critical volume fraction. But, in finite two-dimensional systems, the total oil remaining must be present only in finite clusters of sites, since it is not possible for both the water and the oil phase to percolate simultaneously. In addition, clusters larger than the width of the channel must drain, since they have access to the outside. Thus the remaining oil is the difference between the critical volume fraction and the oil drained. This result can be obtained by summing the total volume over all the finite cluster contributions (of size less than $y = r_s = s^{\sigma\nu}$),

$$V_{\text{oil}} \propto \int_1^{y^{\frac{1}{\sigma\nu}}} s^1 s^{-\tau} ds = 1 - y^{\frac{2-\tau}{\sigma\nu}} \tag{8.16}$$

Using Eq. (1.25), $(\tau - 2)/\sigma = \beta$ one finds that the remaining oil volume must scale as $V_c - y^{-\beta/\nu}$, in agreement with the scaling results of Chandler et al. [4] and with finite-size scaling. Consider that the fraction of sites connected to the infinite cluster is $(p - p_c)^\beta$, which implies a scaling with system size, $y^{-\beta/\nu}$. But the sites not connected to the infinite cluster are those (oil-filled) sites left, $\propto V_c - y^{-\beta/\nu}$.

Our analysis has the additional benefit that the analyses of Chaps. 9 and 10 rely on cluster statistics of percolation based on the same kind of reasoning, but we have been able to show that in the present context they give known results.

Note that, in this chapter, our theoretical calculations were confirmed by comparison with about 50 water retention experiments with associated particle size data, encompassing some 600 individual experimental results in each.

Problems

8.1 Calculate the "bubbling pressure" for a fractal model. Assume that air does not begin to enter (bubble) until the air-allowable volume is a large enough fraction of the porosity to percolate.

8.2 It is a common practice in the porous media community to assume that the interfacial tension is a more fundamental variable than the moisture content. Find a reason why people might assume this. Hint: use the bubbling pressure result from #7.1 and then calculate the pressure at which the water phase would become discontinuous. Assume that both critical volume fractions are 0.1ϕ. You should obtain a ratio for the two pressures of $[(1-0.9\phi)/(1-0.1\phi)]^{1(/3-D)} \approx (1-\phi)^{1/(3-D)}$. For typical soils ($D = 2.8$, $\phi = 0.4$) this ratio is $1/7.6$ (the approximation yields $1/12.9$). Of course this ratio is smaller than the ratio of the smallest to the largest pore size, and thus typical pressure saturation curves do not, in the intermediate saturation regime, contain the full range of pore sizes present.

8.3 Reevaluate the Wilkinson [30] treatment of hysteresis using moisture content as the fundamental percolation variable rather than the pressure. Do his conclusions still hold? What physics could be responsible for the discrepancies between the modified theory and experiment?

8.4 Compare the present derivation of oil residuals with the treatment of Chandler et al. [4]. What does the comparison say about scaling arguments from percolation theory?

References

1. Bauters, T.W.J., DiCarlo, D.A., Steenhuis, T.S., Parlange, J.-Y.: Preferential flow in water-repellent sands. Soil Sci. Soc. Am. J. **62**, 1185–1190 (1998)
2. Bittelli, M., Campbell, G.S., Flury, M.: Characterization of particle-size distribution in soils with a fragmentation model. Soil Sci. Soc. Am. J. **63**, 782–788 (1999)
3. Blank, L.A., Hunt, A.G., Skinner, T.E.: A numerical procedure to calculate hydraulic conductivity for an arbitrary pore size distribution. Vadose Zone J. **7**, 461–472 (2008)
4. Chandler, R., Koplik, J., Lerman, K., Willemsen, J.F.: Capillary displacement and percolation in porous media. J. Fluid Mech. **119**, 249–267 (1982)
5. Clement, E., Baudet, C., Guyon, E., Hulin, J.P.: Invasion front structure in a 3D model porous medium under a hydrostatic pressure gradient. J. Phys. D, Appl. Phys. **20**, 608–615 (1987)
6. Freeman, E.J.: Fractal geometries applied to particle size distributions and related moisture retention measurements at Hanford, Washington. M.A. Thesis, University of Idaho (1995)
7. Gist, G.A., Thompson, A.H., Katz, A.J., Higgins, R.L.: Hydrodynamic dispersion and pore geometry in consolidated rock. Phys. Fluids, A **2**, 1533–1544 (1990)
8. Heiba, A.A., Sahimi, M., Scriven, L.E., Davis, H.T.: Percolation theory of two-phase relative permeability. SPE Reserv. Eng. **7**, 123–132 (1982)
9. Hunt, A.: The calorimetric glass transition: a simple model. Philos. Mag. **64**(5), 563–577 (1991)
10. Hunt, A.G.: Non-Debye relaxation and the glass transition. J. Non-Cryst. Solids **160**, R183–R227 (1993)
11. Hunt, A.G.: Continuum percolation theory for water retention and hydraulic conductivity of fractal soils: 2. Extension to non-equilibrium. Adv. Water Resour. **27**, 245–257 (2004)
12. Hunt, A.G.: Percolative transport and fractal porous media. Chaos Solitons Fractals **19**, 309–325 (2004)
13. Hunt, A.G.: Continuum percolation theory for water retention and hydraulic conductivity of fractal soils: 1. Estimation of the critical volume fraction for percolation. Adv. Water Resour. **27**, 175–183 (2004)

14. Hunt, A.G., Gee, G.W.: Water retention of fractal soil models using continuum percolation theory: tests of Hanford site soils. Vadose Zone J. **1**, 252–260 (2002)
15. Hunt, A.G., Gee, G.W.: Wet-end deviations from scaling of the water retention characteristics of fractal porous media. Vadose Zone J. **2**, 759–765 (2003)
16. Hunt, A.G., Skinner, T.E.: Hydraulic conductivity limited equilibration: effect on water-retention characteristics. Vadose Zone J. **4**, 145–150 (2005)
17. Jerauld, G.R., Hatfield, J.C., Scriven, L.E., Davis, H.T.: Percolation and conduction on Voronoi and triangular networks: a case study in topological disorder. J. Phys. C **17**, 1519–1529 (1984)
18. Khaleel, R., Freeman, E.J.: Variability and scaling of hydraulic properties for 200 area soils, Hanford site. Westinghouse Hanford Company Report WHC-EP-0883 (1995)
19. Khaleel, R., Relyea, J.F.: Variability of Gardner's alpha for coarse-textured sediments. Water Resour. Res. **37**, 1567–1575 (2001)
20. Larson, R.G., Morrow, N.R.: Effects of sample size on capillary pressures in porous media. Powder Technol. **30**, 123–138 (1981)
21. Lenhard, R.J.: Measurement and modeling of 3-phase saturation pressure hysteresis. J. Contam. Hydrol. **9**, 243–269 (1992)
22. Lenhard, R.J., Parker, J.C., Kaluarachchi, J.J.: Comparing simulated and experimental hysteretic 2-phase transient fluid-flow phenomena. Water Resour. Res. **27**, 2113–2124 (1991)
23. Luckner, L., van Genuchten, M.Th., Nielsen, D.R.: A consistent set of parametric models for the two-phase flow of immiscible fluids in the subsurface. Water Resour. Res. **25**, 2187–2193 (1989)
24. Manwart, C., Torquato, S., Hilfer, R.: Stochastic reconstruction of sandstones. Phys. Rev. E **62**, 893–899 (2000)
25. Moldrup, P., Oleson, T., Komatsu, T., Schjoning, P., Rolston, D.E.: Tortuosity, diffusivity, and permeability in the soil liquid and gaseous phases. Soil Sci. Soc. Am. J. **65**, 613–623 (2001)
26. Rieu, M., Sposito, G.: Fractal fragmentation, soil porosity, and soil water properties I. Theory. Soil Sci. Soc. Am. J. **55**, 1231 (1991)
27. Sahimi, M., Yortsos, Y.C.: Applications of fractal geometry to porous media: a review. Paper presented at the 1990 Annual Fall Meeting of the Society of Petroleum Engineers, New Orleans, LA (1990)
28. Schaap, M.G., Shouse, P.J., Meyer, P.D.: Laboratory measurements of the unsaturated hydraulic properties at the vadose zone transport field study site. PNNL Report, 14284, Pacific Northwest National Laboratory, Richland, WA 99352 (2003)
29. van Genuchten, Th.M., Leij, F.J., Yates, S.R.: The RETC code for quantifying the hydraulic functions of unsaturated soils. US EPA 000/091/000, ADA OK, 83 pp. (1991)
30. Wilkinson, D.: Percolation effects in immiscible displacement. Phys. Rev. A **34**, 1380–1391 (1986)
31. Wilkinson, D., Willemsen, J.: Invasion percolation: a new form of percolation theory. J. Phys. A, Math. Gen. **16**, 3365–3376 (1983)

Chapter 9
Applications of the Correlation Length: Scale Effects on Flow

In percolation theory, the fractal nature of large clusters near the percolation threshold underlies some interesting scale dependences of conduction and transport properties. The correlation length gives a measure of the largest length scale at which non-Euclidean, or fractal, geometry effects should be seen. This means that the correlation length must be intimately connected with the quantity known in porous media research communities as a representative elementary volume, or REV. Note that the kind of finite-size scaling results reported in Sect. 2.4 will give results for conduction that decrease with increasing size, however, in view of the fact that the conductivity vanishes with approach to the percolation threshold. However, we can show that calculations of conduction (or flow) based on critical path analysis can, in principle, deliver increases in conductivity or permeability with increasing scale, if the increase in spatial scale brings about an increase in the dimensionality of conduction. This result is based on the strong diminution of p_c with increasing dimensionality. In order to make such comparisons, however, we must be in possession of the tools to calculate an REV, which is based on the correlation length. The actual value of the correlation length will depend on geologic correlations since they can set a fundamental length scale.

Even in the absence of geologic correlations, sedimentary deposits near the percolation threshold will exhibit correlations in medium type. One of the important arguments of the works that this chapter is based on has been that, under common circumstances, a relevant correlation length may be constructed as the product of a geologic factor and a statistical factor from percolation theory. In particular, the correlation length in percolation theory is proportional to a (negative) power of $|p - p_c|$ and a prefactor which, in a bond percolation problem, is proportional to the length of a bond. In a geologic medium described in continuum percolation theory, however, this quantity corresponding to a bond length is actually a geologic correlation length. How these two factors can be separated is discussed below.

A. Hunt et al., *Percolation Theory for Flow in Porous Media*,
Lecture Notes in Physics 880, DOI 10.1007/978-3-319-03771-4_9,

9.1 Representative Elementary Volume (REV)

The correlation length is the system-dependent parameter, which defines the structure of the dominant current-carrying (electric or fluid) paths. Refer back to Fig. 1.3. The typical separation of the nodes is represented in this figure, and this separation is equal to the correlation length, χ. The physical reason for this is that χ describes the size of the largest holes above the percolation threshold. Furthermore, the tortuosity of the backbone of the largest clusters below the percolation threshold is the same as the tortuosity of the links above the percolation threshold. The influence of the blobs in calculating the conductivity is rather secondary since the most resistive elements that cannot be avoided tend to be found in the portions of links without blobs—by definition there is no alternative to the paths through these (except, in the case of critical path analysis, to go to more resistive elements). In fact, as just suggested, χ can be used to describe the structure of such paths in two different contexts: (1) near the percolation transition it gives a characteristic separation of the only possible paths of interconnected medium, which can be used to transport, e.g., air, water, or electrical current, (2) *far from the percolation threshold*, application of critical path analysis involves an optimization which leads to a calculation of the separation of the paths along which the *dominant* transport occurs. In either case, χ^3 is effectively the representative elementary volume, or REV, because in each case χ defines the length scale of the heterogeneity relevant for transport. In earlier chapters critical path analysis was used to generate explicit expressions for the correlation length. As long as the numerical coefficient in the proportionality from percolation theory is not available, however, calculations using the correlation length cannot reliably yield precise numerical coefficients for specific systems so the results are given only in terms of system parameters. In this chapter some systems are treated for which there is little or no information regarding "microscopic" variability, and the expressions derived contain further unknown constants. Thus the development here is only diagnostic and not predictive. In Chap. 5 an example of this type of argument (originally due to Shklovskii and Efros [38]) is given in the problems with an at least semi-quantitative prediction.

9.2 Isolation of Geologic and Percolation Effects on a Correlation Length

We propose that the percolation and geologic effects on a correlation length can be isolated as follows. The research ideas presented in this section have been developed in parallel with Dr. Robert Ritzi and co-workers, and citations to their relevant articles are given.

Consider first a medium which contains a small fraction of sands (<25 %, say) and for which the remainder is composed of finer materials, such as muds. Even though $p < 0.25$ it is nevertheless not unlikely that the sand fraction of the medium is near the percolation threshold. Percolation thresholds tend to be lowered

in strongly correlated systems [19, 25]. Geologically correlated systems are typically characterized by anisotropy while local correlations tend to make the system smaller in a statistical sense. Both anisotropy [11] and small system size [30] tend to reduce p_c.

Discretize a representation of a natural medium in cubic grid blocks. Choose each grid as sand or mud, associating the label chosen with the dominant volume fraction in each block. In one dimension, the percolation probability is one so that in a 1D transect the sand fraction is far below the percolation threshold, and even the mud fraction is not close. Suppose then that one considers the statistics of one-dimensional transects through such a medium. The correlations of the individual grid cells will be at most minimally affected by the percolation variables, so that any correlations are geologic in nature. If the geologic correlation structure is appropriate (for example exponential rather than power-law in form), these correlations will be described by a typical length scale [12, 26], which we can call here, χ_0, and which has insignificant influence from percolation. The composite correlation length in the three-dimensional medium will then be given by the product of the geological factor, χ_0 and a percolation function, $|p - p_c|^{-\nu}$.

9.3 Effects of Dimensional Cross-Overs on Conductivity

A great deal of debate surrounds the issue of whether the hydraulic conductivity can increase with the scale of the measurement. Given the fact that experiment has repeatedly given such results, it seems obvious that the answer is yes. But this does not seem to be the answer from percolation theory. To some this is the major unsolved problem in subsurface hydrology. A few of the examples often quoted are: Bradbury and Muldoon [4], Schad and Teutsch [33], Shouse et al. [39], Rovey and Cherkauer [29], Sanchez-Villa et al. [32], Schulze-Makuch [34], Tidwell and Wilson [43], [44], Schulze-Makuch and Cherkauer [36], Samper-Calvete and Garcia-Vera [31], Schulze-Makuch et al. [35], Davy et al. [7], Paleologos et al. [24], Di Federico and Neuman [8, 9], Di Federico et al. [10], Hunt [13, 14], Chen et al. [6], Martinez-Landa et al. [21]; Zhang et al. [45], Zlotnik et al. [46], Hyun et al. [18], Neuman and Di Federico [23]. Of the above, all publications except that of Shouse et al. [39] deal with geologic scales. Some authors have contested some of the individual experiments (e.g., [5]) and some authors have certainly reported theoretical descriptions for which K diminishes with increasing scale [24]. In Chap. 9 it is shown that the cluster statistics of percolation theory are clearly compatible only with a diminishing value of K with increasing measurement scale. Nevertheless we feel that it is necessary to discover why measurements of the hydraulic conductivity can increase with increasing scale.

Of the above works, Davy et al. [7] and Neuman and co-workers look for theoretical reasons to generate an increase in K with the scale of measurement. The works of Neuman and co-workers are largely based on information from variograms, and a concrete comparison between those works and percolation theoretical works does

not yet exist. Davy et al. [7] propose an increase in connectivity with increasing scale, but their model appears to generate a porosity which increases according to a power of the measurement scale x. There is nothing wrong per se with a porosity which increases with scale; the Rieu and Sposito [28] fractal model would allow an increase of the form $1 - (r_0/x)^{3-D_P}$, if the largest pore radius, r_m, could be proportional to the system size, x. However, a power-law form for the porosity can exceed 1, while the Rieu and Sposito [28] model is limited by $\phi = 1$. This matter becomes partly semantic; it makes some sense to declare that a sample which falls entirely within a given pore (or fracture) does not belong to the medium when the property of interest is the porosity. But it makes no sense to exclude such a region from the hydraulic conductivity. Why? A region of air that surrounded an instrument would not be considered part of a solid medium, but the hydraulic properties of that medium are defined exclusively by the pore space and to leave out the largest pores at the smallest scales is to introduce a scale-dependent bias into the measurement.

There are other reasons for an apparent increase in K with scale x that can be easily discovered within the framework of percolation theory (and one example is given below), but it turns out that such results are not indicative of a scale effect per se. Although the relevance of percolation theory to geologic scales has sometimes been called into question, the same general difficulties to describe the flow and transport in such media exist, e.g., flow channeling [22], which Shah and Yortsos [37] demonstrate is also best treatable in a framework such as that of Katz and Thompson's [20] critical path analysis.

The fact that critical values of the percolation probability, p_c, are such strong functions of dimensionality, together with the fact that for strongly disordered media the "upscaled" value of a conduction or flow property depends so sensitively on p_c means that a cross-over in the dimensionality of conduction can produce a very large effect in the effective transport (or flow) parameter. Thus it is of great importance to be able to identify what physical constraints on conduction lead to dimensional constraints. The important quantity to determine relates, as one might expect, to an REV, or in the language of percolation theory, to the correlation length.

When conduction is isotropic, the analysis is relatively simple and unsurprising. Consider first a cylindrical system, such as a heterogeneous non-metallic wire. How thick can such a wire be before conduction along it is not one-dimensional? The maximum thickness can be obtained by considering an infinitely large and equidimensional system of such material, calculating the correlation length (according to either problem above) and comparing χ with the diameter of the wire, d. If $d > \chi$, the system is not strictly one-dimensional and increasing d values will eventually make the conduction of the system three-dimensional. If $d < \chi$, however, for large lengths, the cylinder exhibits strictly one-dimensional conduction. As an alternative, consider an infiltration experiment, in which a grid is mapped out and metallic plates each some specific length, such as 1 m, are inserted into the soil to divide it into a simple square grid [39]. How small can the separation of these plates be made while maintaining three-dimensional conduction in the vertical direction? Again the answer is based on the comparison of the separation of the dividing plates with the correlation length. However, the depth of insertion of the plates is also an important input. Even if the separation of the plates is smaller than the correlation length,

if the depth is equally small (for isotropic conduction), the problem involves only finite-size effects, not dimensionality effects. Such a simple picture is complicated by anisotropy, but it is nevertheless possible to take a number of anisotropic systems and transform the medium to isotropic form [42]. Such a coordinate transformation affects the volumes of existing or proposed experiments as well, however, and then the problem is to analyze the transformed experimental volumes in terms of the correlation length.

In fact, any of the sort of problems dealt with in this chapter in terms of the correlation length can also be treated in greater depth using the cluster statistics of percolation in subsequent chapters. Nevertheless, when it is possible to make a simple calculation based on the correlation length, the labor saved may be well worth the choice.

For conduction through a rectangular solid to be truly 3D, all dimensions of the solid must be larger than the correlation length, χ. For solid-state physics treatments of the dimensionality of conduction in terms of the correlation length see Shklovskii and Efros [38] and Raikh and Ruzin [27]. In three dimensions χ behaves as,

$$\chi = \chi_0 (p - p_c)^{-\nu} \tag{9.1}$$

where $\nu = 0.88$ [40]. Here χ_0 is a fundamental length, which we take here as being a typical length of a single resistor. An appropriately shaped volume, which is in principle compatible with experiments for treating upscaling in isotropic 3D systems, is a cube. As Tartakovsky and Neuman [42] point out, the axes of anisotropic systems can be rescaled to give equal conductances in each direction. The appropriately shaped upscaling volume for an anisotropic system with, e.g., K values 1000 times larger in the horizontal directions is a rectangular solid with equal horizontal dimensions, but a vertical dimension $1000^{1/2} \approx 31$ smaller [15]. The cross-sectional area on the sides is diminished by a factor $1000^{1/2}$, reducing its conductance accordingly, while the length of the vertical dimension is diminished by the same factor, increasing its conductance by the same factor. This leaves equal conductances in each dimension. The reason why such a "flattened cube" is the appropriate system shape for upscaling, is that the fundamental relationships of the system dimensions to the details of the conduction process cannot change differently in different directions as the scale of the problem is increased. Use of, e.g., a cubic volume for the purposes of scaling up the hydraulic conductivity in the presence of such anisotropy would be equivalent, in the isotropic case, to using a prism with long (vertical) axis 31 times as long as the horizontal axes (Fig. 9.1 from [15]). In such a case it is easily possible for the correlation length to be shorter than the vertical dimension and larger than the horizontal dimensions. This means that for vertical transport, the flow (current) would like to exit the narrow volume, but cannot. Constraining the flow to remain within the volume is a dimensional constraint. If all axes are subsequently lengthened by, say, a factor 31, certainly all dimensions will be larger than the correlation length, whereupon the flow would be 3D, with K as calculated for a 3D medium. This constitutes a change in dimensionality, from 1 to 3, that occurs as a result of the increase in scale, but is not a scale effect per se, since it could be eliminated by choosing the appropriate experimental volume shape.

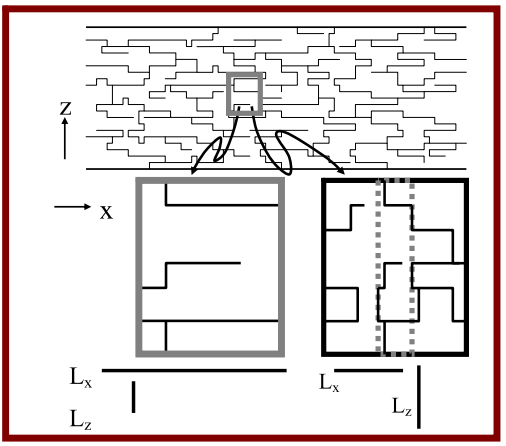

Fig. 9.1 A schematic depiction of a medium with much higher horizontal connectivity than vertical connectivity and the correlation lengths in each direction. A rescaling of length in the horizontal coordinates transforms the system to an isotropic system, but also shrinks the horizontal dimensions of the experimental volume. Now the correlation length is the same in each direction, but it is larger than the horizontal dimension of the experimental volume and smaller than the vertical dimension, providing for 1D conduction

Instead of considering the equidimensional anisotropic case, consider for clarity the transformed medium with elongated volume and isotropic K (Fig. 9.1). Rather than considering flow along the vertical axis to go through a qualitatively defined cross-over from 1D flow to 3D, the method constructed here for solution of this problem is to choose a maximum R, such that the value of the correlation length, χ, is always constrained to be smaller than or equal to the horizontal dimensions of the system. If χ is smaller than the horizontal dimensions, it is certainly smaller than the vertical dimension. This gives a continuous dependence of the effective value of the critical volume fraction and thus of the value of the limiting resistance on the size of the system. In the limit that the system size goes to infinity, this constraint becomes inconsequential and the result must conform to the 3D value of K. In the limit of small system size, p_c must approach 1 and the result for K must conform to the value for 1D flow. χ is constrained to be smaller than the dimensions of the system by the simple matter of making an effective p_c larger than the 3D value, exactly as expected from restricted dimensionality. In such a case the flow paths may appear to be three-dimensional at all scales, but the changing value of p_c is a result of the dimensional cross-over. So now let $\chi = x = V^{1/3}$, the original system size, and calculate how much larger p would have to be than p_c for a given x. The result is [15],

$$p = p_c + \left(\frac{\chi_0}{x}\right)^{\frac{1}{\nu}}; \qquad V = V_c + \left(\frac{\chi_0}{x}\right)^{\frac{1}{\nu}} \tag{9.2}$$

where the second form of the equation is the equivalent form for a continuum with volume fraction, V, replacing p, (and V_c replacing p_c). The reason why the second

form of the equality can be used by analogy is that the correlation length, χ, is expressed in terms of V and V_c for continuum percolation in the same way that it is expressed in terms of p and p_c for bond percolation. Equation (9.2) obviously gives $V = V_c$ for a system of infinite size, $x \to \infty$. For calculations of finite size corrections, Eq. (9.2) implies $p > 1$ in the limit of $x < \chi_0$, an unphysical limit, which can be approximately corrected by a small change in Eq. (9.2) to [15],

$$V = V_c + \left(\frac{\chi_0}{\chi_x + x}\right)^{\frac{1}{\nu}} \tag{9.3}$$

The basis for this modification is the physical requirement that χ be less than $x + \chi_0$, rather than merely x, compensating for the finite separation of resistances arising from their own intrinsic length, χ_0. Such a modification is clearly unnecessary for large x, but, in order for the formulation to make sense at small x it must be added. Equation (9.3), while still approximate, leads to no significant problem with p exceeding 1 as long as $p_c(\alpha_c)$ is very small, as can be the case in highly correlated systems [19, 25] and is assumed to hold here. The limiting value, $p_c = 1$, for small system sizes is a characteristic of strictly 1D conduction, and means that the most resistive element in the system can no longer be avoided. Use of a formulation such as Eq. (9.3) to find the change in V_c for small system sizes has the potential defect that the proportionality for the correlation length is being used in a range where it need not be accurate, far from percolation.

We can apply Eq. (9.3) to the continuum percolation calculation of Rieu and Sposito [28]. The Rieu and Sposito [28] model has been variously applied to soil porosity and to fracture systems. The Rieu and Sposito [28] fractal fragmentation model for soils expresses the total porosity as, $\phi = 1 - (r_0/r_m)^{3-D}$ in terms of the fractal dimensionality, D, and the minimum and maximum radii, r_0 and r_m, over which the fractal description holds. This model can also be used for fracture networks, but in this case r_0 and r_m refer to the smallest and largest fracture apertures, respectively. To calculate the rate-limiting resistance on the critical path one needs an expression for the fractional pore (or fracture) volume, $W(r)$, with pore radius (or fracture aperture) between r and $r + dr$, i.e., the pore volume probability density function. This expression is $W(r) = ((3 - D)/r_m^{3-D})r^{2-D}$ [17], which yields the known porosity, assumed to be the same for the fracture application. In the fully 3D case, under saturated conditions, the Rieu and Sposito model yields for the smallest aperture, r_c, on the optimal system traversing path,

$$V_c = \frac{3 - D}{r_m^{3-D}} \int_{r_c}^{r_m} dr r^{2-D}; \qquad r_c = r_m(1 - V_c)^{1/(3-D)} \tag{9.4}$$

Note that in the limit $V_c \to 0$, $r_c \to r_m$ meaning that with a critical volume fraction of zero, percolation is possible just using the largest fractures. Applied to fracture networks, in which the solid medium is ignored, Eq. (9.4) is best rewritten [15],

$$V_c = \left[\frac{1}{1 - \left(\frac{r_0}{r_m}\right)^{3-D}}\right]\left[\frac{3 - D}{r_m^{3-D}}\right] \int_{r_c}^{r_m} dr r^{2-D} \tag{9.5}$$

where a fraction V_c of the total fracture volume, $1-(r_0/r_m)^{3-D}$, (rather than a fraction of the total system volume), is sufficient to guarantee percolation through the fractures.

In order to find out how the smallest pore size changes as the critical volume fraction approaches 1 (the fully 1D limit), substitute Eq. (9.3) into Eq. (9.5) with the new $V > V_c$ taking the place of V_c, and letting (for convenience and simplicity) the original $V_c \to 0$ for infinite system size,

$$\left(\frac{1}{1-\left[\frac{r_0}{r_m}\right]^{3-D}}\right)\left(\frac{3-D}{r_m^{3-D}}\right)\int_{r_c}^{r_m} dr r^{2-D} = \left(\frac{\chi_0}{\chi_0+x}\right)^{\frac{1}{\nu}} \tag{9.6}$$

Equation (9.6) yields,

$$r_c = r_m\left[1-\left(1-\left[\frac{1}{R}\right]^{3-D}\right)\left(\frac{\chi_0}{\chi_0+x}\right)^{1/\nu}\right]^{\frac{1}{3-D}} \tag{9.7}$$

with $R \equiv r_m/r_0$. Using (for 3D saturated media) $K \propto r_c^2$, consistent with Hunt and Gee [17] (and Katz and Thompson [20], and in fact all the methods summarized by Bernabe and Bruderer [2]), and expressing $K(x)$ in terms of the value $K(3D)$ for $x \to \infty$, valid in 3D one finds [15],

$$\frac{K(x)}{K(3D)} = \left[1-\left(1-\left[\frac{1}{R}\right]^{3-D}\right)\left(\frac{\chi_0}{\chi_x+x}\right)^{1/\nu}\right]^{\frac{2}{3-D}} \tag{9.8}$$

Because Eq. (9.8) is expressed as a ratio of $K(x)/K(3D)$, the complications arising from the fact that even in an infinite system p is slightly larger than p_c can be neglected, just as these same complications were neglected in the calculation of the ratio of the unsaturated to the saturated hydraulic conductivity.

It should be noted that the general framework of the calculation given here would not change if the values of the hydraulic conductivity in the vertical and horizontal dimensions were the same, but the correlations of the hydraulic conductivity in the horizontal direction were much larger than the vertical direction. Use of a correlation length based treatment of a dimensional cross-over would still be appropriate. Now the correlation length from percolation theory would be larger in the horizontal direction than in the vertical because the random selection of a highly conductive element in the horizontal direction would more likely (in comparison with the vertical direction) be associated with other highly conductive elements in the same direction too, not simply because most connections in that direction were larger. Such conditions could be consistent with horizontal layering of sedimentary facies.

Field data from Schulze-Makuch and Cherkauer [36], as well as some other sources [29] are nominally consistent with hydraulic conductivity proportional to power laws of the support volume, $K \propto V^m$, over five to six orders of magnitude of volume V and 3–5 orders of magnitude of K. Reported powers, m, range from 0.5 to nearly 1. Represented as $\log(K)$ vs. $\log(V)$, the data appear to curve towards the horizontal at very small V, and also flatten at large V. Fits with data have simply employed power laws with the above values of m for small V and a horizontal line representing a constant K at large V.

9.4 Comparison with Field Data

In Fig. 9.2 *all* scale-dependent data for K (250 measurements) excluding capacity tests, which showed little trend, from Schulze-Makuch [34] are plotted as log K vs. log V, where V is a water volume, assumed here to be proportional to the solid volume. Almost 200 individual experiments are represented, one of the richest sources of data on this phenomenon. The data from Schulze-Makuch [34] certainly incorporated fracture flow, at least at larger support volumes. To fit these data, $R = 2500$, $D = 2.98$, and $K(3D) = 0.007$ m/s were chosen. This combination of R and D is consistent with a "fracture" porosity of $\phi = 0.14$. However, the result is quite insensitive to the chosen D, and values of 2.97 and 2.95 fit the data equally well. These are consistent with fracture porosity values of $\phi = 0.21$ and 0.32, respectively, meaning that the theory is not particularly sensitive to the value of the porosity chosen. The values of "vuggy" porosity for small *cores* quoted in Schulze-Makuch [34] are 9 % or lower, though these values may account for 90 % of the total core porosity in some cases. A "fracture" porosity is mentioned, but no values are given. The selected value of R implies that if the smallest fracture has an aperture of e.g., 40 μm, the largest has an aperture of 10 cm. While this is certainly a large range, dissolution of fractured carbonates can produce fractures over a wide size range. Although most of the data do appear to fit the same trend, the comparison made here, which uses all the data simultaneously, may not be appropriate. If individual facies were analyzed separately, the range of K values, and thus ratios of r_m to r_0, would be smaller, consistent with smaller porosities.

The horizontal asymptotes in these graphs correspond to ensemble averages for pure 1D ($\alpha_c = 1$) and 3D (with vanishing critical volume fraction) conduction, respectively. The ratio of the values of K in these two asymptotes is, by construction, R^2. If a more realistic finite, but small, value of α_c were chosen, the ratio of the values of K at the asymptotes would be reduced somewhat, since $r_c(3D) < r_m$ in that case.

Clearly some of the data do not follow the theoretical curve plotted. Thus we chose to display the data again (Fig. 9.3), but with the uncertainty generated by finite size complications and described by the cluster statistics of percolation theory (Chap. 10), and for which we displayed the distinct data sets enumerated by Schulze-Makuch. For the uncertainty calculation we simply took the parameters from Chap. 10 (e.g., $D = 2.95$, instead of 2.98), for which little difference in the expected dependence of K on volume can be seen when compared with Fig. 9.2. Here we can see that the uncertainty calculation from Chap. 10 does quite well in describing the variability of K within a given unit or facies (or location), while the outlying values at large V and smaller K, in particular, are also aggregated within given data sets. This result supports our presumption that much of the spread in K values at a given scale comes from the variability in the media investigated.

It is also possible to compare the values of these parameters with parameters from soils, to which the Rieu and Sposito [28] model has been applied. Note that while $D = 2.95$ is larger than typical values quoted (closer to 2.8 for soils [3]), values as high as 2.95 have been reported in Hanford soils [16]. The associated porosity (with

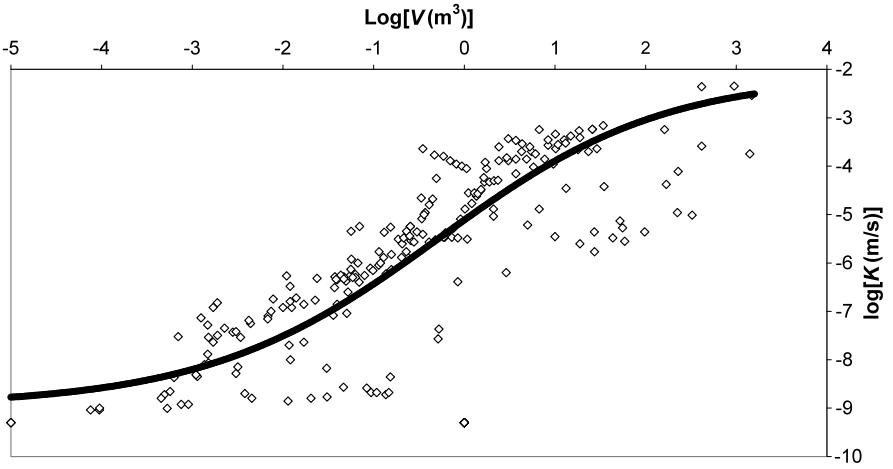

Fig. 9.2 Comparison of the prediction of Eq. (9.8) with the experimental data of Schulze-Makuch [34] for fracture networks in a carbonate aquifer. The experimental data are given by the *open triangles*. The parameters are $D = 2.98$ and $r_m/r_0 = 2500$

one exception) of the 45 Hanford soils ranged from $\phi = 0.24$ to $\phi = 0.54$, with the smaller ϕ values associated with the larger D values. Further, although $R = 5000$ is large, ratios of maximum to minimum pore sizes as high as 250 were described within centimeter sized core samples for Hanford soils. A related implication is that the same physical mechanism as described here could generate a scale effect on K of over four orders of magnitude (up to 250×250) in Hanford soils with significant clay layers as well. See Sect. 12.4 for a treatment of such anisotropy in the Hanford subsurface.

If the present theoretical description forms the basis for the observed scale dependence of K in anisotropic porous media, then it is possible, *in principle*, to conduct experiments in the same media, which do not show a scale effect.

One means to avoid such a scale dependence in anisotropic media would be to use experimental volumes with shapes elongated appropriately (by the square root of the ratio of K values) in the direction(s) of highest K values. However, this can be an easier exercise in lab experiments than it is in the field. Such experimental constructions are mathematically equivalent to isotropic media investigated with equidimensional support volumes, for which K diminishes with increasing size. The reason why K diminishes asymptotically to its infinite system value in that case is, that the dimensional cross-over with increasing system size described here is eliminated when the system is isotropic and the experimental volume equidimensional. The basis for the calculation is that finite size corrections to the infinite system hydraulic conductivity, as calculated from the effects of finite-sized system-spanning clusters, are always positive, but diminish as a negative power of the system size, because of the reduction in cluster numbers with increasing cluster size. These calculations were first given in Hunt [13] and supporting simulations were reported in Hunt [14].

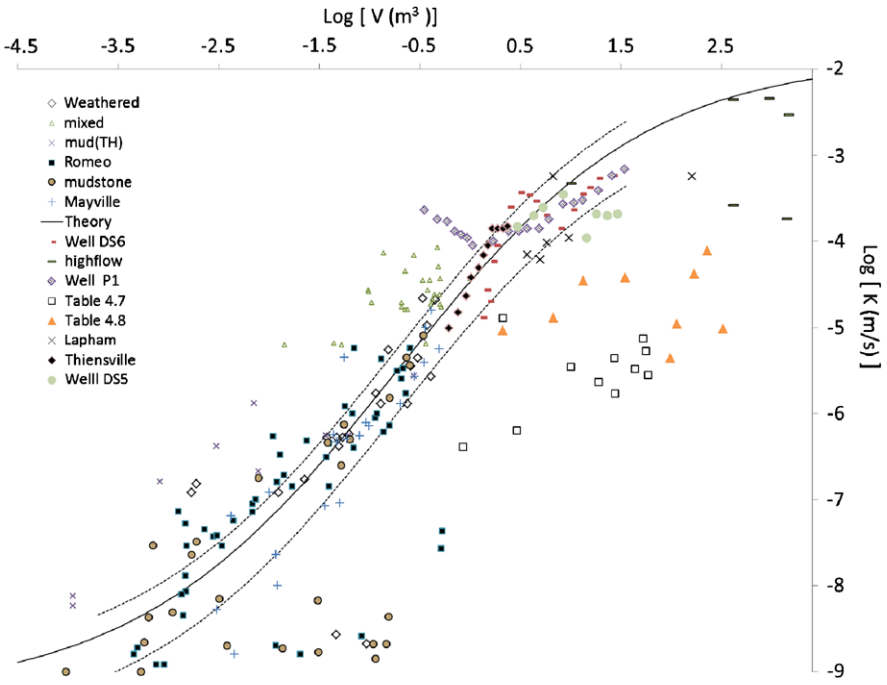

Fig. 9.3 Replot of the data of Fig. 9.2 showing that individual series of data points corresponding to specific experiments do tend to conform to the relatively narrow spread of values predicted for a single particular medium from Chap. 10. In this figure we actually use $D = 2.95$, but the difference between the two predictions is very small, if one compares with Fig. 10.4

This is a fundamental argument for associating the increase in K in anisotropic media with the dimensional cross-over rather than the increase in scale [15].

A second means to avoid seeing a scale effect on K in anisotropic media is to investigate volumes large enough that the dimensional cross-over is not visible (the 296 capacity tests from Table V of [34]). For those data this limit is almost reached as seen in Fig. 9.4. The mean of the slopes in the three cases used for comparison (Table IV.8, IV.7, and Well DS5, also shown in Fig. 9.3) is 0.14. Although the slope in the capacity tests is 0.19, the R^2 value was essentially zero, suggesting that the capacity tests were performed at scales large enough that the dimensionality restrictions did not apply. The purpose of redisplaying the data from Table IV.8 and IV.7 (and Well DS5) is that, whereas their presence helped demonstrate the cross-over to the asymptotic 3-D behavior in Fig. 9.3, their presentation in Fig. 9.4 demonstrates their fundamental consistency with the large amount of additional data from the capacity tests. And the additional data from the capacity tests reveals the large amount of spread in field measurements of the hydraulic conductivity that are not restricted to a given well or facies.

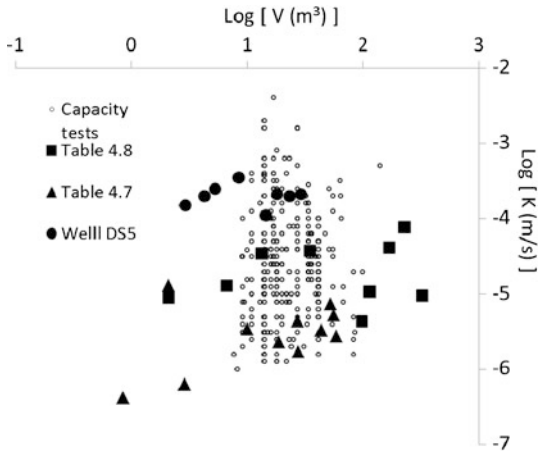

Fig. 9.4 A plot of the capacity tests (also from Schulze-Makuch) at larger typical spatial scales showing the relative insensitivity of the observed data range to the scale of the measurements

9.5 Effects of Hydrophobicity on Water Uptake of Porous Media

It has been regarded as puzzling that the existence of a few hydrophobic particles (ca. 5 %) in a porous medium could prevent water uptake at negative pressures (thus preventing spontaneous uptake of water). The puzzle likely arises from an incorrect perspective. It is true that it does not seem reasonable that a fraction of hydrophobic particles as small as 3–5 % could make an entire medium hydrophobic, but this perspective ignores the need to get the water into the medium. The water follows flow paths, whose separations are governed by the correlation length from percolation theory. *The fact that the pressure at which water normally enters the porous medium corresponds to the percolation transition* means that it is possible that a very small change in conditions can have a large effect on the flow paths.

Consider the following experimental arrangement [1]. From a large quantity of blasting sand a fraction was treated with cyclo-octanol, a chemical with extreme hydrophobic tendencies. This fraction was then mixed in at various fractions from 1 to 8 %. If the concentration of hydrophobic particles is N, and the typical diameter of the particles is d, then the typical separation of such particles must be approximately $(d)N^{-1/3}$. When water enters the medium the separation of the paths of water flow is equal to χ, which must be proportional to $d(\theta - \theta_t)^{-0.88}$. Use of the factor d acknowledges that a fundamental length scale proportional to the particle sizes must exist. Clearly water cannot access the major portion of the medium unless $\chi < (d)N^{-1/3}$, because otherwise it would be impossible to get the water between the hydrophobic particles. But such a small value of the correlation length can only be obtained when the moisture content (or allowed moisture content in the present case) is much larger than the critical moisture content for percolation.

Consider the following thought experiment. Start with a dry medium without hydrophobic particles and begin to decrease the tension, h. When h reaches h_c, defined in the previous chapter, water will begin to enter the medium. However, at this tension the infiltration paths are infinitely far apart. With a slight reduction in h, the path separation drops to, say, somewhere between one and ten per sample. If

even a small fraction of the normal sand grains had been replaced by hydrophobic grains, then these paths would have been interrupted and it would not be possible to bring water to the interior of the medium without running into hydrophobic grains. Water can be forced past hydrophobic grains at sufficiently large positive pressures, but in our case the pressure is still negative. So a further slight reduction in the magnitude of the pressure has little or no effect on the interaction of water with the hydrophobic grains, but it has a large effect on the separation of the infiltration paths, which becomes much smaller. This effect is prominent because the value h_c corresponds to the percolation phase transition. If the value for the correlation length is equated to the separation of the hydrophobic particles one can calculate the smallest value of the effective moisture content, for which the infiltration path separation is small enough to wet the interior. If the value of the moisture content needed is as large as the porosity, then it would be impossible to wet the interior of the system without forcing water past individual hydrophobic grains, which requires a positive pressure. Thus,

$$N^{-\frac{1}{3}} d \approx d(\phi - \theta_t)^{-0.88} \tag{9.9}$$

Solution of Eq. (9.9) for N (and using $\theta_t \approx \phi/10$) yields,

$$N = (0.9\phi)^{2.64} \tag{9.10}$$

Steenhuis et al. [41], which for typical porosities of about 0.4 yields about 0.067. In fact the Bauters et al. [1] sand from the previous section has porosity 0.4 and critical volume fraction 0.048, which would yield a slightly smaller value for N (0.063). Nevertheless one would expect that at a concentration of roughly 6 % hydrophobic particles a typical soil would already become water repellent. Experiment shows that water repellency for the relevant soil from Bauters et al. [1] already sets on at a concentration of about 5.5 % in a soil with porosity 0.4 and critical volume fraction approximately 0.04. Such a close agreement with experiment may be at this stage merely fortuitous, since all numerical constants in Eq. (9.9) have been suppressed. However, it is important that the predicted result, because of the 2.64 power, is much smaller than 1, and is more nearly on the order of 1 %–10 %. Solution of the problem below should help to convince students that the theoretical description is indeed accurate.

Problem

9.1 Suppose you know experimentally the water imbibition curve for a hydrophilic medium (zero percent hydrophobic particles). Using the calculation above for the modification to the effective critical moisture content for percolation (and water uptake) due to the presence of hydrophobic particles, then describe a technique, which would allow you to predict the imbibition curve for your system (with a prescribed fraction of hydrophobic particles). Use the results from Chap. 8 to predict the imbibition curve of any arbitrary medium (without hydrophobic particles) and then apply the procedure you just described to get a

family of imbibition curves with varying fractions of hydrophobic particles. Compare your results with Fig. 10.2.

References

1. Bauters, T.W.J., DiCarlo, D.A., Steenhuis, T.S., Parlange, J.-Y.: Preferential flow in water-repellent sands. Soil Sci. Soc. Am. J. **62**, 1185–1190 (1998)
2. Bernabe, Y., Bruderer, C.: Effect of the variance of pore size distribution on the transport properties of heterogeneous networks. J. Geophys. Res. **103**, 513 (1998)
3. Bittelli, M., Campbell, G.S., Flury, M.: Characterization of particle-size distribution in soils with a fragmentation model. Soil Sci. Soc. Am. J. **63**, 782–788 (1999)
4. Bradbury, K.R., Muldoon, M.A.: Hydraulic conductivity determinations in unlithified glacial and fluvial materials. In: Nielson, D.M., Johnson, A.I. (eds.) Ground Water and Vadose Zone Monitoring. ASTM STP, vol. 1053, pp. 138–151 (1990)
5. Butler, J.J., Healey, J.M.: Relationship between pumping-test and slug-test parameters: scale effect or artifact? Ground Water **36**, 305–313 (1998)
6. Chen, G., Illman, W.A., Thompson, D.L., Vesselinov, V.V., Neuman, S.P.: Geostatistical, type curve and inverse analyses of pneumatic injection tests in unsaturated fractured tuffs at the Apache Leap Research Site near Superior Arizona. In: Faybishenko, B., et al. (eds.) Dynamics of Fluids in Fractured Rocks. Geophysical Monograph, vol. 122, pp. 73–98. AGU, Washington (2000)
7. Davy, P., Bour, O., Darcel, C., De Dreuzy, J.: Permeability of 2D multi-scale fracture networks. Eos Trans. AGU **83**(47) Abstract H71B-0822 (2002)
8. Di Federico, V., Neuman, S.P.: Scaling of random fields by means of truncated power variograms and associated spectra. Water Resour. Res. **33**, 1075–1085 (1997)
9. Di Federico, V., Neuman, S.P.: Flow in multiscale log conductivity fields with truncated power variograms. Water Resour. Res. **34**, 975–987 (1998)
10. Di Federico, V., Neuman, S.P., Tartakovsky, D.M.: Anisotropy, lacunarity, and upscaled conductivity and its autocovariance in multiscale random fields with truncated power variograms. Water Resour. Res. **35**, 2891–2908 (1999)
11. Garboczi, E.J., Snyder, K.A., Douglas, J.F., Thorpe, M.F.: Phys. Rev. E **52**, 819–828 (1995)
12. Guin, A., Ritzi, R.: Studying the effect of correlation and finite-domain size on spatial continuity of permeable sediments. Geophys. Res. Lett. **35**, 10 (2008). doi:10.1029/2007GL032717
13. Hunt, A.G.: Upscaling in subsurface transport using cluster statistics of percolation. Transp. Porous Media **30**(2), 177–198 (1998)
14. Hunt, A.G.: Applications of percolation theory to porous media with distributed local conductances. Adv. Water Resour. **24**(3,4), 279–307 (2001)
15. Hunt, A.G.: Scale-dependent hydraulic conductivity in anisotropic media from dimensional cross-over. Hydrogeol. J. **14**, 499–507 (2006)
16. Hunt, A.G., Gee, G.W.: Water retention of fractal soil models using continuum percolation theory: tests of Hanford Site soils. Vadose Zone J. **1**, 252–260 (2002)
17. Hunt, A.G., Gee, G.W.: Application of critical path analysis to fractal porous media: comparison with examples from the Hanford Site. Adv. Water Resour. **25**, 129–146 (2002)
18. Hyun, Y., Neuman, S.P., Vesselinov, V.V., Illman, W.A., Tartakovsky, D.M., DiFederico, V.: Theoretical interpretation of a pronounced permeability scale-effect in unsaturated fractured tuff. Water Resour. Res. **38**, 1092 (2002)
19. Ioannidis, M.A., Chatzis, I.: The effect of spatial correlations on the accessibility characteristics of three-dimensional cubic networks as related to drainage displacements in porous media. Water Resour. Res. **27**, 1777 (1993)
20. Katz, A.J., Thompson, A.H.: Quantitative prediction of permeability in porous rock. Phys. Rev. B **34**, 8179–8181 (1986)

21. Martinez-Landa, L., Carrera, J., Guimera, J., Vasquez-Suñe, E., Vives, L., Meier, P.: Methodology for the hydraulic characterization of a granitic block. In: Stauffer, F., Kinzelbach, W., Kovar, K., Hoem, E. (eds.) Calibration and Reliability in Groundwater Modeling: Coping with Uncertainty, ModelCARE 99. IAHS Publication, vol. 265, pp. 340–345. IAHS Press, Wallingford (2000)
22. Moreno, L., Tsang, C.F.: Flow channeling in strongly heterogeneous porous media: a numerical study. Water Resour. Res. **30**, 1421 (1994)
23. Neuman, S.P., Di Federico, V.: Multifaceted nature of hydrogeologic scaling and its interpretation. Rev. Geophys. **41**, 1014 (2003)
24. Paleologos, E.K., Neuman, S.P., Tartakovsky, D.M.: Effective hydraulic conductivity of bounded strongly heterogeneous porous media. Water Resour. Res. **32**, 1333–1341 (1996)
25. Prakash, S., Havlin, S., Schwartz, M., Stanley, H.E.: Structural and dynamical properties of long-range correlated percolation. Phys. Rev. B **46**, R1724 (1992)
26. Proce, C.J., Ritzi, R.W., Dominic, D.F., Dai, Z.X.: Modeling multiscale heterogeneity and aquifer interconnectivity. Ground Water **42**, 658–670 (2004)
27. Raikh, M.E., Ruzin, I.P.: Size effect of the longitudinal hopping conduction of a narrow 2-dimensional channel. Phys. Rev. B **4**(2), 11203–11207 (1990)
28. Rieu, M., Sposito, G.: Fractal fragmentation, soil porosity, and soil water properties I. Theory. Soil Sci. Soc. Am. J. **55**, 1231 (1991)
29. Rovey, C.W. II, Cherkauer, D.S.: Scale dependency of hydraulic conductivity measurements. Ground Water **33**, 769–780 (1995)
30. Sahimi, M.: Flow phenomena in rocks—from continuum models to fractals, percolation, cellular automata, and simulated annealing. Rev. Mod. Phys. **65**(4), 1393–1534 (1993)
31. Samper-Calvete, F.J., Garcia-Vera, M.A.: Inverse modeling of groundwater flow in the semiarid evaporitic closed basin of Los Monegros, Spain. Hydrogeol. J. **6**, 33–49 (1998)
32. Sanchez-Villa, X., Carrera, J., Girardi, J.P.: Scale effects in transmissivity. J. Hydrol. **183**, 1–22 (1996)
33. Schad, H., Teutsch, G.: Effects of the investigation scale on pumping test results in heterogeneous porous aquifers. J. Hydrol. **159**, 61–77 (1994)
34. Schulze-Makuch, D.: Facies Dependent Scale Behavior of Hydraulic Conductivity and Longitudinal Dispersivity in the Carbonate Aquifer of Southeastern Wisconsin. Dissertation, University of Wisconsin, Milwaukee (1996)
35. Schulze-Makuch, D., Carlson, D.A., Cherkauer, D.S., Malik, P.: Scale dependency of hydraulic conductivity in heterogeneous media. Ground Water **37**, 904–919 (1999)
36. Schulze-Makuch, D., Cherkauer, D.S.: Variations in hydraulic conductivity with scale of measurement during aquifer tests in heterogeneous, porous, carbonate rocks. Hydrogeol. J. **6**, 204–215 (1998)
37. Shah, C.B., Yortsos, Y.C.: The permeability of strongly disordered systems. Phys. Fluids **8**, 280–282 (1996)
38. Shklovskii, B.I., Efros, A.L.: Electronic Properties of Doped Semiconductors. Springer, Heidelberg (1984)
39. Shouse, P.J., Ellsworth, T.R., Jobes, J.A.: Steady-state infiltration as a function of measurement scale. Soil Sci. **157**, 129–136 (1994)
40. Stauffer, D., Aharony, A.: Introduction to Percolation Theory, 2nd edn. Taylor and Francis, London (1994)
41. Steenhuis, T., Hunt, A.G., Parlange, J.-Y., Ewing, R.P.: Assessment of the application of percolation theory to water-repellent soils. Aust. J. Soil Res. **43**, 357–360 (2005)
42. Tartakovsky, D.M., Neuman, S.P.: Transient effective hydraulic conductivity under slowly and rapidly varying mean gradients in bounded three-dimensional random media. Water Resour. Res. **34**, 21–32 (1998)
43. Tidwell, V.C., Wilson, J.L.: Laboratory method for investigating permeability upscaling. Water Resour. Res. **33**, 1067–1616 (1997)

44. Tidwell, V.C., Wilson, J.L.: Heterogeneity, permeability patterns, and permeability upscaling: physical characterization of a block of Massillon sandstone exhibiting nested scales of heterogeneity. SPE Reserv. Eval. Eng. **3**, 283–291 (2000)
45. Zhang, D., Zhang, R., Chen, S., Soll, W.E.: Pore scale study of flow in porous media: scale dependency, REV, and statistical REV. Geophys. Res. Lett. **27**, 1195–1198 (2000)
46. Zlotnik, V.A., Zurbuchen, B.R., Ptak, T., Teutsch, G.: Support volume and scale effect in hydraulic conductivity: experimental aspects. In: Zhang, D., Winter, C.L. (eds.) Theory Modeling, and Field Investigation in Hydrogeology: A Special Volume in Honor of Shlomo P. Neuman's 60th Birthday, vol. 348, pp. 191–213. Geological Society of America, Boulder (2000)

Chapter 10
Applications of the Cluster Statistics

10.1 Spatial Statistics and Variability of K from Cluster Statistics of Percolation Theory

This chapter presents a conceptually straightforward treatment of spatial correlations of "random" heterogeneous media, but does not intend to capture at this point even a majority of the actual behavior. A great deal of work still needs to be done since what has been accomplished so far neglects the expected geological complications due to patterns of deposition (on a wide range of scales), dewatering, alteration, deformation, and fracture. A fundamental point of this chapter will be that, even if a medium itself does not exhibit correlations, the transport properties of this medium will be correlated over distances which can be very large. In fact a simple physical result emerges, namely that the length scale of correlations in the measurement of a conduction process is directly proportional to the size of the volume of measurement ([2], given in Sect. 10.3 here), known in the hydrologic community as the "support" volume. In other words, the range of the variogram is proportional to the scale of the measurement. This result is observed over 3–4 orders of magnitude of length, i.e. over 10+ orders of magnitude of the volume [6]. When considered in conjunction with scaling of the dispersivity (Chap. 11), for which the support volume also plays a dominant role, and for which the starting point of the derivation is also the cluster statistics of percolation, we suggest that the result for the variogram is a direct consequence of, and clear evidence for, the relevance of percolation theory.

The concepts here will be developed first, however, for simple models of solid state problems, for which initial calculations have already been presented, and for which relatively reliable and simple microscopic models exist. The general approach will combine cluster statistics of percolation theory with critical path analysis. However, the results, which are given in terms of certain length scales (whose calculations were described in Chap. 5), can be easily generalized to hydrologic systems. The purpose of the first section will be to calculate the distribution of electrical conductivity values for a system of cubic shape and linear dimension x.

A. Hunt et al., *Percolation Theory for Flow in Porous Media*,
Lecture Notes in Physics 880, DOI 10.1007/978-3-319-03771-4_10,

The critical subnetwork, which just percolates, is defined by the association of all resistors with resistance values less than or equal to R_c. If another subnetwork is picked by choice of a arbitrary maximum R value such that the maximum $R < R_c$, the largest cluster of interconnected resistors cannot reach infinite size. But it can be large if R is not much less than R_c. Cluster statistics of percolation theory give the occurrence of such clusters. It is necessary for us only to use these statistics to calculate how often such clusters with a given governing R value can occur, and thus how often a finite measurement device or technique will measure the conductivity from a finite cluster with R different from R_c. But in converting the cluster statistics to a form useful for these calculations it is necessary to review some basic scaling arguments and to recall some definitions and values of several length scales.

Take r–E percolation. In Chap. 5, Eq. (5.28) shows that r_m, proportional to the typical hopping distance, is

$$r_m = a\left(\frac{\alpha_c^2}{9\pi}\right)^{\frac{1}{d+1}}\left[\frac{1}{k_B T N(E_f)a^3}\right]^{\frac{1}{d+1}} = a\left[\frac{T_0}{T}\right]^{\frac{1}{d+1}} \tag{10.1}$$

while Eq. (5.25),

$$\frac{E_m}{kT} = \frac{2r_m}{a} \tag{10.2}$$

demonstrates that the range of available hopping energies is proportional to

$$E_m \propto kT\left[\frac{T_0}{T}\right]^{\frac{1}{d+1}} \tag{10.3}$$

Note that the numerical factors of these quantities are not reliable, since important correlations have been excluded from the calculations. In Chap. 5 the bulk separation of maximally valued resistances for r–E percolation was calculated to be,

$$l = a\left(\frac{T_0}{T}\right)^{\frac{1}{d}} \tag{10.4}$$

Below it will be shown how this calculation can be improved in steps. The correlation length evaluated at the optimal resistance for conduction, which will now be denoted as L, was found to be,

$$L = a\left(\frac{T_0}{T}\right)^{\frac{1+\nu}{d+1}} \tag{10.5}$$

Consider a cluster of s elements (volume s) at bond probability p. The purpose here is to relate s to a system length, x, and to relate p to R. Then it will be possible to find the probability that in a system of length x a continuous path can be found with no resistance greater than R, which connects both sides of the system.

It is known [9] that the radius of (distance across) such a cluster is $r_s \propto s^{\sigma\nu}h(z)$, where $z = s^{\sigma}(p - p_c)$. The proportionality constant must include the fac-

tor $a(T_0/T)^{1/4}$, because both the resistance length and the resistance separation are equal to this value. Therefore the relationship must have the following form,

$$r_s = a\left(\frac{T_0}{T}\right)^{\frac{1}{d+1}} s^{\sigma\nu} h(z) \tag{10.6}$$

The function $h(z)$ is not well-known, so that it will be neglected henceforth. Consider the Euclidean distance between maximally valued resistances on such a cluster to be l, then distance across such a cluster, ignoring tortuosity, can be written as Nl, where N is the number of such resistances in a Euclidean length r_s. Therefore,

$$Nl = a\left(\frac{T}{T_0}\right)^{\frac{1}{4}} s^{\sigma\nu} \tag{10.7}$$

The total distance across the cluster is thus the product of a grid scale factor and a percolation function. The following ratio expresses the assumption that the statistical occurrence of critical resistance values on the backbone of the cluster is the same as in the bulk,

$$\frac{N^{\frac{1}{\sigma\nu}}}{s} = \left(\frac{T_0}{T}\right)^{\frac{1}{d+1}} \tag{10.8}$$

since $N^{1/\sigma\nu} = N^{d_f}$ is proportional to the number of critical bonds on the cluster. In accord with the discussion in Chap. 5, the factor on the right hand side of Eq. (10.8) represents $\xi_c^3/\xi_c^4 \propto \xi_c^{-1}$, which is the ratio of a 3-D surface area to its enclosed 4-D volume, where ξ_c gives the linear dimension of the volume. Simultaneous solution of Eq. (10.7) and Eq. (10.8) yields,

$$l = a\left(\frac{T_0}{T}\right)^{(1+\sigma\nu)/(1+d)} \tag{10.9}$$

While the ratio above seems quite different from that in Eq. (10.4), note that $\sigma\nu = 1/d_f$; replacement of $1/d_f$ by $1/d$, would lead to the same result as in Eq. (10.4). One can as a final measure account for the tortuosity of the backbone cluster as well. Remember that the length, Λ, of the tortuous path along the backbone is described by a different exponent than that of the correlation length, $\Lambda \propto (p - p_c)^{-\eta}$, with $\eta = \nu D_{\min}$. This modification includes substituting $(s^{\sigma\nu})^{D_{\min}}$ for $s^{\sigma\nu}$ on the right-hand side of Eq. (10.7)

$$Nl = a\left(\frac{T_0}{T}\right)^{\frac{1}{d+1}} \left(s^{\sigma\nu}\right)^{D_{\min}} \tag{10.10}$$

where N is no longer the Euclidean separation between critical resistances, but the actual number of such resistances along the percolation backbone and l is now their separation in steps along the backbone. One must then also make a corresponding change to Eq. (10.8) so as to make the left-hand side the ratio of $N^{d_f/D_{\min}}$. The result that one obtains is,

$$l = a\left(\frac{T_0}{T}\right)^{\frac{1+D_{\min}/d_f}{1+d}} \tag{10.11}$$

This result was also found in Hunt [1], though it was expressed as

$$l = a\left(\frac{T_0}{T}\right)^{\frac{1+1/\nu d_{\mathrm{f}}}{1+d}} \tag{10.12}$$

as a result of using the exponent $\eta = 1$ (from [9]) without taking advantage of the intervening advances in knowledge of tortuosity (see Sect. 2.1). Numerically the values of the exponent on (T_0/T) for l do not differ greatly, with Eq. (10.4) yielding 0.33, Eq. (10.9) 0.35 and Eq. (10.11) 0.388, although Eq. (10.12) was used (Hunt, 1998) to produce an exponent of 0.365. All four of these values would scarcely be distinguishable in experiment. Note, however, that Eq. (10.5) for L yields an exponent of 0.47, and experiment might distinguish between any of the above values of l and the choice $l = L$. Further, the larger the value of the exponent, owing to the large value of (T_0/T), the larger is the length scale. This makes $L > l$.

Now turn to the cluster statistics

$$n_{\mathrm{s}} = K s^{-\tau} \exp\left\{-\left[s^{\sigma}\left|(p - p_{\mathrm{c}})\right|\right]^{q}\right\} \tag{10.13}$$

K is a (dimensionally-dependent) constant, but the value is of no consequence, since the result will ultimately have to be normalized. Here the absolute value signs are meant to allow the cluster statistics to be applicable on either side of p_{c}. For the Gaussian form, $q = 2$, such a manipulation is not necessary. No solid conclusions with respect to the value of the exponent p are given in Stauffer [9]. The Fisher droplet model gave $q = 1$, but large numerical simulations were very well approximated by $q = 2$ (for which the result was correct on both sides of the percolation threshold), even though theory indicated that the Gaussian form could not be correct (Stauffer). Since the Gaussian form works extremely well, we will use it when making predictions, but when we wish to generate analytic results we use $q = 1$ on account of its simpler manipulation. It is understood, however, that those calculations could probably be modified to yield more accurate results by choice of the Gaussian form. Later in this chapter we show that it is also possible to approximate the cluster statistics by a simple power-law with an abrupt cut-off.

Although it is possible that ultimately predictions of distributions of the values of the conductivity will require a more precise form for the cluster statistics than either choice mentioned, another aspect of the calculation, which has been left out entirely is that the cluster statistics of Eq. (10.13) do not really apply far from percolation. Thus one ought to combine treatments near and far from percolation. The use of any cross-over in functional form would greatly complicate normalization. Here, our development is meant mainly to demonstrate concepts and make it possible to use more simplified cluster statistics; nevertheless the calculations of ensemble means appear to generate verifiable results.

Equation (10.8) implies that $s^{\sigma\nu} \propto N$, but Eq. (10.10), including tortuosity, gives $s^{D_{\min}/d_{\mathrm{f}}} \propto N$. Generating two such expressions derives from two different necessities. In Chap. 5 we spent considerable time treating the optimization of the dc conductivity in an infinite system. In such a case the actual values of the lengths l and L could play key roles, and in that context we needed a separation of resistances on the tortuous path. The decisive point is that if one should find by the argument

of Eq. (10.10) that $l > L$, one would better use percolation scaling concepts to replace l with L. It is probably a contradiction to declare that the correlation length determines the structure of the dc current carrying cluster and then to allow the separation of the critical resistances to exceed that of the nodes. In such a case, the links are made similar to blobs. However, we found that $l < L$ by virtue of its smaller exponent on the temperature-dependent factor. Thus our derivation here provides additional support for our arguments of Chap. 5 that l is not a critical function of $(p - p_c)$. However, in the context of application of cluster statistics, we are more interested in an expression regarding the Euclidean dimension of a cluster. This interest comes from the necessity to compare the actual size of a cluster with a finite system; is the cluster large enough to span the system in question? Thus for transformations of the cluster statistics to useful forms we need the kind of procedure associated with Eq. (10.8).

Now transform $s^{-\tau}$ using Eq. (10.7), $n_s ds = n_N dN$, and the dimensionally dependent scaling relationship (Eq. (1.21)) to N^{-d+1}. Then use $s^{\sigma} = N^{1/\nu}(T_0/T)^{\sigma/(d+1)}$ (from Eq. (10.8)) and the relationship for $p - p_c = k_B T(\xi_c^{d+1} - \xi^{d+1}) \approx (T/T_0)^{1/(d+1)}$ (from Eq. (5.31)) to transform the argument of the exponent in Eq. (10.13) and obtain [1],

$$n_N \propto \frac{1}{N^{d+1} l^d} \exp\left\{-\left[\left(N^{\frac{1}{\nu}}\right)\left(\frac{T_0}{T}\right)^{\frac{\sigma\nu-\nu}{(d+1)\nu}} \ln\left(\frac{R}{R_c}\right)\right]^2\right\}$$
$$= \frac{1}{N^{d+1} l^d} \exp\left\{-\left[\left(\frac{Nl}{L}\right)^{\frac{1}{\nu}} \ln\left(\frac{R}{R_c}\right)\right]^2\right\} \tag{10.14}$$

The combination of exponents on the ratio of the temperatures, is also generated by the ratio l/L, if we use the value for l referred to the Euclidean distance, as argued above. Note that χ is given as proportional to $\chi_0(p - p_c)^{-\nu}$, making it always possible to replace Nl/L with Nl/χ_0 and some numerical constant which, in the case of porous media with their largely unknown distributions, is not likely to be known anyway.

If one expresses $R = R_c \exp(j)$, i.e. one quantizes resistance values in steps of $e = 2.718\ldots$, the following form for $W(N, j)$ results [1],

$$W(N, j) = \frac{1}{N^{d+1} l^d} \exp\left\{-\left[\left(\frac{Nl}{L}\right)^{\frac{1}{\nu}} j\right]^q\right\} \tag{10.15}$$

In the form of Eq. (10.15) contributions to the conductivity may be summed over the index j. Later representation in the form of an integral over R requires the transformation $dj \to dR/R$. Using the cluster statistics in a form like Eq. (10.14) or Eq. (10.15) it is possible to answer a large number of problems.

A cubic volume, $x^3 > L^3$, selected at random, will include some clusters of resistors with, e.g., maximal resistance values less than the critical resistance, which extend from one side of that cube to the other. Such clusters can be defined at all resistance values. Some cubes will contain additional paths (compared with the expected value, $(x/L)^2$) with maximal resistors of the critical resistance value. Other cubes will not contain paths with maximal resistance value R less than or equal to

R_c at all. Such cubes will have a finite probability of being spanned by clusters with $R > R_c$, which are not connected to the critical cluster. The cluster statistics near critical percolation can be used to describe the statistical occurrence of such clusters defined by $R > R_c$ as well.

The calculation of the distribution resistance values for a given cube of dimension x requires summing the statistical occurrence of all cluster sizes, for a given R value, whose lengths exceed x according to the probability that such clusters 'fall' on the volume x^3. The condition

$$N_m l = x \tag{10.16}$$

states explicitly that $N_m l$ is the minimal cluster length which can contribute. The probability that a given cube has conductivity l/Rx^2, where l is the separation of the resistances with the particular value of R chosen, and x^2 is the area normal to the current, is equal to the probability that a cluster with $N > x/l$ is found at the volume x^3. In the following it will be necessary to assume that $x > L$, otherwise the desired statistics for resistance distributions are strongly dependent on the distribution of individual resistances, and thus unrelated to universal cluster statistics. In fact, one way to recognize the value of L from simulations is that the skewness of a distribution of system conductivity values, which is a very rapidly falling function of x for $x < L$, becomes nearly constant for $x > L$ [3].

The probability that a given volume, x^3 will intersect a cluster with linear dimension larger than x (providing the current carrying path) is proportional to the volume, $(Nl)^3$, because it does not matter whether the center of the volume x^3 actually falls on the backbone cluster. It is sufficient that the volume 'cut' the cluster. Thus the probability that a given cubical volume, x^3, is characterized by a maximal resistance, R is proportional to

$$J = \int_{x/l}^{\infty} \frac{dN}{N} \exp\left\{-\left[\left(\frac{Nl}{L}\right)^{\frac{1}{\nu}} \ln\left(\frac{R}{R_c}\right)\right]^q\right\} \tag{10.17}$$

The factor dN/N arises from $(Nl)^3/N^4 l^3$, the numerator resulting from the volume argument above, the denominator from the cluster statistics. In [1] an additional factor $1 - K$ was included to represent the probability that there was no cluster with a smaller R value, which also spanned the volume, but this factor was later argued to be negligible.

Integral (10.17) could be performed relatively easily only in the case that $q = 1$. Since the purposes here are still largely illustrative, this case will be used. Then integral (10.17) yields,

$$J = -\mathrm{Ei}\left\{-\left[\left(\frac{Nl}{L}\right)^{\frac{1}{\nu}} \ln\left(\frac{R_c}{R}\right)\right]\right\} \tag{10.18}$$

where $\mathrm{Ei}(x)$ is the exponential integral of x. Equation (10.18) is in a form, which is not particularly illustrative. But for relatively large values of its argument, $-\mathrm{Ei}(x) \to \exp(-x)/x$ and [1],

$$J = \frac{(L/x)^{1/\nu}\left(\frac{R}{R_c}\right)^{\left(\frac{x}{L}\right)^{\frac{1}{\nu}}}}{\ln\left(\frac{R_c}{R}\right)}, \quad R < R_c \tag{10.19a}$$

$$J = \frac{(L/x)^{1/\nu}\left(\frac{R_c}{R}\right)^{\left(\frac{x}{L}\right)^{\frac{1}{\nu}}}}{\ln\left(\frac{R}{R_c}\right)}, \quad R > R_c \tag{10.19b}$$

$J(R)$ represents an unnormalized distribution of resistance values, but it is possible to find the variance from Eqs. (10.19a), (10.19b) to be $R_c^2(L/x)^2$ (under the condition that $x > 3L$, and approximating $1/\nu$ as 1).

Using the unnormalized distribution (Eqs. (10.19a), (10.19b)) it is possible to calculate approximately the mean value of the conductivity of cubes of dimension x. *Such a calculation applies to any conduction process, thermal, electric, or hydraulic*. The conductivity of a cube of dimension x with a dominant conducting path of length Nl and resistance NR is

$$\sigma = \frac{Nl}{NR}\frac{1}{x^2} \tag{10.20}$$

The mean conductivity of an ensemble of such cubes is an integral over all cubes according to the frequency of their occurrence. The integral over R was split into two parts, $R \le R_c/e$ and $R \ge eR_c$ because of the difference in form of the cluster statistics across $R = R_c$; the case $R = R_c$ was treated separately. The contribution from $R \neq R_c$ was shown to yield a contribution to the dc conductivity, $\Delta\sigma_{dc}$,

$$\left\langle \Delta\sigma_{dc}(x) \right\rangle \propto \sigma_{dc}(\infty)\left[\frac{L}{x}\right]^2\left[1 + \left(\frac{L}{x}\right)^{\frac{1}{\nu}}\right] \tag{10.21}$$

upon ignoring two numerical constants of order unity. The contribution from $R = R_c$ was argued to be of the same form as the first term. The mean conductivity thus diminishes asymptotically with increasing size to its value in the thermodynamic limit, $\sigma_{dc}(\infty)$. The result from Eq. (10.21) is identical to a result for the electrical conductivity of a thin film of thickness x, which can easily be shown to be equivalent to the ensemble mean of the conductivity of a collection of such cubes. The results of Eq. (10.21) were found to be in accord with numerical simulations in [3] for the hydraulic conductivity, though there was some question as to whether both terms were observed.

It was found in [3] that assuming $R = R_0 \exp\xi$, as above together with the Gaussian form for the cluster statistics, which is more accurate than assuming $q = 1$ leads to the result that the distribution of conductivity values is approximately log-normal, at least in the case where $L \approx x$. Clearly, replacing $\ln(R/R_c)$ by $(R - R_c)$ for the case $R = R_0\xi^k$ ($k = 4$ for Poiseuile flow) will make the result more nearly compatible with Gaussian statistics than with a log-normal distribution. At the time of the original publication on conductivity distributions the coincidence that the log-normal distribution appeared to be consistent with Nielsen's results [7] for the distribution of the steady-state unsaturated hydraulic conductivity values in field soils was considered to be significant, especially since the assumed exponential dependence of R on a random variable ξ was consistent with Nielsen's observation that

K was exponentially dependent on the moisture content. In the meantime we recognize that the exponential dependence on a moisture content is not an obvious result, and this question is rather involved. But this topic is discussed further in Chap. 12 in which heterogeneity on more than one scale is treated.

10.2 Cluster Statistics Treatment of Non-equidimensional Volumes and Anisotropy

Most of the material from this section comes from [4] or [5].

An easier means to treat the cluster statistics can be developed, and this treatment is independent of the exact form of the function $f(z)$. Instead of using a particular form for the exponential cut-off, replace $f(z)$ by a sharp cut-off at $s^{\sigma} \propto (p - p_c)^{-1}$. While such an approximation may seem quite rough, it should capture the scaling behavior properly when resulting distributions are normalized, and it should also lead to accurate results for ensemble means. Treating the exponential cut-off as a sharp cut-off,

$$n_N = \frac{1}{N^4 l^3} \quad N < \frac{L}{l} \ln^{\nu}\left(\frac{g_c}{g}\right) \tag{10.22}$$

for the case $g < g_c$ and

$$n_N = \frac{1}{N^4 l^3} \quad N < \frac{L}{l} \ln^{\nu}\left(\frac{g}{g_c}\right) \tag{10.23}$$

for the case $g > g_c$. Both Eq. (10.22) and Eq. (10.23) were written here for the case $R = R_0 \exp(\xi)$ again. One can also write the cluster statistics for the case $R = R_0 \xi^k$, with the results,

$$n_N = \frac{1}{N^4 l^3} \quad N < \frac{L}{l} |V - V_c|^{-\nu} \tag{10.24}$$

Linearize $V - V_c$ for the Rieu and Sposito model (done in Eq. (5.42)) to get

$$|V - V_c| = \frac{3 - D}{3} \left(\frac{g_c}{g_m}\right)^{\frac{3-D}{3}} \frac{|g - g_c|}{g_c} \tag{10.25}$$

using the additional substitution of $(g_c/g_m)^{(3-D)/3}$ for $(r_c/r_m)^{3-D}$. Note that in Chap. 6 the same problem was considered, but with the assumption that the critical volume fraction $V_c \approx 0$. Under such circumstances, $g_c \approx g_m$, and Eq. (10.24) simplifies to,

$$N < \frac{L}{l} |V - V_c|^{-\nu} = \frac{L}{l} \left[\frac{g_c}{|g - g_c|(1 - D/3)}\right]^{\nu} \tag{10.26}$$

It will turn out (in Chap. 11, for example) that a procedure not based on linearization produces much better results. To some degree we continued the linearization here as a tradition, to some degree we were perhaps influenced by the theoretical arguments

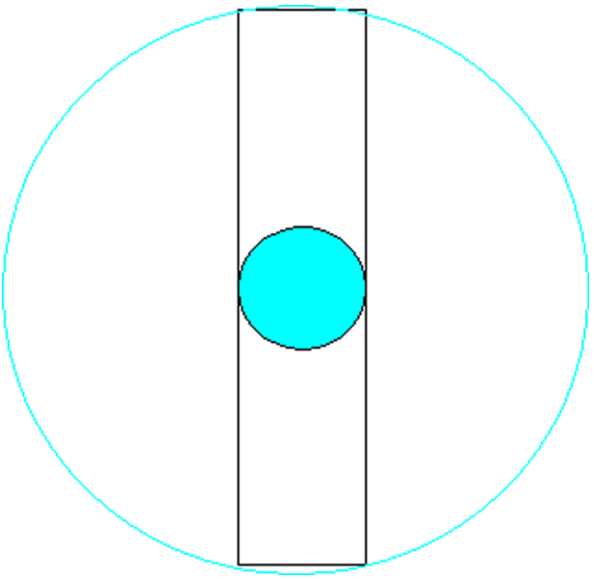

Fig. 10.1 Demonstration that a cluster (filled) of $g < g_c$ (not connected to the infinite cluster) of linear dimension equal to the shortest dimension can force a current to flow through a region of lower conductance, while a cluster (unfilled) with $g > g_c$ must be as long as the largest dimension of the system

that percolation functions and exponents describe behavior precisely only in the asymptotic limit. Nevertheless, such a narrow perspective is much too limiting, and, we can, as usual, apply our results over a much wider range of conditions than merely the asymptotic limits of percolation theory. Accordingly we present here also an analogous result to Eq. (10.26) that is not based on linearization.

$$N < \frac{L}{l}\left|\frac{1}{1-(\frac{g}{g_c})^{1-D/3}}\right|^{\nu} \tag{10.27}$$

Equation (10.27) performs better apparently because, under typical conditions in porous media with D on the order of 2.8 or larger, the very small power $1 - D/3 = 0.067$ or smaller, makes much wider ranges of g fit close to the percolation threshold.

Consider a system with horizontal dimension x and vertical dimension $\varepsilon^{1/2}x$. The factor, $\varepsilon^{1/2}$, can be regarded as arising from a coordinate transformation corresponding to the transformation from an equidimensional volume in an anisotropic medium to a non-equidimensional volume in an isotropic medium (the discussion of the correspondence of $\varepsilon^{1/2}$ to values of K in the anisotropic case will be discussed after the derivation). Systems with characteristic $g < g_c$ can result from clusters of size x or larger, which serve to block the entire volume, but systems with characteristic $g > g_c$ require clusters of linear dimension $\varepsilon^{1/2}x$ or larger (see Fig. 10.1). Using these results one can now follow an analogous procedure to Eq. (10.20) to find $W(g)$ by integrating the product of $(Nl)^3$ and an integrand of the form of the right-hand side of Eq. (10.25). The result is the integral,

$$W(g) \propto \int \frac{dN}{N} \tag{10.28}$$

The question is, what are the limits of such an integral? For either case, $g > g_c$ or $g < g_c$ the upper limit is given by Eq. (10.27). For $g < g_c$, the lower limit is $(x + l)/l$, while for $g > g_c$, the lower limit is $(x\varepsilon^{1/2} + l)/l$. The reason for adding the term l in both cases is to be consistent with the derivation in Chap. 9 which noted that in the limit of small system size x the discretization of the system through the dimensions of the individual resistors could not be neglected. We cannot have cluster sizes smaller than an individual bond length. The results of these integrations are the (unnormalized) expressions for $W(g)$ below,

$$W(g) \propto \ln\left[\left(\frac{L}{l + x\varepsilon^{1/2}}\right)^{\frac{1}{\nu}} \frac{1}{\left(\frac{g}{g_c}\right)^{1-D/3} - 1}\right] \quad g > g_c \tag{10.29}$$

and

$$W(g) \propto \ln\left[\left(\frac{L}{l + x}\right)^{\frac{1}{\nu}} \frac{1}{\left(\frac{g_c}{g}\right)^{1-D/3} - 1}\right] \quad g < g_c \tag{10.30}$$

It is possible to use linearized versions of Eq. (10.29) and Eq. (10.30) to calculate a mean value of the distribution as well as a distribution width in terms of the fundamental formula in terms of the difference of the mean value squared and the square of the mean value. Let

$$A = \left(\frac{L}{l + \varepsilon^{1/2}x}\right)^{\frac{1}{\nu}} \frac{1}{1 - D/3} \tag{10.31}$$

and

$$A' = \left(\frac{L}{x + l}\right)^{\frac{1}{\nu}} \frac{1}{1 - D/3} \tag{10.32}$$

Then it is possible using the linearized versions of Eq. (10.29) and Eq. (10.30) to express an ensemble mean $\langle g \rangle$ as,

$$\langle g \rangle = \lim(\delta \to 0) \frac{\int_{g_c+\delta}^{g_c+Ag_c} g dg \ln\left[\frac{Ag_c}{g-g_c}\right] + \int_{g_c-A'g_c}^{g_c-\delta} g dg \ln\left[\frac{A'g_c}{g_c-g}\right]}{\int_{g_c+\delta}^{g_c+Ag_c} dg \ln\left[\frac{Ag_c}{g-g_c}\right] + \int_{g_c-A'g_c}^{g_c-\delta} dg \ln\left[\frac{A'g_c}{g_c-g}\right]} \tag{10.33}$$

The upper (lower) limit of the first (second) integral is determined by the condition that the upper limit of integral (10.28) be larger than the lower limit. The results were obtained without accounting for any special contribution from $g = g_c$. Evaluation of the integrals leads to,

$$\langle g \rangle = g_c \frac{A + A' + (1/4)A^2 - (1/4)A'^2}{A + A'} = g_c\left[1 + \frac{\left(\frac{L}{\varepsilon^{1/2}x+l}\right)^{\frac{1}{\nu}} - \left(\frac{L}{x+l}\right)^{\frac{1}{\nu}}}{4(1 - D/3)}\right] \tag{10.34}$$

For large values of x it is possible to rewrite this expression as,

$$\langle g_v \rangle = \left[1 + \left(\frac{L}{\varepsilon^{1/2}x + l}\right)^{\frac{1}{\nu}} - \left(\frac{L}{x + l}\right)^{\frac{1}{\nu}}\right]^{\frac{3/4}{3-D}} \tag{10.35}$$

where the subscript v has been added to denote vertical flow. The logic of this particular recombination is that it is, in a sense, an inverse of the expansion of $g^{1-D/3} - g_c^{1-D/3}$; thus it is plausible that a more detailed treatment that did not utilize the linearization in the first place would lead to precisely the same result as Eq. (10.35). Of course this recombination is not unique, but this is a particular case where the recombination is a direct reversal of the linearization of Eq. (5.42). In any case, Eq. (10.34) and Eq. (10.35) are equivalent to lowest order. Further, the results from Eq. (10.35) will be seen to be very nearly identical to the results from Chap. 9 over a wide range of system sizes x. The only purpose is to compare with the calculations of Chap. 9, for which such a linearization was not necessary. Now Eq. (10.35) can be rewritten in the form,

$$\langle g_v \rangle = g_c \left\{ 1 - \left[1 - \left(\frac{1 + x/L}{1 + \varepsilon^{1/2} x/L} \right) \right]^{\frac{1}{\nu}} \left[\frac{1}{1 + x/L} \right]^{\frac{1}{\nu}} \right\}^{\frac{3/4}{3-D}} \tag{10.36}$$

which clarifies the scaling of $\langle g_v \rangle$ with length x as a ratio of x/L.

A similar calculation can be made for an ensemble mean bottleneck conductance for horizontal flow through the system. In this case, however, a cluster of size x is large enough to facilitate flow with a larger g than g_c, but it takes a cluster of size $\varepsilon^{1/2} x$ with maximum $g < g_c$ to block flow. The result is easily deduced from Eq. (10.33) to be,

$$\langle g_h \rangle = g_c \frac{A + A' + (1/4)A'^2 - (1/4)A^2}{A + A'} = g_c \left[1 + \frac{\left(\frac{L}{x+l}\right)^{\frac{1}{\nu}} - \left(\frac{L}{\varepsilon^{1/2}x+l}\right)^{\frac{1}{\nu}}}{4(1 - D/3)} \right] \tag{10.37}$$

where now the subscript h denotes horizontal flow. Equation (10.37) can then also be rewritten in the following form (by the same reversal of linearization as in Eq. (10.34))

$$\langle g_h \rangle = g_c \left\{ 1 + \left[1 - \left(\frac{1 + x/L}{1 + \varepsilon^{1/2} x/L} \right) \right]^{\frac{1}{\nu}} \left[\frac{1}{1 + x/L} \right]^{\frac{1}{\nu}} \right\}^{\frac{3/4}{3-D}} \tag{10.38}$$

Note that $\langle g_h \rangle / \langle g_v \rangle$ is 1 in both the limits of $x \to \infty$ and $x \to 0$. In the limit of an infinite system a critical path may be found equally easily in either the horizontal or the vertical direction and $\langle g_h \rangle / \langle g_v \rangle$ should be 1. However the fact that the ratio of g_h (and g_v) in the limit $x \to \infty$ to its value in the limit $x \to 0$ is also 1 is an artifact of the assumption that $V_c \approx 0$. In the limit $x \to 0$ the present calculation is consistent with the fact that an ensemble mean of systems so small that they are composed of a single element must give the arithmetic mean in either the horizontal or the vertical direction, but the effective hydraulic conductivity of an infinite system is only the arithmetic mean if V_c can be argued or chosen to be zero.

Now how do we actually relate ε to the horizontal and vertical measurements of K? ε is assumed to give a ratio of the characteristic values of horizontal and vertical K measurements. If $V_c = 0$, then it must often be possible to find horizontal paths that connect a system from one side to the other that never have to use any smaller pore (or fracture) radii than r_m. So $K_h \propto r_m^2$ (by the results for the saturated

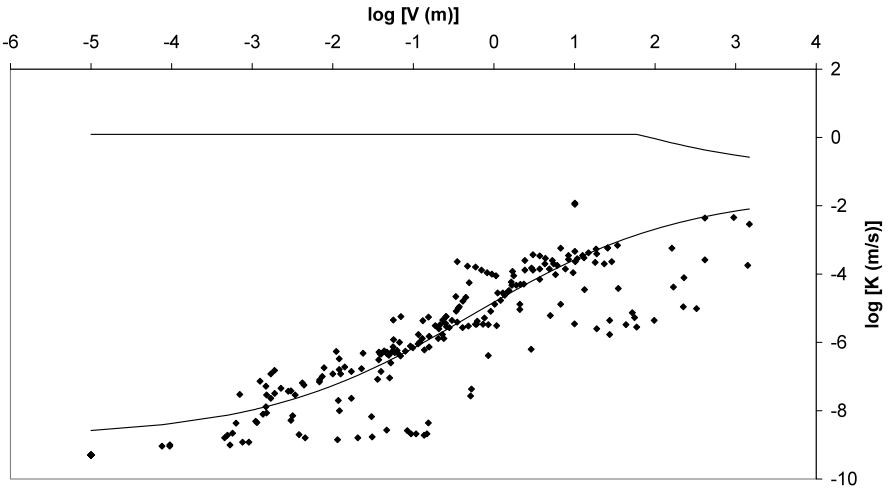

Fig. 10.2 Comparison of the result of Eq. (10.36) for K_v obtained by cluster statistics of percolation with experimental data obtained by Schulze-Makuch [8]. The same values of the parameters, $D = 2.98$, and $r_m/r_0 = \varepsilon^{1/2} = 2500$ were used as in Eq. (9.8) from Chap. 9. Here we show $K_h > K_v$ from Eq. (10.38) for comparison

hydraulic conductivity, Chap. 5). On the other hand, vertical paths in a system small enough to be one dimensional must sample every r value. Thus, effectively, a vertical path has $V_c = 1$ and $K_v = r_0^2$. This means that $\varepsilon^{1/2} \propto (r_m/r_0)$, which is identical to the ratio, R, in Chap. 9. As a consequence, since K_v was shown in Chap. 9 to sweep out the values from r_0^2 through r_m^2, the result for K_h cannot involve a very large enhancement, being at most related to the density of flow path inputs rather than maximally valued resistances to flow. And indeed the maximum enhancement is only about an order of magnitude rather than the 6 orders of magnitude reduction in K_v at the same x value.

After this discussion it is now appropriate to consider how well our results fare in comparison with experiment. We choose the same anisotropic fracture system in a carbonate aquifer [8] as was chosen in Chap. 9. In Fig. 10.2 the result (Eq. (10.36)) for $K_v(x)$ is compared with experiment and found to reproduce experiment approximately equally well as the results from Chap. 9 (and using the same parameters) over a wide range of system sizes. This equivalence was also intended, once again, to demonstrate the redundancy of percolation theory, which allows more than one starting point to calculate the same quantity. Additionally we show the results of Eq. (10.38) for $K_h(x)$. Note that, while K_v is an increasing function of x, K_v is a decreasing function. In these representations L was set equal to 1, making the units of the horizontal scale arbitrary.

In Fig. 10.3 we show a 3-d plot of the results of Eq. (10.29) and Eq. (10.30) for the pdf for measuring conductance value g as function of size, x.

We have [5] developed a scheme to generate a width of a distribution of conductance values that is highly asymmetric, as in Eq. (10.29) and Eq. (10.30). This

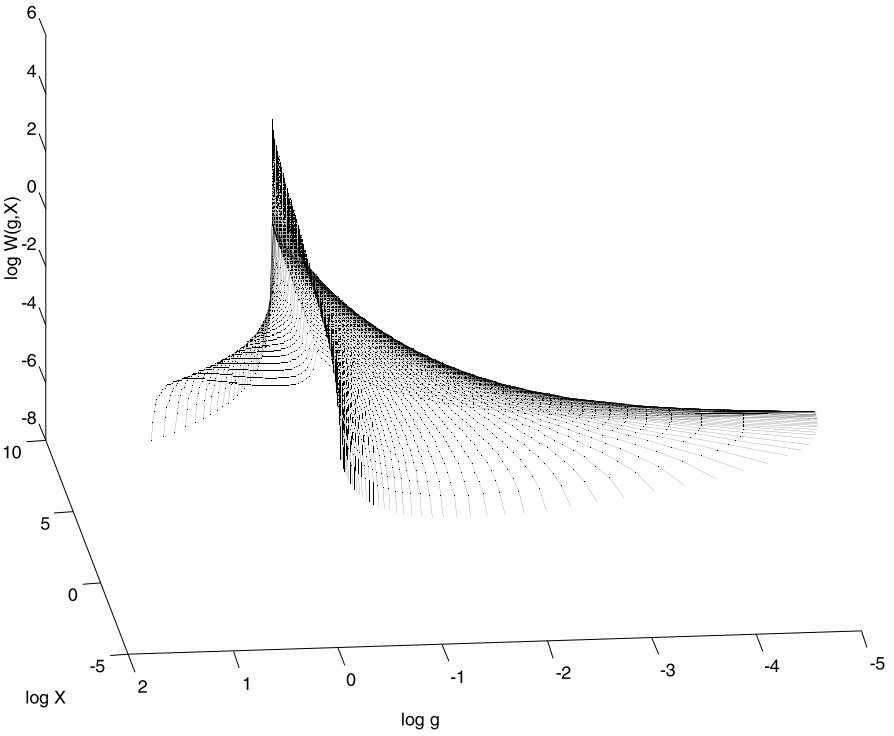

Fig. 10.3 Family of curves describing the distribution of conductance values, $W(g, x)$ as given by the approximation in Eq. (10.29) and Eq. (10.30)

scheme can be described most easily in geometric terms. Emplace a horizontal line of variable height on the graph of $W(g)$. This line will normally intersect $W(g)$ in two points. Choose the height so that the area under $W(g)$ between the two intersection points is 68 % of the total area under $W(g)$, equal to the fractional area within one standard deviation of the mean of a Gaussian distribution. The range of g values between these two intersection points can then serve as a measure of the distribution width. When we calculate this distribution width again for the same parameters as found in Chap. 9, the results can be represented graphically in Fig. 10.4. While the comparisons in Chap. 9 were essentially fits, since the parameters were chosen to fit the data, use of the same parameters here gives Fig. 10.4 at least some of the characteristics of a prediction. Figure 10.5 demonstrates that the distribution width predicted is in accord with field data when specific media are considered individually.

It should be mentioned that the results of this chapter have a potential relevance also to a radioactive waste problem at the Hanford site. Technetium in solution was discharged at the BC Crib site and was expected to drain straight down to the water table. The evidence is that it did not, having encountered a horizontal layer with a large anisotropy in K and spread laterally instead. With increasing time, however,

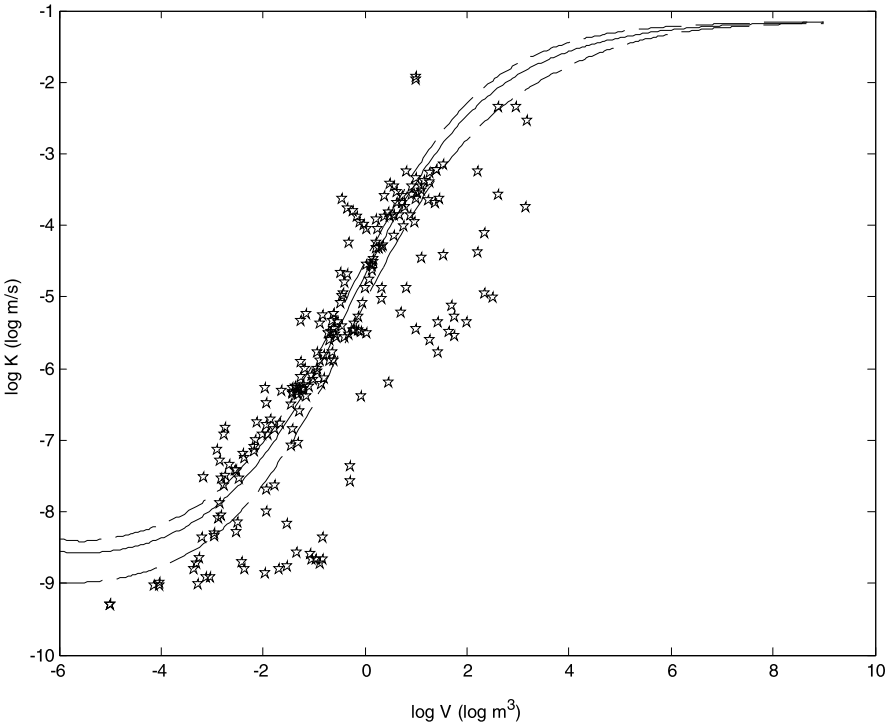

Fig. 10.4 Comparison of the width of the distribution of $W(g)$ values as a function of x with experimental data from Schulze-Makuch [8]. The geometric procedure to calculate the width of the distribution from the approximation given in Eq. (10.29) and Eq. (10.30) is given in the text. The parameters, $D = 2.98$, and $r_m/r_0 = \varepsilon^{1/2} = 2500$ used were again the same values as those chosen in Chap. 9, though in Chap. 9 only the expected value of the conductivity was treated

the effective experimental scale will increase, producing an increase in the expected value of K_v and a decrease in the expected value of K_h. Using the application of the cluster statistics that led to Eq. (10.36) and Eq. (10.38) it should be possible to make a prediction of the length, and thus the time scale, before the probabilities of vertical and horizontal advection are similar and thus evaluate the potential danger of contamination of the water supply in a quantitative way. This question is now addressed in Chap. 12 as it is effectively a problem of multiple scales of heterogeneity.

10.3 Semi-variograms and Cross-Covariance

The semi-variogram for the hydraulic conductivity is defined as,

$$\Gamma_K(h) = \frac{1}{2N(h)} \sum_{j=1}^{N(h)} \left[K(x_j) - K(x_j + h)\right]^2 \tag{10.39}$$

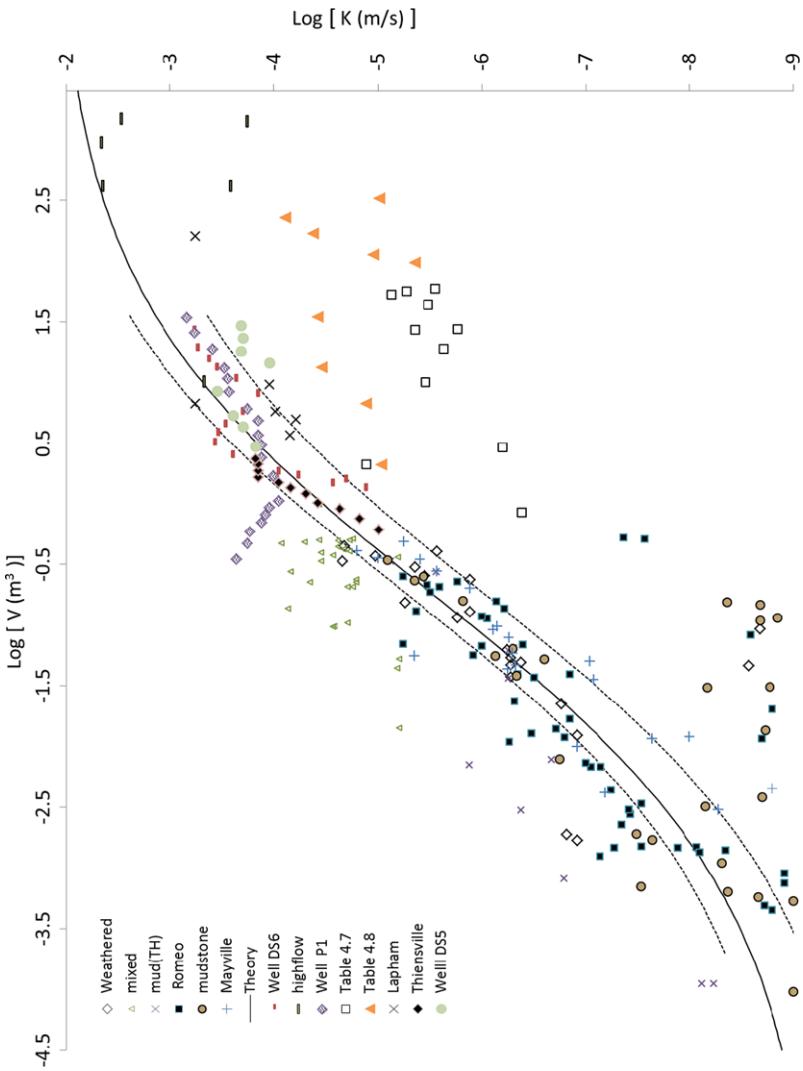

Fig. 10.5 Same as Fig. 9.3 showing that individual series of data points corresponding to specific experiments do tend to conform to the relatively narrow spread of values predicted for a single particular medium from Chap. 10. Here we use $D = 2.95$, but the difference between the two predictions is very small, if one compares with Fig. 10.4

$K(x_j)$ is the value of the hydraulic conductivity at $x = x_j$, $K(x_j + h)$ is its value a distance h from x_j, and $N(h)$ is the number of pairs of points at which measurements are made a distance h apart. For stationary random functions, the semivariogram is related to the covariance, $C_K(h)$, by $\Gamma_K(h) = C_K(0) - C_K(h)$. In practice the semi-variogram (often simply called the variogram) is the product of the variance of K and the difference between 1 and the correlation function of K. The range of the variogram is defined in terms of the length scale which governs the decay of the correlation function.

There are many possible reasons why a random field, such as the hydraulic conductivity, can be correlated from point to point in a geologic porous medium. These include depositional correlations, fractures, folding, etc. There are also reasons that relate to the random combination of highly conducting elements into a larger region of high conductivity. In particular, given the context of this chapter, suppose that a large cluster of resistances of maximum value $R < R_c$ is present in a system of size x. Then a measurement of K in a region of space that covers one part of the cluster will be correlated with a measurement that is made over another part of the cluster. Otherwise, there is no discernible correlation. We can define that probability in terms of conditional probabilities as follows. Start from Eq. (10.18) and write [2],

$$J = \int_{x/l}^{\infty} K\,dN \tag{10.40}$$

where K is the integrand of Eq. (10.18). Equation (10.40) once again gives a (relative) probability that a system of size x has controlling resistance R. The probability that the same cluster determines the resistance after translation a distance h is the (conditional) probability that the cluster that is known to be of minimum size x is actually of size at least $x + h$. This probability is easy to write as [2],

$$P(h) = \frac{\int_{(x+h)/l}^{\infty} K\,dN}{\int_{x/l}^{\infty} K\,dN} \tag{10.41}$$

The variogram, since it measures the lack of correlation, is proportional to the complementary probability, $1 - P(h)$. Using Eq. (10.20ab) the quantity $1 - P(h)$ can be expressed as [2],

$$1 - P(h) = 1 - \left(\frac{x}{x+h}\right) \exp\left[-\left(\frac{x}{l}\right)\left|\ln\left(\frac{R}{R_c}\right)\right|\right] \tag{10.42}$$

Note that Eq. (10.42) is approximate in three respects; one, the cluster statistics of percolation theory are not accurately described by the exponential "Fisher droplet" form used, and two, the approximation for the exponential integral used is an asymptotic limit, and three, cluster statistics far from percolation should be used for R values far from R_c. Again, the main purpose here is instructive. Now the variogram must be obtained by an integral of Eq. (10.42) over the probabil-

ity density for the cluster resistance, R, since clusters of all resistances can occur. Thus [2],

$$\Gamma_K(h) \propto 1 - \int_0^\infty \frac{x}{x+h} \exp\left[-\left(\frac{x}{l}\right)\left|\ln\left(\frac{R}{R_c}\right)\right|\right] W(R,x)dR \tag{10.43}$$

where

$$W(R,x) = \frac{\left(\frac{L}{x}\right)\left(\frac{R}{R_c}\right)^{\frac{x}{L}}/|\ln(R/R_c)|}{\int_0^\infty dR\left(\frac{L}{x}\right)\left(\frac{R}{R_c}\right)^{\frac{x}{L}}/|\ln(R/R_c)|} \tag{10.44}$$

The first term in Eq. (10.43) integrates easily to 1, while the second integrates to $[x/(x+h)]^2$. Thus,

$$\Gamma_K(h) \propto 1 - \left(\frac{x}{x+h}\right)^2 \tag{10.45}$$

Using the representation of the variogram as the product of a spatial dependence and the variance of R yields thus [2],

$$\Gamma_K(h) = R_c^2\left(\frac{L}{x}\right)^2\left[1 - \left(\frac{x}{x+h}\right)\right]^2 \tag{10.46}$$

It is easily determined [3] that Eq. (10.46) for the variogram cannot be precisely correct because its Fourier transform can take on negative values, as can thus the Fourier transform of the correlation function, or the characteristic function. The wiggles in the Fourier transform arise from the lack of continuity of the slope of $\Gamma_K(h)$ in the limit $h \to 0$. Owing to the various approximations, including using an asymptotic expansion for large h in the limit of $h \to 0$, the defect of the derived function in this limit is not really unexpected. Nevertheless Eq. (10.45) clearly shows that the range of the variogram is proportional to x, the linear dimension of the measurement. In strongly heterogeneous media, "a quantitative measure of the range of correlation of a random spatial structure may be calculated from the autocorrelation function. In general the integral scale [this range] is not an intrinsic property of the field, but depends on the scale over which it is measured." In other words, the range is a function only of x. Moreover, Neuman and di Federico [6] present experimental results that demonstrate that the range of the variogram for the hydraulic conductivity is linearly proportional to the measurement length scale over many orders of magnitude of x. So, even in the present approximation, this aspect of experiment is achieved. Further, it was shown in Hunt [2] that Eq. (10.45) resembles the spherical approximation for the variogram.

The cross-covariance is given in terms of the probability that a second volume x at a distance h from a first volume has $R \geq R_2$ if volume 1 has $R \geq R_1$. To write down an expression in terms of cluster statistics, one must make some assumptions regarding the magnitudes of R_1 and R_2. In Hunt [2] it is shown that the cross-covariance is given by,

$$\frac{\int_{R_1}^{\infty} W(R,x)dR \int_{\frac{x+h}{l}}^{\infty} K(R,N)dN}{\int_{R_1}^{\infty} W(R,x)dR \int_{\frac{x}{l}}^{\infty} K(R,N)dN} + \left[\frac{\int_{R_2}^{R_1} W(R,x)dR \int_{\frac{x}{l}}^{\frac{x+h}{l}} K(R,N)dN}{\int_{0}^{\infty} W(R,x)dR \int_{\frac{x}{l}}^{\frac{x+h}{l}} K(R,N)dN}\right]$$
$$\times \left[1 - \frac{\int_{R_1}^{\infty} W(R,x)dR \int_{\frac{x+h}{l}}^{\infty} K(R,N)dN}{\int_{0}^{\infty} W(R,x)dR \int_{\frac{x+h}{l}}^{\infty} K(R,N)dN}\right] \tag{10.47}$$

in the case that $R_1 > R_2 > R_c$. The first term gives, as in the calculation of the variogram above, the probability that the second volume is located on the same cluster of linear dimension $x+h$. In that case $R > R_1$ in the second volume certainly guarantees $R > R_2$. But it is also possible that the second volume is not located on the same cluster (the second factor of the second term); then, however, it may still be located on a cluster of size between x and $x + h$ with controlling resistance somewhere between R_2 and R_1. The cluster must be at least size x in order to control the measurement of volume 2, but cannot be as large as $x + h$, or it will control the measurement of volume 1 as well. If it controlled the measurement of volume 1 as well, then volume 1 would have $R < R_1$. Since the choice of volume 1 and volume 2 is arbitrary, this expression can always serve for cases when both R_1 and R_2 are greater than R_c. The other two cases may be written down analogously (when both resistances are smaller than the critical resistance and when one is larger and one is smaller).

Note that in Hunt [2] the expression corresponding to Eq. (10.47) has several typos, but more importantly the limits on the interior integrals of the first factor of the second term are incorrect.

Problems

10.1 Write analogous expressions for the cross-covariance when both controlling resistance values are smaller than R_c and for the case when they are on opposite sides of R_c.

10.2 Use the cluster statistics of percolation theory to predict the variance of the distribution of K_h and K_v as functions of system size. There are two ways to do this calculation. One is to use the full cluster statistics distribution (with its attendant unknowns). The second way, recommended here, is to use the approximation in the text.

References

1. Hunt, A.G.: Upscaling in subsurface transport using cluster statistics of percolation. Transp. Porous Media **30**(2), 177–198 (1998)
2. Hunt, A.G.: Percolation cluster statistics and conductivity semi-variograms. Transport in Porous Media **39**, 131–141 (2000)

3. Hunt, A.G.: Applications of percolation theory to porous media with distributed local conductances. Adv. Water Resour. **24**(3,4), 279–307 (2001)
4. Hunt, A.G.: Scale-dependent hydraulic conductivity in anisotropic media from dimensional cross-over. Hydrogeol. J. **14**, 499–507 (2006)
5. Hunt, A.G., Blank, L.A., Skinner, T.E.: Distributions of the hydraulic conductivity for single-scale anisotropy. Philos. Mag. **86**, 2407–2428 (2006)
6. Neuman, S.P., Di Federico, V.: Multifaceted nature of hydrogeologic scaling and its interpretation. Rev. Geophys. **41**, 1014 (2003)
7. Nielsen, D.R.: Spatial variability of field-measured soil-water properties. Hilgardia **42**, 215–259 (1973)
8. Schulze-Makuch, D.: Facies Dependent Scale Behavior of Hydraulic Conductivity and Longitudinal Dispersivity in the Carbonate Aquifer of Southeastern Wisconsin. Dissertation, University of Wisconsin, Milwaukee (1996)
9. Stauffer, D.: Scaling theory of percolation clusters. Phys. Rep. **54**, 1–74 (1979)

Chapter 11
Properties Based on Tortuosity

This chapter was originally devoted to the subject of solute dispersion and indeed dispersion still makes up the greater part of the chapter. We have expanded our treatment of dispersion to address a wider range of experimental conditions, including the previously ignored unsaturated case, as well as a wider range of medium models. We have also added comparisons with over 2000 experimental results. We demonstrate that our predicted dependence of typical arrival times on system length explains some long-unexplained results out of dispersive transport in transient photoconductivity. The non-linear dependence of arrival time on distance generates a length dependence of the typical solute velocity (Sect. 11.5), which has implications for the spatio-temporal scaling of reaction rates in porous media as well.

But we have also expanded the chapter to include tortuosity itself. As has been known for decades, the tortuosity of flow or charge transport paths is an important input into calculations of such properties as the permeability and the electrical conductivity. In our presentation of flow and conduction properties (earlier chapters) we did not isolate the effects of tortuosity vis-à-vis connectivity, but instead referred simply to their combined effects as contained in the scaling exponent of the conductivity. But others have not followed this path. Much of the existing work on the relevance of tortuosity to flow derives from a perspective considering flow as chiefly a hydrodynamic problem, with streamlines perturbatively influenced by solid obstacles, frequently spherical. Such investigations typically apply the Navier-Stokes equations or lattice Boltzmann techniques to relatively high porosity models (70–98 %). However, with better computing powers becoming available, lower porosity materials are being included, and it is becoming obvious that percolation theory has a role. Similarly, soil physicists, petroleum engineers, and hydrogeologists each have had their own reasons for defining "tortuosity" factors. Some of the definitions can be seen to be nothing more than quantities describing a deviation between theory and experiment, which are then interpreted as evidence of tortuous paths rather than as revealing weakness in the theory. Others are more physically motivated. In any case, we acknowledge the importance of including some discussion of this literature. In the process we will show that many of the results from simulations conform very closely to percolation theoretical predictions [54], provided

A. Hunt et al., *Percolation Theory for Flow in Porous Media*,
Lecture Notes in Physics 880, DOI 10.1007/978-3-319-03771-4_11,

that the limit $1 - \phi \ll 1$ is not investigated too closely. While this limit of vanishing solid volume fraction is of theoretical interest, it has little utility in studies of natural grain supported media.

11.1 Tortuosity

The purpose of this section is, by invoking concepts from percolation theory, to unify the conceptual understanding of tortuosity. Our review on tortuosity [53] summarizes the current (difficult) state of affairs. While the concept of tortuosity seems straightforward, in practice tortuosity is not consistently defined, and its treatment in the porous media literature is often misleading [44, 108, 140, 168]. Sometimes tortuosity has been defined as a geometrical parameter, other times as a property related to a specific form of transport: hydraulic, electrical, or diffusive [32, 104, 140, 149]. A fundamental question, rarely addressed, is whether tortuosity is an intrinsic property of the medium, of a process within the medium, or neither, being simply an *ad-hoc* parameter used to improve the agreement between theory and experiment. It is typically claimed that tortuosity depends on the type of flow or transport process being studied, and comparisons between predicted and measured fluid flow and transport are used to support that assertion [108, 172]. But such a claim for the nature of tortuosity suggests that its use in practice is often as an adjustable parameter—a "fudge factor"—implying that a clear understanding of tortuosity is lacking. When one considers that the influences of tortuous paths are often invoked to explain discrepancies between experiments and calculations based on the bundle of capillary tubes model [149], the wide range of possible interpretations of tortuosity becomes clear.

It is obvious that flow paths through porous media are not straight, in contrast to the conceptualization of, e.g., electrical current paths in metals. It is also true that many formulations for the electrical or hydraulic conductivity in porous media do not predict experimental results accurately, at any length scale. However, this does not mean, as often assumed, that tortuosity is the only reason for the discrepancy, nor that predictions can be corrected by the simple expedient of incorporating a "tortuosity" factor (originally introduced by Carman [28]). The problem runs far deeper, as noted in Chaps. 3, 5 and 6. Bundles of capillary tube models generate constitutive relations based on arithmetic averaging of local conductances, relegating the role of the heterogeneity to a description of the distribution of tube radii (Sect. 3.5.5). But "standard" methods [27, 112, 169] that calculate hydraulic conductivity, being conceptually based on the capillary bundle, thereby use techniques designed for homogeneous media. Effective hydraulic conductivity values cannot be derived from a geometric or harmonic mean either, nor by a simple generalization such as power-law averaging. Kozeny-Carman [89] formulations of the saturated hydraulic conductivity, for example, have been verified to perform worst of four tested methods when local variability in pore radii is high [17]. The discrepancies are orders of magnitude higher than those given by the critical path formulation

of Katz and Thompson [82]. The use of tortuosity in standard models as a fudge factor to explain the discrepancy between theory and experimental values is quite misleading, as it masks more fundamental issues.

Given this context it may seem unproductive to address studies on "electrical," "hydraulic," or "diffusive" tortuosity. Yet, in the realm of relatively small heterogeneity where simulations or experiments can address the tortuosity accurately, the results seem reasonably compatible with our predictions of geometric tortuosity [53]. In fact, we argue that these four definitions of tortuosity should coincide in the limit of vanishing pore size variability. The details of this argument, based on the trivial topology of a Wheatstone Bridge [54], are outside the scope of the present work. However, we note that the tendency for the various definitions of tortuosity to coincide in the limit of zero pore size variability is in line with our conclusion that universal scaling of the conductivity applies to the hydraulic conductivity as well as the electrical conductivity in such a limit.

11.1.1 Tortuosity Theory

Our discussion of geometrical tortuosity requires two inputs from percolation theory: expressions for the correlation length and the chemical path length. Then we will need the definition of fractal path lengths from Mandelbrot [102].

Percolation theory predicts that in an infinite system, the mean distance between any two sites on the same finite cluster, usually referred to as the correlation length χ, is given by [26, 141, 162]

$$\chi = C|p - p_c|^{-\nu} \tag{11.1}$$

In bond percolation C is proportional to a typical bond length. In Monte Carlo simulations of percolation in the square lattice, Kapitulnik et al. [81] found that $C = 0.85 \pm 0.4$ in units of the bond length. The correlation length is thought to scale with $p - p_c$ in the same way (with the same exponent) as does the Euclidean distance across the largest finite cluster of the connected bonds (sites).

For a fractal path constructed of steps of length ε, the total length of the path $L(\varepsilon)$ would be [102, 173]

$$L(\varepsilon) = x_s^{D_x} \varepsilon^{1-D_x} \tag{11.2}$$

in which D_x is the relevant fractal dimensionality, x_s is the system size, and the subscript "x" stands for either "b", denoting the backbone spanning the network, or "opt", denoting the optimal path. $L(\varepsilon)$ in Eq. (11.2) diverges in the limit $\varepsilon \to 0$ for $D_x > 1$, which is always the case in percolation theory. The backbone is the multiply-connected part of the sample-spanning cluster through which fluid flow occurs, while the optimal path is the most "energetically" favorable path across the system. Lee et al. [93] found that, whereas the fractal dimensionality of the optimal path, D_{opt}, describes the scaling of the most probable traveling *length*, D_b describes the scaling of the most probable traveling *time*. So the models developed below

(Eqs. (11.4) and (11.6)) can describe either a space-based or time-based tortuosity, depending on whether D_x in Eq. (11.2) is replaced by D_{opt} or D_b. The time-based tortuosity will be used in modeling dispersion in flow through porous media, and the arrival times distribution in porous media [52, 73, 75, 76] as shown in Sect. 11.2. The length-based tortuosity is the focus here in Sect. 11.1.

The optimal path fractal dimension D_{opt} is 1.21 in 2D networks, and 1.43 in 3D [31, 129, 160]. The average tortuosity fractal dimension $D_T = 1.10$ reported by Yu and Cheng [177] for 2D simulations is not greatly different from the 2D value of the optimal path dimension ($D_{opt} \approx 1.21$). Note that any lack of resolution at small scales, or limitation in the size of the imaged region, would tend to reduce the value of the *extracted* fractal dimension ($D_T = 1.10$). Other, more detailed comparisons will be given later.

As the percolation threshold is approached for a given network, the correlation length χ diverges, while the individual step (bond) lengths remain constant. If, in accord with the Mandelbrot definition, we suppose that the step lengths approach zero and the largest cluster (or the system size) remains constant, we should choose the individual steps inversely proportional to the correlation length ($\varepsilon \propto \chi^{-1}$). In that case, Eq. (11.2) can be rewritten as

$$L(\chi) \propto x_s^{D_x} \chi^{D_x - 1} = x_s^{D_x} \left[|p - p_c|^{-\nu} \right]^{D_x - 1} \tag{11.3}$$

Because χ is the mean distance between any two sites on the same finite cluster, $L(\chi)$ is the average length of the geometrical path $\langle L_g \rangle$. Thus, following Eq. (11.1), the geometrical tortuosity τ_g is

$$\tau_g(p) \propto |p - p_c|^{\nu(1 - D_x)} \tag{11.4}$$

Equation (11.4) is valid for (1) the case of finite values of the fundamental length scale (i.e. a separation between connected pores), and (2) infinite systems. This requires us to incorporate finite-size scaling into our expression, if we are to compare tortuosity predictions with numerical simulations, which are frequently conducted for systems that are only a few pore separations in length.

Practical application of Eq. (11.4) requires choice of a suitable system parameter in the place of the percolation probability p. For saturation-dependent problems the best choice is the moisture content θ (or, equivalently, the saturation S). In some cases, the porosity may be used. Either way, continuum percolation is the appropriate framework for further development. The question of whether the structure of the resulting continuum percolation representation is more nearly aligned with site or bond percolation, or invasion or random percolation, may determine the choice of the appropriate value of D_b in dispersion, but D_{opt}, relevant for the tortuosity, appears to be less sensitive to this distinction [160]. It is an open question, however, to what degree correlations in the medium may affect the values of D_b and D_{opt} manifest in a given medium. Presumably not all possible media will conform to one of the simple models considered here! However, so far the systems we have investigated do so.

Finite-Size Scaling

The basis of this discussion is the same as in Chap. 9, where we constrained the critical path correlation length to be smaller than the system size by forcing $p > p_c$, and thereby generating a value of the controlling conductance that was smaller than the critical one.

At length scales larger than the correlation length ($x_s > \chi$) the system is macroscopically homogeneous [140] and the geometry is Euclidean, whereas at smaller length scales ($x_s < \chi$) the system is heterogeneous, fractal and statistically self-similar [140]. What this means for finite-sized systems, however, is that it is impossible to distinguish approaches to the percolation threshold closer than the value of p for which $x_s = \chi$. Thus, one can set the system size equal to the correlation length ($x_s = \chi$) to find a particular value of the bond probability, denoted p', which has the following property. All values of p such that $p_c < p < p'$ generate a correlation length larger than the system size, and cannot be distinguished from p_c in a volume as small as the system under consideration. This eliminates system sensitivity to small changes of p in the vicinity of the percolation threshold [45], but very strong dependences on system size emerge for such parameters as diffusion or transport coefficients. Fisher [46] developed finite-size scaling theory, which allows these length dependences to be related to singular behavior of the same property as a function of $p - p_c$. In particular, a property whose dependence on $(p - p_c)$ is of power-law type with power n depends on the system length according to a power law, with the value of the exponent being $-n/\nu$. Thus the tortuosity at the percolation threshold must scale with system size as

$$\tau_g(x_x) \approx (C/x_s)^{1-D_x} \tag{11.5}$$

The theory of finite-size scaling is complicated enough that the precise result for the general function of both system size and the percolation variables is never specified. Yet it is simple enough to devise an expression for the tortuosity that is compatible with both (a) finite-size scaling and (b) the knowledge that in a finite-size system it is impossible to distinguish between a system which is at the percolation threshold, and one which is merely so close that the correlation length is larger than the system size. In the case of geometrical tortuosity we propose the following functional form:

$$\tau_g(p) \propto \left| p - p_c + \left(\frac{C}{x_s}\right)^{1/\nu} \right|^{\nu(1-D_x)} \tag{11.6}$$

Notice that in the limit of large system size ($C \ll x_s$) the above equation converges to Eq. (11.4) for the tortuosity, but for the case $p = p_c$ one retrieves the finite-size scaling result (Eq. (11.5)) for the power-law dependence of the tortuosity on system size.

Continuum Percolation

Wetting or drying processes require pore bodies (sites) or throats (bonds) to be filled by or emptied of water, respectively. Sahimi [142] argued that wetting (e.g., infiltration and imbibition) is a site percolation process, while drying (e.g., drainage)

is a bond percolation process. Hunt [67] argued that, particularly for saturation-dependent problems, it is useful to use a continuum percolation representation with the moisture content playing the role of the percolation variable. To apply Eq. (11.6) to the continuum percolation representation, we replace the variables p and p_c respectively by the water content θ and its critical value for percolation θ_t in the porous medium [67]. This gives

$$\tau_g(\theta) \propto \left| \theta - \theta_t + \left(\frac{C}{x_s} \right)^{1/\nu} \right|^{\nu(1-D_x)} \tag{11.7}$$

We would like to normalize Eq. (11.7) for the tortuosity so that it yields the value of 1 at full saturation, in the limit that the porosity approaches 1. Such a procedure carries the risk associated with extending the simple scaling formulation from percolation to conditions far from the percolation threshold; however, only under such conditions can one make a reasonable comparison with simulations or experiment. But there is an additional problem; when finite-size scaling concepts are used, this leads to a normalization that is size-dependent in principle. We generally want to avoid using a size-dependent normalization, because such a finite-size scaling correction can be readily compromised. But we also recognize that avoiding such complications can lead to a discrepancy of several percent in the limit that porosity approaches one. Accepting these risks, Eq. (11.7) can be rewritten

$$\tau_g(\theta) = \left| \frac{\theta - \theta_t + (C/x_s)^{1/\nu}}{1 - \theta_t} \right|^{\nu(1-D_x)} \tag{11.8}$$

Note that Eq. (11.8), in the case of full saturation and $\theta_t = 0.1\phi$, yields a tortuosity equal to $\phi^{\nu(1-D_{opt})}$. Using the 3D values, $\nu \approx 0.88$ and $D_{opt} \approx 1.43$, generates $0.54 < \tau_g^{-1} < 0.82$ for $0.2 < \phi < 0.6$, a typical range of tortuosity values, at least in unconsolidated media. This range of values is similar to Bear's [13] stated range $0.56 < \tau^{-1} < 0.8$ for saturated media.

In the above expression for the tortuosity, we did not use the finite-size correction in the normalization factor (in the denominator). But when we express the relative tortuosity (compared with its value at full saturation) we should include it, finding

$$\tau_r \equiv \frac{\tau_g(\theta)}{\tau_g|_{\theta=\phi}} = \left| \frac{\theta - \theta_t + (C/x_s)^{1/\nu}}{\phi - \theta_t + (C/x_s)^{1/\nu}} \right|^{\nu(1-D_x)} \tag{11.9}$$

11.1.2 Comparisons of Calculated Tortuosity with Experiment and with Simulations

Equation (11.8) can be compared with a number of different simulation values, including those measured at full saturation for which $\theta = \phi$. Koponen et al. [88] numerically computed the hydraulic tortuosity for flow in a 2D saturated porous medium with a percolation threshold $\theta_t = 0.33$. They used square networks of size 100×100 ($x_s = 100$) for $\phi > 0.55$, and 200×200 ($x_s = 200$) for $\phi < 0.55$. In

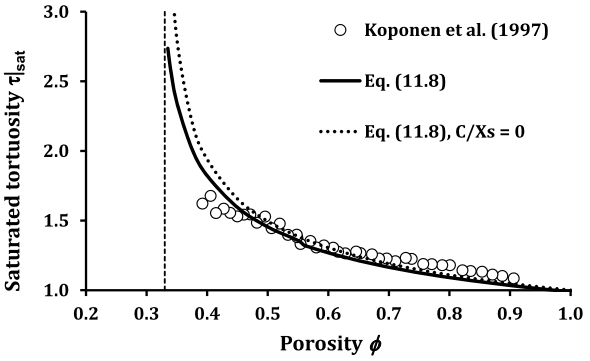

Fig. 11.1 Comparison of numerically obtained "hydraulic tortuosity" [88] with geometric tortuosity calculated from Eq. (11.8). Note that all parameters in Eq. (11.8) are fixed: no parameters were fitted

order to predict tortuosity using Eq. (11.8), for Koponen et al.'s [88] saturated media we set the ratio $C/L_s = 0.0085$ for $\phi > 0.55$, and 0.0043 for $\phi < 0.55$. With all parameters in Eq. (11.8) fixed, the Koponen et al. [88] results follow theory very closely (Fig. 11.1). Here $D_{opt} = 1.21$, $\nu = 4/3$ (the 2D value), and Koponen et al. [88] specify $\theta_t = 0.33$. The error due to ignoring the C/x_s term in the normalization, as discussed above, is a negligible 1 % at $S = 1$: the calculated value is $\tau_g|_\theta = \phi = 0.988$.

Figure 11.1 also shows the case in which the finite-size scaling effect was ignored ($C/x_s = 0$). The comparison demonstrates again how important finite-size effects become as the percolation threshold is approached, even for systems ostensibly as large as 200 elements on a side.

Matyka et al. [104] and Duda et al. [43] tried to account for finite size in modeling tortuosity in saturated media. The Matyka et al. [104] numerical results for the tortuosity as a function of the porosity are compared with Eq. (11.8) where $\theta = \phi$ in Fig. 11.2(a), while the tortuosity as a function of the system size is shown in Fig. 11.2(b). All parameter values are fixed. Although Matyka et al. [104] fitted their numerical results for the system-size dependence of the tortuosity to an exponential function (their Eq. (16)), our Eq. (11.8) does reasonably well in reproducing both behaviors simultaneously. Matyka et al. [104] concluded, presumably in view of their exponential fit to the finite size effects on the tortuosity, that finite-size effects are eliminated above some length scale. However, the existence of clusters at all length scales *at the percolation threshold* means that it is impossible to eliminate such effects in a finite-size system. Moreover, in later work [43], these authors investigated the system-size dependence of the tortuosity at the percolation threshold, and found the power-law divergence predicted in Eq. (11.8). The value of the power that they reported was 0.19, which compares well with our predicted two dimensional value of $1.21 - 1 = 0.21$.

In our analytical derivation of the geometrical tortuosity for saturated porous media ($\tau_g|_{sat}$), Eq. (11.8), based on the optimal percolation path with $D_{opt} = 1.43$ for 3D systems, the exponent is -0.378. This is close to the exponent $\beta = -0.4$ of the power-law function of porosity ($\tau_h|_\theta = \phi = \phi^{-0.4}$) proposed by Mota et al. [111], found from experiments on binary mixtures of spherical particles for saturated hydraulic tortuosity. Figure 11.3 shows good agreement between the results of

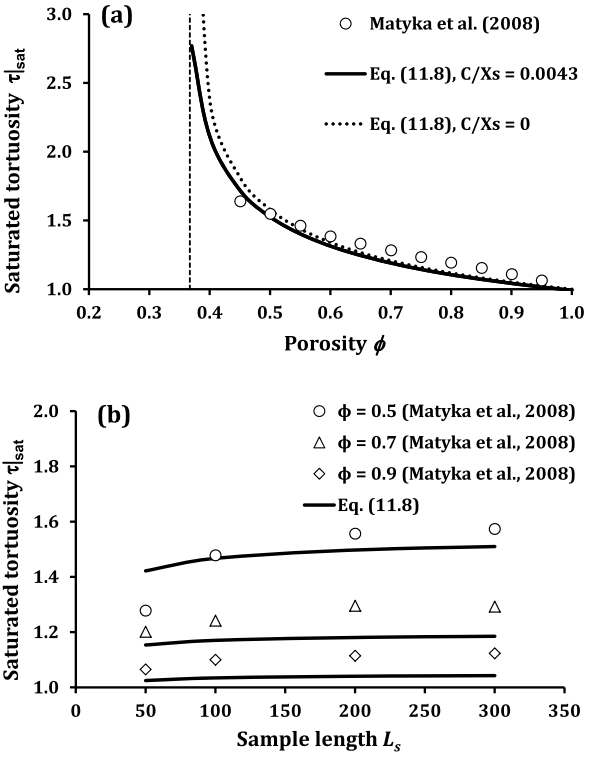

Fig. 11.2 Comparison of the geometric tortuosity prediction of Eq. (11.8) with numerical results from Matyka et al. [104] for both (**a**) the porosity and (**b**) the system size dependence of the tortuosity. Again, no adjustable parameters were used for the comparisons

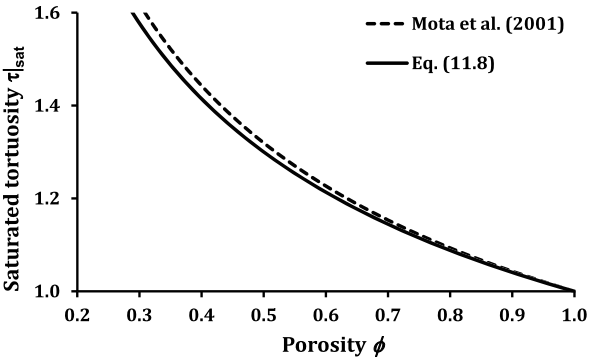

Fig. 11.3 Comparison of the prediction of Eq. (11.8) for the geometric tortuosity with results for the "hydraulic tortuosity" from experiments on binary mixtures of spherical particles. Experimental length scales, much larger than those generated by simulations, permitted neglect of finite-size effects. No adjustable parameters were used

Mota et al.'s [111] model, and the results of calculations based on Eq. (11.8), where $\theta = \phi$ using $\theta_t = 0$ (no percolation threshold consistent with Mota et al. [111]) and $C/x_s = 0$ (negligible finite-size effect, $C \ll x_s$).

Barrande et al. [9] measured the porosity (ϕ) and the formation factor (F) of porous media composed mostly of spherical particles, and calculated the saturated electrical tortuosity from the product of porosity and formation factor ($\tau_e|_\theta = \phi = \phi F$). Their experimental results are compared with the prediction of Eq. (11.8) with

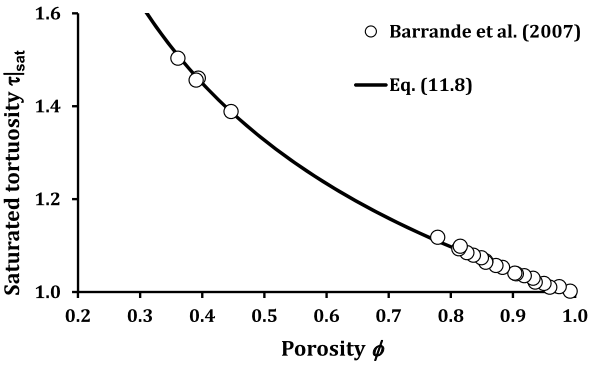

Fig. 11.4 Comparison of the predictions of Eq. (11.8) for the geometrical tortuosity with experimental results for the "electrical tortuosity" as obtained from the product of the porosity and the "formation factor." No adjustable parameters were employed

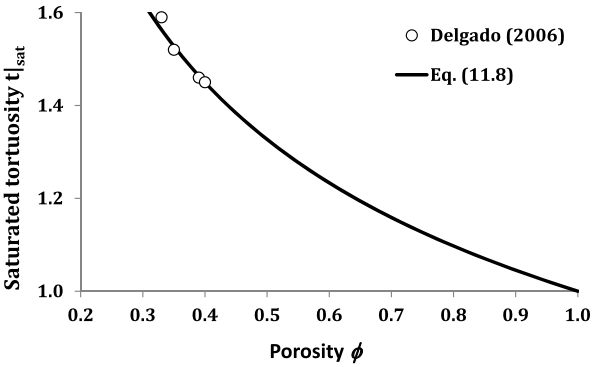

Fig. 11.5 Comparison of the geometrical tortuosity from Eq. (11.8) with experimental results for the "diffusive tortuosity" without use of any adjustable parameters

$\theta = \phi$, $D_{opt} = 1.43$, $\theta_t = 0.1\phi$ (a rule of thumb for coarse soils; Hunt [68]), and $\nu = 0.88$ for 3D systems (Fig. 11.4). The data compare very well with our proposed saturated geometrical tortuosity (Eq. (11.8)).

Delgado [39] measured diffusion both in free fluid (d_f) and in saturated, packed beds of silica sand (d_p) with average diameters of 0.496, 0.297, 0.219, and 0.110 mm. Diffusive tortuosity was calculated using the relationship $\tau_d|_\theta = \phi = d_f/d_p$. Because the sample length, x_s, in Delgado's experiments is larger than 100 mm, almost three orders of magnitude larger than the sand particles (and thus the pore size), and we have no evidence that their porosities approach a threshold value, we assume that the finite-size effect is negligible ($C \ll x_s$). We again set $\theta_t = 0.1\phi$ and used $D_{opt} = 1.43$ and $\nu = 0.88$ for 3D systems, and found excellent match between Eq. (11.8) with $\theta = \phi$, and Delgado's calculated diffusive tortuosity, $\tau_d|_\theta = \phi$ (Fig. 11.5).

In conclusion we note that Eq. (11.8), including numerical constants given either by simulation or experiment, is compatible with all the results from simulation or experiment investigated, even though the focus in generating the data was on conditions far from the percolation threshold. Furthermore, the same equation, using a typical range of porosity values, and applying saturated conditions (neglecting finite-size corrections) yields the observed range of tortuosity values for saturated, natural media cited in [13]. For most natural media, containing thousands or more pores in any direction, finite-size effects will have negligible effects on the tortuosity, so their neglect is legitimate. Percolation concepts appear to give an accurate and comprehensive description of tortuosity.

11.2 Longitudinal Dispersion of Solutes in Porous Media

11.2.1 Scope and Definition

Dispersion is a term which, in the present context, describes the spatial spreading of solutes in porous media under the action of flowing water. This dispersion can be either in the direction of flow (longitudinal) or perpendicular to it (transverse). We focus our attention here on longitudinal dispersion. Compounds dissolved in water in the subsurface are transported by molecular diffusion and advection (motion of the fluid). We address primarily the effects on dispersion from advective flow [52, 73, 74, 76], although we also provide an asymptotic treatment of diffusion [75] valid for relatively high flow velocities. Effects on dispersion from a single capillary tube velocity distribution, known to produce long-tailed arrival time distributions [23], are neglected.

The solutes we consider may be contaminant plumes from any source, radioactive tracers both experimentally and naturally generated, as well as naturally occurring reactants. Solutes may sorb to surfaces, or they may be non-sorbing. We do not specifically incorporate effects of sorption here. However, we will compare our predictions of solute velocities (neglecting diffusion) with experiments (e.g., [42, 97, 124, 146, 174, 181]) on the scaling of solute reactions with space and time scales [77]. The success of these predictions indicates that rates of many reactions in porous media are limited by the transport of reagents to the surface, or of products away from the surface, and that the relevant transport is by advection rather than diffusion.

In order to generate predictive relationships for longitudinal dispersion of solutes, we first calculate the distribution of arrival times, $W(t)$, of solute transported in steady flow [73]. This calculation has a close relationship to that of finding the distribution of hydraulic conductivity values in finite-sized systems [66]. In particular, both are based on the relevance of the cluster statistics of percolation theory to the distribution of water fluxes in terms of the critical flow from critical path analysis. Since the critical flow paths are also tortuous, we must also appeal [73] to scaling arguments of percolation regarding the fractal characteristics of such paths

[93]. Such an application leads directly to a formulation of solute transport in terms of both critical path analysis and percolation scaling. $W(t)$ is given initially for the RS random fractal model of the pore space [134]. Then we extend the result [52] to find the saturation dependence of the arrival time distribution, using the generalized pore-solid fractal (PSF) model [21]. The saturation dependence must be known in order to make comparison with experiments performed under conditions of incomplete saturation.

The present calculations yield asymmetric peaks of $W(t)$ with a long tail. The long-tail behavior is not precisely a power law, though it closely resembles one. This makes our treatment roughly compatible with the framework for the continuous time random walk (CTRW) [15, 150, 151], meaning that some general relationships with CTRW are anticipated, a discussion deferred to the end.

11.2.2 Background Information

Conventional Modeling

A differential equation, commonly called the advection-dispersion equation (or convection-dispersion equation), is widely used to describe effects of both advection and diffusive processes on the spatio-temporal behavior of dissolved solutes (e.g., Sect. 3.4.2, [13, 148]). The equation may be written

$$\frac{\partial C}{\partial t} = \nabla \cdot D_{\mathrm{l}} \nabla C - \boldsymbol{u} \cdot \nabla C \tag{11.10}$$

where $C(x,t)$ is the concentration of the solute, D_{l} is the longitudinal (in the direction of flow) hydrodynamic dispersion coefficient, and $\boldsymbol{u}$ is the velocity of the flow. In the case $\boldsymbol{u} = 0$, the only influence on $C(x,t)$ is the solute's molecular diffusion, D_{s}, and so $D_{\mathrm{l}} = D_{\mathrm{s}}$. But usually D_{l} is found to greatly exceed D_{s}. Further, results of experiments and field observations typically show that D_{l} has a dependence on both spatial and temporal scales. This suggests that describing the relationship between the microscopic process of advection and the macroscopic description of dispersion as simply being analogous to microscopic diffusion is not adequate.

The velocity $\boldsymbol{u}$ is a random field, generated by solution of

$$\nabla \cdot \boldsymbol{u} \propto -\nabla \cdot K \nabla P = 0 \tag{11.11}$$

Here K is the hydraulic conductivity (a random scalar field in isotropic media) and P is the pressure. D_{l} may also be assumed to vary from point to point. Thus, one means to investigate the behavior of solutes in natural porous media is simply to solve numerically Eq. (11.10) and Eq. (11.11) using assumed stochastic variability of the coefficients [36, 37, 47, 49, 138, 175]). Such treatments can address some of the problems of Eq. (11.10), if sufficiently complex media with multi-scale heterogeneity are applied. But more comprehensive comparison [76] of the predictions of "stochastic subsurface hydrology" (for example, [117]) with experiment reveals serious inconsistencies.

A conceptual reason for using critical path analysis and percolation theory rather than a stochastic approach to model fluid flow (and ultimately both solute and particle transport) is the conclusion of Bernabé and Bruderer [17] regarding pore scale upscaling of the hydraulic conductivity:

> At high [relative variance], owing to flow localization, extreme values of [pressure drop squared] occurred at deterministic positions. The flow pattern is so strongly controlled by these huge values [at bottleneck conductances quantified by percolation theory] that a stochastic description becomes inadequate.

If the flow itself cannot be described by stochastic methods, such methods also cannot describe the distribution of particle velocities and path lengths. The pore-scale conclusion of Bernabé and Bruderer [17] is consistent with Shah and Yortsos [156] conclusion that the critical path analysis framework was best suited to explain flow channeling in heterogeneous media at geologic scales, such as that observed by Moreno and Tsang [110]. Our basic method can be applied at either scale.

On the basis of the results and comparisons of this chapter, we argue that the ADE should never be applied at length scales beyond that of a single pore. Nonetheless, treatments of solute transport at larger length scales do need to be consistent with the ADE when reduced to the scale of a single pore.

Quantifying Limitations of the Neglect of Diffusion

Since most of our comparisons with experiment neglect molecular diffusion, it is important first to define the conditions under which it is acceptable to do so. The means to evaluate the relative effects of diffusion [125, 139] are based on the ADE. Under the action of advection, the effects of diffusion appear to be enhanced. The resulting phenomenon is termed hydrodynamic dispersion, but is typically treated mathematically simply as diffusion with a velocity-dependent diffusion coefficient. However, at the scale of a single pore we treat the dispersion term as due to molecular diffusion. The relevance of advection relative to diffusion may then be estimated [125] by use of the Peclet number, $\mathrm{P_e} = Lu/D_\mathrm{s}$, where L is a pore length scale, u is the pore-scale fluid velocity, and D_s is the solute diffusion coefficient. Typically it is assumed that for $\mathrm{P_e} > 100$ diffusion may be neglected, while for $\mathrm{P_e} < 1$ advection may be neglected. In a study related to the present work, Sahimi and Imdakm [145] give $\mathrm{P_e} = 300$ as a lower bound for neglecting diffusion. Clearly we should not exclude the possibility that there is a range of $\mathrm{P_e}$ values greater than 1 for which diffusion cannot be neglected.

Experimental Overview

Based on the success of the approach discussed and expanded on here, Hunt et al. [76] argued that the only term in Eq. (11.10) that was of relevance to the majority of experiments (over 2000 discussed) was the advection term. In fact, it was difficult to

find direct evidence of the importance of diffusion at all. What are the implications of Eq. (11.10)?

Solution of Eq. (11.10) for steady flow in a homogeneous medium leads to Gaussian spreading superimposed in the direction of flow. Natural porous media of interest (rocks, soils, fracture networks) are never homogeneous, and such Gaussian behavior of C is seldom actually inferred or observed [6, 7, 15, 34, 50, 92, 103, 115, 148, 159, 176]. A quantity developed, in the Lagrangian representation, to quantify the discrepancy between experiment and the Gaussian solution, is the longitudinal hydrodynamic dispersion coefficient [35, 36]

$$D_{\mathrm{l}}(t) = \frac{1}{2}\frac{d}{dt}\sigma^2(t) \propto \frac{\sigma^2(t)}{t} \tag{11.12}$$

where the proportionality follows if $\sigma^2(t)$, the variance of the spatial solute distribution, is a power of the time t. For Gaussian dispersion, the linear proportionality $\sigma^2(t) \propto t$ makes $D_{\mathrm{l}}(t)$ time independent. Because field experiments are pinned to an Eulerian representation, $D_{\mathrm{l}}(t)$ may also be reported as the ratio of the variance to the mean *travel length*, l. The two representations of $D_{\mathrm{l}}(t)$ are not always equivalent, since the mean solute velocity, $u_{\mathrm{s}} \equiv l/t$ is not, in general, scale-independent (e.g., [93, 103]). In fact, D_{l} typically increases as a power of time [7, 115, 176]:

$$D_{\mathrm{l}}(t) \approx t^{\delta} \tag{11.13}$$

with $0 < \delta < 1$.

D_{l} increasing as a power of t is considered a difficult point to explain in hydrology. The longitudinal dispersivity, α_{L}, usually given as D_{l}/u, is maybe better expressed as a function of travel distance x, representing the fractional spreading in the direction of travel. Thus, a dispersivity that is proportional to x indicates that the spatial solute distribution has the same appearance at all scales [151]. In fact, a commonly applied rule of thumb is that $\alpha_{\mathrm{L}}(x) = 0.1x$ [50]. In a series of articles on the value of using the Continuous Time Random Walk (CTRW) in solute transport in groundwater, Scher and co-authors have emphasized that the scale invariance of the spatial solute distribution is a result of the waiting time distribution $\psi(t)$ having power-law tails. In the CTRW formulations these tails should have the form $\psi(t) \propto t^{-1-\alpha}$, with general relationships available (see this chapter's Appendix) to predict such phenomena as the temporal scaling of the typical arrival time distribution, or the dispersion coefficient. Our results differ slightly from the exact power-laws proposed in CTRW, however, meaning that the mathematical relationships between CTRW variables do not necessarily hold precisely in our case.

Experiments also reveal other discrepancies with Gaussian spreading. Cortis and Berkowitz [34] point out that several "classical" solute dispersion experiments [80, 118, 119, 148]) show breakthrough curves (BTC) for which Gaussian spreading overestimates the arriving solute flux at both short and at long times. A long-tailed arrival time distribution (for which the variance or even the mean arrival time may not exist) such as we predict will produce a longitudinal dispersion coefficient which increases with system size, and is consistent with the deviations from Gaussian scaling of the BTCs listed by Cortis and Berkowitz [34]. Experimental results

(and practical needs) point to the importance of being able to predict both the entire arrival time distribution, and a spatial distribution of solutes at a given time.

11.2.3 Theoretical Descriptions

There are several ways to approach such problems. One can develop network models that require solutions to systems of difference equations (using, e.g., percolation theory), rather than a single differential equation. This is the approach we follow. One can use numerical or theoretical methods to treat the variability of the coefficients in Eq. (11.10). Or one can seek a mathematical framework, which produces solutions of the type desired. To the third class of approaches belong the Continuous Time Random Walk (CTRW) formulation and fractional differential equations. Thus such power law tails may be described accurately with a fractional advection-dispersion equation, in which integer order derivatives in Eq. (11.10) may be replaced by fractional derivatives [86, 90, 105–107, 122, 147, 178, 179]. While such a formulation can model the long-time behavior, it cannot be used to predict it, unless the order of the derivative can be determined in advance. Further, a fractional differential equation does not appear to generate the appropriate short-time behavior [103]. Additionally, if (as derived here) the long-time tail is not a true power law, then such a method will not quite describe the asymptotic behavior either.

The Continuous Time Random Walk (CTRW) [84, 150, 158] appears to generate the entire arrival time distribution (e.g., [16, 19, 34, 103]) in agreement with experiment (except perhaps at very long times), but like the fractional derivative approaches it is only descriptive. Nevertheless, the CTRW can provide guidance on how to predict large-scale behavior from small-scale observations, on account of the observation that solute distributions tend to maintain the same shape as the plume evolves. But we wish to predict the entire behavior of $C(x,t)$. We believe that this restricts the available options to percolation theory.

Percolation theory has been used before to calculate dispersion related quantities in porous media [5, 10, 63, 87, 93, 98, 123, 129, 145]. But our framework is quite different from earlier ones, because we disentangle the influences of pore-size distribution from the topological complications of the flow paths described in percolation theory. In contrast to the saturation dependence of K, for which different aspects of percolation theory dominate at different saturations, here we find that these different aspects dominate at different time periods. In particular, the pore-size distribution, as expressed through a combination of critical path analysis and cluster statistics of percolation, is important near the peak in the arrival time distribution, while the tortuosity becomes relevant to the long-time asymptotic behavior, and thus to the spatial structure of the dispersion coefficient. Our conclusion regarding the relevance of tortuosity to dispersion on account of the dominance of the critical paths was anticipated in past discussions, at least qualitatively:

> Moreover, the critical path analysis [3] indicates that transport in a well-connected system in which the hydraulic conductivity distribution is broad, is actually dominated by a small

> subset of the system in which the magnitude of the conductivities is larger than a certain threshold. Heterogeneous porous media can therefore be mapped onto equivalent percolation networks. [136]

This evaluation of Rivard and Delay [136] is consistent with decades of publications by Muhammad Sahimi, including Sahimi [140, 142]. However, we do not agree with the quantitative implications of Rivard and Delay's statement that a direct mapping is sufficient. Specifically, if the most permeable portion of the system that just percolates is chosen, the paths of flow are infinitely tortuous; following paths with slightly lower hydraulic conductances would allow solutes to arrive at a much earlier time. Nevertheless, we agree with the general message of Rivard and Delay [136].

Relationship Between Flow and Transport

It is commonly believed that local variability in the hydraulic conductivity of heterogeneous media is a controlling influence on dispersion (see the many texts on stochastic subsurface hydrology, for example [37, 138]). Since it is clear that the solute transport paths are affected by the entire structure of the medium, and not just the statistics of the local conductances, there has been a great deal of work in trying to find the appropriate description of the connectivity of potential flow and transport paths. In the present description, we use percolation theory to give as much of this information as possible. But our focus is not to try to generate a realistic model of the medium. Rather, it is to generate the connectivity and statistics of the hydraulic conductivity simultaneously with the statistics of solute transport. If medium connections are indeed best described by percolation theory, then the precise description of the local variability in permeability becomes secondary. One important consideration is that an appropriate average over the possible transport paths should also generate the hydraulic conductivity.

Consider experiments with wetting fronts in natural media. When the medium itself is fairly homogeneous (such as relatively uniform sand in a sand dune), such wetting fronts are often relatively regular. An interesting result from a particular experiment is that, even though the wetting front was fairly regular, paths of solutes following the fluid could be very irregular [56] (Fig. 11.6). Thus, experiments already suggest that it is appropriate (as in critical path based calculations of the saturated hydraulic conductivity, K) to find K by an optimization between fluid connectivity and pore-size variability, while solute dispersion may better be determined through an enumeration of *all* the paths, including effects of both pore size distribution and connectivity. We suggest that it is the tendency for flow to emphasize the paths of least resistance which makes the cluster statistics of percolation relevant both to the distribution of measured K values and to dispersion of solutes.

We have found [69, 70]) that the distribution of K values in anisotropic fracture networks [152, 154] can be predicted using the cluster statistics of percolation. We now apply the same concepts to find the distribution of global fluxes. We do not seek a distribution of streamline velocities. Note that, in the simplified version of the problem we are considering, solutes are released at one instant in time, even though

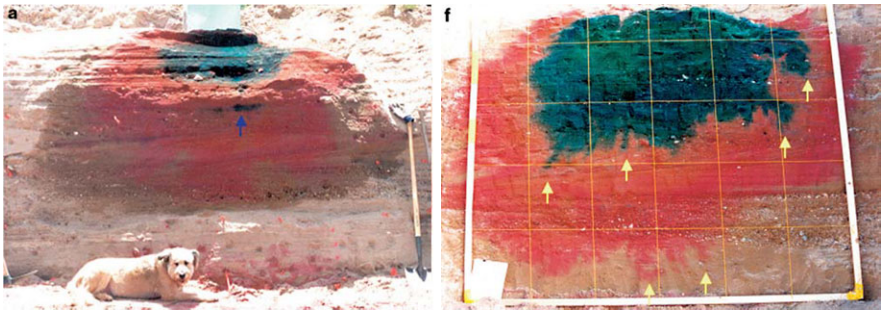

Fig. 11.6 Field experiments [56] reveal a wetting front that is much more regular than solute paths, broadly consistent with calculations of solute transport in terms of an enumeration of all paths, but of the hydraulic conductivity in terms of an optimal path (Figure reprinted with permission from the authors). As pointed out by the authors, these characteristics can be identified much more easily with a color image. The two photographs are taken at different vertical slices in the medium

in experiments solutes are typically released with equal concentration starting at one particular time. We can relate these two procedures using a simple integral. In our picture, the concentration C arriving at any position can be normalized to its original value, making C equivalent to a probability, W. This furthers use of the basic probabilistic transformations on which the derivation is based.

Theoretical Development for Dispersion Based upon the RS Model

The cluster statistics of percolation theory have been applied ([66, 70]; Chap. 10) to the problem of deriving the distribution of controlling resistances (expressed as conductances, $g = R^{-1}$) of clusters of arbitrary length, N. Here N is a number (equal to the number of controlling resistances along one dimension of the cluster); the linear extent of the cluster must be expressed as the product of N and a typical spatial separation, l, of controlling resistances. The volume concentration of clusters of length Nl is then derived from the cluster number n_s by using $n_s ds = n_N \mathrm{d}N$ (see Chap. 10 for definitions for n_s and n_N), and the percolation scaling relationship $(\tau - 1)/\sigma\nu = d$ [161], where d is the dimensionality of the space and τ, σ, and ν are percolation exponents. The result is ([66]; also see previous chapter using the result for $p - p_c$)

$$n_N = \frac{1}{N^{d+1}} \exp\left\{-\left[\left(\frac{Nl}{L}\right)^{\frac{1}{\nu}} \left|1 - \left(\frac{g}{g_c}\right)^{\frac{3-D}{3}}\right|\right]\right\} \tag{11.14}$$

The probability that a given system of Euclidean length, Nl, is spanned by a cluster with controlling conductance g is then proportional to the integral of $N^d n_N$ over clusters of all sizes larger than or equal to the volume in question. The result may be expressed in terms of the exponential integral,

$$\mathrm{Ei}(z) = \int_z^\infty \frac{\exp(-y)}{y} dy \tag{11.15}$$

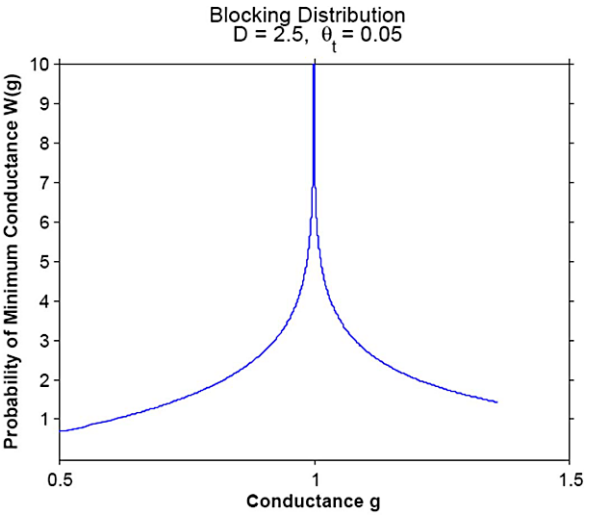

Fig. 11.7 An example of the pdf, $W(g)$, that the controlling (bottleneck) conductance in a system of size x has value g. Horizontal axis is in units of g_c. Fractal dimensionality of the pore space is given

as

$$W(g) \propto \frac{1}{\beta}\mathrm{Ei}\left[\alpha\left(\frac{x}{L}\right)^{\beta}\right] \tag{11.16}$$

where the parameters α and β are given by

$$\alpha = \left|1 - \left(\frac{g}{g_c}\right)^{\frac{3-D}{3}}\right|^2 \quad \text{and} \quad \beta = \frac{2}{v} \tag{11.17}$$

Here x is the linear dimension of the system concerned, L^3 is a representative elementary volume (REV) which represents the smallest volume for which statistical arguments (such as percolation theory) apply, and l is a typical distance between critical resistances, which can be taken to be approximately equal to L. One can then set $L = 1$, meaning that $x = 1$ corresponds to the REV scale. In the limit that the pore size distribution approaches a delta function (no width), the REV scale reduces to the separation of the pores. The result, Eq. (11.16), for $W(g)$ is shown graphically in Fig. 11.7.

An approximation to $W(g)$ from Eq. (11.16) is given by

$$W(g) \propto \ln\left[\left(\frac{L}{l+x}\right)^{1/v} \frac{1}{\left|1 - \left(\frac{g}{g_c}\right)^{\frac{1-D}{3}}\right|}\right] \tag{11.18}$$

Note that $W(g)$ is a function of system size, and thus $W(g)$ can be explicitly represented as $W(g, x)$, or as a conditional probability density function $W(g|x)$. Equation (11.18) shows that the asymptotic behavior of the exponential integral involves a logarithmic divergence in $W(g)$ at $g = g_c = 1$ as shown in Fig. 11.7. Such a logarithmic divergence is integrable, meaning that $W(g)$ is normalizable. This same result may be obtained [70] by replacing the exponential cut-off of the power-law

decay in Eq. (11.14) by a sharp cut-off obtained by setting the argument of the exponential function equal to an arbitrary constant (as implied in [161]).

The solute concentration of the water introduced to the medium can be assumed to be uniform. Thus, although the probability that a given isotropic system is spanned by a cluster of minimum conductance g is given by Eq. (11.17) and Eq. (11.18), the mass of solute transported through such clusters characterized by minimum conductance g must be proportional to the water flux, itself proportional to $gW(g)$. Since $W(g)$ is a sharply peaked function, the effects on a distribution of arrival times, $W(t)$, due to the difference between $W(g)$ and $gW(g)$ is, in most cases, undetectable. Nevertheless, the probability that solute reaches the other end of a system at time t is clearly proportional to the volume of advecting fluid arriving at that time, and the solute arrival time distribution, $W(t)$, is thus proportional to $gW(g)$. The proportionality constant is derived next.

In order to use $W(g)$ to give information on arrival times, we must be able to relate the controlling conductance, g, of a path to the time, t, solute takes to travel along that path, $t(g)$. Here, x may be regarded simply as a parameter, independent of t. Thus the notation suppresses the x-dependence. Then one may use the result

$$gW(g)dg = W(t)dt \quad \text{or} \quad W(t) = \frac{gW(g(t))}{dt/dg} \tag{11.19}$$

In the absence of diffusion, the solution for $t(g)$ is deterministic. Note, however, that since $gW(g)$ is not directly normalized, $W(t)$ must be normalized separately. First we consider the effects of the pore size distribution on $t(g)$, then we proceed to examine the effects of connectivity and tortuosity.

In the following, the treatment of a percolation path as quasi-one-dimensional is not in contradiction to the tortuosity-based arguments; it is merely a first step in finding the influence of the pore-size distribution on the time of transit of a large cluster. Thus we decouple the effects of pore sizes and connectivity. As in an effective resistance, which is the sum of individual resistances along the path, the total *time* of travel is equal to the sum of the travel times through the individual pores along such a quasi-one-dimensional path. This means that it is necessary to find the transit times of individual pores on a path for which the mass flux is defined through the largest resistance on that path.

The time that a solute requires to traverse one pore is proportional to $1/u$, where u is the typical velocity in that pore. Then uA, where A is the cross-sectional area of the pore, must be proportional to Q, where Q is the volume flux of water through the pore. Thus $t \propto r/u \propto rA/Q$, and rA is proportional to r^3, the volume of the pore. Q for all pores along a quasi-one-dimensional critical percolation path is identical and equal to Q_c, which is proportional to g_c. Similarly, Q for all pores along a quasi-one-dimensional path near critical percolation is proportional to g, where g is the controlling (smallest) conductance on such a path. The probability that a given pore has radius r is proportional to r^{-D-1} [71], although the fractional volume in such pores is proportional to $r^3 r^{-D-1} = r^{2-D}$. Q is a volume per unit time, but the time factor is explicitly removed (and called t_0) below so that Q is effectively only a volume. Under those stipulations, Q is r^3, and t_0 is a fundamental pore

time scale. The value of t_0 is not required because only functional dependences are relevant below. Using these inputs it is possible to write the following expression of proportionality:

$$t(r) \propto t_0 \int_{\mathrm{r}}^{r_\mathrm{m}} \frac{r'^3}{Q} \frac{r'^{-D-1}}{r^{-D}} dr' = t_0 \left[\int_{\mathrm{r}}^{r_\mathrm{c}} \frac{r'^3}{Q} \frac{r'^{-D-1}}{r^{-D}} dr' + \int_{r_\mathrm{c}}^{r_\mathrm{m}} \frac{r'^3}{Q} \frac{r'^{-D-1}}{r^{-D}} dr' \right] \tag{11.20}$$

The division of the integral into two terms is useful for expressing the time in terms of the critical time for percolation. The input into Eq. (11.20) is consistent with the assumption that the paths followed by the solute are straight. Equation (11.20) must therefore be modified to account for the effects of the tortuosity as well as the influence of the branching topology on the transit time. The tortuosity was noted to follow

$$\tau_\mathrm{g} \equiv \frac{\Lambda}{\chi} \propto |V - V_\mathrm{c}|^{\nu(1-D_\mathrm{opt})} \tag{11.21}$$

where Λ is the actual (tortuous) path length, V is an arbitrary volume fraction and V_c its critical value for percolation. In the present context V and V_c may be considered to correspond to the volumetric moisture content, θ, and its critical value for percolation, θ_t, even though the specific problem to be addressed here involves saturated conditions. We cite Lee et al. [93] to support our substitution of the exponent D_b in place of the D_opt in Eq. (11.21). The effect of tortuosity is to lengthen each individual time by the factor represented in Eq. (11.21); thus the combined effects of streamline fluxes and tortuosity is given by the product of Eq. (11.20) and Eq. (11.21). An additional factor of $(x/L)^{D_\mathrm{b}}$ enters to give the explicit dependence on the Euclidean measure of the system size, x, in terms of the length, L. Evaluating the integrals in Eq. (11.20) and combining with Eq. (11.21) then yields

$$\begin{aligned} t = \left(\frac{x}{L}\right)^{D_\mathrm{b}} \left(\frac{t_0}{3-D}\right) \left(\frac{1}{r^{3-D}}\right) \left[\left(r_\mathrm{m}^{3-D} - r_\mathrm{c}^{3-D}\right) \right. \\ \left. + \left(r_\mathrm{c}^{3-D} - r^{3-D}\right) \right] \left(\frac{1}{\theta - \theta_\mathrm{t}}\right)^{\nu(D_\mathrm{b}-1)} \end{aligned} \tag{11.22}$$

Equation (11.22) may be further manipulated to yield

$$\begin{aligned} t &= \left(\frac{x}{L}\right)^{D_\mathrm{b}} \left(\frac{t_0}{3-D}\right) \frac{g_\mathrm{c}}{g} \frac{1}{(1-\theta_\mathrm{t})^{\nu(D_\mathrm{b}-1)}} \left[\left(1 + \frac{\theta_\mathrm{t}}{1-\theta_\mathrm{t}}\right) \left(\frac{g_\mathrm{c}}{g}\right)^{\frac{1-D}{3}} - 1 \right] \\ &\quad \times \left[\frac{1}{\left(\frac{g}{g_\mathrm{c}}\right)^{\frac{1-D}{3}} - 1} \right]^{\nu(D_\mathrm{b}-1)} \\ &\equiv t_\mathrm{g} \left(\frac{x}{L}\right)^{D_\mathrm{b}} \end{aligned} \tag{11.23}$$

which serves to define the cluster transit time t_g. The dependence of t_g in Eq. (11.23), which contains a power-law divergence at $g = g_\mathrm{c}$, is depicted in Fig. 11.8.

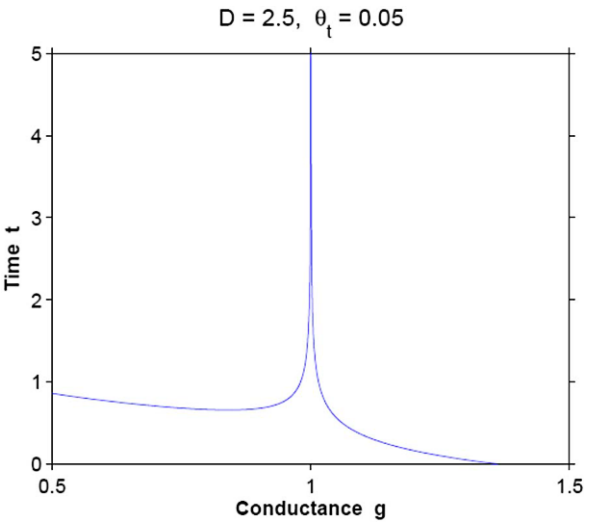

Fig. 11.8 An example of the time, t, of transit through a cluster of minimum conductance, g for specific values of the fractal dimensionality of the pore space and critical volume fraction for percolation. Horizontal axis is in units of g_c

Note that the vicinity of the percolation threshold occurs here in the limit of infinite time. For g near but somewhat less than g_c, there occurs a minimum in $t(g)$. This minimum, broadly speaking, corresponds to the optimal conductance which defines the hydraulic conductivity of an infinite system. How can this be understood?

A non-vanishing K cannot be calculated from a subnetwork of the system, when the subnetwork is just at the percolation threshold. Even though the critical percolation condition defines the most conductive pathways in the system, their spatial separation is equal to χ, which diverges at the percolation threshold, producing an effective conductivity of zero. Thus the network for calculating K must also include a few $g < g_c$ reducing the conductance of each path but greatly increasing the number of effective paths. The system conductivity is then calculated using an optimization procedure [48, 67]. This optimization procedure winds up pinning the controlling g near g_c, similarly to the way the minimum in $t(g)$ is tied to g_c.

Under extreme circumstances of very high disorder in very small systems, this minimum can create a spike in our solutions for $W(t)$; however we do not expect that such a spike (which is a result of $dt/dg = 0$, i.e., many paths with the same arrival time, t) would survive if our calculations take into account the spreading in $W(t)$ due to (for example) the varying velocities within an individual pore. Note as well that in the immediate vicinity of the peak in $t(g)$, the contribution from the variability of the flux (the first factor in square brackets) is negligible in comparison with the tortuosity (the second factor in square brackets), except in the limit of vanishing θ_t. As a consequence, one finds the effects of $t(g)$ on the asymptotic, large time behavior of $W(t)$ to be

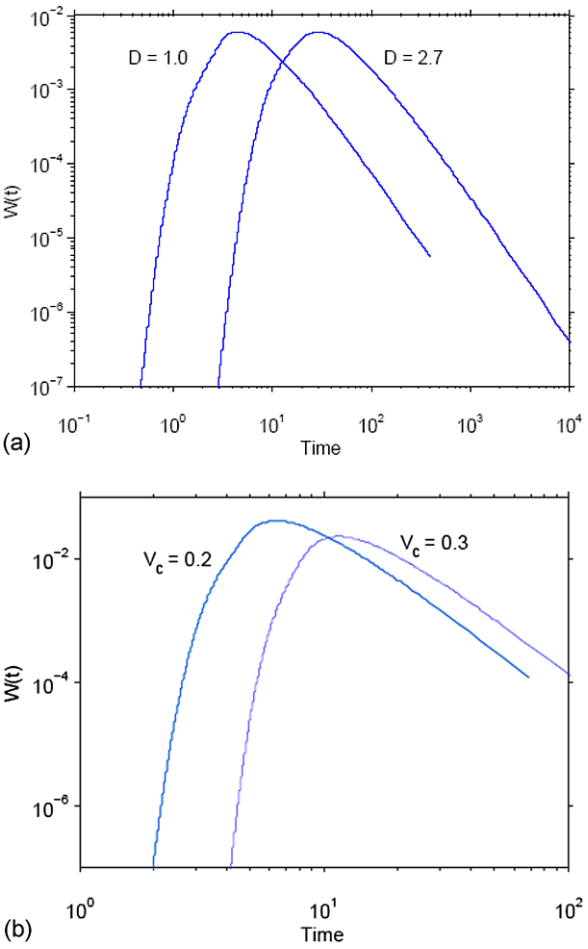

Fig. 11.9 Comparison of the results for the arrival time distribution, $W(t)$, for (**a**) two different values of the fractal dimensionality of the pore space, and (**b**) two different values of the critical volume fraction for percolation

$$W(t) \propto \left[\frac{A}{t}\right]^{\frac{1+(\eta-v)}{\eta-v}} \tag{11.24}$$

with A a constant. However, in the cases we have checked so far, the absolute value of the power predicted by Eq. (11.24) has exceeded by about 0.5 the result generated by numerical analysis of the full distribution. So this estimate is not useful for predictions in finite-sized systems, while we cannot test it in the infinite limit.

A full numerical solution for $W(t)$ from Eq. (11.19), using Eq. (11.23) for $t(g)$, gives the results shown in Fig. 11.9 for two-dimensional random percolation system, for various combinations of fractal dimensionality and critical values of the moisture content. Note the relative insensitivity of the shape of $W(t)$ to variations in system parameters, an important result.

Modification for More Flexible Pore-Size Distribution and Saturation Dependence

We have performed an analogous derivation to that which led to Eq. (11.16) for unsaturated conditions, using the generalized PSF model [21]. The principle reason for using such a strategy is that the PSF model can more easily be fit to a wider range of experimental data, even if its use is not necessarily preferred. Consequently one can obtain all the parameters that are not constrained by percolation theory directly from experimental data for the soil water retention curve. Our result [52] was

$$W_{\mathrm{p}}(g \mid x,\theta) \propto \frac{1}{b}\mathrm{Ei}\left[a\left(\frac{x}{L}\right)^{b}\left(\frac{\beta-\phi+\theta-\theta_{\mathrm{t}}}{\beta-\theta_{\mathrm{t}}}\right)\right] \tag{11.25}$$

Since upper and lower limits to the local conductance distribution have been assumed, the distribution of blocking conductance values given by Eq. (10.25) must have upper and lower limits as well. These are given by

$$g_{\max} = g_{\mathrm{c}}\left[\frac{\beta-\phi+\theta}{\beta-\phi+\theta-\theta_{\mathrm{t}}}\right]^{\frac{3}{3-D}} \tag{11.26a}$$

and

$$g_{\min} = g_{\mathrm{c}}\left[\frac{\beta-\phi}{\beta-\phi+\theta-\theta_{\mathrm{t}}}\right]^{\frac{3}{3-D}} \tag{11.26b}$$

In order to find a distribution of arrival times, we must find the typical arrival time, $t(g|x,\theta)$, as a function of volumetric moisture content θ, travel distance x, and controlling conductance g. Using the PSF model we find

$$t(g \mid x,\theta) = \left[\frac{x}{L}\right]^{D_{\mathrm{b}}} \frac{Dt_0}{3-D}\left[\frac{\left(\frac{g_{\mathrm{c}}}{g}\right)^{\frac{1-D}{3}}\left(\frac{\beta-\phi+\theta}{\beta-\phi+\theta-\theta_{\mathrm{t}}}\right)-1}{1-\left(\frac{g}{g_{\mathrm{c}}}\right)^{\frac{D}{3}}\left(\frac{\beta-\phi+\theta-\theta_{\mathrm{t}}}{\beta-\phi+\theta}\right)^{\frac{D}{3-D}}}\right] \times\left[\frac{1}{(\beta-\phi+\theta-\theta_{\mathrm{t}})^{(D_{\mathrm{b}}-1)\nu}}\right]\left[\frac{1}{\left|1-\left(\frac{g}{g_{\mathrm{c}}}\right)^{\frac{1-D}{3}}\right|}\right]^{(D_{\mathrm{b}}-1)\nu} \tag{11.27}$$

Combining Eq. (11.25) and Eq. (11.27) using the same probabilistic identity (Eq. (11.19)) yields the arrival time distribution. In the case that $\beta = 1$, the PSF model reduces to the RS model (Chap. 4).

There are a few complications in the process just shown. In order to find the arrival time distribution explicitly, one must invert the relationship for $t(g)$ to find $g(t)$. While the former is single-valued, the latter is not; thus it is necessary to apply Eq. (11.19) to every conductance g which defines a cluster with a given t. In fact, as can be seen by examining Fig. 11.8, this inversion may have one, two, or even three solutions. These different solutions, especially at large t values, correspond to different physical situations. A large time can result from a very small controlling conductance, or from a conductance slightly above or below the percolation threshold. Thus, either very tortuous paths, or paths with smaller pore sizes, contribute

Table 11.1 Fractal dimensionality of the backbone on two- and three-dimensional lattices [160]

Percolation variation	D_b	
	2d	3d
Site non-trapping invasion percolation	1.642	1.868
Site trapping invasion percolation	1.217	1.861
Bond trapping invasion percolation	1.217	1.458
Random percolation	1.643	1.870

to $W(t)$ at longer times, while at the very longest times the behavior is controlled by the tortuosity of the paths near the percolation threshold. On the other hand, the short-time behavior is governed by large conductances below the percolation threshold only. The inversion of $t(g)$ near the percolation threshold is also difficult, if one wishes to find an accurate numerical representation of the tail.

In our investigations of the solution that was generated by this process, we saw only a weak dependence on moisture content of the arrival time distribution. But this is only a part of the story. It has been argued ([160], summarizing earlier papers by Muhammad Sahimi and co-workers) that the processes of wetting and drying are fundamentally different percolation processes. According to Sahimi [143], wetting is site invasion percolation with trapping, while drying is bond invasion percolation with trapping. Under full saturation conditions the topology of the system should be consistent with random percolation, since the topological constraints introduced by trapping will have disappeared; moreover the value for D_b from site invasion percolation with trapping is nearly identical to its value from random percolation (Table 11.1), so that even incompletely saturated media on the wetting curve should still be compatible with the choice $D_b = 1.87$. Thus, in three dimensions, we need to use $D_b = 1.46$, for unsaturated conditions under drying and $D_b = 1.87$ otherwise. The value of the exponent ν is, as before, 0.88. The remaining parameters are system specific. If the flow is two-dimensional, for example the well-known case of wall flow in core experiments on very coarse media, one should use $D_b = 1.21$ under conditions of either wetting or drying, and $D_b = 1.6432$ otherwise. In two dimensions, of course, $\nu = 4/3$.

For the purposes of comparison with experiment, variations in the values of D_b that are less than 1 % have been ignored. Thus for each flow configuration, two dimensional or three dimensional, we have distinguished only two possibilities.

11.2.4 Comparison with Simulations

Liu et al. [96] reported on simulations of flow and transport on a 2D percolation structure at the percolation threshold. They did not incorporate any effects of diffusion, nor did they include any effects that would be equivalent to a pore size variability. They solved the Navier-Stokes equations for flow, then used particle tracking methods to determine $W(t)$ (Fig. 11.10). Such a model lends itself to comparison

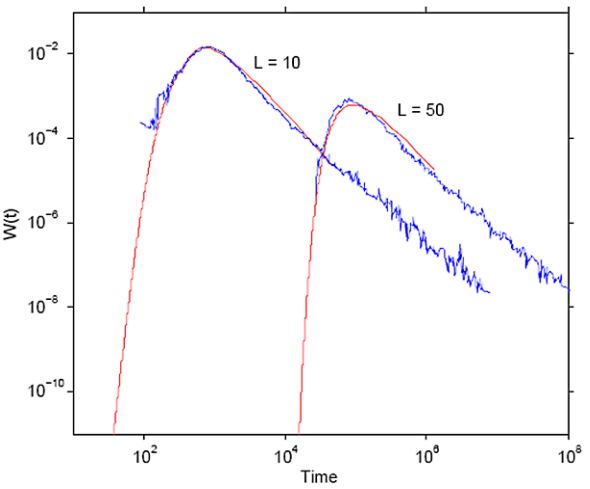

Fig. 11.10 Comparison of the predicted distribution of arrival times with results of numerical simulations by Liu et al. [96]. Both calculation and simulation were done in two dimensions and without accounting for diffusion. Note that three adjustable parameters were used to generate the agreement with spatial system size 10, but the same parameters were used for system size 50. Further, the fractal dimensionality of the pore space used, $D = 1$, corresponds to a system with a very narrow range of pore sizes, generally consistent with the constraints of the simulations, which include no such range

with our predictions, provided we force the model to be consistent with a very narrow range of pore sizes. This restriction is easy to treat using our simple RS model [134]. Further, this model has the smallest number of unknown parameters. In order to fit the curve with our result for $W(t)$ we employed three such parameters: an absolute time scale t_0, the critical volume fraction for percolation θ_t, and the fractal dimensionality of the pore space. These parameters, including $\theta_t = 0.25$, and $D = 1$ (nearly homogeneous), were found by comparison with the curve for $L = 10$, and then our prediction for $L = 50$ was compared with simulation. The two-dimensional values of the parameters $D_b = 1.6432$ and $\nu = 4/3$ were dictated by percolation theoretical arguments made above.

We demonstrated above that $W(t)$ varies little with the pore-space parameters D and V_c; nevertheless, large values of D appropriate for disordered natural media do produce a noticeable downward curvature at larger times, distinct from the numerical simulations. We find that $D = 1$, which for $\phi = 0.5$ would be consistent with $r_0 = r_m/\sqrt{2}$ (a very narrow pore-size distribution), gives a reasonably good shape fit with simulations. Note that in the absence of disorder, the REV length scale is a single pore length, so that a simulation length scale of 1 [96] corresponds exactly to our system length of 1. Larger values of V_c tended to produce a narrower peak: we found that a rather large value, $V_c = 0.25$, produced the closest fit. In retrospect, we may have preferred to see an even larger value (such as 0.5, p_c for a square lattice in 2D), but we have left out numerical constants throughout the derivation, so we find that for an effectively two-parameter fit (the chosen D at very nearly the "ordered"

limit of the RS model is at least somewhat constrained) we have relatively good results. More impressive is that, for exactly the same parameters generated by comparing the $L = 10$ curve with our functional form, we generate almost precisely the correct form for $W(t)$ at $L = 50$, including the appropriate narrowing of the peak on the short-time side.

11.2.5 Comparison with Experiments

Comparison with experiment brings in additional uncertainties. To identify a few, (1) Experimenters typically report a quantity different from $W(t)$, (2) Experimental results include the effects of experimental error, and (3) Experiments cannot turn off the effects of molecular diffusion, though they may be small enough to be negligible. Experimentalists typically measure what is called a breakthrough curve (BTC; see Sect. 3.4.2). An experiment in which solute is transported through a medium by flowing water can be performed in a column of centimeter scale radius and decimeter scale height (in other words, 10^3–10^5 pore separations). Water flow through a system is allowed to reach steady state, i.e., it is uniform in time and nominally uniform in space. Then, starting at time $t = 0$, solute is released at a steady rate into the water flux. The experimenter then measures $1 - C$ as a function of time at the bottom of the column. Note the difference between the typical experimental procedure and a delta-function (pulse) introduction of solute, for which the measured ratio of $C(t)$ at some particular x value to the proportionality constant in front of the delta function corresponds to $W(t)$. The result of the experimental procedure described is a solute flux, which steadily rises to a value of 1.

Since rate of solute release is typically constant, the functional form of the release corresponds to a Heaviside step function, and the temporal dependence of the measured C represents the indefinite integral of $W(t)$, with the BTC being $1 - \int W(t)dt$. The negative of the time derivative of the measured BTC thus corresponds to our $W(t)$. For the purpose of investigating the tail of $W(t)$, it may be preferable to compare theory with this derivative rather than to integrate the theoretical prediction and compare with the BTC. The reason is that the magnitudes of the two terms, 1 and the indefinite integral, are nearly equal. Even roundoff error in the normalization constant will impair accuracy at large t, so we chose instead to compare our expression for $W(t)$ with the negative of the time derivative of the experimental $1 - \int W(t)dt$. That comparison, however, requires choosing some continuous representation of the (discrete) experimental data, which carries some risk of its own.

Cortis and Berkowitz [34] summarize results of three "classical" experiments in solute transport: Scheidegger [148], Nielsen and Biggar [118, 119], and Jardine et al. [80]. We checked first whether our theoretical procedure is generally compatible with these experiments. First we calculate a predicted local power, $\alpha(t) = d(\log[W(t)])/d(\log[t])$ for all times subsequent to the peak. In Fig. 11.11 we see that α at first drops rapidly from zero, then it almost levels off but continues to diminish slowly. This slope can be compared with values of $\beta + 1$ (Margolin and

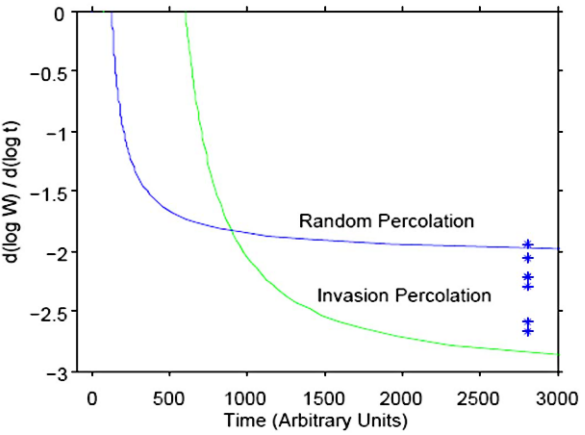

Fig. 11.11 Prediction of local slope of $\log[W(t)]$ vs. $\log[t]$ compared with experimental values for an average slope reported by Cortis and Berkowitz [34]. Predictions are for both random percolation and bond invasion percolation with trapping (relevant to an approach to the critical moisture content for percolation in unsaturated soils), for three-dimensional systems

Berkowitz [103] refer to Shlesinger [158], who showed that if the asymptotic behavior of $W(t)$ is a power law with power α, then the power β that appears in the CTRW is given by $\beta = \alpha - 1$). In Fig. 11.11 we see that the slopes of the two most distinct predictions in three dimensions, random percolation and invasion percolation (on account of the significantly different values of $D_\mathrm{b} = 1.87$ and 1.46 respectively) enclose the reported values of $\beta + 1$. We emphasize, however, that we do not yet know even if all the individual slopes that have been measured can be reproduced by any combination of system-specific parameters that would be reasonable with the appropriate choices of D_b and ν from theory, and we certainly have not tested every individual case to see whether our treatment is predictive. However, since the previous edition we have investigated the case of Jardine et al. [80], and found that our predictions do conform to their observations.

The ideal test would be to find a medium for which the pore-size distribution was known, and then to calculate the arrival time distribution without any unknown parameters. We do not have any such systems available with which to make such useful comparisons.

It is important that the arrival time distribution has a scaling time, t_0, which defines the solute transit time across a relevant pore. In general we cannot calculate this time exactly. However, we assert that it should scale with saturation inversely to the unsaturated value of the hydraulic conductivity, $K(\theta)$. Interestingly, $K(\theta)$ is much more sensitive to the actual saturation value than is the functional form of $W(t)$.

Three soil experiments by Jardine et al. [80] were used to evaluate how the predicted arrival time distribution compares with the experimental measurements. Unfortunately the water retention curve is not available for these datasets. By fitting our model to the numerically calculated arrival time distribution obtained from experiments for the saturated case ($h = 0$ cm), in which $D_b = 1.87$ and $\theta = 0.549$ (Fig. 11.12), we fitted our parameters and found $D = 2.966$, $\theta_\mathrm{t} = 0.15$ and $\beta = 0.8$. As predicted, $D_\mathrm{b} = 1.87$ describes the saturated case very well. We then used these same D, θ_t and β values to predict the arrival time distribution for unsaturated cases ($h = 10$ and 15 cm), changed the value of D_b to 1.46 (from random to invasion per-

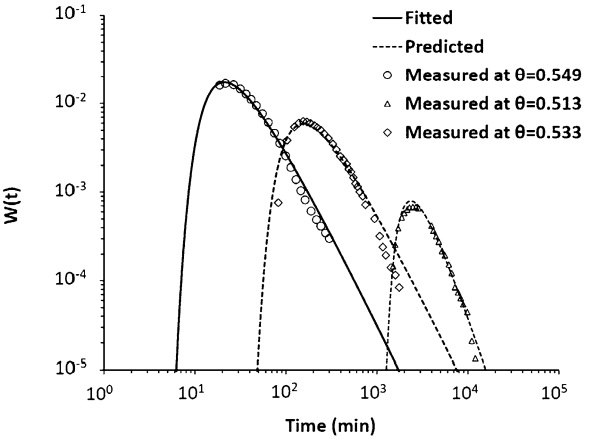

Fig. 11.12 Comparison of the predictions of the saturation dependence of the arrival time distribution with experiments of Jardine et al. [80]. We fitted the first result under saturated conditions ($\theta = 0.549$), but those fit parameters also generated good arrival time distribution shapes at higher tensions, as well as the dependence of the fundamental time scale on saturation (to within typically 8 %)

colation), consistent with the usual experimental practice of producing unsaturated media along drying curves. The results (Fig. 11.12) indicate that $D_b = 1.46$ is an excellent choice for tension $h = 15$ cm (at saturation $S = 0.93$). But the intermediate case at 10 cm tension ($S = 0.97$) is not well described by $D_b = 1.46$; rather, we found that $D_b = 1.87$, the appropriate value for saturated conditions, predicted the arrival time distribution more accurately (Fig. 11.12). Although the experimental arrival time distribution curve actually appears to conform to the random percolation prediction for intermediate time scales, the prediction was not accurate at large time scales, where a smaller value of D_b would have worked better. Thus, at 97 % of saturation, the experimental results still more closely resemble random percolation, except over very long length and time scales, and it is only at saturation as low as 93 % that invasion percolation is clearly a superior choice.

We also found that the typical pore-crossing time t_0 should inversely scale with hydraulic conductivity, $t_0 \propto K^{-1}$, in which K is [52]:

$$K(\theta) = \begin{cases} K_S\left[\frac{\beta-\phi+\theta-\theta_t}{\beta-\theta_t}\right]^{D/(3-D)} & \theta_x \le \theta < \phi \\ K_S\left[\frac{\beta-\phi+\theta-\theta_t}{\beta-\theta_t}\right]^{D/(3-D)}\left(\frac{\theta-\theta_t}{\theta_x-\theta_t}\right)^2 & \theta_t \le \theta < \theta_x \end{cases} \tag{11.28}$$

where K_S is the saturated hydraulic conductivity, and θ_x is the cross-over point on the hydraulic conductivity curve which distinguishes percolation scaling from fractal scaling [51]. Note that Eq. (11.28), in the case that $\beta = \phi$, generates the known form of non-universal scaling of the hydraulic conductivity derived by Balberg [8]. Although this initial analysis does not imply $\beta = \phi$, a second comparison below does.

The time values at the peak of the arrival time distribution (t_p) for $h = 0$, 10, and 15 cm are about 20, 200, and 3000 min, respectively (Fig. 11.12). Therefore, the ratios $t_p(h = 10)/t_p(h = 0)$, $t_p(h = 15)/t_p(h = 10)$, and $t_p(h = 15)/t_p(h = 0)$ would be 10, 15, and 150, respectively. The corresponding ratios, $K(\theta = 0.549)/K(\theta = 0.533) = 8.8$, $K(\theta = 0.533)/K(\theta = 0.513) = 16.4$, and $K(\theta = 0.549)/K(\theta = 0.513) = 144.1$, were calculated using Eq. (11.28) with $D = 2.966$, $\theta_t = 0.15$ and

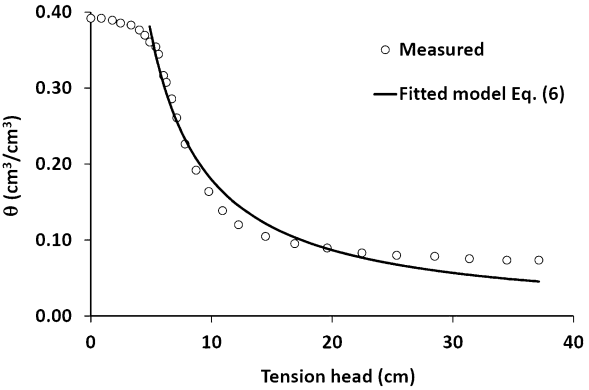

Fig. 11.13 Data from Cherrey et al. [30] for the water retention curve and extraction of the "best fit" set of WRC parameters using the PSF model

$\beta = 0.8$. Accordingly, the discrepancies in the values of t_0 were 12 %, 10 %, and 3 %, respectively. Thus, the same set of system-specific parameters yields both the appropriate shapes of the arrival time distribution, and the scaling of the most likely arrival time, as functions of saturation.

In a second test, we used 6 Hanford sediment experiments measured by Cherrey et al. [30] at different saturations: $\theta = 0.4$ (saturation), 0.237, 0.204, 0.172, 0.139 and 0.126. The measured water retention curve (Fig. 11.13) indicates that the critical water content for percolation θ_t is about 0.074. Fitting the WRC for the generalized PSF model to the measured data yielded $D = 1.95$, $\beta = 0.4$ and $h_{\min} = 4.75$ cm. We used these system-specific parameters to calculate results for $W(t)$, and compared with the experiment (Fig. 11.14). We emphasize that for the case $\beta = \phi$, the generalized PSF model is consistent with non-universal scaling of the hydraulic conductivity. In our comparison with experiment (Fig. 11.14), we used the fundamental time scale, t_0 as a single adjustable parameter, but when we compared the fitted values of t_0 over several orders of magnitude of variability with the predicted scaling of $K(\theta)$, we found the deviations from prediction to be typically only 20 %. Thus we predicted the shape of the distribution very well, and were even able to predict the dependence of the time scale on saturation reasonably well, both within the same framework and without using adjustable parameters. The framing of the problem within critical path analysis leads to a non-universal scaling of $K(\theta)$, even though the dispersion is dominated by quasi-universal exponents of percolation theory. This contrasts with a recent publication of Sahimi [144], where it was argued that non-universality of conduction exponents should produce non-universal behavior in the dispersion as well. We concede that this question is as yet unresolved, though it appears that so far the experimental data favor our theoretical framework.

Although we predict the dependence of the arrival time distribution on saturation very well for the unsaturated medium in this series of experiments, the predicted arrival time distribution for complete saturation, which was narrower than at unsaturated conditions, did not match our predictions at all when we used the exponents from 3D random percolation (Fig. 11.15). Given that the particle size distribution was rather coarse, however, which is known to be a contributing cause for wall flow,

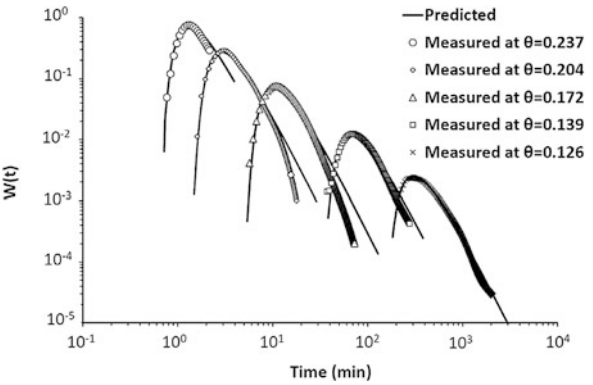

Fig. 11.14 Prediction of the corresponding arrival time distributions as functions of saturation for the medium parameters extracted from Fig. 11.13. One single adjustable parameter, the absolute time scale was used in the comparison, but our result for the saturation dependence of the hydraulic conductivity was able to predict the variation of t_0 over 3 orders of magnitude within a factor 2

we decided to investigate the possibility that the dispersion experiment performed under ostensibly saturated conditions could be influenced by this phenomenon.

The problem in wall flow is that the boundary of the core wall and the medium may be distorted by the presence of many coarse particles, producing a region of higher porosity and, at least near saturation, preferential flow. Given such large pores on the boundary, it may be difficult to maintain the medium at saturation. But because these large pores contribute only a small fraction of the total porosity, they may drain even if the medium as a whole is at, say, 99 % saturation—which is quite difficult to distinguish from 100 % saturation. Since the boundary might thus be unsaturated and its configuration is two-dimensional, but its flow rate nevertheless the fastest, 2D invasion bond percolation with trapping could be the best description. This combination of exponents produced a much closer correspondence with

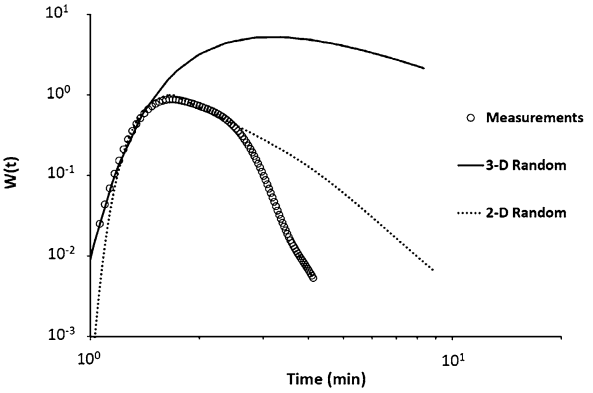

Fig. 11.15 Prediction of the arrival time distribution for the medium of Cherrey et al. [30] when the medium was considered to be fully saturated. In this case it was possible to come close to the actual arrival time distribution only when using percolation exponents appropriate for two-dimensional invasion percolation, suggesting that the experiments were inadvertently conducted under conditions of partially saturated wall flow

experiment (Fig. 11.15), except at large times, where we still overestimate arrival times.

In conclusion, we find that arrival time distributions under saturated conditions should normally have longer tails than during conditions of drying, on account of the more tortuous paths associated with the larger fractal dimensionality of the backbone for random percolation, 1.87, than for invasion bond percolation with trapping, 1.46. However, if preferential flow along the wall can occur, then the wall flow may dominate the arrival time distribution at or near saturation. In such a case a two-dimensional value for D_b should be chosen; for saturated conditions this would be 1.6432, which is still larger than 1.46. However, it is possible that, owing to the much larger pores along the wall, wall flow could dominate even under conditions that make the flow along the walls unsaturated. If the total porosity along the wall is small enough (say 5 %), this part of the medium could be 80 % saturated even though the medium as a whole is 99 % saturated, which would be difficult to distinguish from full saturation. In such cases the appropriate fractal dimensionality to use at ostensibly fully saturated conditions would be two-dimensional invasion percolation, 1.22. The smaller backbone fractal dimension for 2D invasion percolation will produce a much narrower distribution of arrival times for saturated conditions. Further, the relationship between saturated and unsaturated values of the hydraulic conductivity would be complicated, because different pore size distributions as well as different critical volume fractions for percolation would apply. The hydraulic conductivity is much more sensitive to small variations in the characterization of the medium than is the dispersion.

11.3 Spatial Distribution at an Instant in Time and Its Moments

Calculating the spatial distribution, $W(x)$, of solutes at a given time (the "resident concentration" in hydrology terms) is clearly related to calculating the distribution of arrival times at a given point in space (the "flux concentration"). However, we cannot simply integrate over all g holding x constant, since each g value is associated with its own particular velocity, and only one value of g produces a given value of x. On account of the logarithmic dependence of $W(g, x)$, it is not possible to use simple relationships between spatial and temporal scales, as is implied in the publication by Margolin and Berkowitz [103] and the references cited therein.

Consider again the statistics, $W(g, x)$, of clusters of size at least x dominated by minimum conductances g. $W(g, x)$ represents once again the probability that an arbitrary particle will initiate its motion on such a cluster and can also travel at least x on that cluster. If the solute is on a cluster described by $W(g, x)$, then its distance of travel, x, and mean velocity, $\langle u \rangle$, will be related by $x = \langle u \rangle t$, where t is the time since the solute was initially introduced, and $\langle u \rangle$ is dependent on scale, x, as well as on g. For consistency we require this distance x to be identical to x in $W(g, x)$. The pore size dependence of the mean velocity is independent of the distance of

travel, and can be roughly estimated using the framework already introduced above as being inversely proportional to $t(g)$ (in particular as $t_0/t(g)$). Now, $x \propto t^{1/D_b}$, so that $\langle u \rangle = x/t \propto t^{(1/D_b - 1)} \propto x^{1-D_b}$. Using these inputs we find that,

$$\langle u \rangle \propto u_0 \left(\frac{t_0}{t_g}\right)\left(\frac{L}{x}\right)^{D_b - 1} \tag{11.29}$$

where u_0 is a pore scale velocity. Then one can write for the distance traveled,

$$x = \langle u \rangle t = t\left(\frac{L}{t_g}\right)\left(\frac{L}{x}\right)^{D_b - 1} \tag{11.30}$$

where $L \approx u_0 t_0$. Solution of this equation for x/L_0 gives

$$x = L\left(\frac{t}{t_g}\right)^{\frac{1}{D_b}} \tag{11.31}$$

Note that Eq. (11.31) could have been obtained more easily by solving Eq. (11.23) for x, but now we also have an expression (Eq. (11.29)) for solute velocity. The probability that the particle has actually gone this distance x (at time t) is then given by the probability distribution $W(g, x)$ given in Eq. (11.16) and Eq. (11.17), but with the value of $x(t)$ inserted from Eq. (11.31). Then the logarithmic approximation of $W(g, x)$ (Eq. (11.18)) becomes

$$W(g) \propto \ln\left[\left(\frac{L}{l + L\left[\frac{t}{t_g}\right]^{\frac{1}{D_b}}}\right)^{\frac{1}{\nu}} \frac{1}{|1 - \left(\frac{g}{g_c}\right)^{\frac{1-D}{3}}|}\right] \tag{11.32}$$

With $W(g)$ now in a form which expressed both factors in terms of the same g value, we can make a direct translation between $W(g)$ and $W(x)$, similarly to Eq. (11.19):

$$W(x) = \left(\frac{W(g, x(t, g))}{dx/dg}\right) \tag{11.33}$$

where dx/dg is obtained from Eq. (11.27) in terms of dt_g/dg from Eq. (11.23), and where the final step involves solving for g in terms of x and t using Eqs. (11.26a)–(11.26b). Thus the results will include the value of the time as a parameter, just as Eq. (11.19) included the value of the spatial coordinate x as a parameter. Using Eq. (11.29) it is possible to calculate the second moment of the spatial solute distribution $\sigma^2(x)$, with time as a parameter, and the dispersivity α_L as the ratio $\sigma^2(x(t))/tu(t)$. In practice we have simply calculated the dispersivity as $(\langle x^2 \rangle - \langle x \rangle^2)/\langle x \rangle$, where all individual quantities are directly determined from the spatial distribution, although in Sect. 11.8 we show graphically what effect such an approximation has on the dispersivity.

11.4 Comparison of Dispersivity Values with Experiments

First we consider how the dispersion depends on disorder. Our prediction is that the dispersivity first increases with increasing disorder of the medium (or heterogene-

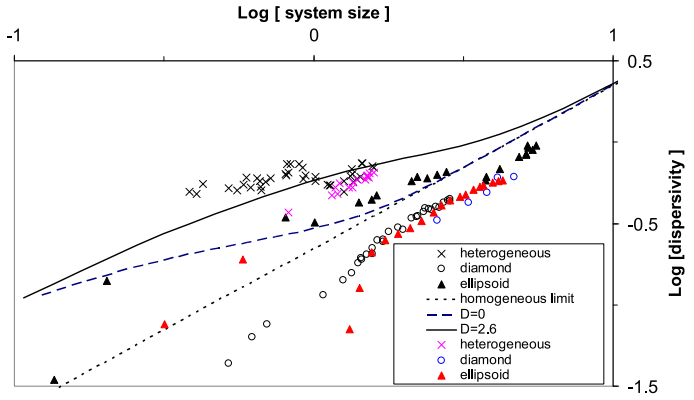

Fig. 11.16 Dispersivity of both relatively homogeneous and "heterogeneous" micromodels as a function of system length. Note that the "diamond" and "ellipsoid" descriptions correspond to nearly homogeneous media, while their dispersivity functions appear roughly compatible with the homogeneous limit from predictions, but the "heterogeneous" medium produces a dispersivity compatible with a much larger fractal dimensionality of the pore space ($D = 2.6$), and thus a relatively wide range of pore sizes

ity), but later diminishes. The increase is only about a half an order of magnitude. We were originally unaware of this non-monotonic behavior [73, 74]. However, it is typically considered that the dispersivity, at least for relatively small flow heterogeneity, is an increasing function of heterogeneity. Under these conditions we cannot make a definitive statement regarding the deviation between our prediction (Hunt et al.'s [76] Fig. 7) and the results from Aggelopoulos and Tsakiroglou [1], for which the dispersivity rises monotonically with increasing heterogeneity, albeit more slowly with continued increase in heterogeneity. Their results are from three different experiments at different scales, so perhaps they should be compared with three different theoretical curves, each with different model characteristics, and each exhibiting a peak at a different value of the conductivity contrast?

We also consider two specific cases [12, 38], for each of which the dispersivity is given for two different magnitudes of heterogeneity. We show that our predictions of the scale dependence of the dispersivity were verified at least approximately in each case (Figs. 11.16 and 11.17). In Fig. 11.16, from micromodel experiments, the homogeneous media are described as "diamond" or ellipsoid. Although we predict the general trends quite well, in order to achieve the agreement seen it was necessary to choose a value of the RS fractal dimensionality D somewhat different than the value we estimated from medium characteristics. The same held true for the experiments in Fig. 11.17, where "channeled" refers to the more disordered medium.

Considerable attention has been paid to the spatial dependence of the dispersivity. It has long been known that measured values of α_L tend to be proportional to the system size. For small distances relative to L the behavior of the dispersivity as a function of length scale is quite non-universal (Fig. 11.18), but its behavior approaches universality with increasing length scale. This universal behavior is consis-

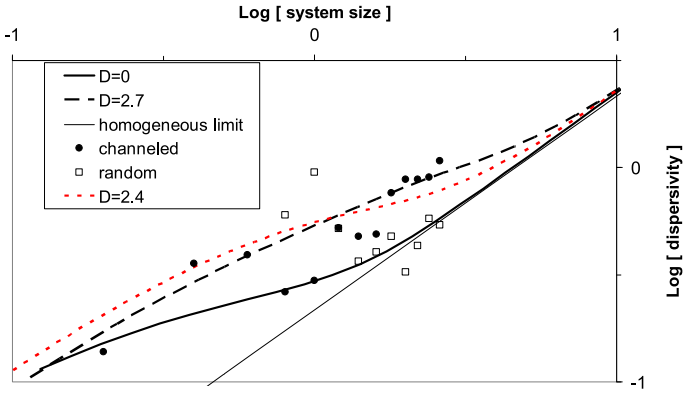

Fig. 11.17 Similar to Fig. 11.16, except that in this case the data are taken at greater length scales and the "channeled" system is macroscopically heterogeneous. Note that the value of the fractal dimensionality predicted from pore space information (2.4) is somewhat smaller than an optimal fit ($D = 2.7$), though still easily distinguished from the more nearly homogeneous system of $D = 0$, which fits the data for the randomized system rather well except for two points

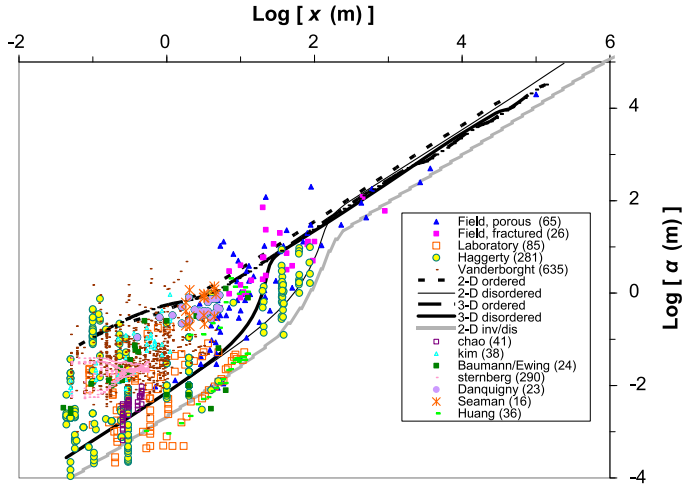

Fig. 11.18 Compilation of approximately 1500 dispersivity measurements from the given sources, compared with the envelope of predicted dispersivity values

tent with a slope slightly larger than 1 (Table 11.2), a result also obtained by Sahimi and Imdakm [145].

The universal behavior derived (see Figs. 11.19, 11.20 and 11.21) is also nearly identical to a rule of thumb ($\alpha \approx 0.1x$) noted in a review [50] of field data for the dispersivity over 20 years ago. Note that at large length scales, the invasion percolation models typically yield slightly smaller dispersivity values (not shown in

Table 11.2 Predicted exponents of dispersivity in the regime of "universal" behavior at large length scales [74]

Model	Invasion				Random			
	2d		3d		2d		3d	
	order	disorder	order	disorder	order	disorder	order	disorder
Slope	1.1	1.09	1.15	1.14	1.07	1.02	1.16	1.13

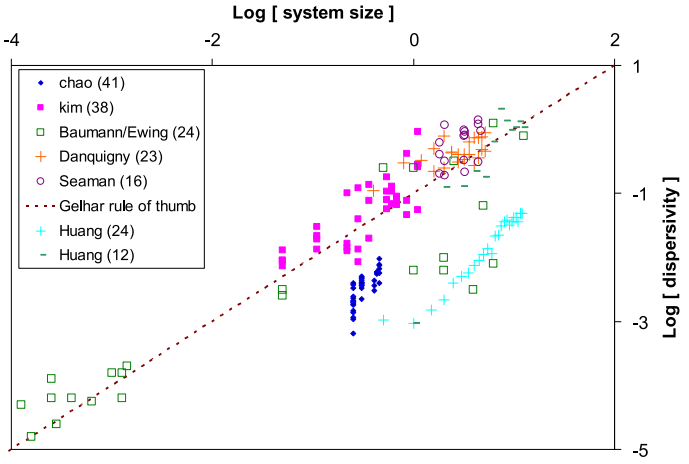

Fig. 11.19 Demonstration that individual experiments at lab (1 m) scales also contain a scale dependence of the dispersivity

detail). This pattern also holds in Fig. 11.21, where we show data over 10 orders of magnitude of length scale.

The envelope of predicted dispersivity values coincides remarkably well (Fig. 11.18). with results from over 1500 experiments [11, 29, 38, 61, 62, 79, 83, 117, 121, 155, 164, 171]. In this figure we chose the same fundamental length scale of $L = 1$ meter for all models and experiments, leading to the agreement shown. This is a point of great significance, to which we will return shortly. Points labeled "field, fractured" and "field, porous," as well as some lab measurements, were compiled by Neuman [115] and Pachepsky et al. [121]. Other references are described explicitly in the figure caption.

Some authors contend that the scale effect on the dispersivity is not seen in individual experiments, and have indeed constructed experimental configurations that do not exhibit such a scale effect (e.g., [164]). However, we point out that all of the experimental results from [164] lie within our envelope of predicted values (Fig. 11.18). Thus it becomes important to document whether the spatial scale effect on the dispersivity is also seen in individual series of experiments. Our results for 7 datasets we investigated are given in Fig. 11.19. Each is in accord with the overall trend (Table 11.3). Other individual datasets that we investigate separately also

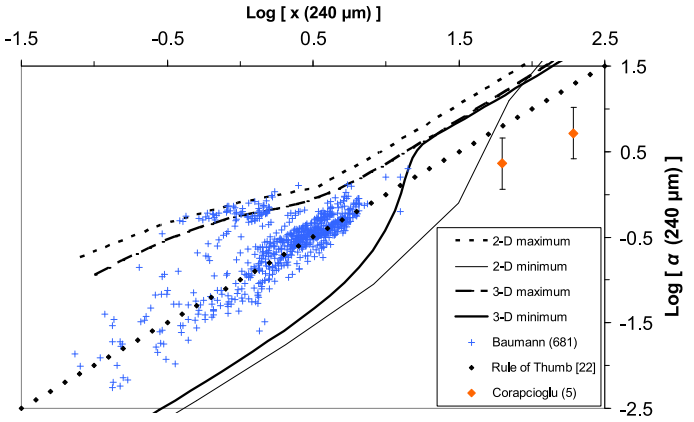

Fig. 11.20 Approximately 680 measurements of the dispersivity of various micromodels from Baumann compared with predictions of the envelope of dispersivity values predicted in percolation theory. The difference between the predictions in Fig. 11.18 and those shown here is that the fundamental length scale has been reduced from 1 m to 240 µm, consistent with the maximum experimental length scale of a few millimeters in the micromodel experiments

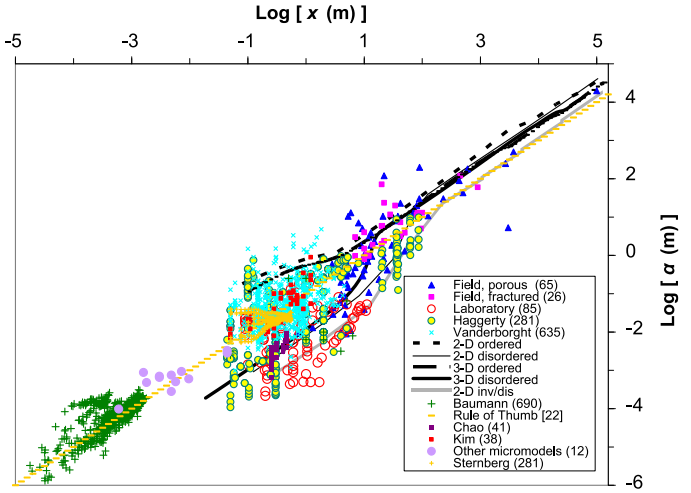

Fig. 11.21 A display of all 2200+ experimental results for the dispersivity showing their general consistency with the rule of thumb from Gelhar et al. [50] and predictions of percolation theory

show this behavior, as do most of the individual datasets compiled in [121] and the 680 experiments reported in [12]. As an additional indication, Fig. 11.19 suggests that the individual dispersivity curves all correspond to one of our predicted cases (compare Fig. 11.18).

Note that the effective slope, found by considering all the experiments in Table 11.3 as a single series, is considerably smaller than Gelhar et al.'s [50] rule of

Table 11.3 Experimental exponents for dispersivity in non-universal regime at short length scales

Data set	# Points	Approximate power	R^2
Chao et al. [29]	41	1.9	0.55
Kim et al. [83]	38	0.99	0.62
Huang et al. [79]	24	0.76	0.82
Danquigny et al. [38]	23	0.51	0.46
Seaman et al. [155]	16	0.88	0.20
Baumann et al. [11]/ Ewing[a]	24	1.5	0.95
Huang et al. [78][b]	12	2.5	0.83
Effective values	174	0.83	0.56

[a]The data from Baumann et al. [11] were combined with data from Robert Ewing that were obtained at a larger length scale

[b]The two series from Huang were distinct and could be treated separately

thumb, which gives a power of 1. But the rule of thumb does a better job of predicting the dispersivity behavior over the scale of the experiments shown, as can be seen (Fig. 11.19); it will continue to do better when more length scales are considered. Our approach does even better, as it is consistent with the tendency of experiments to generate slopes smaller than 1 when their results plot above the rule of thumb line, and slopes larger than 1 when their results plot below the rule of thumb. On the other hand, focusing on too small a range of scales (e.g., field scales; see papers by Neumann) while neglecting other scales (e.g., lab and micromodel scales) allows one to erroneously conclude that the power of the dependence of the dispersivity vs. length scale is much larger than 1. Thus our discussion appears to resolve a conflict between Schulze-Makuch [153] and Neuman [116].

As a further check we can compare our predictions to measured dispersion from micromodels (Fig. 11.20). Baumann et al. [11] conducted 680 experiments over scales of a few microns to about 1500 microns, with the effective pore separation about 1 μm. In Corapcioglou et al. [33], the pore separation was about a millimeter and experiments were conducted at 6 different length scales; unfortunately we could glean with relative certainty only two dispersivity values from their text.

In order to validate our predictions we used a range of D values nearly the same (but slightly smaller, stopping at 2.95 instead of 2.97) as for lab and field scales, as well as the same value of the critical volume fraction for percolation. Since the largest system size in Baumann et al. [11] was on the order of millimeters, one would not expect that a correlation length of 1 m would still be relevant! Changing the micromodel correlation length to 240 μm allows our envelope of predicted dispersivity values to match experiment (Fig. 11.20) quite well: 99.5 % of the micromodel values lie within our predicted bounds. Obviously, the correlation length for data of Corapcioglou et al. [33] should be much larger than for those of Baumann et al. [11], since their glass bead diameters were approximately 1 mm, almost a factor 1000 greater than the fundamental structure in Baumann et al. [11]. If the two data points from Corapcioglou et al. [33] are omitted (because their dispersivity

should not be approaching universal behavior), then our predicted range of values contains nearly 99.8 % of experimental values.

With the change of scale just mentioned, we can combine all the data together in a single figure (Fig. 11.21, which includes a few additional data points such as from Huang et al. [78]). Without the change of scale it would appear that the single choice of length scale would suffice to explain experiments conducted over 10 orders of magnitude of length scales, although the predicted variability at small length scales would be larger than observed. But a change of length scales is necessary, while the different values at the greatly different length scales are at least in accord with what theory predicts. One finds that the asymptotic result from percolation theory—that the dispersivity is roughly linear with length scale—is still consistent with both experiment and Gelhar et al.'s [50] rule of thumb.

11.5 Typical System Crossing Times and the Scaling of Solute Velocities

In the following discussion the mean solute velocity plays an important role. In principle, the tails of the derived arrival time distributions may be so long that a mean arrival time does not exist. But we have defined the mean solute velocity, $\langle u \rangle$, in terms of the spatial moments of the distribution, which are guaranteed to exist. Thus $\langle u \rangle = \langle x \rangle / t$, where t is an input parameter. Similarly, in order to find a typical system crossing time, we have inverted the relationship $\langle x(t) \rangle$ to find how a travel time, $t(\langle x \rangle)$, scales with the distance of travel. Here we compare the latter quantity with results from experiments performed in the late 1970s. We also compare the scaling of the mean solute velocity with time or transport distance with results for the scaling of chemical reaction rates with the same variables. We use the RS model throughout, with realistic variability in the fractal dimension of the pore space. Although we find a large variability in the dispersivity at smaller time scales, there is much less variability in the scaling of the mean transport distance with time. At least at small times, before the behavior of the dispersivity approaches its universal behavior, the time t that is required for solutes to traverse a distance x is dominated by the scaling factor $(x/L)^{D_b}$. But at time scales large enough for the dispersivity to approach its universal behavior, the scaling of time and length changes, as will be seen in comparisons with experiment. In CTRW formalism (see the Appendix), if the tail of the distribution of arrival times is described by the power law $t^{-(1+\alpha)}$, then the scaling of the transit time is given by $(x/L)^{1/\alpha}$. Thus we expect, to a fairly good approximation, that $\alpha = 1/D_b$. However, the discrepancies between the two extracted values of α can be considerable.

11.5.1 Comparison with Typical System Crossing Times in Transient Photoconductivity Experiments

Studies of the transient photoconductivity of amorphous semiconductors and polymers in the 1970's revealed non-Gaussian transport. This behavior showed up both

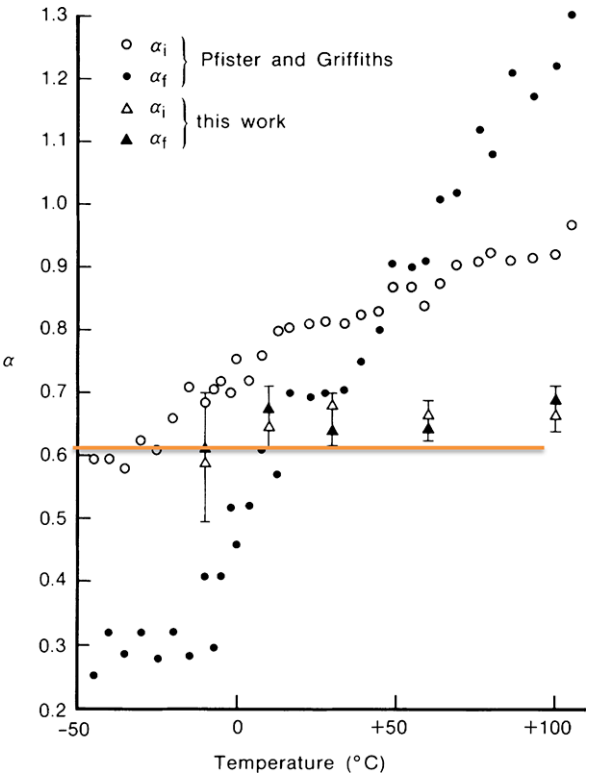

Fig. 11.22 From Bos et al. [22], referring to earlier work of Pfister and Griffiths. The former authors showed that the measurements of the exponent of the tail of the distribution of arrival times were consistent with α near 0.6, independent of temperature. We have added the predicted value of $1/D_b$ for comparison

in long-tailed power-law distributions and in non-trivial behavior of the typical system crossing time. The experiments are described in a review article in *Physics Today* [151].

Theory to explain this transport was mostly based on the continuous time random walk (CTRW), which provided a context to relate the parameters from the different experimental conditions. The *observed* transport was sometimes compatible with Gaussian statistics at high temperatures (compared to, e.g., bandgaps). But mostly it was concluded that the transport was "dispersive," or had power-law tails. In fact the claim was made [126, 128]) that the value of α as obtained from the decay of the photocurrent was a function of temperature. But a second study, on polyvinyl carbazole [128], seemed to show a strong temperature dependence of α, and reported different short time and long time values of α; according to theory they should have been the same. Later experiments [22] on the same material contradicted both aspects of the Pfister and Griffiths study (here shown in Fig. 11.22). Thus the "final" value of α, initially reported as about 0.25 in the low temperature limit, was not confirmed by the later experiments ("this work" in Fig. 11.22), in which both early and late measurements returned about the same value of α, and in which this value was approximately temperature-independent. Our predicted value of approximately $1/D_b = 1/1.64 = 0.61$, shown as a horizontal line, appears to be in accord with the

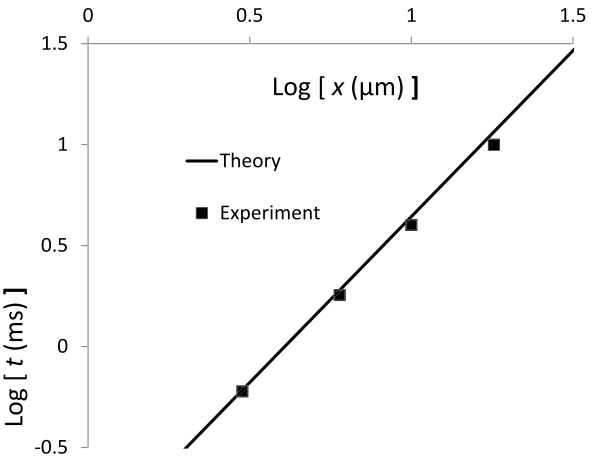

Fig. 11.23 Comparison of the length dependence of the typical arrival time for polyvinyl chloride from Bos et al. [22] with theoretical prediction. The theoretical curve simply scaled t as distance to a power equal to the fractal dimensionality of the backbone

later experimental results from Bos et al. [22]. The later work also reported that 78 room temperature measurements of α returned early-time values of 0.61 ± 0.08.

Note that one can also check directly (Fig. 11.23) to see whether the data from Bos et al. [22] for the time-length scaling agree with theory, which implies that $t \approx x^{1/\alpha} = x^{D_b} = x^{1.64}$. We digitized their Fig. 7, and chose the value of D_b for two-dimensional random percolation. Specifically, we used $t = 0.1x^{1.6432}$, where the numerical constant 0.1 is an adjustable parameter, and found good agreement.

Overall, values of α that were reported tended to cluster around 0.6 and 0.5. These values are slightly confusing when considered directly, but it is interesting that they are almost identical to the scaling exponents reported for silicate weathering rates discussed below (Sect. 11.6). When, instead, we collected the values of exponents that describe the scaling of system transit time with system length at low temperatures, the results were striking (Table 11.4).

In polymer systems (shown in bold) the observed power tends to be near $1.64 = D_b$ for 2D random percolation, while in the remaining systems, the power is near $1.87 = D_b$ for 3D random percolation. For polymers, the hopping conduction is perpendicular to the chains, and is thus restricted to two dimensions, so we should expect values near 1.64. But in amorphous selenium or silicon, we should expect the hopping transport to be fully 3D, giving values near 1.87.

The variability in the power of $t(x)$ that is observed is considerable, however, and needs to be addressed. We suspect that it is due to finite-size and variable disorder, which may confound predictions from ideal scaling arguments. But it might instead be due to the relevance of non-universal exponents of conduction [144], or to variability in D_b. Such variability can arise from e.g., long-range correlations [85]. Since we generated, in the same theoretical framework for which the hydraulic conductivity followed non-universal exponents from percolation theory, the saturation dependence of both t_0 and the full $W(t)$, and since we relate this distribution to the universal exponents of percolation theory, our research does not appear to support the relevance of non-universal exponents of conduction to dispersion. Our perspective here is that variability in time-length scaling is a product of the variable

Table 11.4 Time-length scaling exponents in dispersive transport

Power (lowest temperatures)	Reference	Material
1.64	Bos et al. [22]	Polyvinyl carbazole (78 room temperature measurements)
1.67	Pfister and Griffiths [128]	Carbazole polymers
1.67	Bos et al. [22]	Polyvinyl carbazole
1.81 (next-lowest temperature)	Pfister [126]	a-Se
1.96 (lowest temperature)	Pfister [126]	a-Se
1.82	Pfister and Scher [127]	Not given
2.0	Tiedje [167]	a-Si:H
2.2	Pfister [126] (as given in Scher and Montroll [150])	As_2Se_3

effects of disorder in systems small enough that the region of universal behavior is not reached, and we show next that this variability is exactly what is seen in experiments.

We now show graphically that travel time typically scales with length according to a power equal to, or a little larger than, D_b, depending on the width of the distribution of permeability values. We give a range of values because the dependence of the power on disorder is not monotonic; it contains a maximum, but it does not drop below D_b. The predicted variability in the scaling exponent is 5 % in two dimensions, with values ranging from 1.64 to 1.72, but 21 % in three dimensions, with values from 1.87 to 2.26 (Fig. 11.24). The range of these values could be increased somewhat if a wider range of system lengths were considered, but the scaling also gradually deviates from a power law (Fig. 11.25). The length at which this deviation occurs corresponds to the length scale in groundwater flow where the observed dispersivities trend rapidly upward toward a universal value, many orders of magnitude longer than the smallest relevant system sizes. The observed variability is 2 % in two dimensions, but 21 % in three dimensions. Thus our predictions account for the widely differing ranges of exponents observed in two and three dimensions.

We comment here that there is no reason why percolation concepts cannot be applied to problems of transport in amorphous semiconductors and polymers. In fact, as noted earlier in this book, this is where the applications were first made. However, there is a good reason why the applications described here were not originally attempted for transient photocurrents; in our work we have always defined a medium with local conductance distributions. But in non-equilibrium problems such as the description of the transient photocurrent, the site occupation probabilities by electrons evolve over time as the energy available to the hopping electrons diminishes. With non-equilibrium values of occupation probabilities that are changing in time, it is not strictly valid to define a random impedance network, since the resistance

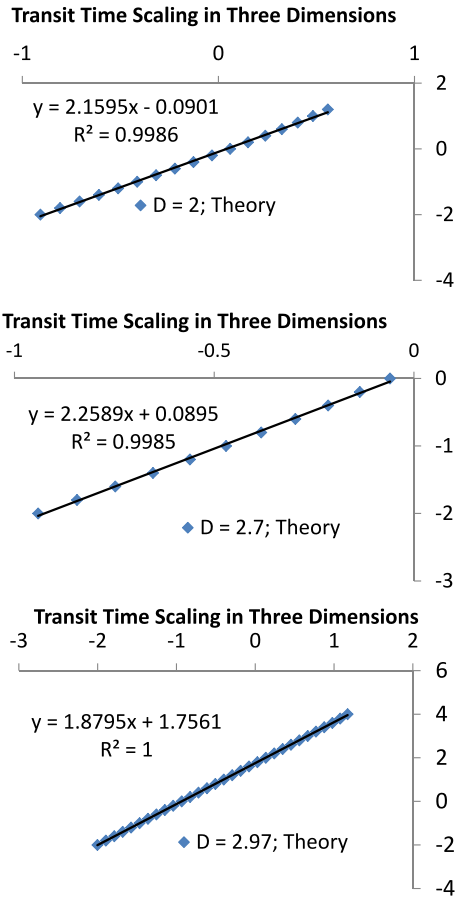

Fig. 11.24 Predicted variation in the scaling of t with x for several values of the pore-space distribution function

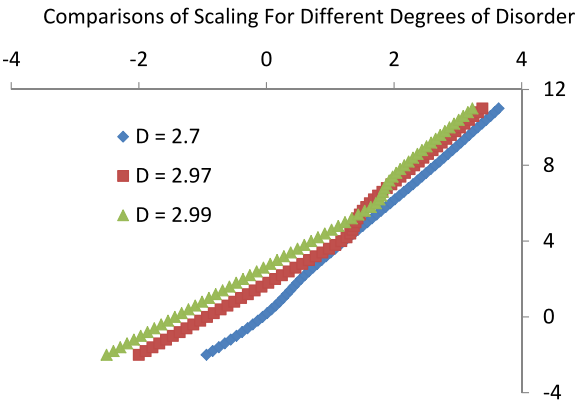

Fig. 11.25 Demonstration that the scaling of the typical arrival time with system length given by a simple power law is only valid over a certain range of system lengths

values would change with the movement of the electrons. Further, until the work of Lee et al. [93] (motivated by petroleum research), relating the scaling of the time exponent to the fractal dimensionality of the backbone, there was little chance to draw the conclusion regarding the relevance of percolation. Thus it can be seen that the field of solid-state physics benefits by the application of percolation concepts to conservative groundwater transport problems, as it was in that context that an explicit and detailed representation for the distribution of arrival times was developed. So it is a logical further step to test whether the results derived for near-equilibrium processes also fit with experiments on systems far from equilibrium, whether of transient photocurrents, or for reactive solute transport. We find that they do in both cases.

11.5.2 Comparison with the Scaling of Chemical Reaction Rates

Data for the scaling of chemical reaction rates with time and space are considered here. These reactions include experimental investigations of uranium dissolution in Hanford sediments, as well as the weathering of silicate minerals *in situ*. Uranium is an example of a groundwater constituent with significant potential implications for human health. The broader importance of understanding silicate weathering may be much greater:

> Slow dissolution of minerals on land and formation of biogenic calcite in the oceans also maintains atmospheric CO_2 concentrations and therefore plays an important role in maintaining global temperatures at levels optimal for the presence of liquid water [18]. In Earth's past, major changes in rock weathering have coincided with periods of mass extinction [2, 157] and reorganization of global biogeochemical cycles [100, 133, 170]

Moreover, the weathering of silicate minerals controls rates of soil formation and surface denudation on the earth's surface [4, 41]. For example, it is known that physical denudation rates are typically proportional to chemical weathering rates [41]. With the additional hypotheses that the predicted transport distance is essentially an equilibration distance, and that this distance can be identified as a weathering depth (e.g., [95]), we can also generate typical landscape denudation rates, and the approximate time scale over which a complete geomorphic reworking of the earth's surface occurs is believed to occur [4].

Weathering reactions take place primarily along phase interfaces in porous media. Such processes are quite complex, requiring, in principle, simultaneous treatment of the chemical equilibration of multiple chemical species, diffusive and advective transport of reagents and reaction products, and changes in the nature of the surface. In view of the complexity of the problem, most approaches simplify some inputs and focus on others [24, 40, 94, 132]. Our approach emphasizes the role of solute transport in limiting reaction rates. Without reagents, the reactions do not occur; without removal of the weathering products, reactions quickly reach equilibrium and cease. We propose that the origin of the observed scaling behavior of the reaction rates is due to a time- (and space-) dependent solute velocity, and to solute

advection rather than diffusion. Thus, whenever chemical reactions are transport-limited, our predicted solute velocity dependence should give the scaling behavior of chemical reaction rates. In fact, this conclusion was generated using hindsight; that diffusion plays little or no role in the reaction rate scaling was not something that we could have assumed *a priori*. Rather, it is a conclusion that results from use of Occam's razor.

In a seminal paper, White and Brantley [174] showed that the scaling of reaction rates, R, in lab experiments yields a different time dependence than do field scale observations. Laboratory experiments generate $R \approx R_0(t/t_0)^{-p}$ with $p = 0.51$, but at the longer time scales extracted from field studies, $p \approx 0.7$. Over the entire 10 orders of magnitude of time scales, from hours to six million years, p is 0.63. Here R_0 is the initial reaction rate at $t = t_0$. The change in slope makes it impossible to predict long-term field reaction rates accurately from shorter term lab experiments without a reliable theory. We will see that this is exactly the behavior that our theory predicts.

The initial time dependence of R is consistent with assuming that weathering rates are diffusion-limited, an appealing assumption. This is easily seen using the relationship $x^2/t = \text{const}$, and then solving for a solute velocity dx/dt as a function of time, $u \approx t^{-0.5}$. However, diffusion control would require that the spatial scaling of the solute velocity be $u \approx x^{-1}$, whereas the observed dependence [100] is actually $R \approx x^{-0.9}$, a small but potentially important distinction. More crucially, diffusion cannot account for the change to a steeper decline of R at later times; thus other influences, such as changes in the surface are often invoked. But if advective solute transport is the limiting factor, then both the cross-over to a steeper slope and the observed dependence on length are automatically generated within our theoretical construction. In fact, percolation theoretical calculations of the solute velocities give the observed scaling of reaction rates with length scales. Finally, percolation theory appears also to generate the observed *increase* in weathering rates with the scale of the measurement.

As a first example, in Fig. 11.26 we reproduce the dependence of reaction rates on "residence time" from [100]. Maher's designations "transport controlled" and "saturation controlled" divide the graph into two regions at 1 yr, according to the theoretical curve she puts through the data points. We compare these observations with the predicted scaling of solute velocity with time. Our predicted scaling of solute velocities, based on a mean solute velocity $d\langle x\rangle/dt$, and one choice of fluid velocity and fundamental reaction rate, does not distinguish between regimes. We assumed 3D random percolation (valid for three-dimensional flow under saturated conditions) and the pore-space fractal dimensionality $D = 2.95$. The correspondence is sufficiently good (Fig. 11.26) to suggest that the distinction is not necessary.

As seen from examination of Fig. 11.26 at large time scales, the predicted mean solute velocity is a non-trivial function of solute transport distance and transport time, and is known precisely only from the numerical solutions outlined in this chapter. The result can be written

$$u(t) = \frac{L}{t_0} f\left(\frac{t}{t_0}\right) \approx u_0 \left(\frac{t}{t_0}\right)^{\frac{1-D_b}{D_b}} \tag{11.34}$$

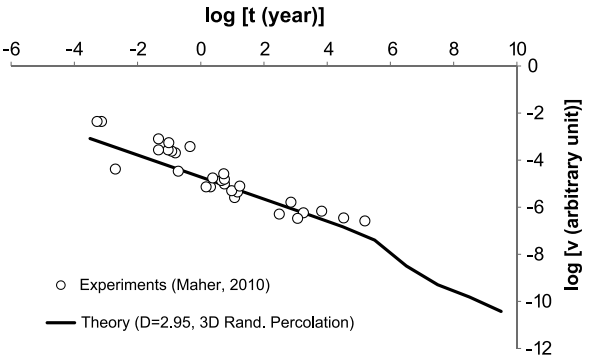

Fig. 11.26 Solute velocity as a function of time used as a proxy for the time dependence of reaction rates in porous media. This shows Maher's distinction between "Transport" and "Saturation" control is unnecessary, as the same function appears to unite both regimes

where it is the form of f that was determined numerically. The approximate equality in Eq. (11.34) is relevant at small time scales, similar to the case of the scaling of system crossing times above. Since reactions on mineral surfaces at the particle scale are the subject here, L must refer to a pore size, while t_0 refers to the time scale required for water (and thus solute) to traverse the pore. Because the upscaled solute velocity diminishes with scale, however, the equality of fluid and solute velocities holds only at the scale of a single pore, where $u_0 \equiv L/t_0$.

Writing the same relationship for the scaling of the reaction rates leads to,

$$R(t) = \frac{R_0}{u'}\frac{L}{t_0} f(t_0) \approx \frac{R_0}{u'}\frac{L}{t_0}\left(\frac{t}{t_0}\right)^{\frac{1-D_\mathrm{b}}{D_\mathrm{b}}} \tag{11.35}$$

where u' is a required scale factor. u' might be proportional to u_0, but it may instead be proportional to a different ratio of a length to time scale. If we assume that u' is proportional to u_0, the number of parameters is reduced, but it is more difficult to explain the experimentally determined [100] proportionality of R to fluid velocity, $u_0 = L/t_0$, in the transport-limited regime, which otherwise "falls out" of Eq. (11.35). The dependence of R_0 on temperature is apparently Arrhenius in form [113]. A drawback of Eq. (10.35) is that the approximate equality holds for specific ranges of time. It would obviously be advantageous to determine R_0 and the prefactor from experiments.

One can also represent the *distance* dependence for reaction rates in the following approximation, consistent with the approximate result in Eq. (11.34) for the time dependence:

$$R(x) \propto \frac{L^{D_\mathrm{b}}}{t_0 D_\mathrm{b}} x^{1-D_\mathrm{b}} \tag{11.36}$$

When Eq. (11.36) is valid (which we shall see is only at shorter length scales), reaction rates decay according to the power $1 - D_\mathrm{b} = -0.87 \approx -0.9$ (in 3D), the dependence seen by Maher [100].

Table 11.5 Comparison of scaling of solute velocities with reaction rates

Observation[a]			Theory		
Mineral	Time-scale (years)	Slope	D	Early slope	Full slope
Fresh Panola Plagioclase	6×10^0	**−0.51**	1.50	**−0.52**	*−0.61*
Plagioclase	3×10^6	*−0.566*	2.50	**−0.49**	*−0.58*
K-Feldspar	3×10^6	*−0.647*	2.90	**−0.48**	*−0.62*
Hornblende	3×10^6	*−0.623*	2.95	**−0.47**	*−0.63*
Biotite	5×10^5	*−0.603*			
Average		−0.61[b]		−0.49	−0.61

[a]Observations are taken from White and Brantley [174]

[b]The average of underlined values

Weathering Rates; Field Data

White and Brantley [174] reported that fresh surfaces of Panola plagioclase (plagioclase being a prominent mineral in continental crustal material) weathered at rates that decayed as the −0.51 power of the time. However, these same authors reported that weathering rates *in situ*, inferred over much longer periods of time (up to about 6 Myr) decayed as the −0.63 power of the time. Our transport theory applied to the RS model is consistent with a solute velocity that, at shorter time scales (up to about 5 decades of time), scales with time according to an exponent whose value lies somewhere between −0.47 and −0.51, depending on the fractal dimension of the pore space (Figs. 11.27 and 11.28). For longer time scales (some 10 decades of time) the scaling exponent changes to a value between −0.61 and −0.63, as shown in the same figures. The values of D chosen for this comparison are between $D = 1.5$ (Fig. 11.28) and $D = 2.95$ (Fig. 11.27), respectively representing quite homogeneous and rather heterogeneous media, although the predictions are little changed by this large difference in D. Thus we account for the reaction rate scaling, regardless whether the medium is homogeneous or heterogeneous. The specific experimental and theoretical exponents are given in Table 11.5. The relative consistency of the exponents across mineral types suggests a physical control, especially since the variability in the experimental values of the exponents, −0.57 to −0.65, differs little from the variability traceable to differences in the medium, −0.58 to −0.63.

The variability in slope in Table 11.5 was generated from a range of D values $1.5 \leq D \leq 2.95$, approximately the same used for the system crossing time for electron transport ($1 \leq D \leq 2.95$), and the observed range in solute dispersivity values. Therefore the same parameters of the same input functions describe the observed variability in time-length scaling in dispersive transport, dispersivity as a function of travel distance, and (as will be shown) reaction rate scaling as a function of time or space. Under conditions of typical porosity, such a range in D corresponds to a range in permeability spreads of from about an order of magnitude to upwards of 5 orders of magnitude. This variation in heterogeneity in permeability describes a

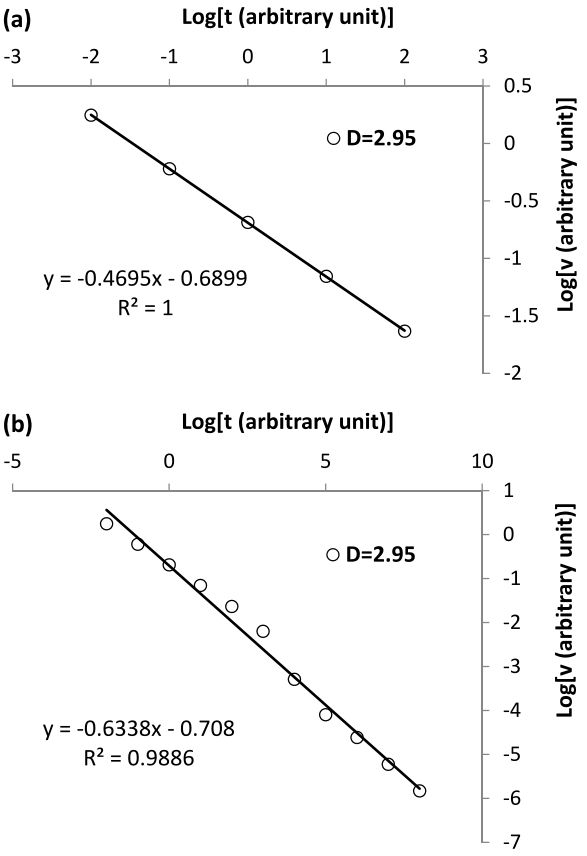

Fig. 11.27 Solute velocity as a function of time for media with a wide range of pore sizes ($D = 2.95$). (**a**) The extracted exponent for the first four orders of magnitude of time; (**b**) a steeper slope that would be consistent with nine orders of magnitude of time variation

rather wide range of natural media, so it is a reasonable choice. But in practice, we find that the results from $D = 2.95$ describe most of the individual experimental data we analyze.

Although it is interesting to extract powers from theory and compare them with experiment, it is much more interesting to compare theoretical and experimental dependences directly. This is done in the following figures. Note that while the theory can provide absolute references to the vertical scale (pore-scale reaction rate) and to the horizontal scale (pore crossing time-scale), these choices typically require more information than is available, particularly for field measurements of weathering rates. Thus in most cases we look for horizontal and vertical scale factors that produce the best fit.

To construct Fig. 11.29, we took the fundamental time unit in the calculations to be years, took the ratio of the measured R to its maximum value (approximately equal to the ratio R/R_0), and adjusted the vertical scale of the calculated u to fall on the experimental curve of the fresh Panola plagioclase, thus interpreting the vertical axis as a solute velocity (with unknown units). We will find that these units are roughly tens of microns per second. The reaction rates were obtained from White

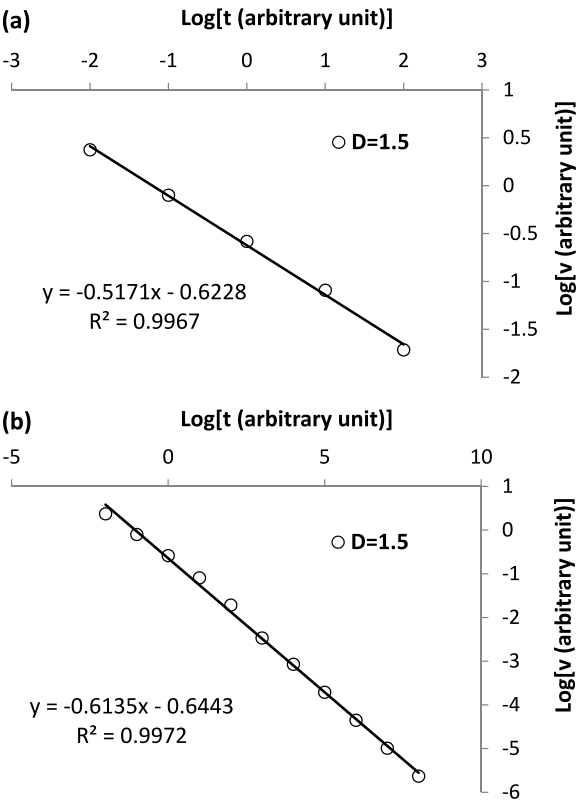

Fig. 11.28 Same as Fig. 11.27, except for a medium with a narrow range of pore sizes ($D = 1.5$)

and Brantley's [174] Tables 4–7, except for FPP (fresh Panola Plagioclase) which was digitized from their Fig. 3. White and Brantley also plotted the FPP sequence simultaneously with the field silicate weathering data, with exactly the same results as our Fig. 11.29. The basalt rind weathering data of Sak et al. [146] is plotted on the same graph. The effective weathering rates in the field over time scales of several million years are about an order of magnitude lower than a value extrapolated from the fresh Panola plagioclase experiments (FPP). It can be seen that our predictions track the trends of the data, but with our assumed range of D values ($D = 1.5$ to $D = 2.95$) we do not generate the variability. Therefore, the observed variability in reaction rates is unlikely to be a result of variability in medium physical characteristics or morphology; rather it is likely due to variability in other factors, such as R_0 and t_0. Using some results of other authors we consider this issue more closely.

Some of the scatter is undoubtedly due to the variability in fluid flow rates, since reaction rates are shown by Maher [100] (her Figs. 4 and 5) to be proportional to flow rates in the transport limited regime (as she asserts, for flow rates greater than 16 m/yr = 0.5 μ/s). At the other extreme, Molin et al. [109] assert that transport control is expected only for flow velocities less than 100 μ/s. This >2 orders of magnitude range of velocities for which reaction rates are considered to be transport limited appears to introduce a roughly two order of magnitude variability in reaction

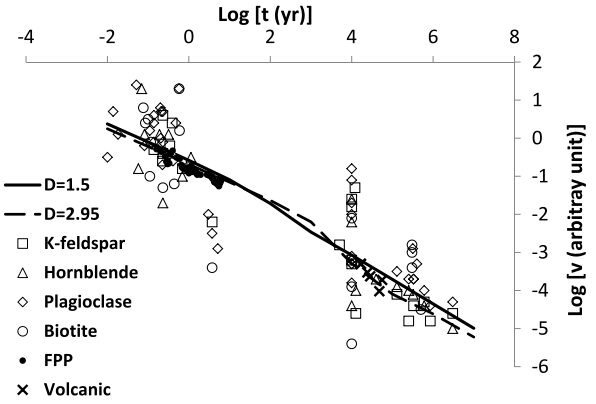

Fig. 11.29 Comparison of all the data, from both experiments (FPP = Fresh Panola Plagioclase), and field measurements of weathering reaction rates. We have again used the mean solute velocity function as a proxy for the reaction rate. Although we do not give units for the velocity, the FPP experiments are consistent with an initial solute velocity equal to the pore-scale fluid velocity, which is about 15 μm/s, meaning that the zero in the *vertical (logarithmic) scale* corresponds to a few tens of micrometers per second. The *vertical scale* for the reaction rates would be roughly normalized to the rate at the scale of a single pore given instant mixing and transport of the reagents and products. This comparison used exponents from 3D random percolation, appropriate for saturated conditions. Two values of D were chosen, corresponding to wide and narrow ranges of pore sizes

rates that is due solely to variability in flow rates. Although we do not know the field flow rates, we can calculate the flow rate (and fundamental time scale) associated with the experiments on the FPP by taking the experimental data in [174] and using that result to estimate error bars on our predictions. In the process we find that the fundamental time scale of FPP experiments is in general accord with our theoretical predictions as well.

White and Brantley [174] crushed 750 g of granite and placed it in a column 100 cm long and 2.4 cm in diameter. Using a density of granite of 2.7 g/cm^3, this gives porosity of about 0.4. At the reported volume flux of 10 ml/hr through this column, one can obtain a pore-scale velocity of about 15 μm/s by using a mass-conservation relationship between flux, area, and velocity, modified by the porosity. Given [174] that the particle sizes range from 0.25 mm to 0.85 mm, one can estimate a typical pore size as 0.3 times the typical particle size [60], about 0.15 mm. So a typical pore crossing time is about 150 μm/15 μm/s = 10 s. With a column length of 100 cm, water encounters between $1000/0.85 = 1176$ and $1000/0.25 = 4000$ particles along the length of the core, and a similar number of pores. Core solute *transit* times of between (10 s) $(1176)^{1.87} = 0.17$ yr and (10 s) $(4000)^{1.87} = 1.7$ yr would be expected, comparable to the range of time values in the experiment [174] that extended from 0.19 yr to 6.2 yr.

The pore-scale flow rate consistent with our graph (calculated above from the laboratory experiments of White and Brantley), 15 μ/s, is about a factor 30 greater than Maher's calculated minimum value; but almost an order of magnitude less than the maximum value given by Molin et al. [109]. Navarre-Sitchler and Brantley [113]

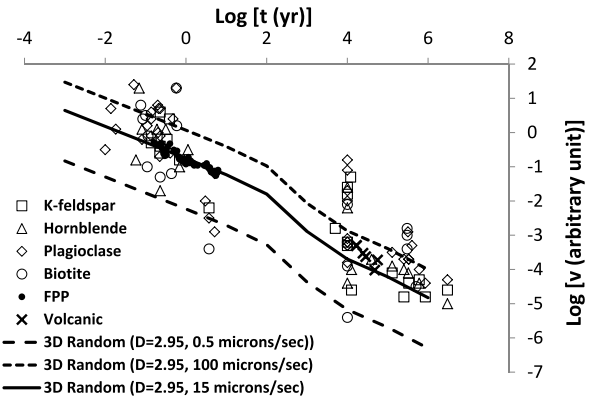

Fig. 11.30 Introduction of approximate error bars associated with the uncertainty in the pore-scale fluid velocity for the range of fluid velocities that is associated with both transport controlled reaction rates [95, 100] and a proportionality of the reaction rates to the fluid velocity, according to Maher [100]

assert that weathering rates at a given spatial scale tend to vary by no more than two orders of magnitude when the temperature variability is controlled for. Thus one *could* estimate a spread of roughly two orders of magnitude centered around the predicted curve as due to variations in velocity, and attribute the remaining uncertainty to variability in temperature. Figure 11.30 shows the uncertainty introduced by a proportionality of reaction rates to the fluid flow rate using the bounding flow rate values quoted from Maher [100] and Molin et al. [109]. However, if u' is not proportional to u_0, our Eq. (11.30) yields a rate prefactor proportional to the fluid velocity, and an additional factor of $t_0^{(1-D_b)/D_b}$. Using $D_b = 1.87$ in 3D leads to a reaction rate proportional only to about the square root of u_0, which would halve the range of R values explained by a variability in u_0, leaving up to one order of magnitude variability accounted for by neither temperature nor flow rate variations.

The data over much of White and Brantley's range show a scatter of one to two orders of magnitude, but at several points, most noticeably at about 10,000 years, scatter exceeds 4 orders of magnitude. From the discussion of Navarre-Sitchler and Brantley [113], most of the remainder of the scatter is probably due to temperature variability. Such variability in temperature would likely be accentuated at around 10 kyear associated with the rapid retreat of the northern continental ice sheets, along whose boundaries most of the measurements relevant for that time frame were made (see Tables 4–7 of White and Brantley [174]).

Despite the large scatter in the data, our theory reproduces the results obtained from the statistical analysis of the observed reactions rates. The observed scatter is approximately what one would expect from weathering rates that are mostly transport-limited. We therefore believe that our results imply that the temporal scaling of reaction rates is due to the time-dependent solute velocity as derived in the percolation theoretical construction.

For additional confirmation, in Maher's [100] Fig. 7 it is shown that observed reaction rates decline approximately as the soil thickness raised to the -0.9 power (for thicknesses of roughly 10 cm to 1 m), as one would expect from using the thickness of the soil cover as a proxy for the transport distance, x. Mean solute

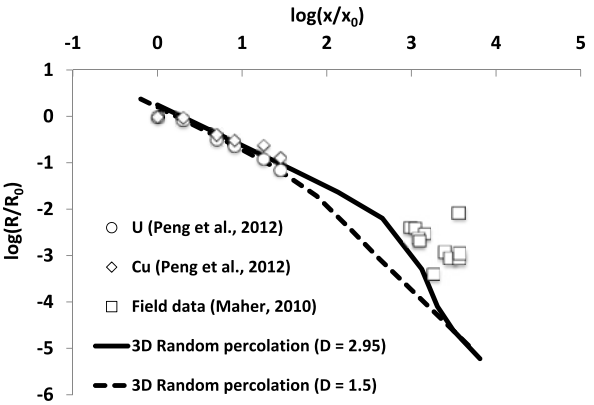

Fig. 11.31 Spatial scaling of reaction rates compared with the spatial scaling of the fluid velocity. In both experiments and field data we were able to normalize to the initial value of the reaction rate, at least approximately. However, values of x_0 for the lab and field data could not be established with certainty. Since the lab data were collected for intraparticle distances, and the field data for interparticle distances, we chose a ratio of x_0 values equal to 10^3. Had we chosen the equally plausible value 10^2, the field data points would have shifted to the left one unit, making the data continuous with the predictions

velocities are proportional to $x/t \approx x/x^{D_b}$ from Eq. (11.34), giving $u \approx x^{-0.87}$. This prediction agrees well with Maher's experimental result. Here our transport distance x corresponds to the length scale known as the weathering front advance in papers on weathering rind formation (e.g., [113, 114, 146]).

We compared data from Maher's [100] Fig. 7 with theory and found reasonable agreement. But since the range of field length scales investigated is quite small, the conclusion might be sensitive to small changes in the actual length or time scales investigated, suggesting that we should extend the range of length scales investigated to include, e.g., laboratory measurements. However, an accurate comparison of this sort requires putting both results on the same plot (Fig. 11.31), meaning that it is important to evaluate the scale constants x_0 and R_0. We normalized the soil weathering rates to the value quoted in [100], but we did not have an exact value for x_0. Then we used experimental data at laboratory (intraparticle) length scales [124]. Peng et al. [124] measured uranium and copper concentrations as functions of depth from the surface of an individual basaltic clast using laser ablation. The depths ranged from 0.6 μm to 29 μm. They reported that the copper and uranium concentrations were highly correlated, so we plotted them together. To this purpose we had to normalize both the copper and the uranium depths and rates to their initial values; those two data series are nearly indistinguishable. Since the requisite value of x_0 would refer to intraparticle flow (very short penetration depths), the same x_0 could not be appropriate for the data we digitized from [100]. Those data refer to interparticle flow through soils over distances up to a meter with pore sizes roughly a particle radius. Thus the ratio of the two length scales we need is the ratio of a particle diameter to that describing the scale of the flow variability within the particle. We used a ratio $x_0(\text{interparticle})/x_0(\text{intraparticle}) = 1\ \text{mm}/1\ \mu\text{m} = 10^3$, but

this argument is only qualitative. If we had used an order of magnitude smaller ratio of fundamental distances, the two data sequences would have followed the same curve; however, we have no reason to prefer that value over the one we did use. Note that the change at larger distances to a more negative slope of the weathering rate as a function of distance should have the tendency to limit depths of weathering within bedrock, unless physical processes are effective at removing the surface.

Now we make some comparisons of actual values of time and length scales related to our choice of axes in Figs. 11.29–11.31. Consider gravity flow (a condition also simulated by White and Brantley [174] for the Panola plagioclase weathering) with a saturated hydraulic conductivity value of 10^{-4} cm/s (the median order of magnitude for crustal materials; [4]). This combination would be consistent with a single pore flow rate of about 1 μm/s, within the fluid velocity limits suggested by Maher [100] and Molin et al. [109] as bounding the transport-limited regime.

Using our *analytical* results for the solute velocity, proportional to $t^{(1-D_b)/D_b}$, a relevant solute transport distance proportional to t^{1/D_b} (compare again with weathering front advance) of 1 μm at 1 s would translate to about 0.5 cm at 1 yr (an order of magnitude smaller than fluid and solute velocities in the fresh Panola plagioclase experiments of White and Brantley [174], to about 4 m at 100 kyr (compare Maher's [100] model results yielding 250 kyr for 2 m), and about 20 m at 1.5 million years. However, the nearly one order of magnitude decrease in effective solute velocity, shown in Fig. 11.28 as occurring at time scales between about 1 kyr and 1 Myr, would typically reduce this weathered depth to several meters at 1.5 Myr, and to about half a meter at 100 kyear. This latter value would be consistent with the Maher [100] model results, and also improve agreement with the results of Lin et al. [95], in which total solute transport distances of up to about a decimeter are associated with time scales of around 100 kyear. By the commonly observed equivalence between chemical weathering depths and physical denudation thicknesses [41], weathering rates in meters per million years lead to similar denudation rates for weathering limited conditions, as obtained through cosmogenic and other methods of dating [4]. Accordingly, for weathering rate limited conditions, grain size transport distances at 1 s can be linked to common landscape surface losses on the order of meters to tens of meters over a time scale roughly equal to the geomorphic age of the earth's surface, 5 Myr [4].

Experiments

Now consider the dependence of uranium reaction rates on time scales from various Hanford experiments. An interesting dependence of U(VI) desorption concentrations on time was obtained by Liu et al. [97]. We digitized the data from Figs. 1–2 of that work. As with the weathering rates above, we assume that the observed concentrations are proportional to the solute velocity. The time span was much shorter than the data summarized by White and Brantley [174], however, covering only

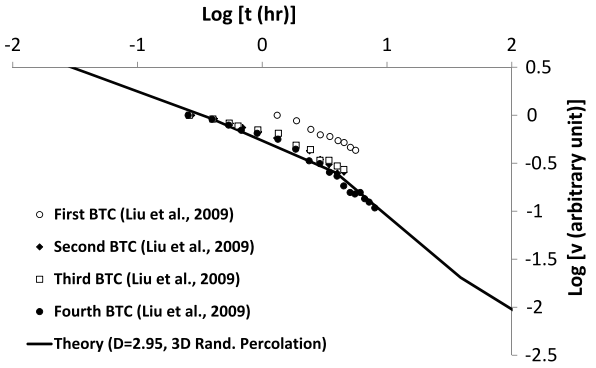

Fig. 11.32 Temporal scaling of reaction rates from the US DOE Hanford site compared with the same solute velocity function in Fig. 11.29 (3D random percolation, $D = 2.95$), but with a different value of the fundamental time scale, appropriate for much higher fluid velocities as well as higher reaction rates. The data appear to show the change of slope that can only be inferred from field data in Fig. 11.29

minutes to hours. This data sequence appears to show (Fig. 11.32) the same kind of cross-over to a steeper slope as seen in White and Brantley's [174] data. This is generally consistent with the value of the controlling rate constant, $10^{-4.29}$, taken from Table 1 of Liu et al. [97], which is five to six orders of magnitude greater than the largest lab values reported by White and Brantley [174]. Consequently, experimental conditions with much greater fluid velocities would still allow for transport-limited reaction rates. If we accordingly change the time axis scale from Fig. 11.29 by a factor of about 10^5, and plot the observed uranium concentrations as a function of time we produce Fig. 11.32. Whereas the weathering rate observations in Fig. 11.29 cover only initial and final slopes, Fig. 11.32 shows the behavior at the predicted slope cross-over. The agreement is less conclusive than we would want, given that we had to use adjustable parameters for the fundamental time and reaction rate scales—a weakness which is reduced in the comparison with the data of Du et al. [42] below. For all the uranium experiment modeling we used the RS model with $D = 2.95$.

In Figs. 11.33–11.35, we examine data from Liu et al. [97], investigating uranium desorption from very coarse sediments. In order to make use of all the breakthrough curves, we normalized the time and concentration values in each to their smallest and largest values, respectively, and plotted the data for later times. We found that the experimental data for the short column could not be fitted to 3D random percolation; the appropriate percolation exponents were those from 2D invasion percolation (Fig. 11.33). This can be understood by appeal to wall flow as the dominant flow mechanism. In very coarse Hanford sediments it is known that flow along the wall of a sediment core can dominate due to the particularly large pore spaces formed along the boundary between the sediment and the wall ([30]; see also discussion of this experiment in [54]).

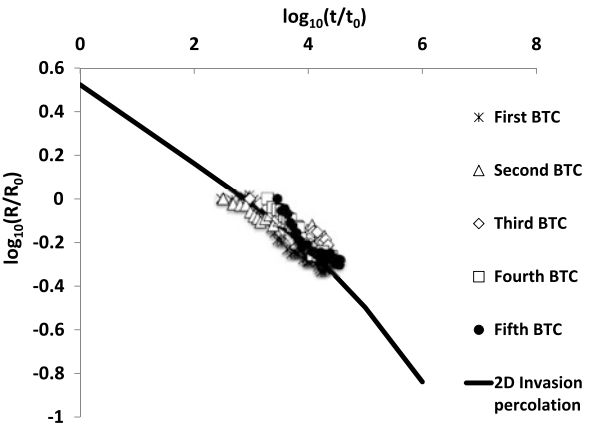

Fig. 11.33 Temporal scaling of reaction rates in a short column of coarse sediments from the US DOE Hanford site compared with 2D invasion percolation scaling ($D = 2.95$) of the solute velocity. Similarly to the experiments of the solute arrival time distribution from Cherrey, our interpretation invokes wall flow as an explanation for the relevance of 2D invasion percolation exponents

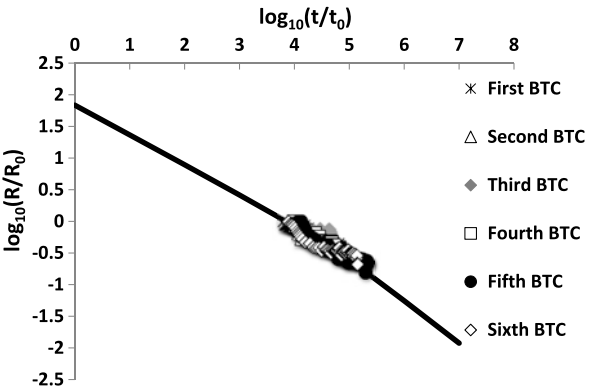

Fig. 11.34 Temporal scaling of reaction rates in a long column of coarse sediments from the US DOE Hanford site compared with 3D random percolation and $D = 2.95$. Although the sediments are the same in Fig. 11.34 as in Fig. 11.33, in this latter case the experiment was performed in a long column

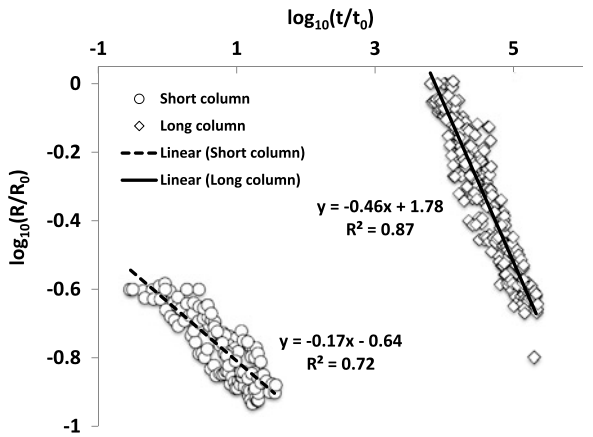

Fig. 11.35 Slopes of reaction rate scaling from the previous two plots. The extracted values, -0.46, and -0.17, compare favorably with the predicted values from Table 11.5 of -0.47 and -0.18, respectively

Table 11.6 Analytical results related to the scaling of solute transport time with distance

Percolation class	Parameter				
	D_b	$u(x)$	$u(t)$	$t(x)$	$x(t)$
2d Random	1.64	$x^{-0.64}$	$t^{-0.39}$	$x^{1.64}$	$t^{0.61}$
3d Random	1.87	$x^{-0.87}$	$t^{-0.47}$	$x^{1.87}$	$t^{0.53}$
2d Invasion	1.22	$x^{-0.22}$	$t^{-0.18}$	$x^{1.22}$	$t^{0.82}$
3d Invasion	1.46	$x^{-0.46}$	$t^{-0.32}$	$x^{1.46}$	$t^{0.68}$

Table 11.7 Calculated fluid flow and particle characteristics for Du et al. [42] experiments

Diameter, µm			Number of particles in 0.5 g	Mean distance between particles, µm	Flow time between particles, s	Column crossing time, hr
Lower bound	Upper bound	Geometric mean				
20	75	38.7	6,202,812	117	28 (3.6)	177
75	500	193.6	49,622	586	141 (73)	43.8
500	2000	1000.0	360	3028	727 (1573)	10.5
20	2000	200.0	45,044	606	145 (78)	42.3
2000	4000	2828.4	16	8563	2055 (11000)	4.2

Data from the long column, however, are consistent with the predictions from 3D random percolation (Fig. 11.34). In Fig. 11.35 we show the slopes of straight lines fitted to the data for both the short and the long column. The short column returns the slope 0.17, while the long column returns the slope 0.46, comparing nicely with the predicted values of 0.18 and 0.47, respectively (see Table 11.6). These analytical values are approximately valid for t values smaller than at the slope break. Again we used the RS model with $D = 2.95$.

Compare the value 0.47, the predicted scaling exponent for $u(t)$ in 3D random percolation (at short time scales), with the theoretical early-time slopes from numerical simulations that range between 0.47 (for large heterogeneity) to 0.52 (small heterogeneity) (Table 11.5). As usual, the details of the medium introduce some variability into the actual values of the exponents.

Next we consider data for uranium elution from Du et al. [42]. These authors report experiments on uranium dissolution, a dependence of uranium concentration that diminishes according to a power of the transport time. The data were collected from elution experiments for five different media with differing particle sizes. In Table 11.7 we use their particle sizes and calculated particle numbers to calculate mean particle separations and the flow time (neglecting effects of stirring). The experiment was performed in a stirred "flow cell" 25 mm tall with 0.5 g of particles in 10 ml of liquid—in other words it was a suspension, not a grain-supported medium. The mean distance between the particles was calculated by assuming the particles were equidistantly dispersed. The static flow time along across a particle was only 5 s for the first entry, a factor 5 smaller than the inter-particle flow time.

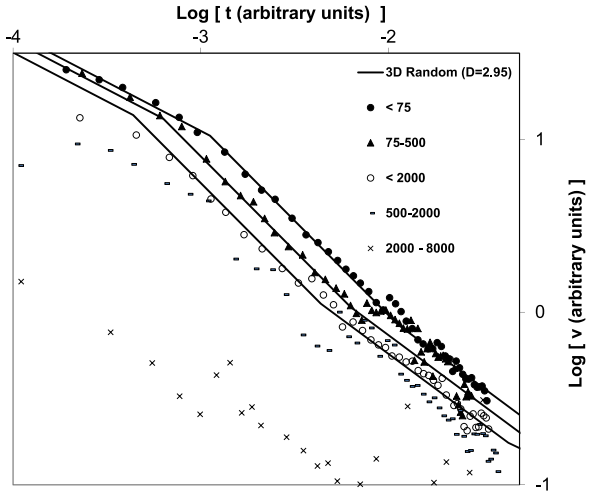

Fig. 11.36 Uranium elution data from Du et al. [42], compared with the same solute velocity function from Fig. 11.29. The elution data were taken separately for five different media with different particle sizes. The time of the first slope cross-over was adjusted to match experiment, and the *vertical scale* was chosen for best fit, but the values of the slopes in all three time ranges were fixed, and the position of the second slope cross-over was fixed by the first. Thus, four different parameters in approximate agreement with experiment were generated by the choice of two fitting parameters for each of the three curves shown. For the largest particle size class, the flow cell contained fewer than 10 particles, so the results of our statistically based theory for interparticle transport could not be applied

The data are plotted and compared with theory in Fig. 11.36. Each theory line uses the solute velocity calculated for $D = 2.95$, with 3D flow under saturated conditions (random percolation). The difference in the three predictions lies solely in the choice of the t_0 and u_0 values, which for three different curves can involve as many as six unknown parameters. Since the fluid velocity u_0 was intended to be the same in all 3 experiments, we used the same value for each, reducing the number of possible adjustable parameter values from six to four. The fundamental time scales used in our numerical calculations, were given in the sixth column of the table (in parentheses), alongside the flow time between particles estimated from the values of their separation and the fluid flow velocity. Note that in most cases, our assumed fundamental time scale is within a factor 2 of the calculated value. Calculation of the typical column traversal time for solutes is in column 7, which generates values in the tens of hours from the product of column 6 and the factor $(25\ \text{mm}/L)^{1.87}$, where L is a particle separation. These values are, with the exception of the first and last entries, near the middle of the experimental values in Fig. 11.36.

The comparison demonstrates that the general behavior of the solute transport in the three columns with smaller grain sizes is well approximated using our calculation. Adjusting two parameters was sufficient to yield three different slope values as well as two cross-over times in each case. For the largest grain sizes (2 to 8 mm) the small number of potential solute paths accentuates fluctuations and renders predic-

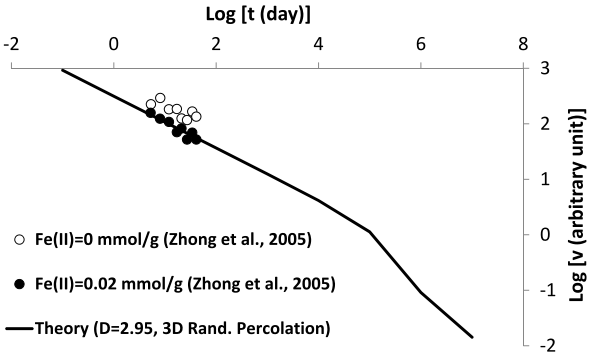

Fig. 11.37 Temporal scaling of iron mobilization for US DOE Hanford site sediments compared with the same solute velocity function as in Figs. 11.26, 11.29, 11.30, 11.31, 11.32, 11.34, and 11.36

tions based on mean solute velocities less useful. Again we used the RS model with $D = 2.95$.

Because the interparticle fluid was stirred, Du et al. [42] interpreted their scale-dependence in terms of diffusion-limited transport within the particles. This interpretation is in accord with the understanding of Noniel et al. [120], whose stirred experiments did not show evidence of transport limited behavior at larger length scales. Consequently, these authors interpreted the results in terms of intra-particle diffusion near the percolation threshold. We argue that the time dependence of the solute transport over lengths equivalent to thousands of particle separations (as in the case of the smallest particles) does not reflect the dynamics of transport within the particles, but rather, the tortuosity of the paths through the porous medium as a whole. Consider also the data for the medium composed of the largest particles. In this one case the experimental length scales do not significantly exceed the diameter of the largest particle, meaning that intraparticle processes can dominate. Here the power observed is nearly -0.5, typical of the early slope regime of our predicted solute velocity curve, but also with pure diffusion which, in the case of the largest particles, could be relevant for the (mostly) intraparticle transport. These reasons, as well as the exceptional agreement with experiment in the cases of the three media with the smallest particles, lead us to favor our interpretation.

Finally we consider the experiments of Zhong et al. [181]. These authors obtain a remobilization rate that decays as $t^{-0.53}$ ($R^2 = 0.89$) or $t^{-0.42}$ ($R^2 = 0.61$). This dependence on time could accord with either diffusion as a limiting mechanism (exponent -0.5), or with our results for transport-limited reaction rates. We compare their remobilization rate with our solute velocity predictions in Fig. 11.37 and find reasonably good agreement.

In this entire series of comparisons we have consistently used the RS model, $D = 2.95$, and 3D random percolation exponents in every case but one. (One would expect 3D random percolation most of the time, and the one case interpreted as 2D invasion percolation was for a coarse Hanford site medium, where wall flow is known to occasionally cause difficulties.) The fact that all the laboratory experiments, and all the field data, were consistent with a single theoretical result (albeit one for which the fundamental time and length scales could be adjusted) is strong

evidence of the relevance to chemical reactions of solute transport by advection. It also adds motivation for calculating the fundamental scaling constants of the results.

Note that Maher [100] ascribes significance to her analyses showing nearly the same reaction rate dependences on both time and distance, at least in what is there denoted as the transport-limited regime. If these two dependences were the same, this would imply that solute velocities were scale-independent. But if solute velocities were scale-independent, then there would be no reason for transport-limitations on reaction rates to introduce the observed scale dependence. But if our analysis is correct, we should expect different powers in these two functions, since the solute velocity is not independent of length scale, even though at small enough length scales it does reduce to the fluid velocity. In our view, analysis of the temporal (Figs. 11.28–11.30 and 11.32–11.37) and spatial (Fig. 11.31) dependences of the reaction rates shows that the two different representations of the data exhibit distinct functional dependences, in accord with our theory.

Sometimes one is interested in the dependence of reaction rates on the scale of measurement, rather than of transport. For example, Navarre-Sitchler and Brantley [113] found a power-law increase of apparent reaction rates with increasing scale of measurement, and interpreted this result in terms of a reaction front with a fractal structure. Such a fractal structure can produce a surface area that grows more rapidly with increasing scale than does a Euclidean object. But percolation theory also generates such a fractal surface, and in principle it is possible to calculate the geometry of such a reaction front within the same theoretical framework that generates the solute velocities. In particular the perimeter of a 3D percolation cluster has *two* contributions [91]: one proportional to the square of the radius, and one proportional to the volume of the cluster. The theoretical results from percolation theory apply only when the linear dimension of such a cluster is at least ten individual units, e.g. bond lengths, pore separations, or a surface roughness scale [67]. Let us define the radius of a large cluster as the correlation length, χ, from percolation theory. Such a large cluster can mark the expansion of the weathering front. The volume of a large three-dimensional percolation cluster is thus proportional to $\chi^{2.5}$ ($M \propto \chi^{d_f}$, where $d_f \approx 2.5$ is the universal mass fractal dimension of large clusters near the percolation threshold; Stauffer and Aharony [162]), meaning that the surface area, A, has two terms: one is proportional to χ^2 and the second is proportional to $\chi^{2.5}$. Thus we have

$$A \approx C\left(\chi^2 + \frac{\chi^{2.5}}{\chi_0^{0.5}}\right) \tag{11.37}$$

where χ_0 is a fundamental length scale which we discuss below.

In Fig. 3 of Navarre-Sitchler and Brantley [113], the reaction rate increases as the 0.33 power of the measurement scale. Their interpretation in terms of a fractal surface allowed extraction of a surface fractal dimension $D_s = 2.33$. Consider alternatively the percolation treatment, Eq. (11.37). Surface areas at the smallest scales are measured by N_2 BET techniques, and thus cannot distinguish length scales smaller than the molecule itself. The linear dimension of a nitrogen molecule is on the order of 10^{-7} mm; we choose χ_0 an order of magnitude larger, 10^{-6} mm. Using the adjustable parameter $C = 10^{-5.5}$, we then generate the comparison in Fig. 11.38. This

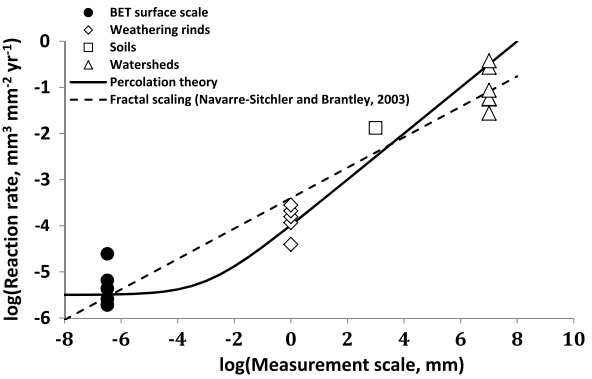

Fig. 11.38 Dependence of weathering rates on length scale, interpreted in terms of a fractal weathering front (from [114]) and interpreted in terms of the surface area of a large cluster using percolation theory. The former employs two adjustable parameters, the slope and the weathering rate prefactor, while the latter employs a single adjustable parameter, the fundamental weathering rate prefactor

figure also shows the result of Navarre-Sitchler and Brantley [113]. Although their result represents a simpler functional form, they require two adjustable parameters; one is the power, the second is the intercept. Ours requires only one, the value of C given above. Thus our result has the advantage of parsimony in addition to the consistency with the theoretical formulation of the solute velocity.

11.6 Dispersion Coefficient as a Function of Time

Theoretical results for $D_l(t)$ are shown in Fig. 11.39. We concentrate on the results obtained for systems with large disorder, i.e., large contrasts in hydraulic conductivity. Using invasion percolation exponents [160] makes $D_l(t)$ a small positive power for all times. Using random percolation exponents [160], $D_l(t)$ is a small positive power for five (three) decades in time in 2D (3D), but diminishes in time thereafter. The values of the approximate early-time powers shown in Fig. 11.39 are 0.372 for 2D random percolation with large disorder, and 0.231 for 3D random percolation with large disorder (using our usual value, $D = 2.95$).

The predicted diminution in $D_l(t)$ at large times should probably be replaced by a constant, representing a kind of universal behavior, because it seems unlikely that the variance of a solute plume can grow more slowly than for a Gaussian process. Such a cross-over at large times to time-independent behavior (argued also in [58, 59, 131]) might be generated from our results by arguments from the central limit theorem. While this comment is somewhat speculative, the time at which this change in behavior occurs does correspond to the solute transport distance at which a cross-over to nearly universal behavior in the scale dependence of the dispersivity actually occurs. Further, the ability to generate a long-tailed distribution in space (as we show below) appears unaffected by the temporal results, as in [180].

Even though our prediction of the dispersion coefficient allows faster than Gaussian increase in $D_l(t)$ for only a limited range of times, it is still useful. A pre-asymptotic regime of three decades of time (3D) corresponds to measurements from 10 minutes to a week, or from 1 day to 1000 days; five decades (2D) corresponds

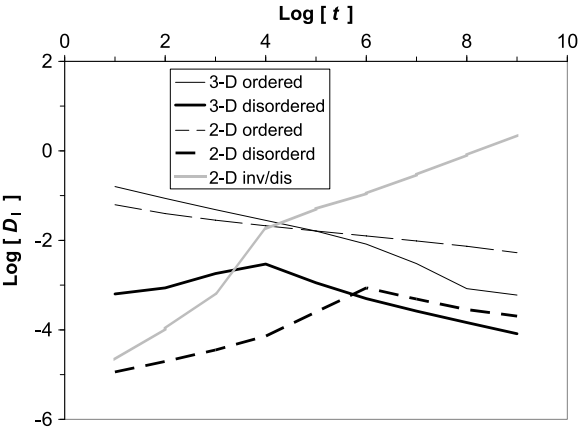

Fig. 11.39 The temporal scaling of the dispersion coefficient D_l for various types of percolation (random unless otherwise specified, otherwise invasion), dimension of the flow (2d or 3D), and both ordered and disordered media

to measurements taken over a period of 10 minutes to two years. In 3D the approximate scale exponent at shorter time scales is 0.231, i.e., $D_l(t) \propto t^{0.231}$, while in 2D $D_l(t)$ in this time range is proportional to $t^{0.372}$. This scaling allows us to compare with experimentally determined results [99, 137, 165, 166] for the variance of a Borden aquifer plume in Fig. 11.40 (below, including further discussion). The 2D result is confirmed separately by comparison with simulations of Rivard and Delay [136] for log-normally distributed conductances. In [136] it was found that D_l scaled as system size to a power between 0.56 and 0.68, which leads to powers of $D_l(t)$ as a function of time [93] between $0.56/D_b = 0.34$ and $0.68/D_b = 0.41$, using the 2D value[82] of D_b as 1.6432 [57]. The result that $D_l(t)$ scales as a small positive power of t is well-known, while the tendency for the rise in $D_l(t)$ to be restricted to a limited time frame is known from modeling:

> It is found that the macroscopic dispersion coefficient increases with time approximately in a power law prior to reaching an asymptotic value, but the spatial distribution of the plume remains non-Gaussian and cannot be described adequately by the advection-dispersion equation. [180]

Our prediction of the variance of a Borden aquifer plume (Fig. 11.40) conform to experiment at least as well as those shown in Neuman and Di Federico's [117] Fig. 13. Actually our results are nearly coincident with theirs, except near $t = 0$ where ours yield a variance of zero. Note that at this stage in the discussion our result is only a one-parameter fit, not a prediction, since we only used the power of t shown in Fig. 11.39, varying the prefactor to improve the match.

When using $L = 1$ meter as the fundamental length scale (see Sect. 11.4), the cross-over to universal behavior occurs at about $10^{1.35} = 22.4$ m in 3D, or 100 m in 2D (Fig. 11.18). Because the change in slope and the cross-over to universal behavior in the dispersivity likely accompany a cross-over to (universal) time-independent D_l, and because this cross-over should occur at the correlation length from percolation theory, we find support for our fundamental hypothesis in new analyses of the Borden aquifer:

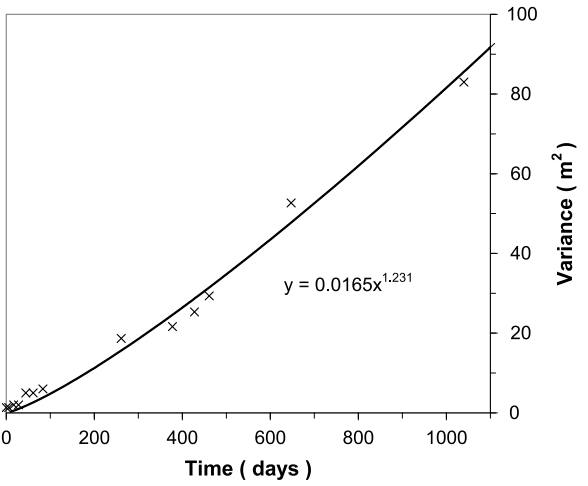

Fig. 11.40 Predicted scaling of the variance of the Borden aquifer plume with no adjustable parameters, compared with actual measurements

> This analysis revealed that macrodispersion at the Borden site is primarily controlled by the proportions, and the mean and variance in length of larger-scale strata of medium sand (M) and strata of fine sand and silt (FZ) [...]. When sampling the pattern in the longitudinal direction, M and FZ couplets repeat at 10 m intervals on average, with a high length variance. To reach a *time-constant* macrodispersivity, the stratal length variability must be fully sampled by the plume [...] beyond an advective distance of about 60 meters, corresponding to about *12 longitudinal transitions* between M and FZ unit types. [130]

Note for further consideration that the proportions of fine sand and silt enter into the calculation of D in the random fractal model ([75] DOE PNNL) of the medium.

How do we work with the universal behavior of dispersivity? We make the underlying assumption (which may be expressed as a hypothesis) that the cause of the uniformity in experimental values of $\alpha(x)$ for large x is the universal behavior that we derived. When experimenters use larger initial solute volumes (larger than the 1 m value we used for all experiments), universal behavior will set on at larger mean transport distances, meaning that the dispersivity at that cross-over will also have to increase. Thus we must first choose an x scale commensurate with the initial solute volume, then adjust α so that the universal portion of the curve is unchanged.

To illustrate, an initial solute volume of 12 m^3 and vertical size 1.6 m [165] should have horizontal dimensions roughly $\sqrt{(12/1.6)} = 2.8$ m each. Thus we rescale the horizontal axis of Fig. 11.18 by a factor 2.8. Now the vertical axis must be rescaled by $2.8^{1.13} = 3.2$ (1.13 is the value of the exponent for 3D random percolation, large disorder, from Table 11.2). Then the cross-over to universal behavior, which in Fig. 11.18 takes place at $x = 10^{1.35} = 22.4$ m and $\alpha = 10^{0.8} = 6.3$ m, should now occur at 22.4×2.8 m $= 64$ m, and α at that point should be 3.2×6.3 m $= 19$ m. The mean solute transport distance after 647 days is about 60 m. The variance of the solute distribution at that cross-over should scale the same way as α, so its value of 29 m^2 (taken from the predicted dispersion coefficient in Fig. 11.40) should be replaced by 93 m^2. The value of 93 m^2 is approximately equal to the variance at 1040 days (84 m^2 from experiment, or 86 m^2 for our fit), mean-

ing that our estimate of α (and the variance) is not reached until the next time step at larger x. But our pre-asymptotic power-law result for $D_1(t)$ using essentially this value of the variance (actually 86 m^2) for 1040 days could fit the variance for the entire range of experimental values (Fig. 11.40) without use of adjustable parameters, and without any knowledge of the structure of the medium!

We interpret the above to mean that, at the time the plume is introduced, it is sampling heterogeneity on the scale of its lateral dimensions, say several meters. Length scales smaller than the plume's initial extent are not particularly relevant. Then when the plume starts to sample much larger scales it is approaching universal behavior anyway, and new heterogeneities do not alter that behavior. This represents the fundamental difference between a theory (ADE) which yields at large scales asymptotic Gaussian behavior in both space and time, and the present theory which (probably) yields Gaussian behavior in time but a continued rise in α. Accordingly we suggest that the experimental scale (initial extent of introduced solute) *does* influence the scale where experiments appear to cross over to universal behavior. This is an important experimental control; in order to translate a curve one decade to the right (one order of magnitude increase in space), one would normally need to increase the initial volume of solution by a factor 1000. The relevance of a fundamental scale factor on a log-log graph that relates to the cube root of the injected volume thus should tend to strongly pin experimental results to a given spatial scale.

How would critical path analysis from percolation theory have addressed this problem before the current research? Hunt [66, 67] suggested that the correlation length of percolation theory should be proportional to a fundamental bond length. Hunt and Idriss [72] then showed that geoindicator statistics applied in 1D could find this fundamental bond length, as almost no system is near the 1D percolation threshold ($p_c = 1$). It is also known [66, 67, 72] that the cube of the percolation correlation length should be a Representative Elementary Volume (REV). Hunt's [67] Fig. 6 showed that critical path analysis for systems with wide ranges of local conductances should have a correlation length roughly 10 times a fundamental bond length. Finally, Ramanathan et al. [130] stated that the fundamental deposits controlling the dispersion were about 5 m in length on average: "M and FZ couplets repeat at 10 m intervals on average." We therefore could have predicted a cross-over to universal behavior at something over 50 m. However, we would not have been able to estimate a dispersivity, or a variance at that scale, nor would we have known the temporal behavior at either larger or smaller length scales.

11.7 Hydraulic Conductivity

While prior calculations have generated the hydraulic conductivity, K, through an optimization of the effects of pore size distributions and the connectivity/tortuosity factor, it should also be possible to find K directly by summing the contributions over all g of $gW(g)t_0/t(g)$. Because there is a local minimum in the arrival time at a g near g_c, and the distribution of g values is sharply peaked at $g = g_c$, the value

of the hydraulic conductivity is controlled by g_c and can be found by optimization. This is an important project that needs to be addressed in the future.

11.8 Asymptotic Treatment of Diffusion Effects

11.8.1 Theoretical Considerations

We treat the effects of diffusion only at the pore scale, again using the RS framework we have used for most of this chapter. Equation (11.10) is, at the pore scale, consistent with treatments based on the Peclet number, P_e. We wish to represent the probability, f, that a particle diffuses off a given path characterized by a given flux at some particular pore with radius r (and length l proportional to r). Equation (11.10) derives from the idea that probability fluxes are proportional to concentration gradients; thus probabilities per unit time for individual particles are constant. This implies that the probability that a particle can exit a given pore by diffusion is the ratio of the advection time, t_A to the molecular diffusion time, t_D. $t_D = D_m/r^2$, while $t_A = r/u$. The inverse ratio of t_D/t_A is known as the Peclet number, P_e:

$$P_e = \frac{r^2/D_m}{r/u} = \frac{ru}{D_m} \tag{11.38}$$

Thus the probability, f_i, that a given particle leaves pore i by diffusion is (also found in [101]),

$$f_i \propto \frac{t_A}{t_D} = \frac{1}{P_e} = \frac{D_m r}{Q} \tag{11.39}$$

where Q is the fluid mass flux through a pore. A compatible result that the time for escape from a dead-end is proportional to P_e was found in Stauffer and Sornette [163], as transition rates and survival times are inverses of each other. The final equality arises from the identity $Q = Au \propto r^2 u$. The assumed proportionality of pore length and radius makes $A/l \propto r$. On a path with conserved Q, the pore with the largest radius provides the best chance to escape on account of its smallest value of P_e. The probability that the particle remains on the flow path at a given pore is $1 - f$. In order to stay on the given flow path it must stay on at every opportunity, which generates a product of $1 - f$ over all the pores along the flow path. If fluid velocities are large, f is so small that we can use the relationship $\exp(-dx) \approx 1 - dx$ to transform the product

$$\prod_i (1 - f_i) \tag{11.40}$$

to

$$\exp\left(-\sum_i f_i\right) = \exp\left(-\sum_i \frac{1}{P_e}\right) \tag{11.41}$$

We can simplify the sum inside the exponential by representing it as the product of a typical value of P_e^{-1} and a number corresponding to the frequency of opportunities to "jump" to another flow path. This number is essentially the number of correlation lengths, χ, traversed, and can be found by taking the product of the number of pores visited on a path $(x/r_m)^{d_{min}}|1-(g/g_c)^{1-D/3}|^{-d_{min}}$ and the fraction of pores that provide close contact with other paths r_m/χ:

$$\exp\left[-\frac{r_m}{\chi}\left(\frac{x}{r_m}\right)^{d_{min}}\left|\frac{1}{(\frac{g}{g_c})^{\frac{1-D}{3}}-1}\right|^{d_{min}}\left(\frac{1}{P_e}\right)\right] \tag{11.42}$$

We chose the scaling exponent d_{min}, which gives the fractal dimensionality of the optimal path [64]. This choice was made because we assumed that the spatial tortuosity factor is relevant to counting the number of opportunities for diffusion-induced transitions off the path. Perhaps the mass fractal dimensionality, D_b, would be a better choice here, but the answer to this question is as yet unknown. In addition to the obvious tendency for factor (11.42) to reduce the contribution of highly tortuous paths (with g near g_c) to large travel times, it also reduces the tendency of very slow paths (with small controlling g and thus small P_e) to contribute to large travel times. There has been some question as to which of these cases was most important to incorporate into dispersion calculations [55, 87, 135], so it is rewarding to find that our calculation scheme accounts for both automatically.

Equation (11.19) must now be multiplied by (11.42) to generate

$$W(t)dt = \frac{gW(g)}{dt/dg}\exp\left[-\frac{r_m}{\chi}\left(\frac{x}{r_m}\right)^{d_{min}}\left|\frac{1}{(\frac{g}{g_c})^{\frac{1-D}{3}}-1}\right|^{d_{min}}\left(\frac{1}{P_e}\right)\right] \tag{11.43}$$

This result is approximate, in principle valid only when P_e is large, because for smaller P_e the escape probability must be treated more carefully. More importantly, for smaller P_e we must account for particles that diffuse *onto* given flow paths as well. Such a treatment is related to a discretized Chapman-Kolmogorov equation, but is more complicated by virtue of the correlation between escape probabilities and the (fractal) length of the path. The continuous time random walk (CTRW) treats these effects consistently with particle conservation, and can even address situations with non-conservative solutes without the kind of approximations that we use here. But an unambiguous correspondence to CTRW does not yet exist.

In order to analyze the effects of an increase in Peclet number, we must at least distinguish between two cases: reduction in the molecular diffusion coefficient, and increase in fluid velocity. In the latter case, an additional effect is that solute particles are advected downstream faster, meaning that large clusters of interconnected resistances become important at smaller times. This effect is easily treated simply by adding a factor of $1/P_e$ to the expression (Eq. (11.23)) for $t(g)$. In Hunt and Skinner [75] this factor was not included, so that derivation is appropriate only for the case of reducing the diffusion constant. In Hunt and Skinner [75] it was found that the slightly superlinear dependence of the dispersion coefficient on Peclet number over the range $1 < P_e < 100$, noted from many experiments and

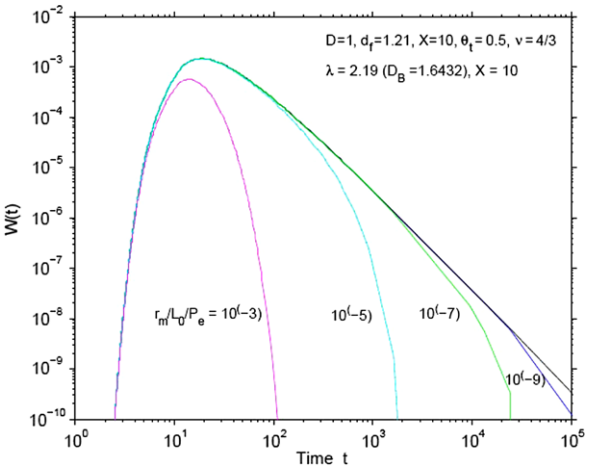

Fig. 11.41 Effects of diffusion on the long-tailed arrival time distribution. Gaussian behavior is approached as the Peclet number P_e diminishes towards 1

simulations [19, 20, 55, 87, 135], was reproduced by our predictions, but that the approximately linear dependence on P_e for higher Peclet numbers was not seen. We will see below that accounting for the reduction in $t(g)$ by the factor $1/P_e$ does not affect the conclusions at small P_e much, but that it helps (under certain circumstances) to bring predictions into accord with observation at larger values of P_e.

11.8.2 Results

The most important effects in either case are that the heavy tails in spatial and temporal distributions disappear (Fig. 11.41) and, as a consequence, the expected Gaussian spreading is eventually recovered [34, 58, 59, 103]. The time at which the effects of diffusion set on diminishes with diminishing Peclet number. As a consequence, the rises in the value of the dispersion coefficient with increasing time, and of the dispersivity with increasing scale, are terminated. In the case of the dispersion coefficient (not shown), the effects are not spectacular, since our theory does not generate an indefinite increase with increasing time anyway. But if diffusion is relevant, at some spatial scale the value of the dispersivity must level off (Fig. 11.42), consistent with Gaussian spreading. This result is simply not seen in the experiments compiled (Fig. 11.18), with the possible exception of one data point. So we conclude that the effects of diffusion are negligible, at least at large spatial scales (upwards of 1 m). While many physicists might find this reasonable, it is quite an unusual conclusion among scientists active in explaining properties of porous media. We also show in Fig. 11.42 the variability introduced into the calculation of the dispersivity by the alternate means of its calculation.

Using parameters representative of disordered media, for four different times we examine the dependence of the logarithm of the dispersion coefficient on the

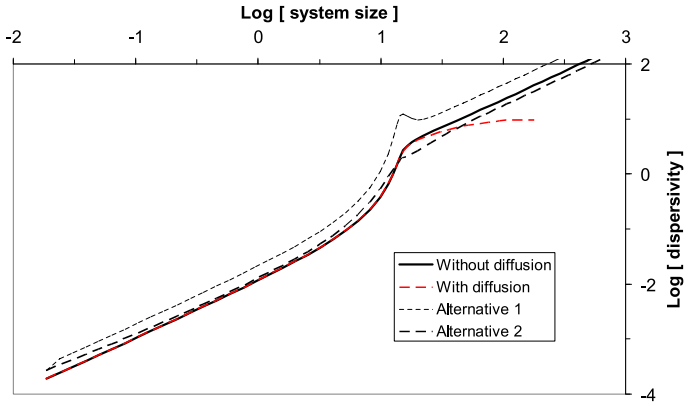

Fig. 11.42 Effects of diffusion on the dispersivity for relatively large Peclet number. Results for two alternative calculations (as well as that of Fig. 11.18) of the dispersivity are shown as well, but for the case of infinite Peclet number

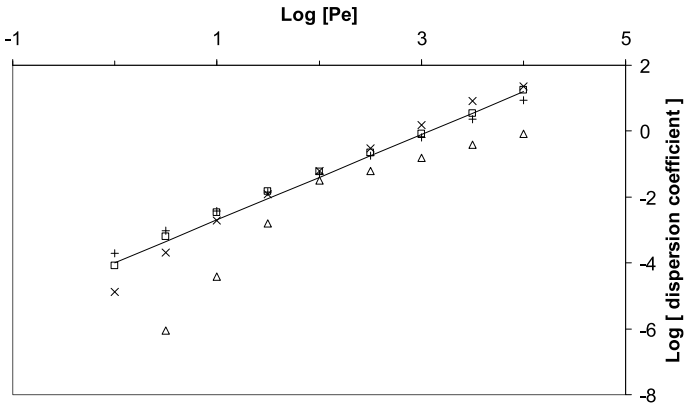

Fig. 11.43 Scaling of the dispersion coefficient with Peclet numbers in the range $1 < P_e < 1000$

logarithm of the Peclet number (Fig. 11.43). As time increases, the initial value of the dispersion coefficient diminishes and the initial slope of D_l (P_e) vs. P_e increases. The range of Peclet numbers plotted is from 1 to 10,000. The straight line has slope of 1.3. The result is a superlinear power, at least for the three small time values, though with slope a little larger than the commonly reported value of 1.2 [19, 20, 55, 87, 135]. For the largest time value, systematic increase of the Peclet number eventually brings the system past the peak in the dispersion coefficient as a function of time, leading to a more complicated (and unverified) dependence of the dispersion coefficient on Peclet number. But for the three smaller time values we see a diminution of the slope of D_l (P_e) vs. P_e, as noted also in [19, 20, 55, 87, 135].

In Hunt and Skinner [75] the dependence of the dispersion coefficient on Peclet number for $1 < P_e < 100$ was very nearly $P_e^{1.2}$, as expected.

11.9 Discussion

In this chapter we have made comparisons of our theoretical predictions of the dispersivity with over 2200 experimental measurements. We have also compared our theoretical predictions of typical solute velocities with over 900 measurements of the spatial and temporal scaling of chemical reactions. In the case of the tortuosity, nearly 100 measured values were discussed. For saturation-dependent dispersion, the number of individual experimental values investigated was almost 500, though in other cases fewer experimental results could be accessed. Altogether, approximately 4000 individual measurements from this chapter confirm our predictions. Two results were unexpected: (1) That experimental results would show so little evidence of the relevance of diffusion in any property, and (2) That the scale of the experimental apparatus would have such a large effect on the dispersivity.

There are still some uncertainties regarding our theoretical development. It appears that we do not predict a monotonically increasing dispersivity with increasing disorder. Experiments may indicate otherwise. We earlier expressed hope [76] that our treatment could be used to inform the choice of exponents in the CTRW, but it does not appear that our results are in accord with that framework for discussion. We attribute the discrepancy to the result in our theory that the long-time tails of the arrival time distribution are not true power laws, but we have as yet no proof. Finally, our theoretical description of dispersion does not incorporate spreads of cluster transit times on single clusters of interconnected conductances. Rather, it incorporates simultaneous treatment of clusters with different controlling conductance values. This is in keeping with a percolation cluster treatment of ac hopping conduction at low frequencies that is known to generate the appropriate frequency dependence of the ac conductivity [65], as well as finite size corrections to infinite size calculations of the dc conductivity. This latter calculation was also tested in the context of porous media [67]. Nevertheless, it is not obvious that the present theoretical treatment must be accurate. Therefore we appeal to its successes in the following areas, demonstrated in this chapter and cited publications. All of these successes stem from the same model, the generalized pore-sold fractal model, and most of them from the subset of parameters that allows the PSF model to reduce to the RS model.

1. We predicted the evolution with system size of the distribution of particle arrival times in 2D simulations at the percolation threshold. The tail of the simulated distribution [96] decayed according to the power, -1.56.
2. The power that was obtained for comparison with the 2D simulations is equal to the observed power for fracture flow, but commonly attributed to diffusive exchange with the rock matrix. Here it should be mentioned that Becker and Shapiro [14], in a stringent test using various solutes with differing diffusion constants, found that matrix diffusion had no effect on the dispersion experiments.
3. We were able to predict the temporal dependence of the variance of the Borden aquifer dispersion tests without use of adjustable parameters, or even detailed knowledge of the subsurface.

4. We could generate the saturation-dependence of the distribution of arrival times observed in two media (including its fundamental time scale), one of which could be predicted without use of adjustable parameters.
5. The prediction of the envelope of dispersivity values over 10 orders of magnitude of length scale was verified.
6. The predictions of the scaling of chemical reaction rates over 13 orders of magnitude of time scale were verified.
7. The predictions of the scaling of chemical reaction rates over approximately 8 orders of magnitude of length scale were verified.
8. The predictions of the (power-law) temporal scaling with system size of the typical arrival time in dispersive transport were verified for both amorphous semiconductors and polymer systems. Here we generated not only the typical values of the power, but its variability as well.
9. The observed Peclet number dependence of the dispersion coefficient was generated by the theory when diffusion was incorporated.
10. Results for the measurement scale dependence of chemical reaction rates were generated using a single unknown parameter.

Can we generate Gaussian dispersion from the present theory? Margolin and Berkowitz [103] note that Gaussian dispersion should result when the first and second moments of the arrival time distribution exist ($\beta > 2$ in CTRW notation). The slope of $W(t)$ for $D_b = 1.46$ is already very nearly -3, which according to CTRW should equal $-(\beta + 1)$; for smaller values of $D_{opt} = 1.217$, such as appropriate for the chemical path length, we should then expect Gaussian dispersion. However, the conditions for which such a choice of fractal dimensionality might be appropriate are not known. We hypothesize that D_{opt} may be appropriate under conditions when the medium is fairly homogeneous both from the standpoint of the pore-size distribution, and from the relevance of any percolation structures. This hypothesis aligns with the arguments of Bruderer-Weng et al. [25], who argue that flow channeling is relevant to long-tailed arrival time distributions, though in our case the actual cause of the long-tailed distributions remains the relevance of the tortuosity of the pathways and the fractal dimensionality of the backbone, while the flow-channeling along such structures arises from a wide range of pore sizes.

Appendix: Basic CTRW and Gaussian Results

For Gaussian dispersion:

$$\langle x \rangle \propto t \tag{11.44}$$

$$\sigma(t) \propto t^{0.5} \tag{11.45}$$

For CRTW:

$$\psi(t) \propto t^{-1-\beta}, \quad t \to \infty \tag{11.46}$$

– If $0 < \beta < 1$

$$\langle x \rangle \propto t^{\beta} \tag{11.47}$$

$$\sigma(t) \propto t^{\beta} \tag{11.48}$$

– If $1 < \beta < 2$

$$\langle x \rangle \propto t \tag{11.49}$$

$$\sigma(t) \propto t^{(3-\beta)/2} \tag{11.50}$$

Sahimi [144]:

– If $0 < \beta < 1$

$$\left\langle x^2 \right\rangle \propto t^{2\beta} \tag{11.51}$$

– If $1 < \beta < 2$

$$\left\langle x^2 \right\rangle \propto t^{3-\beta} \tag{11.52}$$

While our results are compatible with Eq. (11.47) and Eq. (11.48) (within 5 % deviation), we do not find that the long tails of the distribution are compatible with Eq. (11.46) for values of β obtained from either Eq. (11.47) or Eq. (11.48). Here we find discrepancies.

This means that, as yet, we cannot map our treatment of dispersion onto the CTRW. If such a correspondence could be made, the calculation of dispersion for both conservative and non-conservative solutes would be greatly simplified, since the CTRW is already designed to treat either case. In other words, complications due to particle conservation can be incorporated into the CTRW even when some of the particles are adsorbed on surfaces or otherwise lost to the flow, even if subsequent desorption is also possible. Thus an important goal of subsequent research is to investigate more closely the relationship between the present treatment and the CTRW.

References

1. Aggelopoulos, C.A., Tsakiroglou, C.D.: The longitudinal dispersion coefficient of soils as related to the variability of local permeability. Water Air Soil Pollut. **185**, 223–237 (2007)
2. Algeo, T.J., Scheckler, S.E.: Terrestrial-marine teleconnections in the Devonian: links between the evolution of landplants, weathering processes, and marine anoxic events. Philos. Trans. R. Soc. Lond. B, Biol. Sci. **353**, 113–128 (1998)
3. Ambegaokar, V.N., Halperin, B.I., Langer, J.S.: Hopping conductivity in disordered systems. Phys. Rev. B **4**, 2612–2621 (1971)
4. Anderson, R.S., Anderson, S.P.: Geomorphology: The Mechanics and Chemistry of Landscapes. Cambridge Press, New York (2010)
5. Araujo, A.D., Moreira, A.A., Filho, R.N.C., Andrade, J.S. Jr.: Statistics of the critical percolation backbone with spatial long-range correlations. Phys. Rev. E **67**, 027102 (2003)
6. Aronofsky, J.S., Heller, J.P.: A diffusion model to explain mixing of flowing miscible fluids in porous media. Trans. AIME **210**, 345–349 (1957)

7. Arya, A., Hewett, T.A., Larson, R.G., Lake, L.W.: Dispersion and reservoir heterogeneity. SPE Reserv. Eng. **3**, 139–148 (1988)
8. Balberg, I.: Recent developments in continuum percolation. Philos. Mag. B **30**, 991–1003 (1987)
9. Barrande, M., Bouchet, R., Denoyel, R.: Tortuosity of porous particles. Anal. Chem. **79**, 9115–9121 (2007)
10. Barthelemy, M., Buldyrev, S.V., Havlin, S., Stanley, H.E.: Scaling and finite-size effects for the critical backbone. Fractals **11**(supplement), 19–27 (2003)
11. Baumann, T., Müller, S., Niessner, R.: Migration of dissolved heavy metal compounds and PCP in the presence of colloids through a heterogeneous calcareous gravel and a homogeneous quartz sand—pilot scale experiments. Water Res. **36**, 1213 (2002)
12. Baumann, T., Toops, L., Niessner, R.: Colloid dispersion on the pore scale. Water Res. **44**, 1246–1254 (2010)
13. Bear, J.: Dynamics of Fluids in Porous Media. Elsevier, New York (1972)
14. Becker M. W, M.W., Shapiro, A.M.: Tracer transport in fractured crystalline rock: evidence of nondiffusive breakthrough tailing. Water Resour. Res. **36**, 1677–1686 (2000)
15. Berkowitz, B., Scher, H.: On characterization of anomalous dispersion in porous and fractured media. Water Resour. Res. **31**, 1461–1466 (1995)
16. Berkowitz, B., Cortis, A., Dentz, M., et al.: Modeling non-Fickian transport in geological formations as a continuous time random walk. Rev. Geophys. **44**(2), RG2003 (2006)
17. Bernabé, Y., Bruderer, C.: Effect of the variance of pore size distribution on the transport properties of heterogeneous networks. J. Geophys. Res. **103**, 513 (1998)
18. Berner, R.A.: Weathering, plants, and the long-term carbon-cycle. Geochim. Cosmochim. Acta **56**(8), 3225–3231 (1992)
19. Bijeljic, B., Blunt, M.J.: Pore-scale modeling and continuous time random walk analysis of dispersion in porous media. Water Resour. Res. **42**(1), W01202 (2006)
20. Bijeljic, B., Muggeridge, A., Blunt, M.J.: Pore-scale modeling of longitudinal dispersion. Water Resour. Res. **40**(11), W11501 (2004)
21. Bird, N.R.A., Perrier, E., Rieu, M.: The water retention function for a model of soil structure with pore and solid fractal distributions. Eur. J. Soil Sci. **51**, 55–63 (2000)
22. Bos, F.C., Guion, T., Burland, D.M.: Dispersive nature of hole transport in polyvinylcarbazole. Phys. Rev. B **39**, 12633–12641 (1989)
23. Brenner, H.: Macrotransport processes. Langmuir **6**, 1715–1724 (1990)
24. Brantley, S.L., Crane, S.R., Crerar, D., Hellmann, R., Stallard, R.: Dissolution at dislocation etch pits in quartz. Geochim. Cosmochim. Acta **50**, 2349–2361 (1986)
25. Bruderer-Weng, C., Cowie, P., Bernabé, Y., Main, I.: Relating flow channeling to tracer dispersion in heterogeneous networks. Adv. Water Resour. **27**(8), 843–855 (2004)
26. Bunde, A., Havlin, S.: Percolation I. In: Bunde, A., Havlin, S. (eds.) Fractals and Disordered Systems. Springer, Berlin (1996), 408 pp.
27. Burdine, N.T.: Relative permeability calculations from pore-size distribution data. Trans. Am. Inst. Min. Metall. Eng. **198**, 71–77 (1953)
28. Carman, P.C.: Fluid flow through granular beds. Trans. Inst. Chem. Eng., London **15**, 150–166 (1937)
29. Chao, H., Rajaram, H., Illangasekare, T.: Intermediate-scale experiments and numerical simulations of transport under radial flow in a two-dimensional heterogeneous porous medium. Water Resour. Res. **36**, 2869 (2000)
30. Cherrey, K.D., Flury, M., Harsh, J.B.: Nitrate and colloid transport through coarse Hanford sediments under steady state, variably saturated flow. Water Resour. Res. **39**, 1165 (2003)
31. Cieplak, M., Maritan, A., Banavar, J.R.: Invasion percolation and Eden growth: geometry and universality. Phys. Rev. Lett. **76**, 3754–3757 (1996)
32. Clennell, M.B.: Tortuosity: a guide through the maze. In: Lovell, M.A., Harvey, P.K. (eds.) Developments in Petrophysics, vol. 122, pp. 299–344. Geol. Soc., London (1997)
33. Corapcioglu, M.Y., Fedirchuk, P.: Glass bead micromodel study of solute transport. J. Contam. Hydrol. **36**, 209–230 (1999)

34. Cortis, A., Berkowitz, B.: Anomalous transport in "classical" soil and sand columns. Soil Sci. Soc. Am. J. **68**, 1539–1548 (2004)
35. Dagan, G.: Theory of solute transport by groundwater. Annu. Rev. Fluid Mech. **19**, 183–215 (1987)
36. Dagan, G.: Dispersion of a passive solute in nonergodic transport by steady velocity-fields in heterogeneous formations. J. Fluid Mech. **233**, 197–210 (1991)
37. Dagan, G., Neuman, S.P. (eds.): Subsurface Flow and Transport: A Stochastic Approach. Cambridge University Press, Cambridge (1997)
38. Danquigny, C., Ackerer, P., Carlier, J.P.: Laboratory tracer tests on three-dimensional reconstructed heterogeneous porous media. J. Hydrol. **294**, 196 (2004)
39. Delgado, J.M.P.Q.: A simple experimental technique to measure tortuosity in packed beds. Can. J. Chem. Eng. **84**, 651–655 (2006)
40. Dentz, M., Gouze, P., Carrera, J.: Effective non-local reaction kinetics in physicaly and chemically heterogeneous media. J. Contam. Hydrol. **120–121**, 222–236 (2011)
41. Dixon, J.L., Heimsath, A.M., Amundson, R.: The critical role of climate and saprolite weathering in landscape evolution. Earth Surf. Process. Landf. **34**, 1507–1521 (2009)
42. Du, J., Bao, J., Hu, Q., Ewing, R.P.: Uranium release from different size fractions of sediments in Hanford 300 area, Washington, USA. J. Environ. Radioact. **107**, 92–94 (2012)
43. Duda, A., Koza, Z., Matyka, M.: Hydraulic tortuosity in arbitrary porous media flow. Phys. Rev. E **84**, 036319 (2011)
44. Epstein, N.: On tortuosity and the tortuosity factor in flow and diffusion through porous media. Chem. Eng. Sci. **44**, 777–779 (1989)
45. Ewing, R.P., Hu, Q., Liu, C.: Scale dependence of intragranular porosity, tortuosity, and diffusivity. Water Resour. Res. **46**, W06513 (2010). doi:10.1029/2009WR008183
46. Fisher, M.E.: The theory of critical point singularities. In: Green, M.S. (ed.) Critical Phenomena, Proc. 1970 Enrico Fermi Int'l. Sch. Phys., Course No. 51, Varenna, Italy, pp. 1–99. Academic Press, New York (1971)
47. Freeze, R.A.: A stochastic-conceptual analysis of one-dimensional groundwater flow in nonuniform homogeneous media. Water Resour. Res. **11**, 725–741 (1975)
48. Friedman, L., Pollak, M.: The Hall effect in the variable-range hopping system. Philos. Mag. B **44**, 487–507 (1981)
49. Gelhar, L.W., Axness, C.L.: Three-dimensional stochastic analysis of macrodispersion in aquifers. Water Resour. Res. **19**, 161–180 (1983)
50. Gelhar, L., Welty, W.C., Rehfeldt, K.R.: A critical review of data on field-scale dispersion in aquifers. Water Resour. Res. **28**, 1955–1974 (1992)
51. Ghanbarian-Alavijeh, B., Hunt, A.G.: Unsaturated hydraulic conductivity in porous media: percolation theory. Geoderma **187–188**, 77–84 (2012)
52. Ghanbarian-Alavijeh, B., Skinner, T.E., Hunt, A.G.: Saturation dependence of dispersion in porous media. Phys. Rev. E **86**, 066316 (2012)
53. Ghanbarian, B., Hunt, A.G., Ewing, R.P., Sahimi, M.: Tortuosity in porous media: a critical review. Soil Sci. Soc. Am. J. **77**, 1461–1477 (2013). doi:10.2136/sssaj2012.0435
54. Ghanbarian-Alavijeh, B., Hunt, A.G., Sahimi, M., Ewing, R.P., Skinner, T.E.: Percolation theory generates a physically based description of tortuosity in saturated and unsaturated porous media. Soil Sci. Soc. Am. J. (2013). doi:10.2136/sssaj2013.01.0089
55. Gist, G.A., Thompson, A.H., Katz, A.J., Higgins, R.L.: Hydrodynamic dispersion and pore geometry in consolidated rock. Phys. Fluids A **2**, 1533–1544 (1990)
56. Glass, R.J., Brainard, J.R., Yeh, T.-C.J.: Infiltration in unsaturated layered fluvial deposits at Rio Bravo: macroscopic anisotropy and heterogeneous transport. Vadose Zone J. **4**(1), 22–31 (2005)
57. Grassberger, P.: Conductivity exponent and backbone dimension in 2-d percolation. Physica A **262**, 251–263 (1999)
58. Gupta, V., Bhattacharya, R.: Effect of scale on solute-dispersion in saturated porous-media. Adv. Appl. Probab. **16**(1), 18 (1984)

59. Gupta, V., Bhattacharya, R.: A new derivation of the Taylor-Aris theory of solute-dispersion in a capillary. Water Resour. Res. **19**(4), 945–951 (1983)
60. Gvirtzman, H., Roberts, P.V.: Pore scale spatial analysis of two immiscible fluids in porous media. Water Resour. Res. **27**, 1167 (1991)
61. Haggerty, R.: Matrix diffusion: Heavy-tailed residence time distributions and their influence on radionuclide retention. In: Radionuclide Retention in Geologic Media, pp. 81–90, Workshop Proceedings, Oskarshamn, Sweden, 7–9 May 2001, Radioactive Waste Management GEOTRAP Project, Organisation for Economic Cooperation and Development, (2002)
62. Haggerty, R., Harvey, C.F., Freiherr von Schwerin, C., Meigs, L.C.: What controls the apparent timescale of solute mass transfer in aquifers and soils? A comparison of experimental results. Water Resour. Res. **40**, 01510 (2004)
63. Havlin, S., Braunstein, L.A., Buldyrev, S.V., Cohen, R., Kalisky, T., Sreenivasan, S., Stanley, H.E.: Optimal path in random networks with disorder: a mini review. Physica A **346**, 82–92 (2005)
64. Herrmann, H.J., Stanley, H.E.: The fractal dimension of the minimum path in two-dimensional and three-dimensional percolation. J. Phys. A **21**, L829–L833 (1988)
65. Hunt, A.: The low frequency conductivity of the Fermi glass. J. Phys. Condens. Matter **4**(33), 6957–6970 (1992)
66. Hunt, A.G.: Upscaling in subsurface transport using cluster statistics of percolation. Transp. Porous Media **30**(2), 177–198 (1998)
67. Hunt, A.G.: Applications of percolation theory to porous media with distributed local conductances. Adv. Water Resour. **24**(3,4), 279–307 (2001)
68. Hunt, A.G.: Continuum percolation theory for water retention and hydraulic conductivity of fractal soils: 1. Estimation of the critical volume fraction for percolation. Adv. Water Resour. **27**, 175–183 (2004)
69. Hunt, A.G.: Scale-dependent hydraulic conductivity from dimensional cross-over. Hydrogeol. J. **14**(4), 499–507 (2005)
70. Hunt, A.G., Blank, L.A., Skinner, T.E.: Distribution of hydraulic conductivity in single-scale anisotropy. Philos. Mag. **86**(16), 2407–2428 (2006)
71. Hunt, A.G., Gee, G.W.: Water retention of fractal soil models using continuum percolation theory: tests of Hanford site soils. Vadose Zone J. **1**, 252–260 (2002)
72. Hunt, A., Idriss, B.: Percolation-based effective conductivity calculations for bimodal distributions of local conductances. Philos. Mag. **89**(22–24), 1989–2007 (2009)
73. Hunt, A.G., Skinner, T.E.: Longitudinal dispersion of solutes in porous media solely by advection. Philos. Mag. **88**, 2921–2944 (2008)
74. Hunt, A.G., Skinner, T.E.: Predicting dispersion in porous media. Complexity (2010). doi:10.1002/cplx.20322
75. Hunt, A.G., Skinner, T.E.: Incorporation of effects of diffusion into advection-mediated dispersion in porous media. J. Stat. Phys. **140**, 544–564 (2010)
76. Hunt, A.G., Skinner, T.E., Ewing, R.P., Ghanbarian-Alavijeh, B.: Dispersion of solutes in porous media. Eur. Phys. J. B **80**, 411–432 (2011)
77. Hunt, A.G., Skinner, T.E., Ghanbarian, B.: Solute transport predicts scaling of surface reaction rates in porous media: Applications to silicate weathering. Water Resour. Res. (2013, submitted)
78. Huang, W.E., Oswald, S.E., Lerner, D.N., Smith, C.C., Zheng, C.: Dissolved oxygen imaging in a porous medium to investigate biodegradation in a plume with limited electron acceptor supply. Environ. Sci. Technol. **37**, 1905–1911 (2003)
79. Huang, G., Huang, Q., Zhan, H.: Evidence of one-dimensional scale-dependent fractional advection–dispersion. J. Contam. Hydrol. **85**, 53–71 (2006)
80. Jardine, P.M., Jacobs, G.K., Wilson, G.V.: Unsaturated transport processes in undisturbed heterogeneous porous media: 1. Inorganic contaminants. Soil Sci. Soc. Am. J. **57**, 945–953 (1993)
81. Kapitulnik, A., Aharony, A., Deutscher, G., Stauffer, D.: Self-similarity and correlations in percolation. J. Phys. A, Math. Gen. **16**, L269–L274 (1983)

82. Katz, A.J., Thompson, A.H.: Quantitative prediction of permeability in porous rock. Phys. Rev. B **34**, 8179–8181 (1986)
83. Kim, D.-J., Kim, J.-S., Yun, S.-T., Lee, S.-H.: Determination of longitudinal dispersivity in an unconfined sandy aquifer. Hydrol. Process. **16**, 1955 (2002)
84. Kläfter, J., Silbey, R.: Derivation of the continuous-time random walk equation. Phys. Rev. Lett. **44**, 55–58 (1980)
85. Knackstedt, M.A., Sahimi, M., Sheppard, A.P.: Invasion percolation with long-range correlations: first-order phase transition and nonuniversal scaling properties. Phys. Rev. E **61**(5), 4920 (2000)
86. Kohlbecker, M.V., Wheatcraft, S.W., Meerschaert, M.M.: Heavy-tailed log hydraulic conductivity distributions imply heavy-tailed log velocity distributions. Water Resour. Res. **42**(4), W04411 (2006)
87. Koplik, J., Redner, S., Wilkinson, D.: Transport and dispersion in random networks with percolation disorder. Phys. Rev. A **37**, 2619–2636 (1988)
88. Koponen, A., Kataja, M., Timonen, J.: Permeability and effective porosity of porous media. Phys. Rev. E **56**, 3319–3325 (1997)
89. Kozeny, J.: Über Kapillare Leitung des Wasssers im Boden. Sitzungsber. Adak. Wiss. Wien **136**, 271–306 (1927)
90. Krepysheva, N., Di Pietro, L., Neel, M.C.: Space-fractional advection diffusion and reflective boundary condition. Phys. Rev. E **73**(2), 021104 (2006). Part 1
91. Kunz, H., Souillard, B.: Essential singularity in percolation model. Phys. Rev. Lett. **40**, 133–135 (1976)
92. Lallemand-Barres, A., Peaudecerf, P.: Recherche des relations entre la valeur de la dispersivité macroscopique d'un milieu aquifère, ses autres charactéristiques et les conditions de mésure (Research for relations between the macroscopic dispersivity value of an aquifer, its other characteristics and measurement conditions), Bulletin du B. R. G. M. (deuxième série), section III, (4) pp. 227–284 (1978)
93. Lee, Y., Andrade, J.S., Buldyrev, S.V., Dokholoyan, N.V., Havlin, S., King, P.R., Paul, G., Stanley, H.E.: Traveling time and traveling length in critical percolation clusters. Phys. Rev. E **60**(3), 3425–3428 (1999)
94. Li, L., Steefel, C.I., Yang, L.: Scale dependence of mineral dissolution rates within single pores and fractures. Geochim. Cosmochim. Acta **72**, 360–377 (2008)
95. Lin, M., Chabaux, F., Pelt, E., Granet, M., Sak, P.B., Gaillardet, J., Lebedeva, M., Brantley, S.L.: The effect of curvature on weathering rind formation: evidence from uranium-series isotopes in basaltic andesite weathering clasts in Guadeloupe. Geochim. Cosmochim. Acta **80**, 92–107 (2012)
96. Liu, Z.-F., Wang, X.-H., Mao, P., Wu, Q.-S.: Tracer dispersion between two lines in two-dimensional percolation porous media. Chin. Phys. Lett. **20**, 1969–1972 (2003)
97. Liu, C., Shi, Z., Zachara, J.M.: Kinetics of Uranium(VI) desorption from contaminated sediments: effect of geochemical conditions and model evaluation. Environ. Sci. Technol. **43**, 6560–6566 (2009)
98. Lopez, E., Buldyrev, S.V., Barunstein, L.A., Havlin, S., Stanley, H.E.: Possible connection between the optimal path and flow in percolation clusters. Phys. Rev. E **72**, 056131 (2005) (6 pp.)
99. Mackay, D.M., Freyberg, D.L., Roberts, P.B., Cherry, J.A.: A natural gradient experiment on solute transport in a sand aquifer. I. Approach and overview of plume movement. Water Resour. Res. **22**, 2017–2029 (1986)
100. Maher, K.: The dependence of chemical weathering rates on fluid residence time. Earth Planet. Sci. Lett. **294**, 101–110 (2010)
101. Makse, H., Andrade, J.S., Stanley, H.E.: Tracer dispersion in a percolation network with spatial correlations. Phys. Rev. E **61**, 583–586 (2000)
102. Mandelbrot, B.B.: The Fractal Geometry of Nature. Freeman, San Francisco (1983) (468 pp.)

103. Margolin, G., Berkowitz, B.: Application of continuous time random walks to transport in porous media. J. Phys. Chem. B **104**, 3942–3947 (2000)
104. Matyka, M., Khalili, A., Koza, Z.: Tortuosity-porosity relation in porous media flow. Phys. Rev. E **78**, 026306 (2008)
105. Meerschaert, M.M., Benson, D.A., Baumer, B.: Multidimensional advection and fractional dispersion. Phys. Rev. E **59**, 5026–5028 (1999)
106. Meerschaert, M.M., Benson, D.A., Scheffler, H.P., Becker-Kern, P.: Governing equations and solutions of anomalous random walk limits. Phys. Rev. E **66**(6), 060102 (2002). Part 1
107. Meerschaert, M.M., Mortensen, J., Wheatcraft, S.W.: Fractional vector calculus for fractional advection-diffusion. Physica A **367**, 181–190 (2006)
108. Moldrup, P., Oleson, T., Komatsu, T., Schjoning, P., Rolston, D.E.: Tortuosity, diffusivity, and permeability in the soil liquid and gaseous phases. Soil Sci. Soc. Am. J. **65**, 613–623 (2001)
109. Molin, S., Trebotich, D., Steefel, C.I., Shen, C.: An investigation of the effect of pore scale flow on average geochemical reaction rates using direct numerical simulation. Water Resour. Res. **48**, W03527 (2012)
110. Moreno, L., Tsang, C.F.: Flow channeling in strongly heterogeneous porous media: a numerical study. Water Resour. Res. **30**, 1421 (1994)
111. Mota, M., Teixeira, J.A., Yelshin, A.: Binary spherical particle mixed beds porosity and permeability relationship measurement. Trans. Filtr. Soc. **1**, 101–106 (2001)
112. Mualem, Y.: A new model for predicting the hydraulic conductivity of unsaturated porous media. Water Resour. Res. **12**, 513–522 (1976)
113. Navarre-Sitchler, A., Brantley, S.L.: Basalt weathering across scales. Earth Planet. Sci. Lett. **261**(1–2), 321–334 (2007). doi:10.1016/j.epsl.2007.07.010
114. Navarre-Sitchler, A., Steefel, C., Hausrath, E., Brantley, S.L.: Influence of porosity on basalt weathering rates from the clast to watershed scale. Geochim. Cosmochim. Acta **71**(15), A707 (2007)
115. Neuman, S.P.: Universal scaling of hydraulic conductivities and dispersivities in geologic media. Water Resour. Res. **26**, 1749–1758 (1990)
116. Neuman, S.P.: Comment on "Longitudinal dispersivity data and implications for scaling behavior" by Schulze-Makuch. Ground Water **44**, 140–141 (2006) (Author's reply, p. 141)
117. Neuman, S.P., Di Federico, V.: Multifaceted nature of hydrogeologic scaling and its interpretation. Rev. Geophys. **41**(3), 1014 (2003)
118. Nielsen, D.R., Biggar, J.W.: Miscible displacement in soils. I. Experimental information. Soil Sci. Soc. Am. Proc. **25**, 1–5 (1961)
119. Nielsen, D.R., Biggar, J.W.: Miscible displacement in soils. III. Theoretical considerations. Soil Sci. Soc. Am. Proc. **26**, 216–221 (1962)
120. Noniel, C., Steefel, C.I., Yang, L., Ajo-Franklin, J.: Upscaling calcium carbonate precipitation rates from pore to continuum scale. Chem. Geol. **318**, 60–74 (2012)
121. Pachepsky, Ya., Benson, D., Rawls, W.: Simulating scale-dependent solute transport in soils with the fractional advective-dispersive equation. Soil Sci. Soc. Am. J. **64**, 1234–1243 (2000)
122. Park, M., Kleinfelter, N., Cushman, J.H.: Scaling laws and Fokker-Planck equations for 3-dimensional porous media with fractal mesoscale. Multiscale Model. Simul. **4**(4), 1233–1244 (2005)
123. Paul, G., Havlin, S., Stanley, H.E.: Fractal behavior of the shortest path between two lines in percolation systems. Phys. Rev. E **65**, 066105 (2002) (pp. 8)
124. Peng, S., Hu, Q., Ewing, R.P., Liu, C., Zachara, J.M.: Quantitativve 3-d elemental mapping by LA-ICP-MS of a basaltic clast from the Hanford 300 area. Environ. Sci. Technol. **46**, 2025–2032 (2012)
125. Pfannkuch, H.: Contribution à l'étude des déplacements de fluides miscibles dans un milieu poreux (Contribution to the study of the displacement of miscible fluids in a porous medium). Rev. Inst. Fr. Pét. **2**, 18 (1963)
126. Pfister, G.: Pressure-dependent electronic transport in amorphous As_2Se_3. Phys. Rev. Lett. **35**, 1474–1477 (1974)

127. Pfister, G., Scher, H.: Time-dependent electronic transport in amorphous solids—As_2Se_3. Phys. Rev. B **15**, 2062–2083 (1977)
128. Pfister, G., Griffiths, C.H.: Temperature-dependence of transient hole hopping transport in disordered organic solids—carbazole polymers. Phys. Rev. Lett. **40**, 659–662 (1978)
129. Porto, M., Havlin, S., Roman, H.E., Bunde, A.: Probability distribution of the shortest path on the percolation cluster, its backbone, and skeleton. Phys. Rev. E **58**(5), R5205–R5208 (1998)
130. Ramanathan, R., Ritzi, R.W., Huang, C.C.: Linking hierarchical stratal architecture to plume spreading in a Lagrangian-based transport model. Water Resour. Res. **44**, W04503 (2008)
131. Ramirez, J.M., Thomann, E., Wamire, E., Haggerty, R., Wood, B.: A generalized Taylor-Aris formula and skew diffusion. Multiscale Model. Simul. **5**, 786–801 (2006)
132. Raoof, A., Hassanizadeh, S.M.: Upscaling transport of adsorbing solutes in porous media. J. Porous Media **13**, 395–408 (2010)
133. Raymo, M.E.: The Himalayas, organic-carbon burial, and climate in the Miocene. Paleoceanography **9**(3), 399–404 (1994)
134. Rieu, M., Sposito, G.: Fractal fragmentation, soil porosity, and soil water properties. I. Theory. Soil Sci. Soc. Am. J. **55**, 1231 (1991)
135. Rigord, P., Calvo, A., Hulin, J.: Transition to irreversibility for the dispersion of a tracer in porous-media. Phys. Fluids A, Fluid Dyn. **2**(5), 681–687 (1990)
136. Rivard, C., Delay, F.: Simulations of solute transport in fractured porous media using 2D percolation networks with uncorrelated hydraulic conductivity fields. Hydrogeol. J. **12**, 613–627 (2004)
137. Roberts, P.V., Goltz, M.N., Mackay, D.M.: A natural gradient experiment on solute transport in a sand aquifer. III. Retardation estimates and mass balances for organic solutes. Water Resour. Res. **22**, 2047–2058 (1986)
138. Rubin, Y.: Applied Stochastic Hydrogeology. Oxford Univ. Press, London (2003)
139. Saffman, P.G.: A theory of dispersion in a porous medium. J. Fluid Mech. **6**, 321 (1959)
140. Sahimi, M.: Fractal and superdiffusive transport and hydrodynamic dispersion in heterogeneous porous media. Transp. Porous Media **13**, 3–40 (1993)
141. Sahimi, M.: Applications of Percolation Theory. Taylor & Francis, London (1994)
142. Sahimi, M.: Flow and Transport in Porous Media and Fractured Rock. From Classical Methods to Modern Approaches. Wiley/VCH, Weinheim (1995). 500 pp.
143. Sahimi, M.: Flow and Transport in Porous Media and Fractured Rock, 2nd edn. Wiley-VCH, Weinheim (2011). 709 pp.
144. Sahimi, M.: Dispersion in porous media, continuous-time random walk, and percolation. Phys. Rev. E **85**, 016316 (2012)
145. Sahimi, M., Imdakm, A.O.: The effect of morphological disorder on hydrodynamic dispersion in flow through porous media. J. Phys. A, Math. Gen. **21**, 3833–3870 (1988)
146. Sak, P.B., Fisher, D.M., Gardner, T.W., Murphy, K., Brantley, S.L.: Rates of weathering rind formation on Costa Rican basalt. Geochim. Cosmochim. Acta **68**, 1453–1472 (2003)
147. Sanchez, R., Carreras, B.A., van Milligen, B.P.: Fluid limit of nonintegrable continuous-time random walks in terms of fractional differential equations. Phys. Rev. E **71**(1), 011111 (2005). Part 1
148. Scheidegger, A.E.: An evaluation of the accuracy of the diffusivity equation for describing miscible displacement in porous media. In: Proc. Theory of Fluid Flow in Porous Media Conf., Univ. Oklahoma, pp. 101–116 (1959)
149. Scheidegger, A.E.: The Physics of Flow Through Porous Media, 3rd edn. University of Toronto Press, Toronto (1974)
150. Scher, H., Montroll, E.W.: Anomalous transit-time dispersion in amorphous solids. Phys. Rev. B **12**(6), 2455–2477 (1975)
151. Scher, H., Shlesinger, M., Bendler, J.: Time-scale invariance in transport and relaxation. Phys. Today **44**(1), 26–34 (1991). doi:10.1063/1.881289
152. Schulze-Makuch, D.: Facies Dependent Scale Behavior of Hydraulic Conductivity and Longitudinal Dispersivity in the Carbonate Aquifer of Southeastern Wisconsin. Ph.D. Disserta-

tion, University of Wisconsin, Milwaukee (1996)
153. Schulze-Makuch, D.: Longitudinal dispersivity data and implications for scaling behavior. Ground Water **43**, 443–456 (2005)
154. Schulze-Makuch, D., Carlson, D.A., Cherkauer, D.S., Malik, P.: Scale dependency of hydraulic conductivity in heterogeneous media. Ground Water **37**, 904–919 (1999)
155. Seaman, J.C., Bertsch, P.M., Wilson, M., Singer, J., Majs, F., Aburime, S.A.: Tracer migration in a radially divergent flow field: longitudinal dispersivity and anionic tracer retardation. Vadose Zone J. **6**, 373 (2007)
156. Shah, C.B., Yortsos, Y.C.: The permeability of strongly disordered systems. Phys. Fluids **8**, 280–282 (1996)
157. Sheldon, N.D.: Abrupt chemical weathering increase across the Permian–Triassic boundary. Paleogeogr. Paleoclimatol. Paleoecol. **231**(3–4), 315–321 (2006)
158. Shlesinger, M.F.: Asymptotic solutions of continuous-time random walks. J. Stat. Phys. **10**, 421–434 (1974)
159. Silliman, S.E., Simpson, E.S.: Laboratory evidence of the scale effect in dispersion of solutes in porous media. Water Resour. Res. **23**, 1667–1673 (1987)
160. Sheppard, A.P., Knackstedt, M.A., Pinczewski, W.V., Sahimi, M.: Invasion percolation: new algorithms and universality classes. J. Phys. A, Math. Gen. **32**, L521–L529 (1999)
161. Stauffer, D.: Scaling theory of percolation clusters. Phys. Rep. **54**, 1–74 (1979)
162. Stauffer, D., Aharony, A.: Introduction to Percolation Theory, 2nd edn. Taylor and Francis, London (1994)
163. Stauffer, D., Sornette, D.: Log-periodic oscillations for biased diffusion on random lattice. Physica A **252**(3–4), 271–277 (1998)
164. Sternberg, S.P.K., Cushman, J.H., Greenkorn, R.A.: Laboratory observation of nonlocal dispersion. Transp. Porous Media **23**, 135–151 (1996)
165. Sudicky, E.A.: A natural gradient experiment on solute transport in a sand aquifer: spatial variability of hydraulic conductivity and its role in the dispersion process. Water Resour. Res. **22**, 725–741 (1986)
166. Sudicky, E.A., Cherry, J.A., Frind, E.O.: Migration of contaminants in groundwater at a landfill: a case study. IV. A natural gradient dispersion test. J. Hydrol. **63**, 81 (1983)
167. Tiedje, T.: Information about band-tail states from time-of-flight experiments. In: Pankove, J. (ed.) Semiconductors and Semimetals, vol. 21C, p. 207. Academic Press, New York (1984)
168. Tye, F.L.: Tortuosity. J. Power Sources **9**, 89–100 (1983)
169. van Genuchten, M.T.: A closed form equation for predicting the hydraulic conductivity of unsaturated soils. Soil Sci. Soc. Am. J. **44**, 892–898 (1980)
170. Vance, D., Teagle, D.A.H., Foster, G.L.: Variable quaternary chemical weathering fluxes and imbalances in marine geochemical budgets. Nature **458**, 493–496 (2009)
171. Vanderborght, J., Vereecken, H.: Review of dispersivities for transport modeling in soils. Vadose Zone J. **6**, 29–52 (2007)
172. Vervoort, R.W., Cattle, S.R.: Linking hydraulic conductivity and tortuosity parameters to pore space geometry and pore-size distribution. J. Hydrol. **272**, 36–49 (2003)
173. Wheatcraft, S.W., Tyler, S.W.: An explanation of scale-dependent dispersitvity in heterogeneous aquifers using concepts of fractal geometry. Water Resour. Res. **24**, 566–578 (1988)
174. White, A.F., Brantley, S.L.: The effect of time on the weathering rates of silicate minerals. Why do weathering rates differ in the lab and in the field? Chem. Geol. **202**, 479–506 (2003)
175. Winter, C.L., Tartakovsky, D.M., Guadagnini, A.: Moment differential equations for flow in highly heterogeneous porous media. Surv. Geophys. **24**(1), 81–106 (2003)
176. Xu, M., Eckstein, Y.: Use of weighted least-squares method in evaluation of the relationship between dispersivity and field scale. Ground Water **33**, 905–908 (1995)
177. Yu, B., Cheng, P.: A fractal permeability model for bi-dispersed porous media. Int. J. Heat Mass Transf. **45**, 2983–2993 (2002)
178. Zhang, X.X., Crawford, J.W., Deeks, L.K., et al.: A mass balance based numerical method for the fractional advection-diffusion equation: theory and application. Water Resour. Res. **41**(7), W07029 (2005)

179. Zhang, Y., Benson, D.A., Meerschaert, M.M., et al.: Space-fractional advection-dispersion equations with variable parameters: diverse formulas, numerical solutions, and application to the macrodispersion experiment site data. Water Resour. Res. **43**(5), W05439 (2007)
180. Zhang, X., Lv, M.: Persistence of anomalous dispersion in uniform porous media demonstrated by pore-scale simulations. Water Resour. Res. **43**, W07437 (2007)
181. Zhong, L., Liu, C., Zachara, J.M., Kennedy, D.W., Scezcody, J.E., Wood, B.: Oxidative remobilization of biogenic uranium(IV) precipitates: effects of iron(II) and pH. J. Environ. Qual. **34**, 1763–1771 (2005)

Chapter 12
Effects of Multi-scale Heterogeneity

It is commonly believed that problems with multi-scale heterogeneity present the biggest challenge to computation and understanding. A few such problems may be easily treated using percolation theory. We must point out here, however, that in the time since the publication of the second edition of this book, our research alone has called into question many of the assumptions regarding the *role* of multi-scale heterogeneity that is imposed through more complicated models, including some suggestions made in this book. Multi-scale heterogeneity does not need to exist in a medium in order for the dispersivity to be a linear function of length scale and the variogram range to be proportional to the linear dimension of the support volume. In addition, when we actually investigated experiments of the air permeability, k_a, on thirty-seven different media, we were able to find no evidence of the relevance of structural pores to the scaling of k_a with saturation. The simple universal scaling function from percolation appeared to describe soils with and without soil structure equally well. Thus we found no basis for assuming the relevance of a hierarchical model, in which the structural pores could be treated essentially in parallel with the textural pores. One could consequently argue that we should no longer present that treatment of the air permeability here. We keep it, however, for four reasons. One is that, in order to understand why we say that we found no evidence that such a hierarchical model was relevant, it is necessary to see what its predictions are. The second is that such dual porosity models have been around a long time and have been used to try to explain many things—even though our particular results seem to indicate that they are not necessary. The third is that it is instructive to see what self-consistent conclusions one can logically make when addressing problems of more complex media. The fourth is that it is too early to state that such hierarchical models will never be found to be relevant.

Three other problems will be dealt with, one treats a two-scale upscaling problem, where the percolation variable is different at the two scales, the second was only meant to be a schematic treatment of a geologic scale hierarchical problem, but appears to have captured the essence of a "scale effect" on the hydraulic conductivity. The third is a problem of saturation-dependent anisotropy in the hy-

A. Hunt et al., *Percolation Theory for Flow in Porous Media*,
Lecture Notes in Physics 880, DOI 10.1007/978-3-319-03771-4_12,

draulic conductivity at the U.S. Department of Energy Hanford site in Richland, WA.

12.1 Soil Structure

To a physicist without agricultural background the easiest way to imagine a soil with structure is to call back memories of throwing dirt clods. The relatively large spaces between the dirt clods would represent the "structural" pores, while the interior of the dirt clod contains "textural" pores. The soil structure refers to the existence of clods, called "aggregates," and the space between them, and knowledge of the structure implies knowledge of the statistics of the occurrence of aggregates of a given size, structural pores as a function of size, and any spatial correlations in their location. Realistically, however, one is fortunate indeed if one has a measurement of the distribution of structural pore sizes, even though soil structure has been a consistent subject of agricultural and soil physics research for about a half a century (e.g., [26]).

In any discussion of transport properties of such media one runs immediately into a conceptual problem. Imagine that the structural pores are relatively ordered and that they may be connected on a multi-centimeter grid like random resistors. Clearly one can represent the textural pores as shorter resistors (with larger resistance values) inside each grid cell, and allow them to connect to the structural resistances at the boundaries of each grid cell. But can one allow the resistances representing the textural pores in one grid cell to connect to those representing the textural pores in a neighboring grid cell without connecting to the structural pores that divide the cells? This is a critical conceptual problem, and to our knowledge there is no general answer. If one allows such connections, one has what is called a "dual porosity" model [19], if one does not, one has a hierarchical model. Since both types of model are used, there is clearly no general consensus as to what is physically allowed. The difference in transport is as follows. In the hierarchical model, when the saturation drops to the extent that water no longer occupies the structural pores, all processes which require a continuous water phase cease. Since this is clearly not the case in agricultural soils, dual porosity models are more common in the soil science literature. However, in geological applications with different contexts hierarchical models tend to be the rule.

When a dual porosity model is used for soil structure, the percolation treatment is relatively easy; the two contributions to the pore space are simply treated as though they exist in parallel to each other, and there are no additional limitations considered to transferring water between the structural and textural pores. As a consequence the total porosity of the medium is obtained using a sum of the contributions from the structural and textural pores. If both can be treated as fractals, for example, one has,

$$\phi_{\mathrm{s}} = \frac{3 - D_{\mathrm{s}}}{r_{s_{\mathrm{m}}}^{3-D_{\mathrm{s}}}} \int_{r_{s_0}}^{r_{s_{\mathrm{m}}}} r_{\mathrm{s}}^{2-D_{\mathrm{s}}} dr_{\mathrm{s}} \qquad \phi_{\mathrm{t}} = \frac{3 - D_{\mathrm{t}}}{r_{t_{\mathrm{m}}}^{3-D_{\mathrm{t}}}} \int_{r_{t_0}}^{r_{t_{\mathrm{m}}}} r_{\mathrm{t}}^{2-D_{\mathrm{t}}} dr_{\mathrm{t}} \tag{12.1}$$

and

$$\phi = \phi_s + \phi_t \tag{12.2}$$

Here the subscripts s and t stand for structural and textural respectively. As long as the smallest structural pore radius is larger than the largest textural pore, a general procedure can be formulated, which does not make any particular distinction between the two types of pores, except as regards critical volume fractions for percolation. Such values should be treated separately.

For simplicity it will be assumed here that the largest textural pore is smaller than the smallest structural pore. The data, with which the theoretical predictions are compared, will conform to that constraint. Then, as water drains from the medium, it will drain first from the structural pores, before it can begin to drain from the interior of the aggregates; this is simply another consequence of the Young-Laplace relationship between the tension and the pore radius. It is typical for researchers in the field of soil physics to assume that the effects of soil structure are limited to large moisture contents (e.g., [19]). Since we will use the same type model for the structural pores as for the textural pores, we will assume that the critical volume fraction for percolation of the structural pores is approximately $\phi_s/10$, exactly as assumed for textural pores *when the specific surface area is small*. For structural pores, with radii much larger than textural pores, this assumption is realistic. Since structural pores typically account for only about 10 % of the total porosity, $\phi_s/10$ is actually only about $\phi/100$, and can probably be set to zero without serious difficulty. Furthermore, setting the critical volume fraction for the structural pores equal to zero is consistent with the assumption that they do not provide a barrier to water flow at any water content (dual porosity) and with the assumption that they can drain completely. These characteristics also appear to be in accord with experiments generally.

Under the above conditions, the derivation of water retention curves is also brief. For $\theta > \phi_t$, one has,

$$\theta = \frac{3 - D_t}{r_{t_m}^{3-D_t}} \int_{r_{t_0}}^{r_{t_m}} dr_t r_t^{2-D_t} + \frac{3 - D_s}{r_{s_m}^{3-D_s}} \int_{r_{t_0}}^{r_{s>}} dr_s r_s^{2-D_s} \tag{12.3}$$

In Eq. (12.3) $r_{s>}$ refers to the largest structural pore that contains water, and it is given through the usual constraint, $r_{s>} = A/h$, where A is, also as usual, unknown in value. For $\theta < \phi_t$, the result of Chap. 4 applies, using the subscript t for textural pores. The fractal dimensionality of the textural pores is found exactly as already shown in Chap. 4. The fractal dimensionality of the structural pores is found by an analogous procedure, although in this case one often has direct data for the pores themselves, and not for a surrogate, such as the particle size. Since the ratio of smallest to largest particle size is typically assumed to be the same as that for the smallest to the largest pore size, there is no difference in the calculations. However, the scaling formulation for water retention will require the use of a parameter inversely proportional to the largest pore size, h_A, and knowledge of the largest structural pore size, but the largest particle size for the textural pores, makes a finding a relationship between these two quantities difficult without appealing to experiment.

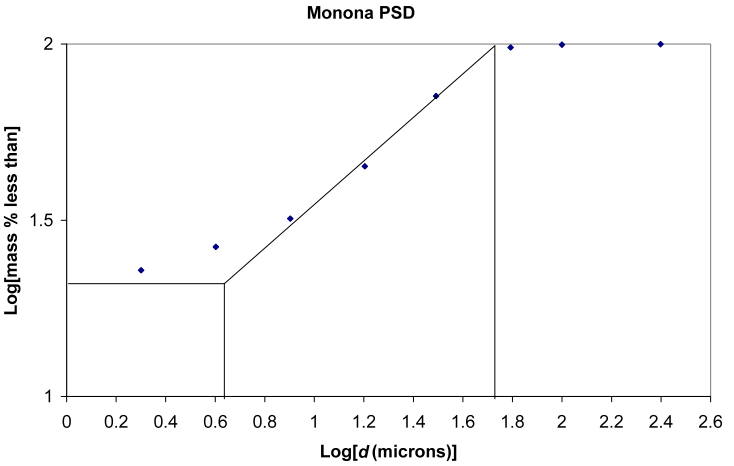

Fig. 12.1 Particle size data for the Monona soil (data unpublished, S. Logsdon)

The hydraulic conductivity is calculated as follows. For moisture contents $\theta \leq \phi_t$, such that the structural pores are empty, the result for K is exactly as in Chap. 5, but with all quantities (fractal dimensionality, critical moisture content, and porosity) referred to the textural pore space. For moisture contents $\theta > \phi_t$, such that some fraction of the structural pores is also wetted, the result for K is a sum of a constant term, corresponding to full saturation of the textural pores, and again a term of the same form as in Chap. 5, but written in terms of the structural quantities. In principle, the hydraulic conductivity for the structural pores should also undergo a cross-over from pore-size dominated to connectivity dominated forms, but in actual comparison with experiment such a cross-over is not included for five reasons: (1) the porosity associated with structural pores is so small (in the case to be considered, 0.04) that division into multiple ranges appears overambitious, (2) the cross-over moisture content depends on the critical volume fraction for percolation, which, though likely very small, is merely assumed to be zero, (3) the connectivity may not be completely percolation dominated, since plant roots (particularly in agricultural soils) may introduce a spatial scale (some regularity in separation), (4) in the range of lowest saturations of the structural pores, where the discrepancy between theory and experiment will be largest, the hydraulic conductivity due to the textural pores will dominate in many cases, (5) in most cases measurements of the hydraulic conductivity will never be accurate and detailed enough to discover the precise form of K in this range of moisture contents.

The particular case considered for comparison with experiment has $\phi_s = 0.04$, $\phi_t = 0.376$. The particle size data (given in Fig. 12.1) yield $D_t = 2.81$. The optical pore size data (given in Fig. 12.2) yield $D_s = 2.979$. The particle size data is nearly identical to the McGee Ranch soil, with $D = 2.81$, $r_m = 54$ μm and $r_0 = 4.3$ μm, so we use the same θ_t value, 0.11. Figure 12.3 shows the comparison between theory and experiment for the water retention curve. In order to obtain the agreement

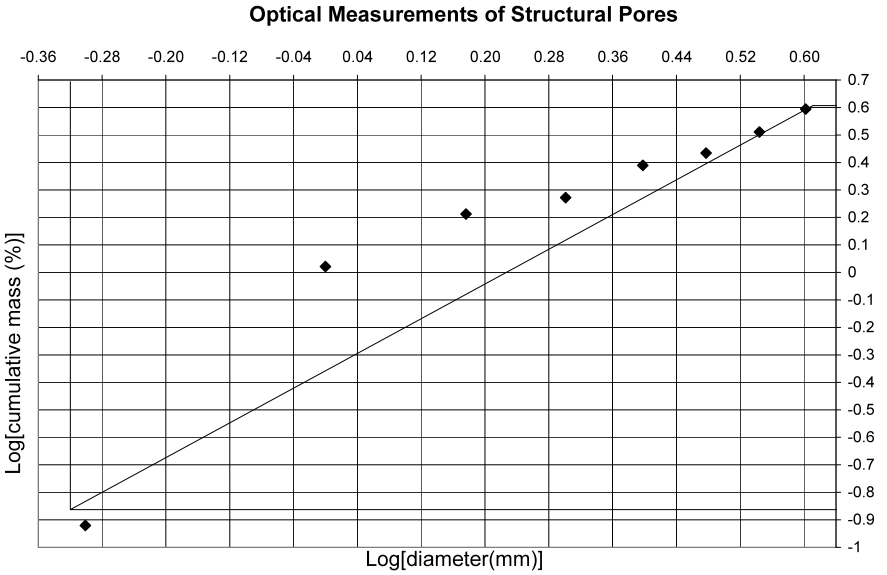

Fig. 12.2 Optical data for structural pores of a soil adjacent to the Monona soil

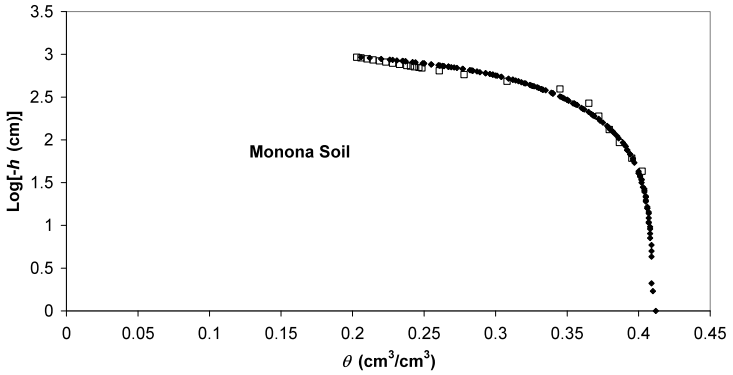

Fig. 12.3 Experimental data for the water retention function of the Monona soil together with the predictions of Eq. (12.3) for both the structural and textural pores separately. Two adjustable parameters, the equivalent air entry pressures for each pore size range, are used

shown, the air entry pressures for the textural and structural pores had to be chosen to be 340 cm and 26 cm, respectively. Thus the ratio of saturated hydraulic conductivities for the structural and textural pores must be assumed to be,

$$\frac{K_{S_s}}{K_{S_t}} = \left(\frac{340}{26}\right)^2 \frac{(1-0)^{\frac{3}{3-2.979}}}{(1-0.11)^{\frac{3}{3-2.81}}} = 1077 \tag{12.4}$$

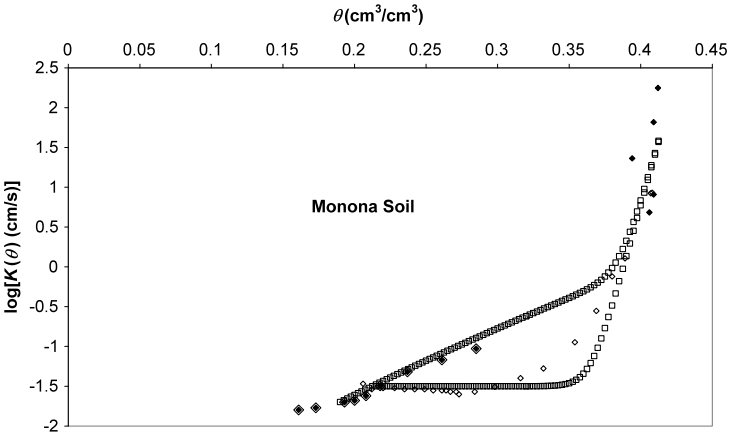

Fig. 12.4 Data for the hydraulic conductivity for several depths of the Monona soil. The predicted hydraulic conductivity from Eq. (6.16) using two parallel contributions, one from the textural pores and one from the structural pores. The porosities and fractal dimensionalities of each are known, and the ratio of the values of K_S is given by Eq. (12.4), so there is only one adjustable parameter in the comparison, the value of K_S for the structural pores. For the soil at the surface the theoretical prediction agrees. However, the experimental data at one depth drop more rapidly than predicted with declining moisture content and then remain constant, even though the moisture content continues to drop

Using these parameters, the hydraulic conductivity may be predicted using one adjustable parameter, K_{S_s}, and the comparison of that prediction with experiment is given in Fig. 12.4. This comparison appears reasonable for a one parameter prediction.

In another exercise consider the effects of the structural pores on the air permeability. In this case, the dual porosity treatment leads to a constant contribution to the air permeability from the structural pores for all water contents less than ϕ_t. This contribution masks the singular behavior of the contribution of the air permeability from the textural pores, and the air permeability appears nearly flat over most of the range of air-filled porosities. Then, for $\theta > \phi_t$, the singular behavior of the air permeability due to the structural pores causes a very rapid drop in air permeability as saturation is approached. The general effects of soil structure on the air permeability and hydraulic conductivity (as functions of saturation) are shown in Fig. 12.5. This result explains the general tendency for the minimal dependence of the air permeability on air-filled porosity for highly structured soils, as well as the perception that the air permeability may be non-zero at full saturation (since it is so difficult to achieve 100 % saturation, particularly with the large hydraulic conductivity associated with such large structural pores).

Note that, as expected with a small range of porosity associated with much larger pores, drainage of these larger pores causes the hydraulic conductivity to fall precipitously over a very small range of moisture contents before it drops more slowly over a wider range of moisture contents associated with the textural pores. This feature is very common among soils; in fact it is so common that the van Genuchten

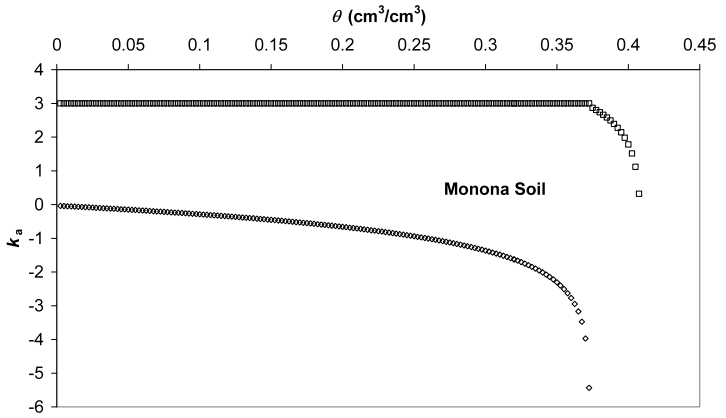

Fig. 12.5 Predictions of the air permeability for the Monona soil. The *open diamonds* describe the result of using Eq. (7.2) for the textural pores only. The *open squares* give the additional contribution from the structural pores

parameterization introduced in Chap. 3 was developed to predict such a change in curvature from positive to negative with diminishing moisture content. However, the van Genuchten parameterization attempts to unite all the ranges of moisture content into one function. It seems obvious that the structural pores need have no specific relationship with the textural pores, while at the dry end complications from incomplete equilibration may be introduced. This leads to major difficulties with the identification of the parameters of the van Genuchten function. See [8] for further comparisons.

Thus it is seen that when two scales of heterogeneity exists, one possible avenue of approach is to use a dual porosity model and apply critical path analysis and percolation scaling to both components of the porosity separately. While this sort of approach may be applicable to three or more scales of heterogeneity as well, the appeal of an approach, which is, (a) simple, (b) physically-based, and (c) parsimonious, diminishes with increasing complexity because of the diminution in parsimony. On the other hand, use of a van Genuchten type argument, which tacitly assumes a correspondence between the parameters of two different types of pores, also becomes less appealing with increasing levels of complexity, because its performance tends to worsen. Clearly any approach to problems with such an increase in complexity is going to suffer from some defect.

12.2 Variable Moisture Content

A significant problem in the soil science community arises from the understanding of the distributions of the saturated and unsaturated hydraulic conductivity. It is frequently assumed that the distribution of the saturated hydraulic conductivity is log-normal, but that the distribution of the unsaturated hydraulic conductivity

values is normal. However, we have seen in Chap. 7 that narrow distributions of measured K values ([13], for example) at low saturations may be more a product of the time limits of the experimenter than of the medium.[1] The often quoted results of Nielsen [18] appear to show that the values of K for steady flow under unsaturated conditions are log-normally distributed, but doubt has been cast on his results for the distribution of K values in the context of the doubt generated by his result that K is exponentially dependent on the moisture content. Most people in the soil science community believe that K is more nearly a power of saturation than an exponential function (as indeed expected from the Rieu and Sposito [22], model considered here in depth). So the question of how K is distributed for saturated and unsaturated conditions is of considerable interest to the soil sciences community.

Since hydraulic conductivity values in *geologic* media are typically spread out over many orders of magnitude, one of the goals of that community for a long time has been to try to "derive" a log-normal distribution for K. Formulations using separation of variables in the macroscopic equations (Laplace's equation), though simple, are clearly unfounded, since such equations tell us nothing about the microscopic details of conduction. We will consider only the soil science problems here.

The results of Chap. 10 appear to imply that, because K_S is determined through Poiseuille flow, it should be (approximately) normally distributed. We believe that the large spread in experimental results for "saturated" conditions is tied to the lack of control over the saturated moisture content (which can generate measurements of the saturated water content of the same sample at different US Department of Energy labs which differ by as much as 20 %). Given the huge effect of structural pores (with only 10 % of the porosity) on K discussed in the previous section, it is easy to comprehend that failure to saturate these pores could lead to huge underestimations of K_S. But, although we believe that complications due to saturation are very likely the cause of these results, first consider the following potential explanation for Nielsen's experiments.

Below is presented a brief description of a compound upscaling procedure, which yields a distribution of unsaturated K values which is (approximately) log-normal for local values of the $K(S)$, which are exponential functions of the moisture content [6]. This result would then be compatible with the conditions of Nielsen's experiments [18].

Rewrite Eq. (6.16) as

$$K(S) = K_S\left[1 - \phi\frac{1-S}{1-\theta_t}\right]^{\frac{3}{3-D_p}} \tag{12.5}$$

In the limit $D_p \to 3$ (with the consequent condition that $\phi \to 0$, Eq. (12.5) yields

$$K(S) = K_S \exp\left[-3\left(\frac{1-S}{1-\theta_t}\right)\ln\left(\frac{r_m}{r_0}\right)\right] \tag{12.6}$$

[1]The fact that these authors tended to replace equilibrium K values less than 5×10^{-8} cm/s with approximately this value (which represented a maximum experimental time) narrowed the widths of their K distributions drastically in the limit of small θ.

Although Rieu and Sposito [22] state explicitly that $D_p < 3$ for their discrete fractal model, there is no reason in a continuum model why $r^3 W(r) = r^{2-D_p}$ cannot be proportional to r^{-1}. In fact using $D_p = 3$ explicitly leads precisely to the result that $K(S)$ is an exponential function of saturation [8], though of not quite the same form as Eq. (12.6).

If one considers the possibility that the moisture content can vary over length scales much smaller than a field measurement (such as Nielsen's), then Eq. (12.6) could describe the local variability of K due to variable saturation. In the case of steady flow, the local moisture contents would not be changed by definition, and one could apply an upscaling procedure to Eq. (11.6). If the local saturations were normally distributed with mean S_m and standard deviation σ_S, then applying critical path analysis [6] to Eq. (12.6) would yield

$$K(S) = K_S \exp\left[-3\left(\frac{1 - S_m - c\sigma_S}{1 - \theta_t}\right)\ln\left(\frac{r_m}{r_0}\right)\right] \tag{12.7}$$

where c is a numerical constant (σ_S was mistakenly referred to in [6], as the variance of S). The value of c would be larger for smaller critical volume fractions. Such values of the critical volume fraction for percolation would not be correlated with θ_t for the critical moisture content at the pore scale. Thus Nielsen's [18] measurements of an (approximately) exponential form for $K(S)$ on a large scale (Eq. (12.7)) could be consistent with an exponential form on a smaller scale as well (Eq. (10.5)), and application of cluster statistics of percolation theory to Eq. (12.6) would yield a distribution of K values that was approximately log-normal (an approximation for at least two reasons, clearly).

But actually Eq. (12.5) can be approximated (to first order) by an exponential dependence of K on S in another limit as well, namely that $S \to 1$ for arbitrary D_p. If the soil is not structured, the fractal dimensionality is likely to be more nearly 2.8 (occasionally as high as 2.9). For the case $D = 2.9$, a variation of the moisture content of 20 %, for $\phi = 0.4$ and $\theta_t = 0.04$, would produce a variation in K of only a factor 50. But in the case of structural pores we found that the fractal dimensionality can be very near 3 (2.98) on account of the small associated porosities. With D so near 3 the exponential approximation is quite accurate. Further, variation of the moisture content of only 10 % (0.04 for a total porosity of 0.4) can cause a variability in K over a factor 500 because of the large power $(3/(3 - D) = 150)$. This range of variability in K is also roughly compatible with a log-normal distribution, and ultimately for much the same reasons as might explain the Nielsen [18] experiments.

Thus it is suggested that measurements of both the saturated and unsaturated hydraulic conductivity distributions can be strongly affected by experimental error: In the first case a relatively narrow distribution can be perceived to be very wide if the moisture content is not controlled carefully, and in the second case a very wide distribution can be perceived as very narrow because of the influence of the time constraints of the experiment.

12.3 A Schematic Hierarchical Problem

Media with geological complexity are difficult even to describe. If the description of a medium is too complex, an analytical application of concepts from percolation theory is not likely to exist. The purpose here is not to address such complications seriously; in fact, we would claim that attributing what seem to be exotic behaviors of the hydraulic conductivity to exotic descriptions of porous media may be misleading. If these "exotic" media appear to produce an increase in K with increasing scale of the medium, then there appears to be a problem of conceptualization. Thus we seek for simpler causes of such apparent scale effects using known physics and idealized, but easily verifiable, models. In Chaps. 8 and 9 the examples of non-equidimensional support volumes and anisotropic hydraulic conductivity fields were treated, and shown to lead to apparent scale effects. In this chapter it will be shown that multiple scales of heterogeneity can also lead to a (mistaken) conclusion that hydraulic conduction becomes easier with increasing length scales.

Consider the following idealized medium [7] composed of seven different types of material, each of which has seven subunits. Let the hydraulic conductivity have a log-uniform distribution in each of the 49 subunits. Make these individual distributions overlap in the following way, The most highly conductive unit has hydraulic conductivities from 2^0 to 2^{-6}, in equal proportions, while the next most conductive unit has hydraulic conductivities from 2^{-3} to 2^{-9}, the third from 2^{-6} to 2^{-12}, etc., as shown in Fig. 12.6. No assumption is made regarding the shapes of the individual volumes, which means that this problem is best treated using continuum percolation theory. If one approaches the upscaling of this medium with a "coarse graining" procedure, then the effective conductivity of each subunit is first found, and then the heterogeneous subunits are replaced with a homogeneous material characterized by the effective subunit conductivity. Since the critical volume fraction for percolation

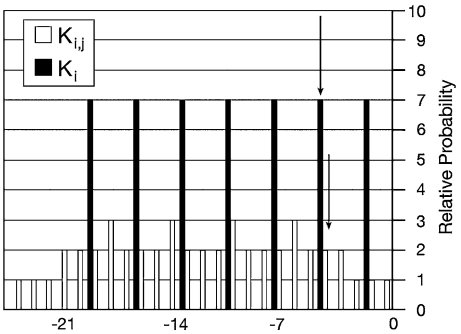

Fig. 12.6 Discrete hydraulic conductivity distributions for two-scale medium as described in text. The *open bars* are the composite distribution of the seven overlapping subunits, each with log-uniform distributions. The *solid bars* are the effective conductivities of each of the subunits, each of which has an equal chance of being encountered. The *arrows* point to the effective conductivity of the system, upscaled from the subunit scale and from the unit scale. The two values are identical (From Hunt [7])

in 3D will be less than 0.5, if repeated often, such a procedure will tend to overestimate the hydraulic conductivity at the largest scales, since most of the volume of any given subunit will have a smaller conductivity than the effective value.

A common value of the critical volume fraction for such continuum problems is ca. 15 % (see Chap. 1 as well), though, as has been seen for problems at the pore scale, even much smaller values can occur. A point of the coarse-graining of such a self-similar medium is that V_c must remain the same at every scale. Applying continuum percolation theory to each of the subunits individually leads to effective K values of 2^{-1}, 2^{-4}, 2^{-7}, 2^{-10}, 2^{-13}, 2^{-16}, and 2^{-19}, as indicated in Fig. 11.6. In each case the quoted value of K is the second largest in the subunit because the volume associated with the largest value of K is only $1/7 \approx 0.143 < 0.15$, and is thus insufficient to "percolate." The median (geometric mean) values of K in each of these units are, however, 2^{-3}, 2^{-6}, 2^{-9}, 2^{-12}, 2^{-15}, 2^{-18}, and 2^{-21}, each a factor 2^2 smaller than the effective K value. If continuum percolation is again applied to the seven units with the above seven K values, the effective K value for the entire medium is 10^{-4}, again the second largest of seven values. Further, if continuum percolation theory is applied to the composite distribution of all 49 subunits simultaneously, the effective K value obtained for the entire medium is also 2^{-4}, provided that the same value, 0.15, is used for V_c. The median, or geometric mean value of the geometric means of the subunits is 2^{-12}, which is too small by a factor of 2^8. Clearly the value of V_c in the latter case may not be quite 0.15. On the other hand, the coarse-graining procedure is also slightly inaccurate. Nevertheless each of these uncertainties is small compared to the error incurred by assuming that the upscaled value of K is closely related to the geometric mean value of K. Further, relating the effective K to the geometric mean value tends to produce an underestimation of K, which grows with increasing scales. The point of this exercise, however, is that the existence of multiple scales of heterogeneity does not lead to an increase in an effective K value with increasing scale, even though certain quantities often taken as predictors of the effective K value do increase with increasing scale.

To make this exercise a little more quantitative we make a specific comparison of the predicted upscaled values of K with the Matheron [16] conjecture, often regarded as a standard means of upscaling K. It was derived specifically for Gaussian random fields in 1 and 2 dimensions, and has been generalized to 3 dimensions, although it has been proved that it cannot be general in 3D. In any case the Matheron conjecture is expressed as follows,

$$K_{\text{eff}} = K_{\text{g}} \exp\left[\sigma^2\left(\frac{1}{2} - \frac{1}{d}\right)\right] \tag{12.8}$$

In this expression K_{g} is the geometric mean, d is the dimensionality of the medium, and σ^2 is the variance of the (log) conductivity distribution. Note that for $d = 2$ the Matheron result yields $K_{\text{eff}} = K_{\text{g}}$, which itself cannot be general as already seen in Chap. 2, as the effective conductivity depends very sensitively on the local connectivity. One can calculate the variance of the conductivity distributions given here very easily and then compare the results of an "enhancement factor," $K_{\text{eff}}/K_{\text{g}}$ for both the Matheron conjecture and continuum percolation. This comparison is given in Table 12.1. This calculation for the Matheron conjecture is not strictly valid, of

Table 12.1 Factors representing enhancement of K relative to geometric mean value. Percolation values are calculated using assumed V_c of 0.15. Values in parentheses calculated from $V_c = 0.06$. Subunit scale is upscaled from the subunit values. Unit scale is upscaled from the unit values. Composite means the entire distribution. Product is the product of the enhancements at the subunit and the unit scales

Method	Subunit scale	Unit scale	Composite	Product
Percolation	2^2 (2^3)	2^6 (2^9)	2^8 (2^{11})	2^8 (2^{12})
Stochastic	$2^{0.53}$	2^7	$2^{6.8}$	$2^{7.53}$

course, since the distributions chosen were log-uniform rather than log-normal. The result is that the Matheron conjecture also tends to underestimate the value of K_{eff}, especially in media with multiple scales of heterogeneity. Furthermore, these underestimations already become noticeable in the case of $V_c = 0.15$. As has been seen, however, at the pore scale V_c can be much smaller than 0.15, and this is likely the case in some geological problems as well, though for some, V_c may also be larger than 0.15. In fact, the point of a small, but growing body of literature is to answer the question of why critical site percolation probabilities are so low in geologic media (most of these works, e.g., [21, 25, 27], divide the medium up into blocks of uniform size and look to correlations in the block conductivities to explain critical percolation probabilities much lower than 0.3116 for a cubic lattice, rather than comparing such probabilities with continuum values, starting from Scher and Zallen [24]). For $V_c = 0.06$, the Matheron conjecture underestimates the hydraulic conductivity by more than four orders of 2, or more than two-thirds the width of an individual subunit distribution.

Note that the value of K at any scale is contained within the distribution of K values at all smaller scales. However, especially for V_c very small, it may be located well into the tail of the distribution. Under such circumstances (if $V_c = 0.05$) limitations in sampling (significantly less than $20 = 1/0.05$ samples) might suggest that the value of K at a larger scale was not represented at all at the smaller scale. So the general implications of continuum percolation theory are that inference of a increase in K with increasing scale may be due to inadequate sampling (in the case of very small V_c) as well as inappropriate inferences due to established methods of inferring K_{eff}.

Figure 12.7 gives a schematic representation of the predicted dependence of measured values of K as a function of scale. This representation is schematic because the representation in terms of system size does not follow automatically from the representation in terms of hierarchical rank (Fig. 12.6). Figure 12.8, from McPherson [17], gives actual K measurements as a function of scale. Note the general similarity.

12.4 A More Realistic Hierarchical Problem

This subsection combines pore scale modeling with geologic scale modeling. In particular, results of pore scale predictions are then used as inputs into geologic

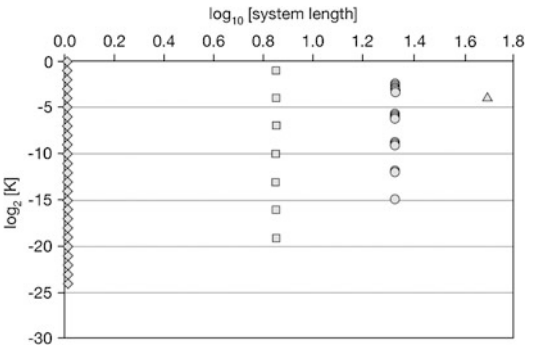

Fig. 12.7 For the system of Fig. 12.6 the distribution of K values as a function of linear scale

scale predictions. The results have practical relevance [12] and turned out to be accurate.

Flow in the subsurface at the U.S. Department of Energy Hanford site under unsaturated conditions shows evidence of anisotropy [31, 33, 34]. This anisotropy is expressed in the predominantly horizontal transport of moisture. Underlying the anisotropic character of the flow is its dependence on anisotropic sedimentary structures on many spatial scales [14, 15]. Any anisotropy in the flow can be logically assumed to lead to anisotropic spreading of contaminants, which appears to have been observed in the case of Technetium [5].

$^{43}Tc_{99}$ is spreading mostly laterally through the U.S. Department of Energy Hanford site sediments. An important question to try to answer is: over what length scale can the transport remain horizontal before the $^{43}Tc_{99}$ is likely to be transported ver-

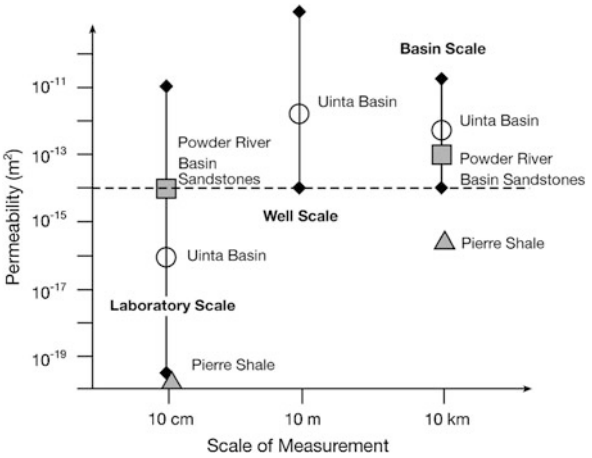

Fig. 12.8 Effect of scale on permeability of rocks in 3 different sedimentary basins in the United States including the Uinta Basin of Utah [32], the Powder River Basin, Wyoming, and the Pierre shale in South Dakota [4]. *Dashed line* at 10^{-14} m^2 indicates average crustal permeability inferred by Brace [3]. *Error bars* associated with Uinta Basin data reflect the full range of permeability evaluated at each scale (reprinted by permission from [17])

tically to the water table. In a medium with sufficient randomness to be treated with the framework of percolation theory, even if anisotropy exists, it must be possible mathematically to transform the medium so as to make it isotropic. In that case, percolation in the vertical and horizontal dimensions must coexist. Practically speaking this means that at some large enough length scale, vertical flow must be as easy as horizontal flow and the Technetium will be transported vertically to the water table. Of course there are many potential vertical transport paths, which might not be treatable in percolation theory, such as vertical conduits known as clastic dikes [29]. If the Technetium transport is controlled by such features (because it occurs at smaller horizontal length scales than what we would predict), our proposed procedure will not be relevant.

An area of the U.S. Department of Energy Hanford called the Vadose Zone Transport Field Study (VZTFS) [30] was selected for study based partly on its earlier study by Sisson and Lu [28], and partly on its potential relevance to the subsurface of the BC Crib area, where the cited Technetium discharge was located. The sediments in the vicinity of the VZTFS consist principally of sand with interstitial silt and silt beds [14, 15]. The hydraulic conductivity is a strongly varying function of moisture content, as we have seen. The Hanford subsurface, located in a semi-arid region, typically has fairly high tensions, h. Thus, at higher tensions in the unsaturated zone, the hydraulic conductivity may be strongly anisotropic as a consequence of the tendency of finer soils to retain more water than coarser ones, and for these soils to have been deposited primarily in horizontal structures. This apparent anisotropy may have some important consequences for the Tc transport.

We proposed Hunt and Skinner [12] the following procedure to address this question:

(1) Use critical path analysis from percolation theory [1, 20] to predict the unsaturated hydraulic conductivity [2, 11] at the sample scale using soil physical information [23] from relevant soils at the U.S. Department of Energy Hanford site, (2) Find the relevant parameters regarding the statistical occurrence and physical extent of such soils [23, 29], (3) Use critical path analysis again together with clusters statistics of percolation theory to predict the distribution of hydraulic conductivity, K, values at geologic scales and with geologic complications such as anisotropy [9, 10], (4) Use sample scale information to generate the appropriate input parameters for the geologic scale treatment, (5) Use the predicted K distribution at geologic scales to estimate the risk involved in a particular solute spill.

Since all the theoretical work is already described in this book, the present discussion can be restricted to finding the necessary input parameters to develop the appropriate output for analysis.

One important input that should be mentioned is that of a quasi-equilibrium assumption; namely that the tension h is constant at a given elevation across soils of different type.

We hypothesized that one could find a distribution of hydraulic conductivity values at a given tension and force that distribution of conductivity values into the form of the Rieu and Sposito [22] distribution.

Specifically we used Eq. (10.7) and Eq. (10.8) to predict the distribution of vertical K values (referenced to the typical horizontal hydraulic conductivity) that one

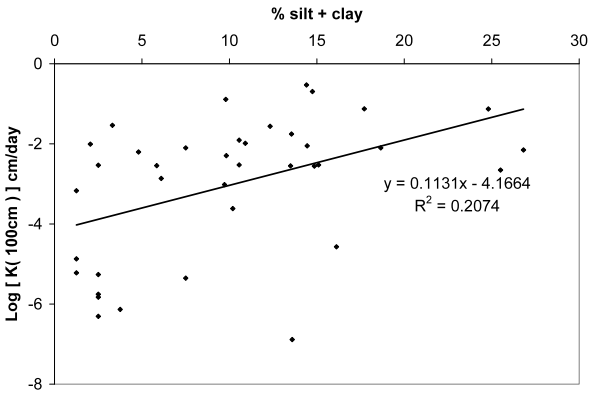

Fig. 12.9 Predicted $K(h = 100\text{ cm})$ for 39 VZTFS soils (source [23]) as a function of fine content percentage (silt + clay). Note that the relationship is very similar if plotted against silt content (not shown). Note also that the R^2 value is lower than if $K(h = 100\text{ cm}/K_S)$ is correlated with fine content since the absolute $K(h = 100\text{ cm})$ depends on K_S as well, and K_S has a slight negative correlation with fine content

would expect to find at a given spatial scale. These equations require several parameters as input, namely an effective porosity, and effective fractal dimensionality, a ratio of a maximum to minimum K, and a relevant length scale. The first three parameters are, as noted previously, not independent as formulated in the Rieu and Sposito model. The next paragraphs will explain how we estimated appropriate parameters, and then we will present the results.

Schaap et al. [23] give particle size data, water retention curves, and the saturated hydraulic conductivity for 53 of 60 soils investigated at the VZTFS site. We took our methods from Chap. 6 [2] to predict the hydraulic conductivity as a function of tension for 39 of these soils. The soils discarded were eliminated due to data problems (cumulative mass fractions with negative slopes, missing saturated values of the hydraulic conductivity, etc.). The reader will note that the following discussion is very practically based, partly because we force data to be compatible with a given subsurface model. Yet we know that the universal aspects of percolation theory tend to make most model characteristics nearly irrelevant, except for the magnitudes of some of the parameters.

We predicted $K(\theta)$ in terms of K_S using the particle size data as a proxy for the pore size data. We matched predicted and observed water retention curves in order to extract h_A, the air entry pressure, and then used the predicted $\theta(h)$ curve together with the predicted $K(\theta)$ and the observed K_S in order to generate K as a function of h without any unknown parameters. We then used summaries of the data to generate our distributions of K values. In fact, we used parameters from these data in order to generate parameters for the K distributions.

Specifically, we produced regressions of $K(h)$ on total silt + clay content for each of three values of h (50 cm, 100 cm, and 200 cm, the latter two in Figs. 12.9 and 12.10). We used the regression equation to generate typical values of K for relatively fine-rich, K_{loam}, and fine-poor, K_{sand}, soils (at two specific values of fine

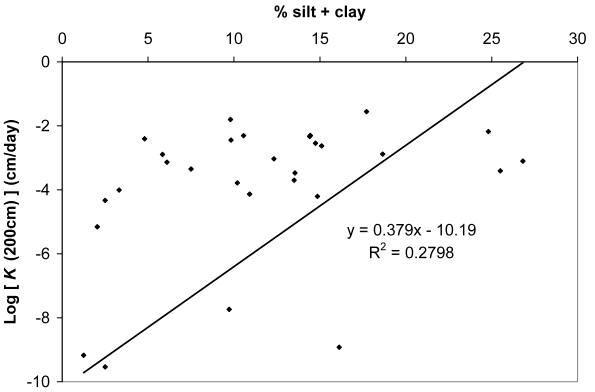

Fig. 12.10 Predicted K ($h = 200$ cm) for 39 VZTFS soils (source [23]) as a function of fine content percentage (silt + clay)

content, 7.6 % and 20.1 %). These two values were identified by taking (arbitrarily) half the maximum fine content (26.8 %) as the value (13.4 %), which distinguishes between fine-rich and fine-poor soils, and then taking the average values of fine content in each range separately. When fine-rich soils had appreciably higher K than fine-poor soils (at $h = 100$ and $h = 200$ cm) we used the ratio $K_{\text{loam}}/K_{\text{sand}}$ in each case to represent the square of the ratio of largest to smallest pore size in the Rieu and Sposito model. The results were $K_{\text{loam}}/K_{\text{sand}} = 54{,}800$ at $h = 200$ cm, and $K_{\text{loam}}/K_{\text{sand}} = 25.8$ at $h = 100$ cm. Clearly the anisotropy at $h = 100$ cm was too small to be relevant. While $h = 200$ cm is too large a tension to be relevant in the field (Rockhold, personal communication, 2008), we also know [11] that the procedures associated with laboratory measurements tend to produce h_{A} values about twice what is usually found in the field. This means that, in fact, the anisotropy that we found for $h = 200$ cm should be relevant for field conditions with $h = 100$ cm. Then we took the fraction of the fine-rich soils as an analogue to the porosity, completing the analogy. In our case 14 out of 39 of these soils had fine content greater than 13.4 %, so we had an effective porosity of 14/39. We then used the relationship $\phi = 1 - (r_0/r_{\text{m}})^{3-D}$ to find the effective fractal dimensionality, D. From this we could use Eqs. (10.7) and (10.8) to produce the final two Figs. 12.11 and 12.12. Note that there is a volume scale in this figure, and that volume scale is relevant. Nevertheless, the amount of work needed to fix that scale using semi-variograms for the hydraulic conductivity (given in [29]) is too great to reproduce here. However, there were at least three distinct spatial scales present in those variograms. We related the smallest scale to the support volume, rather than to relevant structures in the subsurface. When we chose the intermediate volume scale of ca. 40 m^3 (as potentially most suitable to a compound upscaling based on pore-scale results) we generated a prediction [12] that when the Tc plume spreads to about 10,000 m^3, we should expect vertical transport to become about a factor $10^{-1/2} \approx 1/3$ as rapid as horizontal transport. The horizontal scale that we deduced from this was about 70 m. This value appears to be two orders of magnitude too small when compared with field data [5] which appear to show nearly 10 km of predominantly horizontal migration. However, we have subsequently learned (J. Zachara and C. Liu, personal communication, 2011) that the appropriate scale for relevance of vertical transport

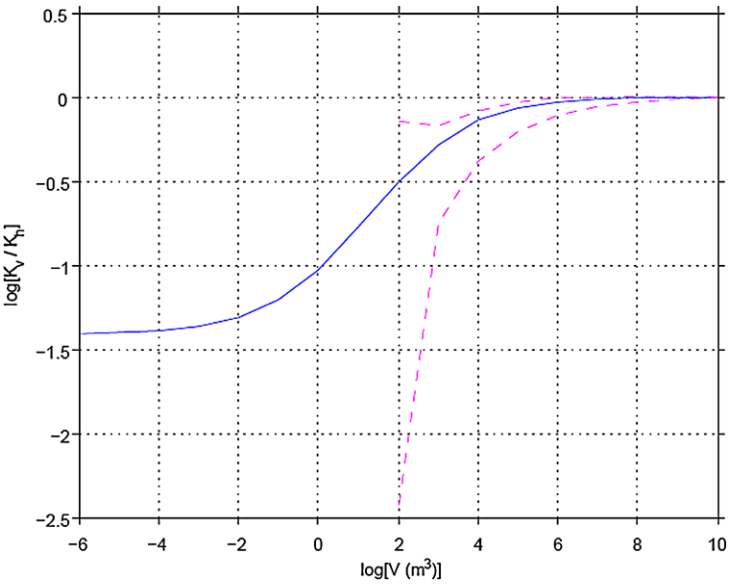

Fig. 12.11 Predicted distribution of K_v values as a function of plume volume for the case that typical conditions favor $h = 100$ cm. In this case $D = 2.72$ and $R = 5.08$. Note that the expected K_v/K_h is ca. $1/5$ at a volume of about 43 $m^3 = 6$ m $\times$ 6 m $\times$ 1.2 m, whereas the expected ratio is ca. $1/3$ at a volume of about 1,000 m^3. Both of these values would be too small to account for significant anisotropy in spreading

is approximately 100 m, and the discrepancy with our purely theoretical predictions [12] was merely 30 %.

Problems

12.1 Repeat the calculations of K for nested heterogeneity that led to the entries of Table 12.1, but using a critical volume fraction of 0.10.

12.2 Allow K to follow a log-uniform distribution with a prescribed width equal to that of the example in Sect. 12.3, and discretize the distribution as in the procedure there. Find the upscaled K as a function of an arbitrary critical volume fraction. Find the value of the critical volume fraction which yields the Matheron conjecture (Eq. (2.30)). How does this critical volume fraction compare with the typical value of about 0.16 quoted in the literature? Is it possible for the Matheron conjecture to be accurate for all values of the width parameter using the same critical volume fraction?

12.3 Consider Problem 12.2 again, but allow nested heterogeneity analogously to the procedure of this chapter. Thus the critical volume fraction is, to a good approximation, independent of scale. Investigate the performance of the Matheron conjecture for the upscaling at both scales; does choice of the critical

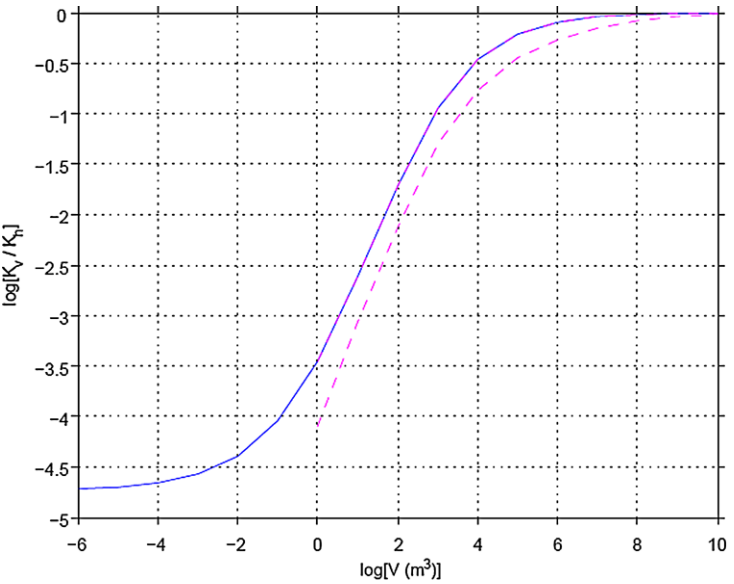

Fig. 12.12 Predicted distribution of K_v values as a function of plume volume for the case that typical conditions favor $h = 200$ cm. In this case $D = 2.918$ and $R = 234$. Note that the expected K_v/K_h is ca. $1/200$ at a volume of about 43 $m^3 = 6$ m $\times$ 6 m $\times$ 1.2 m, whereas the expected ratio is ca. $1/2$ at a volume of about 10,000 m^3. At volumes 10,000 m^3 it is thus relatively common to find K_v values as high as $1/2$ the expected K_h. This implies that a plume spreading through individual soil units of volume 43 m^3 (and length 6 m) can spread to a distance of roughly $(10{,}000/43)^{1/2}6$ m ≈ 100 m in length before it is likely to begin spreading vertically

volume fraction of Problem 12.2, which guarantees equivalence to the Matheron conjecture at the lowest length scale, also guarantee equivalence to the Matheron conjecture at the next higher length scale?

References

1. Ambegaokar, V.N., Halperin, B.I., Langer, J.S.: Hopping conductivity in disordered systems. Phys. Rev. B **4**, 2612–2621 (1971)
2. Blank, L.A., Hunt, A.G., Skinner, T.E.: A numerical procedure to calculate hydraulic conductivity for an arbitrary pore size distribution. Vadose Zone J. **7**, 461–472 (2008)
3. Brace, W.F.: Permeability of crystalline and argillaceous rocks. Int. J. Rock Mech. Min. Sci. **17**, 242–251 (1980)
4. Bredehoeft, J.D.: Groundwater—a review. Rev. Geophys. **21**, 760765 (1983)
5. Cole, C.R., Wurstner, S.K., Bergeron, M.P., Williams, M.D., Thorne, P.D.: Three-dimensional analysis of future groundwater flow conditions and contaminant plume transport in the Hanford site unconfined aquifer system. FY 1996 and 1997 status report, PNNL 11801, Pacific Northwest National Laboratory, Richland, WA 99352 (1997)
6. Hunt, A.G.: Applications of percolation theory to porous media with distributed local conductances. Adv. Water Resour. **24**(3,4), 279–307 (2001)

7. Hunt, A.G.: Some comments on the scale dependence of the hydraulic conductivity in the presence of nested heterogeneity. Adv. Water Resour. **26**, 71–77 (2003)
8. Hunt, A.G.: An explicit derivation of an exponential dependence of the hydraulic conductivity on saturation. Adv. Water Resour. **27**, 197–201 (2004)
9. Hunt, A.G.: Scale-dependent dimensionality cross-over; implications for scale-dependent hydraulic conductivity in anisotropic porous media. Hydrogeol. J. (2005). doi:10.1007/s10040-005-0453-6
10. Hunt, A.G., Blank, L.A., Skinner, T.E.: Distributions of the hydraulic conductivity for single-scale anisotropy. Philos. Mag. **86**, 2407–2428 (2006)
11. Hunt, A.G., Gee, G.W.: Application of critical path analysis to fractal porous media: comparison with examples from the Hanford site. Adv. Water Resour. **25**, 129–146 (2002)
12. Hunt, A.G., Skinner, T.E.: A proposed analysis of saturation-dependent anisotropy for U.S. DOE Hanford site soils. Hydrogeol. J. (2009). doi:10.1007/s10040-009-0499-y
13. Khaleel, R., Relyea, J.F.: Variability of Gardner's alpha for coarse-textured sediments. Water Resour. Res. **37**, 1567–1575 (2001)
14. Last, G.V., Caldwell, T.G.: Core sampling in support of the vadose zone transport field study. PNNL-13454, Pacific Northwest National Laboratory, Richland, WA 99352 (2001)
15. Last, G.V., Caldwell, T.G., Owen, A.T.: Sampling of boreholesWL-3A through -12 in support of the vadose zone transport field study. PNNL-13631, Pacific Northwest National Laboratory, Richland, WA 99352 (2001)
16. Matheron, G.: Elements Pour Une Theorie des Milieux Poreux. Masson et Cie, Paris (1967)
17. McPherson, B.J., the EarthLab Steering Committee: EarthLab: A Subterranean Laboratory and Observatory to Study Microbial Life, Fluid Flow, and Rock Deformation. Geosciences Professional Services, Inc., 60 pp. (2003)
18. Nielsen, D.R.: Spatial variability of field-measured soil-water properties. Hilgardia **42**, 215–259 (1973)
19. Nimmo, J.R.: Modeling structural influences on soil water retention. Soil Sci. Soc. Am. J. **61**, 712–719 (1997)
20. Pollak, M.: A percolation treatment of dc hopping conduction. J. Non-Cryst. Solids **11**, 1–24 (1972). doi:10.1016/0022-3093(72)90304-3
21. Proce, C.J., Ritzi, R.W., Dominic, D.F., Dai, Z.X.: Modeling multiscale heterogeneity and aquifer interconnectivity. Ground Water **42**, 658–670 (2004)
22. Rieu, M., Sposito, G.: Fractal fragmentation, soil porosity, and soil water properties I. Theory. Soil Sci. Soc. Am. J. **55**, 1231 (1991)
23. Schaap, M.G., Shouse, P.J., Meyer, P.D.: Laboratory measurements of the unsaturated hydraulic properties at the vadose zone transport field study site. PNNL Report, 14284, Pacific Northwest National Laboratory, Richland, WA 99352 (2003)
24. Scher, H., Zallen, R.: Critical density in percolation processes. J. Chem. Phys. **53**, 3759 (1970)
25. Shah, C.B., Yortsos, Y.C.: The permeability of strongly disordered systems. Phys. Fluids **8**, 280–282 (1996)
26. Sharma, M.L.: Influence of soil structure on water retention, water movement, and thermodynamic properties of absorbed wate. Ph.D. Thesis, Univ. Hawaii, 190 pp. Univ. Microfilms, Ann Arbor, Mich. (1966) [Diss. Abst. 28 17600B (1966)]
27. Silliman, S.E.: The influence of grid discretization on the percolation probability within discrete random fields. J. Hydrol. **113**, 177–191 (1990)
28. Sisson, J.B., Lu, A.H.: Field calibration of computer models for application to buried liquid discharges: A status report. RHO-ST-46 P. Rockwell Hanford Operations, Richland, WA 99352 (1984)
29. Ward, A.L.: Vadose zone transport field study: Summary report. PNNL Report 15443, Pacific Northwest National Laboratory, Richland, WA 99352 (2006)
30. Ward, A.L., Caldwell, T.G., Gee, G.W.: Vadose Zone Transport field study: soil water content distributions by neutron moderation. PNNL Report 13795, Pacific Northwest National Laboratory, Richland, WA 99352 (2000)

31. Ward, A.L., Zhang, Z.G., Gee, G.W.: Upscaling unsaturated hydraulic parameters for flow through heterogeneous anisotropic sediments. Adv. Water Resour. **29**, 268–280 (2006)
32. Willett, S.D., Chapman, D.S.: Temperatures, fluid flow and the thermal history of the Uinta Basin. In: Collection Colloques et Seminaires—Institut Francais du Petrole, vol. 45. Technip, Paris (1987)
33. Ye, M., Khaleel, R., Yeh, T.-C.: Stochastic analysis of moisture plume dynamics of a field injection experiment. Water Resources Research **41** (2005). doi:10.1029/2004WR003735
34. Yeh, T.-C., Ye, M., Khaleel, R.: Estimation of effective unsaturated hydraulic conductivity tensor using spatial moments of observed moisture plume. Water Resources Research **41** (2005). doi:10.1029/2004WR003736

Chapter 13
Misconceptions

Looking over the research presented in this book, we realize that some in the porous media community will find its implications difficult to accept. Two challenging implications stand out: (1) many concepts that are believed to be understood are actually erroneous, and are hindering progress, and (2) the feeling that some issues are unfathomably complex has caused many to retreat to application-specific empirical models, rather than seeing and addressing the underlying complexity. But our research, with over 9000 comparisons of theory and measurement detailed in this book, shows that some established concepts *should* be replaced, and that complexity *can* be addressed. In that light, here we summarize some misconceptions that we believe are retarding progress in studies of porous media. A few of these have recently been published [2], but this broader summary is new.

It should have been recognized long ago that saturation-dependent properties should be analyzed in terms of percolation theory. The relevant literature traces back to the 1970s, so we have had an unnecessary half-century of persistent confusion and wasted opportunity. The difficulties that arise because percolation theory is ignored in this context are too numerous to count, but some resulting misconceptions are enumerated below. Percolation theory provides a coherent conceptual framework within which many ostensibly disparate processes are seen to have underlying commonalities. The history of science shows the power of unifying concepts to explain, to suggest and guide investigations, and to focus attention on underlying rather than peripheral (or worse, artifactual) issues.

Because percolation theory incorporates scale-dependence considerations, ignoring percolation theory has resulted in a misunderstanding of the nature of parameters. The continuum partial differential equations upon which much research into porous media is based contain parameters whose scale-dependence is not recognized. Their values cannot be calculated within the framework in which they are grounded. Consequently one needs to develop separate "upscaling" approaches for determining what values of a coefficient should be used at a given spatial scale. But the emphasis on the partial differential equations—while ignoring the scale-dependent aspects of their coefficients—betrays a serious lack of understanding of the very processes being modeled. Likewise, the emphasis on measuring the

A. Hunt et al., *Percolation Theory for Flow in Porous Media*,
Lecture Notes in Physics 880, DOI 10.1007/978-3-319-03771-4_13,

coefficients—while ignoring their scale-dependence—leads to research into corrections built on top of misconceptions.

One does not require coefficients (which have an unknown scale dependence) in a partial differential equation, if one is not using a differential equation in the first place. If these coefficients can best be found by using network models and percolation theory, then perhaps one should skip the confusing step of the continuum model and use a network or percolation model at all scales. However, the continuum approach *is* needed in order to get the physics right at the scale of a single pore scale. In some applications, the continuum approach can be extended upward to perhaps ten or even one hundred pores on a side, depending on the equation. Above that scale, a scale-aware approach is required. So (for example) the Advection-Dispersion Equation (ADE) should never be applied above the scale of a single pore. In the case of the Navier-Stokes equations and their lattice Boltzmann equivalent, it is more a question of practicality: for how large a medium is it still possible to generate the appropriate phase boundary conditions?

13.1 Some Misconceptions at the Pore Scale

1. *The water retention curve* (*WRC*) *provides a mathematical transformation of the pore-size distribution*.

This simple transformation implies a medium with the topology of the capillary bundle model. As Wilkinson [6] stated almost 30 years ago, when a porous medium wets (saturation changes from 0 to 1), two percolation transitions are encountered. The first is when the wetting phase percolates; the second is when the non-wetting phase ceases to percolate. Such transitions have profound effects on the pressure-saturation curves, including hysteresis, non-equilibrium behavior, and saturation-dependent finite-size effects. The difficulties extend beyond interpretation of experiments. Each percolation transition is associated with a diverging length scale; if simulations are performed across these transitions, but the results are not analyzed in terms of finite-size scaling, the conclusions will not be reliable. Since the shape of the WRC is affected by phase continuity for each transition, and is particularly affected by finite-size issues, inferring the pore-size distribution from the WRC cannot be valid without addressing complications best handled by percolation theory.

2. *The effects of tortuosity and connectivity on hydraulic conductivity and other properties are not known, justifying use of a phenomenology with adjustable exponent values*.

We have shown by detailed analysis that the universal scaling from percolation theory describes (at least) the saturation dependence of electrical conductivity, air permeability, solute and gas-phase diffusion, and the dry end of unsaturated hydraulic conductivity. We have also demonstrated that simulations and experiments evaluating tortuosity are well described by percolation theory. Because the form and

behavior of these properties is known, accounting for them with empirical or *ad hoc* corrections has no scientific validity.

3. *Two-dimensional models provide a reasonable description of three-dimensional problems*.

It is a fundamental rule of topology that in two dimensions it is impossible for two phases to percolate simultaneously. Consequently, a 2D grain-supported medium cannot support flow. So at the pore-scale, one cannot simultaneously model mechanical and flow properties in 2D. Likewise, in 2D the wetting and non-wetting (e.g., air and water) phases cannot flow simultaneously. Water films around particles would not interconnect, and wetting or drying the medium would produce only one fluid phase transition (or zero if the medium were grain-supported!): the non-wetting phase would cease to percolate at precisely the same saturation at which the wetting phase began to percolate. The problem is fundamentally different in 3D, where continuity of solid and two fluid phases is possible.

4. *Hysteresis in the WRC can be understood by formulating the problem in terms of the water-air interfacial area, for which the equivalent to the WRC becomes single-valued*.

Because one can predict hysteresis by appealing to accessibility and its formulation in percolation theory, hysteresis is already understood. A formal solution was available as early as the early 1980s, and we need not cast about for new solutions. Moreover, percolation considerations suggest that formulating the issue in terms of interfacial area cannot be correct: if a portion of the air infinite cluster loses its connection to the infinite cluster, the interfacial area is little changed, but the system's ability to increase its water content is diminished.

13.2 Some Misconceptions at the Geological Scale

1. *The scale-dependence of dispersivity is based in the evolving nature of the medium with increasing scale*.

The justification for this has been that the ADE cannot yield the observed experimental trends without such an input. However, we find that a medium with a monomodal distribution of local conductances and a single length scale of heterogeneity, treated using basic concepts from critical path analysis and percolation scaling, generates the observed scale-dependent dispersivity over 10 orders of magnitude of length scale. Of course one must choose a different fundamental (input) length scale for micromodel experiments than for field work, but the predicted linear dependence of dispersivity on length scale (in agreement with the Gelhar et al. [1] rule of thumb) was in agreement with experiment over the entire range of experiments investigated. This indicates that attributing this result to multi-scale heterogeneity is a consequence of applying the wrong mathematical model.

2. *Hydraulic conductivity* (K) *should increase with increasing scale because* (a) *the connectivity increases with increasing scale, and* (b) *the largest possible pore* (*or fracture*) *size increases with increasing scale*.

This assertion is supported by appealing to results of calculations of the (usually arithmetic) mean value of the hydraulic conductivity, which are scale-dependent. The upscaled hydraulic conductivity does not relate to the mean value at any smaller scale. Any physical connections that exist at large scales cannot be absent at small scales: they had to pass through the system somewhere! This can be understood most easily in an isotropic medium. However, it is possible to develop such a "scale effect" on K in anisotropic media. Using a transformation in coordinate axes suggested by Tartakovsky and Neuman [5], we showed that the increase in K was a shape effect. (It would also arise in an isotropic medium, but only in the case that the experimental volume was elongated in just one direction. Then if the experimental volume were increased proportionally in all three dimensions, flow would change from one-dimensional to three-dimensional, matching experiment.) As for the argument regarding the relevance of increasing fracture size, it seems clear that the large fractures are in the small systems somewhere too, but they are neglected or underrepresented.

3. *The increase in dispersivity with increasing scale is connected with an increase in hydraulic conductivity with increasing scale*.

See our previous conclusion, that the hydraulic conductivity does not increase with increasing scale. In fact, in isotropic systems, K *diminishes* with increasing length scales, and so does the solute velocity. The reduction in solute velocity with increasing scale is intimately connected with the increase in dispersivity with increasing scale.

4. *Long tails in arrival time distributions in fracture flow experiments are due to retardation from diffusive exchange with the rock matrix, because the ADE predicts Gaussian dispersion*.

This is an example of basing conclusions on the (inevitable) failures of an inappropriate mathematical tool, in this case the ADE. If one considers fractures to support flow through a disordered 2D medium, then the method of Chap. 11 generates the appropriate long-time tails of the arrival time distribution.

13.3 Summary

Forty years ago, percolation theory was an obscure intersection of math and condensed matter physics, with an as-yet unrecognized application in porous media.

Twenty years ago, two of us (AGH and RPE) were independently interested in applying percolation theory to porous media. At that time is was unclear (at least to RPE!) that percolation theory could address the many issues involved. Since we started to collaborate ten years ago, we have continually expanded the range of

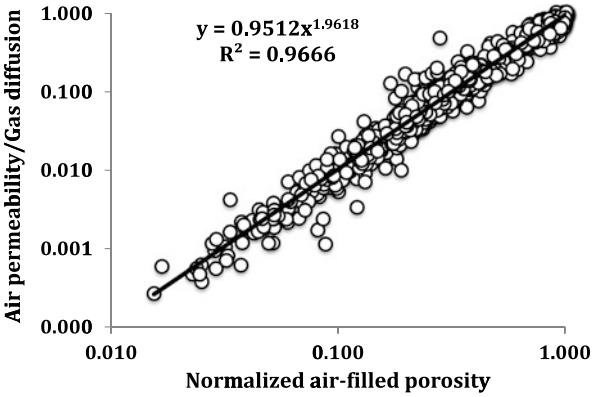

Fig. 13.1 Demonstration of the compatibility of air permeability and gas diffusion data. All data of both processes discussed in Chap. 7 are plotted here. The normalization for gas diffusion was to $\varepsilon = 1$, for the air permeability to $\varepsilon = \varphi$. For the gas diffusion we recognized, as in Fig. 2.1, that the cross-over to linear behavior (at $p = 0.8$) outside the range of observed air-filled porosity values required normalizing the gas diffusion constant to 1.28 times its actual value. Note that over 1000 individual experimental values are plotted on this graph with no selection criteria applied

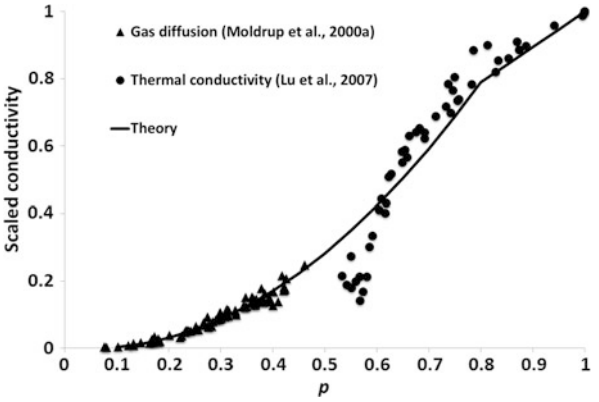

Fig. 13.2 In this figure we selected the first of the Moldrup gas diffusion databases [4] to compare with the thermal conductivity [3]. The comparison would not have been substantially different with any of the other databases. We used the cross-over from the percolation scaling function to effective-medium scaling at $p = 0.8$ as described in Chap. 2

processes and properties that we ask the theory to handle. To date we have not found an issue that could not be clarified by the use of percolation theory.

We offer two final figures (Figs. 13.1 and 13.2), showing that the simple universal scaling law (with appropriate normalization) successfully predicts multiple flow processes. Figure 13.1 demonstrates that the gas diffusion and the air permeability follow the same functional form. We simply took all the data for each, normalized the gas diffusion to its value in air and the air permeability to its value under dry conditions, and plotted them up simultaneously. Even before percolation theory was developed, the electrical conductivity was known to be proportional to the solute diffusion constant. In the 2nd edition of this book, when we had not referred to the effective-medium approximation for the conductivity at high p values, we were not very hopeful that the thermal conductivity could be so easily related to the other

conductivities. However, we now see in Fig. 13.2 that the thermal conductivity, except in a relatively narrow region of p values where the chief change of the medium relates to the elimination of the contact resistance between particles, also fits on the same universal theoretical curve. We should mention that the data of Moldrup et al. [4] are unusually uniform in that each medium has a critical volume fraction near 0.05, which was the mean value of all the Moldrup data. The power of a single theory to describe such apparently disparate processes should not be ignored. Rather, such a unifying framework should guide further investigations into universal behaviors. We anticipate that the theory will help to identify secondary effects that are real rather than artifacts, and to develop physically-based predictive capabilities in the face of once-daunting complexity.

We hope that the tools we present in this book find wide application in soil physics, hydrology, petroleum engineering, and the like. It is now unthinkable to us to work on flow in porous media without using percolation theory. We hope that a further twenty years is not required for that same "phase transition" to take place in the broader porous media community.

References

1. Gelhar, L.W.C., Welty, C., Rehfeldt, K.R.: A critical review of data on field-scale dispersion in aquifers. Water Resour. Res. **28**, 1955–1974 (1992)
2. Hunt, A.G., Ewing, R.P., Horton, R.: What's wrong with soil physics? Soil Sci. Soc. Am. J. **77** (2013). doi:10.2136/sssaj2013.01.0020
3. Lu, S., Ren, T., Gong, Y., Horton, R.: An improved model for predicting soil thermal conductivity from water content at room temperature. Soil Sci. Soc. Am. J. **71**, 8–14 (2007)
4. Moldrup, P., Olesen, T., Gamst, J., Schjønning, P., Yamaguchi, T., Rolston, D.E.: Predicting the gas diffusion coefficient in repacked soil: water-induced linear reduction model. Soil Sci. Soc. Am. J. **64**, 1588–1594 (2000)
5. Tartakovsky, D.M., Neuman, S.P.: Transient effective hydraulic conductivity under slowly and rapidly varying mean gradients in bounded three-dimensional random media. Water Resour. Res. **34**, 21–32 (1998)
6. Wilkinson, D.: Percolation effects in immiscible displacement. Phys. Rev. A **34**, 1380–1391 (1986)

Index

A
A/V, *see* Area
ac, *see* Alternating current
Access, 2, 68, 83–85, 91, 94, 111, 112, 118, 123, 124, 127, 184, 201, 220, 223, 231, 266, 273–277, 294, 308, 398, 431
Activation
  energy, 133, 250, 252, 253, 255–257, 264
ADE, *see* Advection-dispersion equation
Adjustable, *see* Fitting
Adsorb
  coefficient, 68, 76, 77, 86, 220, 342
  see also Sorption
Advection-dispersion equation, 77, 343, 346, 391, 430
  see also Solute
Aggregate, *see* Structure
Agriculture, 65, 86, 410, 412
Aharony, A., 3, 7, 389
Air
  entrapped, 277
  entry, 87, 112, 116, 124, 276, 413, 423
  -filled porosity, 79, 220, 221, 226, 247, 414, 433
  permeability, 45, 73, 144, 157, 159, 160, 219–223, 225, 227, 230, 233, 234, 245–248, 265–268, 409, 414, 415, 430, 433
  pressure, 82, 83, 87, 278
  see also Bubbling
Algorithm, 150, 278–280
Allowed, 14, 17, 29, 47, 83, 84, 141, 171, 193, 198, 260, 274, 275, 278, 279, 284, 293, 308, 357, 389, 410
Amorphous, 46, 60, 140, 250, 369, 371, 372, 399
Amplitude, 251
Analogue, 9, 12, 29, 32, 49, 65, 67, 72, 76, 77, 85, 114, 122, 134, 137, 138, 141, 142, 154, 162, 163, 208, 209, 232, 251–254, 292, 303, 321, 330, 343, 354, 411, 424, 425
Anisotropic, 31, 32, 60, 301, 302, 306, 307, 321, 324, 347, 418, 421, 422, 432
Approximate, 12–14, 17, 24, 28, 30, 85, 103, 112, 115, 136–138, 140, 143, 144, 152, 164, 168, 179, 183–185, 200, 203, 221, 235–237, 241, 252–255, 258, 261, 266, 267, 287, 289, 293, 303, 308, 309, 316, 319, 324, 328, 349, 364, 365, 367, 368, 370, 374, 376–378, 381, 382, 386, 387, 390–392, 395, 396, 398, 399, 411, 416, 417, 425
Archie's law, 41, 78, 157, 159, 166, 178–182, 184, 187, 188, 192, 193, 198, 209, 236, 264–266
Area, 4, 21, 40, 41, 48, 49, 51–53, 61, 66, 68, 69, 71, 73, 78, 122, 157, 159, 161, 162, 164, 189, 190, 220, 235, 237, 243, 244, 258, 263, 285, 286, 290, 291, 301, 315, 318, 325, 350, 380, 389, 390, 411, 422, 431
Arithmetic mean, *see* Mean, arithmetic
Arrival time, *see* Distribution, arrival time
Artificial medium, 207
Aspect ratio, *see* Shape
Average, *see* Mean

B
Backbone, 4–6, 37–39, 41, 62, 63, 139, 147, 165, 298, 315, 318, 335, 355, 362, 371, 374, 399

A. Hunt et al., *Percolation Theory for Flow in Porous Media*,
Lecture Notes in Physics 880, DOI 10.1007/978-3-319-03771-4,

Balberg, 32, 41, 138, 144, 149, 151, 162, 164–167, 169, 178–181, 185, 359
Ball, *see* Sphere
Barrier, 94, 132, 252, 253, 255, 256, 258, 411
Bead, *see* Sphere
Bernabé, 74, 75, 146, 304, 344
Bethe, *see* Lattice, Bethe
Bimodal, 152, 168, 173, 174, 177
Body, *see* Pore, body
Bond
  percolation, 2, 4–6, 8, 9, 13, 22, 28–31, 49, 92, 131, 134, 136, 206, 277, 297, 303, 335, 336, 338, 361, 362
  problem, 2, 3, 6, 22, 49, 131, 136, 277, 297
  red, 4
  see also Percolation
Bottleneck, 46, 149, 164, 166, 173, 177, 200, 203, 221, 253, 258, 267, 323, 344, 349
  see also Limiting
Boundary condition, 77, 430
Breakthrough curve, 76–78, 357
  see also Advection; Dispersion
Brooks, 87, 92, 93, 113, 116, 224
Bruderer, 75, 304, 344, 399
BTC, *see* Breakthrough curve
Bubbling, 87, 289, 294, 295
Bulk density, 63, 64, 121
Bunde, 3, 7, 9, 18, 20, 21, 24, 25

C

Calibrate, 193, 198
Cannonball, 180
  see also Swiss cheese
Capillarybridge, *see* Pendular, structure
  flow, 203, 205, 207, 266, 273, 291
  force, 80
  fringe, 112
  number, 125, 126
  pressure, 79, 80, 111, 116, 122, 125, 126
  rise, 80–82
  tube, 91, 151, 334, 342
  water, 82, 85, 86, 112, 115
  see also Model, capillary tube
Cation, 250, 256, 257
  see also Counterion
Cement, 20
Channel, 294
  distance, 10, 20, 21
  path, 4, 37–39, 335, 399
  see also Tortuosity
Classic, 23, 25, 51, 69, 132, 140, 225, 251, 268, 345, 357
Clay, 64, 65, 73, 90, 92, 132, 169, 179, 187, 188, 192, 196, 219, 220, 229, 237, 238, 240, 241, 249–251, 253–261, 288, 290–292, 306, 423, 424
  see also Hydrated; Smectite
Cluster
  density, 7, 17
  disconnected, 208
  fractal dimension of, 116, 120, 126, 173, 210, 369, 377, 389
  infinite, 4–7, 9, 12, 13, 15–18, 21–25, 30, 37, 40, 42, 44, 49, 51, 62, 83, 94, 136, 137, 139, 208, 244, 273, 275, 294, 306, 314, 316, 321, 335, 336, 352, 398, 431
    strength of, 40
    structure of, 7, 8, 37, 40, 317, 336
  mass, *see* size
  number, 18, 19
  perimeter, 4, 23, 24, 389
  radius, 4, 32, 389
  size, 6, 10, 12, 18, 19, 306, 318, 322
  statistics, 6, 10, 12–18, 20, 22–24, 28, 44, 294, 299, 301, 305, 313, 314, 316–320, 324, 326, 328–330, 342, 346–348, 417
  see also Backbone
Community
  hydrology, 61, 71
  physics, 274
  porous media, 40, 50, 72, 242, 274, 291, 295, 429, 434
  soil physics, 188
  soil science, 61, 69, 415, 416
Complication, 41, 45, 64, 111, 113, 144, 149, 159, 160, 173, 187–189, 198, 203, 214, 219, 221, 228, 234, 258, 275, 277, 278, 284, 304, 305, 313, 338, 346, 354, 400, 415, 416, 418, 422, 430
Compression, 61, 63
Condensed matter, 48, 65, 92, 132, 432
Condition
  boundary, periodic8, 161, 185
  initial, 77
Conductance, *see* Conductivity
Conductivity
  electrical, 2–4, 40, 41, 45, 49, 51, 68, 69, 71, 72, 78, 131, 132, 140, 143, 144, 149, 150, 152, 153, 157–164, 166, 178–181, 183–190, 192–199, 208, 209, 219, 220, 237, 240, 249–255, 260, 261, 264–268, 313, 319, 333–335, 430, 433

equation, 52, 53, 69, 70, 74, 84, 88, 90, 144, 145, 148, 154, 157, 160, 161, 163, 166, 179, 197, 198, 202, 203, 219, 238, 240, 250, 261, 278, 287, 302, 303, 316, 343, 394, 416
hydraulic, 41, 51, 52, 54, 55, 69, 73, 74, 84, 87–91, 113, 124, 138, 143–145, 147–153, 157–161, 163, 166–169, 171, 173, 175–178, 183–185, 188, 200, 202–205, 207, 209, 211, 213, 214, 219, 220, 260, 265–267, 273, 277–279, 285–288, 299–301, 304, 306, 307, 319, 323, 324, 326, 328, 329, 334, 335, 342–344, 346–348, 352, 358–362, 371, 383, 390, 393, 394, 409, 410, 412, 414–420, 422–424, 430, 432
Connection, 2, 26, 27, 50, 59, 60, 65, 67, 78, 84, 93, 124, 131, 158, 161, 187, 254, 265, 283, 304, 347, 410, 431, 432
Connectivity, 1, 3, 40, 46, 52, 55, 70, 71, 79, 86, 89–91, 94, 121, 126, 141, 158, 180, 181, 202, 219, 234, 242, 247, 264, 267, 277, 300, 302, 333, 347, 350, 393, 412, 419, 430, 432
Consensus, 70, 250, 410
Constitutive, 31, 67, 71, 74, 93, 301, 334
Contact
angle, 66, 79–82, 85, 111, 116, 125, 173
resistance, 160, 188, 193, 198, 199, 235, 266, 434
Continuity, 26, 82, 89, 112, 115, 159, 166, 207, 219, 265, 273, 274, 284, 285, 329, 430, 431
Continuous-time random walk, 77, 343, 345, 346, 370, 395
see also Advection; Dispersion
Continuum, *see* Percolation, continuum
Contribute, 4, 9, 32, 40, 41, 54, 70, 73–75, 81, 83, 84, 90, 93, 108, 123, 143, 171, 179, 188–197, 199, 237, 238, 240, 241, 250, 253, 264, 266, 267, 274, 275, 291, 292, 294, 317–319, 322, 352, 355, 360, 361, 389, 393, 395, 410, 414, 415
Convection, *see* Advection
Coordination, *see* Connectivity
Core, 7, 59, 64, 195, 305, 306, 355, 361, 380, 384
Corey, 87, 92, 113, 116, 224
Correlation
function, 7, 9, 21, 328, 329
length, 4, 7–12, 15, 17, 19–22, 24, 25, 27, 28, 33, 38, 40–42, 44, 45, 52–54, 136, 138, 139, 142, 148, 154, 208, 237, 273, 292, 297–304, 308, 309, 314, 315, 317, 335–337, 368, 389, 391, 393, 395
Coulomb
attraction, 258
effect, 258
energy, 250, 255
force, 250
interaction, 250, 251, 258
potential, 255
repulsion, 250
Counterion, 255, 257–259
Coupled transport, 120, 207
CPA, *see* Critical, path
Critical
behavior, 9, 10, 14, 127, 244
bonds, 55, 315
conductance, 47, 49, 51, 145, 153, 163, 237
exponent, 10, 14–16, 18, 25, 27, 32, 33, 38, 43, 44, 47, 166
fraction, 2, 67, 204
frequency, 252, 254, 258–260
path, 9, 45–47, 49–52, 54, 55, 75, 78, 90, 94, 131, 132, 136, 138, 140, 143–146, 148, 151–153, 158, 159, 161, 163, 165–168, 170, 171, 203, 209, 211, 219, 234, 236, 249–251, 253, 255, 258, 264, 266, 267, 283, 297, 298, 300, 303, 313, 323, 334, 337, 342–344, 346, 347, 360, 393, 415, 417, 422, 431
rate, 254
resistance, 54, 134, 135, 151, 154, 179, 254, 315, 317, 330, 349
volume, 31, 32, 90, 94, 144, 145, 148, 173, 180, 181, 188, 191, 193, 197–200, 204, 206, 207, 211, 220, 240, 241, 246, 273, 274, 276, 277, 285, 288, 290, 291, 294, 295, 302–305, 309, 320, 352, 353, 356, 362, 368, 411, 412, 417–419, 425, 426, 434
Crossover, 120, 179, 207, 209, 226, 240, 241, 390, 412
Crystalline, 46, 60, 62, 63, 132, 250, 264
see also Noncrystalline
CTRW, *see* Continuous-time random walk
Cubic, 30, 31, 39, 74, 105, 109, 161, 171, 204, 235, 242, 292, 299, 301, 313, 317, 420
Curve, 48, 76–79, 81–88, 90, 92, 103, 106, 111, 113–124, 126, 159, 167, 169, 173, 174, 176, 184, 187, 190, 198, 199, 206, 209, 210, 222, 226, 232,

234, 246, 253, 262, 267, 273–280, 283–289, 295, 304, 305, 309, 325, 345, 354–360, 364, 367, 371, 375, 378, 381, 383, 384, 387, 388, 392, 393, 411, 412, 423, 430, 434
Cut-off, 15, 110, 164, 165, 316, 320, 349, 350

D
Dangling end, *see* Dead end
Darcy, 72–74
dc, *see* Direct current
Dead end, 4, 5
Decay, 12, 13, 16, 17, 328, 350, 370, 376
Decouple, 350
Degree of saturation, *see* Saturation
Delta, 152, 162, 349, 357
Density, 4, 7, 16, 17, 41, 48, 49, 52, 61, 63, 64, 69, 73, 80, 88, 94, 104, 105, 108, 109, 121, 122, 125, 133, 140, 150, 152, 154, 209, 236, 237, 241, 266, 267, 303, 324, 349, 380
Derivation, 4, 14–16, 19, 22, 29, 42, 55, 56, 72, 111, 162, 164, 165, 173, 179, 184, 187, 295, 313, 317, 321, 322, 339, 348, 354, 356, 395, 411
Derivative, 10, 33, 105, 112, 190, 191, 251, 294, 346, 357
Deviation, 70, 105, 112, 221, 245, 268, 279, 280, 283, 285, 287–290, 325, 333, 364, 372, 400, 417
  see also Dry end; Wet end
Diagenesis, 159, 180, 181
Dielectric, 251, 254, 256, 258
Diffusion
  coefficient, 2, 242, 344, 395
  constant, 42, 44, 148, 160, 167, 243, 244, 247, 249, 395, 398, 433
  gas-phase, 71, 244, 430
  liquid-phase, 71, 208
Diffusion-limited aggregation, 375, 388
Dimensional
  dependence, 18, 24, 51
  one- (1D), 7, 9, 14, 19–23, 33, 41, 47–50, 52, 55, 56, 71, 72, 75, 77, 134, 150, 151, 164, 208, 240, 265, 299, 300, 302–305, 350, 393, 432
  two- (2D), 20, 41, 49–52, 63, 66, 70, 91, 105, 115, 126, 138, 180, 181, 184, 221, 222, 224, 257, 258, 264, 294, 336, 338, 339, 355, 356, 361, 362, 371, 384, 385, 388, 390, 391, 398, 431, 432
  three- (3D), 50, 52, 66, 67, 91, 105, 115, 122, 126, 138, 146, 154, 180–184, 221, 257, 258, 264, 275, 299, 301–305, 336, 338, 339, 341, 360, 371, 375, 376, 380, 381, 384–392, 419, 431
  four- (4D), 25, 142, 154
  invariance, 8, 11
Direct current, 25, 132, 142, 143, 154, 219, 249–261, 316, 317, 319, 351, 398
Disorder, 46, 93, 131, 132, 183, 187, 250–252, 257, 352, 356, 363, 366, 371, 372, 390, 392, 398
Dispersion
  coefficient, 77, 343, 345, 346, 390–392, 396, 397, 399
  longitudinal, 342, 343, 345
  transverse, 342
  see also Advection; Dispersivity; Solute
Dispersivity, 77, 313, 345, 363–369, 377, 390–393, 396–399, 409, 431, 432
Displacement, 60, 75
Distribution
  arrival time, 342, 343, 345, 346, 350, 352–355, 358–362, 369, 373, 385, 393, 396, 398, 399, 432
  frequency, 54, 91, 150, 260, 319, 395, 398
  particle size, 61, 63, 68, 70, 74, 88, 127, 200–202, 260, 277, 360
  pore size, 55, 64, 66–68, 70, 79, 82, 84–90, 92, 103, 108, 111, 114, 126, 158, 163, 168, 171, 178, 181, 184, 199, 201–203, 207, 209, 221, 260, 265, 266, 283, 284, 347, 349, 350, 354, 362, 393
  spatial, 256, 346, 362, 363, 391
  see also Probability density function
Diverge, 7–12, 17, 21, 27, 38, 40, 51, 159, 205, 208, 238, 273, 335, 336, 339, 349, 351, 352
Drain, *see* Drying
Dry end, 85, 86, 112–115, 124, 266, 273, 274, 285, 415, 430
Drying, 1, 62, 68, 82–84, 112, 131, 180, 274–277, 294, 337, 355, 359, 362, 431
Dual
  of a lattice, 92
  porosity, 409–411, 414, 415

E
Edge, 62, 63, 112, 228, 274, 275
Effective medium, 42, 45, 71, 251, 266, 267
Einstein, 42
Electric
  conductance, 150

conductivity, 2–4, 40, 41, 45, 68, 69, 71, 72, 78, 131, 132, 140, 143, 144, 149, 157–161, 163, 164, 178–181, 183–190, 192–199, 208, 209, 219, 240, 249, 250, 252–254, 260, 264–268, 298, 313, 319, 333, 335, 430, 433
dipole, 251, 255
field, 250, 253, 254, 264
potential, 250, 253
resistance, 150, 253, 319
resistivity, 47, 49, 52, 53, 78, 161, 192, 193, 198
Electrokinetic, 157, 160–163, 264, 265, 267
Electromagnetic, 264
Electron, 131, 133, 140, 253, 254, 377
Electroseismic, 219
Empirical, 70, 71, 74, 78, 87, 89, 93, 116, 126, 237, 429, 431
Energy, 18, 33, 63, 68, 69, 79–81, 109, 110, 113, 114, 132, 133, 140–142, 250–253, 255–258, 264, 372, 410, 416, 421, 422
Ensemble, 42, 47, 48, 63, 305, 316, 319, 320, 322, 323
Entrapped, *see* Trap
Equilibrium, 80–83, 85, 111–113, 122, 124, 125, 133, 148, 171, 200, 255, 273–275, 280, 283, 284, 287, 292–294, 374, 416
Ergodic, 292, 293
Euclidean, 4, 7, 10, 13, 17, 20–22, 28, 38, 44, 69, 103, 104, 115, 315, 317, 335, 337, 348, 351, 389
Exchangeable, 43, 77, 195, 256, 398, 432
Experiment, 18, 73, 76, 113, 143, 152, 160, 165, 167, 168, 171, 173, 176, 181, 191, 201, 202, 207, 214, 219, 221, 223, 228, 234, 235, 238, 241, 257, 265, 276–278, 280, 288–290, 293–295, 299, 300, 308, 309, 316, 324, 329, 333, 334, 338, 342–347, 355, 357, 360–362, 368, 369, 378, 380, 384–388, 391, 392, 411, 412, 414, 417, 431, 432
Exponent
critical, 10, 14–16, 18, 25, 27, 32, 33, 38, 43, 44, 47, 166
Fisher, 44, 316, 328
non-universal, 41, 160, 162–164, 180, 181, 191, 371
universal, 160, 163, 181, 199, 207, 231, 265, 371
Exponential
distribution, 14, 15, 18–20, 24, 25
function, 8, 14, 21, 48, 54, 132–134, 137, 141, 143, 144, 146, 153, 293, 339, 350, 416, 417
integral, 318, 328, 348, 349
see also Probability density function, exponential
Extreme value, 41, 47–49, 344

F

Fermi, 132, 140, 141
Film
flow, 84, 86, 148, 159–163, 171, 202–205, 207, 208, 266, 273
thin, 68, 205, 319
Fingering
gravity, 72, 94, 228, 383
viscous, 264, 292–294
Finite-size
effects, 6, 115, 124, 289, 301, 339–342, 430
scaling, *see* Scaling, finite size
Fitting, 71, 118, 121, 123, 191–193, 196–198, 204, 206, 260, 358, 360, 387
Flow, *see* Film
Fluid, 1, 37, 39, 55, 60–63, 65, 67–69, 71–76, 78–80, 82, 86, 89, 93, 94, 103, 112, 115, 122, 125, 126, 144, 158, 160, 161, 188, 190, 208, 220, 240, 265, 266, 284, 298, 334, 335, 341, 342, 344, 347, 350, 375, 376, 379–384, 386–389, 394, 395, 431
Flux, 6, 69, 73, 74, 161, 345, 350, 352, 357, 362, 380, 394
Fortuitous, 309
Fourier, 11, 72, 251, 329
Fractal
characteristics, 8, 9, 44, 92, 127, 166, 342
dimension, 5, 8, 14–17, 20, 28, 37–39, 42, 68, 92, 104–111, 113, 115–122, 126, 165, 173, 177, 184, 185, 187, 202, 209, 210, 261, 274–277, 285, 287, 289, 303, 335, 336, 349, 352, 353, 355, 356, 362, 364, 365, 369, 371, 374, 375, 377, 389, 395, 399, 411, 412, 414, 417, 423, 424
multi, 92
self-similar, 7, 103–106, 126, 161, 176, 187, 213, 337
surface, 261, 389
truncated, 8, 122, 158
Fractional, 6, 31, 66, 112, 164, 303, 325, 345, 346, 350

Fracture, 60, 103, 104, 264, 284, 300, 303–306, 313, 323, 324, 328, 345, 347, 366, 398, 432
Fragmentation, 103, 118, 178, 303
Frequency
  distribution, 54, 91, 150, 260, 319, 395, 398
Function
  exponential, 8, 14, 21, 48, 54, 132–134, 137, 141, 143, 144, 146, 153, 293, 339, 350, 416, 417
  diminishing, 14, 75, 183, 254
  increasing, 161, 283, 324, 364
  monotonic, 75, 151, 152, 161, 283, 364, 372, 398
  non-monotonic, 75, 364
  power-law, 16, 75, 87, 104, 105, 120, 122, 126, 151, 252, 299, 337, 339, 349, 370

G

Gas, 45, 63, 64, 71, 73, 74, 94, 157, 159, 219, 242–244, 246–249, 265–267, 430, 433
  see also Air; Vapor
Gaussian, *see* Probability density function, Gaussian
Geologist, 54, 292, 333
Geology, 32, 54, 55, 61, 62, 69, 71, 73, 79–81, 85, 111, 149, 150, 152, 153, 234, 292, 297–300, 313, 328, 333, 344, 409, 410, 416, 418, 420, 422, 431
Geometric mean, *see* Mean, geometric
Geostatistics, *see* Spatial, statistics
Glass (transition), 264, 292–294
Grain, 11, 60, 64, 65, 67, 82, 91, 180, 181, 187, 202, 207, 234, 235, 237, 266, 275, 284, 309, 334, 383, 386, 387, 418, 419, 431
Granular, *see* Particulate
Gravity, 72, 94, 228, 383
Grid, *see* Lattice

H

Hanford (soil), 109, 110, 113, 114, 167, 168, 185–187, 280, 281, 288–290, 374, 410, 422
Harmonic mean, *see* Mean, harmonic
Havlin, 3, 7, 9, 18, 20, 21, 24, 25, 42, 242
Heat
  capacity, 293
  see also Temperature; Thermal
Heaviside, 357
  see also Delta
Height (of capillary rise), 72, 73, 80, 81, 83–85, 87, 88, 91, 112, 256, 258, 293, 325, 357
Hierarchical, 20, 103, 116, 409, 410, 418, 420
Hole/holes, 2, 3, 6, 7, 11, 94, 138, 298
Hopping
  charge, 132, 251, 255–257
  conduction, 48, 132, 134, 249–251, 255, 257, 258, 314, 371, 398
  electron, 133, 254
  proton, 255, 258
  variable range, 143
Horizontal, 55, 150, 169, 287, 301, 302, 304, 305, 321, 323–326, 349, 352, 370, 378, 392, 421, 422, 424
Humus, *see* Organic (matter)
Hydrated (clay), 188, 219, 249, 260
Hydraulic
  conductance, 144, 148, 160, 162, 213, 347
  gradient, 1, 69, 72, 73, 76, 161, 180, 274, 394
  pressure, 81
  resistance, 74
Hydrogen, 132, 133
Hydrogeology, *see* Hydrology
Hydrologist, 71, 79
Hydrology, 37, 61, 69, 71, 84, 111, 138, 143, 144, 299, 343, 345, 347, 362, 434
Hydrophilic, *see* Wetting
Hydrophobic, *see* Nonwetting
Hyperscaling, 24, 25
Hysteresis, 59, 83–85, 111, 148, 191, 273, 274, 277, 283, 295, 430, 431

I

Ideal (gas law), 244
Imbibition, *see* Wetting
Inconsistency, 40, 45, 61, 71, 77, 90, 112, 138, 274, 343
Infiltration, 300, 308, 309, 337
Infinite
  cluster, 4–7, 12, 13, 17, 18, 22, 23, 37, 40, 42, 51, 62, 83, 94, 136, 137, 208, 244, 273, 275, 294, 321, 431
  size, 4, 7, 15, 16, 30, 44, 49, 103, 133, 303, 314, 398
Ink bottle, 83, 84, 91
Integral, 13, 14, 17, 18, 47, 74, 105, 108, 122, 123, 142, 152, 153, 200, 279, 317–319, 321, 322, 328, 329, 348, 349, 351, 357
Interfacial
  areas, 431
  energy, 79

tension, 221, 295
Invasion, *see* Percolation, invasion
Isotropic, 60, 78, 300–302, 306, 321, 343, 350, 422, 432
see also Anisotropic

K
Katz, 74, 110, 146, 300, 304, 334
Kozeny–Carman, 69, 70, 73–75, 146, 157, 166, 184, 334

L
Laminar, *see* Reynolds number
Laplace, 416
Lattice
anisotropic, 31, 32, 60, 301, 302, 306, 307, 321, 324, 347, 418, 421, 422, 432
BCC, 30, 31
Bethe, 15, 19–24, 277
cubic, 30, 31, 39, 235, 420
dual, 28, 29
FCC, 30, 31
hexagonal, 206
honeycomb, 29–31, 50
infinite, 25, 40
irregular, 64, 66, 177, 347
kagomé, 31
random, 1, 70, 134
regular, 31, 91
square, 2, 4, 5, 13, 28–31, 49, 50, 335, 356
triangular, 25–27, 29–31, 50
Layer, 68, 220, 255–257, 259, 261, 278, 325
Limit, 4, 7, 8, 12, 17, 18, 20, 25, 32, 38, 41, 44, 46–48, 75, 94, 111, 112, 117, 123, 138, 146, 148–150, 159, 164, 166, 167, 178, 179, 188, 190, 198, 199, 221, 236, 237, 240, 241, 243, 245, 246, 253, 254, 261, 287, 290, 302–304, 307, 319, 321–323, 328, 329, 334, 335, 337, 338, 349, 352, 353, 357, 364, 370, 383, 390, 416, 417
Limiting, 12, 32, 44, 46, 48, 50, 51, 53, 54, 91, 122, 137, 148, 149, 152, 159, 253, 255, 256, 302, 303, 321, 374, 375, 388
Linear, 7, 12, 15–17, 28, 38, 44, 45, 48, 72, 77, 78, 104, 105, 144, 188, 189, 199, 205, 206, 235, 237, 238, 240–242, 246, 250, 258, 261–263, 265–267, 313, 315, 318, 321, 329, 330, 345, 348, 349, 369, 389, 396, 409, 421, 431, 433
Link-node-blob, 4, 137
Liquid, 68, 71, 73, 78, 80, 81, 111, 115, 188, 190, 195, 208, 219, 266, 291, 374, 386
Log-normal, 51, 92, 105, 112, 114, 153, 209, 319, 391, 415–417, 420
see also Probability density function, log-normal
Logarithm, 27, 50, 51, 90, 109, 134, 137, 138, 146, 177, 179, 189–191, 236, 254, 293, 349, 362, 363, 380, 396, 397
Loop, 4–6, 20, 138

M
Magnetic, 18, 33, 264, 268
Mandelbrot, 38, 122, 335, 336
Mapping, 92, 103, 279, 300, 347
Mass, 4, 5, 7, 15, 17–20, 22, 37–39, 63–65, 68, 77, 80, 104, 117, 119, 121, 260, 350, 374, 380, 389, 394, 395, 423
Matheron (conjecture), 51, 419, 420, 425, 426
McGee Ranch, 167–169, 187, 201, 279, 288, 412
Mean
arithmetic, 54, 55, 70, 71, 89, 91, 104, 105, 152, 323, 334
cluster size, 20
-field, 20, 22, 23, 25
geometric, 50–52, 65, 70, 71, 386, 419, 420
harmonic, 47, 54, 55, 70, 71, 150, 152, 334
see also Ensemble
Median, 49, 50, 52, 383, 419
Meniscus, 66, 79, 80, 84, 274
Mercury (injection), 85, 86, 111, 124, 182, 273
Model
capillary tube, 91, 151, 334
fractal, 87, 92–94, 103–106, 109, 112, 113, 115, 116, 119, 122, 123, 126, 127, 131, 144, 158, 159, 167, 184, 200–202, 209, 265, 266, 278, 283, 294, 300, 343, 392, 398, 417
network, 59, 91, 92, 126, 131, 138, 161, 162, 242, 277, 346, 430
Rieu and Sposito, 75, 103, 106, 118, 119, 158, 164, 167, 179, 283, 300, 303, 320, 416, 417, 423, 424
Moisture, 45, 54, 55, 62, 63, 90, 112, 113, 148, 149, 158–160, 164–169, 171, 173, 178–180, 188, 193, 200, 203, 204, 206, 209, 211, 212, 214, 226, 228, 231, 232, 237, 238, 241–244, 258, 264, 266, 273–280, 283–285, 287–290, 292, 293, 295, 308, 309, 320, 336, 338, 351, 353–355, 358, 411, 412, 414–417, 421, 422

see also Water
Moldrup, 42, 168, 240, 243–245, 248, 249, 285, 286, 290, 291, 433, 434
Molecule, 68, 76, 256, 258, 389
Moment
first, 22, 33
second, 18, 19, 22, 33, 363
Monodisperse, 203

N
Navier–Stokes, 69, 72, 144, 333, 355, 430
Neighbor
nearest, 4, 6, 22, 23, 25, 26, 30, 31, 48–50, 134
see also Hierarchical
Network, 1–3, 6, 46, 51–53, 59, 60, 65–67, 70, 85, 91, 92, 126, 131, 133–136, 138, 161–163, 179, 236, 242, 258, 264, 265, 277, 291, 335, 336, 346, 352, 372, 430
see also Model
Neutron, 67, 86
Newton, 69, 73
Non-crystalline, 250
Non-equilibrium, 77, 124, 173, 276, 278–280, 283, 372, 430
Non-universal, 3, 41, 93, 144, 149, 158–160, 162–165, 167, 178–181, 185, 190, 191, 204–207, 221, 265, 359, 360, 364, 368, 371
Non-wetting
fluid, 73, 79, 80, 82, 93, 220
phase, 84, 219, 222, 430, 431
Normal, *see* Probability density function, normal
Normalize, 7, 45, 48, 49, 76, 108, 122, 123, 152, 163, 164, 199, 200, 213, 223, 225, 227, 230–234, 243, 244, 246–248, 266, 275, 316, 320, 338, 339, 348–350, 357, 380, 382, 384, 433
Notation, 13, 63, 106, 253, 286, 350, 399
Number, 4, 6, 7, 9, 12, 16–24, 28, 31, 32, 37, 38, 40, 42, 46, 48, 52, 61, 66, 67, 69, 90, 104–106, 113, 116, 117, 119, 121, 125, 126, 134–136, 141, 144, 150, 160, 165, 189, 192, 206, 223, 228, 230, 251, 254, 255, 257, 258, 261, 262, 273, 276, 283, 288, 289, 291, 292, 301, 315, 317, 328, 338, 344, 348, 352, 356, 376, 380, 386, 387, 394–399
Numerical solution, 353, 375

O
Octahedron, 206
Ohm, 40, 72
Oil, 60, 68, 79, 81, 125, 294, 295
see also Petroleum
One dimensional, *see* Dimensional, one- (1D)
Optimal
conductance, 51, 352
length, 5, 208
path, 5, 39, 152, 208, 335, 336, 348, 395
Optimize, 51–54, 56, 65, 113, 137, 138, 141, 145, 146, 153, 190, 194–196, 233, 259, 266, 298, 316, 347, 352, 393, 394
Order of magnitude, 92, 126, 144, 172, 234, 324, 364, 377, 379–381, 383, 389, 393
Organic (matter), 81
Osmotic, 81
Overlap, 32, 132, 133, 136, 254, 418
Oxygen, 256

P
p_c, *see* Critical, probability; Percolation, threshold
Packing
close, 67, 73, 74, 204, 206
Parallel, 41, 53–55, 70, 75, 77, 89, 91, 149–152, 190, 193, 199, 205, 207, 243, 257, 259, 264, 298, 409, 410, 414
Parsimony, 390, 415
Particle
density, 63, 64, 104, 121
radius, 104, 109, 202, 261, 382
size distribution, 61, 63, 68, 70, 74, 88, 127, 200–202, 260, 277, 360
Particulate, 62
Path
chemical, 4, 37–39, 335, 399
lengths, 38, 208, 344, 351
minimal, 148
optimal, 5, 39, 152, 208, 335, 336, 348, 395
pdf, *see* Probability density function
Peclet number, 344, 394–397, 399
Pendular
ring, 235–237
structure, 82, 235, 237, 238, 240, 241, 267, 284
water, 241, 266
Percolation
cluster, 12, 15, 25, 37, 39, 389, 398
continuum, 1, 3, 6, 31, 92, 93, 131, 144, 157, 180, 204, 242, 259, 265, 275,

277, 297, 302, 303, 336–338, 418–420, 429, 430
E-, 140, 251–254
invasion, 1, 39, 60, 83, 85, 274, 355, 358, 359, 361, 362, 365, 384, 385, 388, 390
probability, 9, 17, 21, 25, 29, 30, 47, 50, 55, 131, 299, 300, 336
r-, 48, 132, 133, 135, 142, 143, 153, 251–254
r–*E*, 133, 135, 140, 142, 143, 153, 266, 314
site, 1, 6, 7, 10, 20, 30, 131, 422
theory, 1–4, 6, 7, 9–12, 14–21, 24, 25, 37, 40, 43–46, 51, 55, 59, 60, 62, 65, 70, 72, 75, 78, 90, 92, 113, 131, 134–136, 144, 146, 149, 150, 157–160, 162, 163, 166, 181, 187, 206, 209, 221, 234, 240, 255, 256, 259, 264–268, 274, 275, 277, 287–289, 295, 297–300, 304, 305, 308, 313, 314, 321, 324, 328, 330, 333–335, 342, 344, 346–349, 354, 360, 367, 369, 371, 375, 389–391, 393, 409, 417–420, 422, 423, 429–434
threshold, 3–5, 7–9, 11, 12, 15, 23, 32, 38, 40–42, 44, 45, 49, 51, 52, 54, 91, 127, 131, 134, 138, 148, 149, 152, 153, 158, 168, 179, 188, 189, 195, 205, 208, 214, 221, 226, 227, 231, 234, 236, 237, 240, 245, 246, 248, 251, 255, 264–266, 273, 277, 280, 283, 290, 292, 297–299, 316, 321, 336–340, 342, 347, 352, 354, 355, 388, 389, 393, 398
transition, 3, 11, 13, 46, 254, 273, 285, 287, 288, 298, 308, 430
see also Critical; Trap
Perimeter, 4, 23, 24, 74, 389
Permeability, 45, 62, 68–70, 72–75, 89, 90, 144, 157, 159, 160, 219–223, 225, 227, 229, 230, 233, 234, 245–248, 265–268, 297, 333, 347, 372, 377, 409, 414, 415, 421, 430, 433
see also Conductivity
Permittivity, *see* Dielectric
Petroleum, 61, 68, 69, 78, 79, 86, 89, 92, 111, 188, 333, 374, 434
Phase
air, 84, 90, 113, 219, 220, 222, 273, 274, 289, 431
liquid, 188, 190, 195, 219, 291
non-wetting, 84, 219, 222, 430, 431
solid, 63, 89, 105, 106, 118, 119, 122, 160, 188, 190, 192, 194–196, 199, 220, 234, 240, 241, 266, 291, 431
transition, 11, 292, 309, 431, 434
vapor, 202, 273
wetting, 84, 222, 240, 241, 273, 430, 431
Phenomenology, 76, 87, 91, 93, 112, 166, 188, 189, 237, 241, 244, 251, 430
Phonon, 132, 140, 252, 253, 260
Phyllosilicate, *see* Clay
Physics
condensed matter, 65, 432
soil, *see* Soil, physics
solid state, 1, 143, 313
Poiseuille, 69, 73, 85, 144, 160, 171, 173, 176, 178, 213, 416
Polar, 68, 79
Pore
body, 65, 66, 78, 84, 92, 274
pressure, 161
radius, 66, 75, 84, 108, 111, 115, 116, 123, 126, 127, 144, 146, 158–161, 167, 168, 175, 177, 180, 200, 202, 203, 209–211, 213, 221, 262, 263, 300, 303, 411
-scale, 55, 59, 65, 73, 89, 144, 157, 161, 344, 378, 380, 381, 424, 431
size distribution, 55, 66, 67, 84, 86, 92, 111, 117, 124, 126, 158, 166, 168, 171, 173, 174, 180, 201, 209, 222, 260, 265, 266, 273, 284, 346, 350, 354, 356, 358, 399, 430
space, 1, 3, 55, 63, 67, 79, 86, 103, 106, 108, 110, 111, 121, 126, 148, 159, 161, 164, 171, 175, 179, 182, 188, 193, 201, 202, 206–208, 219, 221, 250, 264, 266, 273, 275–277, 285, 288, 289, 291, 300, 343, 349, 352, 353, 356, 364, 365, 369, 377, 410, 412
structural, 68, 112, 114, 120, 209, 221, 410–413
textural, 120, 209, 410–413
throat, 65, 66, 68, 78, 84, 91, 92, 148, 274
Porosity, 32, 45, 60, 62–64, 66–71, 74, 75, 77–79, 89, 92, 94, 107, 108, 110–113, 116, 117, 119–121, 123, 157–159, 164, 166–169, 178–185, 187, 189–191, 193, 199, 200, 203, 204, 209, 211, 212, 220, 221, 223, 225–228, 232, 236–238, 240–245, 247–249, 264, 266–268, 278, 280, 287, 289, 291, 294, 300, 303, 305, 309, 333, 336, 338–342, 361, 362,

377, 380, 409–412, 414–417, 423, 424, 433
Porous, 1, 3, 4, 6, 7, 31, 32, 37, 40–43, 49, 50, 55, 59–65, 67–82, 84, 91–93, 103–106, 111, 113, 116, 118, 120, 124, 126, 127, 131, 134, 137, 138, 144, 148, 149, 153, 162, 173, 176, 180, 184, 185, 203, 209, 213, 219, 220, 226, 235, 242, 244, 247, 250, 262, 265, 266, 268, 273, 274, 278, 290–295, 297, 306, 308, 317, 321, 328, 333, 334, 336, 338–340, 342, 343, 345–347, 366, 374, 376, 388, 396, 398, 418, 429, 430, 432, 434
Power
  function-law, 104, 105, 339
  see also Probability density function, power-law
Precipitation, 180
Predict, 31, 37, 40, 46, 54, 69–71, 77, 88, 111, 113, 126, 143, 157, 158, 167, 171, 179, 185, 201, 202, 220, 221, 234, 247, 260, 262, 283, 288, 309, 330, 334, 339, 345, 346, 358, 360, 361, 364, 375, 398, 415, 422, 423, 431
Preferential (flow), 361, 362
Pressure
  gas, 63
  hydraulic, 84
  -saturation, 82–85, 87, 88, 91, 106, 111, 273, 275, 278, 283, 430
Probability
  critical, 21, 30, 47, 50, 55, 131
  see also Probability density function
Probability density function
  exponential, 8, 13, 14, 21, 48, 54, 56, 132–134, 137, 141, 143, 144, 146, 147, 153, 250, 253, 254, 258, 260, 263, 293, 299, 318–320, 328, 339, 348–350, 395, 416, 417
  Gaussian, 13, 24, 316, 319, 325, 370, 390, 393, 396, 419
    see also normal
  log-normal, 51, 92, 105, 112, 114, 153, 209, 319, 391, 415–417, 420
  normal
    see also Gaussian
  power-law, 16, 105, 122, 349
  uniform, 49–51, 153, 350, 418, 425
Property
  geometrical, 32, 59, 61, 62, 93, 103, 105, 115, 118, 119, 124, 136, 144, 150, 151, 153, 180, 221, 235, 237, 240, 261, 265, 279, 285, 334–337, 339, 341
  global, 1, 2, 347, 374
  hydraulic, 73, 163, 184, 219, 300, 329, 334
  local, 1, 46, 52, 55, 74, 75, 132, 134, 140, 144, 153, 157, 158, 299, 334, 347, 354, 372, 393, 417, 419, 431
  mechanical, 62, 69, 91, 111, 132, 134, 265, 293, 431
  percolation, *see* Percolation, properties
  physical, 3, 103, 300
  topological, 1, 46, 54, 59, 61, 62, 67, 92, 93, 113, 149, 153, 163, 221, 222, 237, 240, 241, 265, 346, 355
  transport, 1, 3, 9, 37, 55, 60, 67–69, 71, 93, 149, 235, 265, 268, 292, 297, 313, 410
Proton, 250, 255, 257, 258
Pruning, 4, 91, 242

Q

Quantum, 132, 134

R

Radiation, 63, 67, 85, 86
Radius
  of a cluster, 32
  of curvature, 66, 84
  pore, *see* Pore, radius
  of a tube, 54, 80
Random
  field, 52, 328, 343, 419
  walk, 25, 42, 77, 343, 345, 346, 370, 395
Range of validity, 190
Rate-limiting, *see* Limiting
Redundancy, 6, 17, 324
Regions of applicability, 184
Regression, 88, 168, 199, 228, 231, 244, 266, 286–288, 291, 423
Relaxation, 132, 251, 253, 260–263, 293
Renormalization
  group, 11, 25, 264
  scaling, 11, 20, 28
Representative elementary volume and correlation length, 71, 138, 297, 298, 349, 393
Rescaling, *see* Scaling
Residual
  conductivity, 196–198
  oil, 60, 294
  salinity, 188, 195–199
  water, 86, 116, 118, 123, 124, 277, 284, 291

Resistor, 50, 54, 70, 134, 136–138, 141, 151, 152, 165, 258, 301, 314, 317, 322, 410
REV, *see* Representative elementary volume
Reynolds number, 25, 69, 72, 144
Rieu and Sposito, 75, 103, 106, 107, 111, 112, 118, 119, 158, 164, 167, 179, 283, 300, 303, 305, 320, 416, 417, 422–424
Rock
  crystalline, 62, 63, 264
  granite, 60, 62, 380
  pumice, 60, 62, 94, 111
  sandstone, 66, 67, 187, 192, 193, 261, 291
  sedimentary, 191, 304, 421
  tuff, 192, 198, 244
Root mean square (rms), 7, 42,
Rotate, 251, 255
Rough, 15, 28, 81, 82, 116, 123, 125, 255, 275, 320
RS, *see* Rieu and Sposito

S
Sample-spanning, 39, 335
Sampling, 392, 393, 420
Sand, 60, 65, 69, 71, 73, 74, 92, 152, 180, 186, 187, 192–195, 197, 198, 208, 220, 238, 239, 244, 276, 277, 290, 298, 299, 308, 309, 341, 347, 392, 422
Saturate, 184, 416
Saturation, 55, 59, 71, 73, 79, 82–84, 87, 89, 90, 112, 118, 123, 144, 145, 148, 153, 157–160, 163, 164, 167, 170, 175, 178–181, 183–185, 187–189, 191, 198, 199, 201–205, 209, 212, 219–223, 226, 227, 231, 234, 236, 237, 240, 241, 245, 247, 265–267, 273–277, 279, 288, 295, 336, 338, 343, 346, 354, 355, 358–362, 371, 375, 376, 398, 399, 409, 410, 412, 414, 416, 417, 429–431
Scale
  dependent, 300, 305, 320, 362, 429, 431, 432
  independent, 8, 103, 345, 389
  multi- (multiple), 343, 409, 431
Scaling
  cluster, 17
    number, 72
    radius, 73, 75
  exponent, 25, 45, 78, 177, 333, 371, 372, 377, 386, 395
  finite size, 44, 242, 273, 275, 290, 294, 297, 336–339
  fractal, 113, 118, 166, 179, 226, 278–280, 283, 285, 287–290, 359
  function, 409, 433
  law, 15, 16, 20, 433
  percolation, 45, 46, 78, 157, 158, 166, 167, 178, 179, 181, 185, 188–191, 203, 207, 209, 221, 223, 231, 234, 235, 237, 240, 241, 246, 251, 266, 267, 278, 279, 317, 343, 348, 359, 385, 415, 431, 433
  radius, 78, 148, 158–161, 175, 177, 179, 221, 267, 382
  relationship, 14, 17, 18, 20, 24, 25, 28, 33, 317, 348
  spatio-temporal, 333
  see also Upscaling
Scanning curve, *see* Hysteresis
Scher, 31, 94, 204, 345, 372, 420
Seismic, *see* Electroseismic
Semivariogram, *see* Variogram
Separation
  of charge, 255, 264
  of path, 148, 149, 153, 205, 258, 308, 309
Series
  in resistors, 70
  Taylor, *see* Taylor series
Shape, 32, 64, 76–78, 86, 88, 104, 105, 108, 109, 112, 119, 123, 145, 146, 150–152, 173, 174, 177, 203, 204, 278, 279, 283, 301, 313, 346, 356, 360, 430, 432
Shrink, *see* Swelling
Silica, (Silicon), 192, 194, 195, 244, 341, 371
Silt, 65, 92, 124, 169, 186, 187, 238, 240, 241, 290, 392, 422–424
Similar
  self-, 7, 16, 103–106, 126, 161, 176, 177, 187, 213, 274, 337, 419
Simulation, 89, 338, 342, 356
Singly-connected, *see* Dead end
Site
  percolation, 2, 3, 6, 9, 25–27, 31, 39, 131, 133, 136, 337, 420
  problem, 2, 3, 26, 27, 39, 131
  see also Percolation, site
Smectite, 219, 253–256, 258
  see also Clay
Soil
  community, *see* Community, soil science
  physics, 37, 71, 84, 88, 111, 157, 164, 169, 170, 188, 207, 242, 410, 411, 434
  science, 61, 64, 69, 71, 188, 250, 410, 415, 416
  texture, *see* Texture

Solute
dispersion, 9, 37, 78, 333, 345, 347
distribution, 345, 346, 363, 392
arrival time, 342, 343, 345, 346, 350, 358, 369, 373, 385
see also Breakthrough curve
Sorption, 68, 76, 77, 86, 220, 342
Spanning, *see* Samplespanning
Spatial
correlations, 3, 126, 313, 410
statistics, 313
variability, 3, 251, 313, 346
Sphere, 2, 21, 31, 32, 64–67, 74, 75, 91, 133, 136, 154, 193, 203, 235, 240, 241
Sposito, 75, 103, 106, 107, 111, 112, 118, 119, 158, 164, 165, 167, 179, 283, 300, 303, 305, 320, 416, 417, 422–424
Square, 2, 4, 5, 13, 28–31, 42, 49–51, 53, 66, 73, 75, 105, 109, 132, 146, 237, 240, 241, 257, 261, 300, 306, 322, 335, 338, 352, 356, 381, 389, 424
see also Lattice
Stauffer, D., 3, 7, 9, 12, 13, 15, 25, 30, 38, 43, 137, 138, 267, 316, 389, 394
Steady-state, 76, 251, 265, 319
Stochastic, 75, 133, 146, 343, 344, 347, 420
Stokes, 64, 69, 72, 74, 75, 144, 333, 355, 430
Streaming, 163
Streamline, 347, 351
Strength, *see* Cluster, infinite
Structure, 1–4, 7–9, 20, 21, 31, 37, 40, 41, 60, 61, 67, 76, 82, 84, 90, 93, 111, 118, 119, 126, 138, 179, 184, 187, 204, 235, 237, 238, 240, 241, 250, 251, 265–267, 274, 277, 278, 284, 298, 299, 317, 329, 336, 346, 347, 355, 368, 389, 393, 399, 409–411, 414, 417, 421, 422, 424
Sublinear, 235, 240, 241, 250, 252, 254, 277
Superlinear, 262, 277, 395, 397
Surface
area, 4, 21, 61, 68, 73, 122, 159, 162, 164, 189, 220, 243, 244, 263, 285, 286, 290, 291, 315, 389, 390, 411
Swelling
shrink, 74
Swiss cheese, 180
see also Cannonball

T

Taylor series, 21, 23, 24, 27, 136, 257
TDR, *see* Time, -domain reflectometry
Temperature, 80, 81, 132, 133, 140–143, 154, 252, 253, 260, 292, 293, 317, 370–372, 376, 381
see also Heat; Thermal
Tetrahedron, 206
Texture, 64, 65, 74, 186, 187, 196, 209
Thermal, 45, 69, 81, 132, 153, 157, 161, 180, 219, 234–238, 240, 241, 265–267, 284, 319, 433, 434
see also Heat; Temperature
Thompson, 74, 110, 146, 159, 181, 182, 184, 187, 300, 304, 335
Three dimensional, *see* Dimensional, three- (3D)
Threshold, 3–5, 7–9, 11, 12, 15, 23, 32, 38, 40–42, 44, 45, 49, 51, 52, 54, 91, 127, 131, 134, 138, 148, 149, 152, 153, 158, 159, 168, 173, 179, 188, 189, 195, 203, 205, 208, 214, 221, 225–227, 231, 234, 236–241, 243–248, 251, 255, 264–266, 273, 277, 280, 283, 290, 292, 297–299, 316, 321, 336–342, 347, 352, 354, 355, 388, 389, 393, 398
see also Probability, critical
Throat, *see* Pore, throat
Topology, 1–3, 37, 46, 51, 54, 55, 59–62, 67, 70, 92, 93, 113, 131, 149, 151, 153, 158, 163, 166, 195, 219, 221, 222, 236, 237, 240, 241, 265–267, 335, 346, 351, 355, 430, 431
Tortuosity, 20, 37–41, 70, 71, 78, 89–91, 125, 126, 170, 171, 181, 188, 190–192, 198, 199, 235, 242, 243, 267, 268, 298, 315, 316, 333–342, 346, 350–352, 355, 388, 393, 395, 398, 399, 430
see also Chemical, path
Tracer, 76, 342
Transport, 1, 3, 6, 7, 9, 10, 20, 37, 44, 45, 55, 60, 61, 67–71, 77, 79, 89, 91–93, 131, 132, 134, 135, 138, 141, 142, 144, 149, 160, 161, 171, 187, 202–204, 207, 235, 250–252, 255–257, 264, 265, 267, 268, 273, 292, 297, 298, 300, 301, 313, 333, 334, 337, 342–348, 355, 357, 369–372, 374–377, 379–384, 386–390, 392, 399, 410, 421, 422, 424
Trap, 39, 84, 85, 89, 111, 116, 123, 274, 355, 358, 361, 362
Tree, 2, 20, 21
Triangular, *see* Lattice, triangular

Trivial, 11, 27, 335
Tube, *see* Capillary; Poiseuille
Tunnel, 132–134
Two dimensional, *see* Dimensional, two- (2D)

U
Universal, 134, 157–161, 163, 166–168, 179, 181, 183, 185, 188, 189, 191, 196, 199, 204, 206, 207, 214, 219, 221–223, 225, 227, 230–235, 242–246, 248–250, 252, 264–268, 318, 335, 364–366, 369, 371, 372, 389–393, 409, 423, 430, 433, 434
Unsaturated
  diffusion, 430
  electrical conductivity, 144, 163, 430
  flow, 416
  hydraulic conductivity, 84, 88–90, 124, 147, 149, 171, 173, 177, 209, 211, 213, 214, 220, 319, 415, 417, 430
Upscale, 50–52, 54, 55, 70–72, 77, 78, 89, 93, 144, 149, 150, 153, 300, 301, 344, 376, 409, 416–420, 424, 425, 429, 432
  see also Scaling

V
Vadose zone, 422
Van Genuchten, 87, 90, 124, 157, 169, 171, 291, 414, 415
Vanish, 4, 9, 14, 40, 44, 48, 75, 148, 149, 151, 164, 171, 251, 266, 273, 279, 297, 305, 334, 335, 352
Vapor, 60, 81, 85, 202, 273
Variability, 3, 27, 54, 61, 71, 72, 85, 144, 157, 168, 169, 181, 184, 187, 204, 207, 226, 245, 251, 298, 305, 313, 334, 335, 343, 346, 347, 352, 355, 360, 369, 371, 372, 377, 379–382, 386, 392, 396, 399, 417
Variogram, 299, 313, 326–330, 409, 424
Velocity, 38, 69, 72, 73, 75–77, 125, 132, 220, 253, 254, 333, 342–345, 350, 362, 363, 369, 374–378, 380–385, 387–390, 395, 432
Vertical, 55, 73, 80, 83, 113, 150, 168, 169, 300–302, 304, 321, 323, 324, 326, 348, 378, 380, 387, 392, 422, 424
Viscosity, 61, 69, 73, 77, 81, 125, 144, 160, 220, 265
Vug, 305
Vyssotsky, 30, 31, 151, 206

W
Water
  -repellent, *see* Nonwetting
  retention, *see* Pressure, -saturation
  see also Moisture; Wetting
Wave function, 132, 133
Wet end, 83, 87, 88, 112–115, 124, 227, 290
Wetting
  fluid, 1, 73, 79, 80, 82, 86, 93, 125, 220
  front, 1, 347, 348
  phase, 84, 219, 222, 240–241, 273, 430–431
  see also Nonwetting
Width of a distribution, 46, 322, 324, 325

Y
Young–Laplace, *see* Capillary

Z
Zallen, 31, 94, 204, 420